The mineralogical and textural characteristics of copper-gold deposits related to mineral processing attributes

Natalee Kate Bonnici

BSc. (Hons)

School of Earth Sciences

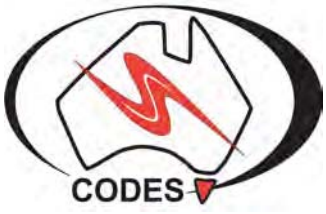

ARC Centre of Excellence in Ore Deposits

A research thesis submitted in complete fulfillment of the requirements for a Doctor of Philosophy degree at the School of Earth Sciences, University of Tasmania

May 2012

Declaration

This thesis contains no material which has been accepted for a degree or diploma by the University or any other institution, except by way of background information and duly acknowledged in the thesis, and to the best of the my knowledge and belief no material previously published or written by another person except where due acknowledgement is made in the text of the thesis, nor does the thesis contain any material that infringes copyright.

Natalee Bonnici

Abstract

The successful liberation of a mineral from its host rock is influenced by the methods of crushing and grinding as well as variability in flotation parameters, all of which are controlled by the mineralogy and textures present in the host rock itself. While it is well known that the mineralogy and texture of a rock influence mineral processing behaviour, previous studies in this field are descriptive, categorical and typically linked to a genetic connotation. In contrast to this, the parameters extracted from physical rock tests are numerical and quantified in a way that can be integrated into a working block model on site. In order to link these two fields together a more quantified approach towards mineralogy and texture is required.

In this thesis, a method for the quantified measurement and characterisation of mineralogical and textural attributes that can be used to predict variability in mineral processing behaviours in copper (Cu)-gold (Au) deposits is presented. The styles of mineralisation selected for the method development of this project were a porphyry Cu-Au deposit (Cadia East, NSW, Australia) and iron oxide-Cu-Au (IOCG; Ernest Henry, QLD, Australia) deposit. The method development sites were selected based on variable mineralogical and textural characteristics, both of which made them more amenable to different measurement techniques used within this research.

Currently there are limited methods for the routine analysis and characterisation of mineralogical and textural attributes prior to the commencement of mining with the purpose of predicting variability in mineral processing behaviours. Recent advances in the field of microscopy linked with increased computer processing capabilities mean that mineralogical and textural parameters can now be quantified more readily. This project investigated the use of advanced microscopy techniques, high resolution digital images and image analysis as tools for quantifying mineralogical and textural attributes at different scales.

Acknowledgements

There are many people that I need to thank, without you this thesis would not have happened.

My supervisors: Julie Hunt, Ron Berry and Steve Walters.

Julie, who has been a fantastic support and friend throughout this whole process, I could not have asked for a more patient supervisor especially in the last two years.

Ron, whose experience and knowledge has been invaluable I am extremely grateful and lucky to have had you as a supervisor.

Steve, whose vision and drive to think outside the box and believe that we could do it has taught me so much.

To all of my supervisors, thank you for all of the time that you have spent helping me to get this thesis completed. Without you all it wouldn't have been possible and for that I am extremely grateful.

I would like to thank the sponsors of the AMIRA P843 project for providing the funding and support for such an amazing and innovative research project.

The staff from Newcrest at Cadia East, Orange and Xstrata at Ernest Henry, Mt. Isa for their technical and on-site support and providing a world class deposits for this research to be undertaken on.

The staff from Mineral Resources Tasmania for their technical support during many months of core logging at Brighton.

Thank you to CODES for providing me the opportunity to work with an amazing group of people that I am going to miss greatly.

To my fellow Gemmers, I have learnt so much working with every one of you. I have had some amazing experiences and great times. Special thanks to Luke Keeney, Simon Mischeaux, Cathy Evans, Adel Vatandhoost, Dee Bradshaw and Tony Kojavic.

To all of my office mates past and present; Adel, Sarah, Reia, Dan and Alexey. Thanks for all the laughs (and patience over the last 12months).

To all the amazing fellow PhD students that I have met and friends I have made. Special thanks to Hiedi P, Anita, Nathan, Lee, Darren, Wjotek, Hiedi B, Jacqueline, Lindsey, Martin, Masoh, Sang, Sue, joe, Andrea, Matt and Rosein. I have no doubt that we will run into each other again.

A huge thanks to Katherine Harris, Hiedi Pass and Helen Thomas whose friendship and support over the past few years I could not have done without. Thank you for just being there to listen and making me laugh when I needed it the most.

And finally, Brendan McGee, my wonderful partner. Thank you. Without you I could not have found the strength to make it to the end. Your patience and unwavering support throughout my whole thesis I will never forget and cannot thankyou enough for.

TABLE OF CONTENTS

List of Appendices

List of Figures

CHAPTER FOUR

CHAPTER FIVE

CHAPTER SIX

List of Tables

CHAPTER FOUR

CHAPTER FIVE

CHAPTER SIX

CHAPTER SEVEN

Chapter One
Introduction

1.1 Problem Statement

The ease with which a mineral is liberated from its host rock and recovered is influenced by the method of crushing and grinding as well as the variability in flotation parameters. Each of these mineral processes is influenced by the mineral constituents of the host rocks and their textures.

While it is well known that the mineralogy and texture of a rock influence mineral processing behaviour, previous studies in this field are descriptive, categorical and typically linked to a genetic interpretation. In contrast to this, the parameters extracted from physical rock tests that are routinely measured by mineral processors are numerical and quantified in a way that can be integrated into a working block model on site. In order to link these two fields together a more quantified approach towards mineralogy and texture is required.

Recent advances in the field of microscopy linked with increased computer processing capabilities mean that mineralogical and textural parameters can be quantified more readily. Previously, these data have been used by mineral processors in the analysis of mine feed, concentrates and tails after mining has commenced. Currently there are limited methods for the routine analysis and characterisation of mineralogical and textural attributes prior to the commencement of mining with the purpose of predicting variability in mineral processing behaviours.

1.2 Aim and Scope

The aim of this study is to establish a method for the quantified measurement and characterisation of mineralogical and textural attributes that can be used to predict variability in mineral processing behaviours in copper (Cu)-gold (Au) deposits. The aim is for this method to be used prior to the commencement of mine site optimisation and planning.

The styles of mineralisation that have been selected for the method development in this project are a porphyry Cu-Au deposit and an iron oxide-Cu-Au (IOCG) deposit. Within Australia these deposits are the largest producers of copper (Geoscience Australia, 2009).

This project investigated the use of advanced microscopy techniques, high resolution digital images and image analysis as tools for quantifying mineralogical and textural attributes at different scales and resolutions. The data obtained from these techniques have been used to provide quantified mineralogical and textural information that can potentially be used predict variability in mineral processing behaviours.

This research forms part of the AMIRA P843 Geometallurgical Mapping and Mine Modelling (GeM‴) project. The GeM‴ project is a large cross-discipline research project being undertaken in the emerging field of 'Geometallurgy'.

1.3 Thesis Overview

The chapter structure of this thesis is:

Chapter one presents the introduction and aims of this project as well as an overview of the two selected study sites: Cadia East and Ernest Henry.

Chapter two is a summary of mineralogical and textural attributes used in the fields of geology and mineral processing and how they are measured. This chapter also provides a review of the literature relevant to the use of mineralogical and textural attributes for the optimisation of mineral processing during comminution, liberation and flotation.

Chapter three provides a description of the systems and techniques that have been used for the analysis of mineralogical and textural characteristics at meso- and micro-scales for different types of rock samples within this research.

Chapter four presents the analysis of meso-scale mineralogical and textural attributes. The meso-scale analysis includes a visual logging system adapted to measure geological attributes that may potentially influence mineral processing behaviours, as well as attributes derived from machine logging of drill-core.

Chapter five presents the quantified micro-scale analysis of intact rock textures and discusses the advantages and disadvantages of using two measurement platforms that are significantly different in resolution, cost and analysis time.

Chapter six presents the micro-scale mineralogical and textural analysis of particulate rock samples carried out using optical microscopy linked with image analysis.

Chapter seven presents the discussion and conclusions for this research which include the integration of meso- and micro-scale textural information as well as recommendations for further work in this field.

1.4 Study sites

Two sites were selected for method development within this project: Cadia East, which is currently in the feasibility stage of mining with production expected to commence in 2012 (Newcrest Mining Limited, 2010), and Ernest Henry, which has been in production since May 1998 and where an underground extension is due to commence production in late 2011 (Xstrata Copper, 2009).

1.4.1 Cadia East, NSW

The Cadia East deposit is a Cu-Au porphyry system that is located in Orange, New South Wales, Australia (Figure 1.1). It is one of six porphyry and skarn style deposits that cluster together to form the Cadia mineralised corridor (Newcrest Mining Staff, 1998; Figure 1.2). The Cadia East ore-body (which also encompasses Cadia Far East) is 600 metres wide and extends 2.5 kilometres along strike and 1.8 kilometres below the surface. Cadia East still remains open to the east, west and at depth. The current mineral resource estimate (2009) is 18.7 million ounces of gold and 3.16 million tonnes of copper with an estimated mine life of 30 years (Newcrest Mining Limited, 2010). Mining is expected to extend from 500 metres to 1650 metres below the surface with an extraction rate of 27 million tonnes of ore per annum.

Geological studies have been undertaken at Cadia East by Wilson (2003) and Kitto (2005). They described the mineralogy and alteration of the upper portions of the Cadia East ore-body using drill-core observations, optical microscopy and scanning electron microscope (SEM) analysis. At the time that these studies were undertaken the decline has reached the deeper portions of the ore-body but was not yet completed. Work undertaken by Wilson (2003) and Kitto (2005) refers only to the upper portions of the deposit. Drill holes collared in the decline (completed in May 2005) are referred to as Cadia East Deeps.

The mineralisation at Cadia East is dominantly hosted by and proximal to the Cadia Far East intrusive complex which comprises monzodiorite, quartz monzodiorite and quartz monzonite intrusive rocks (Kitto, 2005). At shallow levels, the copper mineralisation occurs as disseminated chalcopyrite and minor bornite within the volcaniclastic conglomerates of the Forest Reef Volcanics (Wilson, 2003). At depth, chalcopyrite, bornite, molybdenite, gold and electrum are found in multiple generations of sheeted quartz-calcite veins also within volcanicalstic conglomerates as well as within the monzonitic intrusions of the Cadia Intrusive Complex (Wilson, 2003).

The main alteration stages present at Cadia East are summarised in Table 1.1. It is the alteration stages at Cadia East that control the gangue mineralogy associated with the copper sulphide minerals. The alteration stages described by Wilson (2003) are expressed as pervasive, selectively pervasive, veins and vein selvages. A comparison of the vein assemblages recognised by both Wilson (2003) and Kitto (2005) is presented in Table 1.2. Based on this comparison, the vein assemblages have been grouped into four vein types (A, B, C and D) based on their mineral components rather than their paragenesis, which does not affect mineral processing behaviours. Given that the previous two studies only refer to the upper portions of the ore body, additional analysis of Cadia East veins undertaken during this study has established that there are a number of additional minerals also present (apatite, electrum, hessite, fluorite, tetrahedrite). These have been included in Table 1.3 which presents the mineral components of each vein group. Type examples are shown in Figure 1.3.

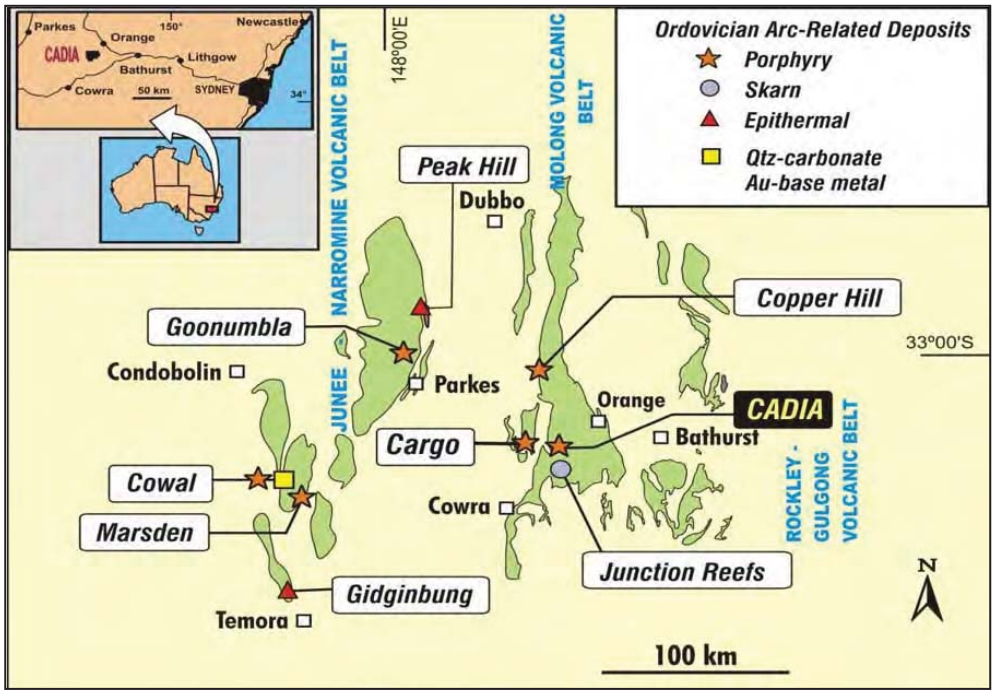

Figure 1.1. Location of the Cadia deposit with respect to the other deposits in the area. Inset shows the location of the Cadia district within Australia and NSW. *Image courtesy of Newcrest Mining Limited.*

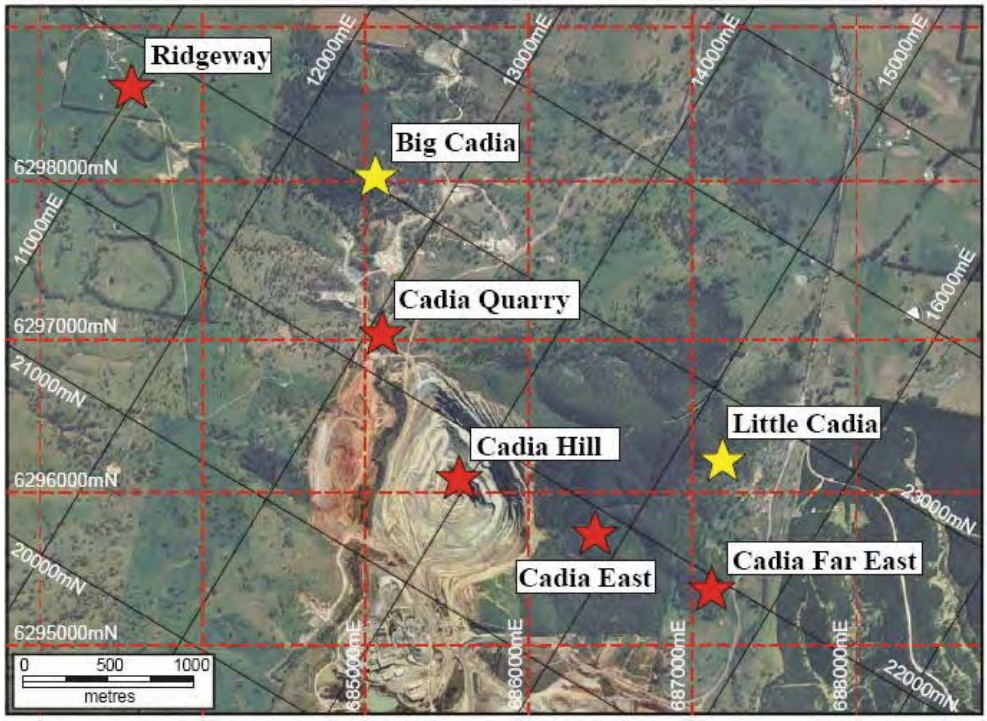

Figure 1.2. Aerial photograph of the porphyry Cu-Au (red stars) and skarn (yellow stars) style deposits within the Cadia mineralised corridor. *Image from* Wilson (2003).

Table 1.1. Main alteration stages defined at Cadia East and their associated mineral assemblages.

Alteration Stages of Cadia East	Mineral components
Sodic	albite
Potassic	orthoclase - magnetite - biotite
Inner Propylitic	albite - actinolite - chlorite
Outer Propylitic	actinolite - chlorite
Phyllic	illite - muscovite ± pyrite ± quartz

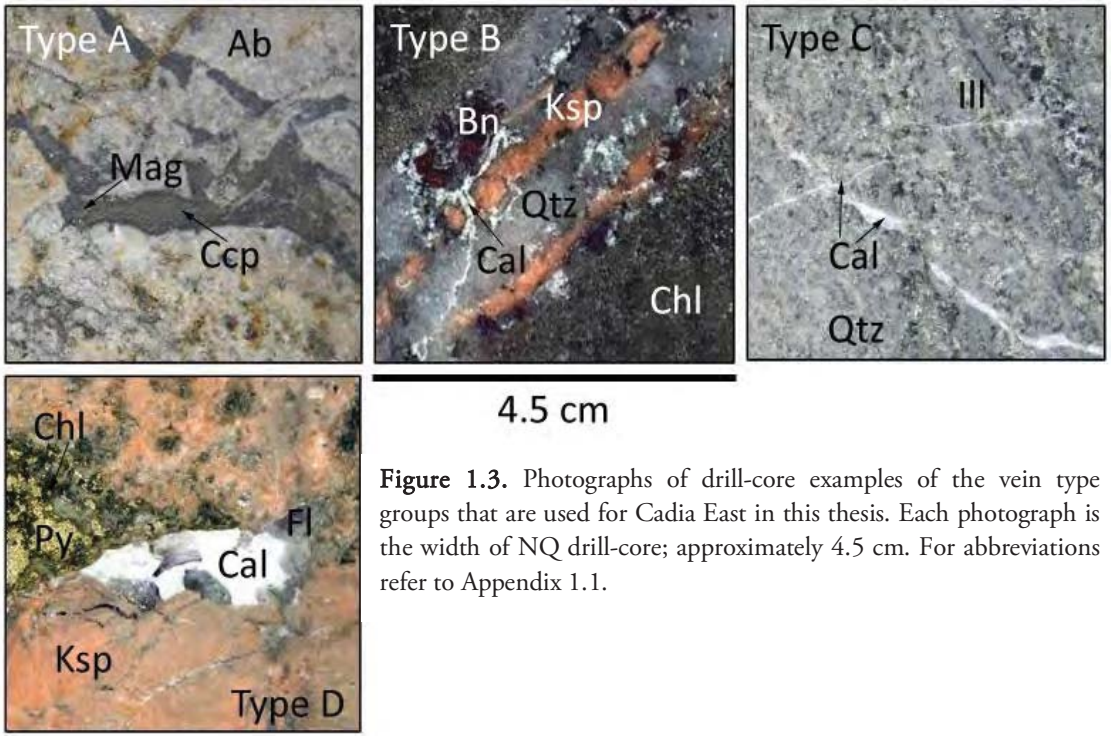

Figure 1.3. Photographs of drill-core examples of the vein type groups that are used for Cadia East in this thesis. Each photograph is the width of NQ drill-core; approximately 4.5 cm. For abbreviations refer to Appendix 1.1.

Table 1.2. Comparison of the vein styles at Cadia East recognised by Wilson (2003) [1] and Kitto (2005) [2]. For the current research each of the vein types has been assigned a group based on similarities in mineral components. These groups (A-D) will be used for Cadia East throughout this thesis (see text for details).

Alteration stage	Vein type (Wilson, 2003)	Vein Type (Kitto, 2005)	Vein mineralogy	Vein Type group
Sodic	CE-1A		magnetite - actinolite ± chalcopyrite ± pyrite ± quartz	A
Sodic	CE-1B		quartz - magnetite - chalcopyrite	A
Potassic (stage I)		Stage 1A	magnetite - quartz - calcite ± chlorite ± chalcopyrite ± pyrite ± albite	A
Potassic (stage I)		Stage 1B	actinolite - pyrite - chalcopyrite - quartz - chlorite - bornite	NIL
Sodic [1] Potassic (stage II) [2]	CE-2 aplitic vein-dykes	Stage 2B	orthoclase (K-feldspar) - quartz ± bornite ± chalcopyrite ± chlorite ± magnetite	A
Sodic	CE-3		quartz - magnetite - chalcopyrite - calcite - biotite	B
Potassic (stage II)	CE-4	Stage 2A	quartz - calcite - chalcopyrite - bornite - molybdenite - gold - chalcocite - digenite - pyrite ± sphalerite [1] ± galena [1]	B
Potasssic (stage III)	CE-5		breccia unit with clasts of CE-4	B
Outer Propylitic [1] Inner Propylitic sub-zone [2]	CE-6	Stage 6A	calcite – prehnite – epidote ± pyrite ± chlorite [2] ± quartz [2]	C
Inner Propylitic sub-zone		Stage 6B	calcite - epidote ± chlorite ± orthoclase (K-feldspar) ± pyrite	C
Phyllic	CE-7		pyrite fault zones	NIL
Phyllic	CE-8		epidote - calcite - fluorite - orthoclase (K-feldspar) - pyrite	C
Post-mineralistaion [1] Calcite [2]	CE-9	Stage 10A	calcite - laumontite ± hematite	C
Calcite		Stage 10B	calcite - fluorite	D

Table 1.3. The Cadia East vein type groups (A-D) that have been produced from a combination of vein styles assemblages established by Wilson (2003), Kitto (2005) as well as within this research[1]. For type examples refer to Figure 1.3.

Cadia East vein type group	Mineral Components
A	Magnetite veins and veinlets with variable quantities of quartz, chalcopyrite, pyrite, calcite, actinolite, chlorite, albite, orthoclase and bornite.
B	Copper and gold mineralised veins which consist of quartz and calcite with variable amounts of chalcopyrite, bornite, digenite, epidote, apatite, fluorite, orthoclase, pyrite and minor amounts of enargite [1], gold, electrum, hessite [1], clausthalite [1], bismuthinite [1] and Hg telluride [1].
C	Calcite veinlets with variable amounts prehnite, epidote, chlorite, quartz, pyrite, laumontite and hematite.
D	Calcite and fluorite veins.

1.4.2 Ernest Henry, QLD

The Ernest Henry deposit is located 38 kilometres northeast of Cloncurry, northwest Queensland, Australia (Ryan, 1998; Figure 1.4). It is the largest IOCG deposit in the Cloncurry district and the second largest within Australia (after Olympic Dam; Mark et. al, 2006). The current mineral resources are 12 Mt at 1% Cu, 0.5 g/T Au and 19% magnetite for the open pit and a probable resource of 72 Mt at 1% Cu, 0.5 g/T Au and 22% magnetite for the underground extension (June, 2009; Xstrata Copper, 2009). The current annual production rate at Ernest Henry is 115 000 tonnes of Cu and 120 000 ounces of gold in concentrate (June, 2009; Xstrata Copper, 2009).

The Ernest Henry ore-body is approximately 250 metres thick, with a width of 300 metres and is open at depth below 1000 metres (Ryan, 1998). The ore-body lies within a southeast-plunging breccia system within a sequence of porphyritic, intermediate volcanic rocks. The economic mineralisation is structurally controlled and lies between a hanging wall sequence of altered volcanic rocks and a footwall sequence of carbonate-altered volcanic rocks and siltstones (Ryan, 1998; Mark et al., 2006).

The breccia body that hosts the mineralisation grades from coherent un-brecciated volcanic rocks through crackle fracture veining to clast supported breccia zones (Strohmayr et al., 1998). The breccia consists of strongly altered felsic volcanic rock fragments supported by a matrix of magnetite, chalcopyrite and carbonate. The copper at Ernest Henry occurs as chalcopyrite, with the gold occurring as a trace component within chalcopyrite and as discrete gold inclusions within the chalcopyrite.

The hydrothermal alteration at Ernest Henry is characterised by four stages: 1. Pre-ore sodic alteration; 2. Potassic alteration; 3. Cu-Au mineralisation (includes syn-ore alteration); 4. Cu-Au mineralisation. The elements and minerals associated with each stage of alteration are summarised in Table 1.4 (Details in Mark et al., 2006).

Figure 1.4. Location of the Ernest Henry deposit (*black box*) with respect to other mineral deposits in the Cloncurry district, northwest Queensland, Australia (Map modified from Syndicated Metals, 2010).

Table 1.4. Summary of the alteration stages and minerals at Ernest Henry based on: Mark et al., 2006 (for element abbreviations refer to Appendix 1.2).

Alteration Stage	Hydrothermal Alteration	Main Chemical Associations	Minerals
Pre-ore Sodic alteration	Albitization	Na	albite, titanate, quartz
	Na-Ca alteration	Na, Ca	actinolite, tremolite, titanate, diopside, albite, scapolite, calcite, apatite, magnetite, pyrite, quartz
	Magnetite - apatite	Fe, P, Mg	magnetite, apatite, actinolite, quartz, calcite
Potassic Alteration	Biotite - magnetite	K, Rb, Fe, Ba, Mn, Cl	biotite, magnetite, K-(Ba) feldspar, titanate, quartz
	Garnet - K-feldspar-biotite	Fe, Mn, K, Ba, Cl, Cu, Co	garnet, biotite, K-feldspar, amphibole, quartz, magnetite, pyrite, chalcopyrite
Syn-ore	Sericite-quartz	K, Rb, Ba, Cl, Cu, Co, Ni, As	K-(Ba) feldspar, quartz, rutile, calcite
	Sericite	K, H	sericite, quartz
Cu-Au mineralisation	Breccia	Fe, K, Ba, S, Cu, Au, Mn, Ca, C, Sr, Co, As, Mo, Sb, U, Ag, F, Cl	magnetite, pyrite, calcite, biotite, K-(Ba) feldspar, chalcopyrite, barite, molybdenite, arsenopyrite, quartz, electrum, garnet, amphibole, rutile, sphalerite, galena, coffinite, monazite
	Late veining	Fe, K, Ba, S, Cu, Au, Mn, Ca, C, Sr, Co, As, Mo, Sb, U, Ag, F, Cl	K-(Ba) feldspar, magnetite, pyrite, chalcopyrite, fluorite, molybdenite, calcite, garnet, quartz, barite, rutile

Chapter Two

Mineralogy and texture in Geometallurgy

2.1 Introduction

This chapter begins with a summary of the emerging field of geometallurgy and descriptions of existing mining operations and the roles of various mining professionals in this field. The existing methods for qualitative and quantitative mineral identification are described followed by the different definitions and classifications of texture in geology and metallurgy. This leads into the introduction of image analysis as a tool used for measuring and quantifying mineralogical and textural attributes. The end of the chapter provides a review of the literature regarding the effect of mineralogy and texture on mineral processing behaviour.

2.2 Geometallurgy

The field of 'geometallurgy' itself is not new, but more recently has been driven by the commercial need to maximize recovery and profit through a more geologically informed approach to metallurgical ore characterisation. Geometallurgy involves the integration of mine geology, process mineralogy, metallurgy, process control, resource modeling and geostatistics. Typically, data from these different aspects of a mine are located in different areas of the mine site or not on site at all. This simple geographical divide is enough to hinder the free flow of ideas between departments and inhibit communication.

The primary aim of a geometallurgical model is to be able to predict mineral processing attributes that affect the value of the mineral resource i.e. throughput and recovery. These attributes can include hardness, grindability, mineral species, mineral grade, mineral and rock texture, deleterious element content, reagent resorption and smelting properties. The measurements of a number of these attributes, such as mineral species and texture, are difficult and can be expensive to undertake on routine basis that is required in order to build a model.

Traditionally, mineral species are identified in drill-core by the mine site geologists with other geological parameters such as primary lithology and alteration style. It is these parameters that often form the basis of metallurgical sampling campaigns, despite rarely being calibrated with or related to mineral processing parameters. Sampling based on predetermined geological boundaries rather than naturally occurring populations that exhibit unique mineral processing properties have the potential to introduce bias and disguise variability during mine site optimization and processing.

Research undertaken within this project investigates techniques and technologies that can be used to provide a quantitative analysis of mineralogy and texture that can potentially be used and integrated into a geometallurgical model. More detailed summaries of the field of geometallurgy can be found in Walters and Kojovic (2006) and Walters (2008).

2.3 Mining Operations

One of the key aspects of geometallurgy is the effective communication between various mine site departments and personnel. An understanding of the role of each department and how they interact with each other is critical in identifying the factors that will impact mineral processing behaviours and improve recovery over the life span of a mine. There are five main stages in the mining life cycle: mineral exploration, deposit evaluation, mine planning, mine construction and operation, and mine closure. The steps involved in each of these stages are summarised in Table 2.1. More detailed summaries regarding mining operations and mineral processing can be found in Jones (1987), Petruk (2005) and Wills and Napier-Munn (2006).

Each of the mining stages that have been outlined in Table 2.1 utilize and rely upon different departments and personnel. It is important to recognize that each of these departments is in fact examining the properties of the same rocks, although from a different perspective. For example, the geologist will recognise features that relate to the formation of the ore deposit, the mining engineer will determine the hardness characteristics of the rock and the metallurgist will determine how to extract the valuable minerals from the rock. Each of these roles relies on each other; the metallurgist will determine the ideal mode of mineral extraction based on the results obtained from the mining engineer. The results obtained from the mining engineer will be a result of the rock minerals and textures which are determined by the geologist. The communication between these departments is critical in identifying the key mineralogical and textural characteristics that influence the mineral processing behaviours. An understanding of the roles that each mining professional has and the processes which they use is extremely important in understanding the geological attributes and how these attributes can influence different mineral processing behaviours. The key roles that are typically undertaken in the mining industry and their responsibilities have been outlined in Table 2.2.

Table 2.1. A summary of the key activities involved the five main stages of mining operations (Australian Government AusAID website, 2010).

Mining stages	Key activities
Mineral Exploration	This stage involves the search for new mineral deposits. Once a new deposit has been identified through drilling and assay, the deposit evaluation can commence.
Deposit Evaluation	Also known as the Feasibility Study, the deposit evaluation involves three critical stages: scoping study, preliminary-feasibility (pre-feasibility) and advanced-feasibility. The **scoping study** provides an initial evaluation of the project. It includes sufficient drilling and sampling to define the ore body, identify technical issues and establish an estimate of the capital and operating costs of the mine. The scoping study will determine whether the project is worth pursuing. The **pre-feasibility** study is crucial for identifying the critical issues that can cause delays and become costly during the feasibility and mining operations stages. This study includes an extensive drilling program and extensive processing test work in order to determine the mining and milling extraction methods and rates, engineering constraints, product recovery, environmental and permitting issues as well as the preliminary capital and operating cost estimates.
Mine Planning	The mine planning is undertaken during the **advanced feasibility** study. The advanced-feasibility study involves the design of the mine, a production schedule, product recoveries, a detailed process flow sheet and the identification of environmental issues as well as a detailed economic model of the project. This study is the final step in determining if the project is worth pursuing. Sufficient information should now have been collected to declare the ore reserves.
Mine construction and operation	The mine construction stage involves the building of infrastructure for both the mining operations and production. The mining operation can extend from only a few years to over a hundred depending on the deposit size. The mining operation involves the extraction, processing and transportation of mineral concentrates to the smelters. There are many factors that need to be taken into consideration during the operational stages of mining that can not only affect the present but may have implications for the future. These include water quality, water quantity, biodiversity issues for local flora and fauna, human rights, waste management, air quality, fisheries and waste water management.
Mine Closure	The mine closure stage involves the dismantling of infrastructure, the reclamation of disturbed areas and the monitoring of water quality and reclaimed areas.

2.4 Mineral Identification

The accurate identification of minerals is an important aspect of many areas in mining. Primarily, mineral identification is undertaken by exploration geologists at the initial stages of deposit discovery and then routinely by mining geologists during the feasibility and operational stages of mining. Misclassified minerals can remain in mine site data bases until a more accurate and comprehensive mineral analysis is undertaken. In extreme cases if minerals remain misclassified or unidentified through to the processing stages, there is the possibility that they may inhibit liberation, flotation and ultimately recovery, resulting in large financial costs for the company.

Geologists use the properties of minerals identified in hand specimen and by optical microscopy to correctly identify minerals. The accurate identification of these properties (see Table 2.3) is dependent on the mineral condition, the size of the mineral and the skill level of the geologist. It is for these reasons that the mining industry has strongly supported research into

developing more accurate methods for the routine identification of minerals. Traditionally, the most accurate mineral identification is undertaken using a scanning electron microscope (SEM) where the mineral identification is based on the chemical composition of the mineral (e.g. Goldstein et al., 1981). In recent years, the introduction of automated SEM platforms (Mineral Liberation Analyser and QEMSCAN) has allowed routine mineral identification to be more accessible and economically viable for research institutions and mining companies (e.g. Goodall and Scales, 2007). An additional advantage of these systems is the production of RGB images (mineral maps) of the sample surface which allows mineral quantities and textural attributes to be quantified using image analysis software. The results can be further compared to mineral processing parameters, such as physical rock properties and liberation potential. Mineral maps, used in conjunction with image analysis (discussed later in this chapter) to extract quantified mineralogical and textural information from rocks, can be used to predict variability in potential mineral processing behaviours (Lastra et al., 1998).

Table 2.2. Summary of the departments involved in mining and the tasks and responsibilities that are undertaken by each profession (1. Berman (Ed), 2001, 2. Gottlieb *et al.*, 2000, 3. Wills and Napier-Munn, 2005).

Department	Job Title	Responsibilities
Geology	Exploration geologist	The exploration geologist is responsible for finding new deposits of economic value, or locating areas for the extension of existing mining operations[1].
	Resource geologist	The resource geologist is responsible for estimating the total minable resource that is available in a deposit, selecting representative samples and creating a block model on which the mining geologist can base their mine planning[1].
	Mining geologist	The mining geologist is responsible for determining the geological aspects of the mine site (i.e. geological maps, mineralogy, fault identification etc.), overseeing drilling activities, controlling the grade of the ore that is sent for processing and understanding the environmental impact issues associated with mining operations[1].
Mineral Processing	Process mineralogist	The process mineralogist is responsible for the identification and analysis of minerals and rocks with respect to various stages of mineral processing, namely ore characterization, representative sample selection, pilot-plant studies, process circuit surveys and routine plant sampling[2].
	Metallurgist	A metallurgist is responsible for refining the process of metal extraction within the mineral processing circuit. This can involve expertise in the fields of froth flotation and leaching dependent of the mill design. Chemical components which include xanthates, dithiophosphates and thionocarbonates are adjusted to improve hydrophilicity, bubble size and ultimately recovery[3].
Engineering	Mining engineer	The mining engineer is responsible for the design of underground and open pit mines. They require information regarding the major structures which include faults and lithologies which exhibit different hardness characteristics. Mining engineers also work in conjunction with mineral processors to design the mineral processing circuit i.e. crushing and grinding circuits[3].
	Blasting engineer	The blasting engineer is responsible for the effective blasting of locations in underground and open pit mines[3].
Geostatistics	Geostatistician	Geostatistics is used to estimate the distributions of variables used in mining. These include grade, hardness, throughput and recovery. The estimates rely on good quality and representative data. The use of data from unrepresentative samples will result in bias and incorrect recovery estimations[1].
Geophysics	Geophysicist	The geophysicist uses techniques such as gravity surveys, magnetic susceptibility and electric resistivity to identify favorable structures and lithologies that may contain ore deposits[1].

2.5 Texture

The term 'texture' is not solely restricted to the fields of geology and mineral processing. The global definition is defined as:

"The distinctive physical composition or structure of something with respect to the size, shape and arrangement of its parts" *Macquarie Dictionary*

This definition can be applied to fields ranging from music and photography, through to materials science and mining. Textural definitions are typically descriptive and categorical which can make them difficult to measure and quantify for research and analysis purposes.

Within the mining industry it is well known that characteristics of texture can cause variability in mineral processing behaviours (e.g. Gaspar and Pinto, 1991; Vink, 1997; Bojcevski et al., 1998). However, the descriptive nature of textural information can make it difficult to quantify and establish which textural attributes can be attributed to certain mineral processing behaviours. This difficulty is further compounded by the lack of a coherent definition for the term 'texture' between geologists, mineral processors and metallurgists. For example:

In geology, texture is defined as:

"The general character of a rock shown by its component particles in terms of grain size and shape, degree of crystallinity and arrangement" *Dictionary of Geology*

In the fields of mineral processing and metallurgy, texture can also be referred to as 'micro-structure' or 'mathematical morphology'. The term 'texture' is applied to the sizes and shapes of particles (broken fragments of rocks) and then extended into the quantity and types of mineral components that make up the particle (Vink, 1997; Bojcevski, 2004). The definitions are typically variable, and it is not uncommon for a study regarding texture compared to a mineral processing parameter to only refer to one aspect of texture, i.e. size or shape. For example, a study undertaken by Cottrell (1975) refers to texture as mineral orientation, and an ore texture study undertaken by Gaspar and Pinto (1991) investigates the influence of modal mineralogy and grain size (described as texture) on ore beneficiation. Much of this confusion between definitions is due to the different uses of textural information between geologists and mineral processors. A geologist describes textures to draw conclusions regarding processes for rock and mineral formation, a mineral processor, metallurgist or mining engineer will measure texture to obtain information for optimizing plant production. The textural classification systems that are used by both geologists and metallurgists have been described in the remainder of this section.

Table 2.3. Mineral features that are used to identify minerals in hand specimen and in optical microscopy (1. MacKenzie and Adams, 1994).

Mineral Feature	Description
Colour	The mineral colour observed in hand specimen. This can be characteristic (e.g. epidote, malachite, sulphur), however many minerals exhibit multiple colours (e.g. fluorite, quartz, sphalerite).
Crystal Habit	Refers to the external form of the crystal. This is different to the crystal cleavage. For example quartz has a prismatic crystal form but exhibits no cleavage, only a conchoidal fracture when broken.
Cleavage	Mineral cleavage is the preferred plane along which a mineral breaks or cleaves. The position of these planes is controlled by the atomic structure of the mineral. Between the planes of cleavage atomic bonds are weak compared to the rest of the crystal structure. Minerals can have up to four cleavage planes at various angles. It is the number of cleavage planes and the angles of the planes that can be used as diagnostic tools. For example, mica minerals have only one plane of cleavage at 180°.[1]
Specific Gravity	The specific gravity refers to the density of mineral relative to the density of water. For example a very dense mineral will feel heavier than expected. This is a typical diagnostic property for barite.
Hardness	The hardness of the mineral is typically used to distinguish minerals that are similar in appearance. Geologists typically use the Moh's hardness scale to determine the mineral hardness compared to the known hardness of common objects (i.e. finger nail, copper coin, builders nail).
Lustre	The term lustre describes the way that light interacts with the surface of a mineral. Examples include adamantine (diamond), resinous (sphalerite), metallic (galena) and greasy (serpentine).
Magnetic Permeability	The magnetic permeability refers to whether a mineral is magnetic. Only the mineral magnetite is strongly magnetic, however, some minerals can be weakly magnetic, e.g. hematite and pyrrhotite.
Crystallinity	Crystallinity refers to the degree to which the crystal exhibits its characteristic features. For example, a perfectly formed crystal is termed 'euhedral', a crystal that has undergone substantial weathering or alteration and no longer exhibits its true crystal form is termed 'anhedral', and degrees between these two are called 'subhedral.'.
Interference Colours	These colours are different to the mineral colour observed in hand specimen and refer to the colour of each mineral in thin section observed with crossed polars. The colour intensity changes as the microscope stage is rotated every 90° and is different for each mineral.[1]
Twinning	Twinning can be observed in hand specimen and under the microscope, it is most common in feldspar minerals and is a result of the rotation of one of the crystal faces around the crystal axis by 180°.[1]
Refractive Index	The refractive index is only observed using an optical microscope and refers to how much the speed of a wave is reduced when it passes through a mineral. Minerals can have up to three refractive indices which result in a refractive index range that can be used as a diagnostic mineral property.[1]
Relief	Relief is only observed using an optical microscope, it refers to the different between the refractive index of a given mineral and its surroundings i.e. other minerals or the mounting medium.[1]
Isotropy	Isotropy refers to minerals that when observed in thin section using an optical microscope under crossed polars have no double refraction. This makes the mineral appear black and is a result of a mineral with a very organized atomic structure. These minerals are called isotropic, common examples include garnet, nepheline and volcanic glass.[1]
Mottled extinction	Mottled extinction is only observed using an optical microscope under cross polarized light and occurs when a mineral does not completely become extinct, but instead appears dark and mottled at the maximum extinction angle. It is typically a diagnostic property of biotite.
Extinction angles	The extinction angle can only be observed in thin section using an optical microscope. It refers to the angle between an extinction position and a well defined direction in a crystal.[1]
Undulose Extinction	Undulose extinction is only observed in thin section using an optical microscope and refers to a whole mineral surface that does not go completely extinct uniformly. This feature is typically diagnostic of quartz and indicates that the mineral has undergone strain.[1]

2.5.1 Scales of Texture

Textural features can be identified and described at three different scales; micro, meso and macro. The type of measurement platform that is being used will influence the scale of textural features that can be observed. Each textural scale and the measurement platforms that are used to observe each scale are described in Table 2.4. Examples of each scale of texture are shown in Figure 2.1.

Table 2.4. The definitions and examples of macro-, meso- and micro- textures scale and the measurement platforms that are used to observe them.

SCALE	Description	Measurement Platforms	Examples
Macro	Macro-texture features are large enough to be observed from a distance. Macro – textures have a scale of metres and kilometers and are used by geologists to classify large features such as lithological units and fault zones (Figure 2.1A).	Regional and pit mapping	Large scale features, including fault structures, lithological units, alteration zones, and fold structures
Meso	Meso-texture features can be determined in hand-specimen. Meso – textures have a reference scale of millimeters or centimeters and are typically used by geologists to log drill-core and document mineralogical and textural features (See Figure 2.1B).	Visual drill-core logging Hylogger Photographs	Millimetre to centimetre scale features, including vein structures, the distributions of minerals, brecciation, foliations, mineral cleavages and sedimentary grading.
Micro	Micro-texture features can only be observed with the aide of a microscope. Micro - textures have a reference scale of microns and are typically used by geologists to identify minerals and textures that can be related to a genetic interpretation (See Figure 2.1C).	Optical Microscope Scanning Electron Microscope (SEM) Mineral Liberation Analyser (MLA) QEMSCAN	Micron to millimeter scale features which include mineral intergrowths, mineral inclusions, the internal structure of veins, mineral cleavages, lineations, sub-grains, alteration haloes and fluid inclusions.

The integration of mineralogical and textural features that are identified at various scales is extremely important in linking geological attributes to mineral processing behaviours. Drill-core logging that is routinely undertaken by geologists typically does not document attributes that are likely to affect mineral processing behaviours other than the abundance of valuable minerals and estimated abundance of vein structures (Walters, 2008; Bonnici et al., 2008). This also applies to mineral processors and metallurgists who typically do not consider geological attributes (such as texture) during the selection of true 'ore types' which will directly impact the design of mining operations. A pioneering study undertaken by Vink (1997) logged the abundance of meso-textures in drill-core, later comparing them to the presence of micro-textures in particulate samples to draw conclusions regarding the liberation potential of each texture. Vink's study recognized the potential of using meso- and micro-textural features as a tool for predicting variability in mineral processing behaviours. The research presented in this thesis builds on the concept presented by Vink through the use of new technology that allows mineralogical and textural features to be routinely measured and quantified using image analysis software.

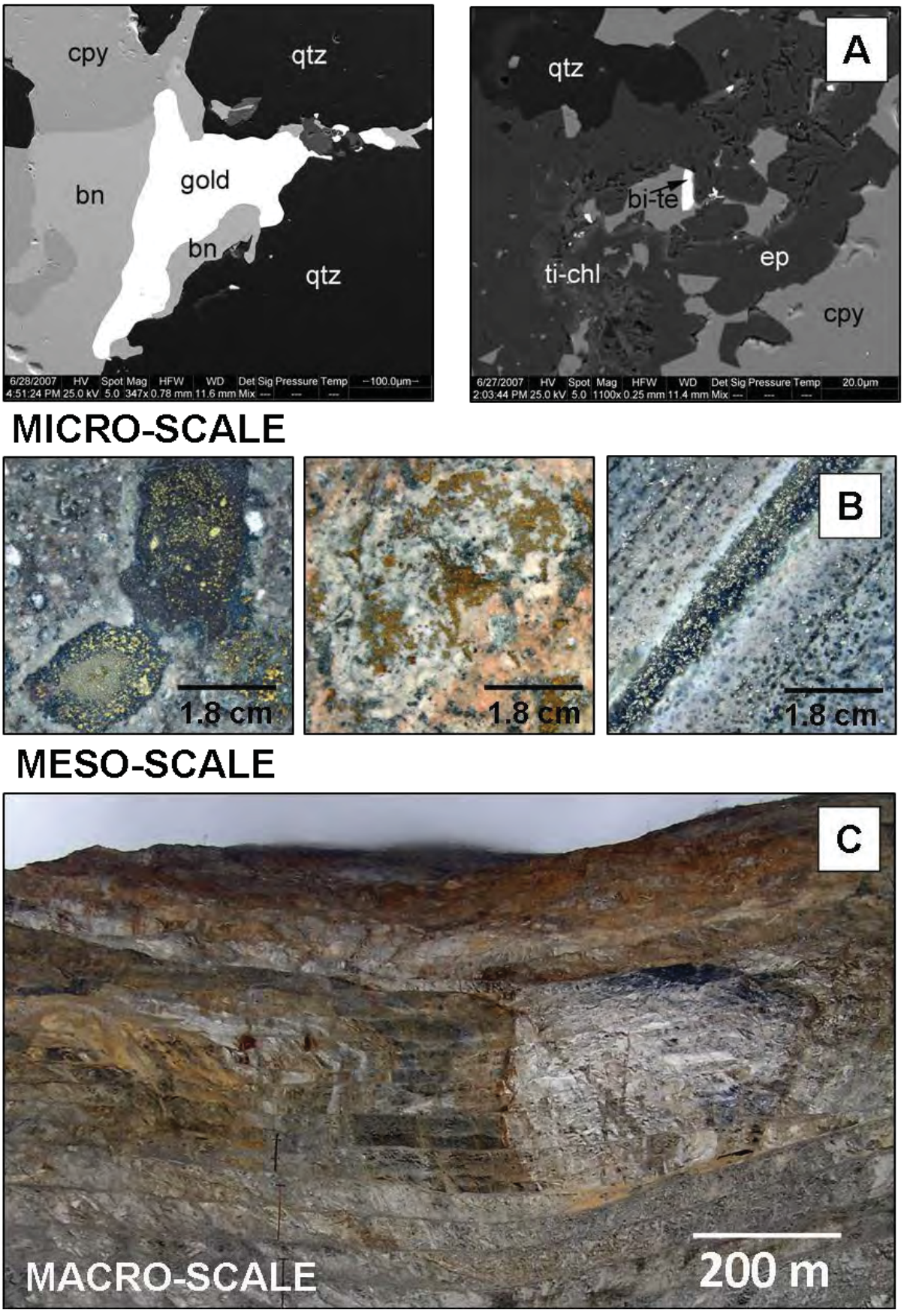

Figure 2.1. Photographs illustrating the scales that texture can be observed. **A.** BSE images showing examples of micro-scale textures. **B.** Images of drill core showing examples of meso-scale textures. **C.** Image of a pit wall showing macro-scale textures.

2.5.2 Textural nomenclature in geology

In the field of geology, classification systems for mineralogical and textural features of a rock can be used either to aid in the naming of the rock or form part of the rock name itself (e.g. porphyritic texture and porphyry [igneous] intrusion). Many of these systems require the visual estimation of mineral abundances and the interpretation of various textural features that are present. These visual estimations and interpretations can be variable between geologists and commonly result in poorly defined qualitative and categorical data. This makes the data difficult to integrate into models to be used by mineral processors for representative sample selection, comparisons to liberation and flotation parameters, and the outcomes of physical testing. In addition to this, different areas within geology have their own classification systems for describing mineralogical and textural attributes. These systems are routinely used on mine-sites and during the exploration process in the geological logging of drill-core. The most commonly used classification systems are summarized in Table 2.5 (more detail can be found in Appendix 2.1).

In addition to the classification systems within different fields of geology there are also wide arrays of nomenclature that refer to the texture of mineral crystals. These textural descriptors typically refer to the size, shape and condition of the mineral grains. The most commonly used textural descriptors are summarized in Table 2.6. As discussed with the textural classification systems, each individual field of geology has its own textural nomenclature that typically implies a genetic connotation. These are outlined in Appendix 2.1.

Table 2.6. Nomenclature used to describe the textures of individual mineral grains (*Summarized from* Gifkins et al., 2005).

Mineral crystal texture	Definition
Acicular	Needle-like crystal shape that can only be observed at the micro-scale.
Angular	Crystals that have clearly defined angular edges and/or shapes.
Botryoidal	Interlocking, rounded crystal masses that resemble the shape of grapes.
Cubic	Crystal shape that resembles a perfect square or cube.
Dendritic	A crystal that develops a branched, tree-like form.
Fibrous	Regular or irregularly thread-like.
Flaky	Plate-like.
Framboidal	Framboidal textures occur in some sedimentary minerals, most commonly pyrite. Framboids are spherical aggregates of equigranular microcrystallites with a diameter of approximately 0.5 μm.
Lathe	A slender elongated form.
Needle-like	A narrow, long and pointed form resembling a needle.
Rhombic	Resembling a rhombic form, the crystal has four sides at unequal angles.
Skeletal	Very similar to dendritic, however the shape has been derived from the degradation of the original crystal.
Spherical	Rounded shape.
Spongy	Refers to a crystal that has rounded holes in it. This typically occurs in pyrite.
Twinning	Crystal twinning occurs when two crystals share some of the same lattice points in a symmetrical manner. This most commonly occurs in feldspar crystals.
Zoned	A crystal that exhibits variable composition along crystal growth bands.

Table 2.5. The most commonly used textural classification systems that are commonly used in various fields of geology.

Field of Geology	Field description	Classification systems	Description	References
Sedimentology	Sedimentary rocks are formed from the accumulation of sediments in water or from air (Nichols, 2009). They are classified based on their mineralogy, clast composition and grain size. In sedimentology, the analysis of changes in clast composition and size are used to determine changes in depositional environments throughout the geological record (Pettijohn et al., 1972; Gladstone and Sparks, 2002; Tamura, 2004), as a measure of modern environments (Dyer, 1970; Allen, 1971; Dowling, 1977; Bryant, 1982; Nickling, 1983; Lancaster, 1986; Kodama, 1994; Livingstone et al., 1999; Cheetham et al., 2008) as well as a measure for sediment transport (Komar, 1977; McClaren and Bowles, 1985; Kleinhans, 2005). Non-clastic sedimentary rocks are either chemical or organic. The most common types of chemical sedimentary rocks are limestones, chert and evaporites (Nichols, 2009).	Udden-Wentworth	Measure of grain or clast size.	Wentworth, 1922 Blair and McPherson, 1999
		Phi scale	A logarithmic form of the Udden-Wenthworth scale. Size is measured in phi (Φ) units.	Krumbein, 1934
		Classification of Terrigenous sediments	Classification based on the grain composition and size.	Pettijohn et al., 1972
		Roundness and Sphericity guide	Measure of grain or clast shape.	Pettijohn et al., 1972
		Guide for sedimentary sorting	Measure of the distribution of grains and clasts throughout the rock	Folk, 1951
		Classification of limestones	Measures the presence of diagenetic cements and minerals.	Wright, 1992 and therin.
Igneous Petrology and Volcanology	Igneous petrology refers to crystalline rocks that have formed from the cooling of magma beneath the earth's surface (McBirney, 2007). These rocks can be termed either intrusive or volcanic (extruded through the earth's crust). Igneous rocks are classified based on their mode of occurrence, chemical composition, textural features and mineralogy. They are named using the Quartz-Alkali feldspar-Plagioclase-Feldspathoid classification (LeMaitre, 2002). Volcanic rocks are named based on the alteration intensity, crystal distribution, texture and mineral assemblage. All of these are included in the rock name as a prefix. The textural nomenclature for volcanology and igneous petrology are detailed in Appendix 2.1.	QAPF classification	The normalised abundances of quartz, alkali-feldspar, plagioclase and feldspathoids are plotted on the QAPF diagram and a rock name is given based on the intrusive or extrusive nature of the rock.	Streckeisen, 1974; *later in* Le Maitre, 2002 Gifkins et al., 2005 British Geological Survey, 1999
Structural geology	Structural geology is the study of rocks that have undergone deformation as a result of tectonic changes.	Fold Morphology	The classification of fold structures based on the shape and amplitude of the fold structure.	Huddleston, 1973
Metamorphic geology	Metamorphic rocks are formed as a result of extreme pressure and/or heat whereby the composition, texture and mineralogy are altered. Metamorphic rock names typically reflect the features that can be observed in the rock. These include the protolith, modal mineral composition and texture which are all included as qualifiers in the rock name. The textural qualifiers for metamorphic rocks and definitions are outlined in Appendix 2.1.	N/A	Metamorphic rocks are classified as foliated or not-foliated. Foliated rocks include a slatey, phyllitic, schistose or gneissic texture. Not-foliated rocks include marble, quartzite or anthracite coal	Bucher and Frey, 1994 British Geological Survey, 1999 Turner and Verhoogen, 1960.

The textural descriptors that are the most important to the research undertaken in this thesis are those used to describe ore textures. Ore textures are widely described by geologists on mine sites and are the most likely classification system to be considered by geologists when selecting ore type samples for metallurgical test work.

Ore textures are characterized based on the valuable minerals (ore minerals) present and their relationships with the other gangue minerals in the ore body (Barton, 1991). Traditionally, an ore texture would only include the textures of the minerals that are of economic value (e.g. Evans, 1993). However, the definition should be extended to include the associated gangue minerals. The minerals that are termed 'gangue' are derived from many of the rock types that have been outlined in Table 2.5 (sedimentary, igneous and metamorphic) and represent the protolith with or without the addition of mineralising fluids. It is not uncommon for rocks that are associated with ore deposits to have undergone intense alteration during the process of ore deposit formation. This process can often overprint original (protolith) textures and form new minerals and textures that are unique to the process of alteration. These zones vary between deposit types and reflect a change in mineralogy due to variations in fluid temperature and composition (see Appendix 2.2 – Alteration zones of porphyry Cu-Au IOCG deposits).

Alteration zones and their minerals are routinely logged during the exploration and mining operation phases. It is the alteration minerals (including ore minerals) and their textures that are the most likely to effect the mineral processing behaviours. For example, a potassic alteration zone, rich in K-feldspar, will be much harder to crush than a phyllic alteration zone that is rich in sericite. A detailed knowledge of these minerals and textures is critical in establishing which factors are most likely to influence the various aspects of the mineral processing operation. In the geological literature, there are specific terms used to describe the intensity and style of the alteration (Table 2.7) as well as the deportment of the ore minerals (Table 2.8). Typically, these terms are logged as an estimated abundance or an abundance range during geological logging. As mentioned previously, these estimates can vary significantly between geologists making it difficult for the data to be integrated into a model. A shift towards the routine, quantified analysis of minerals and their textures at the meso- and micro-scale will allow changes in mineralogy and texture to be further linked to variability in specific mineral processing behaviours. This will allow more informed decisions to be made regarding sample selection for comminution and metallurgical test work and ultimately the optimization of mineral processing circuits.

Table 2.7. Nomenclature for intensity and style of alteration (*Summarised from* Gifkins *et al.*, 2005).

Alteration Intensity	Definition
Pervasive	Extensive alteration that has completely changed the rock composition and texture.
Selectively Pervasive	Selective alteration of pre-existing phases throughout the rock.
Replacement	Existing minerals are replaced by one or more mineral species.
Infill	A mineral or minerals are precipitated from solution into an open space.
Dissolution	Existing minerals are leached and removed by solution with or without replacement.
Static Recrystallisation	Recrystallisation of existing minerals to new grains and/or a change in morphology of the same mineral species or composition.
Dynamic Recrystallisation	Recrystallisation of existing minerals to new grains and/or a change in morphology and/or orientation of the same mineral species or composition.
Deformation	Existing component or texture is rotated, milled, broken, compressed, modified, distorted or fractured.

Table 2.8. Nomenclature for the distribution of ore minerals (*Summarised from* Gifkins *et al.*, 2005).

Ore texture	Definition
Comb	Euhedral crystals growing inwards from the vein wall.
Crustiform	Vein minerals that grow inwards from the vein wall.
Disseminated	Mineralisation that is randomly distributed throughout the rock.
Domainal	The occurrence of patches, pods or groups of clasts within the host rock.
Incomplete infill	The incomplete or partial infilling of veins and cavities with an open vug in the centre.
Layered or banded infill	The deposition of minerals inwards from the cavity or fracture wall to form layers or bands of different minerals.
Massive infill	The continuous deposition of a mineral or aggregate of minerals in a cavity until it is filled.
Overgrowth	A mineral that has precipitated on another crystal.
Pseudomorph	A mineral that takes the crystal form of another mineral. This occurs when a mineral is replaced by another but the dimensions of the crystal do not change.
Sheeted veins	Veins that occur as closely spaced parallel veins. These veins typically contain quartz plus other minerals.
Spherulitic	Aggregate consisting of rounded, ball like structures composed of radiating crystals.
Stockwork veins	An irregular three-dimensional arrangement of veins or veinlets.
Vein	A mineralized zone with a regular development in length, width and depth that is separate from its host rock.
Vein selvage	The replacement of either the entire rock or specific pre-existing phases in restricted areas such as halos around veins.

A number of studies have been undertaken in geology that use quantified textural parameters (most commonly size attributes) to draw conclusions regarding geological processes. For example, in igneous petrology, extensive work has been undertaken investigating the relationship between crystal size distibutions (CSD's) and the rate of crystal nucleation, crystal size and crystal growth rate (Cashman and Marsh, 1988; Cashman and Ferry, 1988; Higgins, 1994; 2000; 2002; 2006; Pan and Higgins, 2002; Higgins and Roberge, 2003; Higgins and Chandrasekharam, 2007 and Mock and Jerram, 2005). More recently, an extensive publication from Higgins (2006a) addressed the theory, applications and the methods for extracting CSDs from thin sections. Alternatively, in the field of structural geology, fabric orientation parameters have been extracted using the equivalent ellipse calculated from scanned digital images (Launeau and Cruden, 1998).

2.5.3 Textural nomenclature in mineral processing

In the field of mineral processing, classification systems for minerals and their textures typically refer to the attributes that are likely to affect the processes of liberation, flotation and ultimately the recovery of the mineral phase of interest (e.g. Bojcevski, 2004; Gaspar and Pinto, 1991). An ideal situation is for the mineral phase of interest to completely liberate during the crushing of the ore i.e. create a mono-minerallic particle (Jones, 1987). This situation is highly unlikely and as a result a particle is classified based on the number of mineral constituents it comprises. Figure 2.2 shows the classification used for particles containing four minerals or less. In theory, the fewer minerals that the particle contains the more likely that the phase of interest will be exposed on the particle surface and the more likely that it will float and be recovered. However, particles with the same shape and mineral abundances can have significantly different mineral processing properties based on their textures (Figure 2.3).

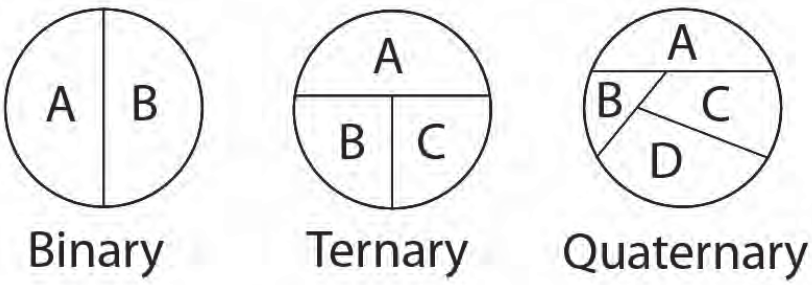

Figure 2.2. The classification used to describe particles compositions (Jones, 1987). Binary particles are composed of two minerals (A and B). Ternary particles are composed of three minerals (A, B and C). Quaternary particles are composed of four minerals (A, B, C and D).

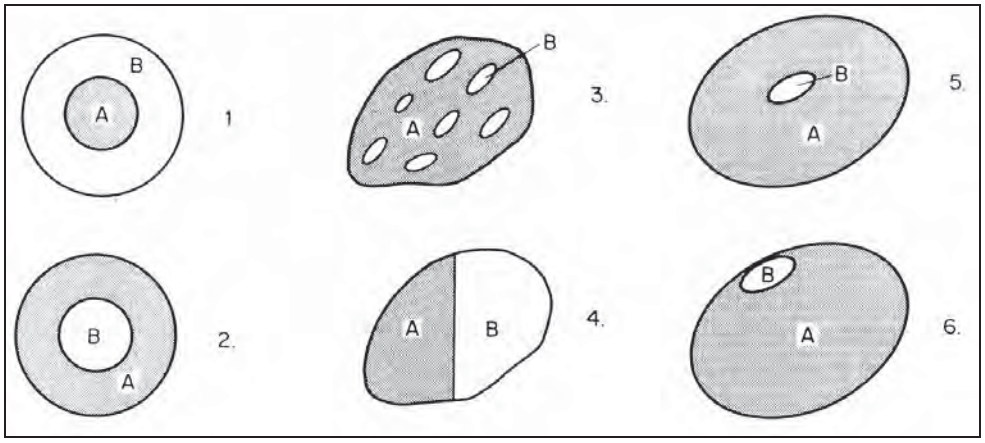

Figure 2.3. Particles of similar size, shape and composition but differing texture. Particles 1 and 2 will have different flotation properties. Particles 3 and 4 are the same size and shape and contain the same proportions of minerals A and B. In particle 4, the minerals A and B are partially liberated, but particle 3 will require a reduction in particle size before the liberation of mineral B can take place. In particle 5, mineral B in not available for attack by any leaching agents, but a similar grain in particle 6 is readily available (*figure taken from* Jones, 1987).

There are a number of terms that are used to describe the distribution of minerals in particles. Typically these refer to location of the valuable phase with respect to the particle surface. The nomenclature that is typically used to describe the particle compositions of most valuable minerals is described in Table 2.9. In addition to these terms, there is separate nomenclature used to classify and describe gold bearing ores (Goodall and Scales, 2007; Table 2.10). This is attributed to the elevated price of gold and its susceptibility to factors such as the nugget effect and gold locked up in the crystal lattice. The degree to which these factors are present within an ore will directly impact the design of the mineral processing circuit.

Table 2.9. The nomenclature used by mineral processors to describe the composition and liberation of particles (*summarized from* Wills and Napier-Munn, 2006).

Particle nomenclature	Definition
Complete liberation	The total liberation of a mineral from its host rock. This will result in a mono-minerallic particle of the valuable phase.
Degree of liberation	The percent of the target mineral exposed on the particle surface.
Locked minerals	Locked minerals refer to valuable phases that are completely enclosed by gangue minerals.
Middlings	Middlings refer to particles that contain locked minerals and will require a reduction in particle size in order to recover the valuable phases.
Refractory ores	Ores which are difficult to treat due to fine dissemination of the minerals, complex mineralogy, or both.

Table 2.10. The nomenclature used by mineral processors to describe gold ores and particles (*summarized from* Vaughan and Kyin (2004) *later in* Goodall and Scales, 2007).

Particle nomenclature	Definition
Complex ores	Gold bearing ores that contain multiple populations of gold that exhibit varying forms of refractivness.
Free-milling	>95% of gold can be recovered using cyanidation.
Mildly refractory	Gold recovery is between 80-95% using cyanidation.
Moderately refractory	Gold recovery is between 50-80% using cyanidation.
Strongly refractory	Gold recovery is <50% using cyanidation.

2.6 Measurements of texture

A qualitative or categorical geological classification (such as those described in section 2.5) is not only difficult to integrate into a model but has not intentionally been established for comparisons against mineral processing properties. In order to undertake a comprehensive **quantitative** analysis of rock, particle or mineral texture, texture needs to be considered in terms of its individual components: size, shape and mineral constituents. This will allow the impact of individual mineralogical or textural characteristics on different mineral processing behaviours to be established. The research that is presented in this thesis relies heavily on quantified textural data and presented in this section are the methods and relevant previous studies for the quantified analysis of the textural attributes: size (section 2.6.1), shape (section 2.6.2), modal mineralogy (section 2.6.3), mineral associations (section 2.6.4) and mineral distribution (section 2.6.5).

2.6.1 Size

The size of a mineral or rock is the most widely used of all the textural parameters (e.g. Jones, 1987, Higgins, 2006a). In many respects it is the easiest to measure. It is a dimensional parameter that can be expressed as a unit of length, area or volume. The ability to quantify size makes it amenable to comparisons with physical rock properties and forms the basis of many routine physical tests that are used in the design and optimization of mineral processing plants (e.g. Wills and Napier-Munn, 2005). Size parameters are obtained from individual minerals as well as rock particles. These data are typically examined as populations of various products created from one sample. For example, a distribution of particle sizes can be produced from the crushed product of a selected drill-core interval. The distribution of particle sizes is a function of the rock hardness, mineral types, mineral form and hardness as well as the rock texture (e.g. Bojcevski, et al., 1998). These distributions can be used to determine the hardness properties of that interval and the energy that will be required to crush this product in the mineral processing circuit (e.g. Wills and Napier-Munn, 2005).

In this research, size parameters have been measured from the mineral and particle features of particulate rock samples as well as the mineral features of intact rocks. Traditionally, size parameters are measured from the planar surfaces of rocks and minerals (Higgins, 2006a). In this thesis, RGB images of planar surfaces have been produced at various magnifications from different measurement platforms. The use of RGB images means that the size parameters can be measured primarily using pixels as a unit measure. The use of image analysis as a technique for quantifying texture will be described in further detail in section 2.8.

The most commonly used measurements of size are area and perimeter (Higgins, 2006a). These can be applied to rocks, minerals or particles as well as other geological features such as faults, veining, lithological units, alteration zones and bedding. Other measurements of size that are used less commonly are the length, width, smallest enclosing ellipse, largest enclosed ellipse and the Feret diameter (Pirard et al., 2004). These measures and their formulae are described in more detail in Table 2.11.

Table 2.11. Formulae and descriptions of the most commonly used measurements of size.

Measurement of Size	Formula	Description	References
Area	The total region enclosed by an objects perimeter. **Square and rectangle** = length x width **Circle or Ellipse** = $r^2\pi$ where r = radius **Triangle** = ½ base length x height	The formula for area is dependent on the object shape.	e.g. Wills and Napier-Munn, 2005
Perimeter	The sum of all object sides.	The perimeter is a measure of the length of an objects boundary.	e.g. Wills and Napier-Munn, 2005
Length Width	The length and width of an object can be calculated using a number of methods: 1. Creating a bounding box around the object and calculating the shortest and longest intercepts 2. Calculating an equivalent ellipse of an object and then calculating the longest and shortest intercepts 3. Calculating the length and width by using the ratio of the eigenvalues of the objects covariance matrix.	Visually, the length and width of an object appears easy to calculate. The length being the longest intercept through the object, and the width being the shortest intercept. In terms of image processing this can become more difficult when processing includes thousands of objects all oriented in varying directs.	Russ et al., 2007 Definiens, 2010
Smallest Enclosing Ellipse	The radius of the smallest circle that can enclose the object.	These parameters are considered a more robust method than area, perimeter and length and width for measuring the size of particles that have undergone sieving (Pirard et al., 2004).	Pirard et al., 2004
Largest Enclosed Ellipse	The radius of the largest circle that can be contained anywhere within the object.		Pirard et al., 2004
Feret Diameter	The distance between two parallel objects that is at a tangent to the object profile and perpendicular to the ocular scale.	Typically, 8 or 16 discrete diameters are taken through the object and the minimum or maximum Feret diameter is used.	Howarth and Rowlands, 1987

In mineral processing, the area and the perimeter are used together to quantify the perimeter complexity and are typically applied to particles (Vink, 1997; Pirard et al, 2004). This is referred to as the Phase Specific Surface Area (PSSA) which is calculated by dividing the perimeter of the object by its area. It is considered that if a particle has a complex perimeter (i.e. high PSSA) then it will have a larger exposed surface area, which will increase the particles potential to float if it contains valuable minerals. For particulate samples, where the size and shape of a mineral or particle has been reduced by the comminution process and the texture partially destroyed, the PSSA is an appropriate measurement of size and perimeter complexity. However, research undertaken within this project found that when the PSSA is applied to intact mineral grains, it is only appropriate for smaller mineral grains. Figure 2.4 shows two examples of objects (measured in pixels) that have a PSSA of

1.38. The larger object (left) has a more complex perimeter than the smaller object on the right. As the area of the mineral increases the PSSA becomes less sensitive to perimeter complexities.

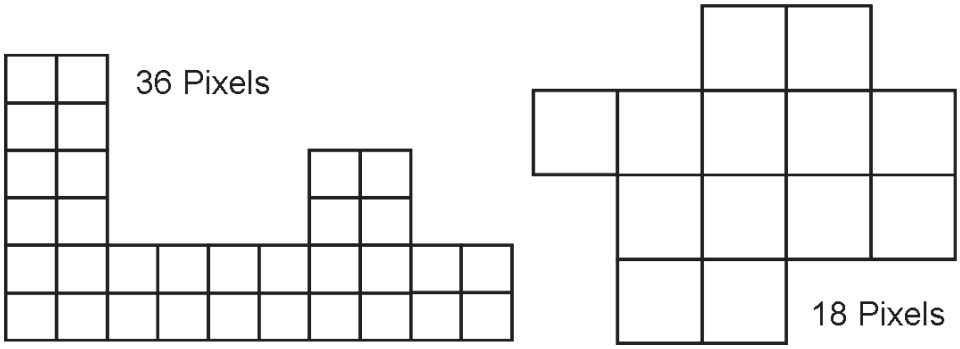

Figure 2.4. PSSA becomes less sensitive to complex perimeters as size increases. The larger object (*left)* has a more complex perimeter than the smaller object (*right*), yet both have a PSSA of 1.38. The pixel size is the same for both objects.

For process mineralogists, who primarily work with particulate samples, the mineral or particle area is typically converted to Equivalent Circle Diameter (D_0; Figure 2.5; e.g. Pirard et al., 2004, Wills and Napier-Munn, 2005. The purpose of this conversion is to produce a distribution of particle sizes that can easily be related to standard sieve sizes (Tyler's √2 sieve series) that are used in the measurement of comminution and grinding products (Grupta and Yan, 2006). It should be recognised that D_0 does not accurately reflect the true diameter of the actual particle that will pass through a given sieve (Wills and Napier-Munn, 2005). Figure 2.5 shows three examples of particle that have similar D_0 values. During actual sieving, it is likely that particles A and B will fall through a smaller diameter sieve, given the right orientation, than that estimated by D_0.

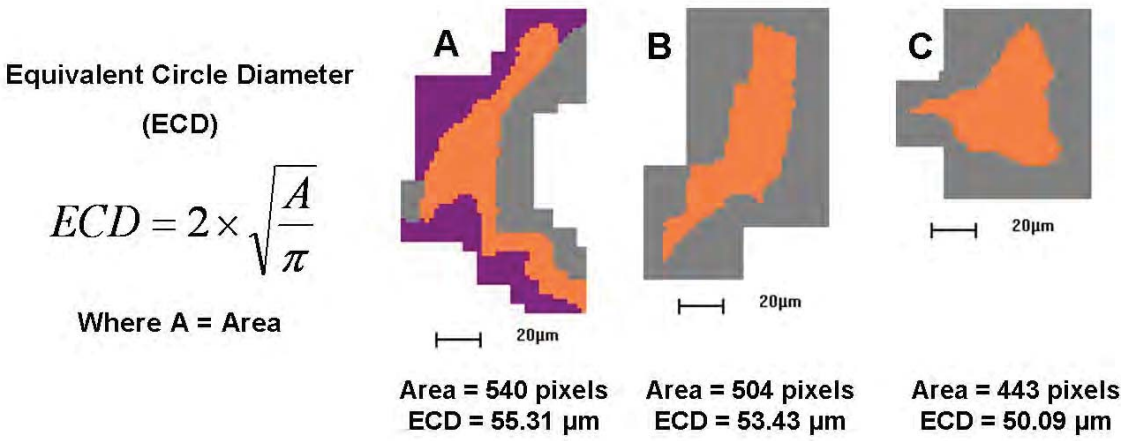

Figure 2.5. Three examples of particles (*orange*) with similar ECDs. The area has been calculated from the number of pixels.

Traditionally, particles that have been sized into fractions using the sieving process are weighed as a proportion of the total sample. The most common method for plotting this data is as a cumulative frequency curve using a semi-logarithmic plot (Wills and Napier-Munn, 2005). However, there have been a number of methods developed with the aim of avoiding congestion and extremities in these plots. The two most widely accepted are the Gates-Gaudin-Scuhmann (Schumann, 1940; later in Wills and Napier-Munn, 2005) and the Rosin and Rammler (1933). Both methods are derived from equations that contract and expand different areas of the graph in

order to produce as close to a straight line as possible (Wills and Napier-Munn, 2005). A straight line is typically considered to be easier to interpret. However, the use of these methods as well as using a cumulative frequency curve rather than a histogram could potentially mask any bimodality that is present in a sample as a result of rock texture. Further detail regarding the Gates-Gaudin-Schuhmann and Rosin and Rammler methods can be found in Harris (1971) and Wills and Napier-Munn (2005).

2.6.2 Shape

The analysis of grain shapes has been widely explored in the field of sedimentary geology (e.g. Ehrlich and Weinberg, 1970; Oakey et al., 2005) and to a lesser extent, igneous petrology (e.g. Triebold et al., 2006). In ore texture studies, shape is often considered indirectly (e.g. Barton, 1991; McArthur, 1996; Ramdhor, 1980; Craig and Vaughan, 1981). For example, an ore texture described as 'a quartz vein exhibiting a comb texture' implies that prismatic crystals are growing in a unidirectional pattern and are perfectly euhedral. To date there are limited examples in the literature regarding ore textures that use quantified shape parameters as part of their textural classification however examples include Donskoi, et al., (2007) and Triffit and Bradshaw, (2008) who examined the effect of mineral shape on the flotation and recovery behaviour at specific sites.

There have been a number of key publications that summarise shape factors and measurements (Serra, 1982; Higgins, 2006a; Pirard and Dislaire, 2005; Pirard, 2005). However, the application of these parameters to real minerals, rather than simulated images of rock particles or mineral grains is limited. Many authors demonstrate the differences in shape descriptors by using a series of manufactured shapes (Rosin, 2003) with only a few showing a practical application of shape analysis using worked examples (Lastra, 2007; Triffett and Bradshaw, 2008). A widely used approach to shape analysis is to use shape descriptors that represent, or are sensitive to, various aspects of simple shapes, e.g. circle, square etc. There are a number of papers that summarise commonly used shape descriptors such as sphericity, rectangularity and elongation and assess the shape measures that are most useful (e.g. Rosin, 1999; 2003, Pirard and Dislaire, 2005). The automatic identification of these shapes can be referred to as 'pattern recognition' and is typically used in the field of 'computer vision' (Rosin, 2003).

The recent increase in the use of automated mineralogy systems has seen the implementation of shape factors into image analysis software (e.g. Higgins, 2006, Russ, 2007). This has been perceived as a huge advantage for the field of mineral processing in terms of the ability to quantify aspects of texture that have traditionally been considered qualitative and descriptive. However, there is a poor understanding of which shape factors are appropriate to use and which other quantifiable parameters they should be compared to or measured against without creating circular arguments. An extensive review of shape factors found in new image analysis systems (which are described later in this chapter) and their interpretations is given by Pourhahramani and Forssberg (2005).

2.6.3 Modal mineralogy

Modal mineralogy is an important factor in determining the ease with which a rock can be crushed and ground in the mineral processing circuit. Traditionally, modal mineralogy was calculated by point counting using optical microscopy methods (e.g. McArthur, 1996) or estimated from hand-specimens samples. The development of Quantitative X-Ray Diffraction (QXRD) analysis has allowed mineral abundances to be determined for powdered materials (Klug and Alexander, 1954;

Copeland and Bragg, 1958). Newer methods in the imaging of planar rock surfaces, and the identification of minerals allows the modal mineralogy to be calculated using a quantitative and unbiased approach.

2.6.4 Mineral associations

The minerals that are associated with a target mineral will have a direct impact on that minerals liberation potential and ultimately flotation and recovery (Petruk, 2005; Bojcevski, 2004; Goodall and Scales, 2007; Becker et al., 2008). There have been a number of studies that have attempted to quantify mineral associations through visual observations using optical microscopy. In particular, a study undertaken by Arif and Baker (2004) characterizes the gold mineralogy based on the mineral associations of 699 native gold grains observed using optical microscopy. These data were used to draw conclusions regarding the source of the gold and select samples for further laser ablation analysis. Like many geological studies, the minerals that have been analysed or included in the study are those that are easily recognized or within the detection limits of optical microscopy analysis. A more automated approach to mineral identification and classification would mean that user error and bias in grain selection could be reduced.

Another study undertaken by Vaughan and Kyin (2004) characterizes mildly refractive ores based on a pyrite, arsenic or antimony association which has implications for the cyanidation of the ores. Vink (1997) and later Bojcevski (2004) created ore texture classifications based on the modal mineralogy and texture of particles and drill core. While the mineral association was recognized as important and considered in their classifications, the ability to routinely quantify this parameter was difficult. It is still time consuming despite improvements in automated microscopy, computer technology and software developments since those studies took place.

2.6.5 Mineral distribution

There are a number of textural terms that are used to describe the distribution of minerals within a rock e.g. disseminated, seriate, aggregate (e.g. Gifkins et al., 2005). Like many other aspects of texture there have been a number of attempts to measure the distribution of minerals in a rock, namely by mathematicians. For example, the proximity of various objects can be measured using co-occurrence matrices (Gay and Latti, 2006). These studies often use simulated images of artificial objects and are restricted by the size of the surface being analysed.

In liberation studies, proximity functions are potentially a useful measure of mineral clustering. For example, if the grain size of the valuable mineral is small, but there are a large number of grains clustered together, then sufficient surface area is still likely to be exposed in order for that mineral to be recovered, for example by flotation. To this author's knowledge there are no examples in the literature of proximity functions that have been used on intact rock samples for the purpose of characterizing liberation potential.

2.7 Texture of intact and particulate rocks

The characteristics of mineral and rock texture can be analysed while the rock is still intact (e.g. drill-core and hand specimen) or broken i.e. as particulates. Intact rock textures are primarily described by geologists from drill-core at the meso scale. This information is typically used to infer formation

conditions as well as for proxies for further ore-deposit exploration. Particulate rocks are observed and described at the micro-scale by mineral processors or metallurgists. Particles can be defined as 'discrete fragments of rock that can contain any number of different minerals' (Jones, 1987) and are primarily used to measure energy requirements and breakage characteristics for mineral processing circuits (Wills and Napier-Munn, 2005) as well as the most suitable mode of mineral extraction and recovery.

In order to integrate mineralogical and textural data that has been measured from both intact and particulate rock samples a number of considerations need to be made. The first consideration is that of scale. Intact rocks can be examined at the macro-, meso- and micro-scales, whereas particulate rocks are typically only observed at the micro-scale. It is therefore likely that the micro-scale analysis of one particle will not be the same as the meso-scale analysis of the same rock over a larger area. This leads to the question of sampling. If data from intact rock analyses are to be compared to analyses undertaken on particulate samples of the same rock, measures need to be taken to ensure that the sample is in fact representative of the intact rock that it was derived from.

The size to which a rock will be crushed for recovery by flotation is the minimum particle size that is required to expose enough of the valuable mineral on the particle surface. This process of mineral liberation destroys the intact rock texture to produce mineralogically simple particles that are more likely to be recovered by flotation. A quantified analysis of the rock and mineral textures prior to breakage can provide valuable information regarding the types of textures and mineral assemblages that are likely to produce various particle sizes and characteristics that are favorable or unfavorable for mineral processing.

2.8 Image analysis as a tool for quantifying mineralogy and texture

Image analysis can be defined as the measurement of geometric features that are exposed on two-dimensional digital images through the use of image analysis software (Jones, 1987). Image analysis is used in a wide range of professions for many tasks that include facial recognition in security systems, automatic number plate recognition, cancer detection through to remote sensing (Russ and Russ, 2007). More recently, advances in the fields of automated microscopy combined with increased computer capabilities have allowed the production of RGB and high resolution images of plane sections cut through rock specimens or mounted mineral particles to be produced more efficiently. These capabilities are a huge development in the ability to quantify minerals and their textures on a fast and routine basis.

There are two main functions of image analysis that will be addressed in this research; the conversion of high resolution optical images to classified images or mineral maps using object-oriented image analysis software (Section 2.8.1) and the extraction of quantified mineralogical and textural data from these images (Section 2.8.2). The application of numerical values to textural parameters that were previously considered qualitative and descriptive allows them to be compared to quantitative measurements that are routinely used by mineral processors.

Another key element to this research is the management of the data that is produced from the analysis of the classified images. In many ways the advances in automated microscopy technology have exceeded the ability to analyze and extract the relevant information from these data sets that

can be practically applied to the everyday procedures undertaken during mining operations (Section 2.8.3).

2.8.1 Object-oriented image analysis software

Object-oriented image analysis refers to software that breaks down an image into individual 'features' or 'blobs'. Features or blobs can be defined as a contiguous group of pixels with the same image properties (Russ and Russ, 2007). Figure 2.6 shows an image that has been segmented into individual objects. A rule set for classification can then be designed by the user by selecting objects that are known to be of a certain class. For example, in an image of a rock surface, objects that are known to be pyrite can be selected and factors that are the most important to the software recognizing other 'like' objects can be ranked i.e. for pyrite, colour, reflectance and shape could be selected. Traditionally, this type of software has been used for the analysis of remote sensing images and biological applications where images of the same area have been imaged under different conditions can all be utilized in the classification process.

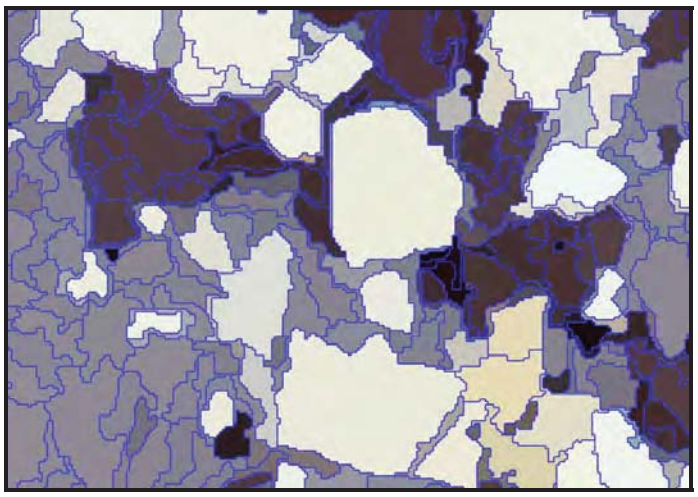

Figure 2.6. Example of an image that has been segmented into individual objects based on colour and image characteristics identified using object-oriented image analysis software.

In this research, classified images have been created from high resolution images of drill-core as well as images of rocks (intact and particulate) under different optical microscopy lighting conditions (reflected light, transmitted light, transmitted light cross-polars and transmitted light crossed polars with 1λ plate). Figure 2.7 shows an example of a high resolution image of a section of drill-core (*left*) and the corresponding classified image (*right*) that has been created using object-oriented image analysis software. The software that has been used to undertake image classification in this project is Definiens (Jyothi et al., 2008; Definiens, 2010). Figure 2.8 illustrates an example of a classified image created using images obtained from an automated optical microscopy system. The image on the *left* is only one of the images used in the image classification. The classified image (*right*) has been produced using mineralogical characteristics that for some minerals can only be observed under variable optical conditions.

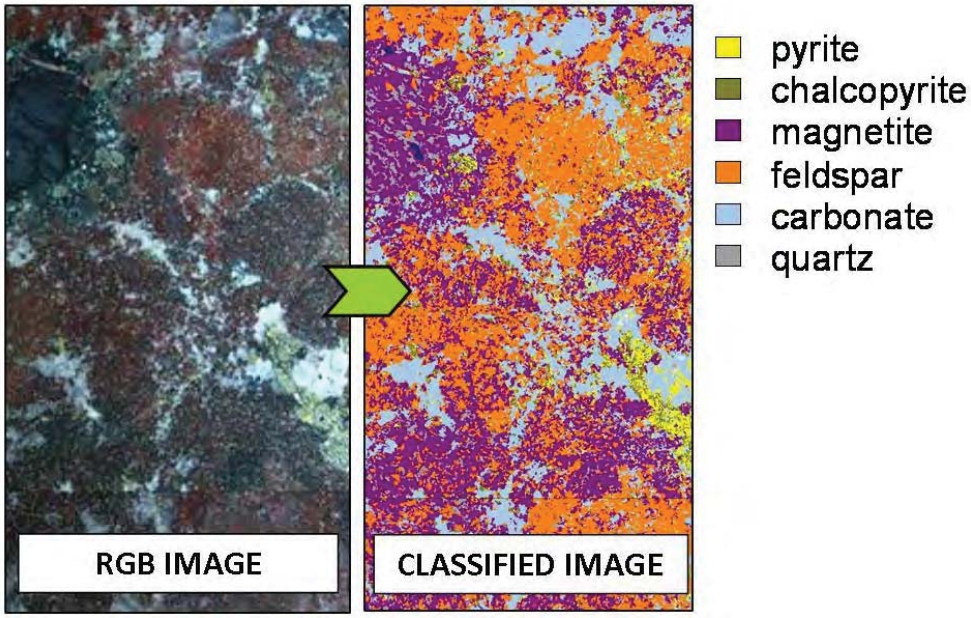

Figure 2.7. This figure illustrates a photograph (*left*) that has been converted into a classified image or mineral map (*right*) using object oriented image analysis software.

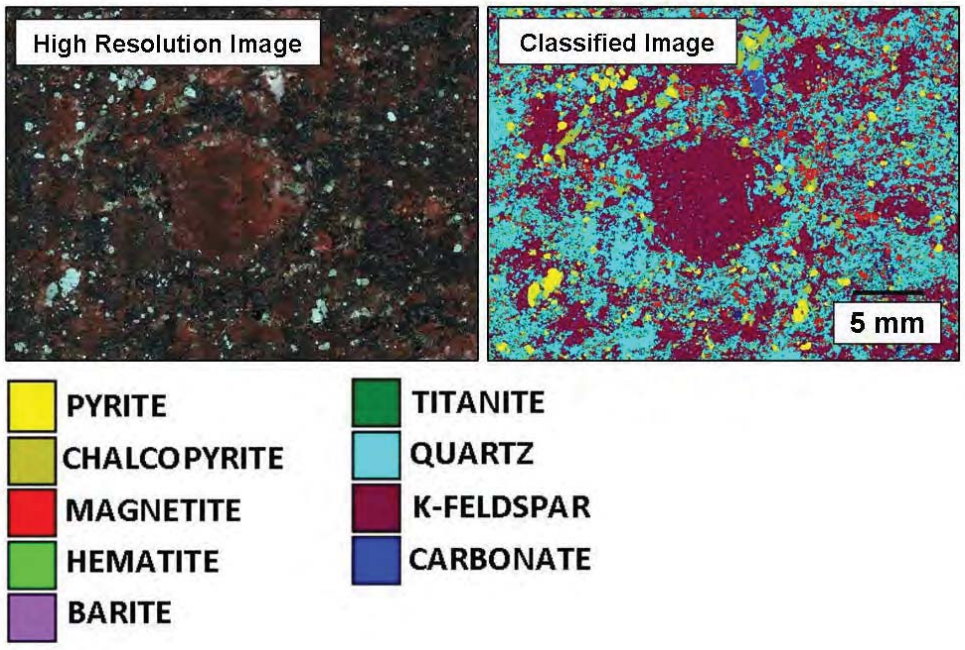

Figure 2.8. The image on the *left* has been taken using an automated optical microscopy system. Using this image and others taken over the same fields under different illumination settings, the classified image on the *right* was produced using image analysis software.

Previously, a number of authors have devised methods for potentially creating mineral maps from images created using optical microscopy (Pirard, et al., 2007; Pirard et al., 2008, Castroviejo, 2009). Research that is currently being undertaken at the University of Liege by Eric Pirard and his research team are using multiple photographs obtained from multispectral optical microscopy imaging to quantitatively discriminate between sulphide mineral species in the visible and near infrared range (400 and 1000 nm; Pirard et al., 2008). The results have proved to be successful in terms of identifying and discriminating between various sulphide minerals, however the method is not suitable for the identification of gangue minerals such as silicates, micas, etc, or the routine production of mineral maps. To this author's knowledge there are currently no existing applications

that produce routine minerals maps from optical microscopy methods where both the valuable and gangue minerals are accounted for. Another system that has been developed by the CSIRO Iron Ore Processing group classifies images obtained by optical micrscopy using in house software called 'Recognition2' (Donskoi et al., 2007). While, the results obtained from this study were found to be successful, Donskoi et al. (2007), noted that much manual retouching of the images was required and are currently working on developing a method for better mineral identification, more comprehensive texture classification and the full automation of image analysis. A detailed summary of the techniques used in this research to produce mineral maps from images produced from optical microscopy (produced in the AMIRA P843 project) have been published by Berry et al., (2008).

Currently, there are no published studies in the literature (outside the AMIRA P843 project) regarding the production of classified mineral maps on continuous sections of drill-core (Figure 2.7; Leigh, 2008, Bonnici et al., 2009). However, the author is aware that mining companies are investing money into further advancing the production of classified mineral maps of drill-core and consulting companies are beginning to offer the classification and quantified analysis of mineralogy and texture in drill-core as a service (e.g. SGS Group). The extraction of mineralogical and textural information using image analysis software is described in the next section (Section 2.8.2).

2.8.2 Data extraction from classified images or mineral maps

The ability to routinely analyze mineralogical and textural information is influenced by a number of factors. These include the image resolution (i.e. meso-scale or micro-scale analysis), instrument precision and accuracy, the speed of analysis and the cost of obtaining this information. Since the development of automated SEM based platforms such as MLA and QEMSCAN (Gu, 2003; Gottlieb et al., 2000), the use of mineral maps as a tool for extracting quantified information regarding mineralogy and texture has increased substantially as computer power increases and the cost of acquiring an automated SEM decreases. Automated SEMs use unique mineral spectra to identify minerals and produce mineral maps at high resolutions (<2 μm). In this thesis, mineral maps have been produced from SEM technology (MLA), as well as optical microscopy and high resolution digital images. The production of classified images across a range of scales allows the extraction of quantified mineralogical and textural data to be extracted using image analysis software.

There most commonly used image analysis software by process mineralogists are those that are built into the MLA and QEMSCAN (MLA Dataview: JKTech, 2010; MinAssist, 2006). These programs are tailored towards the needs of the process mineralogist and metallurgist who can benefit from information regarding chemical assay, modal mineralogy as well as mineralogical and textural information regarding specific mineral phases of interest in particulate samples (Gu, 2003). Previous work has been undertaken by Moen (2006) to create her own classification software for the purpose of creating classified mineral maps from BSE images to further extract quantified mineralogical and textural information. While classified mineral maps were produced, they were found to be time consuming and further work was required for them to be implemented as a routine analysis. Within the AMIRA P843 project, software (texture viewer) has been developed for the purpose of visualizing and sorting minerals and particles as well as extracting quantified mineralogical and textural parameters. More information about Texture Viewer is described in Appendix 2.3.

While the software that is built into the MLA and QEMSCAN can extract quantified mineralogical and textural data, it can only be applied to the classified mineral maps that are produced from these machines. There have been a number of studies that have used selected results

obtained from these software programs to evaluate various stages of mineral processing (e.g. Xiao and Laplante, 2004; Fandrich et al., 2007; Lastra, 2007; Sutherland, 2007; van Alpin, 2007; Dai et al., 2008). Within the project described in this thesis research, classified mineral maps have been produced from a number of sources (automated SEM analysis, optical microscopy, high resolution images) and therefore require software that can extract information from any classified image, regardless of where image is obtained from. The Definiens software that has previously been discussed in terms of producing classified images is also capable of extracting a large range of quantified parameters. This is particularly useful given that the image can be classified and the relevant data extracted simultaneously, making it more amenable to the routine analysis that the mining industry requires.

Image analysis software uses pixel units to measure and quantify mineralogical and textural attributes. In this project, the parameters that have been extracted include measures of modal mineralogy, size, shape, mineral association and mineral distribution. The advantages of using this method is that information can be extracted for the whole image, a selected mineral phase or a selected mineral population. Within the field of image analysis itself, there are a number of techniques that can be used to quantify object characteristics that to this author's knowledge are yet to be applied to the analysis of rocks and minerals. Polygon and skeleton analyses are used to simplify an object but still preserve certain object features (see Figure 2.9). The polygon of an object is produced by the simplification an object (using vectors) in order to reduce the effects of pixel shape (see Figure 2.9). The skeleton of an object is created, through the repeated erosion of all background touching pixels until only a skeleton of the original object remains (Russ, 2007). The polygon of an object will underestimate the complexity of the object's shape, whereas the skeleton of an object will preserve the shape characteristics of the object so that they are more amenable to image analysis. An evaluation of the quantified mineralogical and textural parameters (including polygons and skeletons) that can be extracted using image analysis software is presented in Chapter 3.

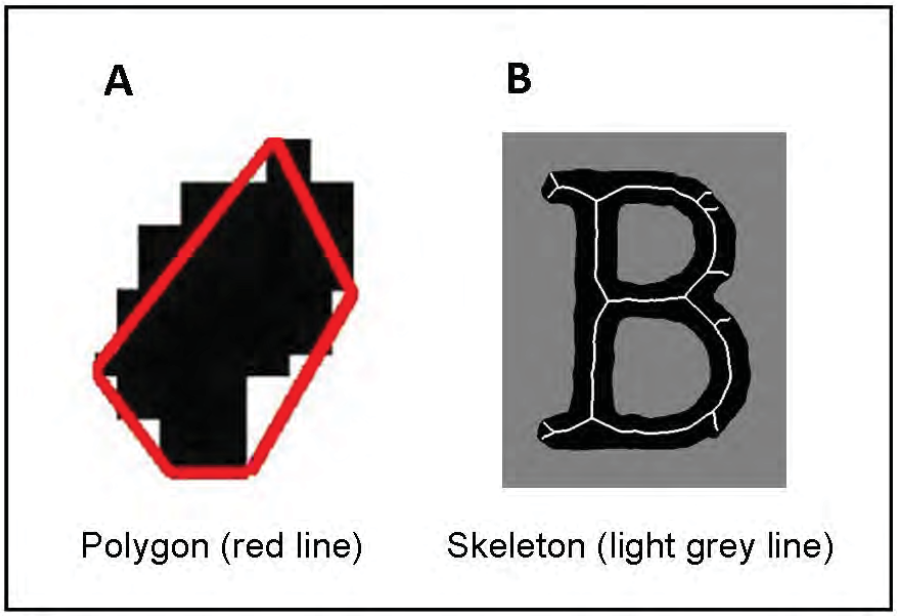

Figure 2.9. Examples of an object that has been converted to a polygon (*red line: left*) and skeleton (*light grey line: right*).

2.8.3 Data management and manipulation

The .csv format used to export results by Definiens allows the data to be easily imported into standard graphing and data visualization programs such as Microsoft Excel and ioGAS. The large files cause problems with many software packages. In this research a combination of Microsoft Excel, ioGAS and DataDesk were used. The IoGAS software has been modified to meet the geometallurgical requirements of the AMIRA P843 project. Now called ioGEM, this software is a powerful data visualization tool which allows the data point size, shape and colour to be systematically assigned to various features within a data set and then be manipulated. This software capability is extremely powerful for the extraction of dominant mineralogical and textural relationships.

Within this research, the dominant mineral associations for each deposit have been established using Principal Components Analysis (PCA) in the software DataDesk. A PCA is a statistical analysis of a data set that extracts the most strongly correlated variables to create a series of principal components. A successful PCA will account for as much of the variability in the data set within the first three principal components. These principal components are then plotted against each other allowing parts of the graph to have unique signature. The use of a PCA enables large data sets to be reduced and tailored to include the most relevant data. A detailed summary of PCA is given by Jolliffe (2002).

The limitations of how much and how quickly data can be manipulated in the field of geometallurgy come from computer and software capabilities. Future advances in these areas will greatly impact the integration of routine mineralogical and textural analysis into the mining industry.

2.8.4 Principles of Stereology

Stereology is the interdisciplinary science of interpreting 3-Dimensional objects from a 2-Dimensional planar surface (see Weibel (1980) for more information). In order for an image or planar surface to be stereologically correct it must obey the principles of stereology. The principles of stereology assume that the material being analysed are completely homogeneous and have been sampled unbiasedly (Latti and Adair, 2001). The principles are as follows:

1. The linear integration principle of Rosiwal $V_V = L_L$ where V_V = volume density and L_L = Intercept length density on line (Weibel, 1980)
2. The point counting principle $V_V = P_P$ where P_P = Point density (Weibel, 1980)

From these principles of stereology it can be assumed that $V_V = L_L = P_P$ (Weibel, 1980). There has been a vast amount of research undertaken in this area, not only in the geological sciences but also the medical sciences. In terms of this research, it is recognised that a 2D surface represented by a classified rock image may not be representative of the 3D object that it was derived from. In this project it is assumed the bias from 2D measurement will affect all samples equally and therefore the ranking of sample will be unchanged. It is impossible to prove this is true for all cases but no discrepancies were detected.

2.9 The impact of texture in mineral processing

The influence of rock texture in mineral processing behaviours has been recognized as an important factor by many authors (Vink, 1997; Petruk, 2005; Bojcevski, 2004; Grupta and Yan, 2006; Wills and Napier-Munn, 2006; Becker et al., 2008; Bonnici et al., 2008; Hunt et al., 2008; Pirard et al., 2008; Triffett and Bradshaw, 2008; Walters, 2008). The mineral processing behaviours considered were; comminution (crushing and grinding), liberation, flotation, and smelting (see section 2.5.3). However, it has only been since the development of automated microscopy systems and the implementation of image analysis software that textural attributes have been able to be quantified at the various stages of mineral processing (Gu, 2003; Gottlieb, et al., 2000). In the past, a number of studies have investigated the influence of various aspects of texture on mineral processing behaviours. Veasey et al. (1989) and Ramadorai et al. (1991) have used the mineralogy of ore types to identify potential metallurgical problems such as abundances of deleterious elements and clay minerals. Various authors have recognized the relationship between grain size and mineral liberation (Craig and Vaughan, 1981; Jones, 1987; Ferrara et al., 1989; Gaspar and Pinto, 1991; Leigh, 1993). Triffett and Bradshaw (2008) used the quantified analysis of shape to distinguish between two different generations of molybdenite that exhibited different flotation characteristics.

A pioneering study by Vink (1997) highlighted the importance of rock textures in mineral processing. He recognized that great confusion existed in the literature regarding the definition of texture both within geology and compared to the field of mineral processing. In his study of the Hilton North deposit, Vink (1997) recognized seven meso-textures and 12 micro-textures. The meso-textures were mapped them throughout the ore-body as percentages. Using visual observations and optical microscopy, Vink (1997) then extracted liberation data from the micro-textures and compared these to the meso-texture classification in order to establish a relationship between the meso-scale textural zoning of the Hilton North deposit and liberation behaviours. It should be noted that within this study Vink (1997) had made attempts to systematically photograph the micro-textures of the Hilton North deposit using the optical microscope. In this very early attempt at automated mineralogy, the technology was not advanced enough and Vink (1997) moved on with his study without the imaging component.

Years later, with the advances in automated SEM technology, Vink's (1997) work was extended in a master's study undertaken by Bojcevski (2004). Bojcevski (2004) established a meso- and micro-textural classification of the George Fisher lead-zinc deposit similar to that of Vink (1997). In this study, seven meso-textures, consisting of variable abundances of galena, sphalerite or pyrite were examined for the presence or absence of the five micro-textures. The micro-textural classification described the distribution of the minerals (massive or banded). Through the use of the emerging MLA system, Bojcevski (2004) was able to undertake a more quantified approach to classifying micro-textures that were then compared to the average head grades as well as the flotation and recovery performance at George Fisher.

While the studies undertaken by Vink (1997) and Bojcevski (2004) went a long way in raising the awareness of the importance of texture in mineral processing behaviours, both studies only considered the mineralogical composition of the particle and the distribution of the valuable minerals. This may have been a function of the texturally simple deposit style that both authors were investigating. Within the present study, the concepts created within the work of Vink (1997) and Bojcevski (2004) will be integrated into meso-scale visual logging of drill-core, high resolution digital

images, automated microscopy and image analysis. This allows the mineralogical and textural attributes that were unable to be easily quantified (e.g. mineral associations, gangue mineralogy, size distributions) at the times of these studies to be tested for their potential impact on mineral processing behaviours. These methods and techniques are presented in Chapter 3.

2.10 Summary

A detailed summary of the emerging field of geometallurgy and the roles that various mining professionals play in producing a successful geometallurgical model have been outlined in this chapter. The nomenclature and classifications systems for describing texture in both geology and mineral processing have been presented and the existing methods for qualitative and quantitative textural analyses have been discussed. Also introduced in this chapter is the use of image analysis software as a tool for routinely quantifying mineralogical and textural attributes at both the meso- and micro-scales. The relevant studies that have used mineralogy, texture and/or image analysis in the fields of geology or mineral processing have been presented. The methods and techniques that have been described in this chapter and will be used in this research are presented in Chapter Three.

Chapter Three
Methodologies

3.1 Introduction

In this chapter, each instrument and technique used in the course of this research is described and discussed in terms of machine resolution, analysis time, cost, instrument limitations and sample requirements. The descriptions and protocols are presented from the largest to the smallest scales (meso- to micro-), beginning with the meso-scale visual drill-core logging (section 3.2), followed by the high resolution drill-core logging system (section 3.3) and then by the optical microscopy analysis (section 3.4) and MLA (section 3.5; Figure 3.1). The final component of the chapter provides an outline of the mineralogical and textural attributes used in this thesis (section 3.6) and descriptions of the mineral processing tests that were collected by other workers on this material (section 3.8). Each of the instruments and techniques used within this research have their advantages as well as their limitations. Some techniques are more amenable to certain ore types than others and where appropriate only the most suitable instruments and techniques have been used.

3.2 Visual (meso-scale) logging of mineralogy and texture

The way that an ore will behave during mineral processing is dependent upon its mineralogical and textural characteristics. How various aspects of texture and to a certain degree, mineralogy effect mineral processing behaviours such as crushing, grinding, liberation and flotation is poorly understood. In early work by Vink (1997), he recognised that textures needed to be measured during geological logging in order to better understand their effect on mineral processing behaviours. He also recognised that multiple textures can occur within one ore type, and this too needed to be taken into consideration during the logging process. In his research Vink (1997) logged a variation of three meso-textures each with a mineralogical descriptor (massive, sphalerite dominated; massive, galena dominated etc.) at the Hilton North deposit. The meso-textures that he used were extremely simple,

which reflected the nature of the ore body and were able to be logged as they occurred down-hole. These textures were then later compared to the results of liberation analysis.

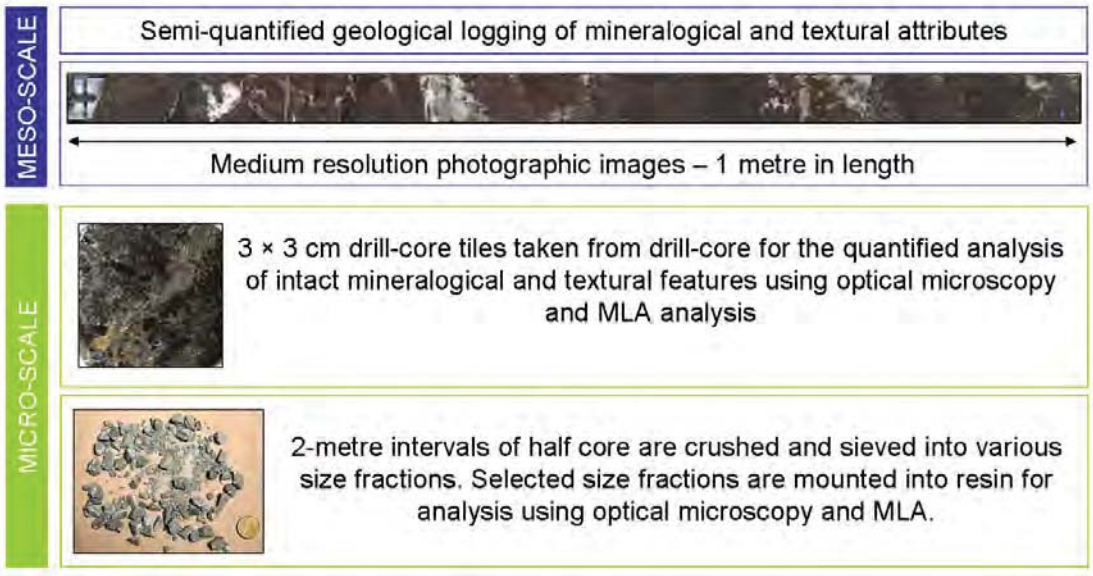

Figure 3.1. Instruments, techniques and sample types that will be used in this research for the analysis of mineralogical and textural attributes at both the meso- and micro-scales.

Within this research, mineralogical and textural attributes will also be logged with the aim of understanding the influence of texture on mineral processing. A different approach to that undertaken by Vink (1997) will be taken in order to accommodate more complex ore systems. Mineralogical and textural attributes (not classes) will be logged as a percentage of the site assay interval (i.e. every 2m for Cadia East and Ernest Henry). The attributes being measured will be based on attributes that can be predicted to affect certain aspects of mineral processing such as comminution, liberation and flotation. The information obtained from textural logging has been used to determine the dominant textural classes present in the examined drill-holes at both Cadia East and Ernest Henry. These classes have been tested against quantified mineralogical data (assays and GEOTEK MSCL data) to assess their validity as independent mineralogical and textural classes that can potentially be compared against the results from mineral processing test work.

3.2.1 On site logging of drill core attributes: Current practice

The logging of geological attributes in drill core is routinely undertaken in both exploration and mining geology. In exploration geology, drill core is typically logged for attributes that will be used to produce models for further exploration targets or constrain where local mineralisation may occur. In mining geology, drill core is logged for mineralisation features as well as structural elements that are likely to affect structural components of the mining operation. Through the life of a deposit it will evolve from being an exploration target, to going through the stages of pre-feasibility, feasibility and finally into production mining. Throughout this process the data extracted from drill core will serve different purposes. It is sensible for the types of geological attributes that are logged to evolve and reflect this change. For the geological logging of diamond drill holes, the attributes are recommended to be routinely measured are listed in Table 3.1. In addition, the intervals in which ore minerals are present require further characterization (Table 3.1).

Table 3.1. Attributes recommended for the routine logging of drill-core for rocks and the ore minerals. Attributes have been summarised from the Field Geologists Guide, Berkman, (2001).

ROUTINE MEASUREMENTS FOR DRILL-CORE LOGGING	
Rock attributes	**Ore mineral attributes**
The length of core drilled	Grain size and relation to other ore minerals
The measured length of core recovered	Orientation of ore minerals and zones of mineralisation
The percent of drill-core recovered	Gangue minerals present
Sampled intervals for assay	Gangue grain size and relation to the ore minerals
A graphic lithological section	Visual estimate of grade as percent metal
Lithology and degree of weathering	
Colour	
Grain size (of dominant minerals)	
Field rock name	
Proportions of rock minerals	
Attitude of bedding or foliation	
Attitude and spacing of joints	
Attitude, width and description of sheared zones	

Each mine site will have their own variation of how these geological attributes are measured and for what purpose. Typically the size of the ore minerals and their relation to the gangue minerals present are documented. However, the minerals are generally listed as simply being present or a rough abundance given e.g. 1-5%. In this case the data is qualitative and not suitable for comparison to other quantitative measures such as assay results.

Within this research a method has been developed to log geological attributes in drill core that are considered to effect mineral processing behaviours such as crushing, grinding, liberation and flotation. These attributes are logged in a way that makes them suitable for comparison to quantitative data such as assay, geophysical and modal mineralogy data. The data measured can also be used to create a visual meso-scale textural classification, as shown in the examples for the Cadia East and Ernest Henry deposits (*see later in* Chapter 4).

3.2.2 On site logging of drill core attributes: New practice

In addition to the usual logging procedure of laying the drill core out areas of good light and marking regions of significance (e.g. lithological boundaries, mineralized zones, changes in alteration minerals etc.), any rock and mineral characteristics that may influence mineral processing behaviours should be noted. The questions that should be considered during this process are outlined in Table 3.2. From these observations, a drill core logging sheet can be designed that will allow the consistent recording of rock and mineral characteristics that may be related to a mineral processing behaviour at a specific ore deposit. Any logging parameters that are selected must be easily and consistently recognisable in the drill core by all geologists on site. If a parameter can not be easily recognised, the results may become skewed and may indicate mineral relationships that do not really exist.

Table 3.2. Questions that need to be regarded when deciding which attributes to measure in drill-core that are considered to affect mineral processing behaviours.

Questions
What valuable minerals are present? e.g. *chalcopyrite or bornite.*
Do any of the valuable minerals phases contain inclusions (elemental or mineral) that could potentially be deleterious? i.e. *arsenopyrite, bismuth, mercury, tellurides, sellenides*.
What is the distribution of the valuable mineral phases? i.e. *disseminated, aggregates, vein style*.
What are the dominant mineral/rock associations of the valuable minerals? i.e. *completely encapsulated in quartz, or intergrown with biotite.*
What are the dominant gangue minerals present?
Are there any sulphide or oxide minerals present as gangue phases? i.e. *pyrite, magnetite, hematite*.
Are there any gangue minerals present that would be deleterious to or hinder mineral processing? i.e. *talc, fluorite, Tetrahedrite.*
Are the dominant gangue minerals hard or soft?
What is the grain size of the valuable minerals and other sulphide minerals?
Are there any other valuable or deleterious mineral phases present within veins? i.e. *free gold, electrum, molybdenite.*
Are there any clay minerals present?
Are there any fault zones present? If so, what is their dominant mineral assemblage?
Is there pyrite present? If so, how much? And where?
Is there magnetite present? If so, how much? And where?
How hard is the rock? Is it uniformly hard or soft?

Each attribute that is recorded, should be measured as either a ratio or a percentage of the assay interval i.e. out of 1 or 100. The attribute should be measured as accurately as possible. This will allow changes in mineralogical and textural attributes to be observed down hole and compared with existing quantified data. Once the logging of drill core attributes has begun, it is likely that new textures or styles of mineralisation will be observed. In this circumstance it is important that new textures are not ignored or misclassified, the logging sheet should be updated to include new information. This method has been undertaken on selected drill-holes at the Cadia East and Ernest Henry deposits and the results and interpretations are presented in Chapter Four.

3.3 High resolution drill-core imaging

In recent years, the increased capabilities of digital cameras have allowed drill-core to be routinely photographed on mine sites. The purpose of this is to ensure that a record is kept prior to rock breakage or the oxidisation processes occurring. To some degree, mineralogical and textural features can be identified from theses images; however unconstrained lighting conditions combined with reflections on wet drill-core and the photographing of whole drill-core trays at one time, mean that the usefulness of the information extracted is limited.

In this research, high resolution imaging is undertaken using the GEOTEK MSCL which is equipped with a camera for core imaging and sensors for measuring P-wave sonic velocity and amplitude, gamma ray attenuation (bulk density), magnetic susceptibility, and electrical resistivity (Figure 3.2; More detail regarding the geophysical capabilities of the GEOTEK MSCL can be found in Vatandoost et al., 2008). Whole or half core is placed into core-boats that systematically feed the core through the logger taking photographs and measurements at specified intervals for each instrument (Figure 3.3). Drill core images were collected under constrained lighting conditions with no image compression artefacts. 24-bit RGB (500 dpi) images were taken every 9 cm along the drill core and stitched together into approximately one metre intervals. The constrained lighting

conditions and exclusion of image compression allows these RGB images to be classified into mineral maps using a rule set created within the Definiens software (see Chapter 2, section 2.8.1). This allows for the fast routine processing of images into mineral maps for the purpose of extracting mineralogical and textural information at the meso-scale.

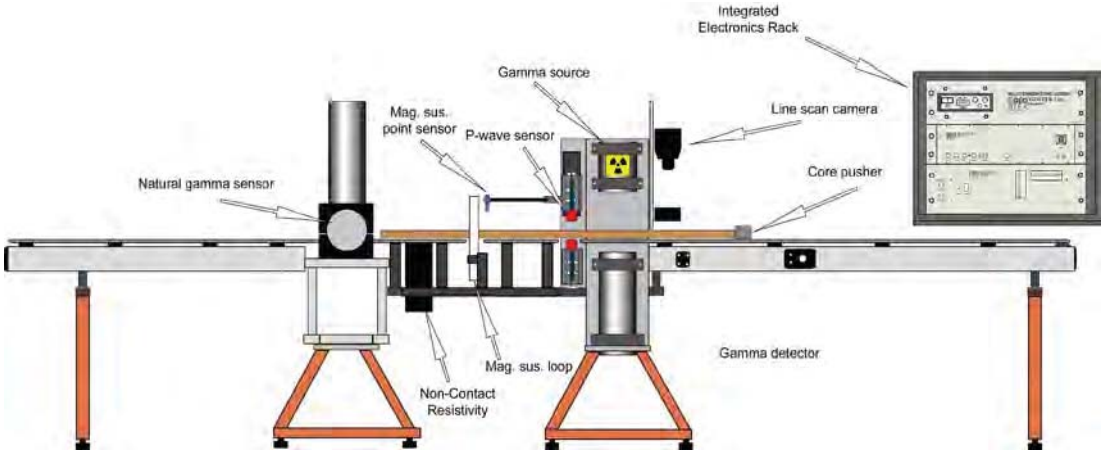

Figure 3.2 Schematic diagram of a GEOTEK MSCL (GEOTEK, 2000).

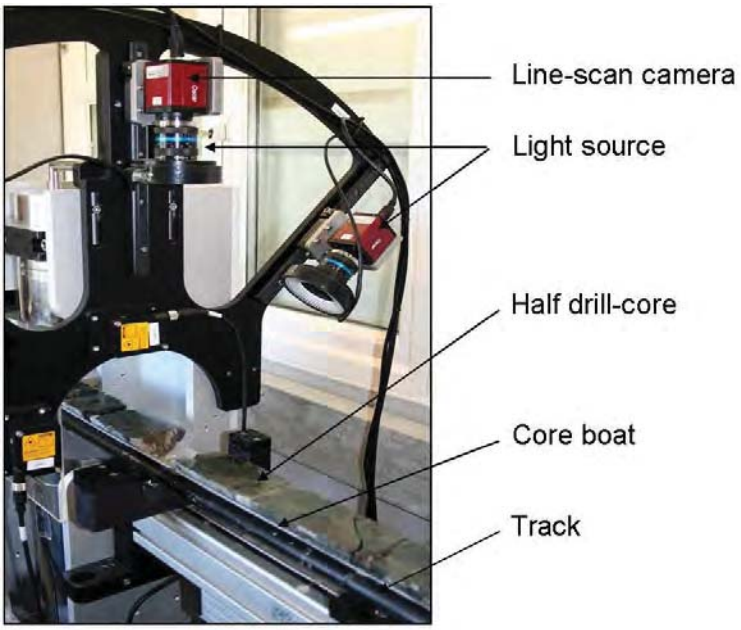

Figure 3.3. GEOTEK MSCL imaging system. Labels show the positions of the line-scan camera (obscured by light source), multiple light sources, half drill-core (photographed wet), core boat and track.

The routine production and extraction of information from meso-scale mineral maps can be used as an early guide for the modal mineralogy and changes in mineralogy down hole in a deposit. They can be used to identify the gangue minerals that are predominantly associated with the valuable mineral phases as well as size and shape data. Having this information prior to commencing metallurgical test work can aide in the selection of more representative ore type samples. Results from the textural analysis of the meso-scale mineral maps have been compared to the outcomes of micro-scale mineralogical and textural analyses performed on drill-core tiles from the corresponding intervals (Chapter seven). The aim is to assess if there are mineralogical and textural characteristics present at the meso-scale that can be used to recognise potential differences in mineral processing

behaviours. In order to do this successfully, the meso-scale information needs to be integrated with more detailed micro-scale analysis. This will assess what level of mineralogical and textural information is lost as the resolution is decreased.

3.3.1 Image acquisition: Procedure of image creation

The high-resolution images of drill-core are acquired at the same time as the measurement of geophysical parameters (see previous section). While, the geophysical results are not directly used in this research, there are steps that need to be taken to ensure the production of good quality images for further classification.

The steps in the production of a typical drill-core image include:

1. Core preparation: Half drill-core that has been produced using a saw (not split). Ideally, the core should be the same width and thickness along the length of the core with no saw or drillers markings.
2. Sections of drill core are placed in order in 1m core boats. The sections of drill-core should be fit together as tightly as possible to ensure that the image produced is as seamless as possible. Where core loss has occurred, the appropriate interval should be left empty.
3. Ensure that all flat surfaces of drill-core are even and parallel with the base.
4. Using a damp cloth, wet the flat surface of the drill-core and ensure that there are no pooled sections of water that may cause areas of reflection in the image.
5. Core boat is loaded onto the track and images are taken every 9cm.
6. Nine cm image sections are stitched together into one metre intervals and exported as .png files (see Figure 3.4).
7. Images are manually edited to mask out fractures, gaps and other artefacts (see Figure 3.4).

Once these steps have been completed the images are ready to undergo the classification process (section 3.3.3) into classified mineral maps.

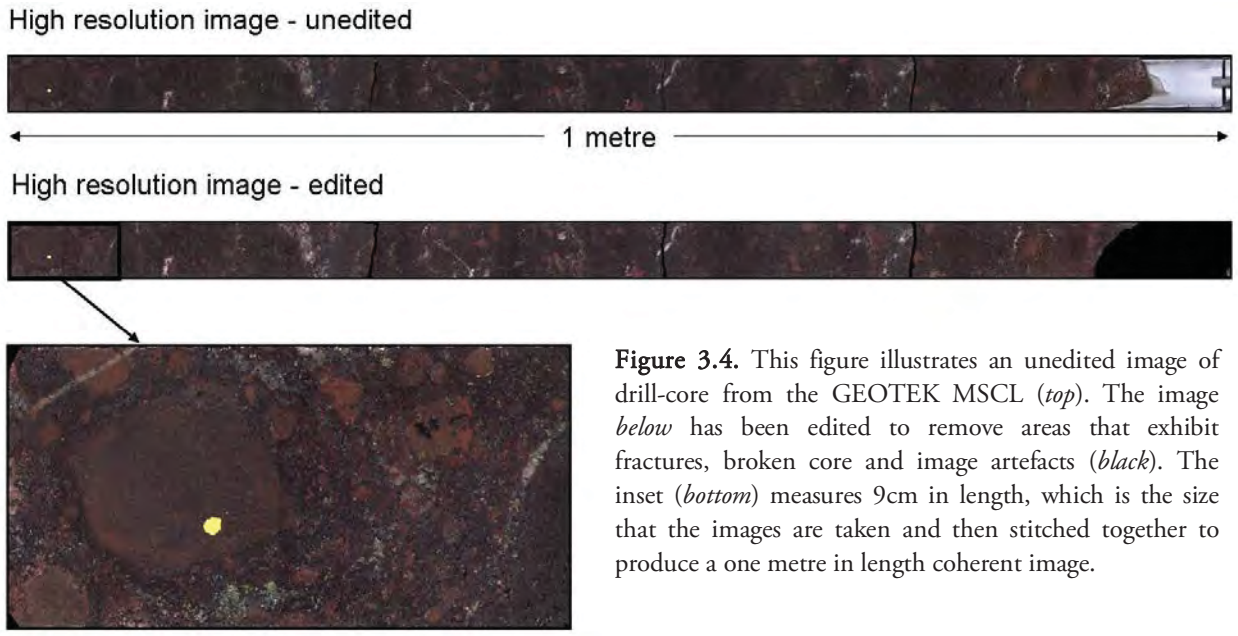

Figure 3.4. This figure illustrates an unedited image of drill-core from the GEOTEK MSCL (*top*). The image *below* has been edited to remove areas that exhibit fractures, broken core and image artefacts (*black*). The inset (*bottom*) measures 9cm in length, which is the size that the images are taken and then stitched together to produce a one metre in length coherent image.

3.3.2 Image Artefacts

Image artefacts occur where there are inconsistencies in the drill-core that is being imaged. These include driller markings, dry core patches, fractures and faults, core boats, rough surfaces, saw marks and image stitching. These artefacts and how they have been controlled in this research are described in Table 3.3.

Table 3.3. Descriptions of image artefacts encountered in the classification of drill-core images and the potential solutions used in this research.

Artefact	Description	Solution
Drillers markings	Lines and dots are left on core by drillers for the geologists for geotechnical measurements (e.g. yellow dot on the image in Figure 3.4).	Classify each colour of driller's pencil. These results can be removed from the data after classification and the extraction.
Dry core patches	These occur when core is moving through the logger and is not monitored to ensure that it remains wet.	Digitally removed prior to classification.
Fractures	Core breakages that occur during drilling.	Digitally removed prior to classification.
Fault zones	Fault zones occur throughout most ore-deposits and can range from cm's to metres in diameter. They consist of broken and soft pieces of core which are not amenable to the image classification process.	Digitally removed prior to classification.
Core boats	Core boats are used to secure the core as it moves through GEOTEK MSCL. Typically the areas between fractures as well as the beginning and end of each metre will be seen in the raw image.	Digitally removed prior to classification or use distinctively coloured core boats.
Rough surfaces	These occur when drill-core is not very competent and the saw is unable to create a clean surface. These also occur when the core fractures and exposes a shallowly dipping surface during drilling.	Digitally removed prior to classification.
Saw marks	Saw marks occur when the core is not cut cleanly and leaves jagged edges on the drill-core.	Where saw marks are extremely bad and create uneven surfaces on drill-core they have been digitally removed prior to classification.
Image stitching	Image stitching artefacts occur after the core has been photographed and the images are being stitched together. The problem is created if the core has moved during between consecutive images being taken. This results in image alignment problems and a linear artefact at the point of image stitching (see Figure 3.5).	These artefacts can influence results by changing the shape of mineral objects (e.g. chalcopyrite) and creating an incorrect classification leading to incorrect results (see inset (*yellow*) in Figure 3.5). The error involved is typically on the scale of tens to hundreds of pixels, which is considered relatively minor in an image of ~ 200 million pixels.

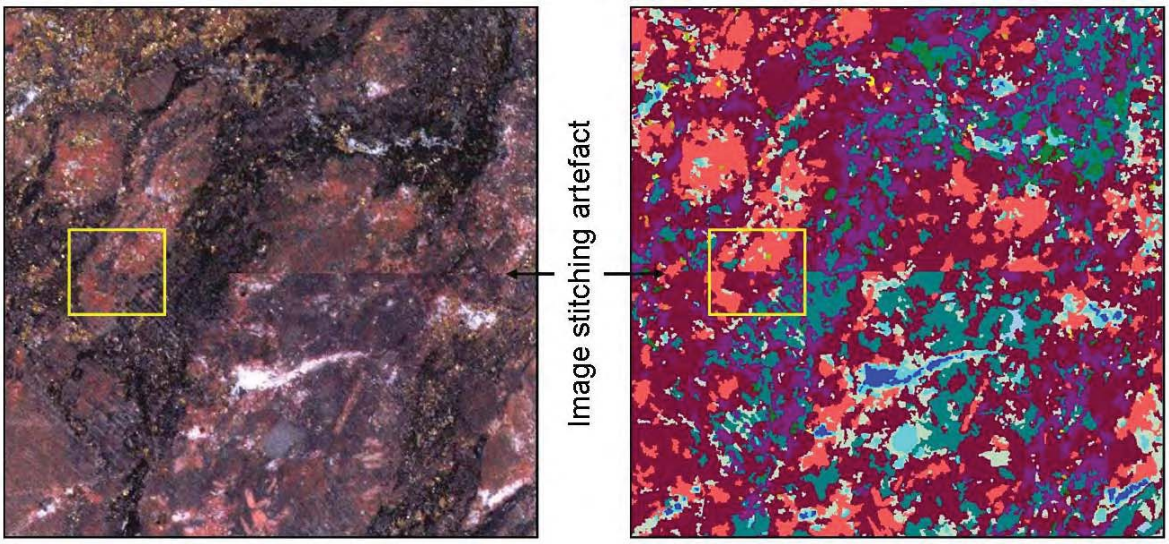

Figure 3.5. Unclassified (*left*) and classified (*right*) images showing the 'image stitching' artefact. The *yellow* inset shows an area where mineral shape and size has been affected by the artefact.

3.3.3 Image classification

The procedure of image classification occurs using the Definiens software. The steps undertaken in creating a typical classified image are as follows:

1. Creating a rule set for image classification: This step should be undertaken by an experienced mineralogist with knowledge about the ore deposit and the minerals that it contains. A rule set can be used on multiple images provided that the lighting conditions and mineralogy does not vary significantly.
2. Image segmentation: This is the first step in creating a rule set. The image is broken down into individual objects based on colour and image characteristics (See Chapter two, section 2.8.1).
3. Selecting minerals for the rule set. The number of minerals or mineral groups should be kept as simple as possible and not exceed approximately 12 minerals. The more minerals or mineral groups that are included in the classification, the more likely that two minerals will share some image characteristics and produce an inaccurate mineral map.
4. Mineral names: Minerals or mineral groups should be named appropriately. If a mineral or mineral group cannot be distinguished from other similar minerals visually, then it should be named to account for this. For example, at Ernest Henry calcite and quartz commonly occur together and without hardness testing can be difficult to tell apart. Therefore, these minerals have been grouped and classified as carbonate/quartz to include other pale and white minerals that cannot be distinguished between visually.
5. Selecting type examples for each mineral or group: Once the image has undergone segmentation, the user can select examples of each mineral or group. Large quantities of examples are selected to ensure that a cross-section of mineralogical variability is included. During the classification process, the software will use these examples to produce a classified mineral map.
6. Comparison of minerals or mineral groups: Minerals or mineral groups that share characteristics should be compared. This is done by observing the histograms that have been created for each group (see Figure 3.6). If the histograms overlap significantly then the software will have difficulty distinguishing between them.
7. Image classification: Once a rule set has been created the image can now be classified into a

mineral map. Once this process has been completed, each mineral or group in the image should be checked for accuracy. If the classification is poor, then the rule set needs to be amended.

8. Routine inspection of images: Classified images need to be routinely checked after the classification procedure has been undertaken. Under circumstances where, the rock types or lighting has significantly changed a modified rule set will need to be created.
9. Extraction of mineralogical and textural information: Mineralogical and textural data can be extracted immediately after the classified mineral map has been produced. This procedure is presented later in the chapter in section 3.6.

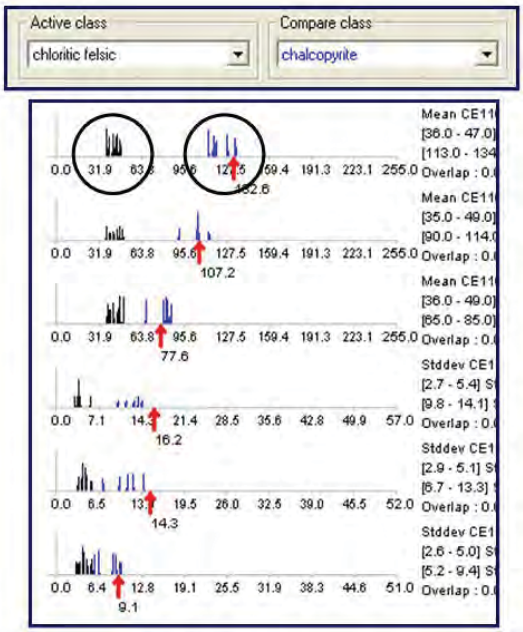

Figure 3.6. Section of a screen shot from Definiens showing a histogram (*black circles*) comparison between two minerals in a rule set. Each graph is a separate image feature. If the histograms overlap, then the software will have difficulty distinguishing between the two minerals or groups during the classification process (*image courtesy of Ron Berry).*

3.3.4 Image acquisition and classification: Cadia East

Cadia East was the first site to undergo machine-based logging with the GEOTEK MSCL. During this process, approximately 1500m of drill-core were photographed at a medium resolution and measured for their petrophysical characteristics. The rock textures were photographed on wet core. This resulted in specular reflectance caused by the direct illumination with the overhead ring flash units. To overcome this, the core was illuminated with only one light at 45°. While, this produced reasonable images, there was variable illumination across the drill-core, which made the classification process extremely time consuming and difficult. The decision was made to use an addition light source and instead perform the meso-scale machine-based textural analysis on the rocks from the Ernest Henry deposit.

3.4 Automated optical microscopy

As described in the previous chapter (Section 2.8), recent advances in digital photography and image processing capabilities have given optical microscopy the capacity to generate mineral maps similar to those generated by the MLA (Berry et al., 2008). Traditionally, optical microscopy is used by geologists to identify minerals in thin sections. However, in recent years with the advances in SEM technology and less emphasis on optical microscopy in university education, the skill of optical mineral identification has decreased significantly.

In a typical optical microscopy analysis, every mineral has unique characteristics (colour, pleochroism, twinning, anisotropy, extinction) when viewed in transmitted-light plane-polarized, transmitted-light crossed-polarized and reflected-light plane polarized (MacKenzie and Adams, 1994). Automated optical microscopy integrated with digital photography allows these views to be systematically photographed frame by frame using an automated stage and inbuilt digital camera. Each frame is photographed and then stitched back together to produce an image of the sample surface (i.e. thin section, grain mount etc.) under various optical conditions.

There have been a number of attempts in recent years to extract quantified mineralogical and textural information using images obtained from optical microscopy. Higgins (2006a) provides a summary of modern optical microscopy techniques in the analysis of minerals and their textures. The automatic recognition of minerals has largely been applied to opaque minerals by using multispectral data to distinguish between minerals with similar reflectance characteristics (Pirard, 2004; Pirard et al., 2007). This work has been expanded by Lane et al. (2008), who use this method combined with commercially available software (developed by SGS mineral services) to produce mineral maps from particulate samples that can undergo routine analysis for locked and complex particle types. Within all these studies, there have been no attempts to quantify gangue related phases that cannot be identified using reflected light microscopy (Berry et al., 2008).

The optical microscopy system used within this project is the Leica DM6000 (Figure 3.7). The protocols and measurement conditions used for this optical system have been established through extensive test work and are described in Appendix 3.2 (Berry et al., 2008). The Leica DM6000 has a high precision stage (<1 micron error in reproducibility) which allows the direct tiling of frames and good registration of multiple images collected. Within this research, images of reflected light (Figure 3.8A), transmitted light (Figure 3.8B), transmitted light crossed polars (Figure 3.8C), transmitted light crossed polars with 1λ plate (Figure 3.8D) have been collected from intact rock tiles and thin sections of particulate samples. These images all provide different information about the minerals present in a sample and have been used together in this research to provide a classified mineral map (Figure 3.8E).

Figure 3.7. Photograph of the Leica DM6000 Automated Optical microscopy system.

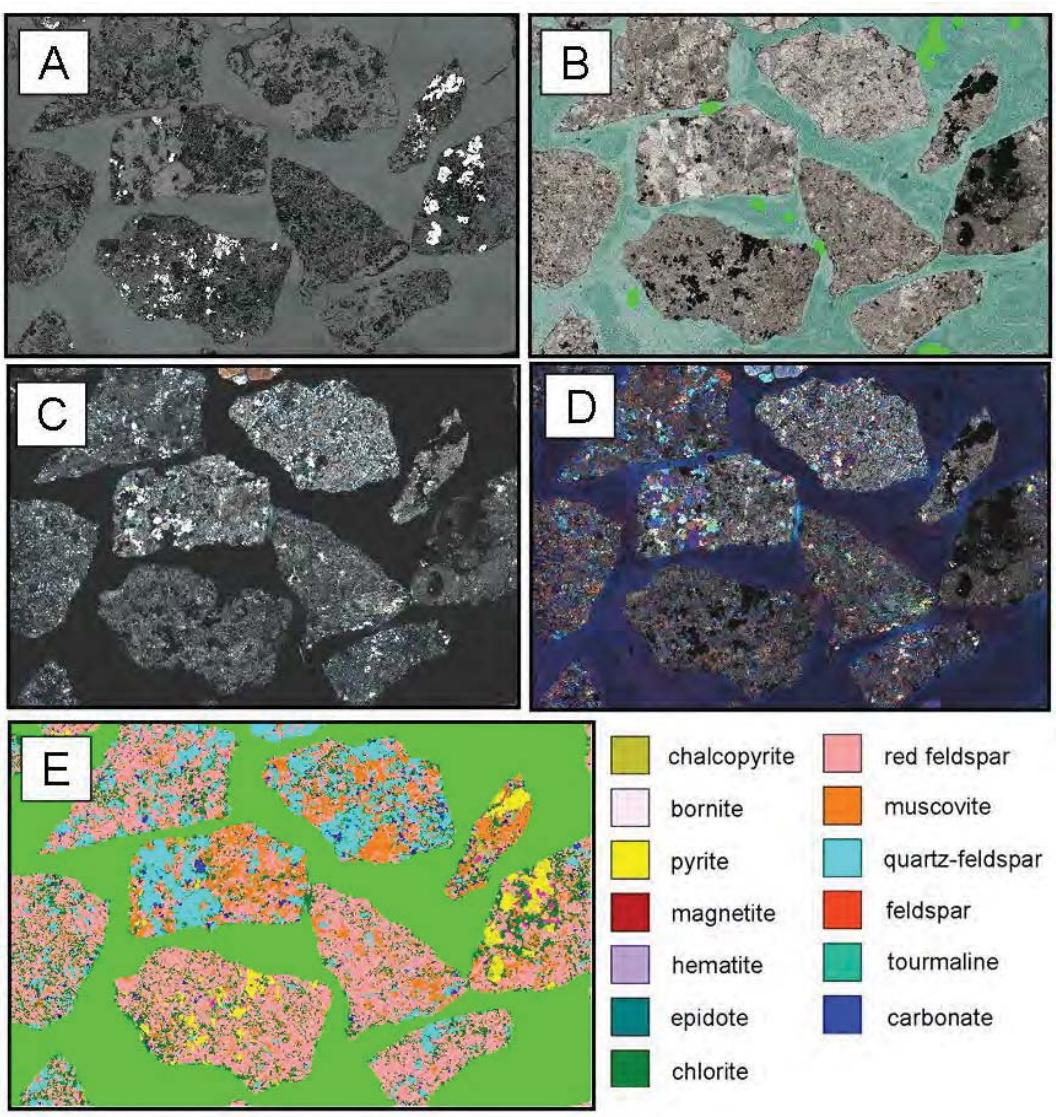

Figure 3.8. **A.** Reflected light image **B.** Transmitted light image **C.** Transmitted light crossed polars image **D.** Transmitted light cross polars image with 1λ plate **E.** Classified image of particulate sample CE143 1362m (*images courtesy of Ron Berry*).

3.4.1 Image acquisition: Procedure for image creation

During the image acquisition stage there are number of factors that are extremely important in the production of a composited image. These include camera alignment with the stage, lighting conditions, condenser and aperture settings, objective lens and camera type. Extensive testing of the settings and configuration of the Leica DM6000 has been undertaken by Assoc. Prof. Ron Berry and are summarised in Appendix 3.2. The typical steps that are taken in the production of images from the optical microscope are:

1. Sample preparation: For analysis using this optical microscopy method, the sample surface needs to be polished and contain no carbon coating.
2. At the beginning of each day, the settings and configurations are checked and recorded (see Appendix 3.2).

3. Samples need to be secured onto the microscope stage to ensure that the sample does not move when the stage is active. This can result in stitching artefacts being produced.
4. The images are recorded using the QWIN software macro provided by Leica. This software allows five channels (each corresponding to different acquisition parameters) to be individually programmed and sequentially analysed. For the thin sections of particulate samples, the transmitted-light plane-polarzied, transmitted-light cross-polarized and reflected light were recorded on 3 channels and the transmitted-light cross-polarized with the 1λ tint plate inserted was recorded on a fourth channel and run separately. For the analysis of rock tile samples, 4 channels were selected the transmitted-light plane-polarzied, transmitted-light cross-polarized, reflected light and reflected light cross-polarized.
5. In the QWIN software, using 'Mosaic Viewer' images are all exported in alphabetical order into folders specific to that sample only.
6. Images are manually inspected for correct mosaicing and the production of images that are suitable to undergo image classification

Once these steps have been completed the images are ready to undergo the classification process (section 3.4.3) into classified mineral maps.

3.4.2 Image artefacts

Image artefacts occur where there are inconsistencies in the drill-core that is being imaged. These include mineral edge effects and image stitching. These artefacts and how they have been controlled in this research are described in Table 3.4.

Table 3.4. Descriptions of image artefacts encountered in the classification of optical microscopy images and the potential solutions used in this research.

Image Artefact	Description	Solution
Mineral Edge effects	Mineral edge effects occur in optical microscopy images when the angle of the mineral in the thin section is not parallel or perpendicular to the thin section surface. Edge effects have been discussed with respect to both optical and SEM based classification systems as an artefact that is a common occurrence and needs to be considered in the analysis of results (Launeau and Cruden, 1998; Berry et al., 2008). The result of the edge effect is an elongate object that is classified as either chalcopyrite or magnetite (see insets in Figure 3.9).	These effects can be manually touched up after classification, however this is time consuming and research into an automated touch up system or amendment to the classification process should be considered in the future.
Image stitching	Image stitching artefacts in classified optical images occur as a result of frame misalignment when the composited image is stitched together. This can be a result of stage or sample movement during the image acquisition process.	See Table 3.3.

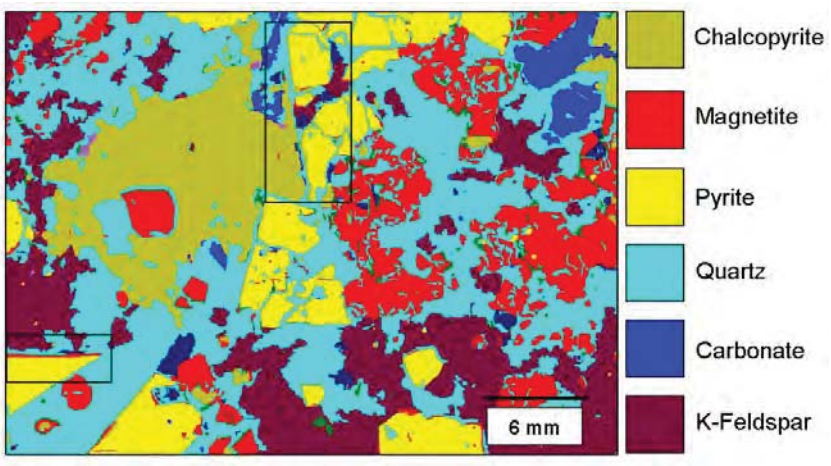

Figure 3.9. The edge effects that occur in classified images obtained from the optical microscopy system. The most common edge effects encountered in this research occur in euhedral pyrite phases where the edges are classified as magnetite or chalcopyrite.

3.4.3 Image classification

The procedure of image classification occurs using the Definiens software. The steps undertaken in creating a typical classified image are as follows:

1-7. These steps are the same as the image classification steps described for core logger images, except that multiple image types of the same sample are used in the classification (see section 3.4.3).

8. Routine inspection of images: Classified images need to be routinely checked after the classification procedure has been undertaken. In the case of the mineral maps produced from optical microscopy, these images can be compared to more accurate mineral maps produced from the MLA of the same image. Figure 3.10 shows a mineral map produced from the optical microscopy images (left) that has been classified with an inaccurate rule set. A comparison with the mineral map produced from the MLA (right) clearly shows that there are problems with the parameters set for magnetite and chalcopyrite in optical microscopy rule set.

9. Extraction of mineralogical and textural information: See section 3.4.3: step 9.

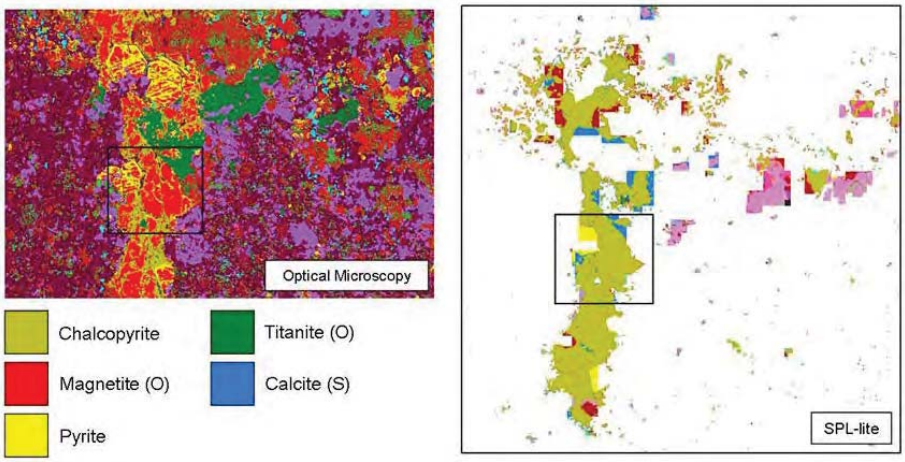

Figure 3.10. A comparison between classified mineral maps produced from the optical microscope (*left*) and the MLA (*right*) in SPL-lite mode. The comparison shows that the rule set used by Definiens to produce the classified image on the left has classified a number of minerals incorrectly when compared to the SPL-lite image on the right. Further investigation showed illumination had changed and a modified rule set was required. O = Optical microscopy image; S = SPL-lite image.

3.5 Mineral Liberation Analyser (MLA)

The MLA is an automated SEM-based system used routinely by mineral processors to obtain detailed mineralogical data for mine feed, concentrate and tails (e.g. Gu, 2003; Fandrich et al., 2007, Goodall and Scales, 2007). MLA techniques are used in this research to obtain mineralogical and textural data for intact and particulate samples of drill core and are described briefly below. The functions and settings of the MLA are described in detail in Appendix 3.3.

3.5.1 MLA Functionalities

The MLA functions are performed using a mineral x-ray spectra analysis. X-ray spectra are acquired using an Energy Dispersive Spectrometer (EDS) and compared against spectra within a 'Mineral Spectra Library' which has been created by the MLA user (see section 3.5.2). Further information regarding the process of spectra collection is detailed in a PhD thesis by Dou (2002).

There are multiple ways in which the mineral spectra are collected using the MLA, depending on the function that is selected. A detailed summary of the MLA functions and their purpose can be found in Fandrich et al., 2007). The functions that have been used within this research are detailed below.

SEM Mode

The MLA in SEM mode allows the MLA user to navigate around a sample and collect mineral spectra from mineral phases of interest. This tool is extremely powerful as it can provide a quantified analysis of a mineral's elemental abundances in seconds. This allows the mineralogy of a sample to be determined quickly and cost effectively. The MLA system contains an inbuilt peak identification software program called EDAX (EDAX, 2008). The EDAX software reports the elemental abundances of a mineral based on the proportion of peaks in the measured mineral spectrum (Figure 3.11).

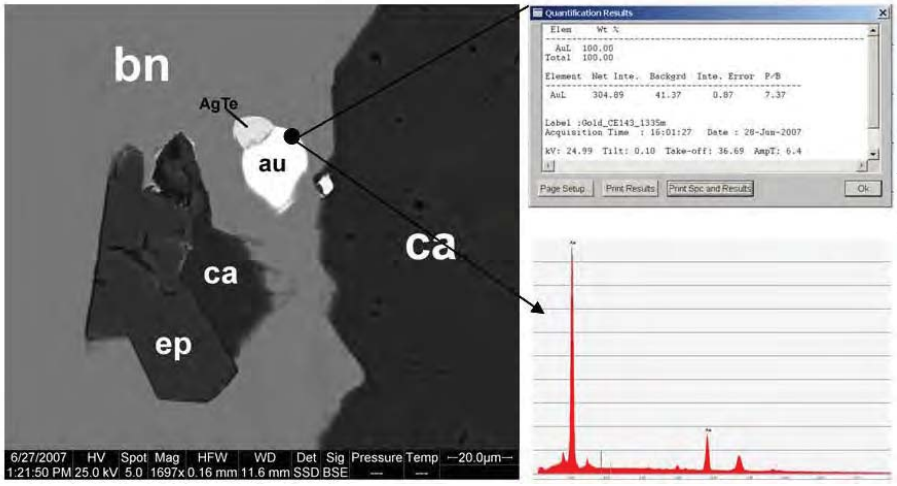

Figure 3.11. Example of an x-ray mineral spectrum obtained from a polished rock surface and the elemental abundances produced by EDAX software (EDAX, 2008; Mineral abbreviations: Appendix 1.1).

In order to extract a representative spectrum for a mineral grain, the grain size of the mineral must be larger than the x-ray beam size. The analysis should be taken at the centre of the grain away from any cracks or boundaries. This reduces noise in the spectrum and avoids any elements that might be included from surrounding minerals. Once a clean mineral spectrum has been collected the EDAX software can be used to calculate the 'quantification results'. From the elemental abundances provided by these results a mineral can be identified. Mineral identification software (e.g. Micronex MinIdent) was used to aid this process.

BSE Images

BSE images are produced through the detection of back scattered electrons within the SEM component of the MLA. The number of back scattered electrons emitted by a mineral in a given time period is directly proportional to the average atomic number of the mineral (Dou, 2002). As the electron beam scans the specimen surface, the intensities of back scattered electrons at different locations form a grey level image (Figure 3.12A). BSE images can be generated from any sample media with a polished and carbon coated surface.

XMOD: X-ray modal: Automated point counting

The XMOD method is an SEM-based point counting method. The MLA in XMOD mode takes an x-ray measurement at a user defined number of points on a given sample. The x-rays are collected in an evenly spaced grid. The white circles in Figure 3.12B each represent an x-ray spot. The x-ray spectrum is matched to spectrum in the mineral spectra library and an estimate of the modal mineralogy in that sample is then given. The XMOD analysis is useful as a measure of modal mineralogy and determining the gangue mineral characteristics.

XBSE analysis

The XBSE measurement collects a series of BSE images; an x-ray spectrum is taken from each region of the image with a different BSE brightness range (Fandrich et al., 2007). The x-ray spectrum is compared against the mineral spectra library and a classified mineral map of the sample is produced (Figure 3.12C). This method is applied to particulate samples. The process requires segmentation of the BSE map into brightness regions (objects). For intact rocks with significant abundance of silicate minerals the segmentation method in the present software version is inefficient. XBSE was not used for intact texture in the present project.

SPL-lite: Sparse Phase Liberation analysis

The SPL-lite technique is a specialized form of XBSE analysis in which only those minerals that are in a BSE brightness range selected by the user are analysed. The MLA identifies areas that have pixels in the user defined BSE brightness range and collects an x-ray spectrum from each mineral in that area and the immediate area surrounding that mineral (the size of this area is defined by the user). The collected x-rays are compared against the mineral spectra library and a classified mineral map is produced. Figure 3.12D illustrates a mineral map from an SPL-lite classification set to a BSE brightness of chalcopyrite and higher. The advantage of this setting is that all minerals that have a greater atomic mass (and hence a brighter BSE brightness level) than chalcopyrite are typically sulphides or valuable minerals such as gold, electrum and tellurides.

The SPL technique was primarily developed to classify particulate samples where the phase of interest is present at low levels (0.01 to 1.0%). By only classifying areas of the target mineral the MLA system is able to measure a greater number of grains in a given time period. Within this research, this technique was primarily used to analyse intact tiles of drill core rather than particulate samples. The textures of the valuable minerals are intact which allows these images to be used to extract information regarding texture prior to breakage.

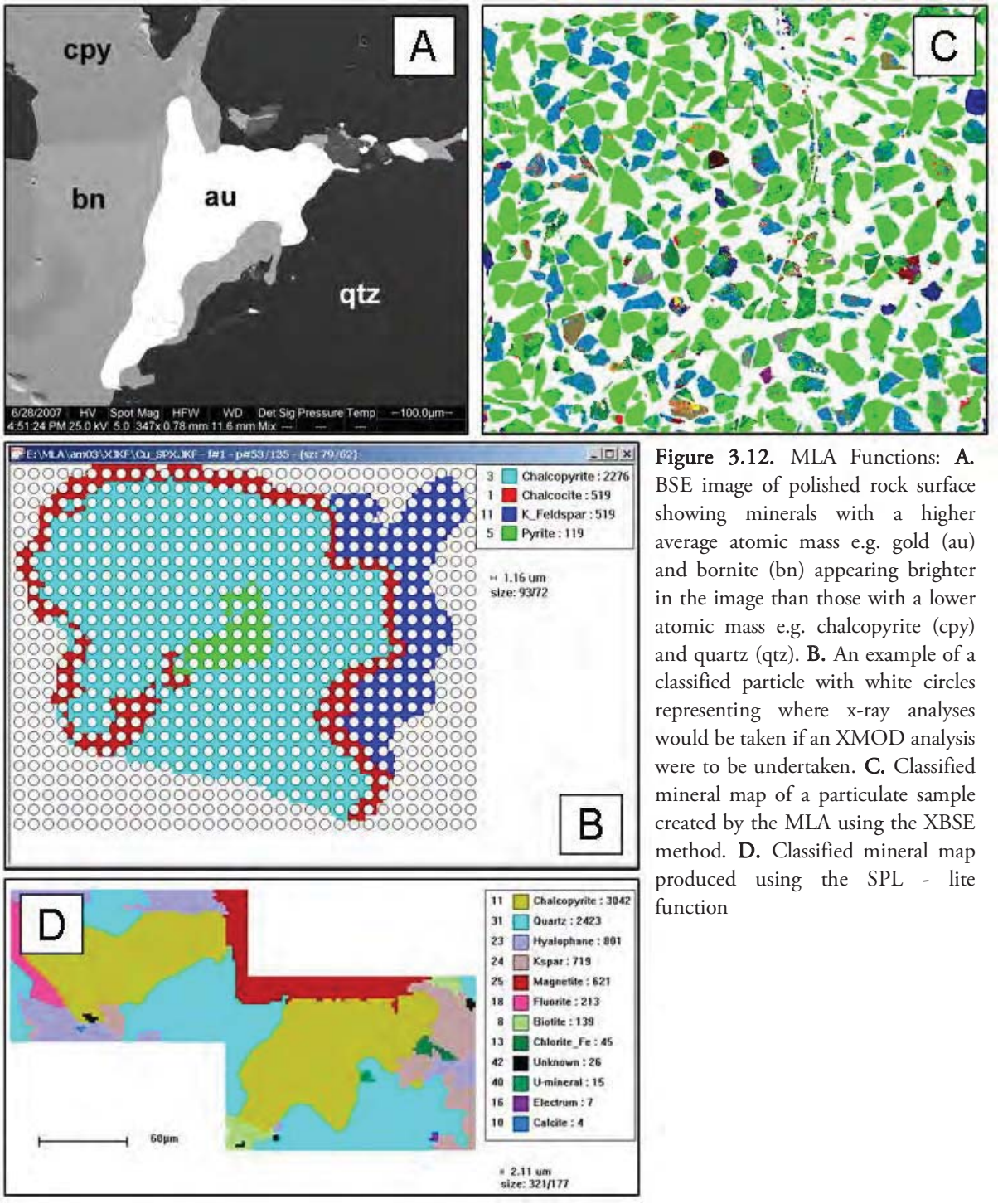

Figure 3.12. MLA Functions: **A.** BSE image of polished rock surface showing minerals with a higher average atomic mass e.g. gold (au) and bornite (bn) appearing brighter in the image than those with a lower atomic mass e.g. chalcopyrite (cpy) and quartz (qtz). **B.** An example of a classified particle with white circles representing where x-ray analyses would be taken if an XMOD analysis were to be undertaken. **C.** Classified mineral map of a particulate sample created by the MLA using the XBSE method. **D.** Classified mineral map produced using the SPL - lite function

3.5.2 Creating a mineral spectra library

A mineral spectra library is required for each ore deposit being analysed with the MLA. The mineral spectra library is required in order to undertake the classification step of the data processing, i.e. matching a spectrum obtained from an x-ray analysis to one stored in the mineral spectra library. The EDAX control software within the MLA is controlled by the user to identify and name the minerals that are present in a sample (Figure 3.13A). The MLA standards program is used to store the spectra that can be later used to classify samples from that ore deposit (Figure 3.13B).

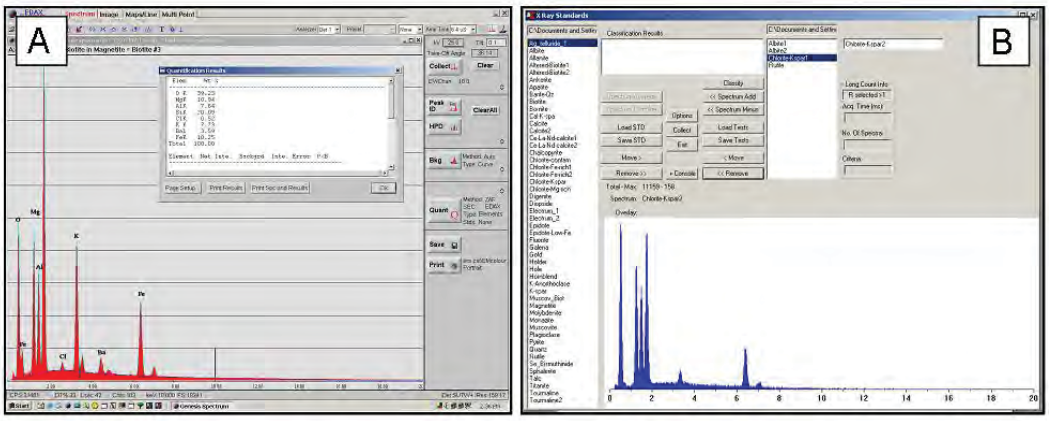

Figure 3.13.A. EDAX control software which is used to view and quantify spectra. **B.** Screen shot from the MLA standard program.

The creation of the mineral spectra library is an important step in the MLA's analytical procedure. The quality of the results obtained from an MLA analysis is only as good as the library that is used to classify them. There are a number of areas that need to be considered prior to and during the creation of the mineral spectra library. These are outlined in Table 3.6 and described in further detail in Appendix 3.4. Based on this information a method has been developed within this research that allows the MLA user to create a mineral spectra library that is representative of the samples that are being analysed. This method is described below and in further detail in Appendix 3.4.

Creating a representative mineral spectra library

The creation of the mineral spectra library by the MLA user should be considered the weakest link in this quantitative method. The MLA analysis itself is quantitative, it is however the interpretation of and the selection of mineral spectra that will be stored in the library that is prone to human error. Figure 3.15 illustrates the results of an XMOD analysis undertaken on the same sample but classified with mineral spectra libraries created by two different users (Table 3.5). The outcomes of this test indicate that the results can vary significantly if a spectrum is saved into the library that is not representative of the sample. Within this project a method has been developed that allows the MLA user to test if the minerals that have been saved into the mineral spectra library are in fact representative of their sample. The method is based on the results of the MLA XMOD analysis method and the manipulation of the spectral fitting algorithm found in the MLA data processing software 'Particle X'.

Table 3.5. Four mineral spectra measured from the same grain with variable amounts of Na-K-Al.

Element	Mineral Spectrum 1	Mineral Spectrum 2	Mineral Spectrum 3	Mineral Spectrum 4
O	50.27	50.43	50.64	52.00
Na	7.96	8.09	7.37	6.35
Al	10.67	10.44	10.82	11.35
Si	31.10	31.04	29.72	27.76
K	0.00	0.00	1.46	2.55

Table 3.6. A brief description of the areas that need to be consideration prior to and during the creation of the mineral spectra library.

	Description	Implications for MLA analysis	Recommendations
IONIC SUBSTITUTION	A solid solution series is the compositional range between end-member minerals that share the same basic formula that experience the substitution of elements in one or more atomic series (Klein et al, 1977) e.g. the plagioclase minerals albite ($NaAlSi_3O_8$) and anorthite ($CaAlSi_2O_8$) experience a complete shift between Na^+ in the albite and the Ca^{2+} in the anorthite. As Ca^{2+} increases, Na^+ decreases and the plagioclase accommodates this in the crystal structure by reducing the number of silicon atoms in its crystal lattice.	Minerals in solid solution series will exhibit similar mineral spectra with slight variations in elemental peak intensities. Problems arise when there are varying degrees of elemental abundances between two compositional end members. The spectrum can be measured accurately, however when it is compared to a spectrum in the mineral spectrum library it may be in the middle of two compositional end members and result in a misclassification. Table 3.7 shows variable elemental abundances for four mineral spectra that have been measured from the same grain.	The recommendations for ionic substitution and Alteration minerals are the same: **1.** During the classification process, the user can define how tightly a measured spectrum should match a spectrum from the mineral spectra library. It is recommended that the user select a fit of 1^{-30}. This number refers to a tightness of fit produced from a spectral fitting algorithm. This algorithm is proprietry, however it is understood that a tighter fit would produce a larger number i.e. 1^{-10} and a looser fit would produce a smaller number i.e. 1^{-90}. Reducing the tightness of fit would allow any variants of a spectrum to be classified incorrectly resulting in inaccurate results for minerals not part of a solid solution series, but consisting of the same elements e.g. chalcopyrite ($CuFeS_2$) and bornite (Cu_5FeS_4). **2.** Select mineral spectra that are similar to all variants of a solid solution series. It is suggested that the minimum number of spectra for one mineral are included in the library as possible. For example, if five types of albite are selected, and there is a chemical variation across one albite grain then classified image produced will be unusable. Figure 3.14B illustrates a classified image that has resulted from two mineral spectra in the same library being too similar. The MLA measures x-rays of minerals one frame at a time and then stitches them back together at the end in order to produce a complete image. If there is a compositional variation within a mineral phase, then giving the spectral matching software has too many options resulting in the same mineral being classified differently between frames. It is recommended that only end member compositions are used in the mineral spectra library. If classified images are still producing a high number of unknown areas, then a median composition between end members should be selected.
ALTERATION MINERALOGY	Alteration is defined as the change in the mineralogical or chemical composition of a rock caused by the circulation of solutions or fluids (e.g. Gifkins et al., 2005).	The problems encountered with alteration minerals are similar to those encountered with minerals that exist in a solid solution series. Alteration events often occur over extended periods of time where new minerals are formed and/ or existing ones start to change their composition towards being in equilibrium with their new surroundings. An example of this is shown in Figure 3.14A; Ti-rich biotite replaces biotite and later illite/muscovite destroys a pre-existing K-feldspar-quartz assemblage.	
FINE-GRAINED MINERALS	One of the limitations of this technique is reached when analysing fine-grained minerals. For the purpose of this research fine-grained minerals are minerals that are smaller than the width of the x-ray beam + 5 µm to allow for the beam spread. Typically these are grains approximately < 11-12 µm in diameter for a spot size of 6 to 7 units.	The problems that are encountered by the MLA include being unable to extract a clean mineral spectrum for storage in the mineral spectra library and the beam size exceeding grain size, causing measurements to be taken across boundaries. In additional if a sample contains fine-grained minerals that have a similar BSE range, then the MLA will have difficulty recognising that the minerals are different. This will result in the occurrence of false boundaries (Figure 3.14C) and the mineral spectrum will be measured from the centre of the false grain. This means that any mineral that falls within the false boundary will later be classified as whatever the measured spectrum in the centre is classified as. It may be a mixed spectrum, or the entire region will be incorrectly classified as one mineral.	Whilst there are no direct solutions for the problems caused by fine-grained minerals and ores, the following are recommended: **1.** While collecting the mineral spectrum for the mineral spectra library, the instrument magnification should be as high as possible while still being able to retain a sharp focus on the mineral (Figure 3.14D). **2.** For grains that are smaller than the beam size, if the mineral is of importance i.e. a valuable phase, then the user would need to assess whether using a smaller beam size would be a viable option given that this slows the processing time down significantly and thus increases the cost of analysis. **3.** For XMOD analyses there are always a small proportion of minerals that are unknown or invalid due to measurements being contaminated. In these cases the user can either reduce the 'tightness of fit' of the spectral fitting algorithm to incorporate more of the unknown minerals or manually classify any unknown spectra. The latter of these options is extremely time consuming.
SPECTRA LIBRARY	The construction of a representative library is iterative and ongoing. As new samples are classified with the MLA, minerals not yet in the mineral spectra library will appear as unknown minerals. These minerals can be manually checked by the user to determine if they are unknown minerals or mixed spectra.	If all the samples are not constantly re-classified as the library is updated then samples from earlier analysis cannot be compared to samples analysed with a later mineral spectra library.	Updating the mineral spectra library will reduce the number of unknown and misclassified minerals in a MLA analysis and improve the accuracy of the user's results.

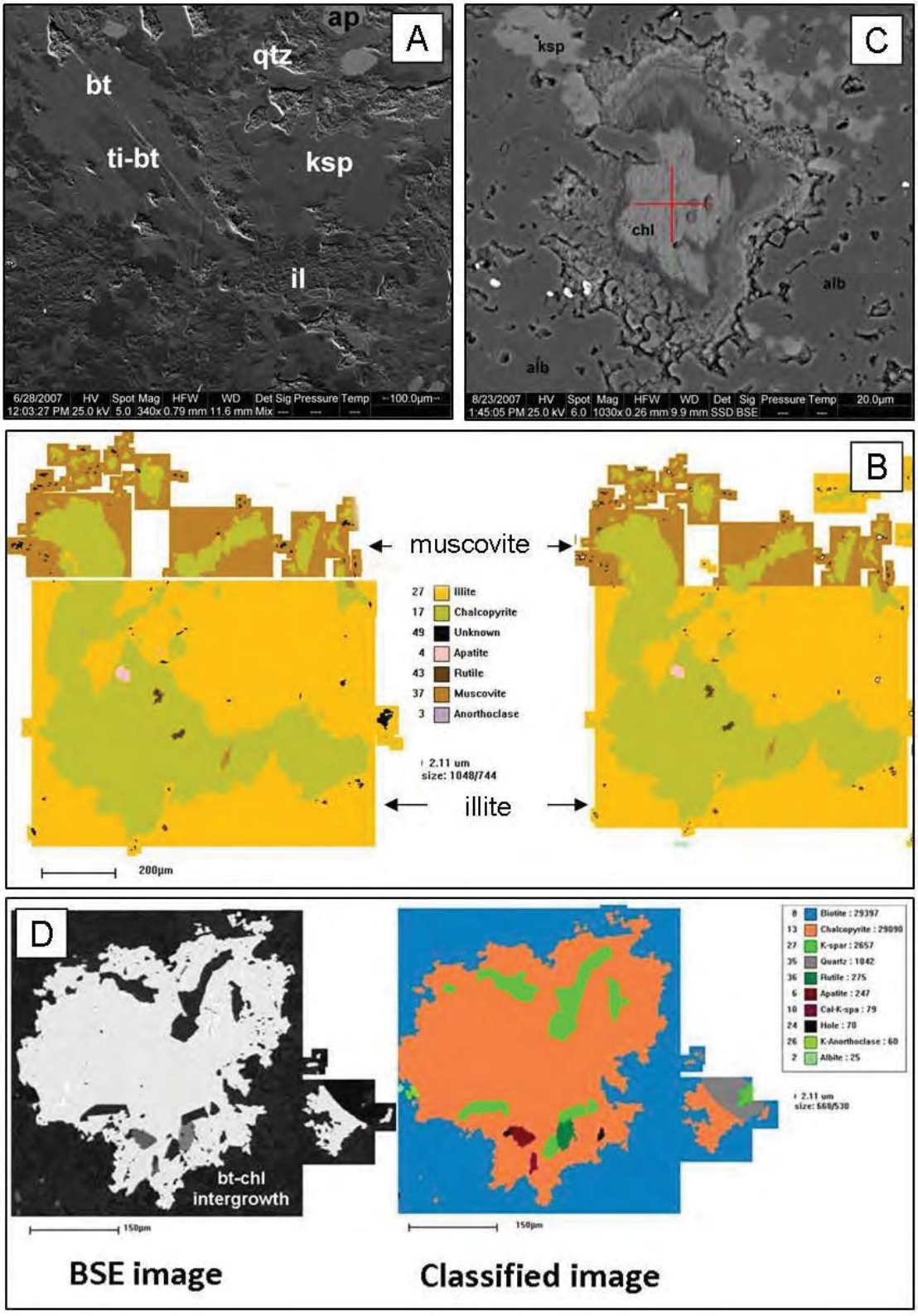

Figure 3.14A. BSE image showing alteration mineralogy. **Figure 3.14B** Classified mineral maps produced from the MLA in SPL-lite mode. The unstitched image (*left*) shows the same mineral being classified as muscovite and illite in different frames. This has resulted in the stitched image (*right*) being classified with incorrectly. **Figure 3.14C** BSE image of fine-grained chlorite with a flat surface at the centre of the grain suitable for x-ray measurement. The mineral can be seen to degrade at the grain boundaries. *Red Cross* is where x-ray is recommended to be taken. **Figure 3.14D.** BSE image (*left*) of chalcopyrite enclosed by biotite (bt) – chlorite (chl) intergrowth. The intergrowth (*right*) is only classified as biotite (*blue*). For mineral abbreviations refer to Appendix 1.1.

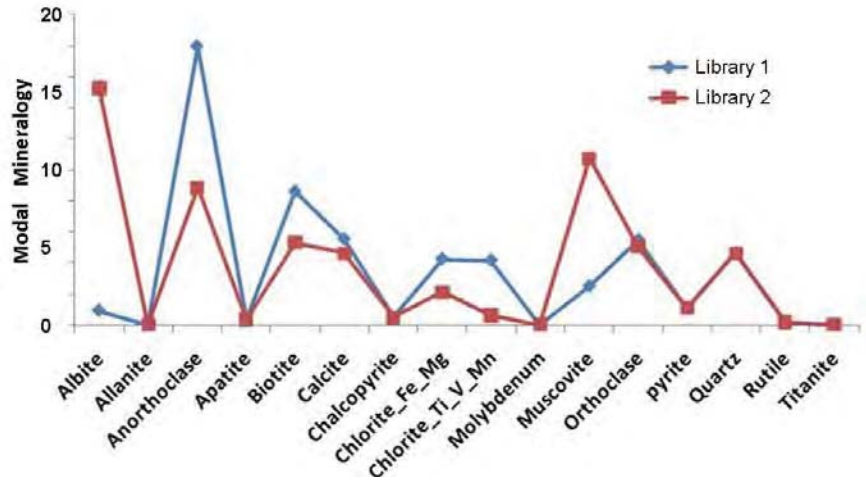

Figure 3.15. The modal mineralogy obtained using the MLA (in XMOD mode) for the same sample but two mineral spectra libraries that have been created by two different users.

Prior to the classification process 'Particle X' will allow the user to vary the tightness of fit of the spectral fitting algorithm. The recommended tightness of fit in the MLA user manual is 1^{-30} (MLA System User Operating Manual Module 3 – X-ray standard collection, 2005). In theory, if a mineral spectrum is representative of the mineral in the sample then the results returned from an XMOD analysis as the tightness of fit is weakened, will not change. For example, if an unrepresentative epidote spectrum is saved into the mineral spectra library during the classification procedure, only the epidote end members that are within the tightness of fit range will be classified as epidote, the remaining epidote will remain unclassified. If the tightness of fit is reduced and the sample is re-classified then some of the unclassified epidote grains will be then be classified as epidote. Therefore, for a truly representative mineral spectrum, the number of classified minerals should change very little before flattening out when the tightness of fit is reduced (Figure 3.16).

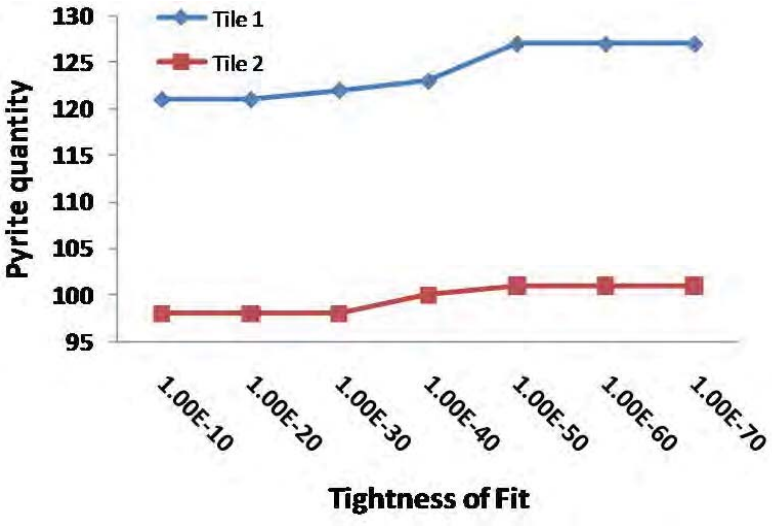

Figure 3.16. Changes in pyrite content of two samples from Cadia East at varying tightness of fit levels.

For minerals that are likely to contain variable trace elements (silicates, micas etc.) even within one sample, a representative mineral spectrum would increase slightly as the tightness of fit is reduced. If there is a significant increase in mineral abundance as the fit is decreased, then it may indicate that there is more than one end member of that mineral and two mineral spectra end members may be required. Figure 3.17A illustrates a sharp increase in epidote abundance as the tightness of fit is decreased. This is the result of an unrepresentative mineral spectrum. Figure 3.17B illustrates a slight increase in epidote abundance, the result of a representative mineral spectrum.

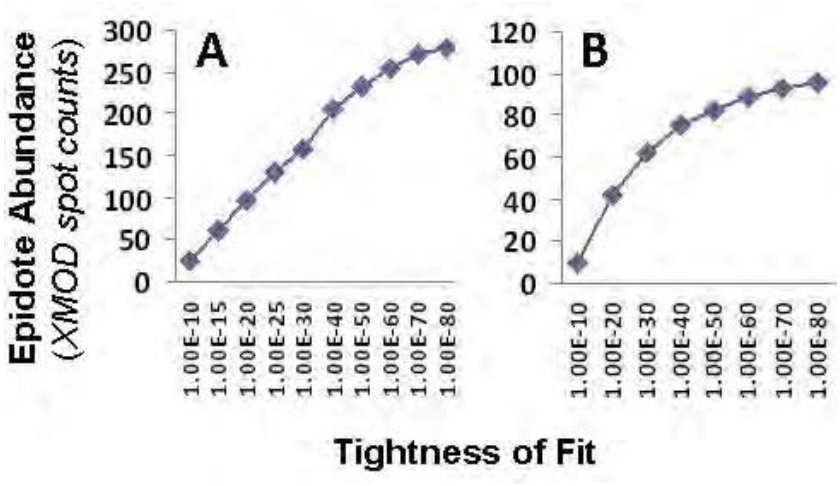

Figure 3.17A. Epidote abundance calculated from XMOD analysis at variable tightness of fit levels for an unrepresentative mineral spectrum **B**. Epidote abundance calculated from XMOD analysis at variable tightness of fit levels for a representative mineral spectrum.

All minerals in the Cadia East mineral spectra library have undergone testing using this method to ensure that they are representative of the samples being analysed.

XMOD analysis versus traditional point counting methods

One the advantages of an XMOD analysis is the grid approach which has been established to produce unbiased results. Previous authors have discussed the fundamental statistics that are required regarding a modal analysis by the means of point counting (e.g. Chayes, 1956; Moen, 2006). The number of points that are required for analysis and the associated error are dependent on the mineral abundance of the sample (Chayes, 1956; Hasofer, 1963). If the percentage of a mineral is known, then theoretically the error derived from the point counting method can be calculated based on the number of counts. This method for calculating error may have been suffice for Moen's work, which is primarily in the heavy minerals industry where samples are relatively homogeneous compared to distribution of minerals in complex ore systems (Solomon, 1963). Figure 3.18 illustrates the total number of points required for the acceptable error at specific mineral quantities. If the sample is completely homogeneous then the point count will represent the actual mineral abundance of the sample. However, consider a complex ore system where minerals can occur as aggregates, complex intergrowths and as fine disseminations all within the same sample. The mineral abundances calculated from such a sample are likely to be regularly over or underestimated. For example, Table 3.7 shows examples of chalcopyrite abundance calculated from both XMOD and SPL-lite methods for disseminated, clotted and vein chalcopyrite assemblages at Cadia East. The SPL-lite mineral percents have been calculated as a percent of the image area in order to be compared to the results of the XMOD analysis. The examples that are predominantly fine-grained disseminated chalcopyrite are underestimated in eight out of the 10 examples. Only one example produced the same mineral abundance for both techniques. Based on these results, the XMOD is considered most representative of the minerals in a sample that are not smaller than the step size between points or the beam diameter of the x-ray (see Appendix 3.5).

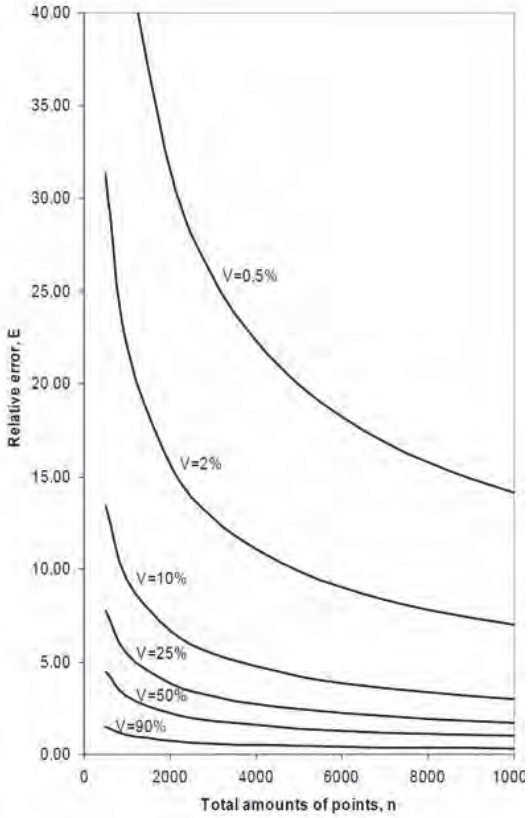

Figure 3.18. (*left*) (taken from Moen, 2006) illustrates the error associated with various numbers of points for samples of a given grade. This graph assumes a homogenous sample.

Table 3.7. Examples of the chalcopyrite abundances calculated by two MLA methods. The XMOD results are calculated using an x-ray point count of the sample in a grid approach. The SPL-lite method calculated the actual area of chalcopyrite in the sample image.

Disseminated (<6mm)			Clotted (>6mm)			Vein hosted		
Example	XMOD %	SPL-lite %	Example	XMOD %	SPL-lite %	Example	XMOD %	SPL-lite %
CE082 285	0.06	0.09	CE109 309	4.51	4.62	CE098 355	4.54	4.88
CE082 301	0.47	0.40	CE109 319	3.11	3.26	CE109 443	0.65	0.65
CE098 177	3.32	2.97	CE109 327	1.92	1.96	CE143 1121	2.74	2.78
CE098 233	2.79	3.02	CE109 337	3.43	3.42	CE143 1177	0.02	0.03
CE098 271	6.25	6.62	CE109 485	1.47	1.20	CE143 1227	0.85	0.76
CE109 219	0.67	0.70	CE110 271	2.41	2.46	CE143 1265	0.83	0.75
CE109 237	0.42	0.45	CE110 411	4.27	4.31	CE143 1357	3.68	3.72
CE110 281	0.32	0.38	CE110 441	15.35	15.18	CE143 1371	0.14	0.16
CE110 383	0.61	0.60	CE143 1165	1.61	1.36	CE143 1441	1.00	0.96
CE143 1233	0.18	0.15	CE143 1241	2.70	1.63	CE143 1465	0.43	0.02

3.5.3 Image collection and classification

The image and spectra collection is undertaken by the MLA and the classification process is undertaken by the 'MLA Particle X' software. This means that once the image and the spectra have been collected, the sample can classified repeatedly using different mineral spectra library without having to re-run the sample. The steps undertaken in a typical single analysis include:

1. Sample preparation: Drill core tiles and thin sections are polished and carbon coated.
2. MLA method selection: The methods are selected based on:
    - The types of minerals that are present i.e. common minerals such as bornite, chalcopyrite or rarer minerals such as gold or electrum.

- The quantity of the minerals in the sample i.e. how much of the total surface of the sample does the mineral cover.
- The time and cost of analysis.

3. MLA setup: The setup conditions used within this thesis were based on extensive test work undertaken by Dr. Maya Kamnetsky as part of the AMIRA P843. These tests are outlined in Appendix 3.5.
4. Create a representative spectral library for the deposit using the recommendations outlined in section 3.5.2.
5. MLA analysis is undertaken. The XMOD analysis produces a BSE image as well as a point count of the sample surface. The SPL-lite analysis produces a classified image of all minerals with a BSE range of 200 - 255 i.e. a BSE range above and including chalcopyrite.
6. Classification: During the classification procedure the set up conditions need to be specified. These include beam size, image resolution, run-time (if a limit is to be applied), voltage, collection time and brightness and contrast settings. The set up conditions for the XMOD and MLA analyses undertaken in this research are detailed in Appendix 3.6.
7. Post production: Once the images have been acquired from the MLA and the classification process has been completed the images are reduced and undergo a clean up process. This includes selecting only regions that contain the minerals of interest e.g. For Cadia East copper minerals, gold minerals and rare phases were selected. This reduces the file size as well as the time taken to extract mineralogical and textural data later using Definiens. An inspection of the image also includes identifying unclassified minerals.
8. End results: XMOD results are exported as .csv files and converted into modal abundances. SPL-lite images are exported as bitmaps and are now ready to be imported into Definiens where mineralogical and textural data can extracted.

3.5.4 Integrating MLA and Optical Microscopy

Within this research the MLA and optical microscope have been used for different purposes as well as to cross-checking results. The MLA has a higher resolution, is more accurate and more expensive than the classification of optical microscopy images. However, the optical microscope allows polymorphic minerals such as pyrite-marcasite as well as hematite and magnetite to be distinguished from one another visually. Before the results of these images can be compared or integrated, the sizes of the classified images from both of these techniques needs to be considered. The images that are produced using the optical microscopy system are restricted to an area of 2.28 × 1.52 cm. This means that in order to make a direct comparison between images of the resolution of the microscope and identification capabilities of the image analysis software with the MLA results. The MLA images which measure 3 × 3 cm will need to be cropped down to the same area as the optical images (Figure 3.19).

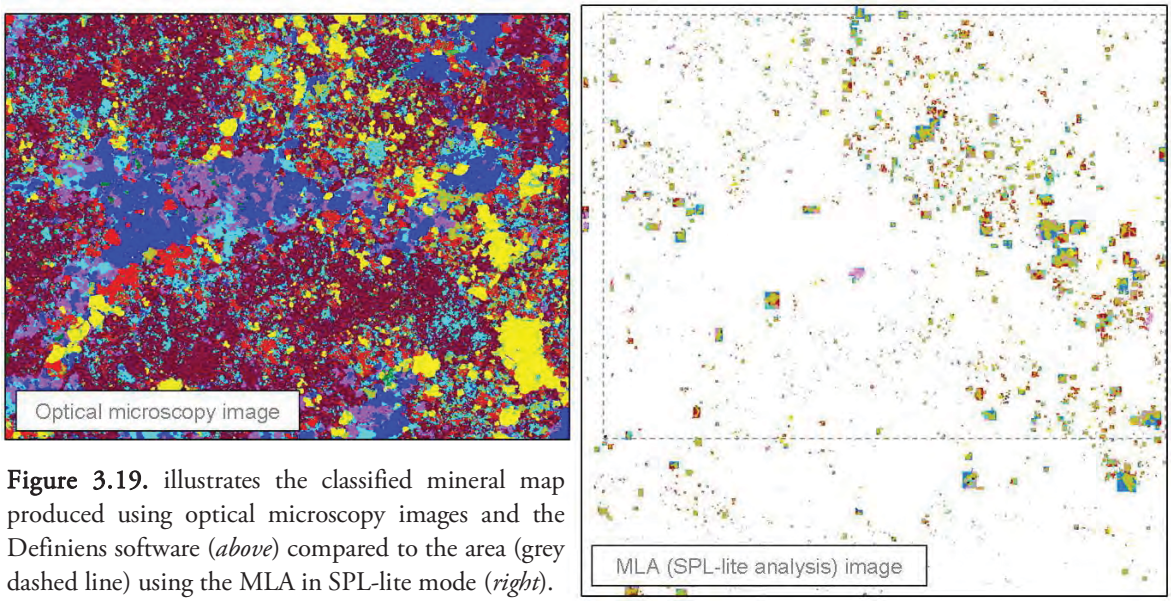

Figure 3.19. illustrates the classified mineral map produced using optical microscopy images and the Definiens software (*above*) compared to the area (grey dashed line) using the MLA in SPL-lite mode (*right*).

3.6 Extracting quantified mineralogy and texture from classified mineral maps

The extraction of mineralogical and textural attributes using object-oriented image analysis software has been described previously in Chapter 2, section 2.8.1. The use of Definiens allows a large range of attributes to be extracted for mineralogy and texture. A summary of these attributes are outlined in Appendix 3.6. Given the large number of samples and the number of different image sources that have been used in this research, it would unrealistic and out of the scope of this project to extract information about every attribute that can be extracted using Definiens. In this research only the mineralogical and textural attributes that are considered to be useful in determining differences in mineral processing behaviours have been analysed. These attributes are listed in Table 3.8.

Table 3.8. The mineralogical and textural attributes that have been used in this research.

Aspect of texture	Attributes that have been extracted
Modal Mineralogy	Percentage of minerals in each image/sample.
Mineral Associations	Percentage of minerals in a one, five and ten pixel rim of the valuable phases.
Size	Area, diameter, length, width, largest enclosed circle, smallest enclosing circle.
Shape	Shape Index, Roundness, Elliptical Fit.
Mineral Distribution	Distance to nearest phase.

It is clear that the analysis of mineralogy and texture through the use of classified mineral maps is a huge improvement on the traditional qualitative analyses that have previously been performed. However, it should be considered that through the production of classified mineral maps, in some cases the grain boundaries cannot be distinguished. Figure 3.20A shows a number of chalcopyrite grains with their grain boundaries touching. Figure 3.20B shows the classified image of this same area. Given that the classification of these grains is based purely on Back Scatter Electron (BSE) brightness and X-rays, the mineral grain boundaries are not distinguished rather the entire area of a group of grains is identified. Therefore for the remainder of this thesis the term 'PhReg' will be used instead of 'grain' or 'mineral' to indicate the statistics related to a contiguous region of a mineral and not to a grain in the strict sense.

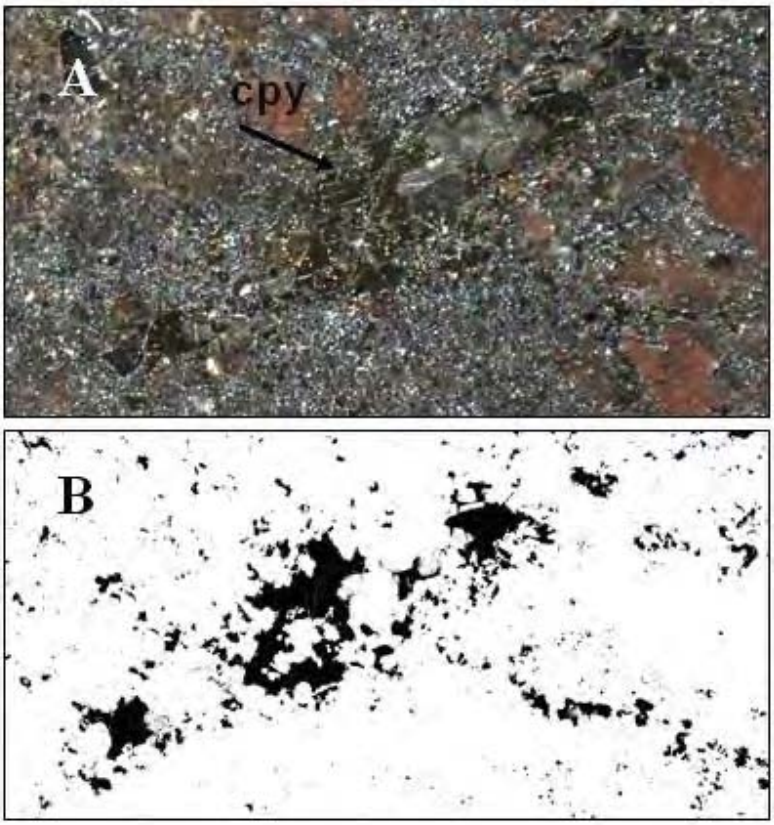

Figure 3.20. Unclassified (**A**) and classified (**B**) images of the same sample. The top image shows chalcopyrite grains with distinct grain boundaries, however when classified with a SEM-MLA system, the grain boundaries between adjacent chalcopyrite grains cannot be distinguished

3.7 Mineral abundances calculated from Assays

The modal mineralogy for several minerals can be calculated from the chemical assays that are routinely undertaken on-site. The number of minerals that can be calculated is dependent upon the elements that are routinely assayed for and the number of minerals present in the deposit that contain unique elements in their crystal lattice (i.e. no other minerals contain that element). This approach has been undertaken in this research for both Cadia East and Ernest Henry. The method for calculating mineral abundances from assay will be outlined in this section using a worked example from Cadia East (CE109: 442-444m).

3.7.1 Calculating mineral abundances from chemical assays: An example from Cadia East

The elements that are routinely assayed for at Cadia East are copper (Cu), Copper extracted from Cyanide leaching (CuCN), gold (Au), molybdenum (Mo), Lead (Pb), Zinc (Zn), Iron (Fe), and Sulphur (S). The minerals at Cadia East that can be attributed to these elements were determined by extensive SEM analysis and are outlined in Table 3.9.

Table 3.9. Common and rare minerals that contain can be attributes to elements assayed for at Cadia East.

Element	Common minerals	Rare minerals
Cu	Chalcopyrite, Bornite	Digenite, Tetrahedrite, Tennanite
CuCN	Bornite	Digenite, Tetrahedrite, Tennanite
Mo	Molybdenite	
Pb	Clausthalite	Galena
Zn		Sphalerite
S	Chalcopyrite, Bornite, Molybdenite, Pyrite	Digenite, Tetrahedrite, Tennanite, Galena, Sphalerite, Barite
Fe	Magnetite, K-feldspar, Albite, Biotite, Chlorite, Epidote, Pyrite, Chalcopyrite, Bornite	Digenite, Tetrahedrite, Tennanite

The assay results for CE109: 442-444m are:

Cu	5380 ppm	CuCN	284 ppm
Mo	909 ppm	S	8450 ppm
Fe	31000 ppm	Zn	41 ppm
Pb	1 ppm		

The first mineral abundances to be calculated are those that have one assayed element that does not overlap with another mineral. At Cadia East these are molybdenite, sphalerite and clausthalite (PbSe). Despite both clausthalite and galena occurring as minor inclusions in copper sulphides, SEM analysis indicates that galena is rare compared to clausthalite. For every mineral's abundance that is calculated, the other elements in each equation that are also present in the assay analysis need be adjusted accordingly. For example, based on the molecular weights of both molybdenum (Mo) and sulphur (S), for each 1ppm of Mo attributed to molybdenite (MoS_2), 0.67 ppm of S will be deducted from the total S assay. The mineral abundances for molybdenite, sphalerite and clausthalite were calculated using the following formula:

$$\text{Mineral Abundance} = \frac{\text{Element 1 (ppm)} + \text{Element 2 (ppm)} \times \left(\frac{\text{Molecular Weight of Element 2}}{\text{Molecular Weight of Element 1}} \right)}{10\,000}$$

For Cadia East where the majority of the copper mineralisation is contained in chalcopyrite and bornite, the CuCN concentration is used as an estimate for the bornite abundance. The CuCN leach will dissolve out a number of copper sulphide and copper oxide minerals, however, it does not leach out chalcopyrite. SEM and MLA analysis indicate that bornite mineralisation can occur in exsolution with digenite, however this is not common. For example, routine MLA-XMOD analysis of 23 samples that contained bornite, showed that digenite occurred in only four of these samples. Hence, the CuCN values can be used to determine bornite content.

To calculate the mineral abundance of chalcopyrite the total Cu assay value is adjusted by deducting the CuCN assay value. In cases where the CuCN value exceeds the total Cu assay, these results are considered inappropriate to use and were discounted. The estimated mineral abundances for CE109 442-444m are given in Table 3.10.

Table 3.10. Estimated mineral abundances calculated from elemental assay data at Cadia East. CE109 442-444 m. Mineral abbreviations as in Appendix 1.1.

Mineral	Assay Element	Assay ppm	Calculated Mineral elements (ppm)	Mineral Abundance (%)	Assay Balance						
					Cu	CuCN	S	Fe	Mo	Pb	Zn
Mo	Mo	909	**Mo** 909 **S** 607.5	0.15	5380	284	7842.5	31000	0	1	41
Sp	Zn	41	**Zn** 41 **S** 20.10	0.0061	5380	284	7822.4	31000	0	1	0
Chl	Pb	1	**Pb** 1 **Se** 0.38	0.00014	5380	284	7822.4	31000	0	0	0
Bn	CuCN	284	**Cu** 284 **Fe** 49.92 **S** 114.69	0.045	5096	0	7707.7	30980	0	0	0
Ccp	Cu	5096	**Cu** 5096 **Fe** 4479 **S** 5142	1.47	0	0	2566.0	26501	0	0	0
Py	S	2566	**S** 2566 **Fe** 2235	0.48	0	0	0	24266	0	0	0

The mineral abundances for chalcopyrite, bornite, pyrite, molybdenite, sphalerite and clausthalite have been calculated from assay data for CE082, CE098 and CE143 (Appendix 3.8). Any samples that were found to contain errors have been removed (CE082 298, 302 and 306).

3.7.2 Mineral abundances calculated from assay data: Ernest Henry

The mineralogy at Ernest Henry has been defined using detailed SEM (MLA) analysis. The dominant and rare mineral phases at Ernest Henry are displayed in Table 3.11. These will determine which minerals can be calculated from elemental assays at Ernest Henry. The elements that are assayed at Ernest Henry are Arsenic (As), Gold (Au), Cobalt (Co), Copper (Cu), Iron (Fe), Molybdenum (Mo), Nickel (Ni) and Sulphur (S). The mineral abundances that have been calculated are chalcopyrite, pentlandite, arsenopyrite and molybdenite (Appendix 3.9). If Barium (Ba) were also assayed then barite and pyrite abundances would also be able to be calculated.

Table 3.11. Dominant and Rare mineral phases for Ernest Henry

Element	Common minerals	Rare minerals
As		Arsenopyrite, sulpharsenite, cobaltite
Au		Electrum, gold
Co		Sulpharsenite, cobaltite
Cu	Chalcopyrite	Bornite
Fe	Magnetite, biotite, chlorite, pyrite, K-feldspar	Arsenopyrite, allanite, serpentine, sulpharsenite
Mo		Molybdenite
Ni		Pentlandite
S	Barite, pyrite, chalcopyrite	Arsenopyrite, sulpharsenite, sphalerite

3.8 Measuring for Mineral Processing attributes

The results of large and small scale physical tests undertaken at the Julius Krütschnitt Minerals Resource Centre (JKMRC) at the University of Queensland on the same drill-core are briefly described in Table 3.12 and Appendix 3.7, 3.8 and 3.9.

Table 3.12. Summary of the physical tests that have been used for comparisons with mineralogical and textural data within this research. Further detail regarding these methods can be found in Appendices 3.8, 3.9 and 3.10.

Physical Test	Units	Scale	Description
EQUOtip	Ls (Leeb hardness unit)	Small	The EQUOtip is a portable electronically controlled velocity rebound tester (Verwaal and Mulder, 1993). It is a non destructive method for observing changes in rock hardness down hole (See Appendix 3.7).
JK Comminution Index (JKCI)	No units	Small	The JKCI uses an algorithm that involves examining breakage distributions size by size and examining the fines generated (See Appendix 3.8)
JK Rapid Breakage Tester (JKRBT)	kWh/t (as well as the a*b parameters used by JKMRC)	Small	Developed at the JKMRC as part of the AMIRA P9N research the JKRBT tests particles across a wide range of sizes using precise energy inputs (See Appendix 3.9).
Point Load Test	MPa and compressive strength	Small	A geomechanical test used to measure rock fragmentation strength (Broch and Franklin, 1972). The PLT measures the Point Load Strength (Is) of the rock sample.
Drop Weight Test	kWh/t	Large	Developed at JKMRC, the DWT is combined with a data reduction technique determines the relationship between the specific energy input and resultant product size (Napier-Munn et al., 1996).

3.9 Summary

Described in this chapter are the methods, technologies and associated protocols that have been used within this thesis. The typical procedures have been described for the meso-scale visual drill-core logging; the creation of meso-scale mineral maps using the GEOTEK Multi-Sensor Core-Logger (MSCL); the creation of mineral maps using images created using automated microscopy; and the classification and creation of mineral maps using the Mineral Liberation Analyser (MLA). Also listed in this section are the large and small scale physical tests that the results from this thesis will be compared to.

Chapter Four

Mineralogy and texture: Meso-scale

4.1 Introduction

Presented in this chapter are the results of visual and machine-based logging (high resolution digital images) of mineralogical and textural attributes in drill-core for the Cadia East and Ernest Henry mineral deposits. The results are presented as follows:

- 4.2. Results of visual logging of drill-core: Cadia East
- 4.3. Results of visual logging of drill-core: Ernest Henry
- 4.4. Results of machine-based logging: Ernest Henry
- 4.5. Interpretations of meso-scale mineralogy and texture from Cadia East
- 4.6. Interpretations of meso-scale mineralogy and texture from Ernest Henry
- 4.7. Comparison of meso-scale techniques

The methods of both meso-scale logging techniques are described in Chapter 3, sections 3.2 and 3.3. Results of the visual logging of drill-core have been used to create textural classes that are predicted to have unique mineral processing properties. These classes have potentially been compared to both qualitative and quantitative data, which include chemical assays, mineral assays (see method in Chapter 3, section 3.7), on-site geology logs and the results of machine based logging (Ernest Henry only, section 4.6: this chapter).

The quantified mineralogical and textural data obtained from the machine-based logging of drill-core have been used to examine changes in the modal mineralogy, grain size and mineral associations of the valuable minerals for six drill-holes from Ernest Henry. These data were used to observe changes that could be related to liberation potential, grinding and flotation behaviours of an ore. This may result in a more informed selection of samples for metallurgical testing as well as the integration of knowledge between geologists and metallurgists working on site.

4.2 Results of visual logging of drill-core: Cadia East

Based on the method described in Chapter 3, Section 3.2, mineralogical and textural attributes that are considered to potentially influence mineral processing behaviours have been logged for three drill-holes at Cadia East (CE082, CE098, CE143; Figure 4.1). The three holes were selected for textural logging in order to represent a wide range of minerals and textures present in Cadia East. The mineralogical and textural attributes selected to be logged are described in Table 4.1. Each attribute and its variants have been measured as a percentage (unless otherwise stated) of each two metre interval that coincides with the Cadia East assay and geology logging intervals. This allows the results of the visual logging to be compared against other qualitative and quantitative measures that have been produced by site.

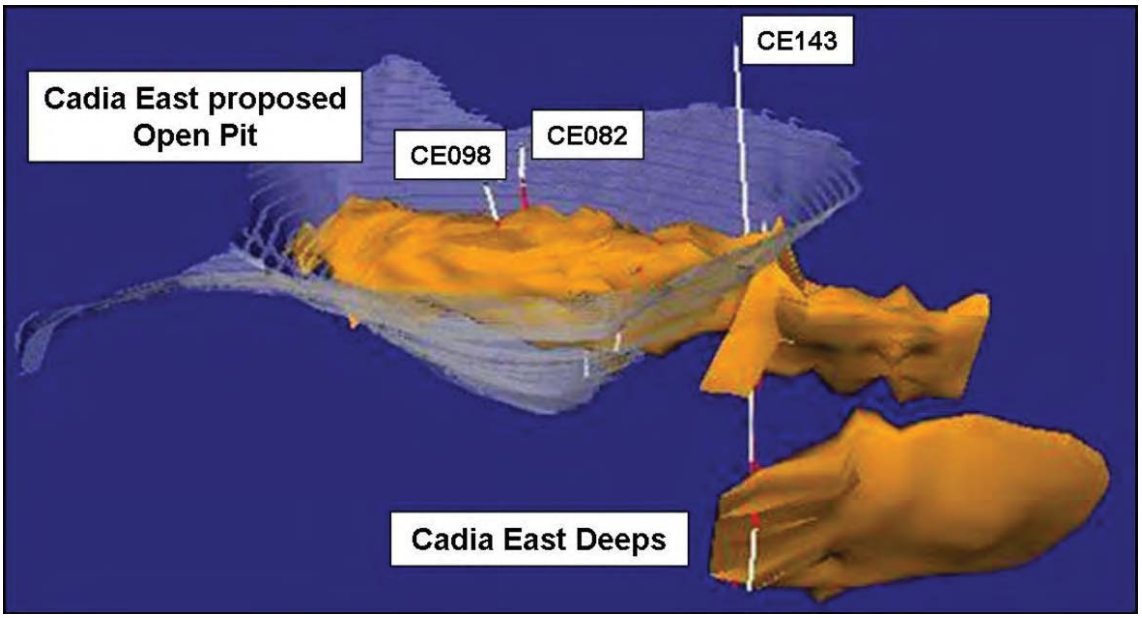

Figure 4.1. Copper grade shell (*yellow*) for Cadia East illustrating the location of the drill-holes that have undergone visual logging of drill-core attributes. *Image from Newcrest Ltd.*

The results obtained during the logging of attributes related to the valuable mineral phases only (chalcopyrite and bornite) are presented in section 4.2.1. This is followed by the logging of attributes related to gangue mineralogy and their textures in section 4.2.2.

All mineral abbreviations used in this chapter are defined in Appendix 1.1.

Microsoft Excel spreadsheets containing the detailed textural logging data for CE082, CE098 and CE143 are in Appendix 4.1.

Table 4.1. List of mineralogical and textural attributes that have been selected for drill-core logging at Cadia East. The attributes were chosen based on their predicted potential impact on mineral processing behaviours.

Attribute	Variant	Description
1. Valuable minerals present	Chalcopyrite	The dominant valuable minerals that are present.
	Bornite	
2. Distribution of valuable minerals	Fine-grained disseminations	Disseminated chalcopyrite or bornite with an approximate diameter <6mm (Figure 4.2A).
	Coarse-grained aggregates	Aggregates of chalcopyrite or bornite with an approximate diameter >6mm (Figure 4.2B).
	Vein-hosted	Chalcopyrite or bornite hosted in veins, typically of quartz-calcite composition (Type B see Chapter one, section 1.4.1; Figure 4.2C).
3. Deportment of non-vein sulphide species	Mafic minerals	Fine to coarse-grained disseminated chalcopyrite or bornite associated with mafic minerals, typically chlorite, biotite, magnetite or epidote (Figure 4.2D).
	Felsic minerals	Fine to coarse-grained disseminated chalcopyrite or bornite associated with felsic minerals, typically albite, K-feldspar, quartz, sericite or calcite (Figure 4.2E).
	Mafic layers	Fine-grained disseminations of chalcopyrite or bornite within the mafic layers of the volcanoclastic sandstone unit (Figure 4.2F).
4. Valuable mineral species only hosted by veins	Chalcopyrite	Chalcopyrite and/or bornite hosted within veins, typically occurring with quartz ± calcite ± epidote.
	Bornite	
5. Non-vein valuable mineral species	Chalcopyrite	The percentage of the total copper sulphides (chalcopyrite plus bornite) that chalcopyrite comprises of the interval.
	Bornite	The percentage of the total copper sulphides (chalcopyrite plus bornite) that bornite comprises of the interval.
6. Dominant gangue mineral types	Albite ± K-feldspar ± quartz	Albite ± K-feldspar ± quartz occur as pervasive gangue alteration. Each mineral can occur by itself or together (Figure 4.2G).
	Chlorite-biotite	Biotite and chlorite occur as fine-grained intergrowths in matrix material and also form rounded clots with chalcopyrite (Figure 4.2H and Figure 4.2D respectively).
	Chlorite-magnetite ± biotite	Chlorite and magnetite occur together as rounded clots and as matrix minerals in volcanoclastic breccia units (Figure 4.2I).
	Albite ± K-feldspar ± quartz clots/clasts in a matrix of chlorite-biotite	Clasts of Albite ± K-feldspar ± quartz in a matrix of chlorite-biotite (Figure 4.2J).
7. Vein minerals (*measured as present or absent*)	Fluorite 1	Fluorite 1 occurs in minor quantities in veins with quartz-calcite ± chalcopyrite ± bornite ± molybdenite ± pyrite (Figure 4.3A).
	Fluorite 2	Fluorite 2 occurs in clots with calcite that cross-cut earlier mineralisation and textures (Figure 4.3B).
	Molybdenite	Molybdenite occurs in minor quantities in veins with quartz-calcite ± chalcopyrite ± bornite ± molybdenite ± pyrite (Figure 4.3C).
8. Pyrite: Chalcopyrite ratio	N/A	The ratio of chalcopyrite and pyrite in the measured interval. Primarily, this measure was undertaken visually. However, later developments in mineral assays allowed this to be undertaken more accurately (see Section 4.6). Examples of varying pyrite: chalcopyrite ratios are shown in Figures 4.3 D,E and F.

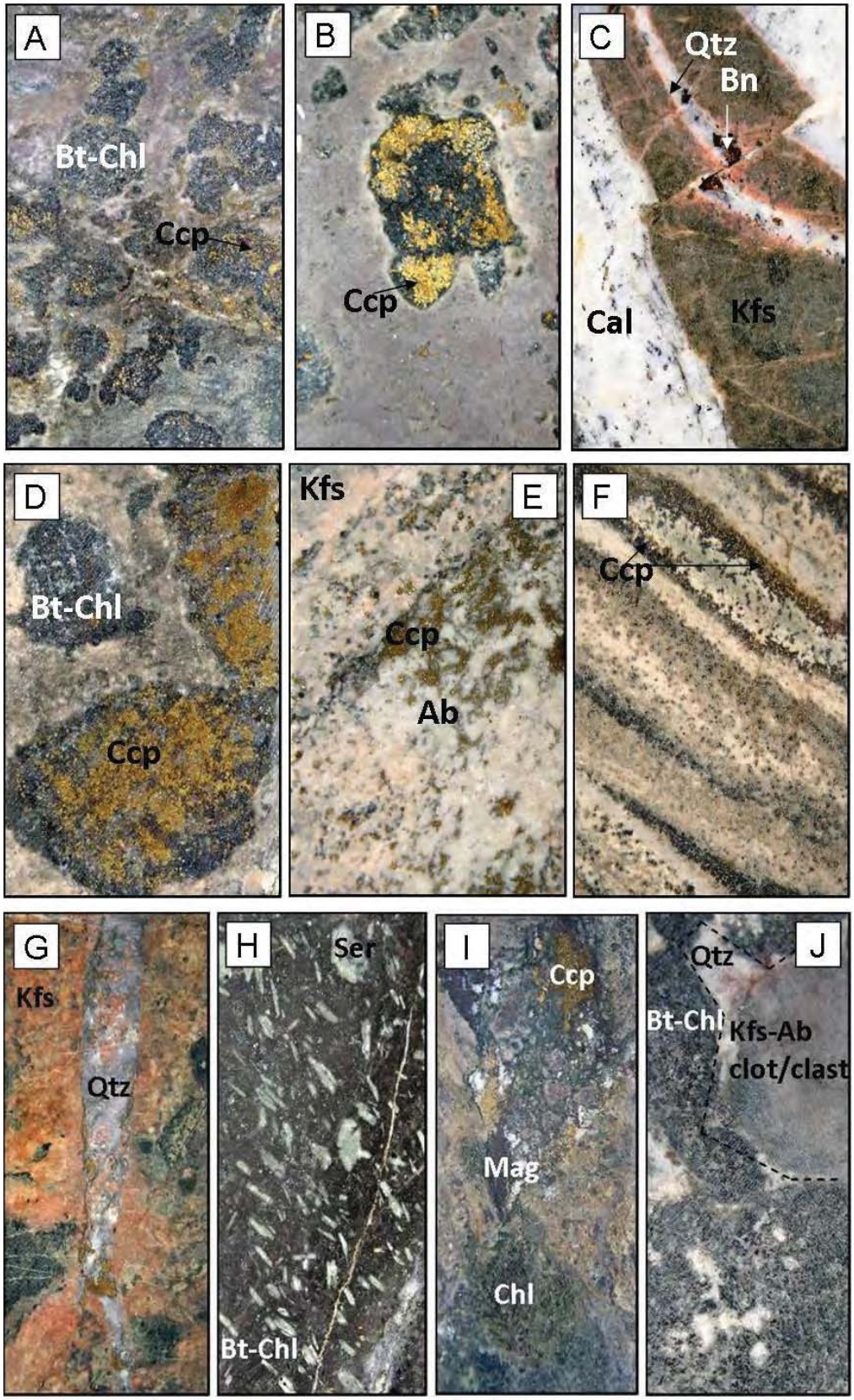

Figure 4.2. Examples of visually logged drill-core attributes for Cadia East. All images are the width of NQ core (5.5 cm) **A.** Fine-grained disseminated chalcopyrite in chlorite-biotite clots **B.** Coarse-grained aggregates of chalcopyrite in a rounded clot of chlorite-biotite **C.** Vein-hosted bornite **D.** Chalcopyrite with a chlorite and biotite mineral association **E.** Chalcopyrite with an albite and K-feldspar mineral association **F.** Chalcopyrite hosted in mafic layers of a volcanoclastic sandstone **G.** Albite ± K-feldspar ± quartz gangue **H.** Biotite and chlorite gangue **I.** Magnetite-chlorite gangue **J.** Albite ± K-feldspar ± quartz clots/clasts in a matrix of chlorite and biotite. *For mineral abbreviations refer to Appendix 1.1.*

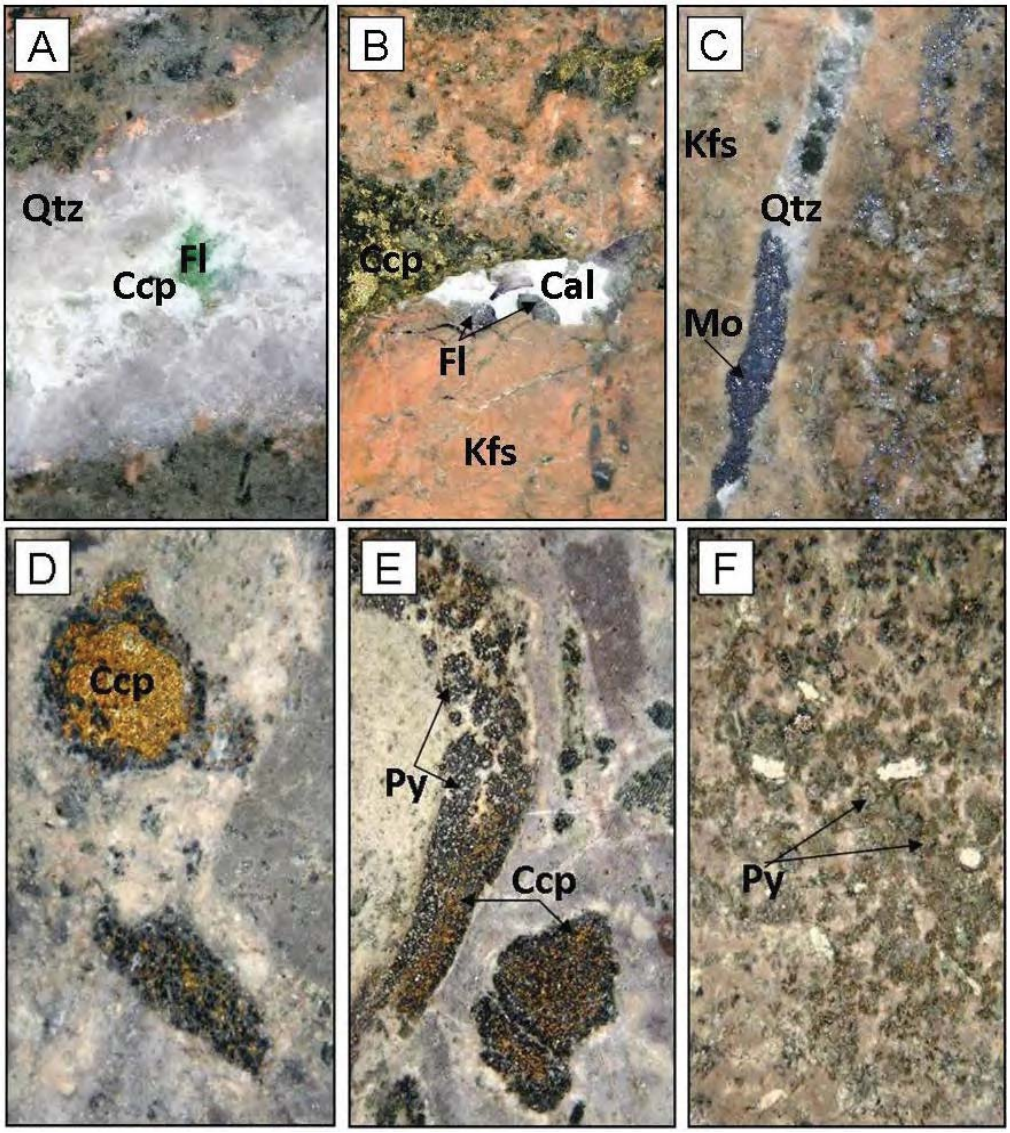

Figure 4.3. Examples of visually logged drill-core attributes for Cadia East. All images are the width of NQ core (5.5 cm) **A.** Fluorite 1 **B.** Fluorite 2 **C.** Molybdenite **D.** 100:1 chalcopyrite: pyrite ratio **E.** 60:40 chalcopyrite: pyrite ratio **F.** 0:100 chalcopyrite: pyrite ratio. *For mineral abbreviations refer to Appendix 1.1.*

4.2.1 Valuable mineral phases and textures

The valuable minerals at Cadia East that can be identified at the meso-scale are chalcopyrite and bornite. Presented in this section are the results for the visual logging of drill-core attributes related to these mineral phases only. The logged attributes include numbers one to five outlined in Table 4.1.

Variability in the distribution (location) of the copper-sulphide minerals is predicted to correspond with a variation in the grain size and the minerals that they are associated with. For example, Cu-sulphide minerals that are hosted in veins are typically observed to have a coarser grain-size than those that occur as fine-grained disseminations. Figure 4.4 illustrates the changes in the distribution of copper-sulphide minerals down-hole for CE082, CE098 and CE143. In all three drill-holes the proportion of coarse-grained aggregates increases with depth before becoming dominated by vein-hosted mineralisation. For drill-hole CE082, fine-grained disseminations are the most dominant between 116 and 176 metres depth. This is followed by an increase in the

abundance of coarse-grained aggregates of Cu-sulphide minerals to 218 metres where the remainder of the drill-hole is dominated by vein-hosted Cu-sulphide minerals increases until 308 metres. Drill-hole CE098 progressively decreases in fine-grained disseminations and increases in coarse-grained aggregates between 142 and 246 metres. This is followed by an increase in vein hosted Cu-sulphides up to 346 metres depth where this becomes the dominant distribution style until 390 metres. For CE143, the Cu-sulphide minerals are predominantly vein hosted with localised areas of fine-grained disseminations and coarse-grained aggregates between 1108 and 1212 metres depth as well as 1218 and 1288 metres depth.

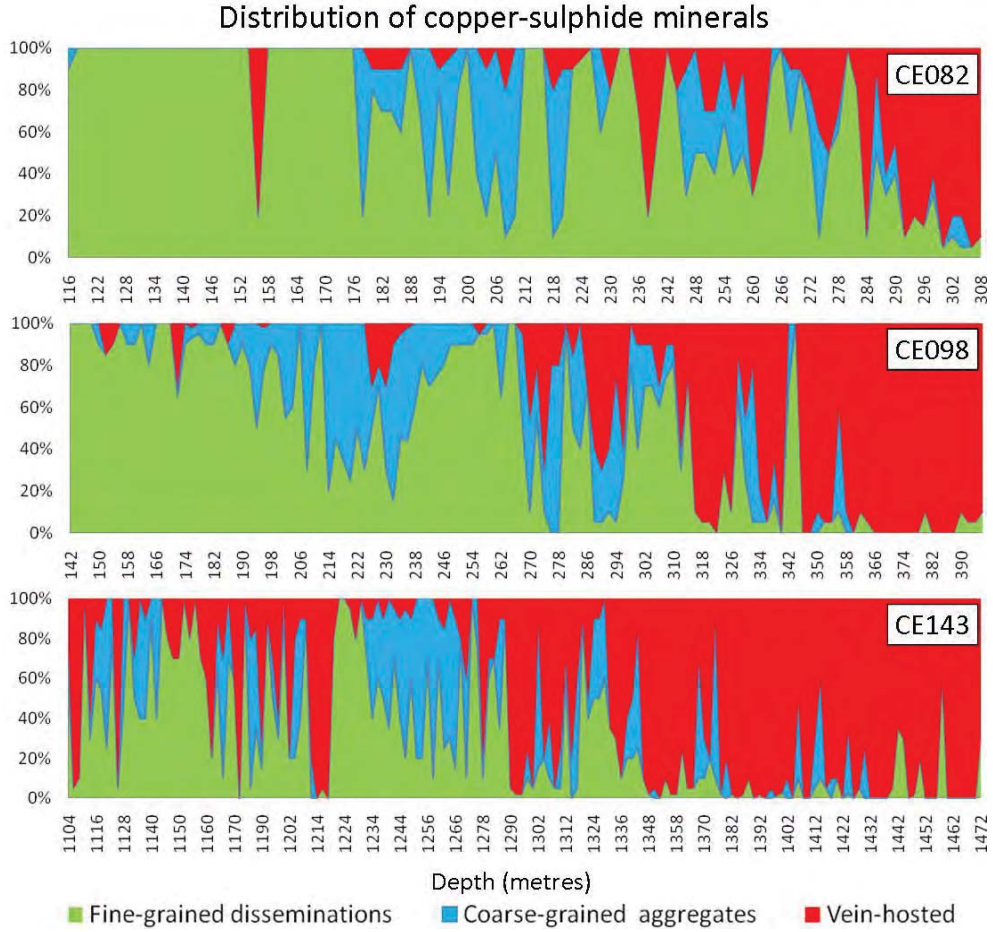

Figure 4.4. Down-hole plots illustrating the changes in the distribution of copper-sulphide minerals (chalcopyrite and bornite) for drill-holes CE082, CE098 and CE143. Examples of these attributes are illustrated in Figure 4.2A, B and C.

The copper-sulphide minerals that are hosted within veins typically exhibit similar gangue mineral associations (i.e. quartz-calcite ± epidote ± pyrite) throughout the Cadia East deposit. The fine-grained disseminations and the coarse-grained aggregates however occur in direct contact with both mafic and felsic minerals (see Table 4.1; Figure 4.2D and Figure 4.2E). These changes are illustrated in down-hole plots in Figure 4.5. These plots show that there is a strong preferential association with mafic minerals compared to the felsic minerals for the fine-grained disseminations and coarse-grained aggregates. In addition to this the proportions of chalcopyrite and bornite (as fine-grained disseminations or coarse-grained aggregates) have also been logged and are shown in Figure 4.6.

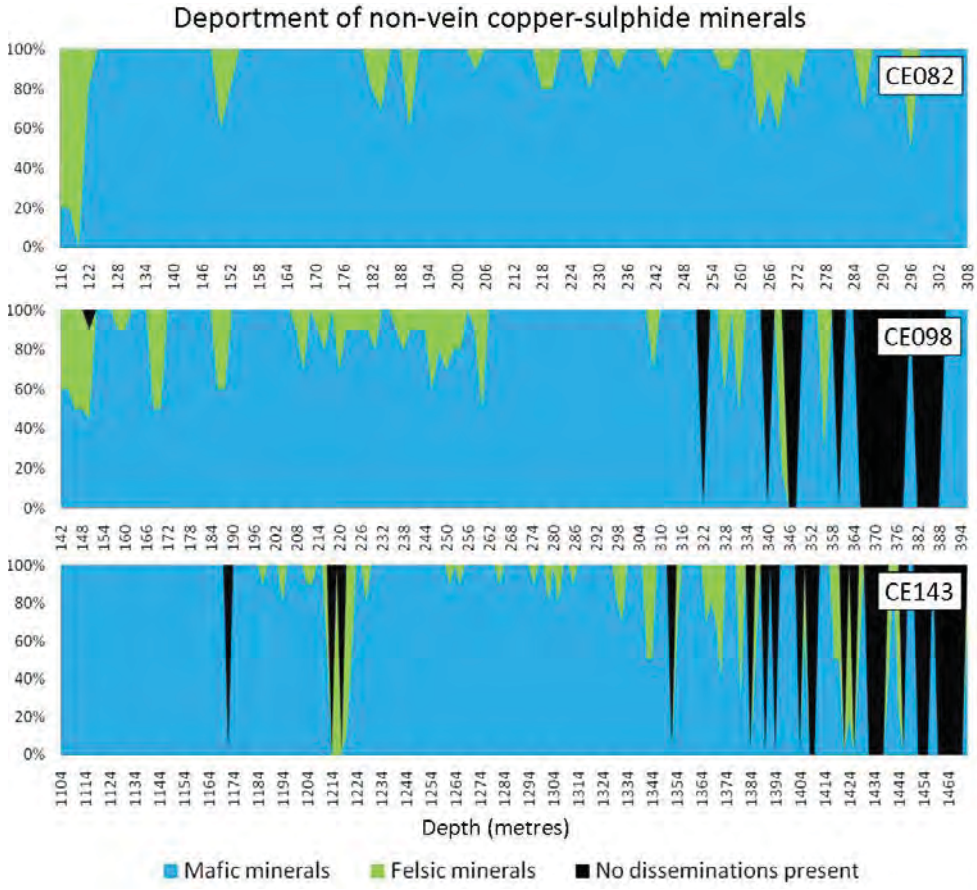

Figure 4.5. Down-hole plots illustrating the changes in the gangue minerals associated with copper-sulphide minerals for the fine-grained disseminated and coarse-grained aggregates in drill-holes CE082, CE098 and CE143.

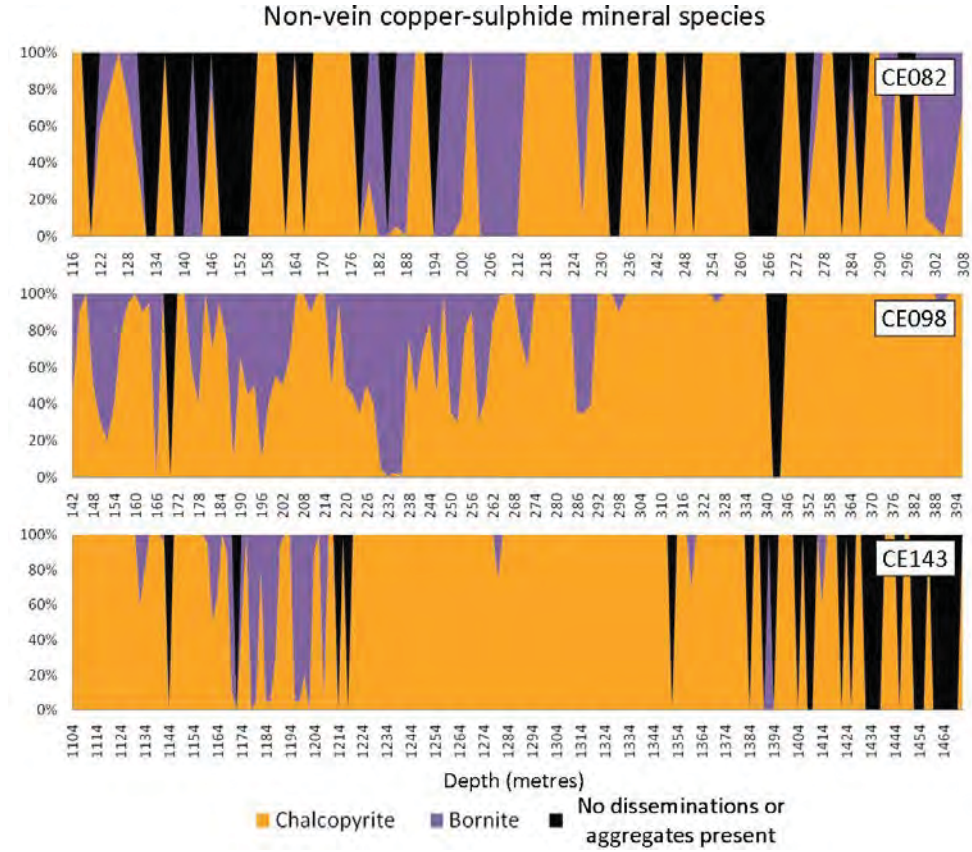

Figure 4.6. Down-hole plots illustrating the changes in copper-sulphide mineral species for the fine-grained disseminated and coarse-grained aggregates in drill-holes CE082, CE098 and CE143. Intervals where there are no disseminations or aggregates present indicate that the Cu-sulphide minerals are hosted by veins only.

Figure 4.7 shows the down-hole changes of the copper-sulphide mineral species hosted within mineralized veins. It is clear that for CE082 and CE098 chalcopyrite is the dominant vein-hosted valuable mineral, with bornite becoming more abundant between 1164 and 1200m and 1284 and 1400m in CE143.

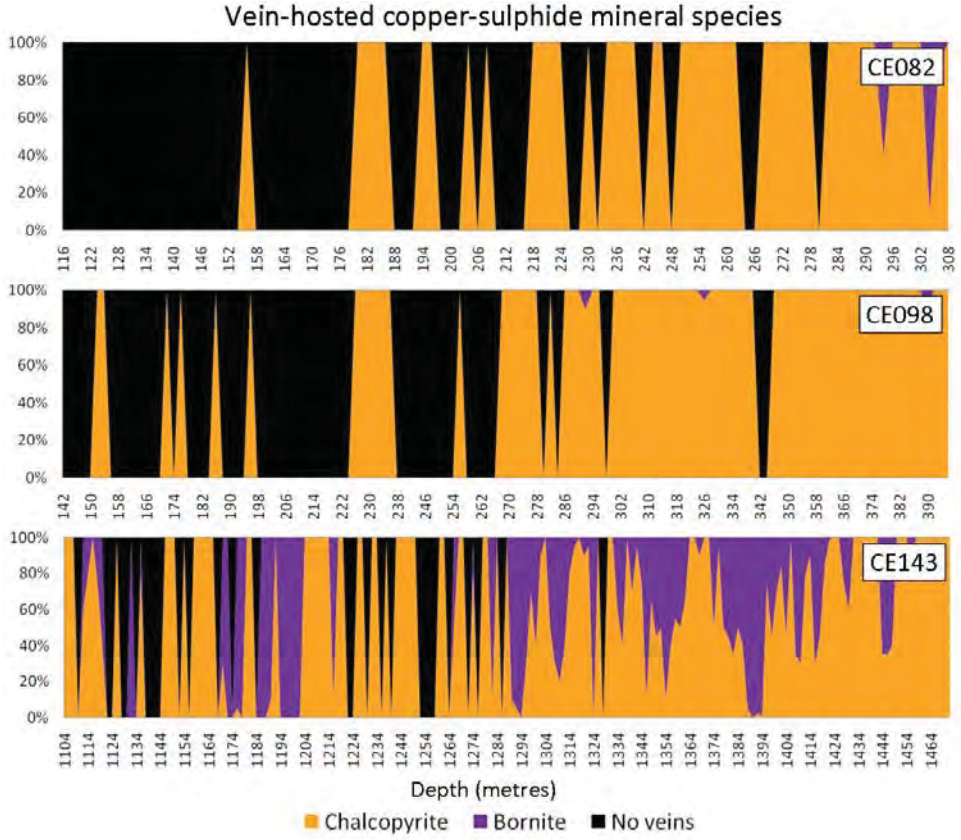

Figure 4.7. Down-hole plots illustrating the changes in copper-sulphide mineral species for the vein-hosted mineralisation in drill-holes CE082, CE098 and CE143.

4.2.2 Gangue mineral phases and textures

Presented in this section are the results for the logging of rock characteristics and gangue minerals in drill-core. The logged attributes include numbers six to eight in Table 4.1.

At Cadia East, the dominant gangue minerals were observed and grouped based not only on the minerals that commonly occur together, but also as minerals that can be assumed to have similar processing behaviours i.e. the similar hardness. The changes observed in gangue mineralogy are predicted to reflect the ease with which a rock is likely to crush and grind. For example, it can be assumed that rocks with an increased content of chlorite-biotite will be softer to crush than those that have a high albite, K-feldspar or quartz content. It can also be expected that areas with clots or clasts of albite, K-feldspar or quartz with a biotite-chlorite matrix will be easy to crush initially but harder to grind.

Figure 4.8 shows the down-hole distribution of gangue mineral groups estimated during visual logging (see Table 4.1). Drill-hole CE082 is dominated by albite-K-feldspar-quartz clasts with a chlorite and biotite matrix up to 170 metres depth before becoming dominant in chlorite-magnetite. A similar chlorite-magnetite signature is observed in the deeper portions of drill-hole CE098, however this section (after 286 metres depth) exhibits a higher proportion of chlorite-biotite minerals. Drill-hole CE143 contains more competent minerals, i.e. high proportions of albite-k-feldspar and quartz minerals intercalated with sections of chlorite-biotite and chlorite-magnetite.

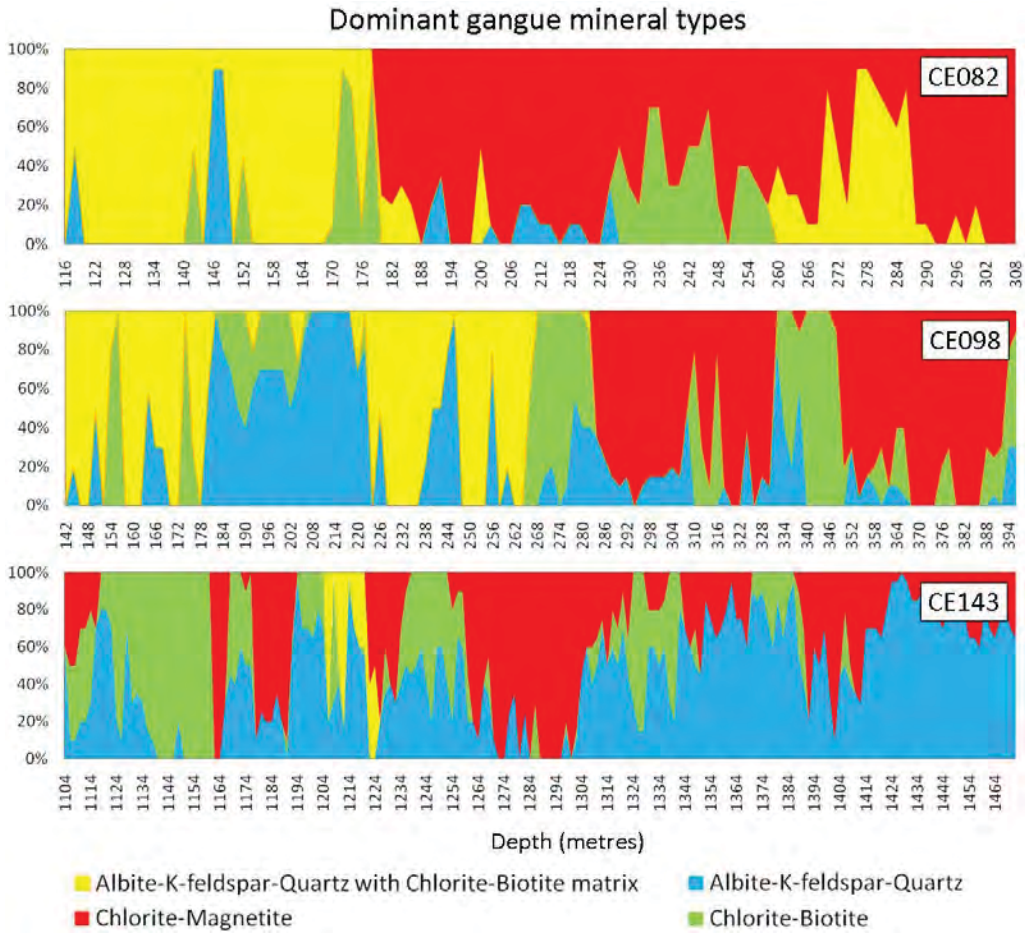

Figure 4.8. Down holes plots illustrating the changes in the visual estimates of the percentage of gangue mineralogy for the drill holes CE082, CE098 and CE143.

The pyrite to chalcopyrite ratio is an important attribute when considering the acid producing potential of ore (Johnson and Hallberg, 2005). Despite a rock being of a minable grade for copper or gold, if there is a large quantity of pyrite in an ore it may not be economical to mine because it can potentially cause problems for liberation, flotation chemistry and/or copper concentrate quality and if not managed properly, environmental problems (e.g. Petruk, 2005). Figure 4.9 illustrates the down-hole proportions of chalcopyrite and pyrite. For CE082 and CE098 there is a high proportion of pyrite compared to chalcopyrite in the upper portions of these drill-holes.

During the logging of drill-core from Cadia East, minerals that have the potential to be deleterious were recognised and documented every time they occurred. These minerals include two generations of fluorite, one that occurs in veins with chalcopyrite and bornite (Fluorite 1) and another that occurs with calcite as clots that cross-cut earlier mineralisation and textures (Fluorite 2).

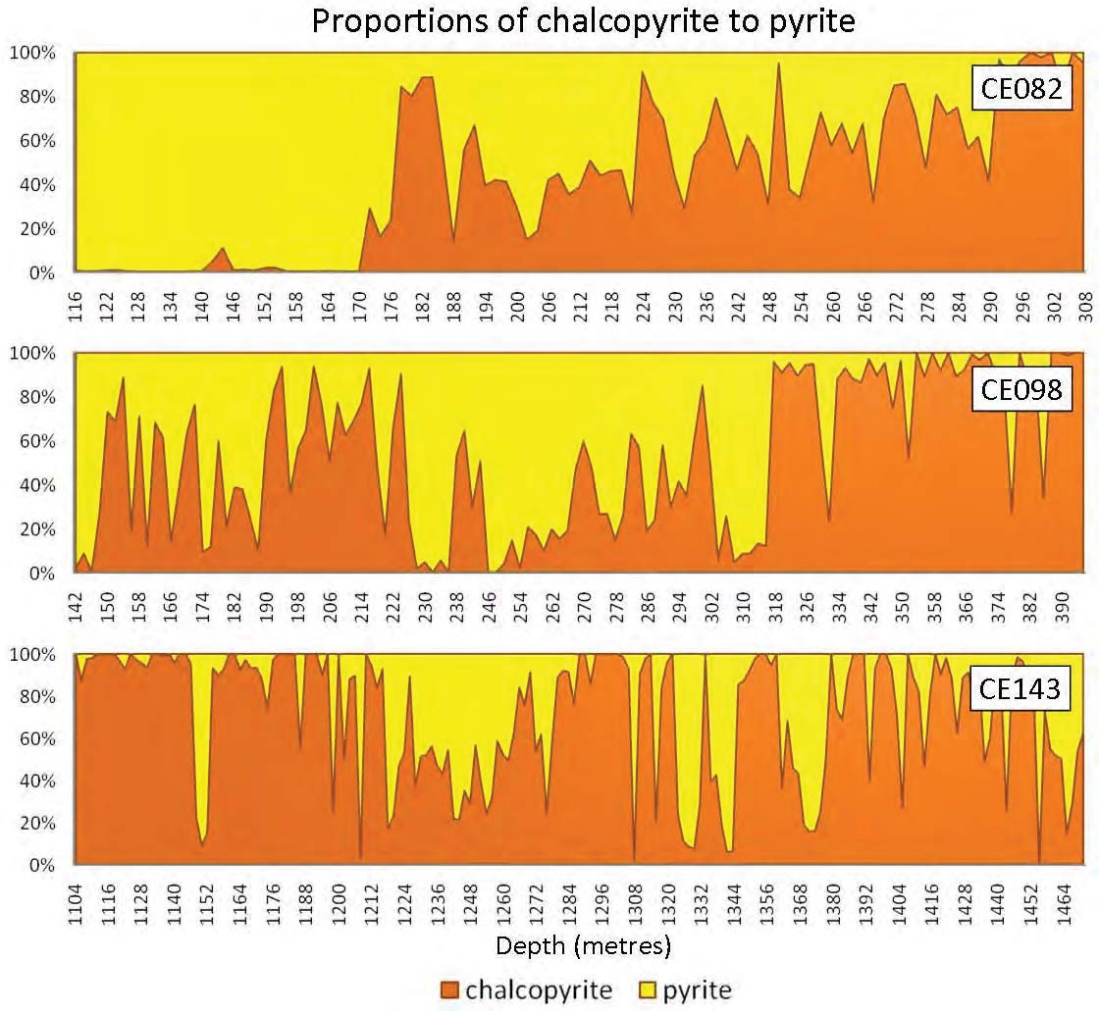

Figure 4.9. Down holes plots illustrating the changes in visual estimates of chalcopyrite: pyrite ratio for the drill holes CE082, CE098 and CE143.

4.2.3 Summary

Mineralogical and textural attributes have been measured at Cadia East based on the method described in Chapter 3, section 3.2. The drill-holes CE082, CE098 and CE143 were selected because they show the maximum mineralogical and textural variability. The results presented in this section have been used to create textural classes for Cadia East that are predicted to have unique mineral processing behaviours. These will be presented in Chapter 4.5.

4.3 Visual-based mineralogical and textural logging: Ernest Henry

Visual logging of mineralogical and textural characteristics was also undertaken on drill-core from the Ernest Henry IOCG deposit which contains very different minerals and textures than those of Cadia East. Based on the method described in Chapter 3, Section 3.2, mineralogical and textural attributes that are considered to potentially influence mineral processing behaviours have been logged for the drill-hole EH635 and the sampled intervals of EH432, EH446, EH556, EH574 and EH633 (Figure 4.10). The mineralogical and textural attributes that have been selected to be logged

are described in Table 4.2. Each attribute and its variants have been measured as a percentage (unless otherwise stated) of each two metre interval that coincides with the Ernest Henry assay and geology logging intervals.

The results obtained during the logging of mineralogical and textural attributes related to chalcopyrite only are presented first in section 4.3.1. This is followed by the results of the logging of gangue mineralogy and their textures which are presented in section 4.3.2.

All mineral abbreviations used in this chapter are outlined in Appendix 1.1.

Microsoft Excel spreadsheets containing the detailed textural logging data for EH432, EH446, EH556, EH574, EH633 and EH635 are in Appendix 4.2.

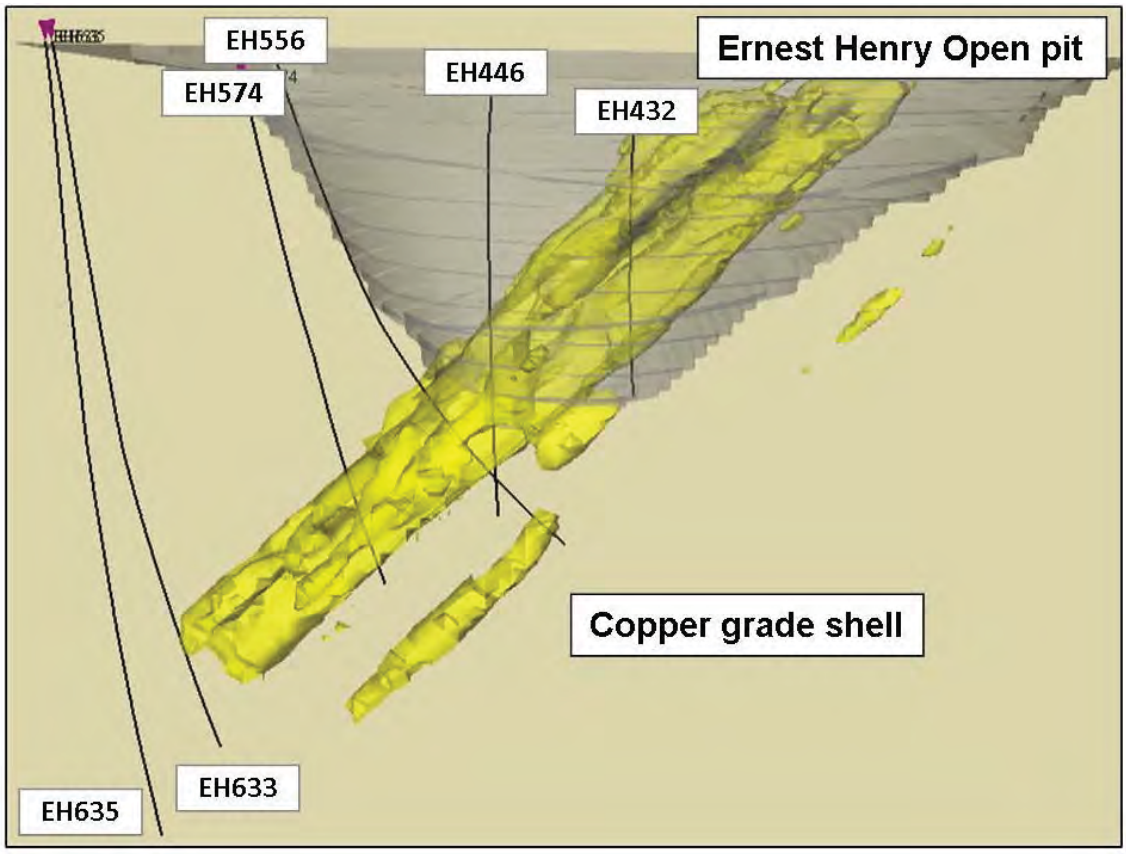

Figure 4.10. Open pit, copper grade shell and selected drill-hole locations for Ernest Henry. *Image from Xstrata Ltd.*

Table 4.2. Mineralogical and textural attributes that have been selected for drill-core logging at Ernest Henry. The attributes have been determined based on their potential impact on mineral processing behaviours.

Attribute	Variant	Description
1. Chalcopyrite deportment	Fragmental	Fragmental units refer to lithological units where the mineralisation occurs as fine to coarse-grained interstitial chalcopyrite between well-defined clasts of hematite dusted feldspar (albite or K-feldspar) with fine-grained magnetite (Figure 4.11A). Unit is measured as an estimated percentage of the logged interval.
	Mottled	Fragmental unit consisting of predominantly feldspar or magnetite with fine-grained chalcopyrite. Clasts are not well defined and the rock has a mottled appearance (Figure 4.11B). Unit is measured as an estimated percentage of the logged interval.
	Massive	Massive magnetite or feldspar with very fine-grained (<1mm) chalcopyrite (Figure 4.11C and D). Unit is measured as an estimated percentage of the logged interval.
2. Mineralised clots	N/A	Mineralised clots form in the matrix of the fragmental units and consist of chalcopyrite, pyrite, carbonate, magnetite and quartz. They have been estimated as an percentage of the logged interval (Figure 4.11E).
3. Chalcopyrite to pyrite ratio	N/A	The ratio of chalcopyrite and pyrite in the measured interval. Primarily, this measure was undertaken visually. However, later developments in mineral assays allowed this to be undertaken more accurately (see Section 4.6).
4. Vein mineral species	Barite, carbonate, chalcopyrite, magnetite, pyrite, quartz, siderite.	Estimated as a percentage of the mineral species present in each interval.
5. Carbonate veinlets	Also occur with varying quantities of chalcopyrite, pyrite, magnetite, siderite, quartz, barite, carbonate.	Calcite occur as irregular shaped veinlets that cross-cut pre-existing textures and fabrics. Varying quantities of other minerals may be a result of remobilised mineralisation. They have been measured as percentage of the logged interval (Figure 4.11F).
6. Modal mineralogy	Actinolite, apatite, carbonate, chlorite, chalcopyrite, feldspar, magnetite, pyrite, quartz, tourmaline.	Abundance of each mineral is estimated as a percentage.
7. Matrix composition	Matrix and clasts.	Percentage of matrix and clast material in the fragmental components of each interval.
8. Specular Hematite	Measured as nil, minor or visible grains.	Describes the degree of hematite alteration present.

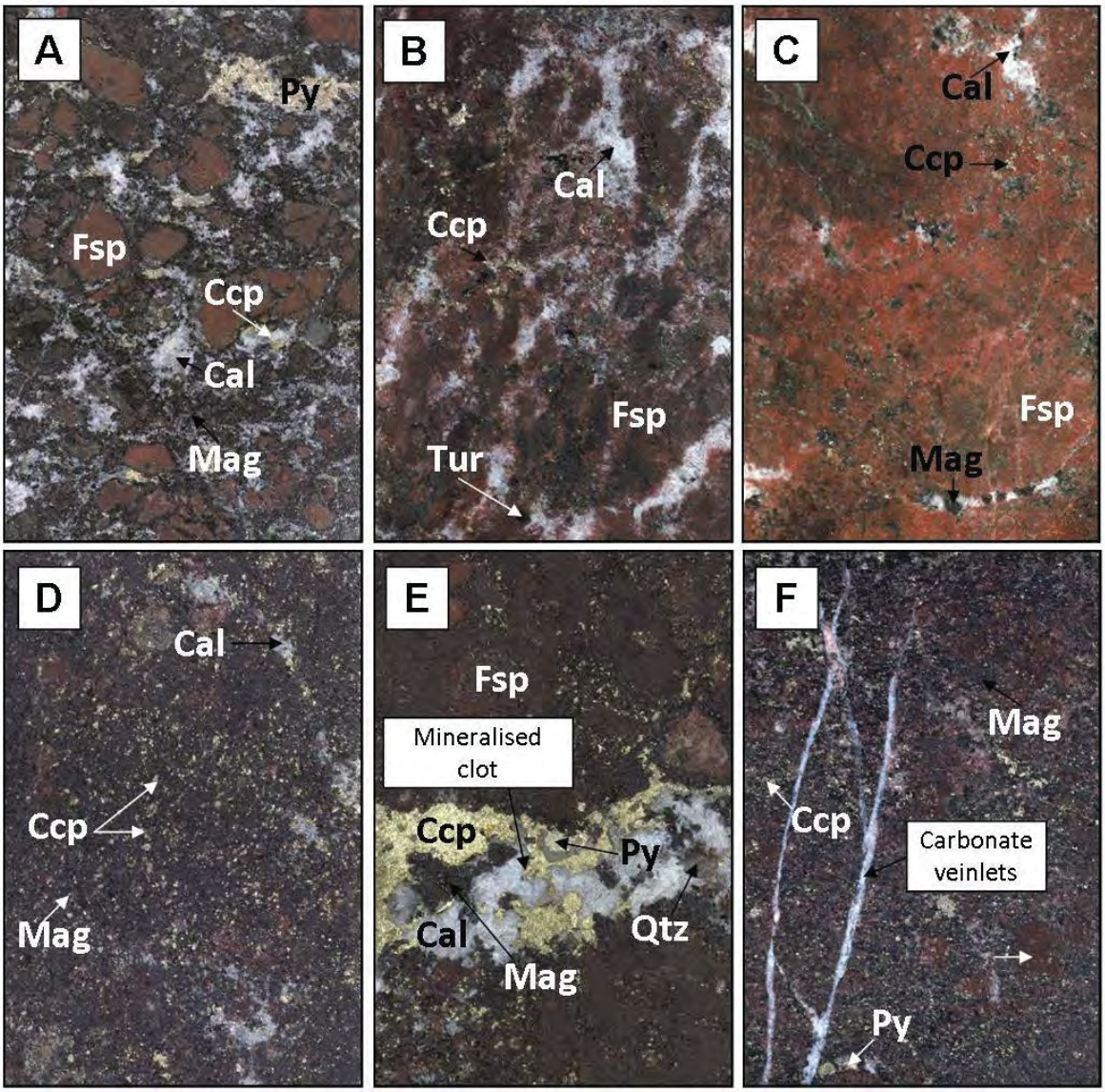

Figure 4.11. Examples of visually logged drill-core attributes for Ernest Henry. All images are the width of NQ core (5.5 cm in diameter) **A.** Example of a fragmental unit with clearly defined clast edges and fine-grained chalcopyrite in the matrix **B.** Example of a mottled texture with fine-grained chalcopyrite and clasts edges that are not clearly defined **C.** Example of massive feldspar with fine-grained chalcopyrite **D**. Example of massive magnetite with fine-grained chalcopyrite **E**. Example of a mineralised clot with coarse grained chalcopyrite **F**. Example of carbonate veinlets cross-cutting pre-existing minerals and textures. *For mineral abbreviations refer to Appendix 1.1.*

4.3.1 Chalcopyrite textures

The valuable copper sulphide mineral at Ernest Henry that can be identified at the meso-scale or in hand specimen is chalcopyrite. Presented in this section are the results for the visual logging of drill-core attributes related to chalcopyrite for drill-hole EH635. EH635 is the example used in this project to investigate the minerals and textures that could be present in the proposed Ernest Henry underground extension. The logged attributes include numbers one to three outlined in Table 4.2.

As at Cadia East, the variability in the grain size of chalcopyrite is predicted to result in differences in the minerals that they are associated with (See Figure 4.11A, B and C). Figure 4.12A illustrates the changes in the distribution of chalcopyrite down-hole for EH635. This drill-hole is dominated by rocks with a mottled texture with local regions consisting of massive and fragmental

textures. The mottled texture broadly corresponds with an increase in mineralised clots (Figure 4.12B). As previously discussed in section 4.2.2, an elevated abundance of pyrite can influence the flotation and smelting processes (Petruk, 2005). The abundance of pyrite compared to chalcopyrite is shown in Figure 4.12C. An increase in chalcopyrite compared to pyrite is observed between 820 and 1110 metres.

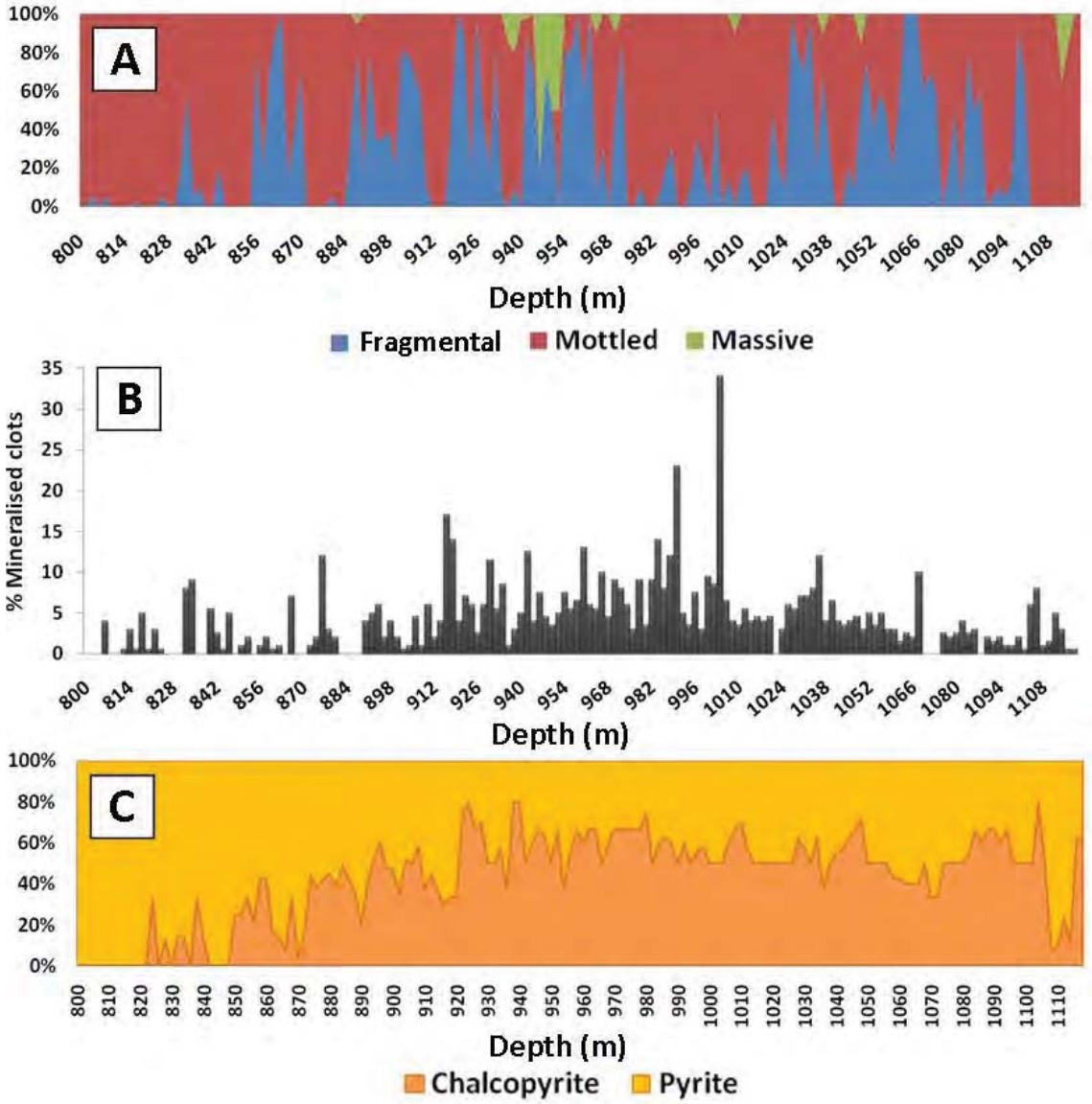

Figure 4.12. Down-hole plots for EH635 illustrating the changes in: **A.** distribution of chalcopyrite **B.** the abundance of mineralized clots **C.** chalcopyrite to pyrite ratio.

4.3.2 Gangue mineral phases and textures

Presented in this section are the results for the logging of rock characteristics and gangue minerals in drill-core for EH635. The logged attributes include numbers four to nine in Table 4.2.

The down-hole changes in the estimated modal mineralogy for EH635 are shown in Figure 4.13A and indicate that the dominant gangue minerals are magnetite, feldspar and carbonate minerals respectively. The region between 800 and 965 metres is dominated by magnetite (50-70%) before becoming rich in feldspar between 965 and 1118 metres (40-70%).

The percentages of matrix to clast material present in rocks exhibiting fragmental and mottled textures are shown in Figure 4.13B. The composition of the matrix material has also been logged and is shown in Figure 4.13C. The regions between 870 and 970 metres as well as 985 and 1080 metres exhibit a matrix that is dominated by magnetite, whereas all other zones are dominated by carbonate minerals.

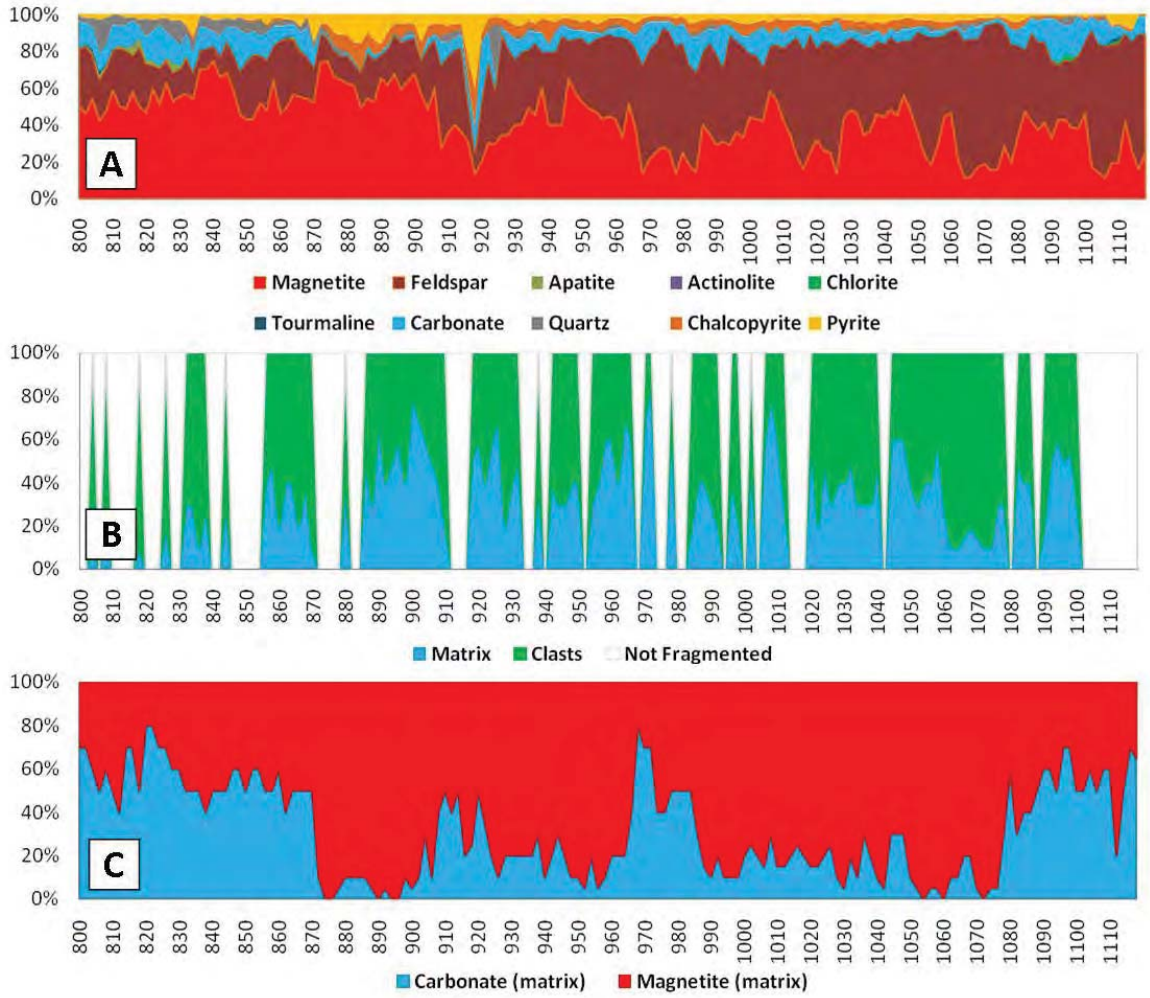

Figure 4.13. Down-hole plots for EH635 illustrating the changes in: **A.** Modal mineralogy **B.** the ratio of clasts to matrix material **C.** composition of matrix material.

4.3.3 Summary

Mineralogical and textural attributes have been measured at Ernest Henry based on the method described in Chapter 3, section 3.2. The drill-hole EH635 was selected for detailed logging as this represented the minerals and textures that will potentially be encountered in the underground extension planned for Ernest Henry. The results presented in this section have been used to create textural classes for Ernest Henry that are predicted to have unique mineral processing behaviours. These will be presented in Chapter 4.8.

4.4 Results for machine-based logging of Drill-core: Ernest Henry

Machine-based logging has been undertaken on drill-core from six holes (EH432, EH446, EH556, EH574, EH633 and EH635) from the Ernest Henry IOCG deposit. In total 1774 metres of medium-resolution digital images have been produced using the GEOTEK MSCL and the procedures outlined in Chapter 3, section 3.3. The classification and extraction of quantified mineralogical and textural information from these images was undertaken using the Definiens (Table 4.3). The results are summarised here and the detailed results are listed in appendices:

4.3: Modal Mineralogy calculated from drill-core images: Ernest Henry

4.4 to 4.9: Mineralogical and textural attributes calculated from drill-core images for drill-holes EH432, EH446, EH556, EH574, EH633 and EH635 respectively.

Table 4.3. Drill-holes and meterages that have been photographed using the GEOTEK MSCL for Ernest Henry as well as the mineralogical and textural attributes that have been measured.

Drill Hole	From	To	Whole Rock	Chalcopyrite
EH432	150m	400m	Modal Mineralogy	Area Length and width Minerals Associated with chalcopyrite Preferential chalcopyrite deportment Chalcopyrite distribution
EH446	300m	600m		
EH556	450m	750m		
EH574	544m	810m		
EH633	858m	1166m		
EH635	800m	1120m		

The interpretations of the results presented in this section will be discussed later in this chapter in section 4.8.

4.4.1 Ernest Henry Mineral Categories

The rule set for the production of classified mineral maps at Ernest Henry was defined by Berry (2008). The minerals that have been used in the Ernest Henry classification and the colours that they have been assigned to are summarised in Table 4.4. Examples of the medium resolution photographic images and the corresponding mineral maps are shown in Figure 4.14. Figure 4.14A and 4.14B illustrate examples of the red feldspar, magnetite, magnetite/chlorite, magnetite/feldspar, chalcopyrite, pyrite, quartz and carbonate/quartz mineral classes prior to and after classification. Figure 4.14C and 4.14D show the unclassified and classified images respectively with examples of the mineral categories red feldspar, feldspar/magnetite, felsic, carbonate/quartz, chalcopyrite, pyrite and quartz.

At Ernest Henry, there are a number of mineralogical and textural features that are amenable to identification using image analysis. Table 4.5 summarises these features for each mineral class.

Table 4.4. The minerals groupings and RGB colours that have been used in the classification of images at Ernest Henry.

Mineral Category	Minerals included in classification	RGB colour
Carbonate/Quartz	Calcite, quartz, barite	0, 0, 255
Pyrite	Pyrite	255, 255, 0
Red Feldspar (K-feldspar)	K-feldspar	255, 87, 87
Chalcopyrite	Chalcopyrite	163, 192, 0
Chlorite	Chlorite, actinolite, magnetite	0, 128, 0
Felsic	Calcite, quartz, barite, feldspar, siderite	192, 220, 192
Magnetite	Magnetite, hematite	128, 0, 128
Magnetite/Chlorite	Magnetite, chlorite	0, 128, 128
Magnetite/feldspar	Magnetite, K-feldspar	128, 0, 59
Quartz	Quartz	0, 255, 255

Table 4.5. Mineralogical and textural features that can be identified using image analysis for each of the mineral categories at Ernest Henry.

Mineral category	Mineralogical and textural features
Carbonate/Quartz	The carbonate-quartz category typically represents the calcite-quartz crystals that make up the matrix material in rocks that exhibit fragmental and mottled textures.
Pyrite	The classification for pyrite is most representative of the coarser grains that are present in mineralized clots. The classification does not recognise the extremely fine and disseminated pyrite that can be smaller than the pixel size.
Red Feldspar (K-feldspar or albite)	The red feldspar classification typically represents the well-defined red clasts in the fragmental units.
Chalcopyrite	The classification for chalcopyrite is most representative of the coarser grains that occur in mineralised clots and can include minor amounts of fine-grained disseminated pyrite if the crystals are oriented in a way that it appears to be darker than normal.
Chlorite	The chlorite classification identifies all of the green colourations in the images. This includes chlorite, actinolite and in some areas feldspar minerals that have a dark green chlorite.
Felsic	The felsic classification represents all of the felsic minerals that have an opaque white colouration. This can include quartz, calcite, unstained feldspar, barite and siderite.
Magnetite	The magnetite classification represents euhedral, black crystals of magnetite that typically occur in the matrix material of rocks with the fragmental or mottled texture.
Magnetite/Chlorite	The magnetite/chlorite classification is dominantly fine-grained magnetite that occurs in matrix material with very minor amounts of chlorite alteration.
Magnetite/feldspar	The magnetite/feldspar class is predominantly red rock that has been darkened by the presence of fine-grained magnetite alteration.
Quartz	The quartz class includes euhedral grey to transparent quartz crystals that occur as veins or as matrix material.

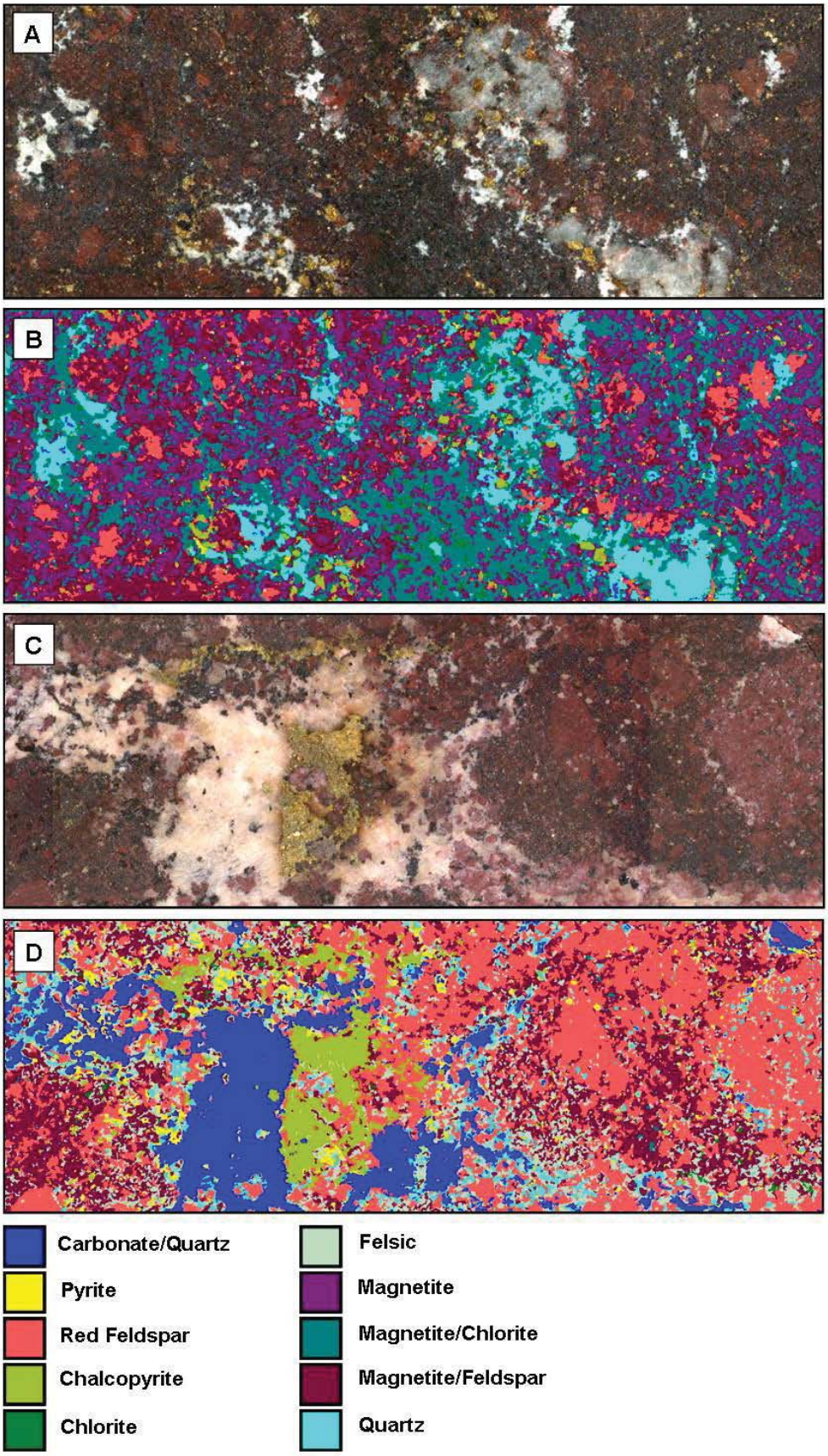

Figure 4.14A. EH574 684.15-684.30m. Unclassified photographic image of drill-core **B.** Classified mineral map of 4.14A **C.** EH432 226.65-226.80m. Unclassified photographic image of drill-core **D.** Classified mineral map of 4.14C.

4.4.2 Modal Mineralogy

Based on Table 4.5 the following groupings were created to reflect the minerals that exhibit similar colour characteristics, overlap in the classification (Carbonate and quartz minerals, magnetite and chlorite) or will exhibit similar hardness characteristics (the feldspar minerals). This will simplify and more effectively show changes in modal mineralogy down-hole:

MgChl	magnetite + magnetite/chlorite + chlorite
Fsp	magnetite/feldspar + red feldspar + felsic
CaQtz	carbonate/quartz + quartz
Chalcopyrite	chalcopyrite
Pyrite	pyrite

These groupings have been used to observe the changes in mineral class abundance down-hole. The modal mineralogy has been calculated based on these groupings for all six drill-holes from Ernest Henry. The down-hole plots shown in Figure 4.15 have been used to identify combinations of minerals that most commonly occur together. Examples of these combinations have been labelled A-E and are described below. Group D refers to a generation of chalcopyrite that has previously been described in the visual logging at Ernest Henry. Group D can occur with any of the groups A, B, C and E. Figure 4.16 shows the distribution of the groups A-E for drill-hole EH635. This figure shows, that for drill-hole EH635 there are continuous zones of A and B, which are both feldspar dominant groups. There are localised areas of group E, which indicates an increase in magnetite and chlorite minerals. Group D predominantly occurs with groups B and E.

Combinations of Groups

A Fsp (>60%) + MgChl
B Fsp (>60%) + CaQtz
C MgChl (>60%) + CaQtz
D (Chalcopyrite + Pyrite) >5%
E Fsp (40-60%) + MgChl (40-60%)

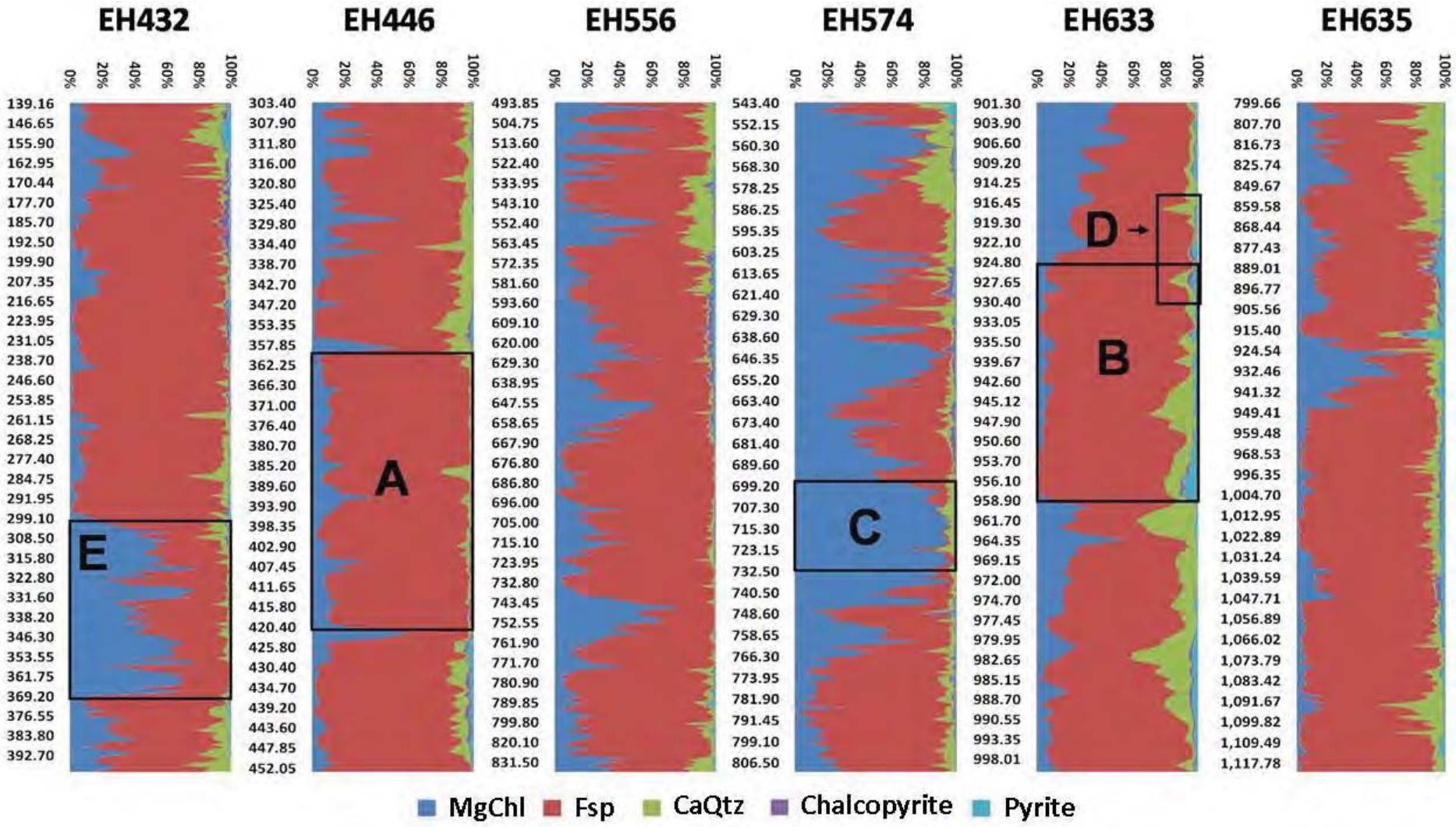

Figure 4.15. EH635. Down-hole modal abundance for EH432, EH446, EH556, EH574, EH633 and EH635 for the groupings MgChl, Fsp, CaQtz, Chalcopyrite and Pyrite calculated from classified mineral maps of drill-core. Labels A to E indicate areas of varying mineralogical composition: A - Fsp (>60%) + MgChl; B - Fsp (>60%) + CaQtz; C - MgChl (>60%) + CaQtz ; D- (Chalcopyrite + Pyrite) >5%; E - Fsp (40-60%) + MgChl (40-60%).

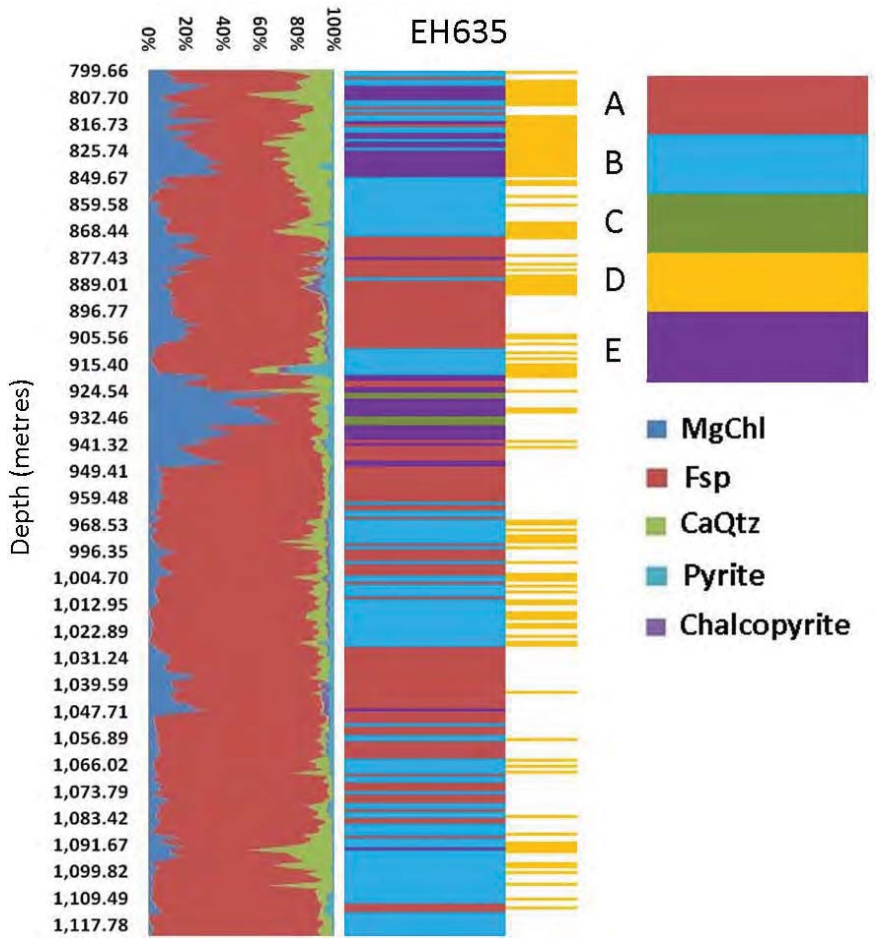

Figure 4.16. The down-hole distribution of modal mineralogy and mineral group combinations (A-E) for drill-hole EH635. The modal mineralogy has been calculated from the classified images of drill-core.

4.4.3 Chalcopyrite size

The size of each chalcopyrite PhReg (see Chapter 3, section 3.6) has been measured from the classified images of drill-core from the six drill-holes from Ernest Henry (see Table 4.3). All of the attributes were extracted using the Definiens Developer software and follow the processes outlined in Chapter 3, section 3.3 and section 3.6.

Presented in this section are the results for area, length and width of chalcopyrite. In this section (and the following: 4.4.4 Minerals associated with chalcopyrite) four examples of drill-core images are used to demonstrate the textural attributes that have been used throughout this research.

The four examples correspond to the dominant mineral combinations that were identified from the down-hole plots in Figure 4.15. The examples are A, C and E with the combinations B and D occurring together (see previous section). These examples are described in Table 4.6 and sections of the corresponding unclassified and classified mineral maps are shown in Figure 4.17. The remainder of the data extracted from the drill core images from all six drill-holes are in Appendices 4.4 - 4.9. These data will be used later to validate the outcomes of the meso-scale visual logging (section 4.6).

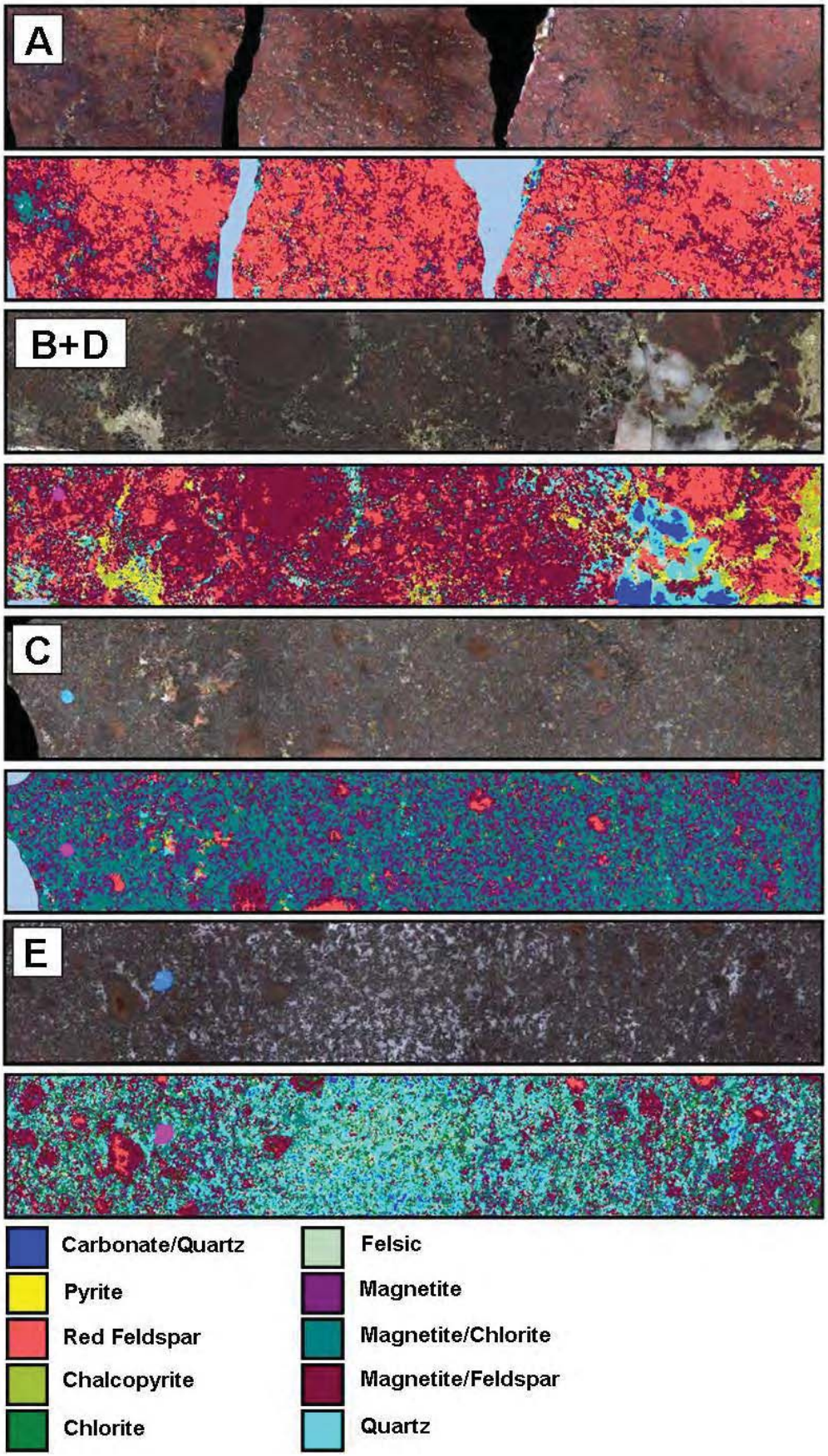

Figure 4.17. Unclassified (*upper*) and classified (*lower*) images that have been used for the analysis of chalcopyrite PhRegs. Each image shows an example of the mineral dominant mineral combinations discussed in the previous section (4.4.2) For image depths see Table 4.6. All images have a height of 5.5cm.

Table 4.6. The sample numbers, image length and number of chalcopyrite PhReg's for each of the examples **A**, **B/D**, **C** and **E** that will be presented in this section and section 4.5.4.

Example	Sample #	Image length	# of chalcopyrite PhReg's extracted
A	EH446 364.00m	85 cm	1649
B/D	EH633 926.70m	95 cm	3483
C	EH574 706.40m	90 cm	1615
E	EH432 305.80m	85 cm	1711

Area

The area of each chalcopyrite PhReg (see Chapter 3, section 3.6) has been converted from a pixel to an Equivalent Circle Diameter (ECD; µm) measurement. The cumulative ECD distribution for combination groups A, B/D, C and E are presented in Figure 4.18. Where multiple generations of chalcopyrite occur together (i.e. disseminated and clotted), a cumulative distribution curve will mask any bimodality. In order to observe bimodal generations of size, the data were plotted as a weighted histogram (Figure 4.19).

The cumulative size distributions shown in Figure 4.18 show two distinct trends. Graphs A, C and E all exhibit similar curves that indicate that >80% of the chalcopyrite PhRegs have ECD >150 microns. The size distribution shown in graph B/D indicates a coarser size population where >80% of the recognised chalcopyrite PhRegs are > 300 microns. In Figure 4.19 it is clearly seen that in samples A, C and E a majority of the chalcopyrite occurs within the 300-600 µm size fractions. However, samples C and E contain a larger proportion of coarse (>1200µm) chalcopyrite (~16%) than sample A (~5%). For sample B/D, 63% of the chalcopyrite has an ECD >1200 µm and ~32% has an ECD between 300 and 1200 µm indicating multiple chalcopyrite size populations.

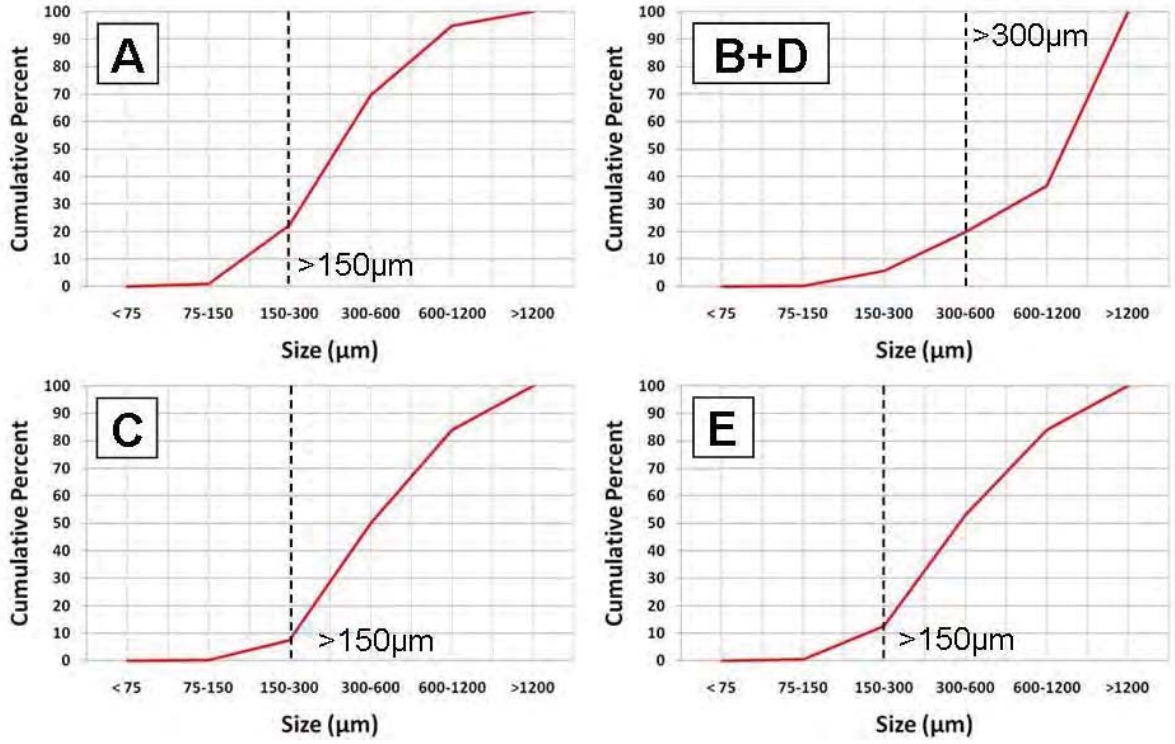

Figure 4.18. Cumulate ECD distributions measured from drill-core images for **A.** EH446 364.00m **B and D.** EH 633 926. **C.** EH574 706.40m **E.** EH432 305.80m

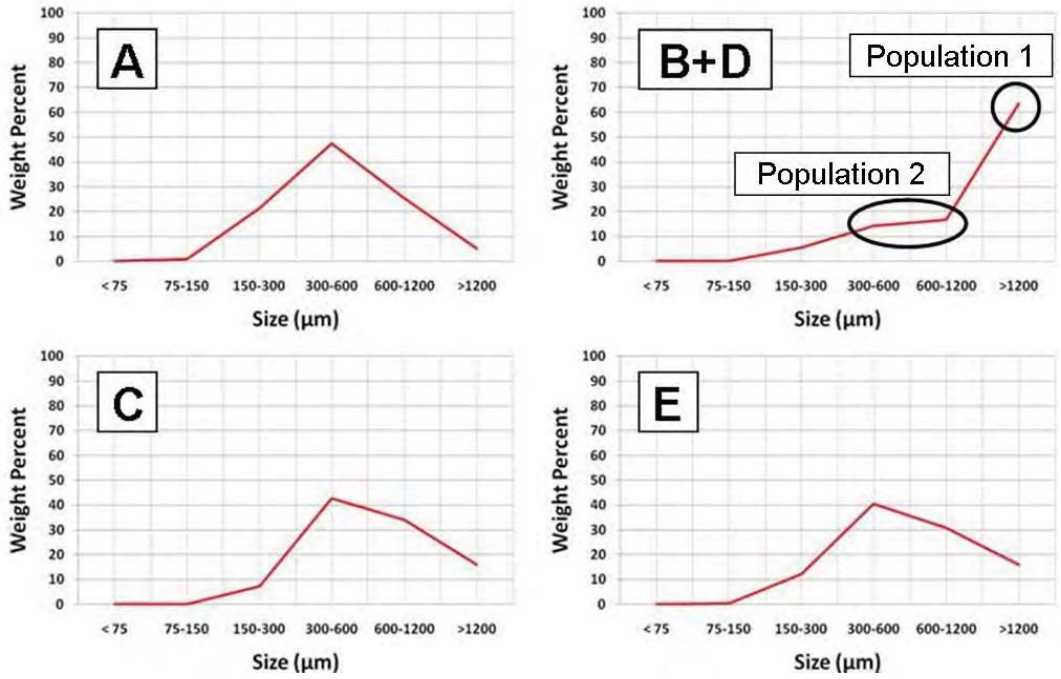

Figure 4.19. ECD size distribution curves showing the normalized area percentage of chalcopyrite phases for different ECD size ranges measured from classified images of drill-core. The examples used (A, B/D, C and E) correspond to the examples used in Figure 4.17. The black circles in B represent separate size populations of chalcopyrite (bimodality).

Length and Width

The length and width has been calculated for each chalcopyrite PhReg in each image. All length and width data for the chalcopyrite extracted from each image have been plotted on the template shown in Figure 4.20. When considering the bounding box approximation used by Definiens and the equivalent ellipse approximation used by other image analysis software, the width is always going to be the shorter of two rectangle or ellipse lengths, and the length is always going to be the longer of two rectangle or ellipse lengths. This means that no data will plot to the left of a line with the gradient equal to one on a length versus width plot. As data plots further away from the gradient =1 line the more elongate an object is. As data plots to the right of the diagram, the larger the chalcopyrite object is. This allows for the entire population of chalcopyrite PhRegs to be observed in one diagram. Conclusions regarding the elongation of chalcopyrite can be made based on where the length and width data plot on this Figure.

The length and width of the chalcopyrite extracted from each of the image examples of A, B/D, C and E (Figure 4.15) are plotted in Figure 4.21. Examples A, C and E all exhibit chalcopyrite populations that predominantly have a length: width ratio between 1:1 and 3:1 and a length of <100 pixels. Example B/D however, exhibits a number of large objects (*black circles*) and one point that has a length > 600 pixels and a length to width ratio of 4:1.

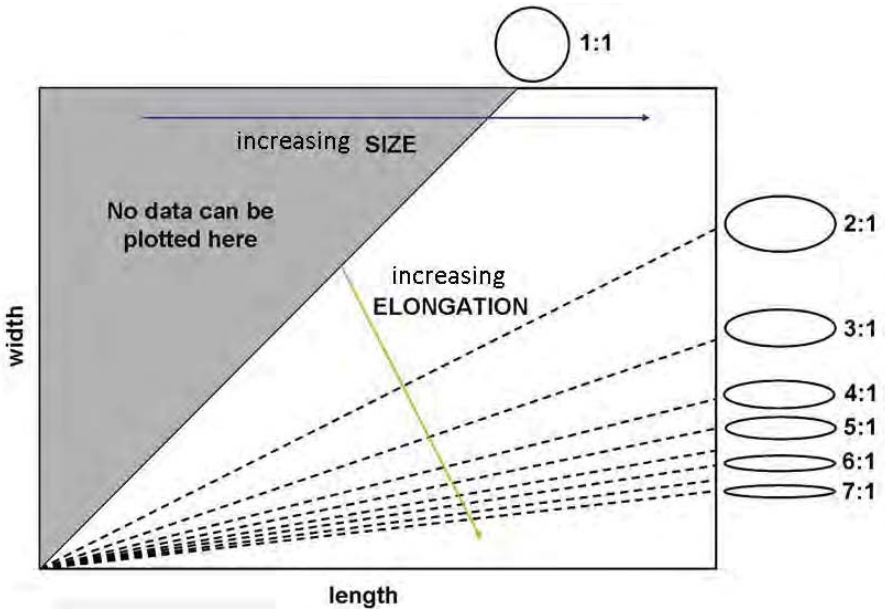

Figure 4.20. Template for length and width data that can be used to make size and shape interpretations about populations of objects. Ratios indicate Length: Width.

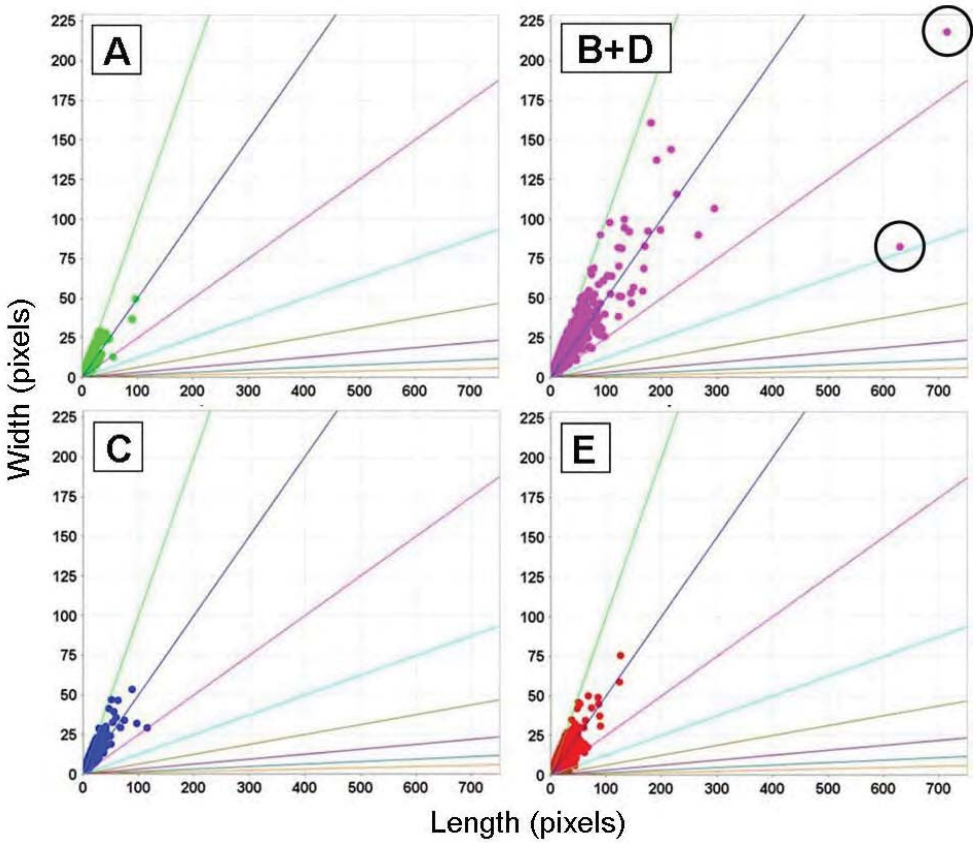

Figure 4.21. Length and width data for examples A, B/D, C and E (Table 4.6). Examples A, C and E all have similar length to width ratio ranges (1:1 to 3:1). Example B/D contains a number of larger more elongate mineral PhRegs.

4.4.4 Minerals associated with chalcopyrite

For the meso-scale images at Ernest Henry, the minerals present in a 5 pixel rim around the chalcopyrite have been extracted (Figure 4.22). These rims represent the minerals within the 250

microns surrounding the chalcopyrite PhReg. The minerals are reported as a proportion of the rim, totalling to the value of one. The minerals associated with each chalcopyrite PhReg have been weighted against the total area of chalcopyrite in each of the corresponding images. This ensures that the results are not biased towards smaller chalcopyrites that only comprise a small part of the total sample population. Each PhReg has been classified based on its dominant mineral associations. Where there is no mineral group that comprises >50% of the 5 pixel rim, the term 'mixed' has been assigned.

Figure 4.23 shows the dominant minerals that are associated with chalcopyrite for the four examples described in Table 4.6. Examples A, B/D and E all contain chalcopyrite with a dominant Fsp association, however example A contains 95% Fsp whereas B/D contains 77% with 10% of the chalcopyrite associated with pyrite. For the chalcopyrite in example E, 52% is associated with Fsp, with 24% exhibiting a dominant mixed association. All of these differ significantly from example C where 89% of the chalcopyrite is dominantly associated with MgChl.

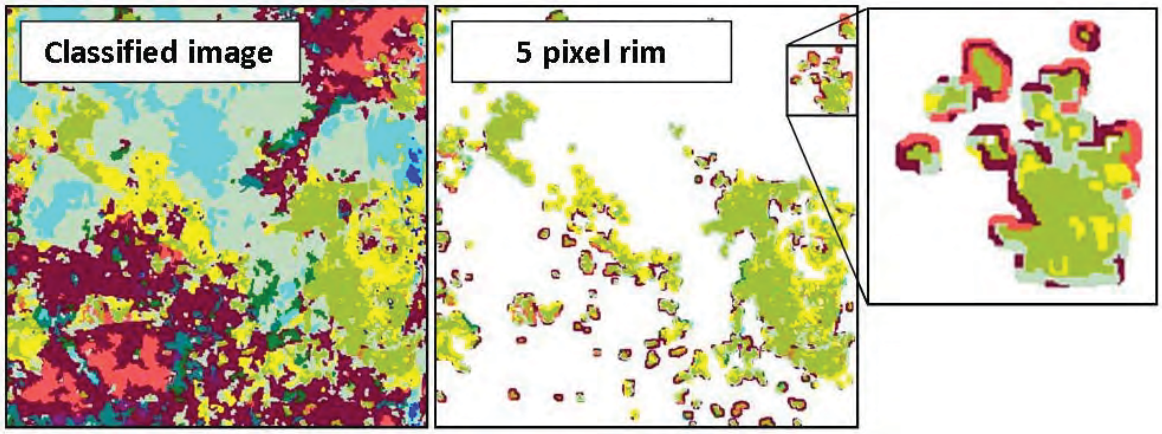

Figure 4.22. Examples of a 5 pixel (250 μm) rim which was used to extract mineral association data from classified images.

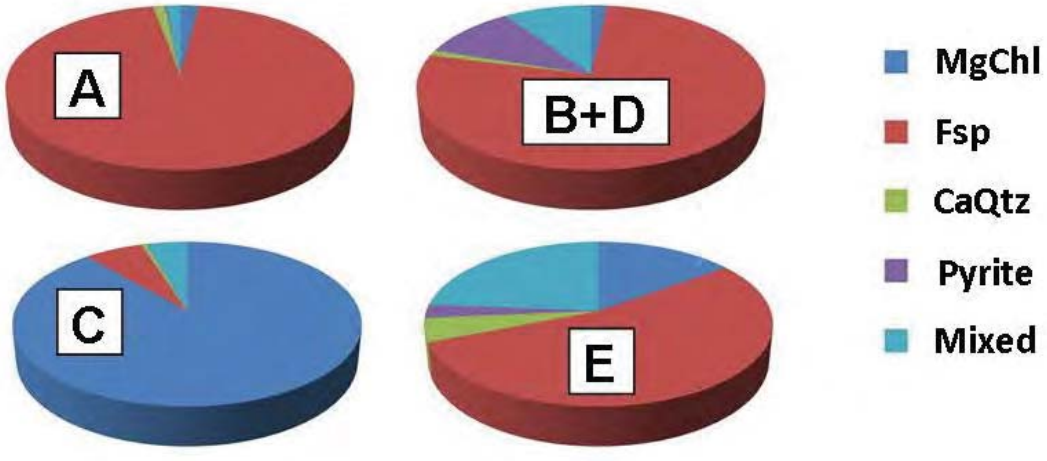

Figure 4.23. Dominant chalcopyrite examples for A, B /D, C and E.

The minerals that are associated with chalcopyrite have also been determined for different size ranges of chalcopyrite within the same example. This will determine whether the chalcopyrite association varies with PhReg size. Chalcopyrite PhRegs for each example have been grouped into fine-grained (<150 μm ECD); medium-grained (150-600 μm ECD) and coarse-grained (>600 μm

ECD). The graphs in Figure 4.24 illustrate the changes in the percentage of MgChl, Fsp, CaQtz and Pyrite associated with chalcopyrite of different sizes for examples A, B/D, C and E. Each chalcopyrite PhReg within each size fraction has been weighted against the total chalcopyrite to ensure that each population remains unbiased (i.e. not skewed towards chalcopyrite with a size of only 1 pixel). The data for these figures are presented in Table 4.7.

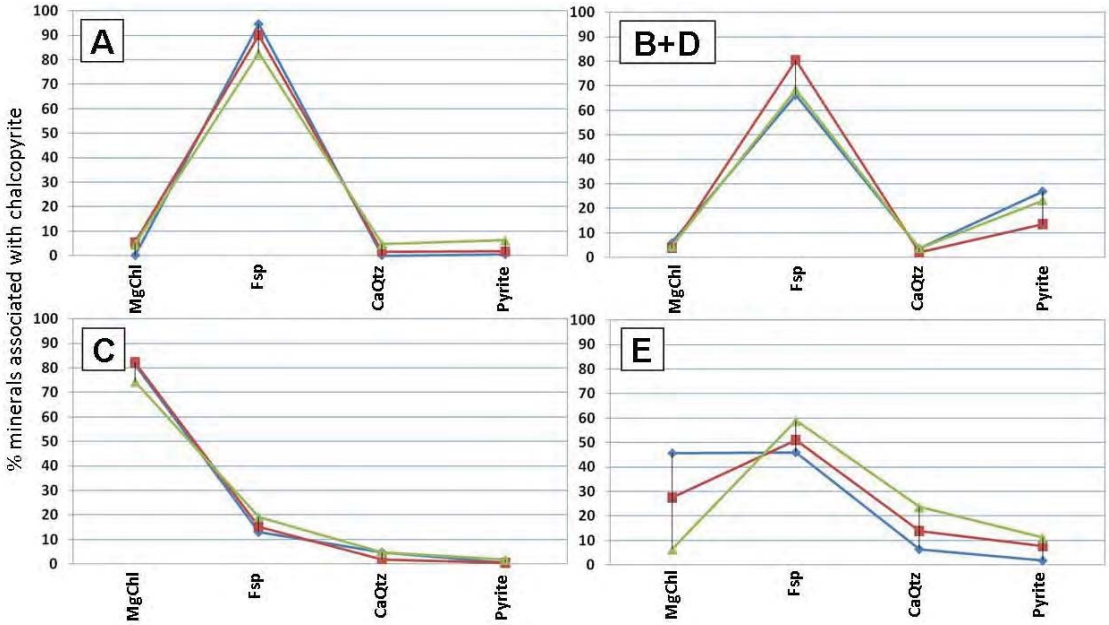

Figure 4.24. Changes in mineral groups associated with chalcopyrite for examples A, B/D, C and E (See Figure 4.15). Each example has been divided into size fractions; fine (< 150 μm ECD; *blue*), medium (150-600 μm ECD; *red*) and coarse (>600 μm ECD; *green*).

Table 4.7. Data for the changes in minerals associated with chalcopyrite for fine (<150 μm), medium (150-600 μm) and coarse (> 600 μm) PhReg sizes shown in Figure 4.23.

Example	Chalcopyrite Size fraction	Percent of sample	Mineral Groups			
			MgChl	Fsp	CaQtz	Pyrite
A	Fine	0.90	0.03	0.86	3.62×10^{-3}	3.72×10^{-3}
	Medium	68.66	3.64	62.66	1.16	1.21
	Coarse	30.40	1.41	1.52	25.53	1.94
B/D	Fine	0.17	0.01	54.68	0.01	0.05
	Medium	19.69	0.74	15.68	0.42	2.85
	Coarse	80.14	3.46	0.10	3.06	18.95
C	Fine	0.02	0.10	0.02	0.01	6.30×10^{-4}
	Medium	49.97	41.11	7.64	0.97	0.24
	Coarse	49.91	37.15	9.60	2.30	0.85
E	Fine	0.41	0.18	0.18	0.03	0.01
	Medium	52.27	14.20	26.82	7.24	4.01
	Coarse	47.32	3.00	28.00	11.11	5.21

In order to determine whether chalcopyrite is preferentially associated with particular minerals (higher level of association than expected by random distribution), the dominant mineral associations of each example (Figure 4.23) is compared against the modal mineralogy for the corresponding interval. This will determine if disseminated or clotted chalcopyrite at Ernest Henry exhibit a preferential deportment or association with any of the gangue minerals. If there is no preferential deportment then the minerals associated with chalcopyrite will reflect the modal mineralogy of the corresponding interval. Figure 4.25 will be used as a template for interpreting mineral deportment. In this template, if a mineral plots to the left of the blue line (where the

gradient is equal to one) then there is a negative mineral deportment i.e. chalcopyrite is not preferentially associated with that mineral. If the mineral plots to the right of the blue line, then there is a preferential deportment or association with that mineral. If the mineral plots along the blue line, then the chalcopyrite associations reflect the modal mineralogy of the host rock.

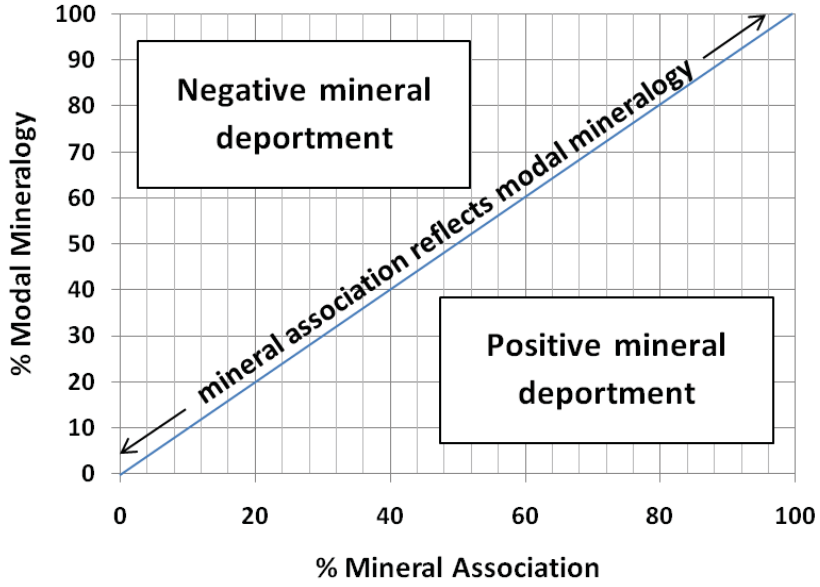

Figure 4.25. Template for interpreting preferential mineral deportment of valuable phases. If the mineral data plots along the *blue* line then the mineral associations reflect the modal mineralogy of the rock and there is no preferential deportment. If the mineral data plots to the left of the *blue* line then there is negative deportment. If it plots to the right of the *blue* line then there is positive mineral deportment.

In order to compare the modal mineralogy to the chalcopyrite association in the 5 pixel rims, the chalcopyrite abundance needed to be deducted from the modal mineralogy and normalised. This ensures that the mineral class abundances calculated in the modal mineralogy are not underestimated. The graphs for the chalcopyrite deportment for the examples A, B/D, C and E are shown in Figure 4.26. The mineral classes associated with the chalcopyrite PhReg for examples A and C both plot close to the blue line and therefore reflect the modal mineralogy of the rock. Example B/D exhibits minor positive deportment with Fsp. In example E chalcopyrite PhRegs show a negative deportment with MgChl and CaQtz mineral classes.

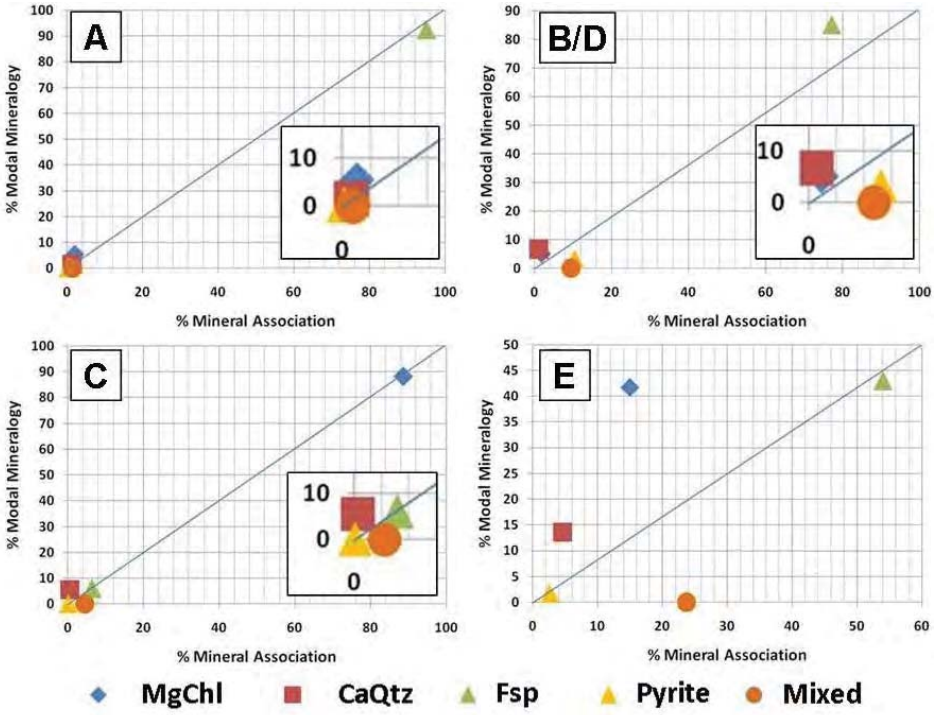

Figure 4.26. Plots illustrating chalcopyrite mineral association versus modal mineralogy. Positions of the minerals indicate a negative or positive deportment of chalcopyrite with the surrounding minerals or an association that reflects the modal mineralogy of the rock (As in Figure 4.25). Insets show clusters of mineral classes from the bottom left corners of examples A, B/D and C.

4.4.5 Distribution of chalcopyrite

The distribution of chalcopyrite grains in a rock can affect the floatability of a particle (Jones, 1987). For example, chalcopyrite grains that are smaller than the target grind size of an ore can still be recovered by flotation if the grains are clustered together enough to expose sufficient surface area of chalcopyrite to the flotation bubble. The distribution of chalcopyrite phases can be measured using a 'nearest neighbour' approach (Gay and Latti, 2006). For each chalcopyrite PhReg present in core-logger images the distance to the nearest chalcopyrite grain has been measured in pixels. This measurement can be considered a measure of how clustered together the chalcopyrite phases are. The average distance to the nearest chalcopyrite phase has been measured for various sizes of chalcopyrite in examples A, B/D, C and E (Figure 4.27). The averages have not been weighted against size as this would bias the results to reflect the distance of only the larger phases in each population.

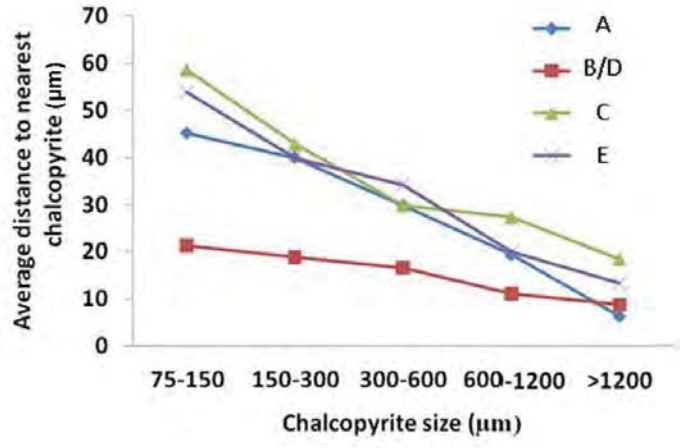

Figure 4.27. The average distance to the nearest chalcopyrite PhReg for examples **A**, **B/D**, **C** and **E** for different size of chalcopyrite.

Figure 4.27 suggests that for each example the average distance to the nearest chalcopyrite phase decreases as the phase size increases. In order to assess if larger chalcopyrite phases are more likely to be closer to another chalcopyrite than the smaller phases the average distance to the nearest chalcopyrite phase for each of the examples A, B/D, C and E have been compared to the chalcopyrite abundance calculated from the classified images of the corresponding interval (Figure 4.28). This will test whether this trend is true or an artefact of increasing chalcopyrite grade i.e. the higher the grade, the less distance there is between chalcopyrite phases.

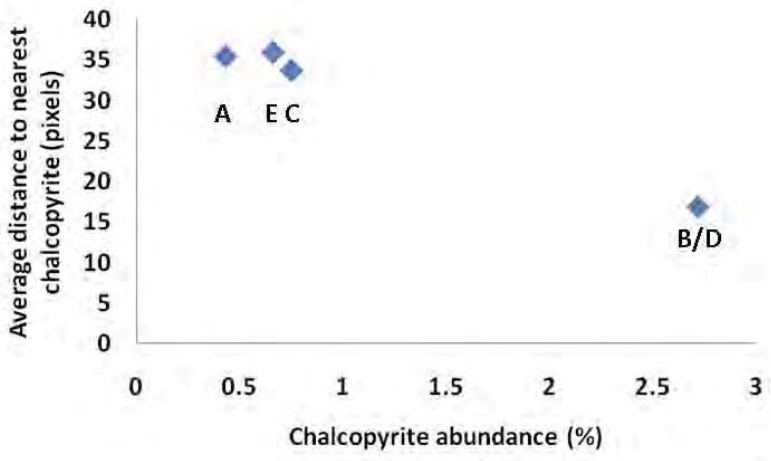

Figure 4.28. The average distance to the nearest chalcopyrite PhReg for examples A, B/D, C and E versus the corresponding chalcopyrite grade calculated from classified core images.

The average distance to the nearest chalcopyrite PhReg and the corresponding chalcopyrite grade calculated from the classified core images have been plotted in Figure 4.29 for drill-holeEH446 (168 classified images). The distance to the nearest chalcopyrite PhReg decreases exponentially as the chalcopyrite abundance increases. The direction that the points deviate away from this trend can be used to interpret whether the chalcopyrite phases are clustered together (*blue* arrows) or more widely dispersed (*green* arrow).

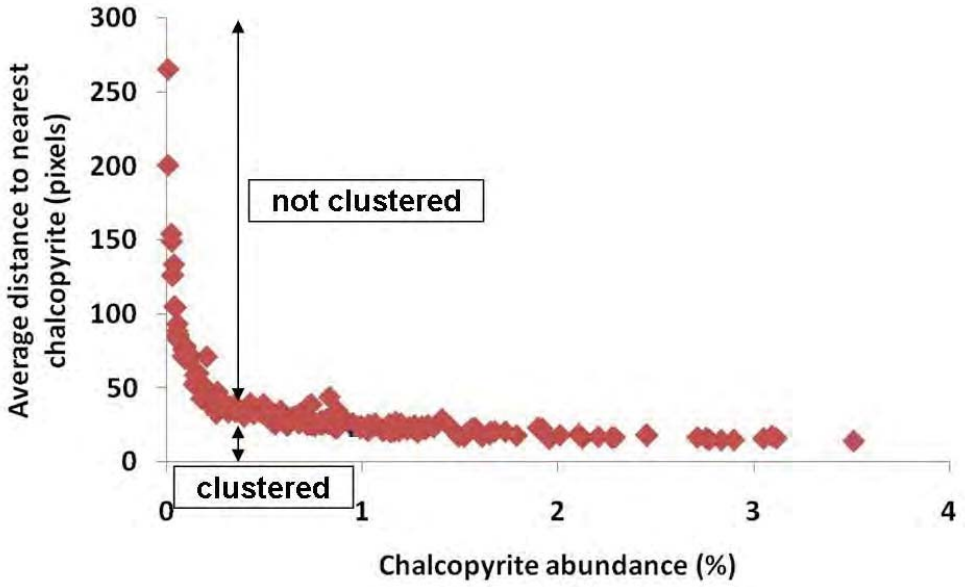

Figure 4.29. The average distance to the nearest chalcopyrite for all classified images in EH446 versus the corresponding chalcopyrite abundance calculated from the same images. The blue arrows indicate where points will plot if the chalcopyrite is clustered, the green arrows indicate chalcopyrites that are more widely dispersed.

4.4.6 Summary

Mineralogical and textural attributes have been extracted from classified images of drill-core from Ernest Henry. The procedures for this method are outlined in Chapter 3, section 3.3. From the six drill-holes (EH432, EH446, EH556, EH574, EH633 and EH635), four samples were selected to demonstrate the mineralogical and textural analysis that has been used throughout this project. The selection of samples reflects the most commonly occurring mineralogical signatures observed in the sampled drill-holes at Ernest Henry (see section 4.4.2).

The mineralogical and textural attributes that have been measured are area, length, width, modal mineralogy, chalcopyrite mineral associations and chalcopyrite distribution. The interpretations and results of all of the data extracted from drill-core images are presented later in this chapter (section 4.5.2).

4.5 Interpretations of meso-scale mineralogy and texture from Cadia East

The aim of the visual logging of drill-core presented in section 3.2 was to develop a method for the identification of mineralogical and textural attributes that are predicted to influence mineral processing behaviours. In this section, these results have been used to create textural classes that are considered to be unique with respect to different aspects of mineral processing. In order to establish if these classes are in fact unique, comparisons have been made to both chemical and mineral assays (see Chapter 3, section 3.7) as well as drill-core logging from site geologists.

4.5.1 Interpretations of meso-scale visual-logging

In section 4.2, data was presented from the visual logging of meso-scale mineralogical and textural attributes. Here these attributes are compared with assays for Cu, Au, Mo, Pb and Zn in order to determine if there is an existing relationship with particular mineralogical and textural features of the rock.

For the drill-holes CE082, CE098 and CE143 the distribution of copper sulphide minerals has been logged (see section 4.2, Figure 4.2A, B and C). This attribute is considered a measure of approximate grain-size as well as the copper sulphide mineral distribution. Figure 4.30 illustrates the median grades of Au, Cu, CuCN, Mo, Fe, S, Zn and Pb for the 2 metre intervals that were logged as predominantly (>70%) fine-grained disseminations, coarse-grained aggregates or vein-hosted. Where there was not one dominant distribution of copper-sulphide minerals the interval was termed ‘mixed’.

The intervals that are predominantly vein-hosted display higher Au and CuCN grades and lower S, Zn and Mo grades than the intervals that are predominantly fine-grained disseminations or coarse-grained aggregates. The intervals that consist of predominantly coarse-grained aggregates have the highest Cu, Mo and Fe grades with the intervals that are predominantly fine-grained disseminations having the highest Zn and Pb grades and the lowest Au, Cu and CuCN grades. The overall spread of the data and statistics for Figure 4.30 are present in Table 4.8.

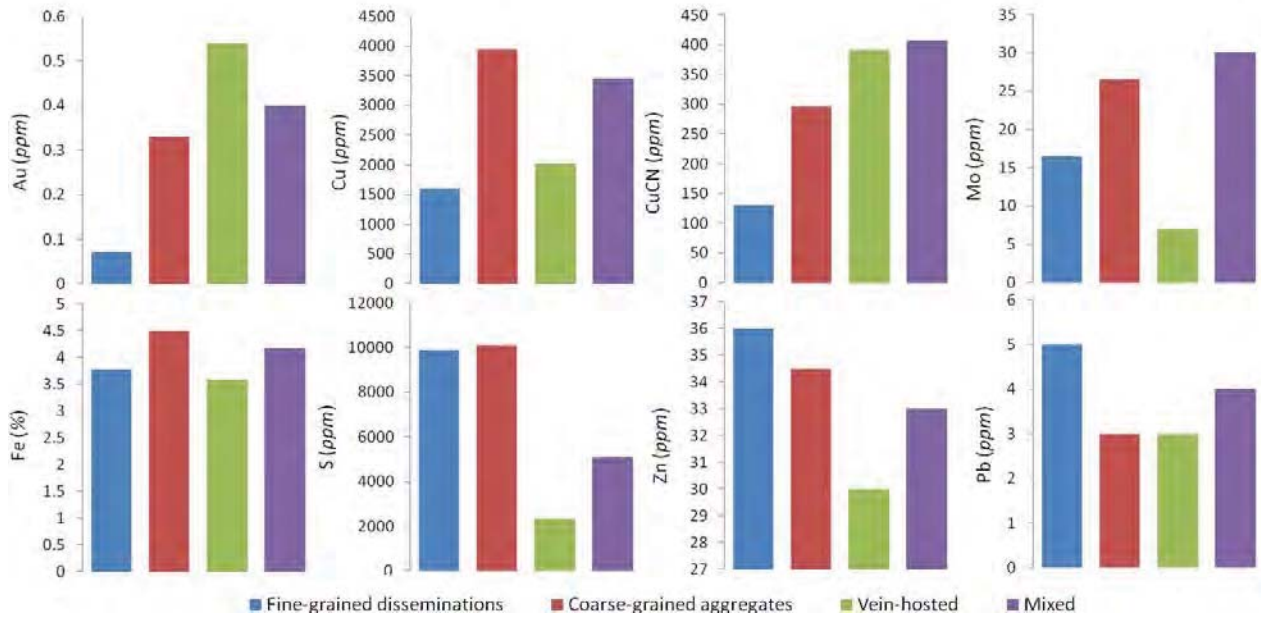

Figure 4.30. Histograms showing the median assay grades divided by the distribution of the copper-sulphide minerals (see section 3.2, this chapter). Assay data for CE082, CE098 and CE143 were provided by Newcrest Ltd.

Table 4.8. Statistical data for the assay grades divided by the distribution of copper-sulphide minerals for CE082, CE098 and CE143. Assay data provided by Newcrest Ltd.

	N	Au (ppm)	Cu (ppm)	CuCN (ppm)	Mo (ppm)	S (ppm)	Fe (%)	Zn (ppm)	Pb (ppm)
All 2 metre intervals									
Average	407	0.67	3310	783	44.51	10319	3.97	49.45	6.82
Standard Deviation		1.05	2986	1335	64.23	13874	1.59	110.75	14.44
Median		0.24	2340	275	17	4700	3.80	33	4
Fine-grained disseminations of Cu-sulphide minerals									
Average	142	0.24	2800	379	40.00	15233	3.77	56.82	6.63
Standard Deviation		0.492	3148	1000	57.13	13999	1.60	116.47	9.59
Median		0.07	1593	130	16.50	9875	3.78	36.00	5.00
Coarse-grained aggregates of Cu-sulphide minerals									
Average	26	0.51	4955	604	42.50	11958	4.40	37.19	5.08
Standard Deviation		0.63	3524	913	44.07	10486	1.59	15.37	6.61
Median		0.33	3945	296	26.50	10100	4.49	34.50	3.00
Vein Hosted Cu-sulphide minerals									
Average	125	1.21	2630	989	32.88	4028	3.78	46.38	5.93
Standard Deviation		1.48	1963	1371	56.92	6562	1.40	139.51	15.89
Median		0.54	2020	392	7.00	2370	3.59	30.00	3.00
Mixed Cu-sulphide minerals									
Average	114	0.65	4314	1102	59.79	10723	4.33	46.42	8.42
Standard Deviation		0.78	3194	1594	79.71	17339	1.69	74.92	18.55
Median		0.40	3455	407	30.00	5095	4.17	33.00	4.00

In section 4.5, the elements obtained from assays have been used to calculate the abundance of a number of minerals. For Cadia East, these minerals are chalcopyrite, bornite, pyrite, molybdenite, clausthalite (PbSe) and sphalerite. These calculated mineral abundances have been compared against the results of the visual logging. This will determine if any relationships exist between the quantified mineralogical data determined from assay and the visually logged attributes that were estimated based on their potential to influence mineral processing behaviours.

Figure 4.31 shows the percentages of chalcopyrite and bornite calculated from assay for each of the dominant gangue mineral types described from the meso-scale visual logging (see section 4.2, figure 4.2G, H, I and J). This figure shows that bornite is the most abundant in the intervals that have been logged as predominantly (>70%) chlorite-magnetite and albite-K-feldspar-quartz. Chalcopyrite is the most abundant in the intervals logged as albite-K-feldspar-quartz clasts with a matrix of chlorite-biotite. The intervals logged as chlorite-biotite contain minor abundances of both chalcopyrite and bornite and the lowest grades of chalcopyrite and bornite.

The abundance of pyrite in an ore as well as its proximity to the valuable mineral phases is important when considering the mineral processing potential and recovery of an ore. Figure 4.32 shows the calculated abundances of pyrite and chalcopyrite from assay for each of the different copper sulphide mineral distributions determined from the meso-scale visual logging (i.e. fine-grained disseminations, coarse-grained aggregates and vein-hosted). This figure shows that for the vein-hosted copper sulphide minerals there is only minor pyrite compared to chalcopyrite, except for several outliers which can be attributed to the presence of phyllic fault zones rich in pyrite (Wilson, 2003). For the fine-grained disseminations there appears to be a group that has low chalcopyrite and high pyrite (*red circle*) as well as a group that exhibits high chalcopyrite with a relatively low abundance of pyrite (*blue circle*). For the coarse-grained aggregates the pyrite abundance does not exceed the chalcopyrite abundance (except for one outlier).

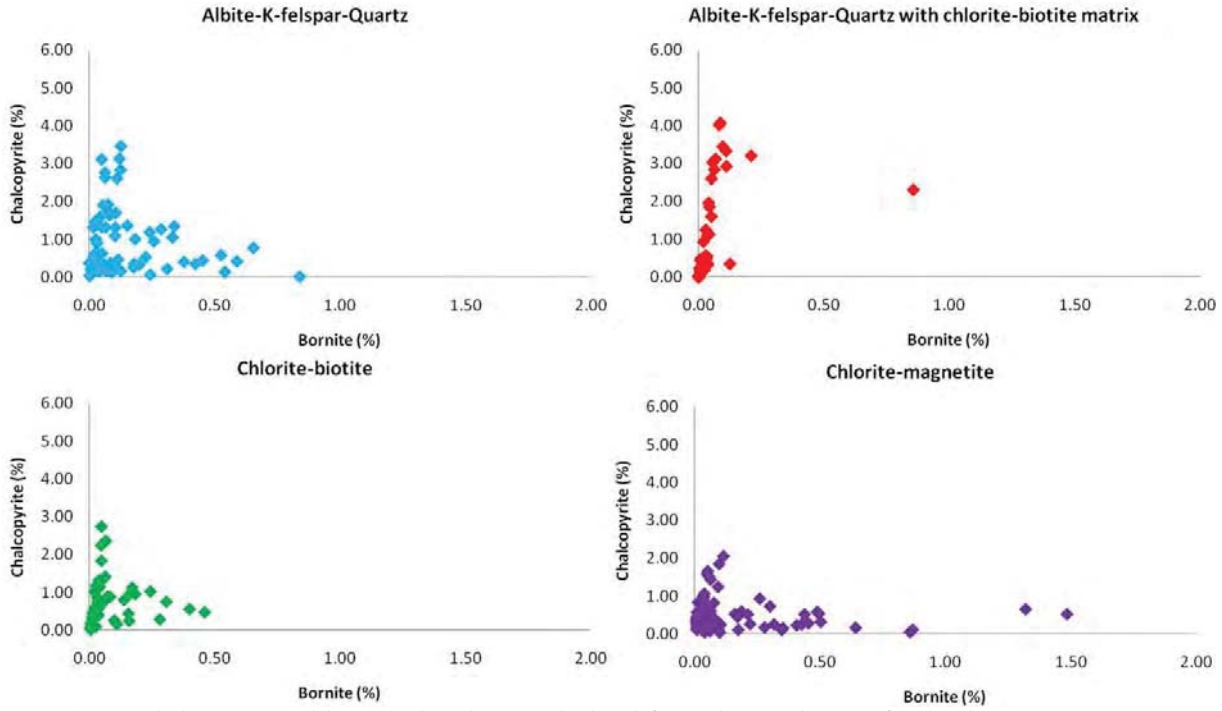

Figure 4.31. Chalcopyrite and bornite abundances calculated from elemental assays for the dominant (>70%) gangue mineral types (see section 4.2). Drill-holes CE082, CE098 and CE143. N = 298.

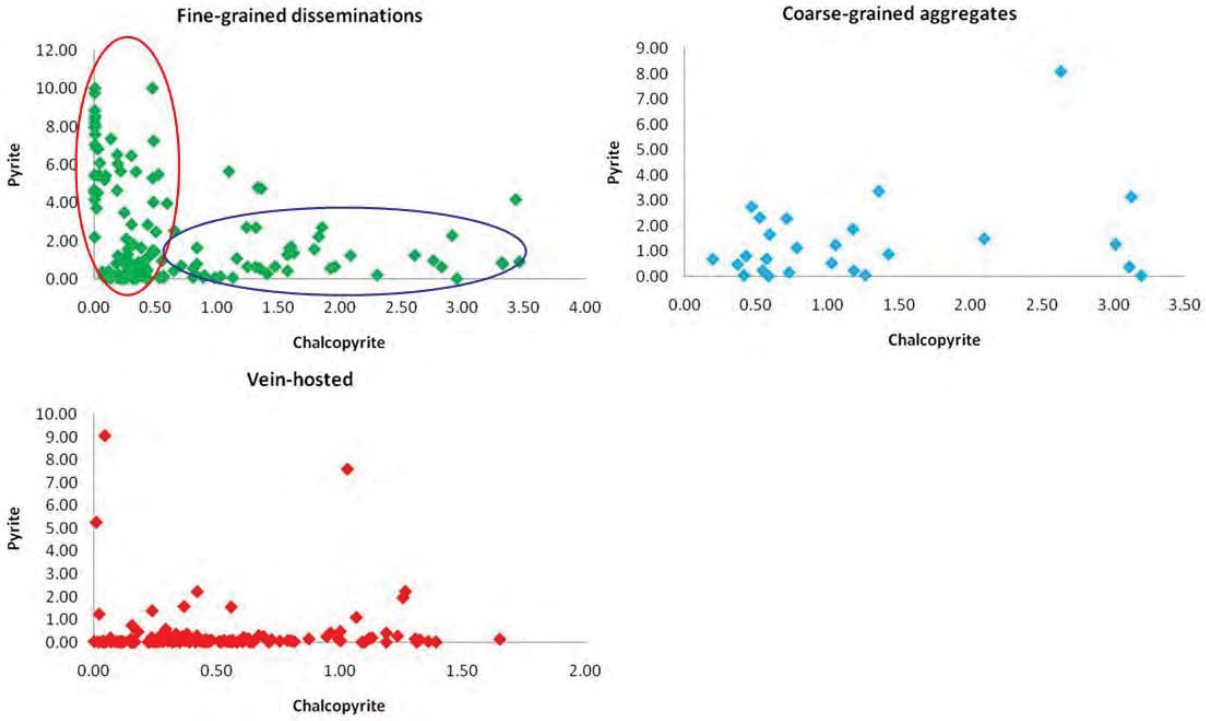

Figure 4.32. Chalcopyrite and pyrite abundances calculated from elemental assays for the dominant (>70%) distribution styles of the Cu sulphide minerals. (see section 4.2). Drill-holes CE082, CE098 and CE143. N = 293.

The determination of mineral species from assay can also be used to identify potential mineral associations for valuable mineral phases. Figure 4.33 illustrates the chalcopyrite and bornite abundances down-hole for CE143 plotted with the assay data for Au. These down-hole plots indicate areas where gold has a strong correlation with chalcopyrite (*green circles*) and bornite (*blue circles*). These data can be valuable in determining the dominant gold mineral associations for an ore type as well as where potential samples can be taken from for gold analyses.

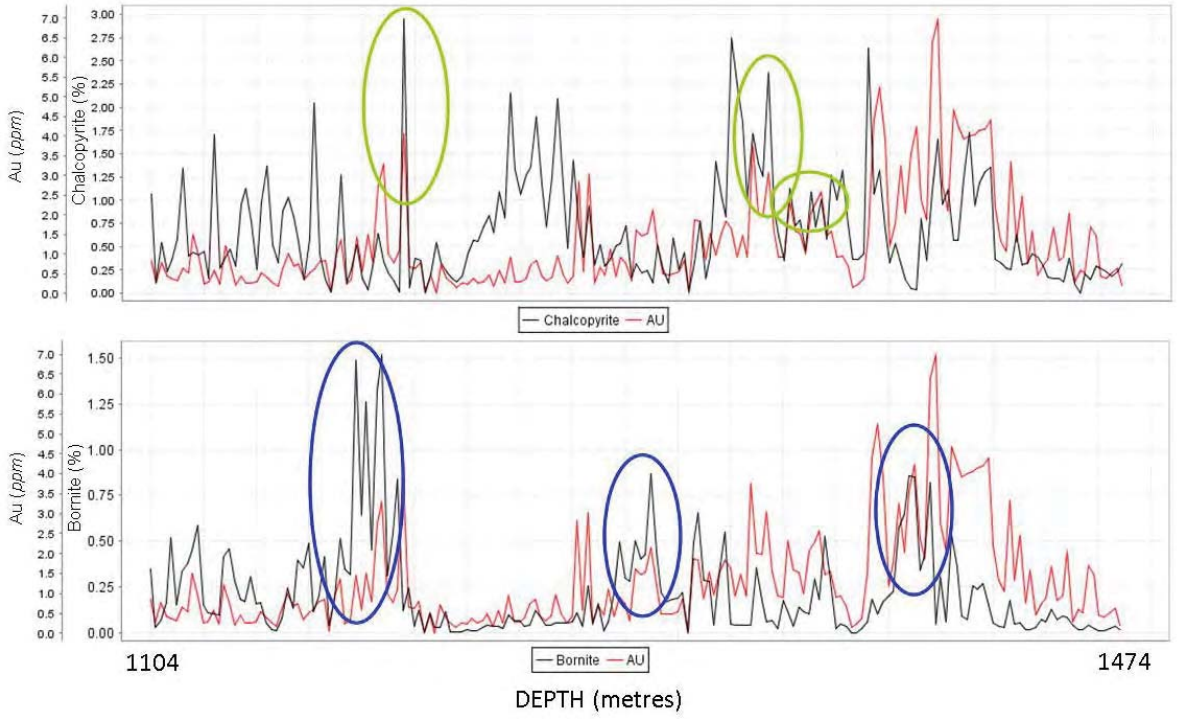

Figure 4.33. Calculated mineral abundances of chalcopyrite and bornite plotted with gold assay for CE143. Green circles indicate a gold-chalcopyrite correlation, blue circle indicate a gold-bornite correlation.

The mineral types that are directly associated with the chalcopyrite and bornite have also been logged. These are considered to directly affect the liberation potential of the valuable mineral phases. For the vein-hosted chalcopyrite and bornite, it is expected that the mineral associations will predominantly consist of quartz, calcite, epidote, fluorite and pyrite as well as other vein forming minerals that cannot be observed in hand specimen. For the fine-grained disseminations and coarse-grained aggregates, the chalcopyrite and bornite were observed to be associated with mafic minerals and less commonly felsic minerals. The types of mafic minerals that occur with chalcopyrite and bornite change with zones of alteration; however the textures remain predominantly the same. For example, the mafic minerals can include biotite, (potassic alteration), magnetite (potassic alteration) or epidote (propylitic and potassic alteration). This is also true where chalcopyrite disseminations and aggregates occur with felsic minerals. At Cadia East, the felsic minerals include albite (sodic alteration), K-feldspar (potassic alteration), sericite and quartz (phyllic alteration) which are also variable between different alteration zones (Wilson, 2003). It is proposed that for the fine-grained disseminations and coarse-grained aggregates of chalcopyrite and bornite, that the minerals directly associated with them and hence the most likely to influence their liberation potential are controlled by changes in alteration minerals. This will be investigated further using micro-scale analyses which are presented in Chapter 5.

4.5.2 The creation of meso-scale textural classes

The data from the visual logging of drill-core has been interrogated in order to determine the dominant mineralogical relationships and textures of the valuable minerals that are predicted to have unique mineral processing behaviours. The mineralogical and textural properties that were considered important at Cadia East have been used to determine meso-scale classes with potential differences in mineral processing behaviours. These are:

- Three styles of Cu-sulphide mineralisation: (1) fine-grained disseminations, (2) coarse-grained aggregates and (3) vein-hosted.
- Three dominant styles of gangue mineralogy that reflect the changes in alteration minerals: (1) mafic minerals (chlorite, biotite and epidote), (2) mafic minerals and magnetite, (3) felsic minerals (albite, K-feldspar and quartz).
- Four lithology styles: (1) fragmental (conglomerate and volcanoclastic), (2) fault zones (laumontitic, chloritic), (3) intrusive volcanic units and (4) the upper pyritic cap unit.

These properties and how they were used to define independent meso-scale textural classes are shown as a decision tree in Figure 4.34. There are four major textural classes and 13 sub-classes therein that have been created. These are described in Table 4.9 and photographic examples are shown in Figures 4.35 and 4.36. For each texture class the predicted mineral processing behaviours are listed in Table 4.10. For example, the gangue mineralogy of a rock can be considered to have the most effect on the initial rock crushing (e.g. King, 2001). The minerals in direct contact with the valuable mineral phases can be predicted to affect the grindability, liberation potential and flotability of an ore (e.g. Gaudin, 1957; King, 2001; Petruk, 2005). The size of the valuable mineral phase can be expected to affect the liberation potential and recovery (Jones, 1987).

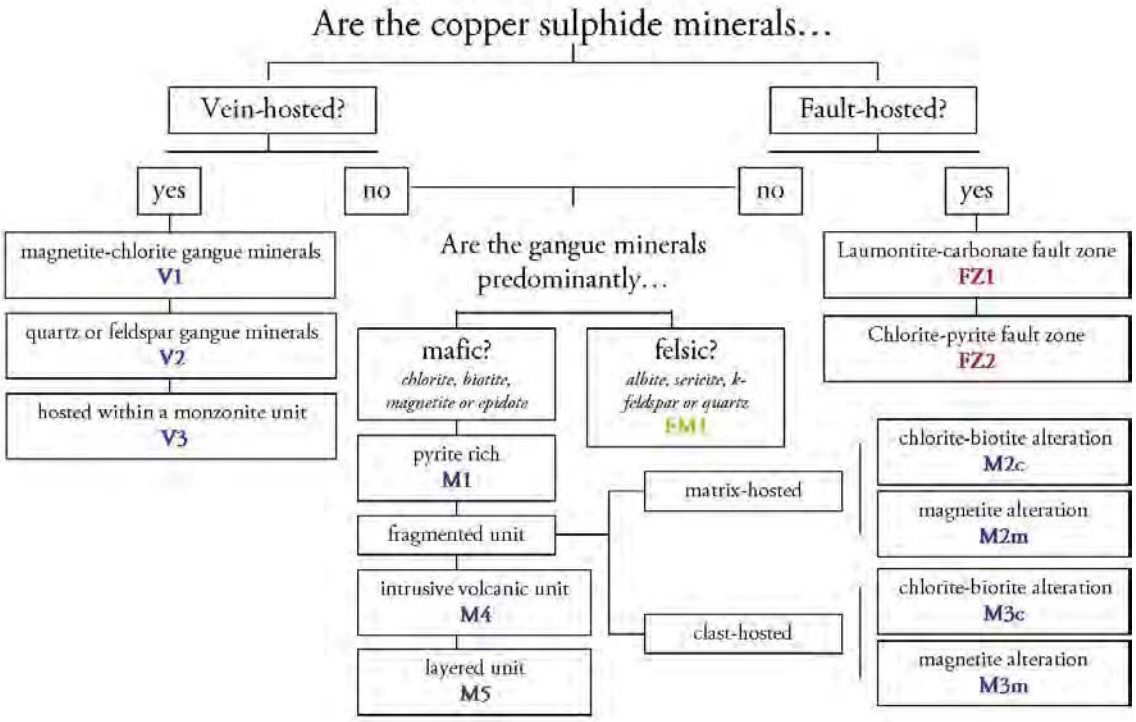

Figure 4.34. Decision tree illustrating the properties that were used to define the textural classes at Cadia East. The four major textural groups are vein-hosted (*purple text*), fault-hosted (*red text*), mafic gangue minerals (*blue text*) and felsic gangue minerals (*green text*).

A percentage of each textural class has been assigned to each two metre assay interval for drill-holes CE082, CE098 and CE143. These textural classes have been compared against grade and other geological attributes in order to assess if the class is unique and should remain part of the classification. Only the intervals that consist of 100% one class will be used to ensure that quantified measurements can be assigned to pure end-members only. All other intervals will be assigned the term 'mixture', allowing the validity of each group to be tested against existing assay data, on-site drill-core logs as well as new data that has been generated within this project (optical and MLA microscopy). In addition to the three drill-holes that have been described in this chapter, additional sampled intervals (approximately one every 10 metres) have been selected for analysis from the drill-holes CE109 and CE110.

The abundance of each textural class per two metre interval has been estimated and is given in Appendix 4.10.

Table 4.9. Mineralogical and textural characteristics of the meso-scale textural classes defined for Cadia East.

Major groups	Sub groups	Description
MAFIC HOSTED	**M1**	Pyrite is the dominant sulphide mineral. Chalcopyrite is fine-grained (<0.5mm) and typically associated with pyrite and the gangue minerals quartz - K-feldspar - chlorite/biotite - illite/muscovite in the upper lithological units (logged as volcanoclastic, volcanoclastic conglomerate and bedded volcanoclastic) of Cadia East (Figure 4.35A).
	M2m	Chalcopyrite with minor pyrite are the dominant sulphide minerals. Chalcopyrite typically occurs as fine-grained dissemination to coarse-grained aggregates (<35mm) in the matrix of breccia and conglomerate lithologies. It occurs with biotite-chlorite-magnetite ± illite-muscovite ± albite (Figure 4.35B).
	M2c	Same as M2m with **no** magnetite (Figure 4.35C).
	M3m	Chalcopyrite with minor bornite are the dominant sulphide minerals. Chalcopyrite and bornite typically occur as small aggregates of chalcopyrite (<8mm) coarsening up to 25mm in clots of chlorite-biotite-magnetite surrounded by K-feldspar-albite ± quartz (Figure 4.35D).
	M3c	Chalcopyrite is the dominant sulphide with minor occurrances of bornite and pyrite. Chalcopyrite occurs as fine-disseminations coarsening to large coarse- aggregates up to 20cm in clots of biotite-chlorite surrounded by K-feldspar-albite ± quartz (Figure 4.35E).
	M4	Chalcopyrite with minor pyrite are the dominant sulphide minerals. This texture is characterised by chalcopyrite that occurs as fine-grained disseminations in the igneous intrusions that occur in the upper portions of Cadia East (clinopyroxene porphyry, feldspar porphyry; Figure 4.35F).
	M5	Chalcopyrite with minor pyrite are the dominant sulphide minerals. This texture is characterised by chalcopyrite that occurs as fine-grained disseminations within the mafic laminations of the volcanoclastic sandstone units in the upper portions of Cadia East (Figure 4.35G).
FELSIC HOSTED	**FM1**	Chalcopyrite with minor bornite are the dominant sulphide minerals. Chalcopyrite occurs as aggregates of fine-grained to coarse-grained irregular clots with minor chlorite-biotite and typically associated with albite, K-feldspar or quartz (Figure 4.35H).
VEIN HOSTED	**V1**	Chalcopyrite and minor bornite are the dominant sulphide minerals. This texture is characterised by chalcopyrite in quartz – calcite ± bornite ± epidote veins hosted by a magnetite-chlorite gangue (Figure 4.35I).
	V2	Chalcopyrite and bornite are the dominant sulphide minerals, molybdenite occurs in minor amounts. This texture is characterised by chalcopyrite and bornite in quartz – calcite ± bornite ± epidote veins hosted by a quartz-K-feldspar gangue (Figure 4.36A).
	V3	Chalcopyrite is the dominant sulphide mineral. There are little or no non-vein sulphides present. This texture is characterised by chalcopyrite in quartz – calcite ± bornite ± epidote veins hosted within the monzonitic intrusion in Cadia East Deeps (Figure 4.36B).
FAULT HOSTED	**FZ1**	Chalcopyrite and pyrite are the dominant sulphide minerals. This texture is characterised by fine-grained to coarse-grained chalcopyrite hosted in a chloritic fault zone (Figure 4.36C).
	FZ2	Chalcopyrite and pyrite are the dominant sulphide minerals. This texture is characterised by fine-grained to coarse-grained chalcopyrite hosted in a calcite-laumontite-illite ± chlorite fault zone (Figure 4.36D).

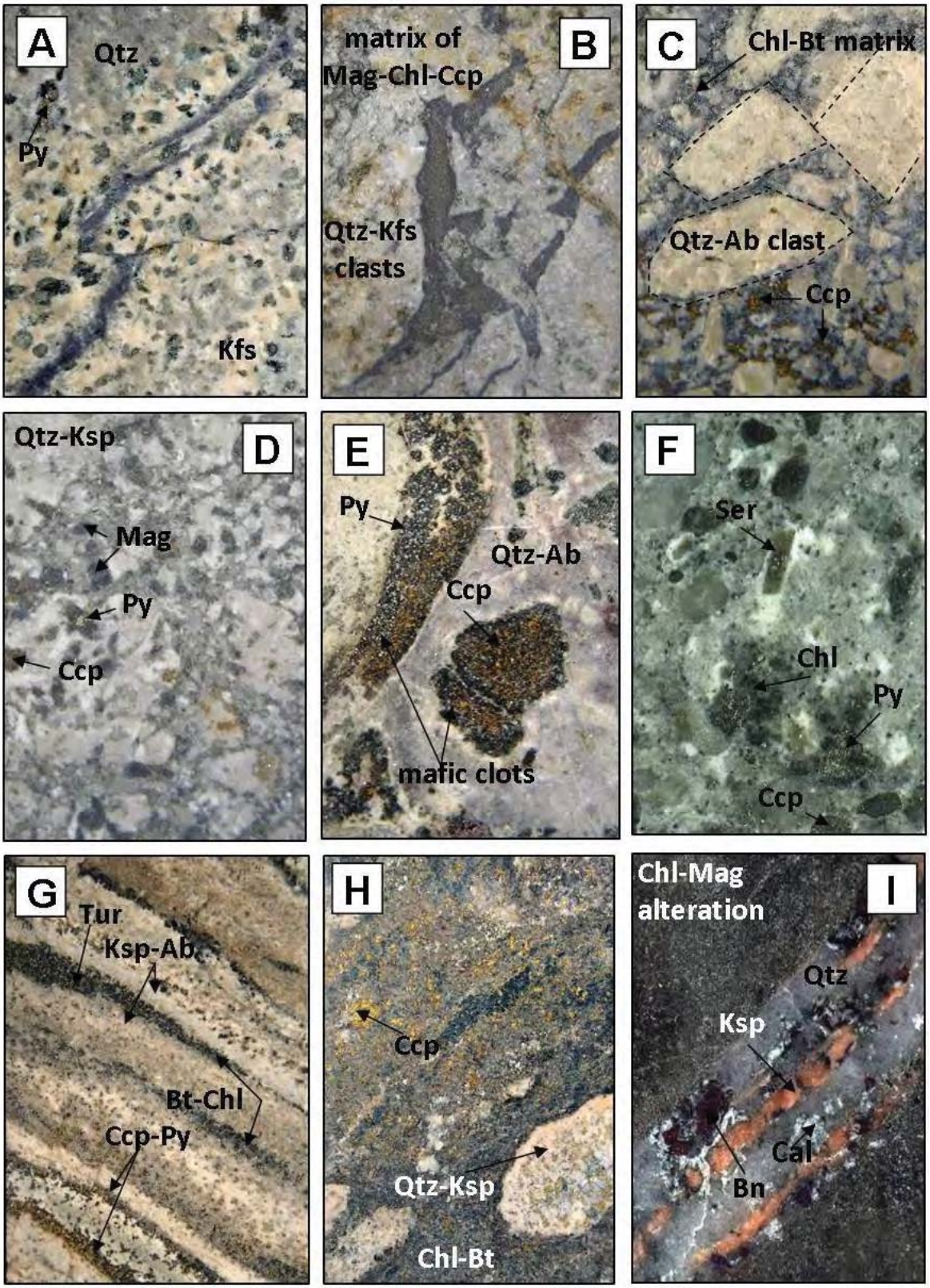

Figure 4.35. Cadia East texture classes (NQ core width - 5.5cm) **A** M1: chaclopyrite with mafic mineral association and high pyrite content **B** M2m: Chalcopyrite in a magnetite-chlorite matrix **C** M2c: Chalcopyrite in a chlorite-biotite matrix **D** M3m: Chalcopyrite hosted by clasts that have undergone magnetite alteration **E** M3c: Chalcopyrite hosted by clots of biotite-chlorite **F** M4: Chalcopyrite hosted by a feldspar-porphyry unit **G** M5: Chalcopyrite hosted within mafic layers of a volcaniclastic sand stone units **H** FM1: fine- and coarse-grained chalcopyrite associated with quartz and K-feldspar **I** V1: Chalcopyrite and bornite hosted in veins that cross-cut chlorite-magnetite gangue. For mineral abbreviations refer to Appendix 1.1.

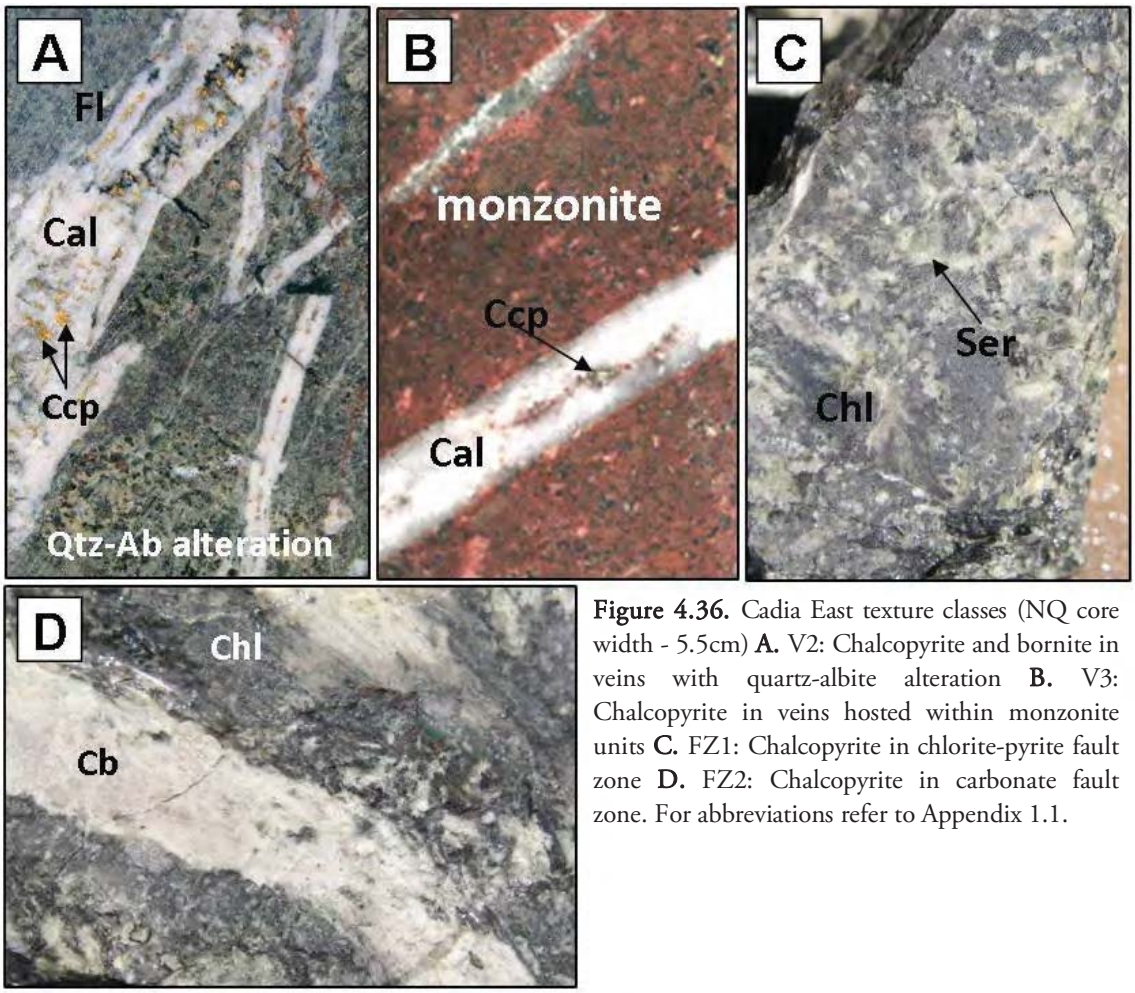

Figure 4.36. Cadia East texture classes (NQ core width - 5.5cm) **A.** V2: Chalcopyrite and bornite in veins with quartz-albite alteration **B.** V3: Chalcopyrite in veins hosted within monzonite units **C.** FZ1: Chalcopyrite in chlorite-pyrite fault zone **D.** FZ2: Chalcopyrite in carbonate fault zone. For abbreviations refer to Appendix 1.1.

Spatial Continuity of textural classes

The spatial continuity of the meso-scale textural classes has been examined in order to determine whether the classes occur over sufficient lengths to be suitable as a predictive tool for differences in mineral processing behaviours. For example, if a number of textures have been classified, but are randomly distributed throughout a deposit, then the spatial continuity of the textures will be smaller than a minable bench (typically on the scales of tens of metres) and therefore cannot be used in a working block model. Figure 4.37 illustrates the spatial continuity of the textural classes for CE082, CE098 and CE143. For CE082 there are two continuous zones of M1 (54 metres) and M2m (104 metres). For CE098 and CE143 the textures are less continuous and contain a higher proportion of mixed classes. CE098 contains a continuous length of the V1 texture class (52 metres). The remainder of the hole consists of M2C and M3c occurring intermittently with small zones of M4. CE143 contains a continuous length of the V3 texture which continues to depth (at least 62 metres). The remainder of the drill-hole consists of localized patches of V1 and V2 with small zones of M2m, M2c, M2m, M3c and M4.

Table 4.10. The predicted mineral processing characteristics of meso-scale textural classes for Cadia East.

Textural Class	Predicted effect on mineral processing
M1	High pyrite content can potentially affect flotation and grinding (Petruk, 2005). Pervasive silica and K-feldspar alteration is predicted to produce a competent, hard rock which has implications for crushability (Napier-Munn et al., 2005). The fine grain size of chalcopyrite and low abundance is predicted to hinder the liberation potential and recovery (Jones, 1987).
M2m	Chalcopyrite associated with magnetite-chlorite-biotite may have implications for liberation potential. The selective magnetite-chlorite-biotite alteration of the matrix material and quartz-K-feldspar-albite alteration of clasts is predicted to produce an ore type that is soft to crush and hard to grind. The difference in hardness between the two rock components (matrix and clast) will allow this weaknesses to be exploited during the crushing process, but can potentially result in coarse rock fragments that may require substantial energy to grind and recover valuable minerals (Gaudin, 1957).
M2c	Chalcopyrite associated with chlorite-biotite is predicted to have implications for liberation potential. Fine-grained mica minerals that are in direct contact with valuable phases could affect liberation potential as micas have the propensity to smear during grinding rather than break (Jones, 1987, Petruk, 2005). The selective chlorite-biotite alteration of the matrix material and quartz-K-feldspar-albite alteration of clast is predicted to produce an ore type that is soft to crush and hard to grind (Gaudin, 1957; see M2m).
M3m	Chalcopyrite associated with magnetite-chlorite-biotite clots may influence liberation potential and grinding behaviour (See M2c). The matrix of quartz, K-feldspar or albite alteration is predicted to increase the rock competency which will require substantial energy to crush (Napier-Munn et al., 2005).
M3c	The chalcopyrite in this texture is fine and coarse grained and occurs as aggregates, it is predicted that aggregate (clustering) nature of the chalcopyrite will improve the liberation potential of the fine grains (Gaudin, 1957). The coarse grained chalcopyrite can be assumed to break easily during crushing and expose enough free particle surface to be easily recovered during flotation. The matrix of quartz, K-feldspar or albite alteration is predicted to increase the rocks competency (hardness) which will require substantial energy to crush (Napier-Munn et al., 2005).
M4	The chalcopyrite in this texture is fine-grained and disseminated throughout intrusive igneous rocks that have been pervasively altered by quartz, K-feldspar or albite. It is predicted that this rock will be competent and hard which can require substantial energy during crushing (Napier-Munn et al., 2005). The fine-grained nature of the chalcopyrite is predicted to reduce the liberation potential of the chalcopyrite (Jones, 1987).
M5	The chalcopyrite in this rock forms fine to coarse grained clots that are hosted in the mafic (chlorite-biotite tourmaline) layers of the volcanoclastic sandstone units. The other layers are typically more competent quartz, albite or K-feldspar. The difference in hardness between the two rock components (mafic and felsic layers) will allow this weaknesses to be exploited during the crushing process, but can potentially result in coarse rock fragments that may require substantial energy to grind and recover valuable minerals (Gaudin, 1957).
FM1	The chalcopyrite in this texture is coarse, it typically occurs with the fine-grained intergrowths of chlorite-biotite that are observed in M3c, however the Cu grade is elevated and the coarse grained clots are now in direct contact with the pervasive quartz, albite or K-feldspar alteration. The coarse-grained nature of the chalcopyrite is predicted to be easy to liberate (Jones, 1987).
V1	Both chalcopyrite and bornite are hosted in veins which are typically in direct contact with the minerals quartz-calcite ± epidote ± fluorite. The chalcopyrite is mostly coarse which is predicted to improve the liberation potential of this texture class (Jones, 1987). The host rock is altered by magnetite which is predicted to crush differently than the rocks hosting the V2 and V3 textures.
V2	Both chalcopyrite and bornite are hosted in veins which are typically in direct contact with the minerals quartz-calcite ± epidote ± fluorite. The chalcopyrite is mostly coarse which is predicted to improve the liberation potential of this texture class (Jones, 1987). The host rock is pervasively altered by quartz which is expected to increase the hardness of the rock and require more energy to crush (Napier-Munn et al., 2005).
V3	Both chalcopyrite and bornite are hosted in veins which are typically in direct contact with the minerals quartz-calcite ± epidote ± fluorite. The chalcopyrite is mostly coarse which is predicted to improve the liberation potential of this texture class (Jones, 1987). The veins are hosted by a monzonite intrusion which has undergone intense K-feldspar alteration which is expected to increase the hardness of the rock and require more energy to crush (Napier-Munn et al., 2005).
FZ1	Chalcopyrite occurs as disseminations or fragments of other textures in a fault zone dominated by chlorite and pyrite. These fault zones are extremely soft and contain minerals that are likely to crush easily and smear during grinding (Napier-Munn et al., 2005). It is not known yet whether these fault zones will contain clay minerals that can form mineral coatings during the flotation process (Petruk, 2005). At Cadia East, fault zones have a softening effect that extends to 50m from the fault zone itself.
FZ2	Chalcopyrite occurs as disseminations or fragments of other textures in a fault zone dominated by carbonate and laumontite. These fault zones have direct implications for crushability. They also cause intense carbonate veining in the surrounding area which is predicted to reduce the rock competency and making it easier to crush (Napier-Munn et al., 2005).

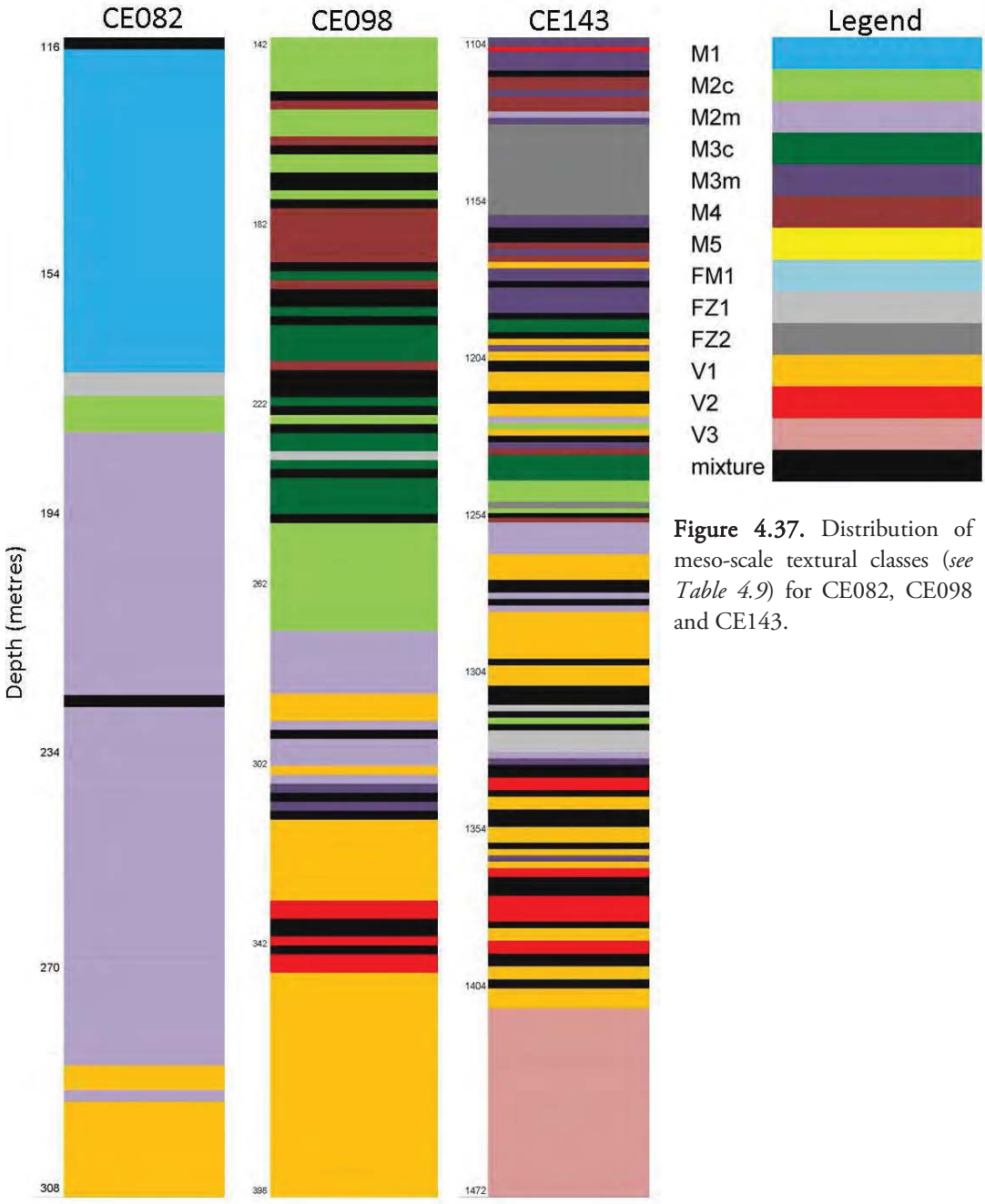

Figure 4.37. Distribution of meso-scale textural classes (*see Table 4.9*) for CE082, CE098 and CE143.

Each of the intermittent zones of textural classes are neighboring classes that predominantly contain similar minerals (e.g. M2c, M3c and M4: chlorite, biotite, feldspar) and belong to the same major textural groups (see Table 4.9). It is how these minerals are distributed throughout the rock that has led them to be classified as different classes. Further investigation will determine if these classes are unique and occur sporadically or whether some classes exhibit similar mineral processing behaviours and can be grouped together.

Textural classes related to assay data

In this section the meso-scale textural classes have been compared against the corresponding elemental assay data as well as the mineral abundances that were calculated from the same data. The mean, median and standard deviations for Au, Cu, CuCN, Mo, S, Fe, Zn, Pb as well as the

calculated bornite, chalcopyrite, molybdenite and pyrite abundances from assays are given in Table 4.11 for each textural class.

Table 4.11. The mean, median and mode for the elemental and mineral assays for each of the Cadia East texture classes.

Textural class		N	Assay (*ppm*)								Mineralogy (*calculated from assay*)			
			Au	Cu	CuCN	Mo	S	Fe (%)	Zn	Pb	Bn	Ccp	Mb	Py
M1	Mean	31	0.02	386.77	42.35	10.97	30574	3.15	48.68	6.35	0.01	0.10	0.00	5.65
	Median		0.01	37.00	5.00	1.00	29200	3.16	45.00	5.00	0.00	0.01	0.00	5.42
	StDev		0.02	793.90	105.61	24.37	13165	1.03	22.94	9.94	0.02	0.20	0.00	2.53
M2c	Mean	36	0.27	3976	514.61	47.78	16591	3.33	40.81	6.36	0.08	1.00	0.01	2.41
	Median		0.08	2540	172.50	25.50	14800	3.59	35.00	5.00	0.03	0.67	0.00	1.78
	StDev		0.41	3777	1265	62.52	10664	1.23	20.59	4.30	0.20	0.91	0.01	2.12
M2m	Mean	77	0.19	2156	247.66	21.97	5547	5.06	39.27	7.27	0.04	0.55	0.01	0.65
	Median		0.05	1750	170.00	13.00	4180	4.80	36.00	5.00	0.03	0.45	0.01	0.44
	StDev		0.54	1400	401.79	37.08	4501	1.29	12.31	10.76	0.06	0.37	0.00	0.73
M3c	Mean	25	0.38	7174	613.84	83.32	13892	2.75	40.60	16.48	0.10	1.89	0.01	1.31
	Median		0.26	6690	421.00	55.00	13550	2.18	28.00	5.00	0.07	1.83	0.01	0.89
	StDev		0.28	4437	709.58	73.31	7878	1.45	36.44	44.55	0.11	1.30	0.01	1.34
M3m	Mean	22	0.71	3755	2258	98.23	6373	4.51	63.68	4.91	0.36	0.43	0.01	0.74
	Median		0.51	2910	2101	73.50	2350	4.59	27.50	2.00	0.33	0.31	0.01	0.00
	StDev		0.64	2554	2281	100.60	12075	1.15	161.26	8.92	0.36	0.39	0.01	2.26
M4	Mean	19	0.39	4650	731.79	81.53	9826	2.83	43.58	8.58	0.12	1.13	0.01	1.04
	Median		0.21	4390	323.00	63.00	9630	2.67	30.00	5.00	0.05	1.09	0.01	0.77
	StDev		0.40	2944	902.73	69.06	7360	1.19	67.50	16.27	0.14	0.92	0.01	1.23
M5	Mean	2	0.45	4898	388.00	63.00	16875	2.44	16.50	1.50	0.06	1.30	0.01	2.27
	Median		0.45	4898	388.00	63.00	16875	2.44	16.50	1.50	0.06	1.30	0.01	2.27
	StDev		0.59	4826	267.29	77.78	6399	0.72	4.95	0.71	0.04	1.32	0.01	2.08
FM1	Mean	19	0.40	10798	527.26	178.37	17890	2.90	32.21	11.63	0.08	2.97	0.02	1.35
	Median		0.32	9195	445.50	140.50	17675	2.73	25.50	7.00	0.07	2.51	0.02	1.34
	StDev		0.28	6032	338.93	162.70	7907	0.96	30.57	11.30	0.05	1.67	0.02	0.84
V1	Mean	89	0.88	2707	913.22	49.06	3864	4.69	53.85	7.35	0.14	0.53	0.01	0.33
	Median		0.24	2290	387.00	24.00	2370	4.31	32.00	3.00	0.06	0.43	0.00	0.03
	StDev		1.40	1978	1198	102.75	5801	1.55	163.79	23.27	0.19	0.46	0.01	1.02
V2	Mean	15	1.82	3408	1142	65.20	9044	3.09	35.80	4.27	0.18	0.65	0.01	1.18
	Median		0.93	3490	446.00	4.00	4200	2.45	36.00	4.00	0.07	0.62	0.00	0.15
	StDev		1.87	1578	1778	95.34	14296	1.41	10.14	2.09	0.28	0.43	0.01	2.68
V3	Mean	30	1.64	1981	475.03	3.80	3002	2.76	22.90	4.03	0.08	0.44	0.00	0.24
	Median		1.19	1320	307.00	3.00	2100	2.81	20.00	4.00	0.05	0.30	0.00	0.10
	StDev		1.35	1805	466.03	4.03	3194	0.70	10.38	1.52	0.07	0.43	0.00	0.42
FZ1	Mean	7	0.57	4503	454.14	75.21	29117	4.42	108.36	6.07	0.07	1.17	0.01	4.64
	Median		0.47	4095	290.50	39.00	8875	3.07	38.50	3.50	0.05	0.99	0.01	0.69
	StDev		0.43	3612	440.21	87.33	39281	3.12	249.34	5.61	0.07	1.03	0.01	7.14
FZ2	Mean	17	0.56	4409	1584.4	118.60	7370	3.20	174.60	62.70	0.25	0.82	0.02	0.71
	Median		0.49	4520	1461.5	119.50	3500	3.02	22.00	2.00	0.23	0.78	0.02	0.00
	StDev		0.31	826.66	902.51	56.57	9985	0.82	476.30	190.55	0.14	0.41	0.01	1.65

Based on the mineral abundances calculated from assays for bornite, chalcopyrite, pyrite and molybdenite, Figure 4.38 shows boxplots for each of the textural classes at Cadia East. This figure shows that FM1 and M3c have the highest grade of chalcopyrite and FZ2 and M3m have the highest grade of bornite of the 13 textural classes. The vein-hosted classes (V1, V2, V3) exhibit grades of 0 - 1.5% and 0 - 0.3% for chalcopyrite and bornite respectively, with only small interquartile ranges. As expected, the FZ1 and M1 classes exhibit the highest abundance of pyrite. For molybdenite, the highest grade was observed in the FM1 texture.

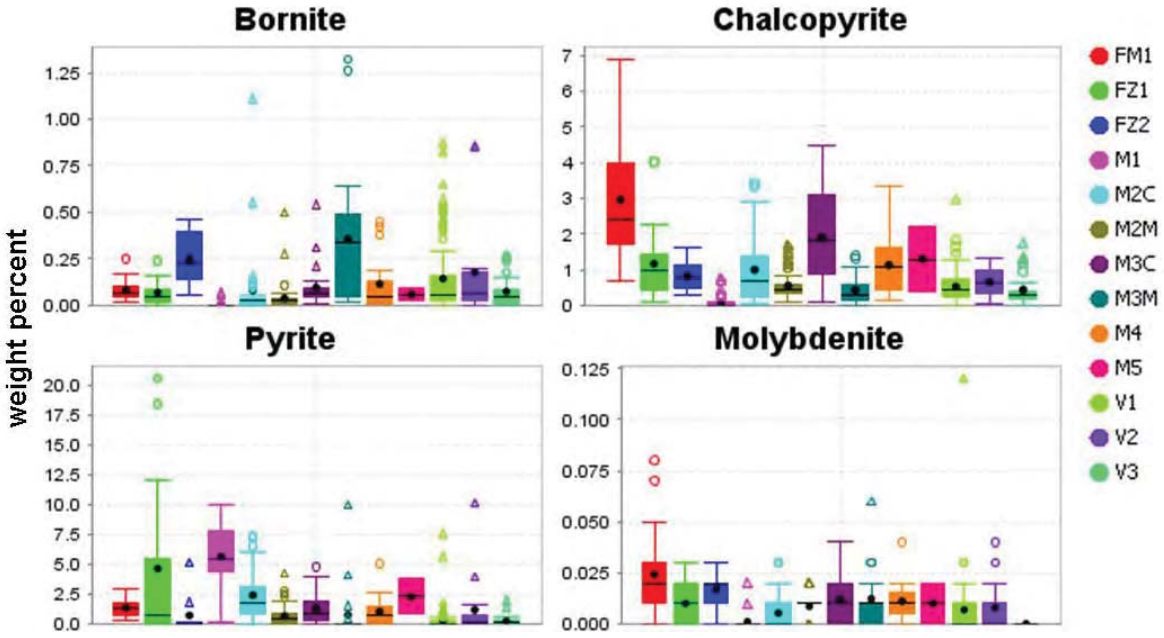

Figure 4.38. Boxplots for chalcopyrite, bornite, pyrite and molybdenite abundances calculated from assays for each texture class from Cadia East.

The location of gold minerals in any deposit type can be difficult to determine without the microscopic analysis of a large number of samples. Au can be associated with a large number of elements (e.g. Cu, Ag, Te; Petruk, 2005); however this does not mean that they occur as part of the same mineral. For example, Au can be associated with Cu in a vein dominated system. However, the gold minerals do not necessarily have to occur as inclusions within the Cu minerals or as part the lattice. They can occur with other vein minerals, or in the vein selvage itself. Figure 4.39 illustrates the Au and Cu grades plotted for each of the textural classes. The classes have been plotted separately in order to better observe any existing trends. In this figure, the vein-hosted texture-classes (V1, V2, and V3) are shown to have a positive Au and Cu trend with more Au occurring in the classes than any of the others. This does not mean there is not gold hosted by any of the other textures, in fact the plots for the mafic- and felsic-hosted textures show two distinct trends: high Cu with low Au, and Au increasing with Cu.

The Cu-sulphide species for each texture are shown in Figure 4.40. This figure shows that the vein-hosted texture classes, V1 and V2 as well as M3m and Fz2 have elevated abundances of bornite.

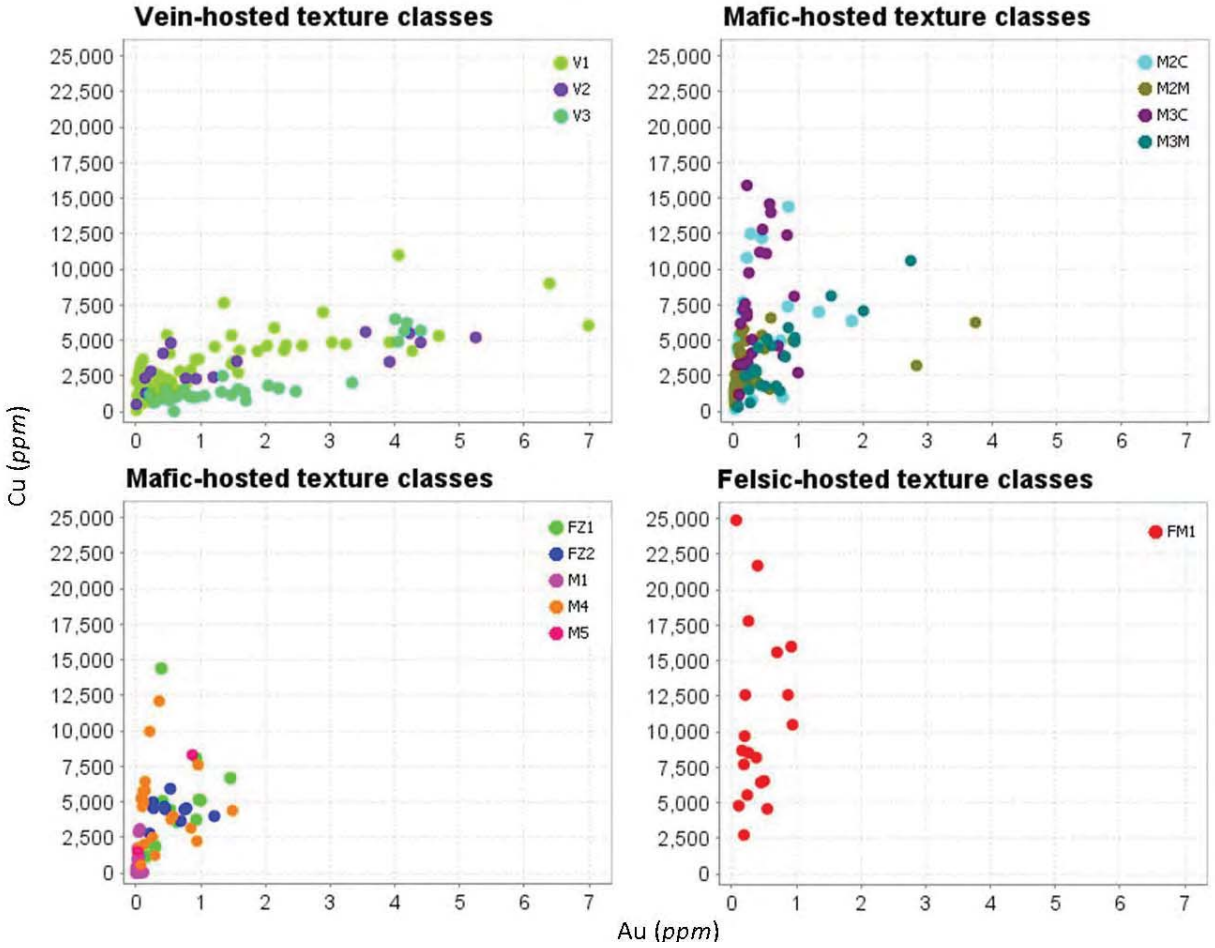

Figure 4.39. Au (ppm) versus Cu (ppm) for each of the meso-scale textures classes from Cadia East.

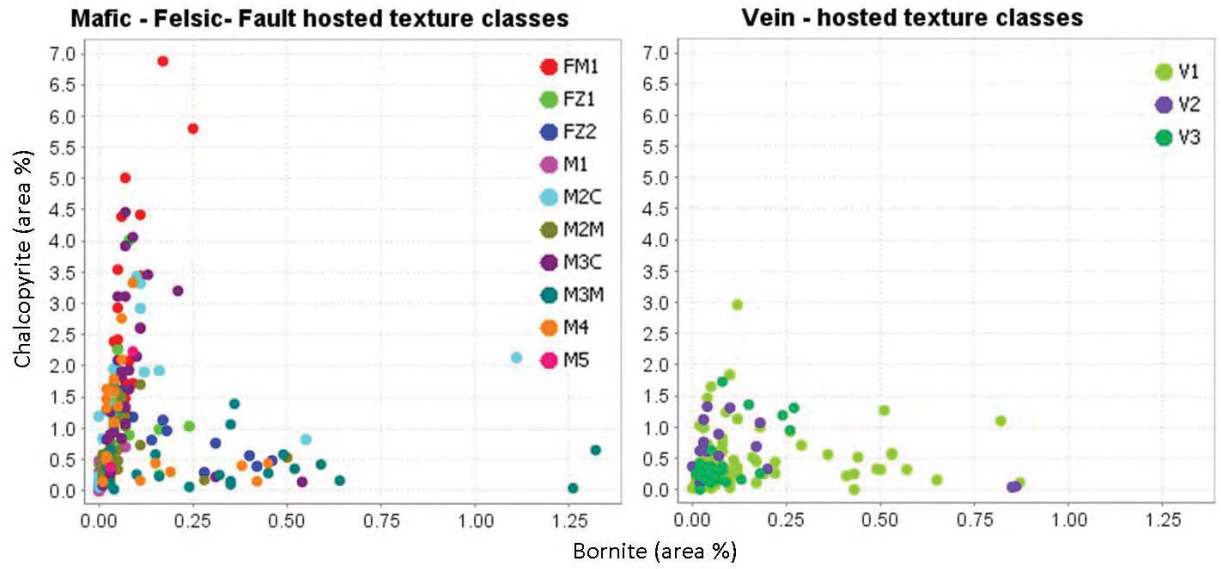

Figure 4.40. Graphs showing bornite (*area percent*) versus chalcopyrite (*area percent*) for each of the meso-scale texture classes from Cadia East. The mineral weight percentages have been calculated from assay.

From the elemental assays, the Fe % and the S (ppm) can be used to display trends related to the presence of the minerals magnetite and pyrite. For example, samples that are rich in pyrite with minor occurrences of magnetite will plot on a trend extending from (0,0) to the top right corner of a graph of S (ppm) versus Fe %. This trend is observed in texture classes M1 and FZ1 in Figure 4.41.

Alternatively, samples rich in magnetite will plot along a vertical line to the left of the graph. This trend is observed in the texture classes V1, M2m and M3m (Figure 4.39). All other samples rich in Fe bearing minerals such as feldspars, biotite, epidote etc. will plot between these trends.

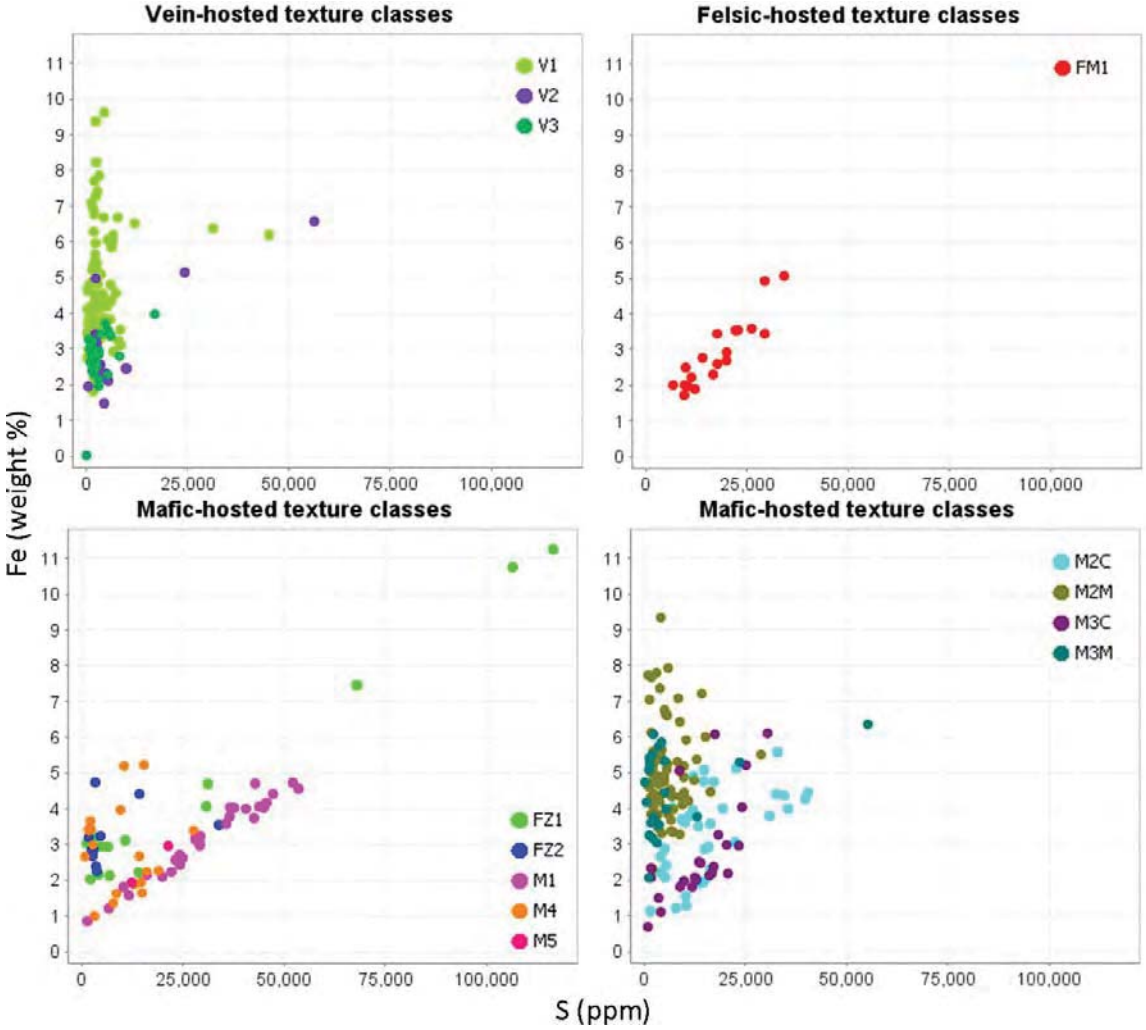

Figure 4.41. Graphs showing S (*ppm*) versus Fe (*percent*) for each of the meso-scale texture classes from Cadia East. Element abundances have been obtained from site assays.

Texture classes related to on-site geological logging

During the development of the visual logging method, it was proposed that lithology and other geological boundaries are not ideal as proxies for selecting zones with different mineral processing behaviours. In this section, the meso-scale texture classes have been compared against selected attributes obtained from geology drill-hole logs from site. Shown in Table 4.12 are the percentages of the different lithologies, alteration styles and major alteration minerals for each texture class logged by the Cadia East geologists. The definitions of each alteration style at Cadia East are presented in Table 4.13. Where a single lithology, alteration style or major alteration mineral exceeds 80% it is highlighted *green*. Apart from the M1 and V3 texture classes, which were characterised by an alteration style and lithology respectively, only three textures contained one dominant alteration style or mineral.

Table 4.12. The percentages of each lithology, alteration style and major alteration mineral logged by the Cadia East geologists for each of the textural classes defined by the meso-scale logging method used in this project. Where a texture class consists of >80% of one lithology, alteration style or alteration style it is highlighted *green.*

Texture classes	M1	M2c	M2m	M3c	M3m	M4	M5	FM1	FZ1	FZ2	V1	V2	V3
n	31	36	77	25	22	19	2	19	7	17	89	15	30
Lithology													
Pyroxene-Feldspar Porphyry	0	14	32	0	0	32	0	16	0	0	3	0	0
Feldspar Porphyry	0	6	0	0	5	0	0	0	0	65	7	40	3
Volcaniclastics – conglomerate	78	47	55	64	45	21	0	74	29	0	18	0	0
Volcaniclastics – bedded	6	8	0	0	0	0	50	0	0	0	24	20	0
Volcaniclastics – Angular fragments	0	3	0	0	0	5	0	0	0	0	0	0	0
Volcanicalstic	0	14	3	20	27	16	0	10	57	0	11	33	0
Volcanics - massice	0	0	7	0	0	5	0	0	0	0	26	0	0
Breccia	10	0	0	0	0	0	0	0	0	0	0	0	0
Fault – cataclasite	0	0	0	0	0	0	0	0	14	0	0	0	0
Fault – structure	0	0	0	0	0	11	0	0	0	6	1	0	0
Mixed	6	8	0	8	23	5	50	0	0	29	8	7	7
Monzonite	0	0	0	0	0	0	0	0	0	0	0	0	90
Altered/ Not identifiable	0	0	0	8	0	5	0	0	0	0	0	0	0
Alteration Style													
Albite/Pyrite Sodic	10	3	0	20	0	5	50	47	0	0	0	0	0
Pervasive potassic	0	6	0	16	14	5	0	5.5	14	0	20	40	100
Phyllic cap	90	42	0	40	0	32	50	21	43	0	0	0	0
Inner Propylitic	0	31	96	8	68	37	0	0	0	88	35	50	0
Regional Propylitic	0	0	0	0	0	0	0	0	0	0	0	0	0
Skarn-peripheral	0	0	0	0	0	0	0	0	0	0	25	0	0
Transitional	0	10	0	12	0	21	0	21	0	0	0	0	0
Unknown	0	8	4	0	14	0	0	5.5	43	12	19	20	0
Mixed	0	0	0	4	4	0	0	0	0	0	1	0	0
Major Alteration mineral													
Albite	0	0	0	0	4.5	0	0	0	0	24	2	0	0
Biotite	0	6	0	16	9	5	0	0	14	0	8	20	0
Carbonate	0	0	0	0	0	0	0	0	0	0	0	0	0
Chlorite	0	28	51	4	23	0	0	5.5	14	0	53	33	0
Epidote	0	8	0	0	0	0	0	0	0	0	0	0	0
K-feldspar	0	0	1	8	36	32	0	0	0	48	2	0	0
Magnetite	0	3	8	16	9	11	0	0	0	0	19	0	0
Pyrite	0	0	1	0	0	0	0	0	44	0	0	0	0
Reddening	0	0	36	0	0	0	0	5.5	0	0	8	13	94
Sericite	0	19	0	4	4.5	11	0	0	0	0	5	7	0
Silica	10	22	0	48	0	41	50	89	14	6	2	20	3
Silica/Abite	90	6	0	0	0	0	0	0	14	0	0	0	0
Mixed	0	8	3	4	14	0	50	0	0	24	1	7	3

Table 4.13. Descriptions of the alteration styles used in the logging of drill-core at Cadia East. *Descriptions courtesy of Newcrest Ltd.*

Alteration code	Alteration style	Minerals
Ap	Albite/Pyrite Sodic	Albite-quartz-sericite-pyrite
Kp	Pervasive potassic	Biotite-actinolite-magnetite-K-feldspar-albite
Pc	Phyllic cap	Sericite-albite-quartz-pyrite-tourmaline
Pi	Inner Propylitic	Reddening, chlorite, epidote, magnetite, K-feldspar, albite
Pr	Regional Propylitic	Chlorite-epidote-carbonate-prehnite
Sp	Skarn-peripheral	Epidote-carbonate-magnetite-chlorite
Tr	Transitional (Sodic to Propylitic)	See Ap, Pi and Pr (*above*)

The presence of disseminated magnetite has also been logged by the site geologists. Figure 4.42 shows the estimated abundance of disseminated magnetite for each of the textural classes, ranked from the lowest to highest abundance (*N Score*). Based on the site drill-core logs, texture classes M2m, M3m and V1 are predominantly logged as having disseminated magnetite. While this

is expected, it also confirms that there are attributes present in the existing drill-core logs that can be useful if the presence of magnetite is confirmed as affecting any aspect of mineral processing behaviours.

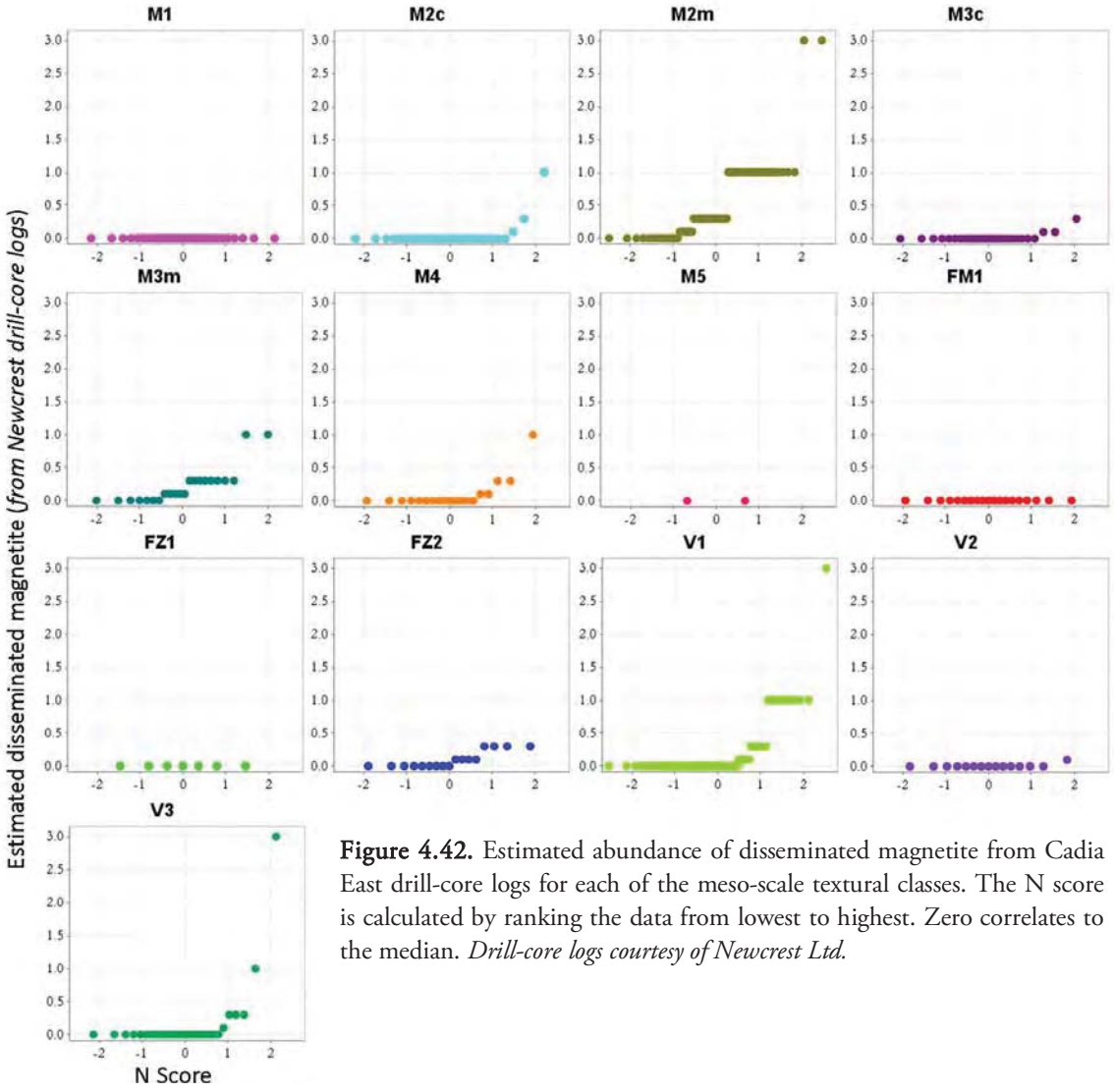

Figure 4.42. Estimated abundance of disseminated magnetite from Cadia East drill-core logs for each of the meso-scale textural classes. The N score is calculated by ranking the data from lowest to highest. Zero correlates to the median. *Drill-core logs courtesy of Newcrest Ltd.*

4.5.3 Summary

An interpretation of the meso-scale mineralogical and textural analysis for Cadia East has been presented in section 4.5. In this section, only the results of the meso-scale visual logging were considered due to the images of drill-core at Cadia East not being of a standard that can be used for classification purposes in this research.

The visually logged mineralogical and textural attributes from Cadia East were chosen to help identify possible rock characteristics that may to influence mineral processing behaviours. These properties are the size and distribution of the valuable minerals, chalcopyrite and bornite; the lithology styles i.e. fragmental, faulted, intrusive volcanic and pyrite rich (see Table 4.10); and the dominant gangue mineral types. Based on these properties, four major and thirteen sub- texture classes were identified (see Table 4.9). As a result, each two-metre interval from drill-holes CE082, CE110 and CE143 were assigned a texture class or mixture of texture classes. The distribution of the

texture classes has been presented for CE082, CE110 and CE143 in order to determine if these classes were spatially continuous or sparsely distributed. In addition to this, the results of elemental assays, the mineral abundances calculated from assays and the geological logging previously undertaken by the site geologists at Cadia East have been compared to each of the meso-scale texture classes. This allows any of these classes that have unique quantifiable attributes that can be used as a proxy for texture to be determined.

4.6 Interpretations from Ernest Henry

As discussed in the previous section for Cadia East (section 4.5), the aim of the visual logging of drill-core was to establish a method for identifying mineralogical and textural attributes that have the potential to influence mineral processing behaviours. In this section for Ernest Henry, the textural classes created from visual logging have been compared to the results of mineralogical and textural attributes extracted from the classified images of drill-core as well as chemical and mineral assays (see Chapter 3, section, 3.7), and drill-core logging from site geologists.

4.6.1 Interpretations of meso-scale visual-logging

In section 4.3, data was presented from the visual logging of meso-scale mineralogical and textural attributes. Here these attributes are compared with the mineral abundances calculated from assays for chalcopyrite, molybdenite, pentlandite and aresenopyrite. The distribution of these mineral abundances down-hole is shown for EH635 in Figure 4.43. A comparison of the distribution of chalcopyrite down-hole to the estimates from the visual logging of chalcopyrite clots shows that similar trends are observed (see Figure 4.12B).

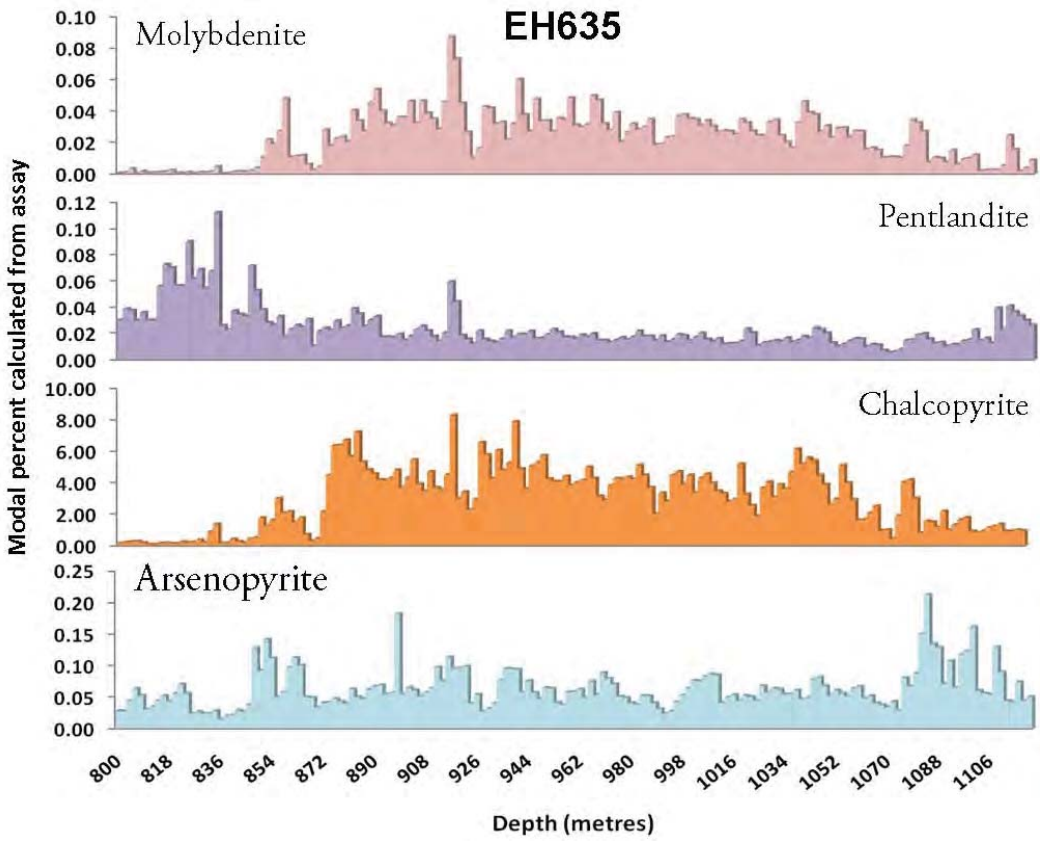

Figure 4.43. EH635 down-hole mineral abundances for **A.** molybdenite **B.** pentlandite **C.** chalcopyrite **D.** arsenopyrite.

It has been proposed that a majority of the Cu grade at Ernest Henry is hosted by the mineralised clots. The presence of mineralised clots (Figure 4.11E) is observed to be more abundant in the rocks exhibiting fragmental and mottled textures (see Figure 4.11A and B). Table 4.14 shows the mean, median and standard deviations of the Cu, Au, S, Fe, Mo, As, Co, Ni as well as chalcopyrite assay grades for intervals that have been logged as > 3% mineralised clots, <3% mineralised clots and no mineralised clots. For example, the median grades for Au, Cu, Mo and Fe increase with the presence of mineralised clots. The median for Au in intervals with no mineralised clots is 0.17 ppm compared to 0.69 ppm for intervals with > 3.00% mineralised clots.

Table 4.14. The mean, median and standard deviation (Stdev) of elemental and mineral assays for each meter intervals logged as >3.00%, 0 ≤ 3.00% and 0.00% mineralised clots. For mineral abbreviations see Appendix 1.1.

Percent mineralised clots	Statistics	N	Cu (ppm)	Au (ppm)	S (ppm)	Fe (%)	Mo (ppm)	As (ppm)	Co (ppm)	Ni (ppm)	Ccp (%)
0.00	Mean	73	8050	0.38	33278	18.09	125	385	477	103	2.32
	Median		5200	0.17	24300	16.56	59	240	430	55	1.50
	Stdev		7743	0.41	26853	7.82	129	487	369	193	2.24
0 ≤ 3.00	Mean	102	9666	0.46	34330	20.48	151	362	510	73	2.79
	Median		7550	0.34	32050	20.47	153	294	513	60	2.18
	Stdev		7009	0.40	17352	8.18	103	238	233	48	2.02
> 3.00	Mean	120	13803	0.70	45418	24.57	233	296	561	69	3.99
	Median		13850	0.69	38800	24.65	235	263	496	57	4.00
	Stdev		5786	0.34	26426	6.09	113	146	296	45	1.67

At Ernest Henry, two trends for the distribution of gold minerals have been observed. Figure 4.44 shows Au versus chalcopyrite (calculated from assays) for six drill-holes. This figure shows two distinct trends that are both associated with an increase of chalcopyrite. Given that both Au associations are with chalcopyrite, the different trends may be a result of different chalcopyrite textures which supports the results shown in Table 4.14. As with Cadia East, the exact mineral associations will require further micro-scale analysis.

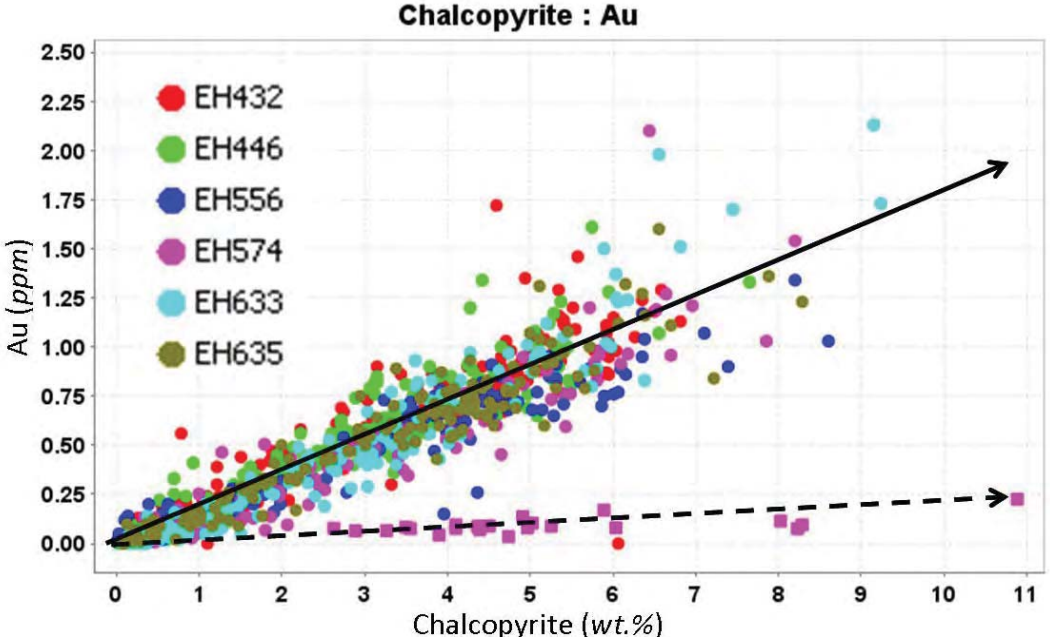

Figure 4.44. Chalcopyrite abundance (calculated from assay) plotted against Au grade (ppm) for drill holes EH432, EH446, EH556, EH574, EH633 and EH635. Each point represents a two-metre assay interval. There are two distinct gold-chalcopyrite trends shown by the solid and dashed arrows. n=1235.

4.6.2 The creation of meso-scale textural classes

The data from the visual logging of drill-core has been interrogated in order to determine the dominant mineralogical relationships and textures that have the potential to affect the processing and recovery of the valuable minerals. These relationships have been used to determine meso-scale classes for Ernest Henry. These are:

- Three dominant gangue textures: (1) fragmental (clasts and matrix clearly defined), (2) mottled (clast textures have been destroyed by alteration) and (3) massive (rock is dominated by one mineral).
- Four dominant styles of gangue mineralogy: (1) feldspar, (2) calcite (with minor quartz), (3) magnetite and (4) pyrite.
- Two dominant chalcopyrite sizes: (1) coarse-grained mineralised clots and (2) fine- to coarse-grained disseminations.

These properties and how they were used to define independent meso-scale textural classes are shown as a decision tree in Figure 4.45. This resulted in three major textural classes with nine sub-groups. Examples of the classes are shown in Figure 4.46. The nine sub-groups represent the competency of the rock and the dominant gangue minerals. Each of these classes was assigned one of two suffixes which represent sulphide deportment (D – disseminated, C – clotted). The meso-scale textural classes for Ernest Henry and their predicted influence on the mineral processing behaviours are described in Table 4.15.

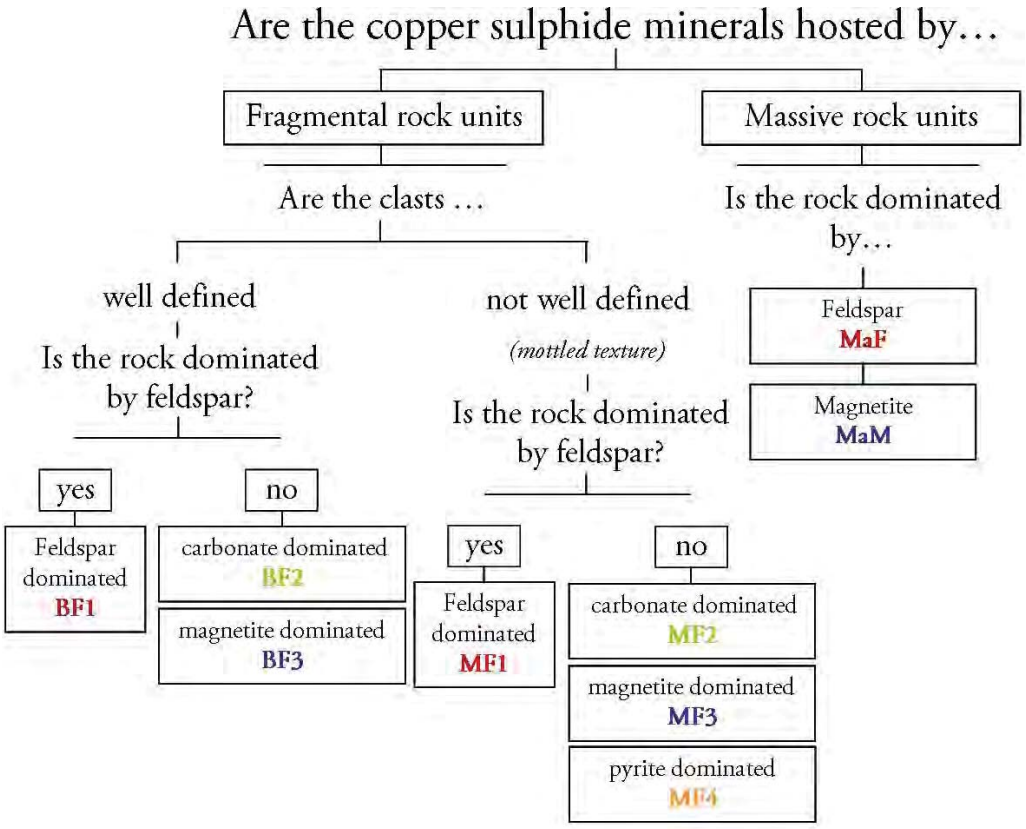

Figure 4.45. Decision tree illustrating the meso-scale mineralogical and textural features at Ernest Henry.

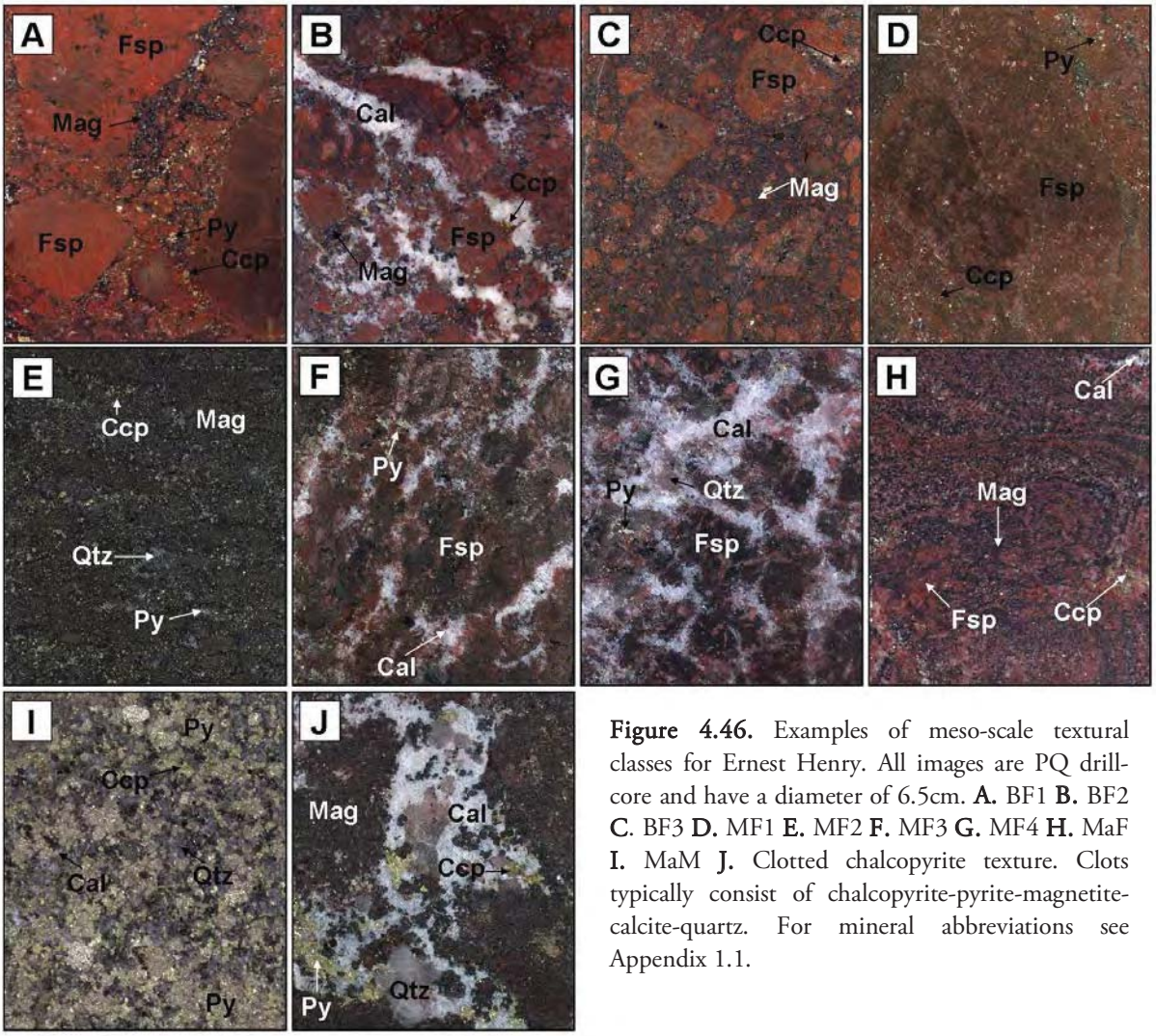

Figure 4.46. Examples of meso-scale textural classes for Ernest Henry. All images are PQ drill-core and have a diameter of 6.5cm. **A.** BF1 **B.** BF2 **C.** BF3 **D.** MF1 **E.** MF2 **F.** MF3 **G.** MF4 **H.** MaF **I.** MaM **J.** Clotted chalcopyrite texture. Clots typically consist of chalcopyrite-pyrite-magnetite-calcite-quartz. For mineral abbreviations see Appendix 1.1.

The percentage of each textural class in each two metre assay interval has been logged for the drill-hole EH635 and the sampled intervals of drill-holes EH432, EH446, EH556, EH574 and EH633. These textural classes have been compared against the mineralogical and textural attributes that were extracted from the classified images of drill-core. This will determine if each of the meso-scale visual classes exhibits quantifiable attributes that allow them to be recognised from data extracted from the classified images. Only the intervals that consist of 100% one class are used to ensure that quantified measurements can be assigned to pure end-members. All other intervals were assigned the term 'mixture'.

For the textural class assignments for each two metre interval see Appendix 4.10.

Table 4.15. Meso-scale textural classes for Ernest Henry, their descriptions and potential impact on mineral processing behaviours.

Textural Class	Description based on visual logging	Expected effect on mineral processing
BF1	Fragmental unit with well defined feldspar clasts. Rock is predominantly feldspar (Figure 4.46A).	Brecciated texture may result in easier crushing; more competent clasts of feldspar can be predicted to make grinding difficult (Napier-Munn et al., 2005).
BF2	Fragmental unit with well defined feldspar clasts. Matrix dominated by carbonate minerals and minor quartz (Figure 4.46B).	Brecciated texture may result in easier crushing; more competent clasts of feldspar can be predicted to make grinding difficult. Matrix of calcite may have a softening effect on the rock (Petruk, 2005).
BF3	Fragmental unit with well defined feldspar clasts. Matrix dominated by magnetite (Figure 4.46C).	Brecciated texture and magnetite matrix may result in easier crushing (Gaudin, 1957); more competent clasts of feldspar can be predicted to make grinding difficult (Napier-Munn et al., 2005).
MF1	Fragmental unit with clast edges not defined clearly giving the rock a mottled appearance. Rock is predominantly feldspar (Figure 4.46D).	Mottled texture is predicted to be more competent than the breccia textures. High feldspar content indicates a hard rock that could be potentially difficult to crush (Napier-Munn et al., 2005).
MF2	Fragmental unit with clast edges not defined clearly giving the rock a mottled appearance. Matrix is dominated by carbonate minerals and minor quartz (Figure 4.46E).	Mottled texture is predicted to be more competent than the breccia textures. Matrix calcite could have a softening effect on the crushability (Napier-Munn et al., 2005).
MF3	Fragmental unit with clast edges not defined clearly giving the rock a mottled appearance. Matrix is dominated by magnetite (Figure 4.46F).	Mottled texture is predicted to be more competent than the breccia textures. Matrix magnetite could have a softening effect on the crushability but be difficult to grind (Gaudin, 1957).
MF4	Fragmental unit with clast edges not defined clearly giving the rock a mottled appearance. Matrix is dominated by pyrite (Figure 4.46G).	Mottled texture is predicted to be more competent than the breccia textures. High content of matrix pyrite could influence grinding and flotation behaviour (Petruk, 2005).
MaF	Massive unit dominated by feldspar minerals (Figure 4.46H).	Rock will be hard to crush and grind (Napier-Munn et al., 2005). Chalcopyrite is typically very fine-grained which will affect liberation potential and floatability.
MaM	Massive unit dominated by magnetite (Figure 4.46I).	Rock could potentially be easy to crush but difficult to grind (Napier-Munn et al., 2005).
(*textural class*).D	Fine-grained to coarse-grained disseminated chalcopyrite. Typically occurs with disseminations of pyrite (Figure 4.46I)	Fine-grained generations of disseminated chalcopyrite are likely to be more difficult to liberate and recover than the clotted generation of chalcopyrite (Jones, 1987).
(*textural class*).C	Coarse aggregates (clots) of chalcopyrite with magnetite-calcite-quartz-pyrite phenocrysts. Typically occurs in the matrix of fragmental units (Figure 4.46J)	Clotted chalcopyrite is very coarse grained and can be predicted to liberate and float easily (Jones, 1987).

4.6.3 Interpretations of meso-scale machine-based logging

In this section, the quantified mineralogical and textural attributes will be compared to the meso-scale visual logging that has been presented in the previous sections (4.3 and 4.5). The objectives will be to test whether the 18 textural classes (9 classes with a C or D suffix: see Table 4.15) identified through visual logging can be defined purely using the quantified mineralogical and textural data extracted from the classified images of drill-core. The mineralogical and textural data for 1454 classified images (Appendices 4.3 - 4.9) of drill-core from Ernest Henry have been examined in order to determine whether these textural classes can be recognised.

The distinguishing features of the meso-scale textural classes can be broken down into three main components: the gangue mineral texture (fragmental or massive), the gangue mineral types and size of the chalcopyrite grains. How these components can be distinguished using the mineralogical and textural features that have been extracted from the classified images (section 4.5) are presented in Table 4.16.

Table 4.16. The three major components of the Ernest Henry meso-scale texture classes and the features that can be used from the classified images of drill-core to distinguish between them.

Textural class components	Textural classes that component is associated with	Mineralogical and textural attributes extracted from classified images to distinguish between classes
Gangue mineral texture	(1) Fragmental (clasts and matrix clearly defined): BF1, BF2, BF3, BF4. (2) Mottled (clast textures have been destroyed by alteration): MF1, MF2, MF3. (3) (3) Massive (rock is dominated by one mineral): MaF, MaM	Modal mineralogy: can be used to distinguish between massive and fragmental gangue textures. Massive texture classes will consist of predominantly one mineral class (MgChl or Fsp).
Styles of gangue mineralogy	(1) Feldspar: MaF, BF1, MF1 (2) Calcite (with minor quartz): BF2, MF2 (3) Magnetite: MaM, BF3, MF3 (4) Pyrite: MF4	Modal mineralogy: can be used to define the texture classes MaF and MaM using a percentage threshold. Modal mineralogy: can be used to determine the dominant matrix minerals of the fragmental textures given that the clasts present are composed of feldspar minerals.
Chalcopyrite size	(1) Coarse-grained: Clotted: (C) (2) Fine-grained: Disseminated: (D)	Chalcopyrite length and width: Two generations of chalcopyrite were easily distinguished on length versus width plots (see Figure 4.21). Classified images containing clotted chalcopyrite PhRegs will exhibit outliers. Chalcopyrite area: Disseminated and clotted chalcopyrite was shown to exhibit two different trends when plotted as a cumulative distribution curve (Figure 4.18 and a weighted histogram (Figure 4.19).

The simplest meso-scale texture classes to distinguish between are those that can be determined by their gangue mineralogy. A flow chart shown in Figure 4.47 shows the meso-scale textural classes that can be determined using the modal mineralogy calculated from the classified images. The mineral thresholds have been determined based on the estimated modal mineralogy determined during the initial logging of mineralogical textural attributes (see section 4.3). The clotted (C) or disseminated (D) suffix can be determined using the length and width ratio of chalcopyrite. This however, does make the assumption that the mineralised clot contains at least one coarse-grained chalcopyrite grain. Where the length of any chalcopyrite PhReg exceeds 150 microns the image is classified as clotted. Where no chalcopyrite PhReg's exceeding 150 microns the image is classified as 'disseminated'.

Based on the flow chart in Figure 4.47, each classified image from the drill-holes EH432, EH446, EH556, EH574, EH633 and EH635 have been assigned a texture class (1454 images). At this stage the difference between the BF (Brecciated – clasts well defined) and the MF (Mottled – clasts not well defined) cannot be determined using only the results of the classified images. To overcome this, the BF1, BF2, BF3, MF1, MF2 and MF3 classes have been combined as outlined in Table 4.17.

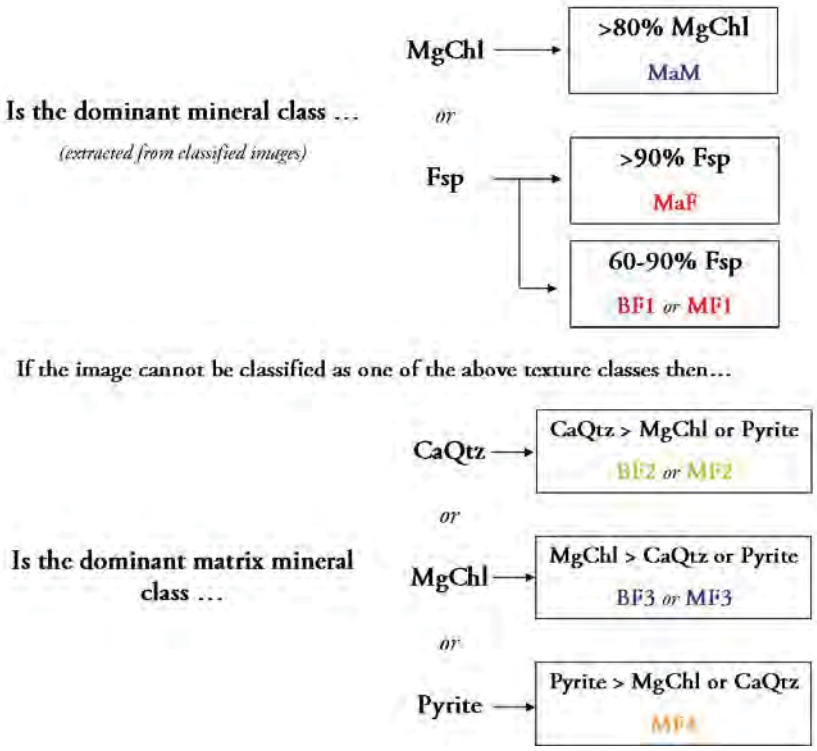

Figure 4.47. Flow chart for the identification of meso-scale textural classes using modal mineralogy calculated from the classified images of drill-core from Ernest Henry.

Table 4.17. Meso-scale texture classes from machine-based and visually based drill-core logging.

Machine-based texture class	Visually based texture class	Number of images
MaF	MaF	145
MaM	MaM	60
F1	BF1, MF1	37
F2	BF2, MF2	251
F3	BF3, MF3	951
MF4	MF4	11

In this section, a detailed textural analysis of each machine-based class is presented (see section 4.3). 15 examples of each class have been selected (except for MF4) and where possible both clotted and disseminated examples have been used (see Table 4.18). These analyses are followed by a summary of the modal mineralogy, chalcopyrite PhReg associations as well as a chalcopyrite size analysis for all of the images classified from the six drill-holes that have been analysed at Ernest Henry.

Chalcopyrite PhReg Size

The chalcopyrite PhReg sizes are presented as cumulative Equivalent Circle Diameter (ECD), histograms of ECD, and length and width for each of the machine-based textural classes outlined in Table 4.17 (see section 4.3, *this chapter*). The examples used for each texture class and the size data used in their analysis are shown in Table 4.18.

As described previously in section 4.3, the cumulative ECD is commonly used by process mineralogists to observe the distribution of mineral or particle sizes in a sample (Petruk, 2005). In Figure 4.48, the distribution of chalcopyrite PhReg size is shown to steeply increase between 150 and 1200 μm for the examples classified as disseminated (*blue lines*). The examples of classified

images that exhibit clotted chalcopyrite are shown by the *green lines* and steeply increase between 600 to >1200 μm. The texture classes MaF, F1, F2 and MF4 all exhibit trends that indicate >80% of chalcopyrite PhReg ECDs are between 150 and 1200 μm with 0-20% >1200 μm for the disseminated examples. The texture classes MaM, F1, F2 and MF4 exhibit trends that indicate 70-80% of the chalcopyrite PhReg ECD's are >600 μm for the clotted chalcopyrite examples. For the texture classes F3 and MaM, the cumulative distribution trends for several examples (EH574 645.40, EH574 736.15, EH574 761.20, EH635 925.52) do not follow the trends described previously. This suggests that these examples may exhibit multiple chalcopyrite size populations (bimodality).

Bimodal size populations are easier to observe as distribution curves of PhReg size ranges (see section 4.3). Figure 4.49 shows the distribution curves of chalcopyrite PhReg sizes for the selected examples of the meso-scale texture classes. The fine-grained disseminated examples (*blue* lines) show two different PhReg size distributions:

- 30-50% chalcopyrite PhReg ECD between 300 and 600 μm: observed in texture classes MaF, F1 and MF4.
- 40-90% chalcopyrite PhReg ECD between 300 and 1200 μm: observed in texture class F3.

The coarse-grained clotted chalcopyrite examples all show a sharp increase from 600 μm (>70% chalcopyrite >600 μm: see texture classes MaM, F3 and F2).

The examples that were predicted to exhibit bimodal chalcopyrite size populations based on their cumulative frequency distributions (Figure 4.48) are shown to exhibit two peaks (*black circles*) in the corresponding size distribution curves.

Table 4.18. The mineralogical and textural attributes extracted from the selected examples of machine-based meso-scale texture classes.

Class	Example	N	Chalcopyrite Phase Size (μm)						Length: Width ratio median	Maximum Length (pixels)	Disseminated (D) or clotted (C)	Chalcopyrite mineral associations: average wt. %				Modal Mineralogy percents calculated from meso-scale classified images				
			<75	75-150	150-300	300-600	600-1200	>1200				MgChl	CaQtz	Fsp	Pyrite	MgChl	Fsp	CaQtz	Ccp	Pyrite
MaM	EH574 645.40	866	0.01	1.16	26.88	49.42	18.19	4.34	1.33	60.00	D	88.60	0.26	10.77	0.37	96.59	1.95	1.22	0.17	0.07
	EH574 646.35	3301	0.00	0.29	11.89	29.37	28.84	29.61	1.33	188.45	C	70.59	1.29	24.89	3.24	87.02	9.67	1.36	1.33	0.62
	EH574 712.60	284	0.00	0.06	3.25	10.07	18.12	69.39	1.33	169.00	C	66.19	2.42	29.33	2.06	96.76	0.95	1.88	0.32	0.09
	EH574 713.55	517	0.00	1.41	5.45	14.85	18.17	60.12	1.33	389.69	C	67.40	2.09	23.54	6.96	93.79	1.15	3.93	0.97	0.17
	EH574 714.40	379	0.00	0.10	2.69	18.41	30.72	48.08	1.33	126.00	D	72.91	1.38	24.99	0.71	96.57	1.37	1.64	0.35	0.06
	EH574 715.30	386	0.00	0.10	2.16	9.43	19.43	68.85	1.33	439.00	C	71.39	2.75	23.89	1.97	95.25	1.28	2.81	0.52	0.14
	EH574 717.95	67	0.00	0.33	10.15	21.10	52.70	15.73	1.27	44.66	D	56.25	3.38	35.84	4.54	95.32	1.93	3.69	0.03	0.03
	EH574 719.75	153	0.04	0.24	9.10	25.33	38.12	27.16	1.33	60.96	D	53.97	5.63	37.25	3.15	94.69	1.92	3.27	0.07	0.04
	EH574 720.60	172	0.02	0.56	12.46	11.10	17.53	58.34	1.33	112.00	D	32.70	0.88	65.80	0.62	94.88	1.68	3.31	0.08	0.05
	EH574 725.75	40	0.00	1.04	5.76	24.79	40.74	27.68	1.33	68.96	D	41.57	4.03	53.86	0.54	94.93	1.68	3.33	0.04	0.01
	EH574 728.20	167	0.00	1.04	15.29	42.31	41.36	0.00	1.33	44.00	D	77.71	0.92	21.16	0.20	94.25	4.82	0.85	0.05	0.03
	EH574 729.15	277	0.00	0.26	6.51	21.81	47.75	23.66	1.33	98.56	D	63.85	1.32	34.38	0.45	95.66	3.26	0.86	0.18	0.04
	EH574 729.95	178	0.00	0.75	13.81	29.28	40.03	16.13	1.23	51.10	D	68.53	0.25	31.13	0.08	97.06	1.83	1.02	0.06	0.02
	EH574 736.15	130	0.00	1.50	27.11	40.08	31.32	0.00	1.25	31.59	D	82.31	1.28	15.59	0.82	95.45	3.57	0.92	0.03	0.04
	EH574 737.00	213	0.03	0.61	11.23	31.75	17.62	38.77	1.33	111.07	D	54.88	1.22	42.99	0.90	95.47	3.25	1.14	0.08	0.06
MaF	EH432 231.05	7287	0.00	0.52	29.63	46.20	14.33	9.32	1.33	140.75	D	5.23	0.54	92.72	1.51	6.31	91.21	0.47	1.50	0.52
	EH432 232.00	4767	0.00	0.96	33.85	42.52	10.16	12.51	1.27	126.00	D	5.15	0.57	93.25	1.03	6.49	91.64	0.44	0.96	0.47
	EH446 306.10	413	0.00	1.40	25.03	48.30	21.00	4.27	1.25	36.00	D	5.00	0.55	93.41	1.03	6.44	92.16	1.07	0.21	0.13
	EH446 364.85	1860	0.00	1.32	20.91	42.83	30.15	4.79	1.29	61.41	D	5.61	0.85	91.52	2.02	6.61	91.74	0.68	0.54	0.43
	EH446 378.15	989	0.01	1.04	21.65	48.11	25.35	3.84	1.33	64.09	D	6.19	0.95	91.18	1.68	7.00	91.27	1.21	0.35	0.18
	EH446 382.60	1427	0.00	1.30	21.47	42.92	24.34	9.97	1.31	83.38	D	5.83	1.20	91.14	1.83	7.22	91.35	0.79	0.42	0.22
	EH446 398.35	1996	0.01	0.57	15.79	37.54	26.80	19.28	1.33	139.50	D	5.93	1.31	90.78	1.98	6.81	91.37	0.85	0.64	0.33
	EH446 452.05	1277	0.00	1.51	27.55	41.43	22.35	7.16	1.29	66.00	D	5.44	0.84	92.26	1.46	6.95	92.14	0.47	0.28	0.17
	EH556 669.50	748	0.00	0.00	14.71	48.80	23.75	12.73	1.33	74.00	D	3.01	0.13	95.13	1.73	7.39	91.92	0.23	0.26	0.20
	EH556 676.80	618	0.00	0.00	14.67	49.49	33.74	3.11	1.33	60.00	D	5.05	0.09	93.97	0.88	6.60	92.45	0.65	0.21	0.10
	EH556 677.00	271	0.00	0.00	9.50	33.38	32.01	25.10	1.33	77.25	D	4.86	0.09	93.33	1.72	7.48	91.73	0.33	0.35	0.11
	EH556 684.15	308	0.00	0.00	28.51	53.59	17.89	0.00	1.25	35.19	D	3.77	0.19	95.78	0.26	6.96	92.73	0.19	0.07	0.05
	EH556 694.20	1523	0.00	0.77	22.92	48.51	22.07	5.73	1.25	52.00	D	6.16	0.52	92.78	0.53	7.34	91.59	0.54	0.36	0.16
	EH635 1072.07	585	0.00	1.49	24.15	33.01	19.45	21.90	1.33	81.14	D	5.53	2.40	80.00	12.07	7.15	91.03	1.10	0.13	0.59
	EH635 1075.51	592	0.00	1.90	27.26	36.49	18.70	15.65	1.29	65.13	D	11.28	1.92	79.21	7.58	6.40	91.87	1.09	0.14	0.51
F1	EH432 247.55	3241	0.00	0.26	13.33	32.81	18.23	35.37	1.25	413.18	C	1.79	16.48	80.21	1.52	1.69	88.30	8.40	1.26	0.35
	EH446 346.30	1208	0.00	0.56	16.04	40.62	27.56	15.22	1.33	88.56	D	1.83	6.79	90.13	1.26	2.00	86.94	10.52	0.40	0.14
	EH556 513.60	448	0.00	0.00	21.39	56.65	21.96	0.00	1.29	38.57	D	2.91	2.72	92.07	2.30	3.22	89.56	6.91	0.12	0.19
	EH556 780.90	884	0.00	0.23	5.24	21.49	40.00	42.03	1.40	184.00	C	7.88	5.85	81.23	5.03	2.85	88.30	7.27	0.68	0.90
	EH574 771.60	2744	0.00	0.21	5.07	20.74	31.93	42.06	1.40	191.00	C	13.41	4.54	78.21	3.83	7.08	90.15	1.62	0.62	0.53

Class	Example	N	Chalcopyrite Phase Size (μm)						Length: Width ratio median	Maximum Length (pixels)	Disseminated (D) or clotted (C)	Chalcopyrite mineral associations: average wt. %				Modal Mineralogy percents calculated from meso-scale classified images				
			<75	75-150	150-300	300-600	600-1200	>1200				MgChl	CaQtz	Fsp	Pyrite	MgChl	Fsp	CaQtz	Ccp	Pyrite
	EH574 772.60	297	0.00	0.46	8.45	26.60	25.60	38.89	1.40	199.81	C	11.18	2.95	79.27	6.60	7.13	80.44	11.72	0.25	0.46
	EH574 775.85	1135	0.00	0.22	6.07	29.04	32.97	31.69	1.39	190.00	C	11.44	3.51	77.53	7.52	6.12	83.56	9.06	0.71	0.54
	EH574 788.75	2743	0.00	0.12	3.68	22.08	36.36	37.76	1.41	191.00	C	9.31	3.59	85.10	1.99	4.37	88.85	3.97	2.22	0.59
	EH635 1022.89	5069	0.00	0.49	18.53	41.69	22.61	16.69	1.33	124.46	D	1.72	4.79	86.13	7.37	1.48	90.62	4.35	1.42	2.14
	EH635 1065.10	1568	0.01	0.66	15.85	33.47	33.55	16.48	1.33	163.62	C	3.02	8.17	72.48	16.33	2.72	83.98	10.60	0.54	2.16
	EH635 1066.02	1417	0.01	0.97	24.07	45.54	16.63	12.78	1.33	125.59	D	3.88	3.49	80.89	11.74	2.57	88.82	6.89	0.33	1.39
	EH635 1066.89	297	0.00	0.46	8.45	26.60	25.59	38.89	1.40	199.81	C	11.18	2.95	79.27	6.60	3.76	85.82	7.58	0.52	2.32
	EH635 1073.79	323	0.03	3.38	40.50	35.49	20.59	0.00	1.33	36.51	D	4.74	5.26	80.74	9.26	6.68	89.57	3.19	0.05	0.51
	EH635 1108.51	1931	0.00	1.13	20.90	43.79	26.22	7.96	1.33	111.63	D	1.93	5.32	71.06	21.69	2.52	88.28	5.25	0.52	3.43
	EH635 1110.47	2422	0.01	1.51	27.44	50.68	16.35	4.01	1.33	76.84	D	2.21	4.44	74.35	19.00	2.11	88.89	4.42	0.51	4.08
F2	EH432 168.62	4888	0.00	0.19	8.86	26.81	29.21	34.93	1.33	313.60	C	13.15	19.89	59.13	7.83	20.62	47.87	27.49	2.39	1.63
	EH432 381.90	585	0.00	0.45	5.85	15.19	27.13	51.38	1.40	254.76	C	15.86	10.79	62.49	10.85	19.53	57.46	22.07	0.42	0.52
	EH432 396.40	337	0.00	2.45	32.32	40.23	25.01	0.00	1.33	49.46	D	24.32	19.29	51.43	4.96	26.66	42.43	30.63	0.06	0.22
	EH556 547.70	883	0.00	0.00	10.87	39.24	30.93	18.97	1.33	96.95	D	11.16	6.08	75.26	7.51	23.62	51.04	24.00	0.38	0.97
	EH574 626.80	952	0.00	0.12	5.54	20.19	21.71	52.43	1.33	296.26	C	25.07	5.04	56.69	13.20	35.65	26.43	36.75	0.67	0.49
	EH633 917.30	825	0.00	0.17	3.06	8.97	14.65	73.15	1.5	284.19	C	2.64	17.67	65.79	13.89	20.43	56.34	21.26	1.04	0.94
	EH633 961.00	270	0.00	0.63	10.76	20.11	25.16	43.34	1.33	117.96	D	5.11	22.84	52.55	19.50	21.20	48.00	29.81	0.11	0.87
	EH633 961.70	663	0.00	1.01	19.24	46.65	20.05	13.04	1.69	78.72	D	6.35	41.00	32.84	19.80	25.88	35.94	36.73	0.16	1.29
	EH633 963.55	663	0.01	2.37	19.76	35.79	24.94	17.12	1.33	81.00	D	5.16	21.31	48.25	25.28	26.42	44.46	27.48	0.21	1.43
	EH635 820.24	684	0.00	5.42	52.44	35.26	6.88	0.00	1.33	31.00	D	7.56	17.95	46.35	28.13	20.43	46.54	31.45	0.07	1.51
	EH635 823.04	604	0.02	2.56	35.00	32.34	18.74	11.33	1.33	61.90	D	6.11	41.85	29.76	22.28	22.89	38.69	36.76	0.11	1.55
	EH635 825.74	100	0.00	3.52	34.27	30.23	10.64	21.33	1.33	110.53	D	8.48	11.34	58.50	21.68	25.68	45.60	27.53	0.09	1.10
	EH635 831.54	592	0.02	4.01	44.29	32.51	13.89	5.28	1.33	49.00	D	20.73	21.48	45.24	12.54	30.85	35.56	32.66	0.08	0.84
	EH635 924.54	401	0.01	2.03	22.67	38.36	26.28	10.64	1.33	66.00	D	10.14	9.27	30.72	49.87	31.37	22.37	42.67	0.18	3.40
	EH635 1092.58	1384	0.00	0.72	22.23	47.55	20.77	8.72	1.33	65.28	D	10.68	23.11	55.94	10.27	19.20	51.89	27.48	0.35	1.08
F3	EH432 319.60	346	0.00	0.21	7.57	42.84	43.50	5.88	1.38	44.90	D	58.08	1.57	37.27	3.08	77.76	20.32	1.44	0.24	0.24
	EH432 320.50	631	0.00	0.06	12.12	43.10	39.31	5.41	1.40	57.61	D	38.87	2.07	51.42	7.63	61.79	34.26	2.54	0.38	1.04
	EH432 327.65	1254	0.00	0.92	24.48	41.41	22.29	10.89	1.33	72.00	D	42.60	1.18	54.58	1.64	78.13	19.98	1.26	0.41	0.22
	EH432 355.45	455	0.01	0.76	15.06	30.73	29.22	24.21	1.33	89.00	D	24.85	4.00	66.98	4.16	77.86	20.55	1.19	0.15	0.24
	EH432 356.40	455	0.01	1.10	16.74	29.46	36.76	15.93	1.40	62.00	D	36.72	2.72	55.89	4.67	76.97	22.26	0.53	0.14	0.09
	EH556 745.00	103	0.00	1.39	16.80	36.58	31.36	13.88	1.50	37.00	D	34.50	0.71	60.53	4.26	76.55	23.11	0.25	0.03	0.06
	EH574 554.05	908	0.00	0.52	7.06	20.09	18.29	54.04	1.33	283.00	C	62.07	4.49	27.22	6.21	77.89	1.63	19.35	0.71	0.42
	EH574 557.65	1211	0.00	0.16	7.58	27.63	28.36	36.27	1.33	211.13	C	67.87	11.20	17.58	3.35	78.65	2.85	17.21	0.76	0.53
	EH574 614.60	1302	0.00	0.12	5.45	17.74	32.44	44.25	1.33	110.89	D	51.47	1.42	41.78	5.32	78.25	18.92	1.38	1.06	0.40
	EH574 633.40	850	0.00	0.25	8.63	25.92	27.09	38.11	1.33	124.66	D	64.17	2.93	29.87	3.03	77.00	16.90	5.07	0.68	0.35
	EH574 640.85	3449	0.00	0.08	5.30	24.66	38.39	31.56	1.33	127.15	D	78.86	0.72	19.20	1.22	78.18	18.43	1.06	2.08	0.25
	EH574 654.40	1908	0.00	0.18	7.62	24.29	22.40	45.51	1.33	476.69	C	53.85	2.15	38.58	5.42	76.45	17.36	4.22	1.25	0.72

Class	Example	N	Chalcopyrite Phase Size (μm)						Length: Width ratio median	Maximum Length (pixels)	Disseminated (D) or clotted (C)	Chalcopyrite mineral associations: average wt. %				Modal Mineralogy percents calculated from meso-scale classified images				
			<75	75-150	150-300	300-600	600-1200	>1200				MgChl	CaQtz	Fsp	Pyrite	MgChl	Fsp	CaQtz	Ccp	Pyrite
	EH574 700.10	1064	0.00	0.08	3.29	15.32	24.29	57.01	1.33	288.03	C	63.27	4.72	28.40	3.62	79.18	16.09	3.41	1.04	0.28
	EH574 761.20	318	0.00	1.83	52.57	25.18	20.42	0.00	1.25	36.71	D	64.24	2.93	29.37	3.47	76.95	19.59	3.20	0.04	0.22
	EH635 925.52	109	0.13	10.20	54.08	12.12	23.47	0.00	1.5	29.00	D	43.29	9.31	23.87	23.53	77.13	15.77	6.94	0.01	0.14
MF4	EH432 148.45	3738	0.00	0.25	11.77	35.20	29.95	22.83	1.42	124.22	D	4.77	3.48	80.29	11.46	6.07	80.64	5.54	1.57	6.17
	EH574 543.40	1373	0.00	0.07	3.81	20.70	28.07	47.35	1.57	177.48	C	64.85	22.11	9.45	3.59	18.87	48.14	8.73	1.15	23.11
	EH633 957.95	8363	0.00	0.67	13.68	42.28	36.59	6.77	1.55	94.48	D	1.79	2.69	69.39	26.13	1.19	79.34	7.36	2.53	9.58
	EH635 882.65	12824	0.00	0.44	12.37	36.31	34.54	16.34	1.54	237.75	C	4.17	1.20	70.33	24.30	7.27	74.27	2.54	5.10	10.82
	EH635 889.91	13111	0.00	0.26	5.96	19.23	29.00	45.55	1.50	288.46	C	2.66	1.53	68.77	27.05	6.75	74.71	1.17	9.02	8.34
	EH635 915.40	6388	0.00	1.11	23.99	46.13	20.42	8.33	1.50	99.76	D	1.27	5.11	78.52	15.11	2.47	85.95	5.01	1.37	5.20
	EH635 916.30	13382	0.00	0.71	11.34	31.32	35.36	21.27	1.60	173.00	C	1.35	4.72	55.01	38.92	3.58	59.78	6.58	5.08	24.97
	EH635 917.20	12193	0.00	0.44	8.19	26.74	35.17	29.46	1.50	190.40	C	2.48	9.09	56.91	31.52	4.54	50.43	14.86	5.87	24.29
	EH635 918.10	10877	0.00	0.49	8.20	24.52	33.05	33.73	1.52	217.52	C	2.34	8.61	51.94	37.11	4.44	52.11	14.41	5.55	23.48
	EH635 1112.44	2690	0.00	1.71	30.70	48.23	17.89	1.48	1.50	51.70	D	3.15	3.80	71.88	21.17	3.47	90.20	1.74	0.47	4.12

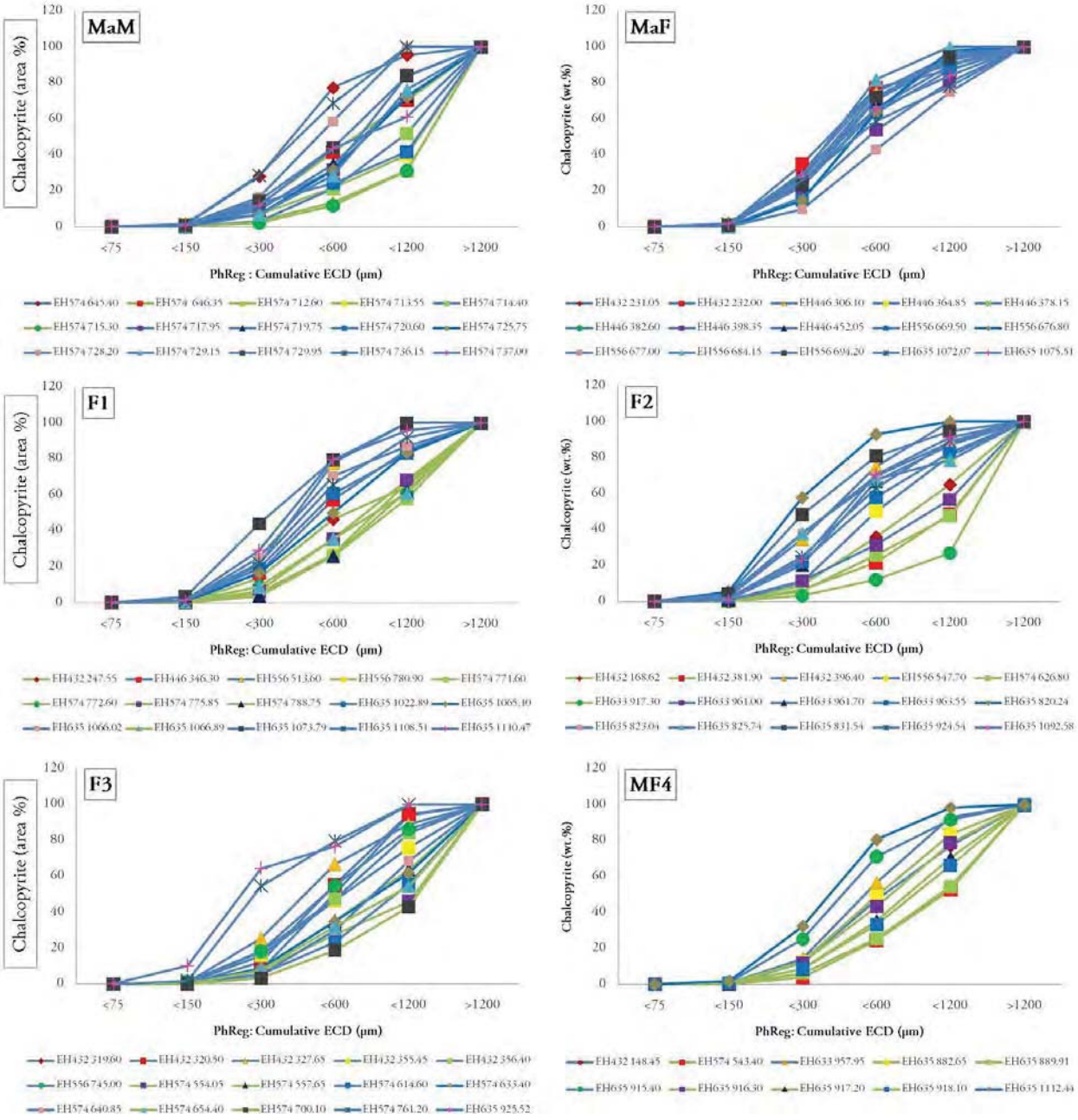

Figure 4.48. The cumulative ECD distribution curves for chalcopyrite PhRegs for the meso-scale machine-based texture classes MaM, MaF, F1, F2, F3 and MF4. Each example represents the chalcopyrite PhRegs extracted from one classified image. Each chalcopyrite has been weighted against the total chalcopyrite in that image. *Blue lines* – disseminated examples; *Green examples* – clotted examples.

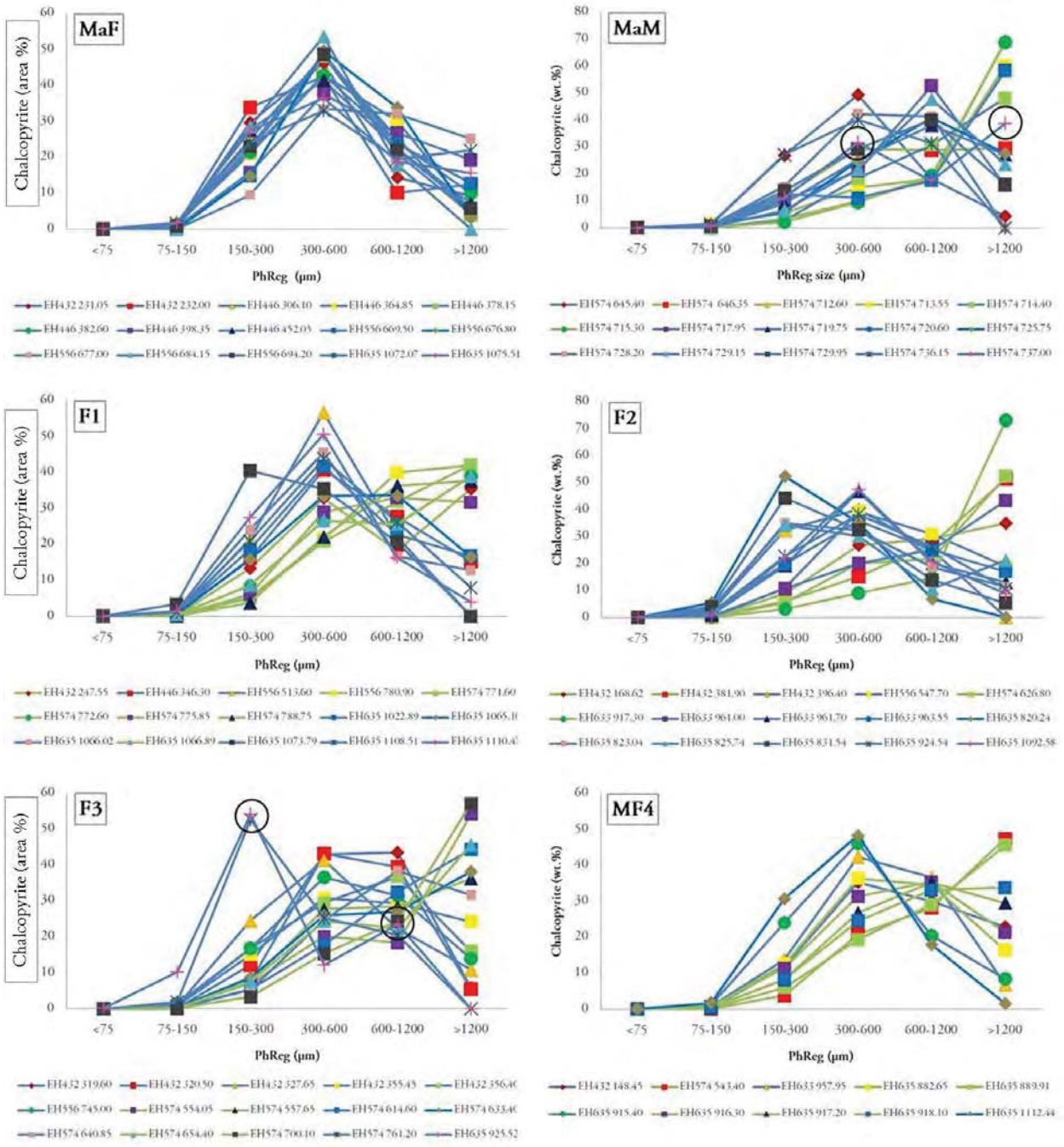

Figure 4.49. Size distribution curves showing the ECD distribution for chalcopyrite PhRegs for the meso-scale machine-based texture classes MaM, MaF, F1, F2, F3 and MF4. Each example represents the chalcopyrite PhRegs extracted from one classified image. Each chalcopyrite has been weighted against the total chalcopyrite in that image. *Blue lines* – disseminated examples; *Green examples* – clotted examples.

The maximum length and corresponding width were used to determine if an image should be classified as disseminated or clotted chalcopyrite. If the length of the largest chalcopyrite PhReg is >150 µm then the image was classified as C (clotted – coarse grained). If the length of the largest chalcopyrite PhReg is <150 µm then the image was classified as D (disseminated – fine-grained). Figure 4.50 shows the maximum length of chalcopyrite PhRegs and their corresponding width for the examples in each of the meso-scale texture.

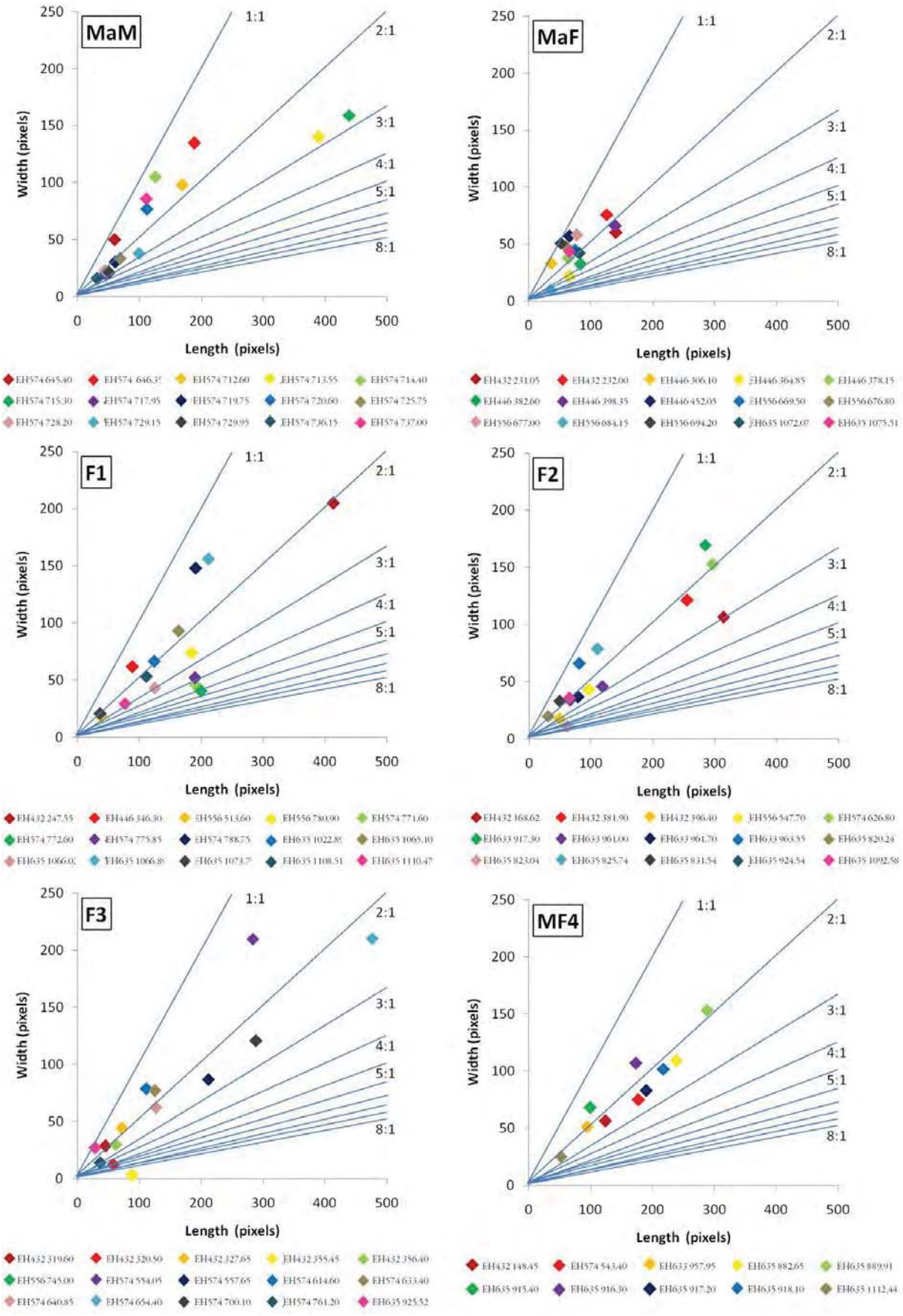

Figure 4.50. Length and width for chalcopyrite PhRegs for the meso-scale machine-based texture classes MaM, MaF, F1, F2, F3 and MF4. Each example represents the chalcopyrite PhRegs extracted from one classified image.

Mineral groups associated with chalcopyrite

The mineral groups that are associated with chalcopyrite have been measured by calculating the abundance of mineral groups in the 5 pixel rim surrounding the chalcopyrite PhReg (see Figure 4.22). The results of the examples selected for each texture class (Table 4.18) are shown as box plots in Figure 4.51. This figure shows that for the texture classes MaF, F1 and F2 the chalcopyrite PhRegs are dominantly associated with the Fsp mineral group. For the texture class MaM chalcopyrite PhRegs are predominantly associated with MgChl and lesser Fsp mineral groups. The chalcopyrite PhRegs in texture class F3 are associated with the MgChl and Fsp mineral groups. For the texture class MF4, the chalcopyrite PhRegs are predominantly associated with Fsp with lesser Pyrite.

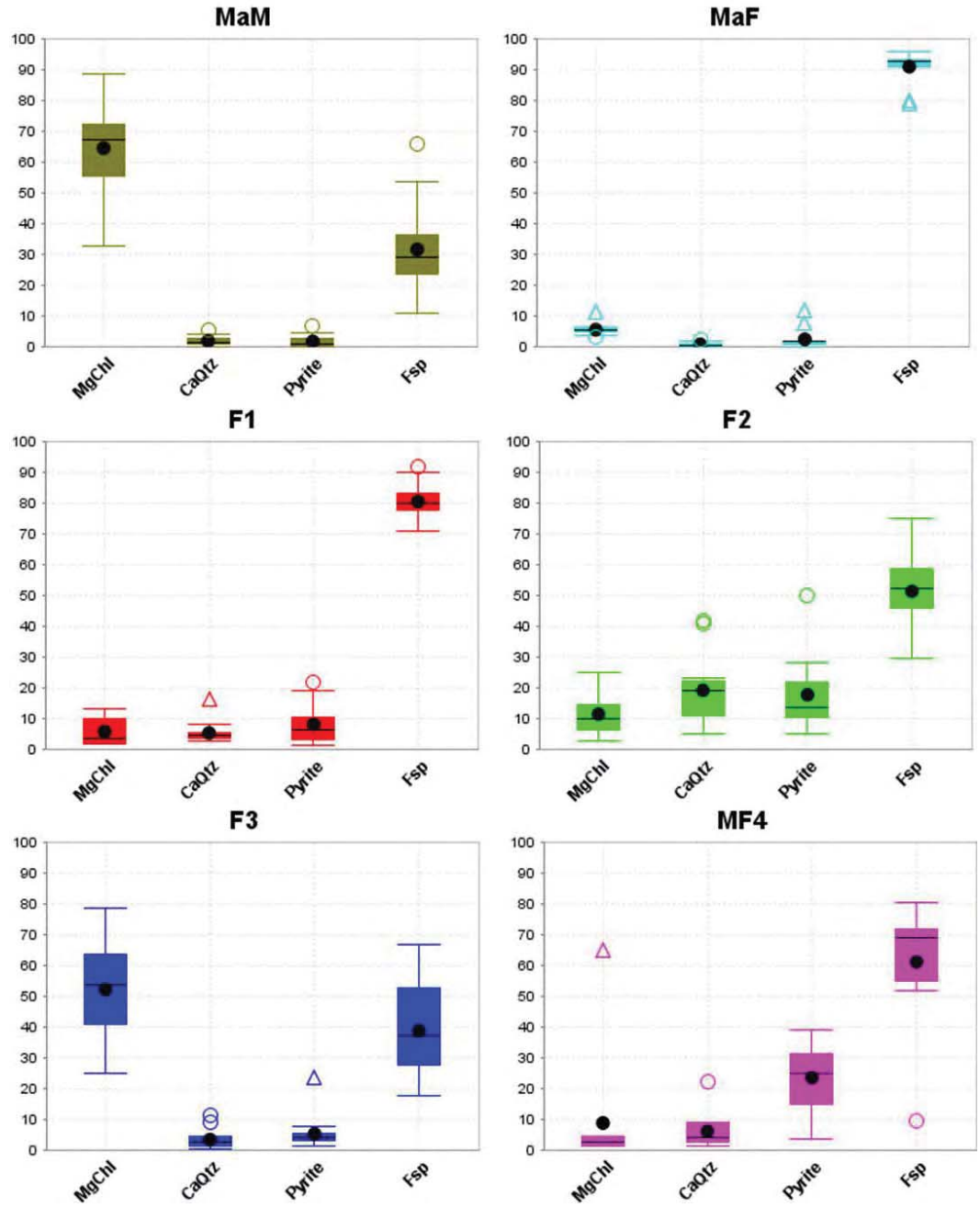

Figure 4.51. Abundance of minerals associated with chalcopyrite for the meso-scale machine-based texture classes MaM, MaF, F1, F2, F3 and MF4. Each box plot represents the examples outlined in Table 4.18 for each texture class.

Taking into consideration that the distribution curves of PhReg size (Figure 4.49) showed that some examples exhibit bimodal size populations, it is possible that these chalcopyrite populations can also exhibit different mineral associations. Figure 4.52 shows the mineral group abundances associated with chalcopyrite for fine- (<150 µm ECD), medium- (150-600 µm ECD) and coarse-grained (>600 µm ECD) PhRegs. This allows the changes in the minerals associated with chalcopyrite of different size ranges to be observed. The data used to produce this figure are presented in Table 4.19.

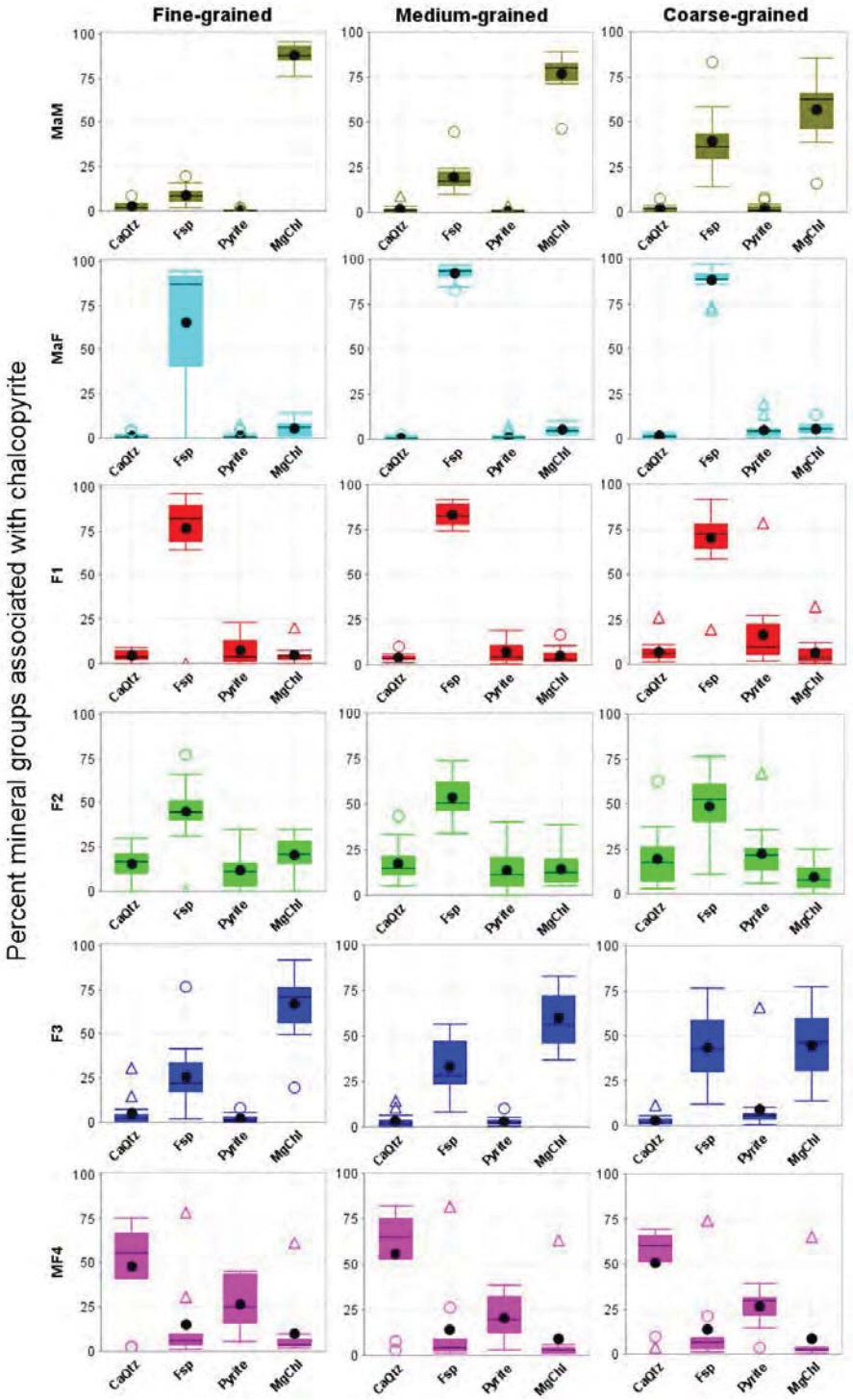

Figure 4.52. Abundance of minerals associated with chalcopyrite PhRegs of different size fractions for the meso-scale machine-based texture classes MaM, MaF, F1, F2, F3 and MF4.

Table 4.19. Abundances of mineral groups associated with chalcopyrite for examples of the texture classes MaF, MaM, F1, F2, F3 and MF4. NIL refers to images that had no chalcopyrite PhRegs of a given size fraction in the classified image.

Texture class	Example	Fine-grained				Medium-grained				Coarse-grained			
	Chalcopyrite Association	MgChl	CaQtz	Fsp	Pyrite	MgChl	CaQtz	Fsp	Pyrite	MgChl	CaQtz	Fsp	Pyrite
MaM	EH574 645.40	93.43	2.04	4.21	0.33	89.45	0.21	9.91	0.43	85.44	0.33	14.05	0.18
	EH574 646.35	86.52	0.94	9.82	2.72	71.50	0.81	15.52	1.48	62.46	1.62	31.47	4.36
	EH574 712.60	94.21	1.31	4.48	0.00	82.41	1.04	15.35	0.68	63.65	2.62	31.47	2.67
	EH574 713.55	95.66	1.86	2.37	0.10	82.47	1.60	14.82	1.11	65.34	2.20	24.63	7.84
	EH574 714.40	87.64	0.81	10.82	0.73	84.17	1.25	14.22	0.37	69.68	1.45	28.06	0.80
	EH574 715.30	80.29	1.38	15.83	2.50	82.74	1.08	14.76	1.41	69.89	2.99	25.09	2.04
	EH574 717.95	90.69	0.62	8.69	0.00	73.53	3.41	22.87	0.19	48.22	3.39	41.82	6.58
	EH574 719.75	94.07	4.27	1.67	0.00	71.49	3.20	21.57	3.74	44.95	6.99	45.08	2.98
	EH574 720.60	89.23	4.63	6.14	0.00	74.75	2.25	22.41	0.60	15.95	0.43	83.01	0.61
	EH574 725.75	80.66	8.75	10.59	0.00	46.41	8.79	44.80	0.00	38.81	1.81	58.60	0.78
	EH574 728.20	85.80	3.32	10.89	0.00	84.48	0.81	14.56	0.16	66.55	1.10	32.08	0.26
	EH574 729.15	84.04	1.93	13.96	0.07	76.69	0.57	22.40	0.34	58.43	1.62	39.47	0.49
	EH574 729.95	92.43	0.73	6.84	0.00	80.36	0.24	19.22	0.19	59.16	0.26	40.58	0.00
	EH574 736.15	86.26	4.25	7.72	1.77	81.08	0.88	17.60	0.43	62.96	0.38	36.48	0.17
	EH574 737.00	76.30	3.63	19.73	0.33	72.95	1.32	24.70	1.04	40.42	1.16	57.61	0.81
	DATA RANGE	**76.30-95.66**	**0.62-8.75**	**1.67-19.73**	**0.00-2.72**	**46.41-89.45**	**0.21-8.79**	**9.91-44.80**	**0.00-3.74**	**15.95-85.44**	**0.26-6.99**	**14.05-83.01**	**0.00-7.84**
MaF	EH432 231.05	5.78	0.29	93.35	0.58	4.50	0.24	94.94	0.62	7.47	1.53	86.26	4.74
	EH432 232.00	6.07	0.92	92.63	0.37	4.95	0.36	93.89	0.80	6.42	1.39	88.47	3.72
	EH446 306.10	2.70	1.93	94.65	0.73	2.34	0.70	96.45	0.51	0.39	2.19	97.05	0.36
	EH446 364.85	7.64	0.21	90.30	1.86	5.89	0.84	91.41	1.86	4.30	2.00	88.00	5.69
	EH446 378.15	9.50	0.98	88.65	0.86	7.26	0.66	91.09	1.00	5.41	2.77	87.79	4.03
	EH446 382.60	8.62	0.71	90.51	0.16	7.22	1.05	90.39	1.34	3.27	3.92	88.41	4.41
	EH446 398.35	9.43	0.86	87.05	2.66	6.98	1.36	89.73	1.91	4.93	2.89	87.98	4.21
	EH446 452.05	5.54	0.55	93.55	0.36	4.64	0.76	93.82	0.78	3.10	2.06	90.56	4.28
	EH556 669.50	NIL	NIL	NIL	NIL	3.75	0.09	95.01	1.14	1.65	0.20	95.31	2.84
	EH556 676.80	NIL	NIL	NIL	NIL	3.71	0.11	95.54	0.65	7.51	0.07	91.06	1.36
	EH556 677.00	NIL	NIL	NIL	NIL	3.84	0.11	94.79	1.25	5.52	0.09	92.29	2.09
	EH556 684.15	NIL	NIL	NIL	NIL	2.79	0.25	96.74	0.22	7.99	0.11	91.49	0.42
	EH556 694.20	14.03	2.13	83.44	0.39	6.30	0.46	92.90	0.34	5.64	0.65	92.66	1.05
	EH635 1072.07	6.13	4.62	82.03	7.21	6.44	1.71	84.56	7.29	4.15	3.32	73.36	19.17
	EH635 1075.51	7.14	3.93	84.84	4.08	10.26	2.15	82.96	4.64	13.11	1.35	71.96	13.58
	DATA RANGE	**2.70-14.03**	**0.21-4.62**	**82.03-93.55**	**0.16-7.21**	**2.34-10.26**	**0.09-2.15**	**82.96-96.74**	**0.22-7.29**	**0.39-7.99**	**0.07-3.92**	**73.36-97.05**	**0.36-19.17**
F1	EH432 247.55	3.18	0.28	96.24	0.30	1.94	5.26	92.00	0.81	1.66	26.20	69.91	2.23
	EH446 346.30	4.05	1.29	93.75	0.91	1.56	6.03	91.42	0.98	1.99	7.93	88.36	1.72
	EH556 513.60	NIL	NIL	NIL	NIL	2.73	3.57	91.74	1.96	3.58	1.23	91.66	3.54
	EH556 780.90	3.95	5.06	89.82	1.17	5.43	10.37	75.89	8.30	2.01	8.89	76.65	12.45
	EH574 771.60	20.03	8.61	68.39	2.97	16.65	1.30	79.00	3.05	32.13	1.91	58.32	7.64
	EH574 772.60	1.13	2.88	94.71	1.28	9.13	2.88	83.50	4.48	12.27	3.05	77.19	7.50
	EH574 775.85	5.36	1.98	88.63	4.02	10.52	2.50	82.82	4.15	11.76	3.93	75.07	9.24
	EH574 788.75	7.03	3.75	88.76	0.46	8.21	2.91	87.32	1.57	9.76	3.80	84.29	2.14
	EH635 1022.89	1.74	2.43	87.85	7.97	1.69	3.19	90.89	4.22	1.73	7.24	78.61	12.42
	EH635 1065.10	5.14	4.52	69.49	20.85	2.47	5.36	79.70	12.46	3.50	10.93	65.15	20.43
	EH635 1066.02	1.53	8.96	82.29	7.22	3.00	2.64	88.33	6.04	5.89	5.83	62.38	25.90
	EH635 1066.89	3.25	3.53	75.45	17.77	3.62	2.43	77.30	16.64	0.81	1.18	19.58	78.42
	EH635 1073.79	7.70	8.82	78.57	4.91	4.18	3.81	82.65	9.36	7.30	10.58	72.53	9.60
	EH635 1108.51	4.49	6.77	69.16	19.58	1.91	4.55	74.52	19.02	1.85	6.73	64.33	27.09
	EH635 1110.47	4.31	7.96	64.61	23.12	2.39	4.54	75.64	17.43	1.65	3.76	69.73	24.86
	DATA RANGE	**1.13-20.03**	**0.28-8.96**	**64.61-96.24**	**0.30-23.12**	**1.56-16.65**	**1.30-10.37**	**74.52-92.00**	**0.81-19.02**	**0.81-32.13**	**1.18-26.20**	**58.32-91.66**	**1.72-27.09**
F2	EH432 168.62	20.08	1.76	77.17	0.99	20.50	7.57	69.52	2.40	8.98	26.42	53.83	10.77
	EH432 381.90	31.94	10.35	53.54	1.19	23.35	11.38	58.11	0.07	13.74	10.68	63.74	11.85
	EH432 396.40	34.88	20.14	44.49	0.49	25.84	20.38	49.01	4.77	18.37	14.65	60.67	6.30
	EH556 547.70	NIL	NIL	NIL	NIL	13.51	6.71	73.88	5.57	7.97	5.72	76.49	9.82
	EH574 626.80	31.91	8.53	54.46	5.09	38.77	5.15	50.64	5.45	19.59	5.07	58.79	16.54
	EH633 917.30	7.97	9.98	66.36	15.69	5.31	12.26	70.94	11.50	2.24	18.36	65.18	14.22

Texture class	Example	Fine-grained				Medium-grained				Coarse-grained			
	Chalcopyrite Association	MgChl	CaQtz	Fsp	Pyrite	MgChl	CaQtz	Fsp	Pyrite	MgChl	CaQtz	Fsp	Pyrite
	EH633 961.00	31.24	18.48	40.47	9.80	6.74	12.89	65.75	14.62	4.09	27.21	46.99	21.71
	EH633 961.70	21.05	30.30	41.14	6.14	7.24	43.27	37.22	12.18	3.81	37.13	23.72	35.33
	EH633 963.55	17.38	12.35	48.13	22.13	8.94	18.46	50.82	21.77	1.55	24.52	44.21	29.72
	EH635 820.24	8.76	17.64	48.04	25.55	6.86	18.69	45.77	28.68	15.38	8.77	52.32	23.53
	EH635 823.04	21.56	22.02	40.29	16.13	8.07	33.33	37.80	20.80	0.20	62.58	11.11	26.11
	EH635 825.74	14.27	25.14	45.01	15.59	6.84	14.70	57.72	20.74	11.00	3.15	61.61	24.24
	EH635 831.54	23.15	23.49	37.73	14.09	19.40	22.54	47.67	10.39	24.69	17.55	36.17	21.59
	EH635 924.54	19.42	14.54	31.12	34.92	13.52	11.91	34.23	40.33	3.66	5.19	24.30	66.84
	EH635 1092.58	24.67	16.83	47.72	10.78	12.27	22.33	57.67	7.72	6.46	25.05	51.72	16.77
	DATA RANGE	**7.97-34.88**	**1.76-30.30**	**31.12-77.17**	**0.49-34.92**	**5.31-38.77**	**5.15-43.27**	**34.23-73.88**	**0.07-40.33**	**0.20-24.69**	**3.15-62.58**	**11.11-76.49**	**6.30-66.84**
F3	EH432 319.60	74.11	1.34	21.82	2.73	56.28	2.34	38.56	2.82	58.53	0.96	37.30	3.20
	EH432 320.50	19.89	3.70	76.40	0.00	45.31	1.27	47.88	5.54	30.26	3.00	56.52	10.22
	EH432 327.65	63.67	1.98	34.02	0.33	51.71	1.14	46.32	0.83	21.00	1.27	74.44	3.28
	EH432 355.45	58.13	7.30	33.27	1.31	36.93	3.96	56.83	2.28	13.93	3.97	76.29	5.81
	EH432 356.40	54.47	1.80	41.45	2.29	45.14	0.82	50.48	3.57	32.21	1.63	59.96	6.19
	EH556 745.00	68.09	1.77	30.14	0.00	41.29	0.72	54.65	3.35	31.41	1.44	60.83	6.32
	EH574 554.05	91.69	5.15	1.88	1.28	82.64	6.84	8.24	2.28	55.03	3.67	33.77	7.53
	EH574 557.65	80.78	15.03	3.76	0.43	76.07	10.48	11.55	1.89	63.04	11.57	21.18	4.21
	EH574 614.60	54.19	2.61	34.90	8.30	53.75	1.20	40.35	4.70	50.52	1.48	42.42	5.58
	EH574 633.40	74.62	0.56	21.63	3.19	67.91	1.93	28.65	1.52	62.15	3.47	30.52	3.87
	EH574 640.85	71.41	1.37	25.42	1.79	82.51	0.51	16.00	0.97	77.09	0.80	20.74	1.37
	EH574 654.40	73.48	1.39	21.30	3.82	69.88	2.80	25.56	1.75	45.87	1.82	45.00	7.31
	EH574 700.10	77.30	1.49	19.88	1.33	74.01	1.30	23.08	1.62	60.76	5.42	29.70	4.12
	EH574 761.20	91.71	1.44	6.85	0.00	68.41	2.92	24.43	4.25	46.26	3.06	49.74	0.93
	EH635 925.52	49.51	30.48	14.25	5.76	47.39	14.04	28.24	10.33	21.67	0.00	12.31	66.02
	DATA RANGE	**19.89-91.71**	**0.56-30.48**	**1.88-76.40**	**0.00-8.30**	**36.93-82.64**	**0.51-14.04**	**8.24-56.83**	**0.83-10.33**	**13.93-77.09**	**0.00-11.57**	**20.74-76.29**	**0.93-66.02**
MF4	EH432 148.45	10.08	2.80	78.36	5.78	5.91	3.20	81.37	7.27	3.42	3.52	74.28	14.49
	EH574 543.40	61.16	2.59	30.55	5.69	62.90	8.05	26.16	2.90	65.27	9.91	20.97	3.85
	EH633 934.70	8.00	77.27	6.56	8.17	3.78	65.87	3.48	26.87	1.87	37.84	2.98	57.31
	EH633 957.95	2.09	64.37	2.79	30.74	1.69	74.08	2.22	22.00	1.92	63.46	3.29	31.33
	EH635 882.65	4.76	68.95	1.45	24.84	4.49	75.24	0.99	19.27	3.86	65.67	1.41	29.06
	EH635 889.91	6.86	65.10	4.02	24.01	3.92	78.61	1.16	16.31	2.22	65.51	1.64	30.63
	EH635 915.40	3.76	75.68	4.28	16.27	1.43	82.39	3.72	12.45	0.77	69.15	8.51	21.56
	EH635 916.30	1.59	47.16	6.86	44.39	1.62	55.02	4.77	38.59	1.14	55.10	4.65	39.11
	EH635 917.20	3.34	44.37	8.65	43.66	3.12	55.91	8.56	32.41	2.14	57.52	9.38	30.96
	EH635 918.10	3.64	41.11	9.64	45.62	3.21	53.09	8.81	34.89	1.90	51.46	8.51	38.13
	EH635 1112.44	3.02	66.64	5.28	25.07	3.20	73.41	3.49	19.90	2.95	66.07	4.95	26.02
	DATA RANGE	**1.59-61.16**	**2.59-75.68**	**1.45-78.36**	**5.69-45.62**	**1.43-62.90**	**3.20-82.39**	**0.99-81.37**	**2.90-38.59**	**0.77-65.27**	**3.52-69.15**	**1.41-74.28**	**3.85-57.31**

Figure 4.52 shows a decrease in the mineral groups MgChl and increase in Fsp associated with chalcopyrite as the PhReg size increases for the texture class MaM. This trend is reversed for the texture class MaF which shows a minor decrease and increase in Fsp and MgChl respectively. Both texture classes F1 and F2 (which Fsp is the dominant gangue mineral) show a higher abundance of Fsp associated with the medium-grained chalcopyrite than the fine- and coarse-grained PhReg size fractions. Texture class F3 shows a decrease in MgChl and increase in Fsp associated with chalcopyrite as the PhReg size increases. The MF4 texture class shows an increase in median pyrite associated with chalcopyrite as PhReg size increases.

The changes in the abundance of different mineral (groups) associated with chalcopyrite of various size ranges were shown in Figure 4.52. This data shows that there are two dominant mineral associations with chalcopyrite that change with size. As the chalcopyrite PhReg size increases, the mineral (groups) associated with chalcopyrite change from reflecting the dominant gangue or

alteration mineralogy to reflecting the mineralogy of the coarse-grained mineralized clots (carbonate-quartz-magnetite-pyrite-chalcopyrite).

Comparison of meso-scale machine-based textural classes

Previously in this section, mineralogical and textural attributes from 15 examples of each meso-scale texture class were examined. The aim was to establish if the textural classes defined using data only extracted from classified images have unique mineralogical and textural characteristics which may have an impact on mineral processing behaviours. In this section, a comparison of the textural attributes of each class will be presented using all of the classified images obtained from the six drill-holes examined from Ernest Henry (1454 images). These data will be used to assess if there are unique mineralogical and textural signatures present that can be used to identify potential differences in mineral processing behaviours.

The modal mineralogy for each of the texture classes is expected to be variable for each class given that it is one of the determining factors for assigning an interval to a given class. The averages and standard deviations of the mineral group modal abundances are summarised in Table 4.20 and illustrated as box plots in Figure 4.53. Shown in this figure is that while there are some significant differences in modal mineralogy between texture classes, some of the classes do exhibit similar averages and ranges for some mineral groups (i.e. F2, F3 and MF4 have similar ranges in Fsp abundance). This may result in similar behaviours of some aspects of mineral processing behaviours (Table 4.21) For example; the abundance of mineral in the bulk rock will provide an indication of a rock's physical properties (i.e. hardness). These bulk properties will affect the ease at which a rock is broken down in the comminution circuit. The easier a rock is to crush or grind, the less power that is required by the comminution circuit to process the ore (Napier-Munn et al, 2005).

Table 4.20. Average and standard deviation (σ) of the modal mineralogy of the meso-scale machine-based texture classes.

Texture class	n	Fsp		MgChl		Chalcopyrite		Pyrite		CaQtz	
		mean	σ	mean	σ	mean	σ	mean	σ	mean	σ
MaM	145	6.09	4.55	88.90	5.11	0.77	1.07	0.28	0.28	3.97	3.35
MaF	60	93.58	1.98	3.42	2.00	0.84	0.81	0.61	0.58	1.55	1.42
F1	37	85.12	4.56	7.20	4.79	0.81	0.62	1.04	0.96	5.84	2.63
F2	251	75.35	13.03	7.39	6.12	0.98	0.96	1.78	1.43	14.50	8.53
F3	950	64.35	20.76	28.62	19.49	1.07	1.33	1.06	1.19	4.90	5.38
MF4	11	71.20	15.76	5.71	4.72	3.57	2.70	13.12	8.86	6.40	4.74

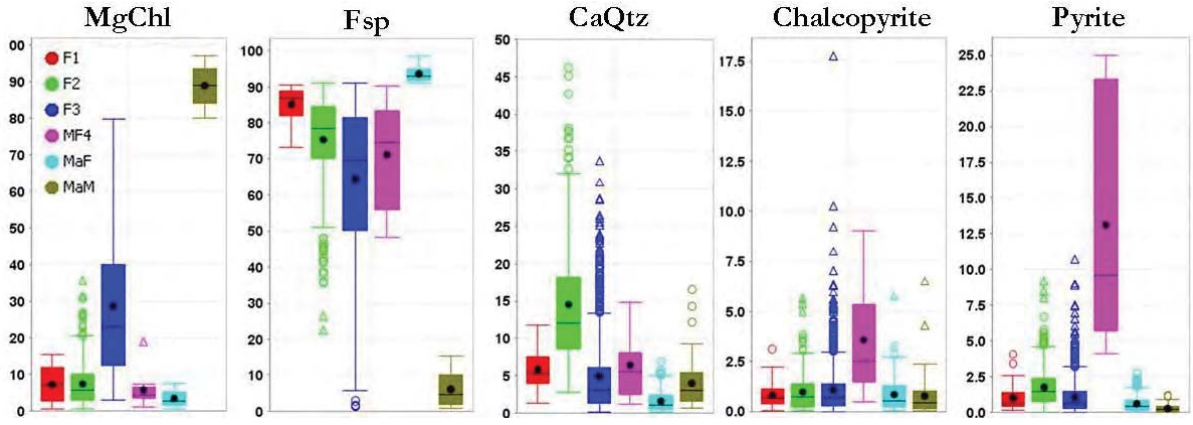

Figure 4.53. Box plots illustrating the mean (*black* line), median (*black* circle) and range of the mineral abundances for each of the texture classes.

Table 4.21. The modal mineralogy characteristics and the potential impacts on mineral processing behaviours for the meso-scale machine-based texture classes defined for Ernest Henry.

Texture Class	Distinguishing Features	Impact on mineral processing behaviour
MaM	Highest abundance of magnetite and lowest abundance of pyrite and feldspar.	High magnetite content can result in an ore that is hard to crush and grind (Napier-Munn et al., 2005) and possibly require more energy to operate the mill.
MaF	Highest abundance of feldspar and lowest abundance of carbonate/quartz and magnetite.	Feldspar is extremely hard. Ores with this texture can be predicted to be difficult to crush and grind (Napier-Munn et al., 2005) and require more energy to liberate the chalcopyrite from the ore.
F1	High abundance of feldspar minerals (80-90%) with most intervals containing 3-12% magnetite and 4-8% carbonate/quartz.	High abundance of feldspar can potentially impact the grinding and possibly the crushing behaviour depending on its distribution. The magnetite and carbonate/quartz content may aide initial breakage.
F2	Highest abundance of carbonate/quartz and pyrite (after MF4).	The high/abundance of carbonate/quartz minerals present as matrix material between clasts comprising of feldspar may aide in initial rock breakage. Abundance of pyrite can cause the production of a contaminated copper concentrate if it is picked up by flotation bubbles.
F3	High abundance of magnetite, 12-40% for most intervals.	Presence of magnetite can potentially result in a different in the crushing and grinding behaviour of an ore compared to the feldspar rich texture classes.
MF4	Highest abundance of pyrite and chalcopyrite.	High pyrite content can increase the possibility of pyrite floating with chalcopyrite and producing a contaminated copper concentrate (Petruk, 2005).

The distribution of the chalcopyrite PhReg size based on area for each texture class is shown in Figure 4.54. This figure shows that for the intervals classified with the suffix 'disseminated', all texture classes except MaM exhibit similar trends in their size distribution curves. 38-45% of the chalcopyrite PhRegs have an ECD of 300-600 µm and 26-30% have an ECD of 600-1200 µm (see Table 4.22). For the texture classes that contain 'clotted' chalcopyrite, the PhReg size distribution curves show that these classes also contain between 20-30% of the 'disseminated' chalcopyrite population (*black circle*). Texture classes F1(C) and MF4(C) are shown to exhibit similar trends with 35.6 % and 32.05 % of chalcopyrite PhRegs exceeding 1200 µm ECD. Texture class MaM(C) has the highest weight percent of coarse-grained chalcopyrite, with MaF(C), F2(C) and F3(C) all displaying bimodal size distribution curves with 32.50-41.00 % chalcopyrite exceeding an ECD of 1200 µm.

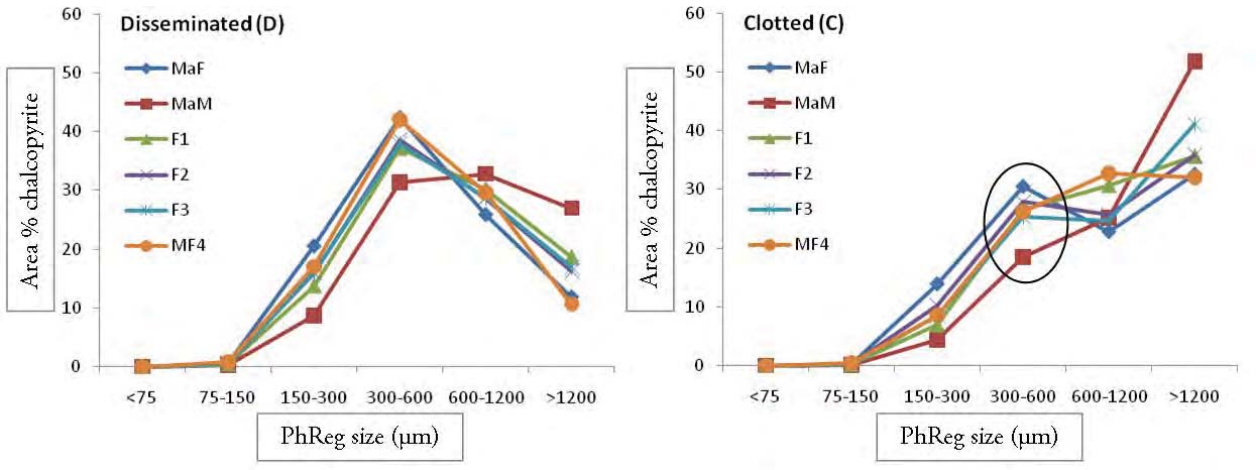

Figure 4.54. PhReg ECD size distribution curves showing the distribution of chalcopyrite size for each of the machine-based meso-scale texture classes. Chalcopyrite PhRegs have been normalised against the total chalcopyrite for each class. For n PhRegs for each texture class refer to Table 4.22.

Based on the size distributions shown in Figure 4.54 it can be proposed that the texture class MaM(C) will have the highest potential for liberation assuming the larger chalcopyrite is easier to liberate; followed by F1(C) and MF4 (C); MaF(C), F2(C) and F3(C); MaM(D) then MaF(D), F1(D), F2(D), F3(D) and MF4(D).

The minerals that are associated with chalcopyrite are also extremely important for liberation potential as well as level of grinding that will be required for the optimal liberation and recovery of chalcopyrite. Figure 4.55 shows the weighted average of each mineral group associated with chalcopyrite for each of the meso-scale texture classes (see also section 4.4.4, this chapter). This figure shows that there is little difference between the mineral associations of the 'disseminated' and 'clotted' classes (except for MF4). It is expected that this is due to the bimodal distributions observed in clotted textural classes Figure 4.54. As a result, the abundances of minerals associated with different size fractions of chalcopyrite have been calculated for each texture class and are shown in Table 4.22 and Figure 4.56. The size fractions are fine-grained (<150 µm ECD); medium-grained (150-600 µm ECD); coarse-grained (>600 µm ECD).

Table 4.22. PhReg size distributions and abundances of mineral groups that are associated with chalcopyrite for each of the texture classes that can be distinguished using the meso-scale machine based analysis.

Texture Class	MaF		MaM		F1		F2		F3		MF4	
	D	C	D	C	D	C	D	C	D	C	D	C
PhReg (n)	236690	125935	22785	42403	32280	27429	280270	300860	925429	1215574	21175	63754
Percent Area – ECD												
<75 µm	1.36 $\times10^3$	5.57 $\times10^4$	2.43 $\times10^3$	7.11 $\times10^4$	1.25 $\times10^3$	9.07 $\times10^4$	1.76 $\times10^3$	5.45 $\times10^4$	1.73 $\times10^3$	4.87 $\times10^4$	1.61 $\times10^3$	8.32 $\times10^4$
75-150 µm	0.56	0.32	0.24	0.11	0.46	0.20	0.60	0.30	0.52	0.20	0.76	0.43
150-300 µm	20.47	13.87	8.69	4.41	13.70	6.96	15.95	10.29	15.98	8.55	17.04	8.56
300-600 µm	42.32	30.47	31.3	18.47	37.14	26.48	38.59	27.85	37.91	25.38	41.95	26.22
600-1200 µm	25.82	22.78	32.8	25.19	30.12	30.70	28.66	25.72	28.71	24.61	29.63	32.74
>1200 µm	11.82	32.56	26.96	51.81	18.59	35.67	16.20	35.84	16.88	41.07	10.63	32.05
Area percent mineral groups associated with chalcopyrite												
CaQtz	1.83	2.16	2.93	2.14	4.42	4.42	3.66	9.00	6.20	2.72	3.48	5.29
MgCh	3.33	2.27	63.39	64.09	9.60	9.47	4.43	3.74	16.42	17.89	2.45	4.68
Fsp	90.00	88.36	30.04	27.75	76.88	76.32	72.06	71.42	71.53	67.20	72.92	57.59
Pyrite	2.94	3.69	1.98	3.35	7.23	6.71	10.85	12.04	6.33	7.79	19.18	29.48
Chalcopyrite	1.90	3.54	1.66	2.67	1.86	3.08	2.39	3.80	2.47	4.39	1.98	2.96
Area percent mineral groups associated with chalcopyrite : Fine-grained chalcopyrite (<150 µm)												
PhReg (n)	9636	3929	748	1070	1457	833	15034	11670	41819	37699	1352	3955
CaQtz	1.54	1.37	4.06	2.61	5.32	3.57	8.24	5.19	3.41	2.61	3.66	6.14
MgCh	4.60	3.30	78.11	74.43	6.85	7.56	6.70	5.03	20.44	17.44	3.40	3.76
Fsp	90.28	91.66	13.87	15.29	74.03	78.49	70.99	75.06	67.97	68.82	67.65	47.66
Pyrite	1.92	1.74	1.36	2.88	10.72	6.15	11.22	10.56	5.90	7.22	21.81	35.23
Chalcopyrite	1.66	1.93	2.59	4.79	3.08	4.23	2.85	4.16	2.29	3.91	3.49	7.21
Area percent mineral groups associated with chalcopyrite : Medium-grained chalcopyrite (150-600 µm)												
PhReg (n)	211989	103916	18703	32729	27628	22008	241419	254548	778128	1045472	18084	50103
CaQtz	1.12	0.77	2.17	1.40	3.64	2.99	8.45	5.65	2.45	1.62	2.93	5.01
MgCh	3.06	2.06	74.13	76.15	7.06	7.59	4.99	4.14	17.76	18.6	2.58	4.64
Fsp	92.58	93.44	21.02	18.53	81.71	82.99	76.54	80.22	73.59	72.57	76.73	60.54
Pyrite	1.77	1.58	1.28	1.83	5.92	4.07	8.02	7.13	4.28	4.38	15.97	26.36
Chalcopyrite	1.47	2.16	1.40	2.08	1.66	2.36	2.01	2.86	1.93	2.83	1.79	3.45
Area percent mineral groups associated with chalcopyrite : Coarse-grained chalcopyrite (>600 µm)												
PhReg (n)	15065	9875	3334	8604	3195	4588	23817	346642	105482	160538	1739	9696
CaQtz	3.04	3.28	3.44	2.36	5.22	5.14	12.49	11.10	4.19	3.29	4.27	5.43
MgCh	3.77	2.43	56.13	60.49	12.28	10.42	3.73	3.49	14.80	17.53	2.24	4.71
Fsp	85.58	84.26	36.15	30.50	71.87	72.95	66.64	65.95	69.15	64.43	67.42	56.08
Pyrite	4.96	5.38	2.45	3.81	8.56	8.05	14.28	15.08	8.76	9.56	23.84	31.12
Chalcopyrite	2.64	4.65	1.83	2.85	2.07	3.44	2.86	4.38	3.09	5.20	2.23	2.67

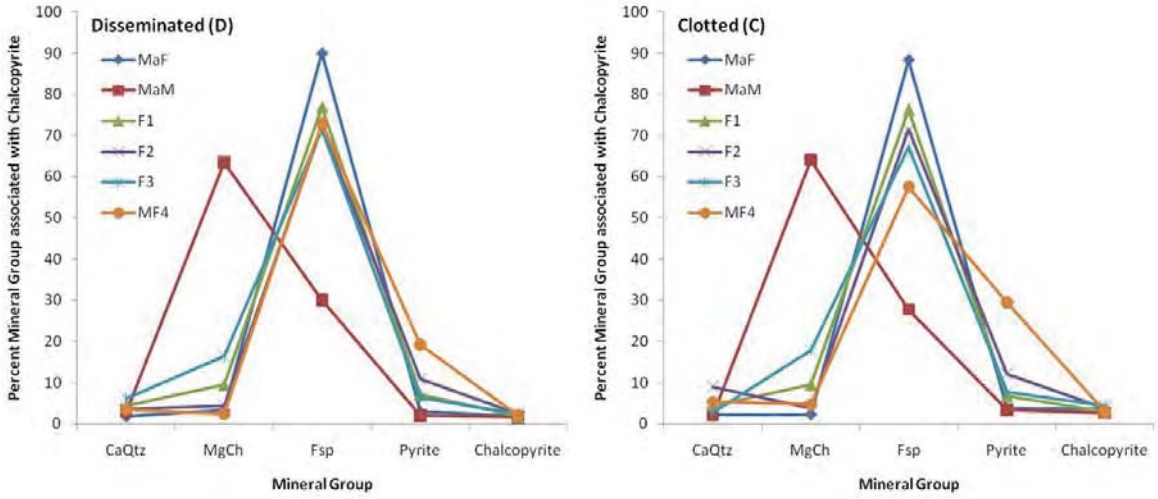

Figure 4.55. Abundances of mineral groups associated with chalcopyrite for each of the machine based meso-scale texture classes. Chalcopyrite PhRegs have been weighted against the total chalcopyrite for each class. For n PhRegs for each texture class refer to Table 4.22.

Figure 4.56 shows that for the 'disseminated' texture classes, most of the mineral groups associated with chalcopyrite are similar to those shown in Figure 4.55 (not texture class MaM). For the 'clotted' texture classes, MaF and F3 both showed an increase in the abundance of CaQtz and Pyrite associated with chalcopyrite as the chalcopyrite size increased. For F1, F2 and MF4 (also 'clotted') the abundance of chalcopyrite associated with the mineral group Fsp is highest for the medium-grained chalcopyrite. These changes indicate that as the chalcopyrite PhReg size increases, there is more chalcopyrite associated with the mineral groups that comprise the mineralized clots (CaQtz, Pyrite, Chalcopyrite and lesser Fsp). This change is the most pronounced in the texture class MaM which is predominantly massive MgChl. As the chalcopyrite PhReg size increases, the chalcopyrite associated with MgChl (for both disseminated and clotted) decreases and the abundance of chalcopyrite associated with Fsp, CaQtz and Pyrite starts to increase. The predicted impacts that each of the mineral groups will have on the liberation potential of chalcopyrite are presented in Table 4.23.

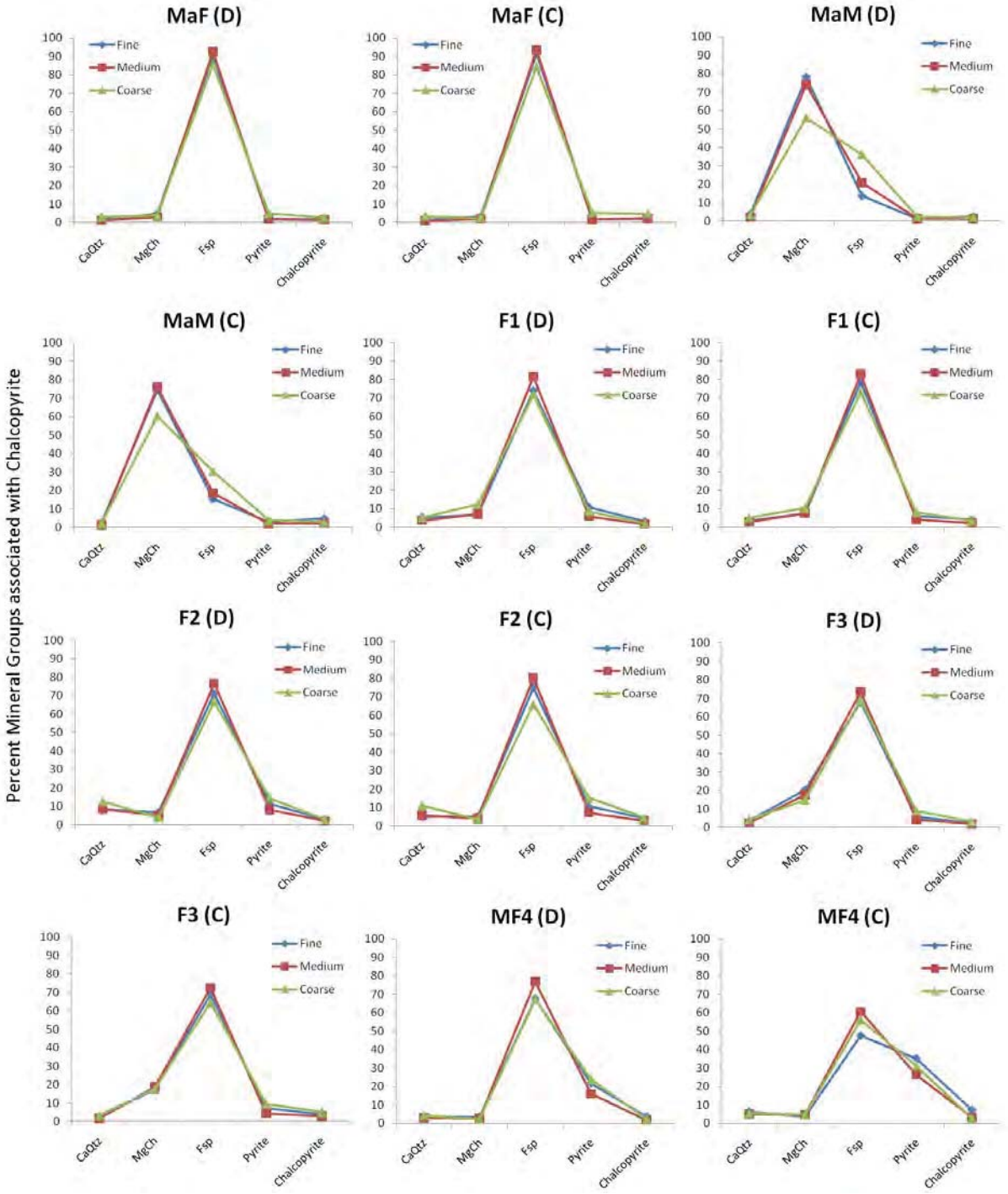

Figure 4.56. Abundance of mineral groups surrounding fine-, medium- and coarse chalcopyrite PhRegs for each machine based meso-scale texture class. Mineral group abundances have been calculated using the mineral group proportions present in the 5 pixel rim surrounding each chalcopyrite PhReg. Each chalcopyrite PhReg has been weighted against the total chalcopyrite for each class and size-range.

Table 4.23. The predicted impacts of mineral groups associated with chalcopyrite on the liberation potential and mineral processing behaviour of chalcopyrite in Ernest Henry examples.

Mineral Group	Texture classes with high (>60%) abundance of mineral group associated with chalcopyrite.	Texture classes with moderate (10-60%) abundance of mineral group associated with chalcopyrite.	Texture classes with minor (<10%) abundance of mineral group associated with chalcopyrite.	Potential impact on chalcopyrite liberation.
CaQtz			MaF (D), MaF (C), F1 (D), F1 (C), F2 (D), F2 (C), F3 (D), F3 (C), MF4 (D), MF4 (C), MaM (D), MaM (C).	The carbonate component of the CaQtz mineral group is expected to have a softening effect on the rock, however the quartz component is expected to be hard and cleanly liberate where it is in contact with chalcopyrite.
MgChl	MaM (D), MaM (C).	F3 (D), F3 (C).	MaF (D), MaF (C), F1 (D), F1 (C), F2 (D), F2 (C), MF4 (D), MF4 (C).	The magnetite component of the MgChl group is expected to be hard and cleanly liberate from chalcopyrite, however the chlorite component is expected to be soft and potential remain locked with the chalcopyrite during liberation.
Fsp	MaF (D), MaF (C), F1 (D), F1 (C), F2 (D), F2 (C), F3 (D), F3 (C), MF4 (D).	MF4 (C), MaM (D), MaM (C).		Fsp is predicted to be hard and require more energy to grind than the other mineral groups.
Pyrite		MF4 (D), MF4 (C), F2 (D), F2 (C).	MaF (D), MaF (C), F1 (D), F1 (C), F3 (D), F3 (C), MaM (D), MaM (C).	Can potentially stay locked with chalcopyrite and contaminate the copper concentrate.
Chalcopyrite			MaF (D), MaF (C), F1 (D), F1 (C), F2 (D), F2 (C), F3 (D), F3 (C), MF4 (D), MF4 (C), MaM (D), MaM (C).	Indicates that other chalcopyrite PhRegs are proximal to existing grains (potential clustering).

Spatial distribution of textural classes

The ultimate aim of creating a meso-scale classification is to establish if potential differences in mineral processing behaviours can be predicted prior to metallurgical testing and mining. The classification that has been presented in this section shows that a number of classes can be distinguished using the data extracted from the classified images of drill-core. These classes exhibit different mineral compositions as well as different chalcopyrite sizes and mineral relationships. All of these characteristics contribute to the ease with which a rock is crushed and minerals are liberated in the mineral processing circuit. If however, the textural classes are not spatially coherent and typically occur at a scale that is less than that of a mining bench (typically 20-50 metres), then the textures that are being processed will become blended and difficult to monitor.

The spatial distribution of the six machine based meso-scale texture classes (MaM, MaF, F1, F2, F3 and MF4; not including the PhReg size suffix) are shown in Figure 4.57 for the drill- holes EH432, EH446, EH556, EH574, EH633 and EH635. The most dominant machine based meso-texture within the six holes is F3 which comprises 65% of the classified intervals. F2 typically occurs interlayered with F3 intervals between 1 and 20 metres thick. Both F2 and F3 have similar distributions to the mineral group Fsp with a variation in other gangue minerals (typically in the matrix of the fragmental units). MaF occurs as sections ranging from 1-35 metres thick. Both texture classes F1 and MF4 only occur as small sections ranging from 1-18 metres thick.

The machine based meso-scale texture classes defined in this section will be compared against micro-scale mineralogical and textural data obtained from the MLA and optical microscopy analysis of drill-core tiles. This will determine if the mineralogical and textural results obtained from the meso-scale analysis are observed at micro-scale.

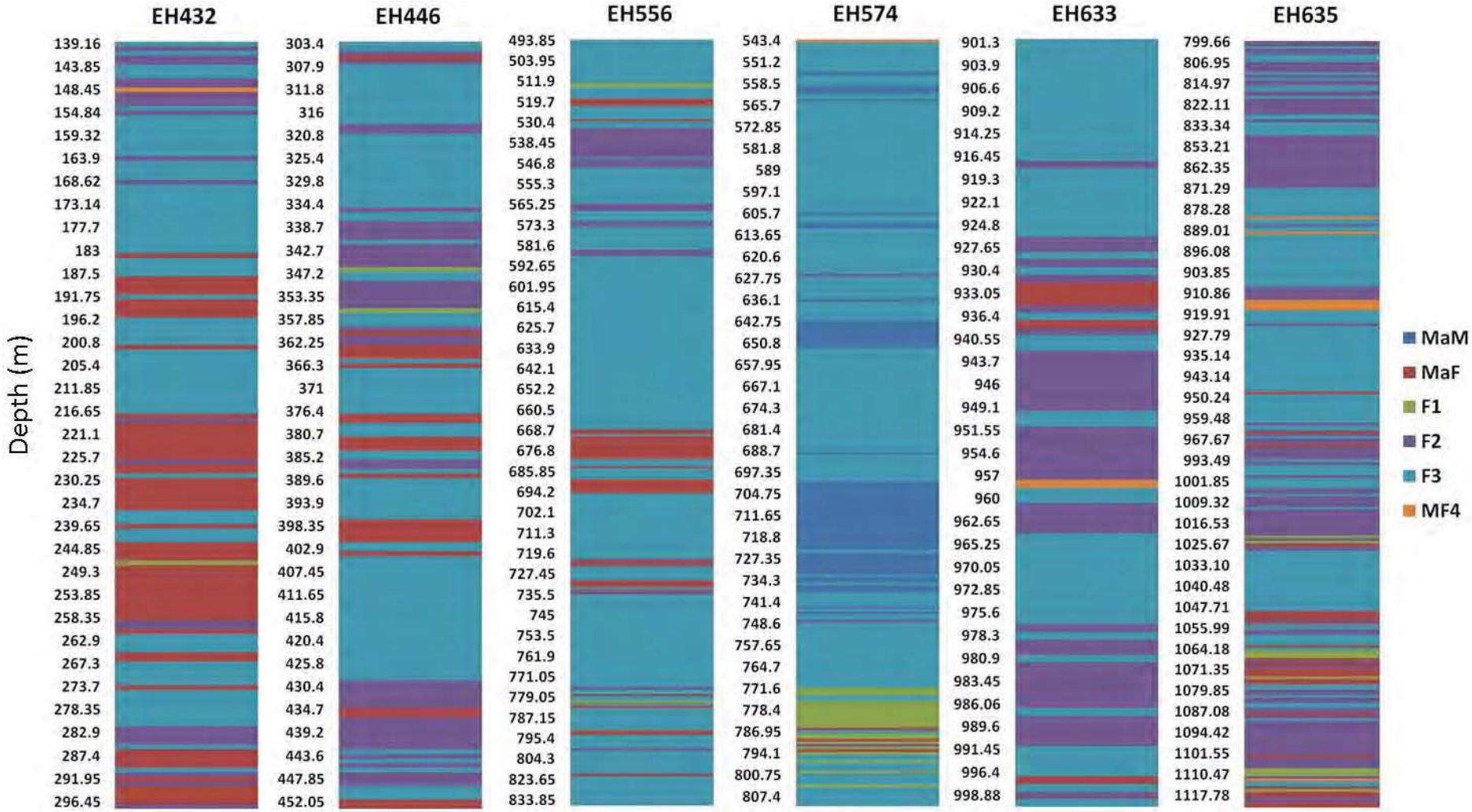

Figure 4.57. The spatial distribution of the machine based meso-scale textural classes at Ernest Henry for EH432, EH446, EH556, EH574, EH633 and EH635.

Meso-scale textural classes compared to lithology

The modal mineralogy calculated from classified core images has been compared to lithologies that have been logged by site geologists at Ernest Henry. There are 13 different lithologies present in the six drill holes that have been analysed in this study. The abbreviations and the site descriptions for these lithologies are presented in Table 4.24. Figure 4.58 illustrates examples of each of these. The most common lithologies present in the six drill holes are fv2, fv1, mmb, amv2 and fv respectively. The modal percent for each of the five mineral groups (Chalcopyrite, Pyrite, CaQtz, MgChl, Fsp) are plotted in Figure 4.59 for each lithology. This figure shows that the modal percentages of each mineral group are highly variable within most of the lithologies. Lithologies amv1 and fv3 have the least variability in their mineralogy (i.e. few outliers and small interquartile range) and are both dominated by feldspar minerals. Given the highly variable mineral abundances across most lithologies, the lithological units and boundaries are probably not good constraints for selecting samples for metallurgical performance.

Table 4.24. Abbreviations and logging descriptions for Ernest Henry lithologies present in EH432, EH446, EH556, EH574, EH633 and EH635.

Lithology	Description
amv	Altered mafic volcanics, generally phenocryst poor, very fine to fine grained, variably amygdaloidal, massive to banded volcanic rock (Figure 4.58A). n = 23
amv1	Altered fractured mafic volcanics - brittle fracturing, clast supported, can be overprinting alteration (Figure 4.58B). n = 27
amv2	Altered mosaic mafic volcanics – matrix supported breccia with moderate to strong digestion of clasts (Figure 4.58C). n = 88
fv	Felsic volcanics – not fractures, veined or brecciated (Figure 4.58D). n = 75
fv1	Fractured felsic volcanics – brittle fracturing, clast supported, can be overprinting alteration (Figure 4.58E). n = 127
fv2	Mosaic felsic volcanics – matrix supported breccia with moderate to strong digestion of clasts (Figure 4.58F). n = 786
fv3	Lithic felsic volcanics – generally matrix supported with aligned clasts (Figure 4.58G). n = 46
iv	Intermediate volcanics – massive to banded rock (Figure 4.58H). n = 83
iv1	Intermediate volcanics – brittle fracturing, clast supported (Figure 4.58I). n= 32
iv2	Intermediate volcanics – matrix supported breccia (Figure 4.58J). n = 39
mmb	Marble matrix breccias – massive carbonate rock. Generally reserved for the footwall of the mineralised zone, contains 'swirly' textures (Figure 4.58K). n = 115
sch3	Weakly to moderate foliated schist (Figure 4.58L). n = 11
vn	Vein. n = 2

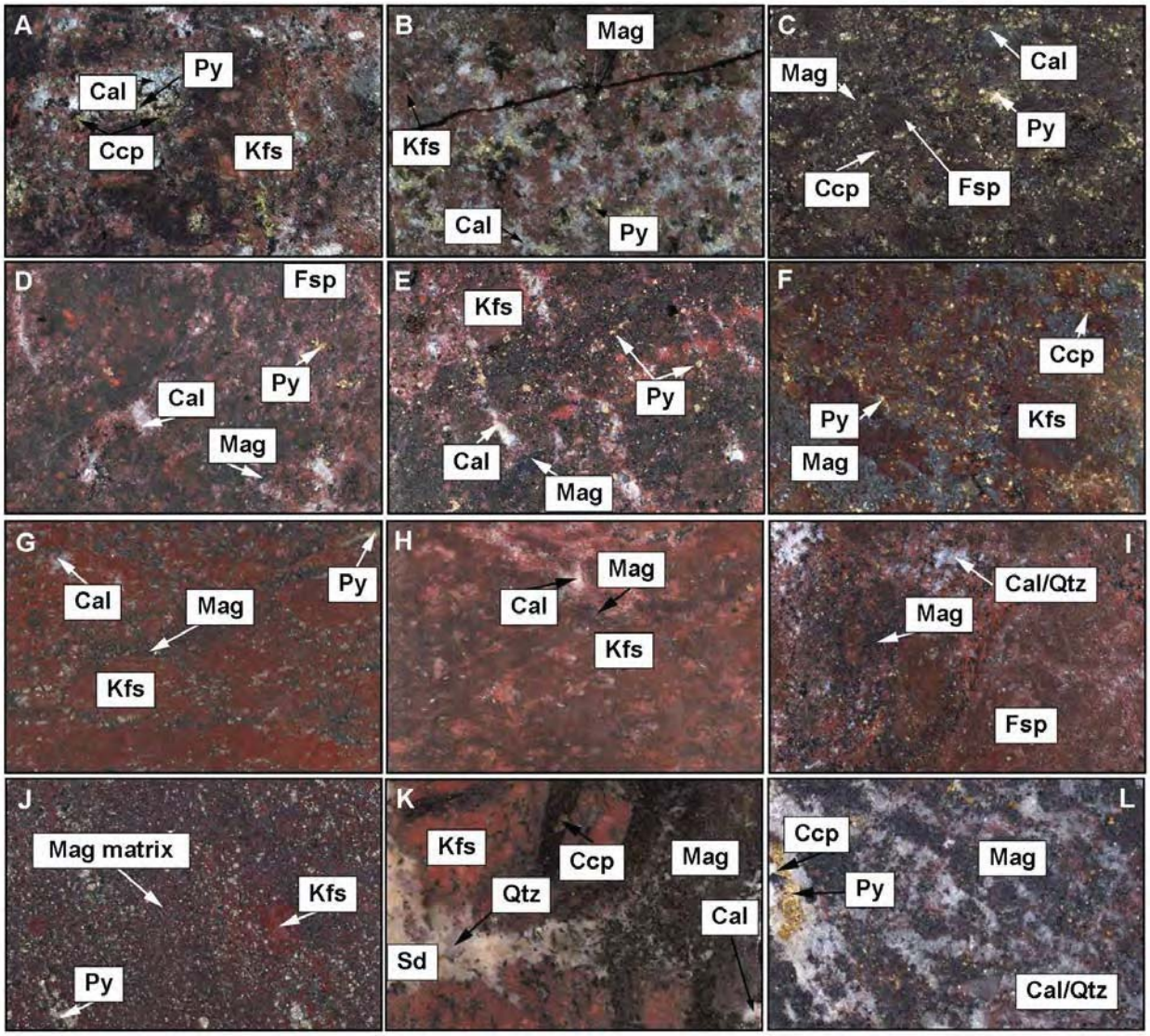

Figure 4.58. Photographs illustrating the lithologies logged by site geologists for the drill holes selected for analysis in this project. All photographs taken using the GEOTEK MSCL **A.** EH633 961m; amv lithology **B.** EH635 852.33m; amv1 lithology **C.** EH635 873.95m; amv2 lithology **D.** EH556 523.25m fv lithology **E.** EH556 531.25m; fv1 lithology **F.** EH556 591.65m; fv2 lithology **G.** EH635 1083.42m; fv3 lithology **H.** EH556 821.00m; iv lithology **I.** EH635 1097.18m; iv1 lithology **J.** EH635 1113.42m; iv2 lithology **K.** EH432 373.90m; mmb lithology **L.** EH556 557.10m sch3 lithology. All image widths are 5.5cm. *For mineral abbreviations refer to Appendix 1.1.*

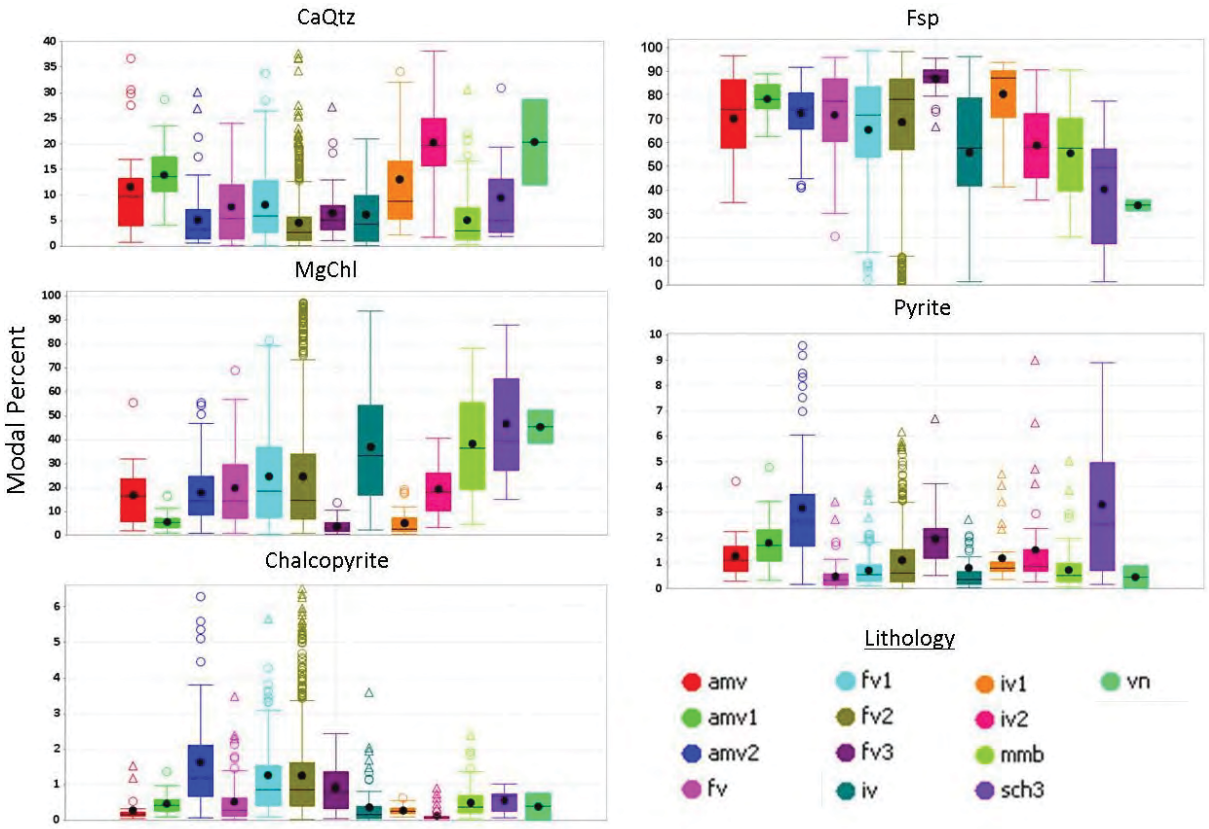

Figure 4.59. Boxplots illustrating the modal mineralogy for lithologiocal units logged by site-geologists. Percentages of mineral classes calculated from classified images for the lithologies described in Table 4.24.

4.6.4 Summary

The interpretations of the meso-scale mineralogical and textural analysis for Ernest Henry have been presented in section 4.6. In this section both the meso-scale visual logging results and automated classification of drill-core images were considered.

The visually logged mineralogical and textural attributes from Ernest Henry were correlated with the rock properties that were predicted to influence different aspects of mineral processing behaviours. These properties are the gangue mineral textures i.e. massive and fragmental; the dominant gangue minerals (feldspar, calcite, quartz, magnetite, pyrite); and the size of the valuable mineral phase chalcopyrite. Based on these properties, 9 texture classes, each with a suffix for size (disseminated or clotted) were identified (see Table 4.15). As a result, each two-metre interval from drill-hole EH635 and each sampled interval from drill holes EH432, EH446, EH556, EH574 and EH633 were assigned a texture class or mixture of texture classes.

The results of the visual logging have been compared to the mineralogical and textural data that have been extracted from the classified images of drill-core. In total 1454 images of drill-core were classified. From these images the mineral groups MgChl, CaQtz, Pyrite, Fsp and chalcopyrite were identified (see section 4.4.2) and the following attributes measured: modal mineralogy, chalcopyrite area (measured as an equivalent circle diameter), chalcopyrite length and the gangue mineral groups associated with chalcopyrite (calculated from the 5 pixel rim surrounding chalcopyrite). Using the mineralogical and textural attributes extracted from the classified images of drill-core, three of the meso-scale visual classes are able to be distinguished (MaF, MaM and MF4)

and the remaining six grouped into three classes (Six classes in total: MF1 and BF1 → F1; MF2 and BF2 → F2; MF3 and BF3 → F3). The grain-size suffix was determined using length as a threshold (>150 pixels length = clotted; <150 pixels length = disseminated). 15 examples of each texture class were selected for mineralogical and textural analysis in order to determine which parameters had the most potential predicting differences in mineral processing behaviours. These parameters are modal mineralogy, area (measured as an equivalent circle diameter) and the gangue mineral groups associated with chalcopyrite.

The data for all of the chalcopyrite objects (3 295 584 PhRegs) were combined and the modal mineralogy, area and gangue minerals associated with chalcopyrite were calculated for each of the machine-based meso-scale texture classes (section 4.6.4). The spatial distribution of each class down-hole was also observed in order to determine if the texture classes occurred as coherent sections or were sparsely distributed. The results and interpretations that have been presented in this section will be compared against higher resolution and more accurate micro-scale analysis in Chapter 5. This will determine whether meso-scale features identified in drill-core can be used as a proxy for more detailed micro-scale mineralogical analyses.

4.7 Comparison of meso-scale techniques

A comparison of both meso-scale logging techniques that have been described in this chapter and how they can potentially be used together are described in Chapter 7 (The integration of meso- and micro-scale techniques). In this chapter the integration of the visual and machine-based logging techniques will also be compared to the results of the micro-scale mineralogical and textural analyses that are presented in the next two chapters (Chapter 5: Mineralogy and texture of intact rocks: micro-scale and Chapter 6: Mineralogy and texture of particulate rocks: micro-scale).

4.8 Summary

Knowledge of rock characteristics can lead to an improved understanding of a rock's potential processing performance. Primarily in mining, this understanding begins at the meso-scale with drill-core. In this chapter, results and interpretations for two methods for measuring meso-scale mineralogical and textural attributes have been presented: The visual logging of mineralogy and texture predicted to potentially influence mineral processing behaviours (crushing, grinding, liberation, flotation: section 4.2 and 4.3); and the machine-based logging of mineralogy and texture using mineral maps created from medium resolution photographs of drill-core in conjunction with object-oriented image analysis software (section 4.6). Both meso-scale methods were applied at Ernest Henry, however only the visual logging method was applied to Cadia East.

The method for the visual logging of mineralogical and textural attributes in drill-core is outlined in Chapter 3, section 3.2. This method was developed with the aim of being suitable across different deposits and deposit styles. The types of attributes that were measured at both deposits in this study were considerably different despite the dominant copper sulphide mineral (chalcopyrite) being the same at both deposits. The dominant gangue mineral phases present at both deposits are significantly different. Cadia East is dominated by feldspar, quartz, biotite, chlorite, illite and muscovite, whereas at Ernest Henry the dominant gangue minerals are feldspar, magnetite, calcite, quartz and pyrite. The distributions of the copper sulphide minerals as well as the gangue minerals are also different for both deposits. In this chapter these data were used to create a number of

textural classes that were considered to have unique mineralogical and textural characteristics that could potentially correlate with mineral processing behaviours. These classes do not correlate with existing drill-core logging undertaken by site geologists. They correlate better with elemental and mineral assay data. More detailed (and accurate) micro-scale analyses are tested against these classes in the next two chapters.

The method for the production of meso-scale mineral maps and the extraction of quantified mineralogical and textural attributes is outlined in Chapter 3, sections 3.3. This method was applied to Ernest Henry, where 1774 metres of drill-core from drill-holes EH432, EH446, EH556, EH574, EH633 and EH635 were photographed using the GEOTEK MSCL and classified into mineral maps using the Definiens software. The production of minerals maps from drill-core has allowed quantified meso-scale mineralogical and textural attributes to be extracted. For Ernest Henry, the attributes that have been extracted are modal mineralogy, chalcopyrite area, length and width of chalcopyrite and the minerals associated with chalcopyrite. Four examples were selected based on differences in gangue mineralogy and were used to show the mineralogical and textural analysis undertaken on each image. The data extracted from all of the images was used to determine whether the classes established from visual logging of drill-core could be identified using the quantified data extracted from mineral maps. For Ernest Henry, 6 of the 9 textural classes could be identified. The mineralogical and textural attributes that have been extracted from the meso-scale mineral maps will also be extracted from the micro-scale mineral maps and presented in the next chapter. A comparison of these techniques is presented in Chapter 7.

Chapter Five

Mineralogy and texture of intact rocks: Micro-scale

5.1 Introduction

Presented in this chapter are the results of the micro-scale mineralogical and textural analysis undertaken using automated optical microscopy and the Mineral Liberation Analyser (MLA) for the Cadia East and Ernest Henry mineral deposits. The results are presented as follows:

- 5.2. Results of optical microscopy analysis: Ernest Henry.
- 5.3. Results of MLA analysis: Cadia East.
- 5.4. Results of MLA analysis: Ernest Henry.
- 5.5. Summary of micro-scale mineralogy and texture: Ernest Henry.
- 5.6. Summary of micro-scale mineralogy and texture: Cadia East.
- 5.7. Conclusions

The methods of both micro-scale analytical techniques have been described in Chapter 3, sections 3.4 and 3.5. Here the quantified results from the analysis of high resolution classified images obtained from optical microscopy and MLA have been used to compare with the mineralogical and textural attributes that were previously recognised in drill-core at the meso-scale, as well as to search for other micro-scale attributes that are predicted to effect mineral processing behaviours. The results have been analysed using a range of statistical methods including Principal Components Analysis (PCA) in order to identify naturally occurring mineralogical relationships at both Cadia East and Ernest Henry. These data have also been compared to other quantified results including chemical and mineral assays (see Chapter 3, section 3.7). With respect to the optical microscopy analyses, these have been undertaken on samples from both Ernest Henry and Cadia East, however the analysis of cm-scale intact mineral textures (from drill-core tiles, see Chapter 3, Figure 3.1) has only been undertaken on samples from Ernest Henry. The samples analysed from Cadia East are coarse

particulates (-3mm + 400 μm) and the results are presented separately in Chapter 6. MLA analysis has been undertaken on intact textures for both deposits.

5.2 Results of optical microscopy analysis: Ernest Henry

Based on the method described in Chapter 3, section 3.4, high resolution optical microscopy images of drill-core tiles have been produced for rock samples from Ernest Henry. In total, 406 drill-core tiles have been taken from drill-holes EH432, EH446, EH556, EH574, EH633 and EH635 (see Chapter 4, Figure 4.10). The classification and extraction of quantified mineralogical and textural information from these images was undertaken using Definiens software (Table 5.1). The results are summarised in this section and detailed in the following appendices:

Appendix 5.1 Modal mineralogy calculated from classified images of drill-core tiles: Ernest Henry

Appendix 5.2 Mineralogical and textural attributes of chalcopyrite calculated from classified images of drill-core tiles: Ernest Henry

From the 406 drill-core tiles, thirty examples of mineral maps obtained from the optical microscope have been selected for a detailed mineralogical and textural analysis (Table 5.2, see also Figure 4.52 *later in this chapter*). These samples were selected based on the surviving texture classes that were defined by the meso-scale visual and machine based logging presented in the previous chapter (section 4.4).

Table 5.1. Drill-holes, meterages and number of tiles that have been sampled and photographed using the Leica DM6000 optical microscope for Ernest Henry as well as the mineralogical and textural attributes that have been measured from the classified images.

Drill Hole	From	To	# of tiles	Rock	Chalcopyrite
EH432	150m	400m	70	Modal Mineralogy	Area Length and width Minerals associated with chalcopyrite
EH446	300m	600m	74		
EH556	450m	750m	91		
EH574	544m	810m	73		
EH633	858m	1166m	32		
EH635	800m	1120m	66		

Table 5.2. Drill-hole numbers, depths and number of chalcopyrite (ccp) PhRegs for the 30 core tile samples presented in this section. Examples were chosen from three categories (mottled – fine-grained; mottled – coarse grained; and massive) as defined in Chapter 4, section 4.6.

Mottled (Fine-grained)				Mottled (Coarse-grained)				Massive			
	Example	Texture	# ccp PhRegs		Example	Texture	# ccp PhRegs		Example	Texture	# ccp PhRegs
1	EH432 253.15	F3	3468	11	EH432 376.10	F1	5815	21	EH432 213.07	MaM	2702
2	EH446 353.00	F3	6037	12	EH432 377.00	F1	2611	22	EH446 395.35	MaF	1866
3	EH556 592.00	F3	670	13	EH446 386.10	F3	4530	23	EH574 765.00	MaM	6842
4	EH556 706.05	F3	2219	14	EH446 399.00	F1	2873	24	EH574 783.00	MaF	1721
5	EH574 578.90	F2	1685	15	EH446 471.50	F3	7218	25	EH574 798.00	MaF	142
6	EH574 586.00	F2	5566	16	EH574 596.00	F1	5646	26	EH574 800.00	MaF	354
7	EH574 594.00	F2	5734	17	EH633 999.00	F2	2740	27	EH633 887.00	MaM	8337
8	EH633 879.00	MF4	4757	18	EH635 923.00	F3	2174	28	EH633 915.00	MaM	4375
9	EH635 919.00	MF4	6793	19	EH635 945.00	F3	5469	29	EH633 1159.00	MaF	1475
10	EH635 921.00	F2	4302	20	EH635 985.00	F3	3840	30	EH635 933.00	MaM	4398

5.2.1 Ernest Henry mineral categories

For the classification of drill-core tiles, the minerals and mineral groups that are able to be identified were restricted to those that could be identified using reflected light microscopy and those that can easily be distinguished based on their colour. The rule set for the production of classified mineral maps was defined by Ass. Prof. Ron Berry, these are outlined in Table 5.3. Given that the images taken using the optical microscope have been taken on intact rock tiles and not as thin sections, the silicate and mica minerals are not able to be identified using their characteristic optical properties. The oxide and sulphide minerals however display their unique reflected light signatures, making them easier to identify. An examples of a high resolution reflected light image and the corresponding mineral map are shown in Figures 5.1A and 5.1B respectively. The mineral maps of the 30 examples that have been selected for detailed analyses are shown in Figure 5.2.

Table 5.3. The minerals and mineral groups used in the classification of optical microscopy images as well as the possible minerals that could be included in the classification and the corresponding RGB colours.

Mineral Category	Minerals included in classification	RGB colour
Barite	barite	192, 87, 255
Carbonate minerals	calcite, dolomite	0, 0, 255
Chalcopyrite	chalcopyrite	192, 192, 0
Hematite	hematite	0, 255, 0
Mafic minerals	biotite, chlorite, tourmaline	86, 128, 0
Magnetite	magnetite	255, 0, 0
Pyrite	pyrite	255, 255, 0
Quartz	quartz with lesser feldspar and carbonate minerals	0, 255, 255
Red Feldspar	k-feldspar, albite	128, 0, 59
Titanite	titanite	0, 128, 0
Pit		0, 0, 128
Unclassified		0, 0, 0

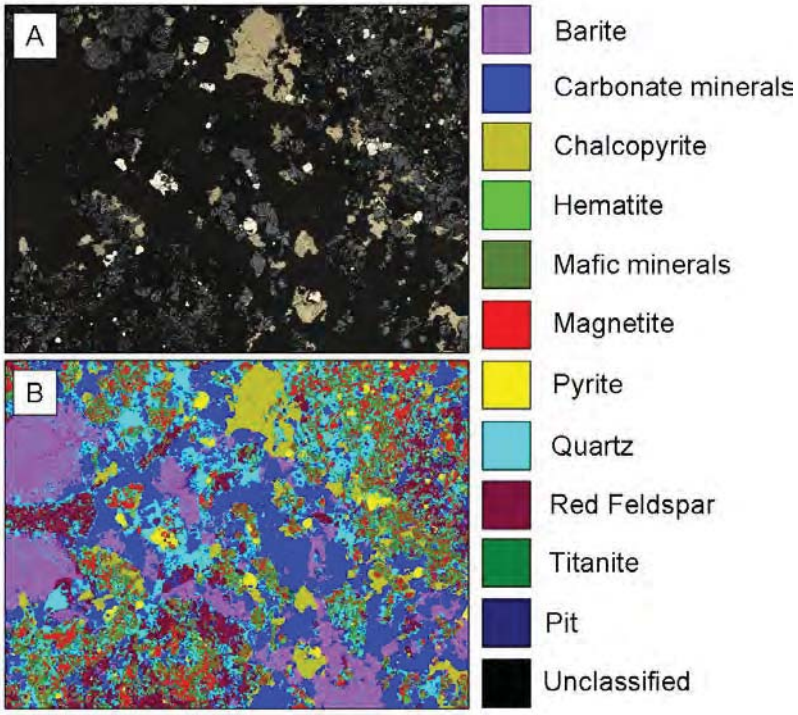

Figure 5.1. EH635 985m. **A.** High resolution reflected light image **B.** Mineral map produced from the classification of reflected light, reflected light crossed polars. Classified images were produced using Definiens and have a width of 2.5 cm.

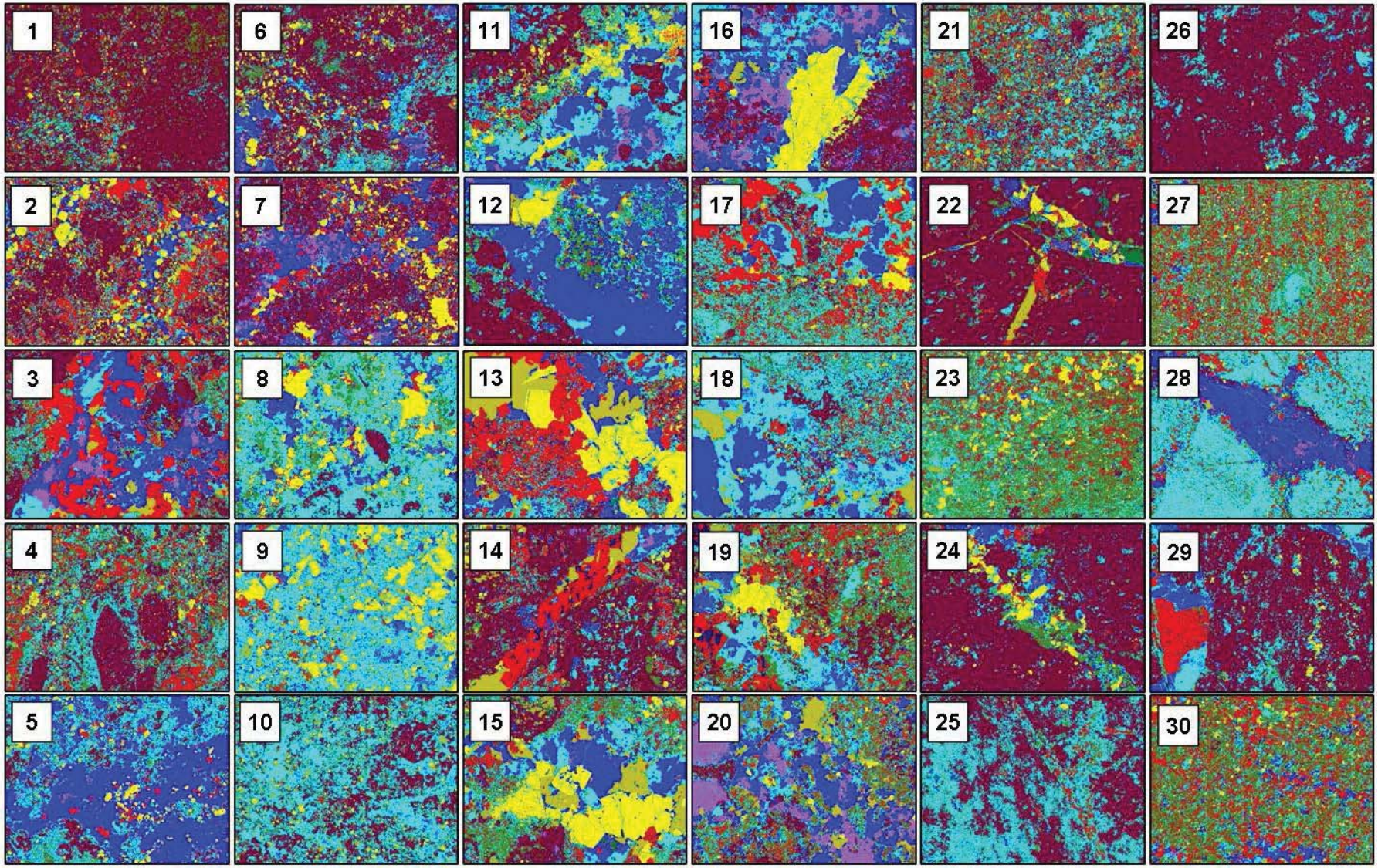

Figure 5.2. Mineral maps of the 30 Ernest Henry examples that are presented in section 5.2 (Table 5.3). All images have a width of 3cm. *For mineral key see Figure 5.1.*

5.2.2 Modal Mineralogy

The modal mineralogy calculated from optical microscopy mineral maps is not representative of 2m intervals unlike the modal mineralogy calculated from the meso-scale mineral maps that were presented in the previous chapter which were able to be to used observe changes in mineral groups with depth (see Chapter 4, section 4.5.2). The optical microscope images represent the combinations of minerals that typically occur together at a much higher resolution than the meso-scale millimetres and are therefore considered more to be more accurate. Shown in Figure 5.3 are the mineral abundances (presented as pie charts) calculated from the minerals maps for the thirty selected examples. This figure shows that there are several common mineral signatures present:

- Abundant Red feldspar: > 50% (i.e. examples 1, 6, 14, 22, 24, 26, 29)
- Abundant Quartz: > 40% (i.e. examples 4, 8, 9, 10, 11, 18, 21, 25, 28)
- Abundant Magnetite: > 25% (i.e. examples 3, 7, 13, 27, 30)
- Abundant Pyrite: > 10% (i.e. examples 8, 13, 15, 16)

While a visual estimate provides a broad overview of the mineralogy, simply observing the mineral abundances of each mineral map independently does not provide information regarding the common mineral relationships (combinations) that occur between these minerals. In order to determine what these relationships are a Principal Components Analysis (PCA) has been performed on the mineral abundances calculated from all of the optical microscopy mineral maps (406 images; see Table 5.1; Appendix 5.2). The PCA determined that 67.1% of the variability in mineral abundances can be accounted for within the first four principal components (see Chapter 2, section 2.8.3). The minerals and mineral groups used in this analysis are shown in Table 5.4 with the corresponding data for each principal component. Scatter plots of the first four principal components are shown in Figure 5.4 (PC1 and PC2) and Figure 5.5 (PC3 and PC4). Labelled on the scatter plots are areas where a sample rich in a particular mineral would plot. Based on the results presented in Table 5.4, Figure 5.4 and Figure 5.5, the most commonly occurring mineralogical signatures are:

- Red Feldspar (PC3)
- Quartz (PC2)
- Barite and carbonate minerals (PC1, PC3 and PC4)
- Magnetite, hematite and mafic minerals (PC1)
- Chalcopyrite, pyrite, magnetite and hematite (PC2)
- Pyrite and chalcopyrite (PC4, PC2, and PC9)
- Barite and hematite (PC4)

Also shown in the PCA are the minerals or mineral groups that are not likely to occur together. For example, PC1 indicates that Barite and Carbonate minerals occur together (or may reflect the difficulty in distinguishing these minerals from each other using optical microscopy) as will magnetite, mafic minerals, hematite and red feldspar, but not in the same sample. PC2 indicates that chalcopyrite, pyrite, magnetite and hematite will occur together but not in the same sample as quartz. The percentage of the mineralogical variability that each principal component represents is given by the 'variance proportion' in Table 5.4.

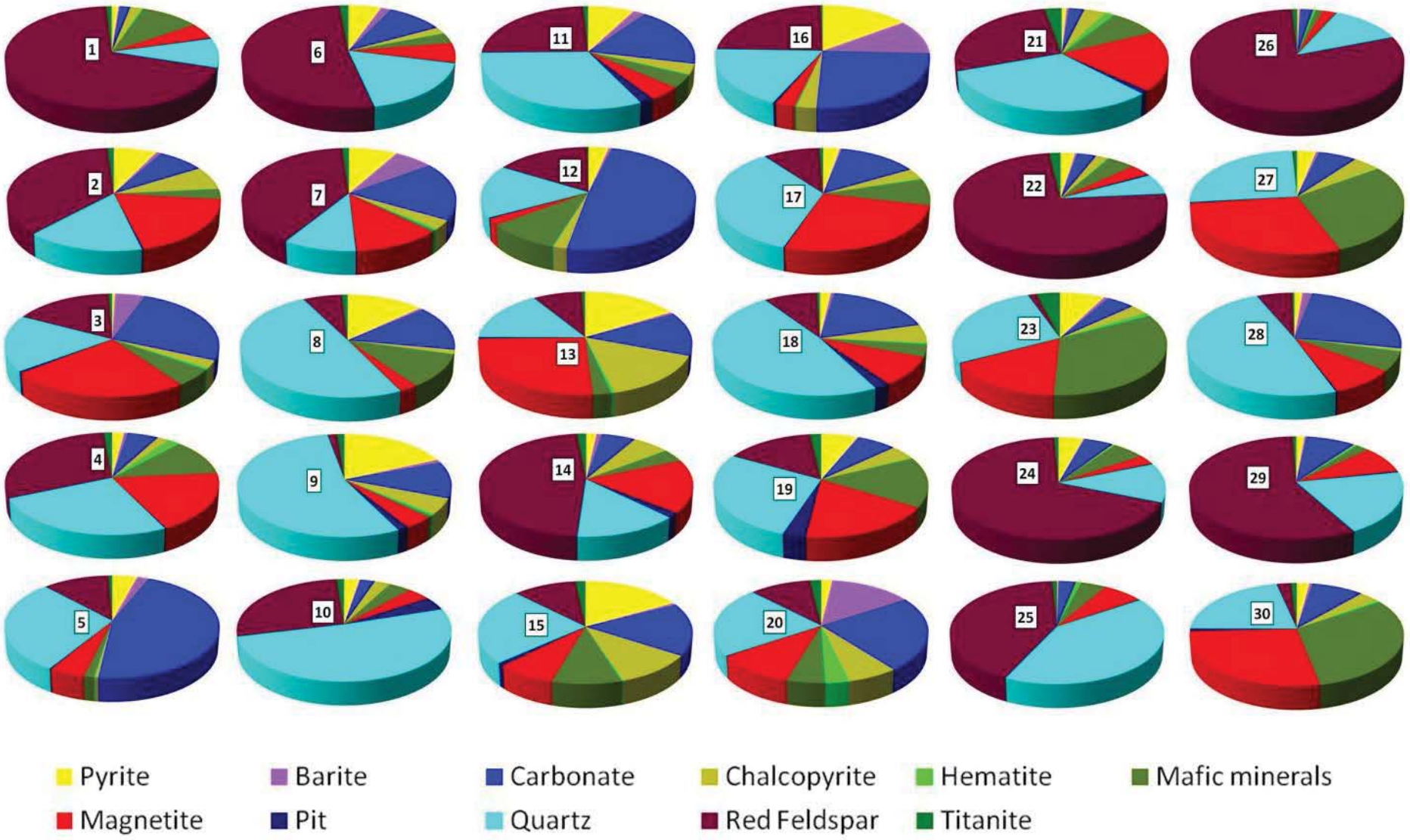

Figure 5.3. Modal mineralogy calculated from classified mineral maps for the 30 selected examples for Ernest Henry (Table 5.2).

Table 5.4. Minerals and mineral groups used in the PCA of the mineral abundances determined from optical microscopy mineral maps. PC refers to Principal Component. n = 398 images.

Mineral	PC1	PC2	PC3	PC4	PC5	PC6	PC7	PC8	PC9
Pyrite	0.183	0.259	-0.111	0.599	-0.668	0.203	0.112	-0.058	0.159
Barite	0.406	0.219	-0.337	-0.360	0.043	0.0	0.140	-0.713	0.119
Carbonate Minerals	0.480	-0.062	-0.430	-0.223	-0.037	-0.093	-0.148	0.601	0.372
Chalcopyrite	-0.034	0.358	-0.217	0.492	0.591	-0.324	0.319	0.067	0.143
Magnetite	-0.416	0.401	-0.183	-0.019	0.112	0.266	-0.657	-0.084	0.333
Mafic Minerals	-0.493	-0.244	-0.191	-0.110	-0.338	-0.575	0.150	-0.133	0.405
Quartz	-0.068	-0.602	-0.140	0.198	0.254	0.540	0.193	-0.137	0.403
Red feldspar	-0.230	0.138	0.743	-0.063	0.057	-0.090	0.015	-0.039	0.599
Hematite	-0.312	0.389	-0.017	-0.404	-0.086	0.380	0.594	0.279	0.077
Variance Proportion	**20.3**	**18.3**	**17.0**	**11.5**	**9.9**	**8.6**	**7.6**	**6.5**	**0.3**

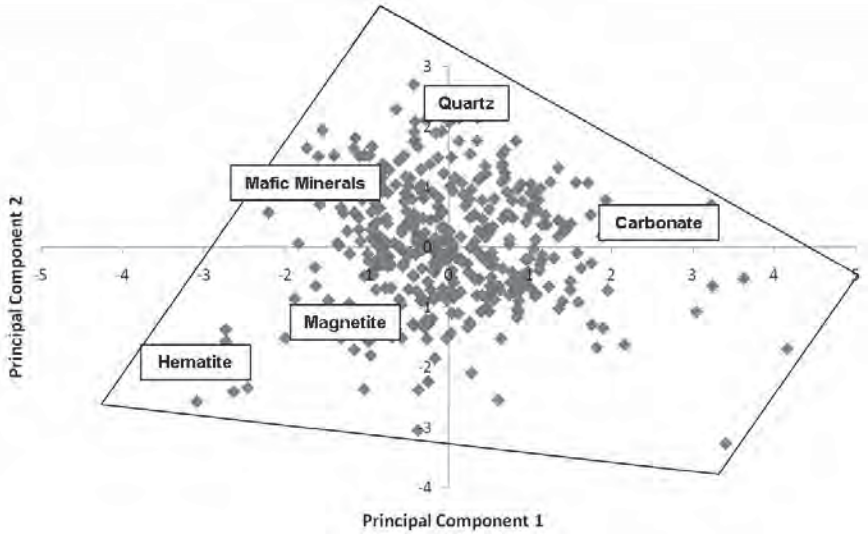

Figure 5.4. Scatter plot showing Principal Component 1 versus Principal Component 2 for the PCA undertaken on mineral abundances calculated from optical microscopy mineral maps. Mineral labels indicate where a sample abundant in that mineral will plot. n= 406 images.

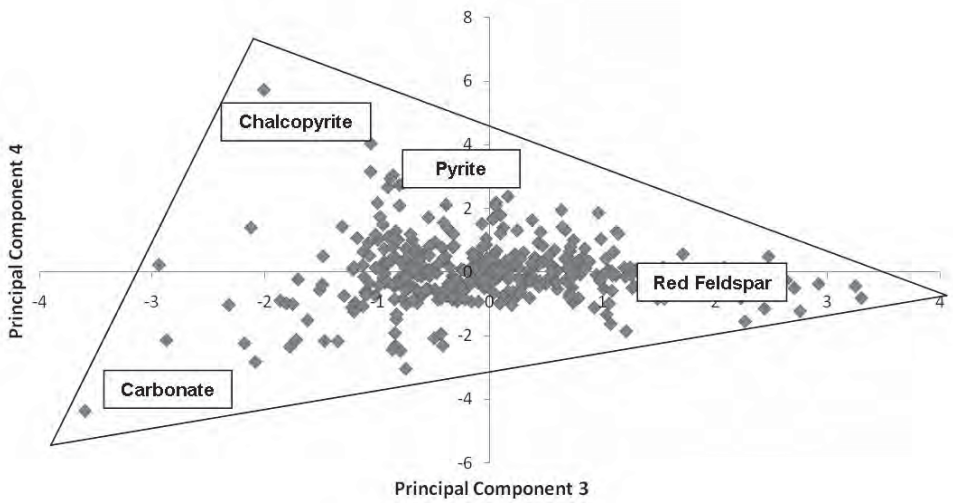

Figure 5.5. Scatter plot showing Principal Component 3 versus Principal Component 4 for the PCA undertaken on mineral abundances calculated from optical microscopy mineral maps. Mineral labels indicate where a sample abundant in that mineral will plot. n= 406 images.

5.2.3 Chalcopyrite size

The size of each chalcopyrite PhReg has been measured from the mineral maps produced from optical microscopy images of 406 drill-core tiles from Ernest Henry (see Table 5.1). All of the attributes were extracted using Definiens Developer software and follows the methods outlined in chapter 3.4.1. Presented here are the results for area, length and width of chalcopyrite in the samples outlined in Table 5.2.

Area

The area of each chalcopyrite PhReg has been converted from a pixel to an equivalent circle diameter (ECD; μm). The ECD size distributions are presented as size distribution curves (Figure 5.6 – *left*) as well as cumulative size distributions (Figure 5.6 – *right*) for examples the meso-scale fine-grained mottled texture classes, coarse-grained mottled texture classes and the massive texture classes (see Table 5.2). Each example has been coloured based on the meso-scale texture class assigned from the meso-scale machine-based logging as described in Chapter 4, section 4.6 (F1 - Orange; F2 - Green; F3 - Blue; MF4 - Red; MaM - Purple; MaF - Olive).

Figure 5.6 shows that for the examples selected from each meso-scale texture class the cumulative distribution curves (*right)* do not exhibit similar size distribution trends. For example, EH556 592.00 has been classified as fine-grained based on the chalcopyrite size measured from the corresponding meso-scale image. However, the cumulative size distribution calculated at the micro-scale suggests a coarse-grained signature with 36% of the chalcopyrite exceeding an ECD of >1200 μm. This signature is likely to reflect one coarse-grain within the sample given that the other 9 examples which exhibit no chalcopyrite with an ECD >1200 μm.

The size distribution curves are better for showing examples that exhibit bimodal size distributions than the cumulative equivalent. For example, EH432 377.00 (Figure 5.6B), EH635 919.00, EH635 945.00 (Figures 5.6A and B) contains both fine and coarse chalcopyrite resulting in bimodal distribution curves. In order to better observe the true size distribution trends for chalcopyrite, the drill-core tiles have been grouped based on similar size distribution trends. Figures 5.7 and 5.8 show the distributions presented as size distribution trends and as cumulative size distributions respectively. Three distinct size distribution trends have been recognised as well as two bimodal size distributions (Table 5.5).

Table 5.5. Characteristics of chalcopyrite PhReg size distribution trends. Area is measured as an Equivalent Circle Diameter.

ECD Trend	Characteristics
1	Fine-grained. Chalcopyrite ECD <1200 μm. 30-80% of chalcopyrite has an ECD <75 μm.
2	Fine-medium grained. 60-80% of chalcopyrite has an ECD of 75-600 μm.
3	Coarse-grained. 35-80% chalcopyrite has an ECD >1200 μm.
4	Bimodal distribution. 10-46% of chalcopyrite has an ECD of <75 μm with no chalcopyrite exceeding an ECD of 1200 μm.
5	No dominant size fraction. No size fraction exceeds 30%.

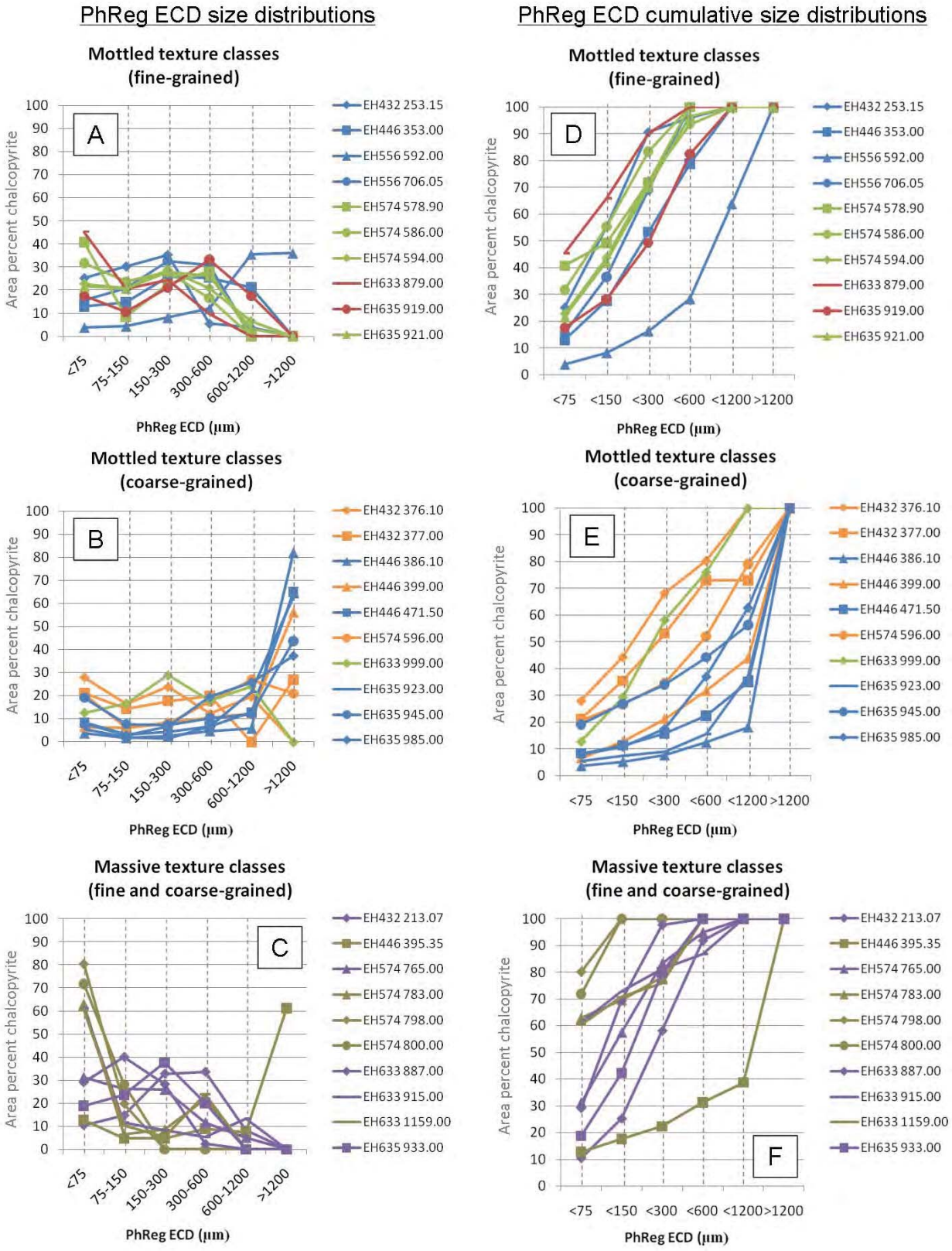

Figure 5.6. PhReg size distribution curves of chalcopyrite measured from optical microscopy mineral maps and converted to an ECD. Each example has been coloured based on the corresponding meso-scale texture class assigned to the sampled interval (F1 - Orange; F2 - Green; F3 - Blue; MF4 - Red; MaM - Purple; MaF - Olive), as described in Chapter 4, section 4.6).

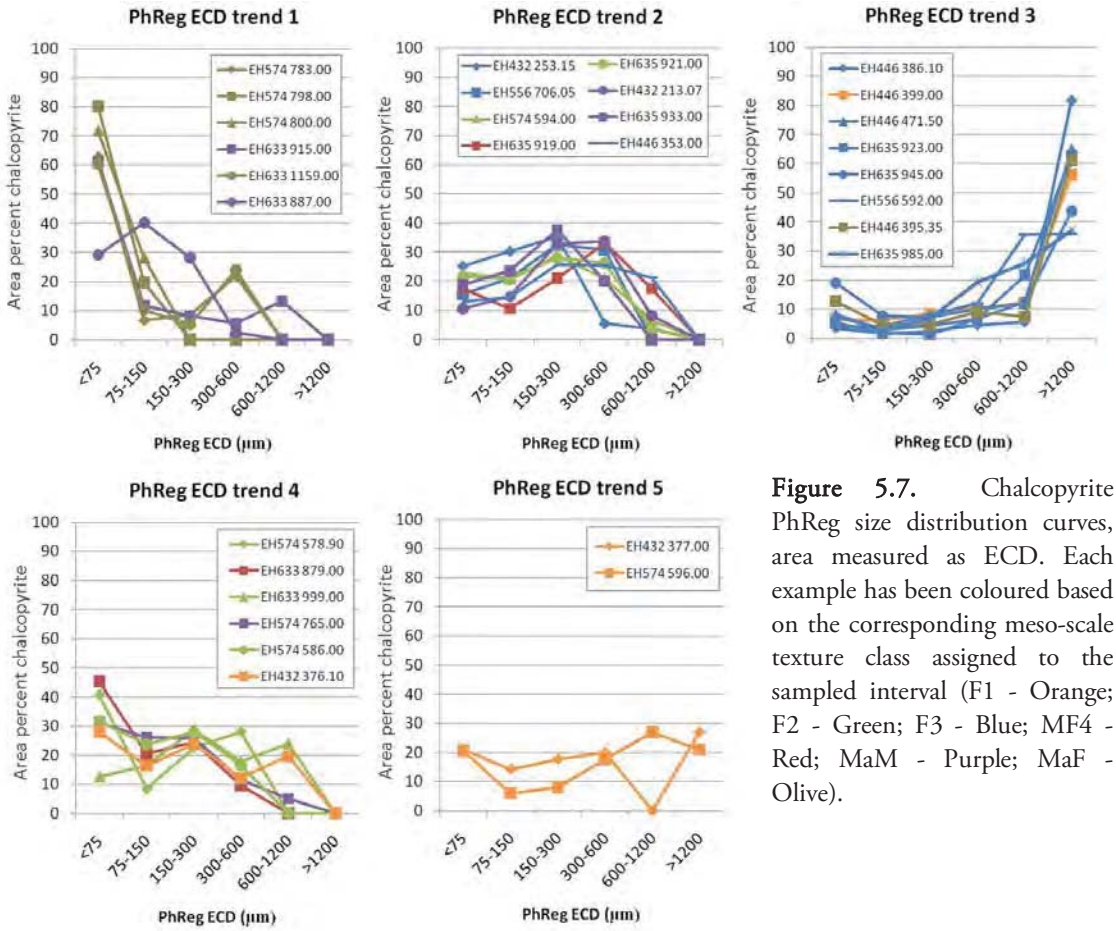

Figure 5.7. Chalcopyrite PhReg size distribution curves, area measured as ECD. Each example has been coloured based on the corresponding meso-scale texture class assigned to the sampled interval (F1 - Orange; F2 - Green; F3 - Blue; MF4 - Red; MaM - Purple; MaF - Olive).

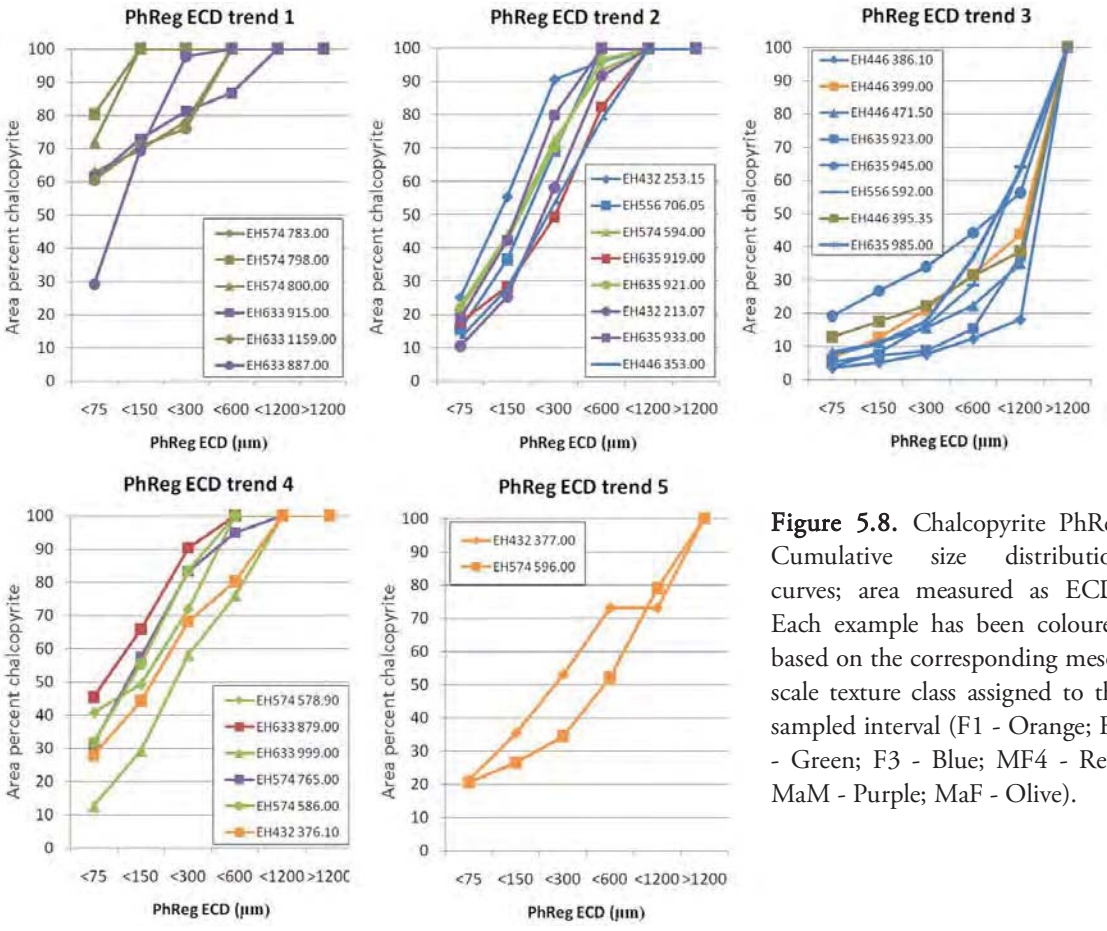

Figure 5.8. Chalcopyrite PhReg Cumulative size distribution curves; area measured as ECD. Each example has been coloured based on the corresponding meso-scale texture class assigned to the sampled interval (F1 - Orange; F2 - Green; F3 - Blue; MF4 - Red; MaM - Purple; MaF - Olive).

Length and width

During the meso-scale machine-based analyses (Chapter 4, section 4.4), the maximum length and corresponding width has been used to determine whether a sample exhibits coarse grained or fine grained chalcopyrite. Here the maximum length and width has been calculated from each of the 30 selected examples outlined in Table 5.2 and presented in Figure 5.9. Figure 5.9 shows that both the massive and fine-grained mottled examples contain finer-grained chalcopyrite than the coarse-grained mottled examples. However, a large majority of both of the mottled examples plot between the 1:1 and 2:1 ranges on the length verses width plot (See Chapter 4, Figure 4.20). The examples that plot further out (towards the bottom right) represent more elongate (vein) chalcopyrite PhRegs. These examples are EH446 399.00 (2:1); EH635 933.00 (2:1); EH574 765.00 (3:1); EH633 1159.00 (4:1); EH446 395.35 (4:1).

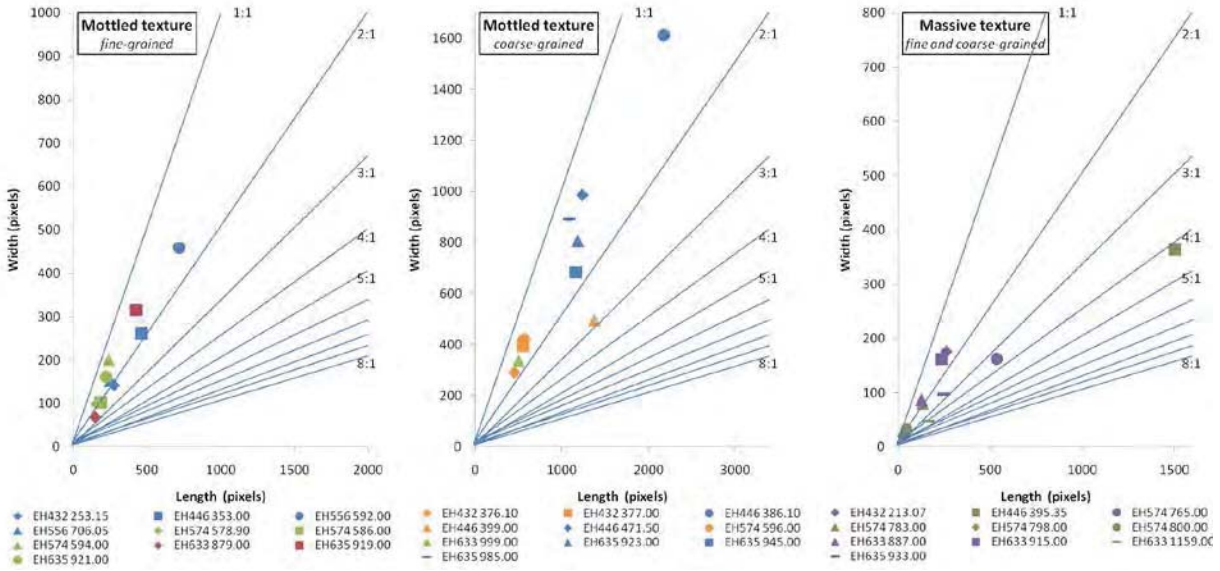

Figure 5.9. Maximum chalcopyrite PhReg length and corresponding width for drill-core tile examples presented in Table 5.2.

5.2.4 Minerals associated with chalcopyrite

Unlike the meso-scale mineral maps, the minerals associated with chalcopyrite at the micro-scale (optical microscopy) have been calculated from the minerals present in a one pixel rim surrounding the chalcopyrite PhReg (see Chapter 4, section 4.4.4). These rims represent the minerals within the 3.97 microns surrounding the chalcopyrite PhReg. The mineral associations are reported as a proportion of the total rim, totalling to the value of one. The minerals associated with each chalcopyrite PhReg have been weighted against the total area of chalcopyrite in each of the corresponding images in order not to bias the results towards the smaller chalcopyrite PhRegs. Using all of the chalcopyrite PhRegs from EH635 (n = 326 421), a PCA was undertaken to establish the most common minerals that are associated with chalcopyrite. The PCA determined that the first four principal components account for 69.70% of the variability in minerals associated with chalcopyrite (Appendix 5.2). Table 5.6 shows the weighting of each of the minerals or mineral groups in each of the principal components. The minerals barite and titanite were removed from the PCA during the initial stage of the analysis because they were found to account for very little of the variability in the minerals associated with chalcopyrite. Figure 5.10 shows the principal components

presented as density plots. Where minerals or mineral groups occur together tie lines can be seen between them. For example, quartz and carbonate minerals; pyrite and carbonate minerals; quartz and mafic minerals. These density plots can be used to illustrate which minerals are associated with chalcopyrite for individual mineral maps or as shown in Figure 5.10 a large number of samples. This is particularly useful for showing samples that may consist of multiple textures and hence several generations of chalcopyrite with varying mineralogical associations. Where particular mineral relationships occur more often, these relationships will account for more of the variability within the sample and therefore account for more of the variance population.

Table 5.6. Principal components calculated for the minerals associated with chalcopyrite for EH635. Data extracted from classified optical microscopy images for EH635. n = 326 421.

Mineral	PC1	PC2	PC3	PC4	PC5	PC6	PC7
Pyrite	0.204	0.840	0.138	-0.030	0.033	0.166	-0.452
Carbonate Minerals	-0.184	-0.083	-0.655	-0.291	-0.470	0.345	-0.325
Magnetite	0.572	-0.465	0.324	-0.359	-0.022	0.034	-0.471
Mafic Minerals	0.231	0.063	-0.307	0.223	-0.272	-0.825	-0.210
Quartz	0.147	-0.220	-0.114	0.838	0.081	0.343	-0.301
Red feldspar	-0.154	-0.071	-0.389	-0.173	0.824	-0.146	-0.301
Hematite	-0.706	-0.121	0.434	0.061	-0.137	-0.182	-0.493
Variance Proportion	20.0	17.8	16.3	15.6	15.4	14.2	0.7

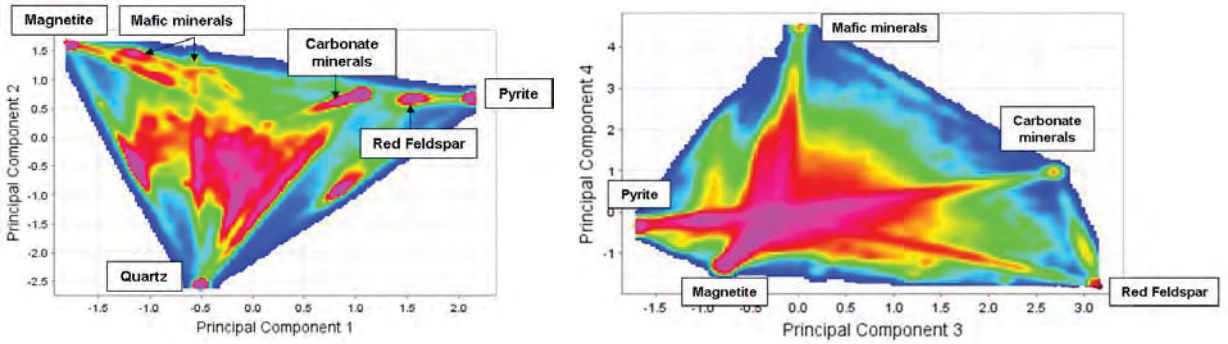

Figure 5.10. The first four principal components shown as density plots illustrating the most common minerals associated with chalcopyrite. The PCA was undertaken using the chalcopyrite PhRegs measured from the optical microscopy images from EH635 (see Table 5.6). n = 326 421chalcopyrite PhRegs from all 66 drill-core tiles.

The minerals directly associated with chalcopyrite are predicted to have a strong influence on the liberation potential of chalcopyrite. For each selected example, a density plot illustrating principal component one versus principal component two has been produced and is shown in Figure 5.11. This allows the most dominant minerals associated with chalcopyrite for each example to be determined. Based on Figure 5.11, the PCA shows that the chalcopyrite in examples 20, 27, 30 have a strong association with magnetite and mafic minerals; 1, 2, 4, 6, 7, 8, 10, 11, 13, 14 and 15 have a strong association with quartz, pyrite and carbonate minerals; 16, 22, 24 and 29 have a strong association with red feldspar; 3, 5, 9 and 18 have a strong association red feldspar and quartz.

The size analysis of chalcopyrite size presented in the previous section showed that there are multiple size populations of chalcopyrite (fine, medium and coarse). Given that some examples have shown that bimodal populations are present, it may also be possible that chalcopyrite populations exhibit different mineralogical associations for different size ranges. Four examples from Figure 5.11 (2, 9, 10 and 30) have been selected based on exhibiting different mineral associations with chalcopyrite (Table 5.7). These examples have been used to determine whether the minerals associated with chalcopyrite change with chalcopyrite size. Figure 5.12 shows line plots of the

minerals associated with fine (< 150 μm), medium (150-300 μm) and coarse (> 300 μm) sizes fractions of chalcopyrite. The green circles represent minerals whose associated abundance with chalcopyrite increases with chalcopyrite size. The red circles represent minerals whose associated abundance with chalcopyrite decreases as chalcopyrite increases. Most notably, the chalcopyrite PhRegs associated with the carbonate minerals and quartz increases with size for three of the examples (2, 9 and 30) and the proportion of pyrite associated with chalcopyrite decreases as chalcopyrite size increases for all four examples.

Table 5.7. Changes in the abundance of minerals associated with different sizes of chalcopyrite (ccp) PhRegs for examples 2, 9, 10 and 30 (see Figure 5.2 and Table 5.2). Shaded areas indicate significant changes in percent of a mineral associated with chalcopyrite.

Example	Ccp PhReg size	Percent of mineral associated with chalcopyrite								
		Pyrite (py)	Carbonate minerals (carb)	Quartz (qtz)	Magnetite (mag)	Barite	Hematite	Mafic minerals	Red Feldspar (fsp)	Titanite
2 (qtz-carb-py)	Fine	12.35	13.74	19.65	15.99	2.06	0.57	3.27	28.31	4.03
	Medium	1.17	21.52	23.27	16.58	3.55	0.75	4.06	24.33	4.71
	Coarse	1.13	24.28	28.08	16.87	3.63	0.19	5.40	16.87	3.34
	Total	10.18	16.12	20.69	15.55	2.57	0.56	3.54	26.79	4.00
9 (red fsp-qtz)	Fine	37.87	9.86	37.26	7.33	1.24	1.97	1.38	0.64	1.95
	Medium	6.24	18.27	50.97	10.46	3.18	2.77	2.76	1.31	3.45
	Coarse	6.74	19.77	51.79	5.77	4.16	4.18	2.30	1.40	3.61
	Total	32.05	11.54	39.85	7.86	1.80	2.20	1.62	0.80	2.28
10 (qtz-carb-py-red fsp)	Fine	15.71	10.11	45.21	6.19	1.90	1.26	5.91	8.84	3.18
	Medium	4.27	15.37	54.88	4.16	2.91	2.05	6.12	5.33	3.71
	Coarse	5.31	13.89	51.49	0.63	8.17	1.31	7.83	7.49	3.77
	Total	15.05	11.06	46.84	6.09	2.04	1.40	5.74	8.40	3.37
30 (mag-mafic minerals)	Fine	5.82	13.51	24.51	24.60	2.30	2.23	23.24	1.08	2.23
	Medium	2.57	21.70	27.90	16.26	3.21	2.56	20.11	1.77	3.67
	Coarse	Nil	Nil	Nil	Nil	Nil	Nil	Nil	Nil	Nil
	Total	6.84	13.83	23.58	26.22	2.09	2.56	21.24	1.06	2.57

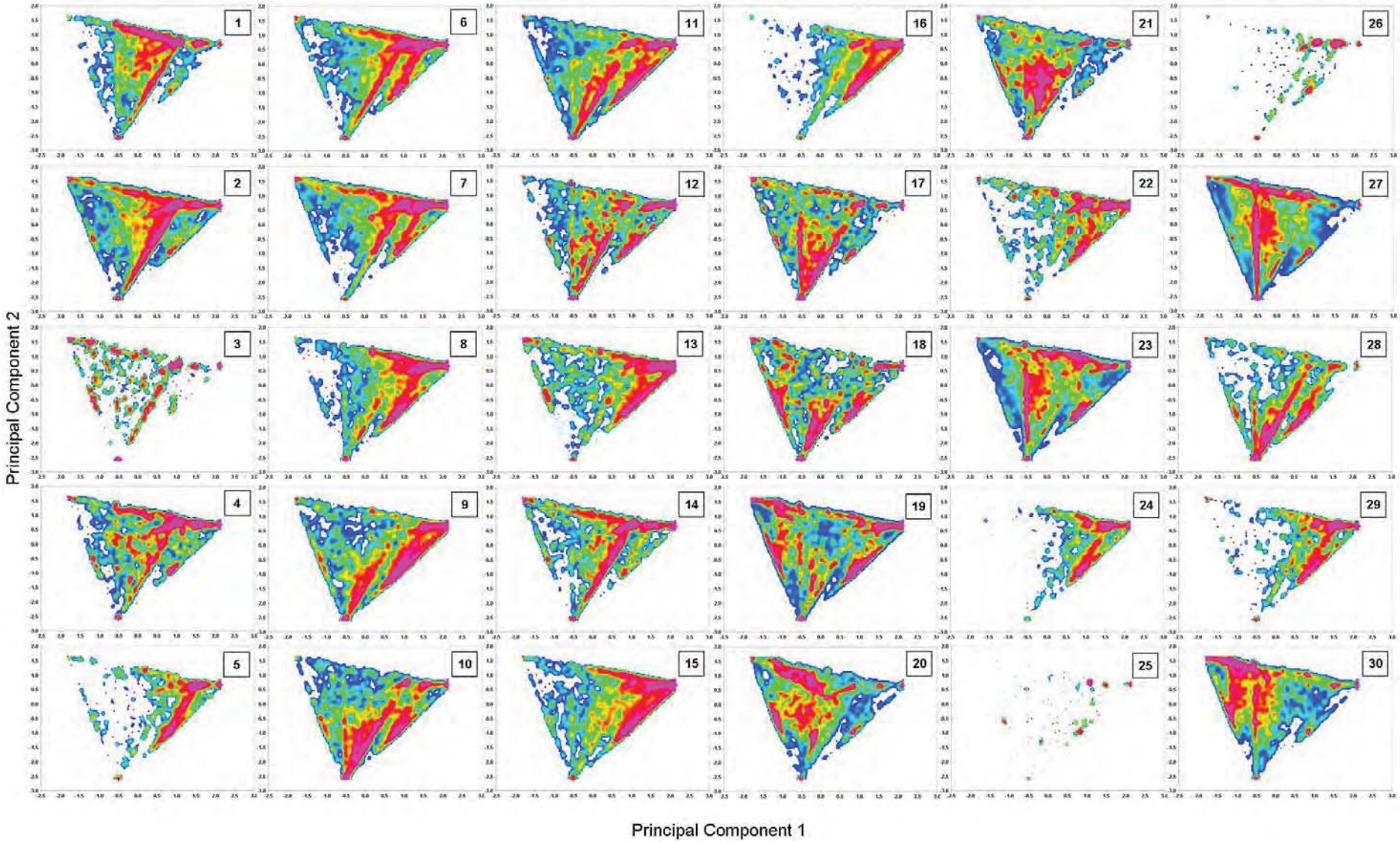

Figure 5.11. Principal Component 1 versus Principal Component 2 diagrams for the 30 examples of optical microscopy mineral maps from Ernest Henry listed in Table 5.2. Density plots illustrate the minerals that are associated with chalcopyrite from image. See Figure 5.10 for location of mineral densities.

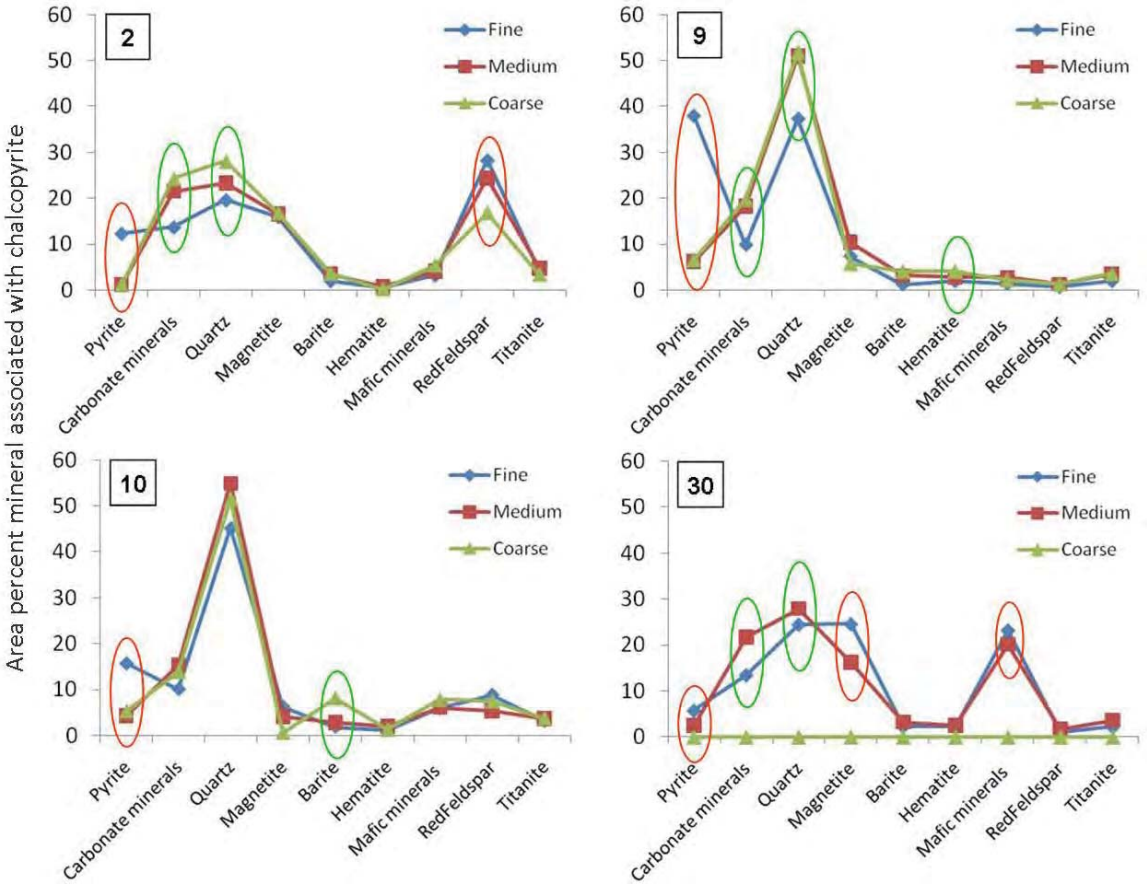

Figure 5.12. Plots illustrating the changes in abundances of minerals associated with different chalcopyrite PhReg size intervals for examples 2, 9, 10 and 30 (see Figure 5.2 and Table 5.2). Fine - <150 μm ECD, Medium – 150-600 μm ECD, Coarse >600 μm ECD. *Red* circles – Percent mineral associated with chalcopyrite increases as chalcopyrite size decreases. *Green* circles – Percent mineral associated with chalcopyrite increases with chalcopyrite size.

5.2.5 Summary

398 drill-core tiles have been photographed using the Leica DM6000 optical microscope (see Chapter 3, section 3.4. These images have been classified into mineral maps and mineralogical and textural information was extracted using the Definiens Developer software. 10 minerals or mineral groups were identified: chalcopyrite, pyrite, magnetite, mafic minerals, carbonate minerals, quartz, red feldspar, hematite, barite and titanate. The mineralogical and textural information extracted were modal mineralogy, area, length and width and the minerals associated with chalcopyrite. Thirty examples were selected for detailed analysis in this chapter. The examples were selected based on the meso-scale machine-based textural classification undertaken in the previous chapter (mottled: fine-grained, mottled: coarse-grained, massive).

In order to establish the most prominent mineralogical signatures a Principal Components Analysis (PCA) was undertaken on the results of the modal mineralogy. This determined that the dominant mineralogical signatures were: red feldspar; quartz; barite-carbonate minerals; magnetite-hematite-mafic minerals; chalcopyrite-pyrite-magnetite-hematite; pyrite-chalcopyrite.

The size of chalcopyrite has been measured as an equivalent circle diameter (ECD) and presented as size distribution curves and cumulative size distribution curves. From these results three

trends and two bimodal distributions were identified (Table 5.5). A summary of these results plus MLA micro-scale analyses for Ernest Henry are presented later in this chapter in section 5.5.

5.3 Results of MLA analysis: Cadia East

Based on the method described in Chapter 3, section 3.5, classified mineral maps of drill-core tiles have been produced for rock samples from Cadia East using the SEM-MLA. In total, 130 drill-core tiles from drill-holes CE082, CE098, CE109, CE110 and CE143 (see Chapter 4, Figure 4.1) have undergone MLA analysis with particular emphasis on chalcopyrite, bornite, molybdenite and gold. The extraction of quantified mineralogical and textural information from these images was undertaken using Definiens image analysis software. The results are summarised in this section and are given in more detail in the following appendices:

- 5.3 Mineral spectra library: Cadia East
- 5.4 Modal mineralogy calculated from XMOD analysis of drill-core: Cadia East
- 5.5 Mineralogical and textural attributes of chalcopyrite calculated from SPL-lite analysis of drill-core: Cadia East
- 5.6 Mineralogical and textural attributes of bornite calculated from SPL-lite analysis of drill-core: Cadia East
- 5.7 Mineralogical and textural attributes of molybdenite calculated from SPL-lite analysis of drill-core: Cadia East
- 5.8 Mineralogical and textural attributes of gold, electrum and hessite.
- 5.9 Analysis of shape attributes: Cadia East

From the 130 drill-core tiles, thirty examples obtained from MLA analysis have been selected for detailed mineralogical and textural analysis. These examples were selected based on the meso-scale textures that were defined in the previous chapter (sections 4.2 and 4.5). Ten each of fine-grained disseminated, coarse-grained aggregates, and vein-hosted rock tile examples were chosen that each contains > 100 chalcopyrite PhRegs (Table 5.8; Figure 5.13).

Table 5.8. 30 examples of drill-core tiles selected for detailed micro-scale mineralogical and textural analysis and the number of chalcopyrite, bornite and molybdenite PhRegs extracted from each. For mineral abbreviations refer to Appendix 1.1.

Fine-grained disseminated				Coarse-grained aggregates				Vein hosted			
Example (N)	Ccp	Bn	Mb	Example (N)	Ccp	Bn	Mb	Example (N)	Ccp	Bn	Mb
CE082 285	2151	nil	19	CE109 309	8144	nil	104	CE098 355	1202	59	6
CE082 301	2024	28	42	CE109 319	3393	3	63	CE109 443	2951	nil	nil
CE098 177	6244	nil	50	CE109 327	1891	2	55	CE143 1121	3411	4355	nil
CE098 233	4737	nil	32	CE109 337	6683	1	132	CE143 1177	125	5609	127
CE098 271	15249	nil	72	CE109 485	1019	94	35	CE143 1227	4626	nil	37
CE109 219	1742	2	196	CE110 271	1801	1	102	CE143 1265	3390	nil	nil
CE109 237	1122	nil	655	CE110 411	7770	nil	183	CE143 1357	2284	553	nil
CE110 281	2184	1	90	CE110 441	24523	3	61	CE143 1371	1296	nil	nil
CE110 383	762	nil	16	CE143 1165	2400	19373	186	CE143 1441	2620	46	nil
CE143 1233	2330	nil	nil	CE143 1241	19571	29	nil	CE143 1465	3900	nil	nil

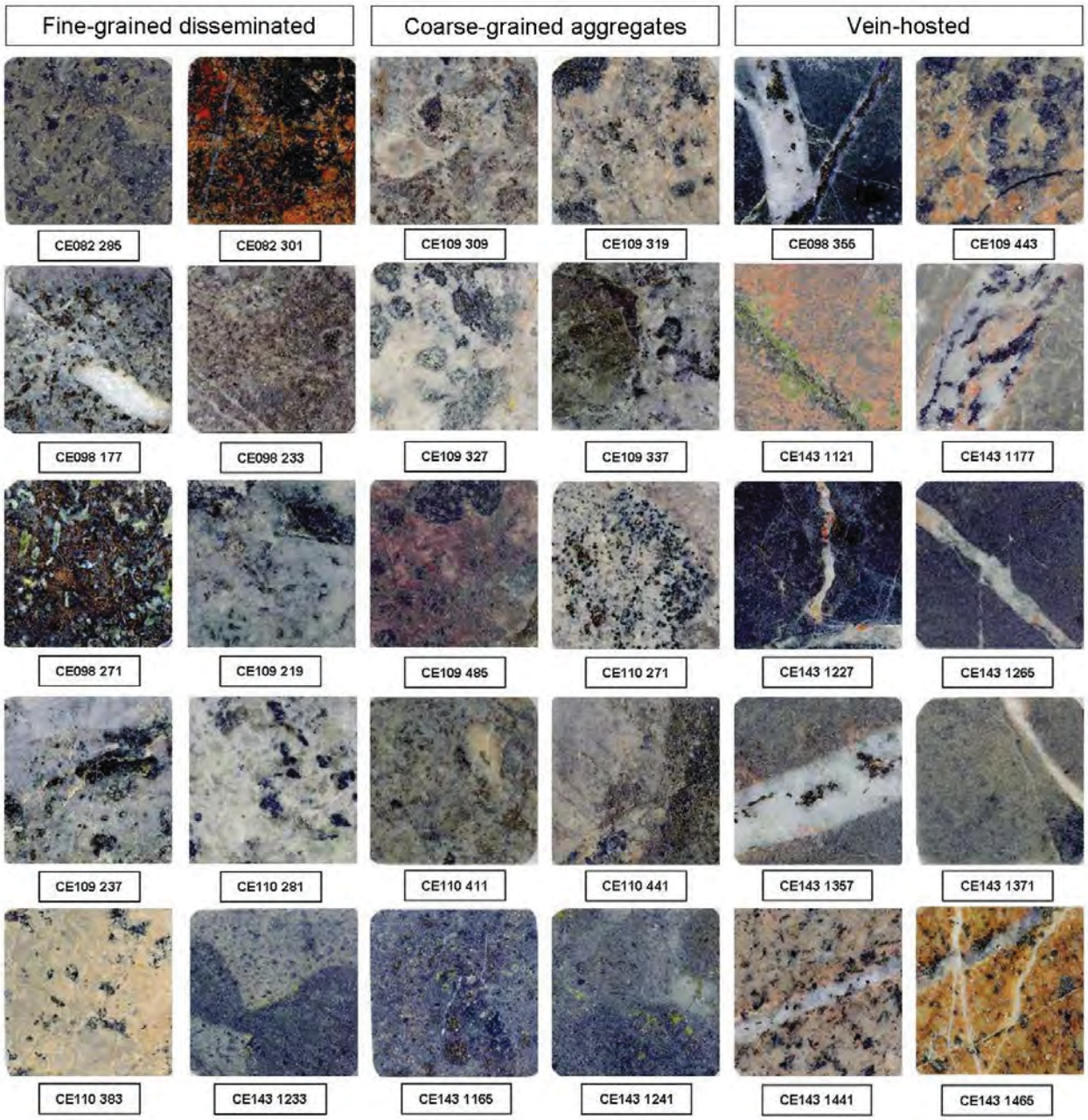

Figure 5.13. Scanned photographs of the 30 drill-core tiles that have been selected for detailed analysis for Cadia East. Each tile is 3 × 3 cm.

The Cadia East mineralogy has been determined using the MLA in the automated SEM mode (MLA-SEM). A library of mineral spectra has been compiled according to the methods and procedures outlined in Chapter 3, section 3.5.2 (section 5.3.2; Appendix 5.3). This process has allowed a thorough understanding of the mineralogical and textural relationships present at Cadia East to be determined. A summary of the Cadia East mineralogy and textures are presented in section 5.3.1.

For the thirty examples from Cadia East selected for detailed MLA analysis, the results are presented as follows:

- 5.3.3 XMOD analysis: modal mineralogy.
- 5.3.4 Size analysis of Cu-sulphide minerals (chalcopyrite and bornite): measured as Equivalent Circle Diameter (ECD), Length and Width, Phase Specific Surface Area (PSSA) and smallest enclosed circle.
- 5.3.5 Gangue minerals associated with Cu-sulphide minerals and molybdenite
- 5.3.6 Shape analysis: undertaken on 30 individual chalcopyrite PhRegs of varying shape and size.
- 5.3.7 Analysis of gold and silver bearing minerals.

5.3.1 Cadia East mineralogy

Previous studies undertaken at Cadia East by Wilson (2003) and Kitto (2005) have defined the mineralogy of the upper portions of the Cadia East ore body based on observations in drill core, optical microscopy and SEM analysis. At the time of these studies, a decline into the Cadia East ore body had not yet been completed and access to drill-core for the deeper portions of the ore body were not available. The mineralogy at Cadia East as determined within this study will be presented as sulphide minerals, feldspar minerals, carbonate minerals, oxide minerals, silicates, others and rare minerals (gold, silver and tellurides) as shown in Table 5.9.

Table 5.9. Cadia East mineralogy determined using the MLA in SEM mode.

Mineral		Meso-scale	Micro-scale
Sulphide Minerals	Chalcopyrite	Chalcopyrite is the main copper bearing mineral at Cadia East and occurs in all depths of the ore deposit. In drill core, chalcopyrite occurs as fine-grained (<2mm diameter) disseminations (Figure 5.14A), coarse-grained (cm - 10's of cms diameter) clots (Figure 5.14B), in Type B veins (Figure 5.14C) where it is much coarser (cms to tens of cms), and less commonly in Type A and D veinlets. Observations in this research suggest that in the upper portions of the ore body chalcopyrite is typically fine-grained and becomes coarser with depth, before predominantly occurring in vein assemblages in Cadia East Deeps.	Under high magnification, the disseminations of chalcopyrite are irregular and globular in shape (Figure 5.14D), coarse- aggregates of chalcopyrite grains are irregularly shaped and branching (Figure 5.14E). Chalcopyrite in Type B veins typically occurs interstitially between neighbouring, more competent minerals such as quartz, epidote and pyrite. As a result, the grain shape of the chalcopyrite commonly represents the inverse of its neighbouring minerals (Figure 5.14F).
	Bornite	Bornite at Cadia East is predominantly hosted by Type B veins (Figure 5.15A). Type B veins hosting bornite are common in the Inner Propylitic and Potassic alteration zones (Kitto, 2005). Bornite as minor disseminations (<2mm diameter) occurs in the upper Inner Propylitic alteration zone.	At the micro-scale vein-hosted bornite exhibits a similar habit to chalcopyrite (Figure 5.15B) and can be observed in exsolution with chalcopyrite (Figure 5.15E) as well as digenite (Figure 5.15C). Observations in this research indicate where bornite is present in Type B veins the presence of gold, electrum and telluride minerals increases. However, this does not mean that these minerals are always hosted by bornite.
	Digenite	Not observed in hand specimen.	The digenite is fine-grained (<500µm) and typically occurs in exsolution with bornite (Figure 5.15C) in Type B vein assemblages.
	Molybdenite	Molybdenite occurs as fine-grained (<1mm diameter) disseminations, in Type B vein assemblages and is also seen in shear zones associated with faulting (Figure 5.15D).	At high magnification, the molybdenite grains are lathe shaped and euhedral (Figure 5.14E).
	Tetrahedrite minerals	Not observed in hand specimen.	The Tetrahedrite minerals were only observed at the micro scale in minor amounts with chalcopyrite in the upper portion of the deposit. These minerals include tetrahedrite, tennanite and enargite.
	Pyrite	There are several generations of pyrite at Cadia East (Wilson, 2003, Kitto, 2005); Coarse-grained clots and fine-grained disseminations in the pyrite cap zone in the upper portion of the ore body (Figure 5.15F), it also occurs in Type B vein assemblages (Figure 5.16A), as late stage thick (<10cm diameter) veins and disseminations associated with fault zones.	At the micro-scale, pyrite occurs as euhedral to subhedral disseminated grains with quartz, K-feldspar and albite. In addition to this pyrite also occurs as coarse-grained aggregates with chalcopyrite-chlorite-biotite.Within the pyrite cap zone exhibits the similar mineral inclusions to the chalcopyrite and bornite in Cadia East Deeps i.e.clausthalite (Figure 5.16B), hessite, gold (Figure 5.16C), electrum etc.
	Galena	Not observed in hand specimen.	Galena was only observed at the micro-scale where it occurs as small euhedral inclusions in chalcopyrite and bornite in Type B veins, or as small grains in the vein selvage.
	Barite	Not observed in hand specimen.	The Barite at Cadia East was only observed at the micro-scale. It occurs as small inclusions in sulphide minerals (<40µm) and as free euhedral grains.
Feldspar Minerals	K-Feldspar	The K-feldspar at Cadia East occurs within most depths of the ore deposit. In drill-core it is characterised by pervasive pink iron alteration which can vary in intensity (Figure 5.16D).	At high magnification, K-feldspar was observed with albite or quartz. There are five dominant textural variations: 1. K-feldspar and albite with irregular sub-rounded contacts (Figure 5.16E). 2. Sub-rounded fragments of textural variation 1 in a matrix of illite-muscovite. 3. K-feldspar and quartz with irregular sub-rounded contacts (Figure 5.16F). 4. Sub-angular fragments of textural variation 3 in a matrix of chlorite-biotite. K-feldspar in vein selvages which can host gold, electrum, hessite and clausthalite (Figure 5.17A).
	Albite	At Cadia East, albite occurs in the pyrite cap and deeper potassic alteration zones (Kitto, 2005). In drill core it is white-cream in colour (Figure 5.17B) and cannot be distinguished from K-feldspar unless stained with sodium cobaltinitrate.	At high magnification, albite was observed as irregular grains with K-feldspar (Figure 5.16D) and quartz.
	Plagioclase	Not observed in hand specimen.	The plagioclase at Cadia East typically occurs within the feldspar-porphyry rock unit. The plagioclase is difficult to identify in drill core, and typically occurs as remnant cores (Figure 5.17C) of euhedral crystals that have been pseudomorphed by K-feldspar or albite (Figure 5.17D).
Mica minerals	Biotite	In drill core, biotite is black, fine-grained (<1mm) and shredded in appearance. It can be seen in the matrix material of the breccia units (Figure 5.17E) as well as in rounded clots with biotite-chalcopyrite ± magnetite (Figure 5.17F). There are three dominant compositions of biotite at Cadia East, Mg-rich, Fe-rich and Ti-bearing biotite.	At high magnification biotite is typically observed intergrown with or being replaced by chlorite (see Chapter 3, Figure 3.15C)
	Illite/ Muscovite	In drill core, illite and muscovite are white to cream, very fine-grained with a rough, soft texture. Throughout Cadia East the chemical composition of illite and muscovite is variable between the two end	Under the microscope, where muscovite grains are present they are cleaner and more euhedral than the very fine-grained, grungy appearing illite (Figure 5.16B). The illite/muscovite alteration has a shreddy

Mineral		Meso-scale	Micro-scale
		members.	appearance that permeates through the rock replacing the pre-existing textures.
	Chlorite	Chlorite alteration is very common in the rocks at Cadia East (Wilson, 2003). In drill core it is typically fine-grained, soft and dark-green to black in colour. It is present in a number of forms: 1. with biotite ± magnetite ± chalcopyrite as coarse clots in the conglomerate lithologies (Figure 5.14B) 2. in the matrix in breccia lithologies (Figure 5.14C) 3. as a dominant mineral in fault zones (Figure 5.18A)	At high magnification chlorite can be observed to be gradually replacing pre-existing textures and minerals within the rock (Figure 5.18B).
Carbonate minerals	Calcite	There are four main occurrences of calcite observed at Cadia East. The most dominant occurrence is in Type B veins. The calcite is a bright white, often standing out next to the transparent grey quartz (Figure 5.14C). There are two occurrences of late-stage calcite that cross-cut the rock fabric: Calcite in Type C veinlets which are typically only mm's in diameter and contain minor chalcopyrite (Figure 5.18C), and calcite-fluorite clots in Type D veins. The clots are rounded and pinch out in sections and usually only a few cm's in diameter but can locally reach <10 cms (Figure 5.18D).	In Type B vein assemblages calcite fills spaces between more competent minerals in the vein assemblage such as quartz, epidote, pyrite and apatite (Figure 5.15D). The fourth occurrence of calcite (see meso-scale description) is typically only observed under high magnification in the cores of biotite-chlorite-chalcopyrite ± magnetite clots. Figure 5.17E shows a chalcopyrite clot with a core of magnetite and calcite, encompassed by an intergrowth of biotite and chlorite.
	Rare Earth Element calcite	Not observed in hand specimen.	At Cadia East, REE calcite occurs in minor amounts with K-feldspar-chlorite and rutile. It was only observed using a microscope (Figure 5.18E). X-ray analysis indicates that the REEs present are La, Ce and Nd.
	Anhydrite	Not observed in hand specimen.	Anhydrite at Cadia East is rare and was only observed at the micro-scale. Figure 5.18F illustrates anhydrite occurring in a calcite-quartz-fluorite vein assemblage.
Oxide minerals	Magnetite	In drill core four main types of magnetite are visible: 1. Magnetite-biotite-chlorite clots which can host chalcopyrite. The magnetite is often too small to see, but can be detected using a magnet in hand specimen. 2. Coarse magnetite with biotite-chlorite between clasts of K-feldspar and albite in breccia hosted lithologies (Figure 5.17E) 3. Type A veinlets (Figure 5.19A). These veinlets are typically <14mm in diameter with minor amounts of chalcopyrite. 4. Skarn style magnetite. This magnetite is massive and often associated with garnet and epidote.	At the micro-scale, magnetite grains are subhedral and typically between 100 and 400 μm in diameter (Figure 5.19B).
	Hematite	Hematite can be observed in core as 'hematite dusting' in feldspar minerals (Figure 5.16D) and as in Type C veinlets (Figure 5.19C) with calcite and laumontite as well as hematite rims on magnetite.	Cannot be distinguished from magnetite using the MLA.
	Rutile	Not observed in hand specimen.	The rutile at Cadia East was only observed at the micro-scale. It is typically <100 μm across and occurs with or proximal to Ti-biotite (Figure 5.19D) and as small grains (<200μm) within Type B veins (Figure 5.19E).
	Titanite	Not observed in hand specimen.	The titanate at Cadia East is only visible at the mi cro-scale. It occurs as linear grains along the planar cleavages of chlorite (Figure 5.20D).
Silicate minerals	Quartz	At Cadia East quartz is observed in Type B veins (Figure 5.14C) and as a pervasive silica alteration (Figure 5.19D) in the Pyrite Cap and parts of the Inner Propylitic alteration zones (Wilson, 2003). In Type B veins, quartz is colourless to grey and forms subhedral to euhedral grains along straight edged vein boundaries. Pervasive silica alteration is characterised by its cream/grey matte appearance and hardness, with individual quartz crystals not visible.	At the micro-scale, quartz and K-feldspar occur together filling in areas around small clots of sulphide minerals (Figure 5.19F) in the upper Pyrite Cap alteration zone of the ore-body as well as in the vein selvages and surrounding the monzonite intrusion in Cadia East Deeps. In Type B veins, prismatic quartz crystals predominantly occur along the edges of the veins (Figure 5.19E) with chalcopyrite-bornite and calcite interstitially filling the remaining area.
	Epidote (clinozoisite)	There are two main occurrences of epidote at Cadia East, firstly as prismatic, pistachio green crystals in Type B veins (Figure 5.20A) and secondly as grungy anhedral crystals in the potassic alteration zone (Figure 5.20B). The latter occurs with small clots of biotite and chalcopyrite, the number of these clots present increases with the intensity of the potassic alteration.	In Type B veins, epidote is typically associated with quartz, calcite, bornite and chalcopyrite and can host inclusions of hessite, electrum and gold (Figure 5.20C).
	Tourmaline	The tourmaline at Cadia East in confined to the Pyrite Cap alteration zone and the volcaniclastic sandstone unit (Wilson, 2003). It is characterised by bands of small rounded aggregates of black needle-like crystals (Figure 5.19A).	Not observed in using the MLA.

Mineral		Meso-scale	Micro-scale
	Allanite	Not observed in hand specimen.	Allanite occurs in only minor amounts and observed at the micro-scale. The mineral spectrum for allanite indicates that it contains the REE's Ce, Nd and La.
Rare/ valuable minerals	Gold and electrum	Not observed in hand specimen.	The gold and electrum at Cadia East was predominantly observed at the micro-scale. X-ray analysis of electrum grains allows an estimate of the gold fineness to be calculated. Other than the 100% Au there are two types of electrum, one with approximately 10% Ag and one with approximately 30% Ag. Analysis of gold and electrum in this study found that as well as occurring as rounded inclusions (typically <20 μm diameter) in bornite and chalcopyrite of Type B veins (Figure 5.20F), gold and electrum also occurred: • at grain boundaries between chalcopyrite and other minerals in Type B veins (Figure 5.21A) • in K-feldspar in the selvages of veins (Figure 5.17A) • as inclusions in epidote and quartz within Type B veins (Figure 5.20C) • as free gold in K-feldspar Preliminary observations also noted the presence of other inclusions where gold and electrum were present. These are predominantly Hessite and Clausthalite. Analysis of the shallower portions of the ore-body where there is low gold and copper grades found that gold and electrum occurred as inclusions in pyrite (Figure 5.16B; 5.16C) and chalcopyrite. Gold and electrum were also found proximal to inclusions of hessite and clausthalite.
	Hessite	Not observed in hand specimen.	The Hessite at Cadia East was only observed at the micro-scale. It typically forms rounded blebs between 5 and 25 μm diameter in and proximal to chalcopyrite and bornite minerals (Figure 5.21B). It has been observed at all depths at Cadia East. In chalcopyrite and bornite, hessite does occur with other rare phases including electrum and clausthalite (Figure 5.21B).
	Clausthalite	Not observed in hand specimen.	Clausthalite at Cadia East only be seen at the micro-scale. It is very common as small (<10 μm) rounded inclusions in and proximal to chalcopyrite, bornite and pyrite. Inclusions can be as few as one or two per grain (Figure 5.21B) or at times appear as dense fine-grained inclusions in the host mineral (Figure 5.21C).
	Monazite	Not observed in hand specimen.	Monazite at Cadia East only be observed at the micro-scale. It contains REE's of La, Ce and Nd and forms as small irregular grains in illite biotite/chlorite, quartz as well as inclusions in minerals within Type B veins (Figure 5.21D).
	Bismuthinite and Hawleyite	Not observed in hand specimen.	Bismuth and mercury tellurides at Cadia East are rare. They are only be observed at the micro-scale and occur as small inclusions in chalcopyrite and bornite. Bismuthinite occurs as small lathe shaped inclusions (Figure 5.21E) in chalcopyrite and bornite, and only been observed in the deeper portions of the ore-body at Cadia East. Hawleyite occurs as irregular shaped inclusions in and proximal to chalcopyrite also in the deeper part of the ore-body. Both bismuth and mercury are considered deleterious elements.
Others	Fluorite	The fluorite in Type D veins can be colourless, green, or purple and forms euhedral crystals that cross-cut all rock fabrics (Figure 5.18D).	There are two generations of fluorite at Cadia East. The first was only observed at the micro-scale as small grains within Type B veins (Figure 5.14F). The second occurs in Type D veins.
	Apatite	Not observed in hand specimen.	There are two generations of apatite at Cadia East; both only observed at the micro-scale. The first generation form small euhedral and subhedral grains in Type B veins (Figure 5.17C). The second forms larger anhedral grains associated with disseminated and coarse-grained aggregates of chalcopyrite (Figure 5.20E).

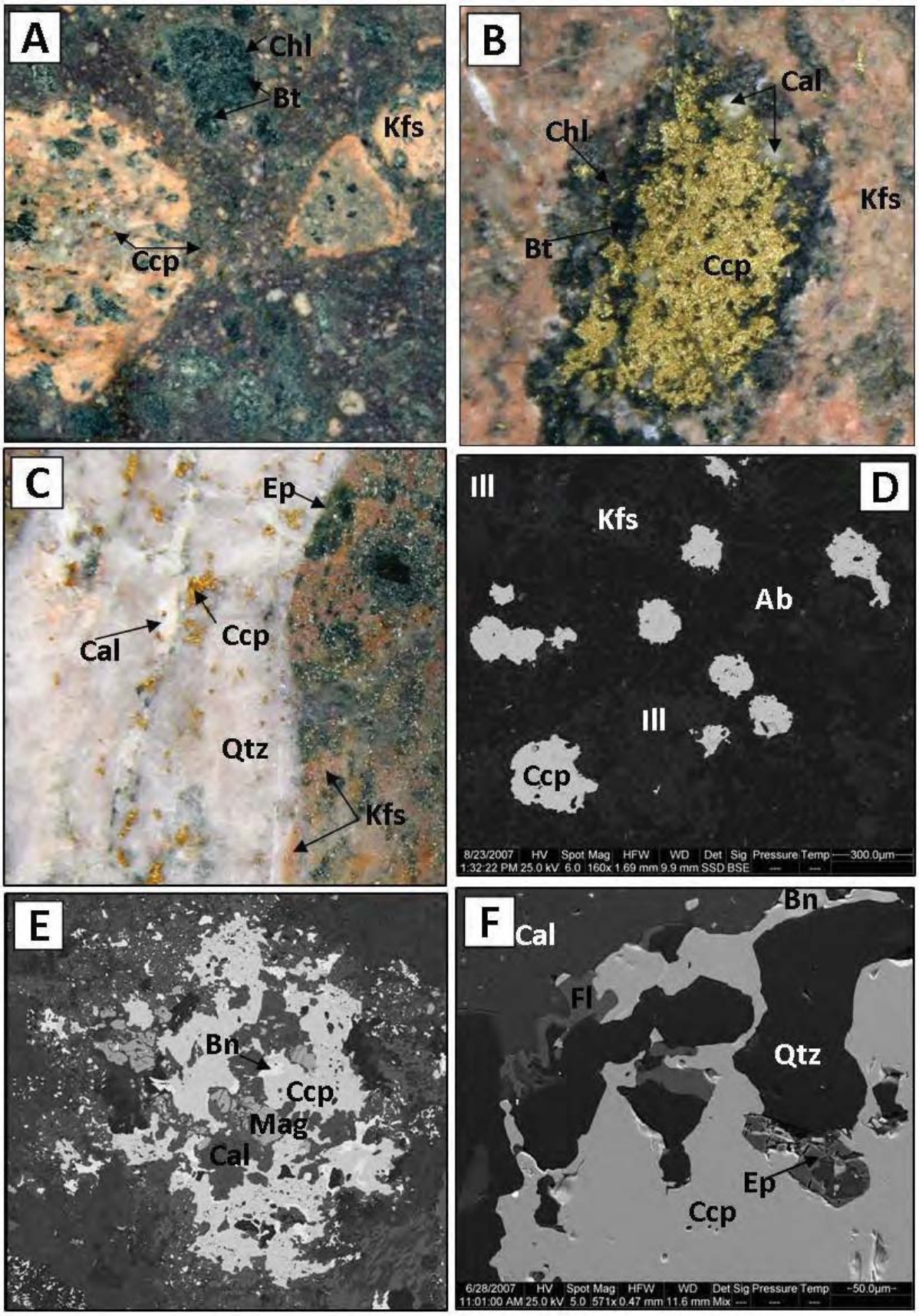

Figure 5.14. Photographs of **A.** Fine-grained (disseminated) chalcopyrite **B.** Coarse-grained (aggregates) chalcopyrite **C.** Chalcopyrite hosted by a sheeted vein. Width of each photograph is 5.5 cm. BSE images of **D.** Fine-grained disseminated chalcopyrite **E.** coarse-grained aggregates of chalcopyrite **F.** Chalcopyrite in a sheeted vein. *For mineral abbreviations refer to Appendix 1.1.*

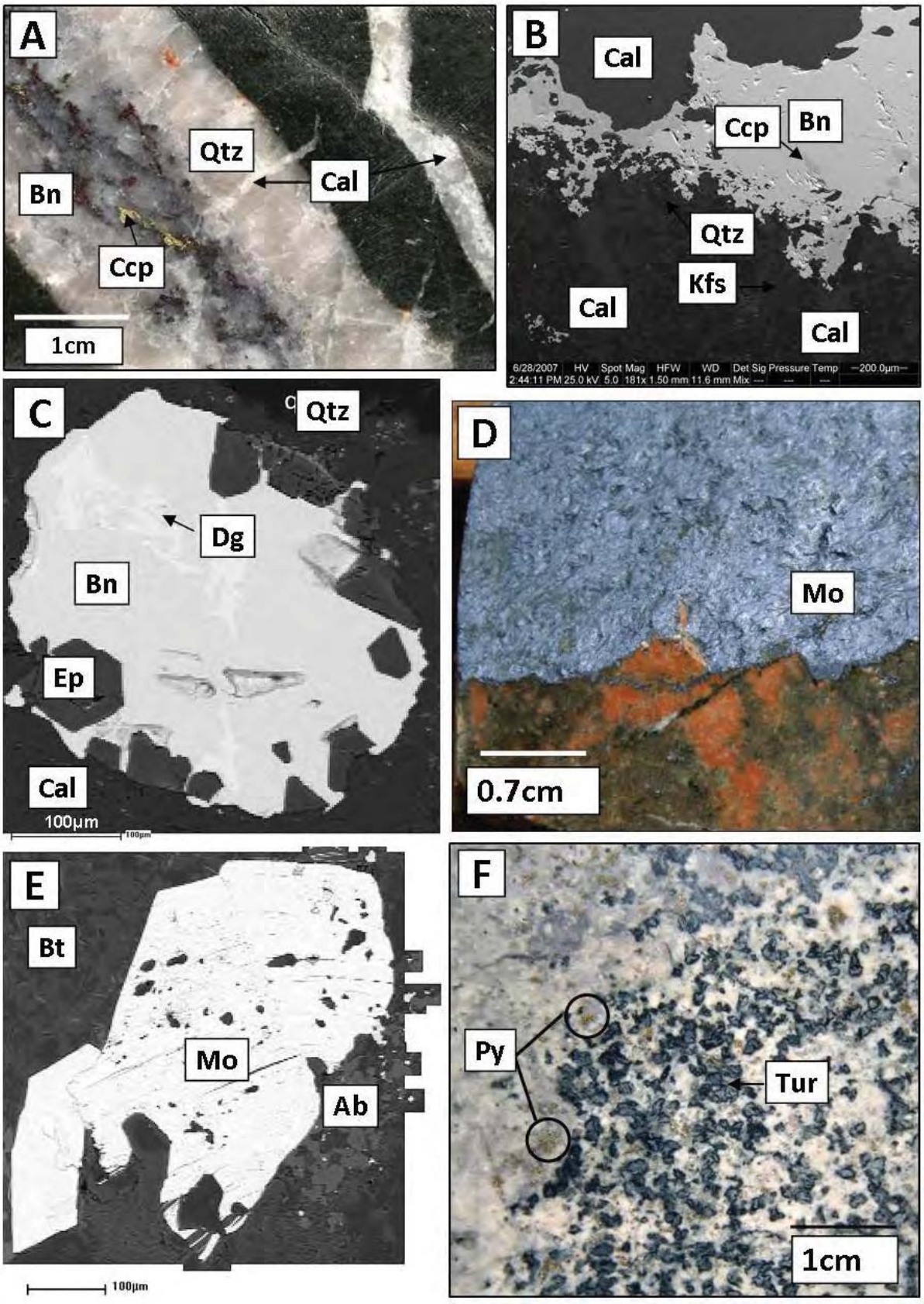

Figure 5.15A. Photograph of bornite in Type B vein with chalcopyrite, quartz and calcite **B.** CE 143 1381.50m. BSE image of Type B vein and gangue mineral boundary. Bornite is filling areas between grains of calcite **C.** CE143 1177m. Bornite in exsolution with digenite **D.** Photograph of molybdenite in a shear zone **E.** CE 143 1165m. BSE image of a molybdenite grain enclosed by biotite and albite **F.** CE110 192m. Fine-grained clots of disseminated pyrite from 'pyrite cap' alteration zone. *For mineral abbreviations see Appendix 1.1.*

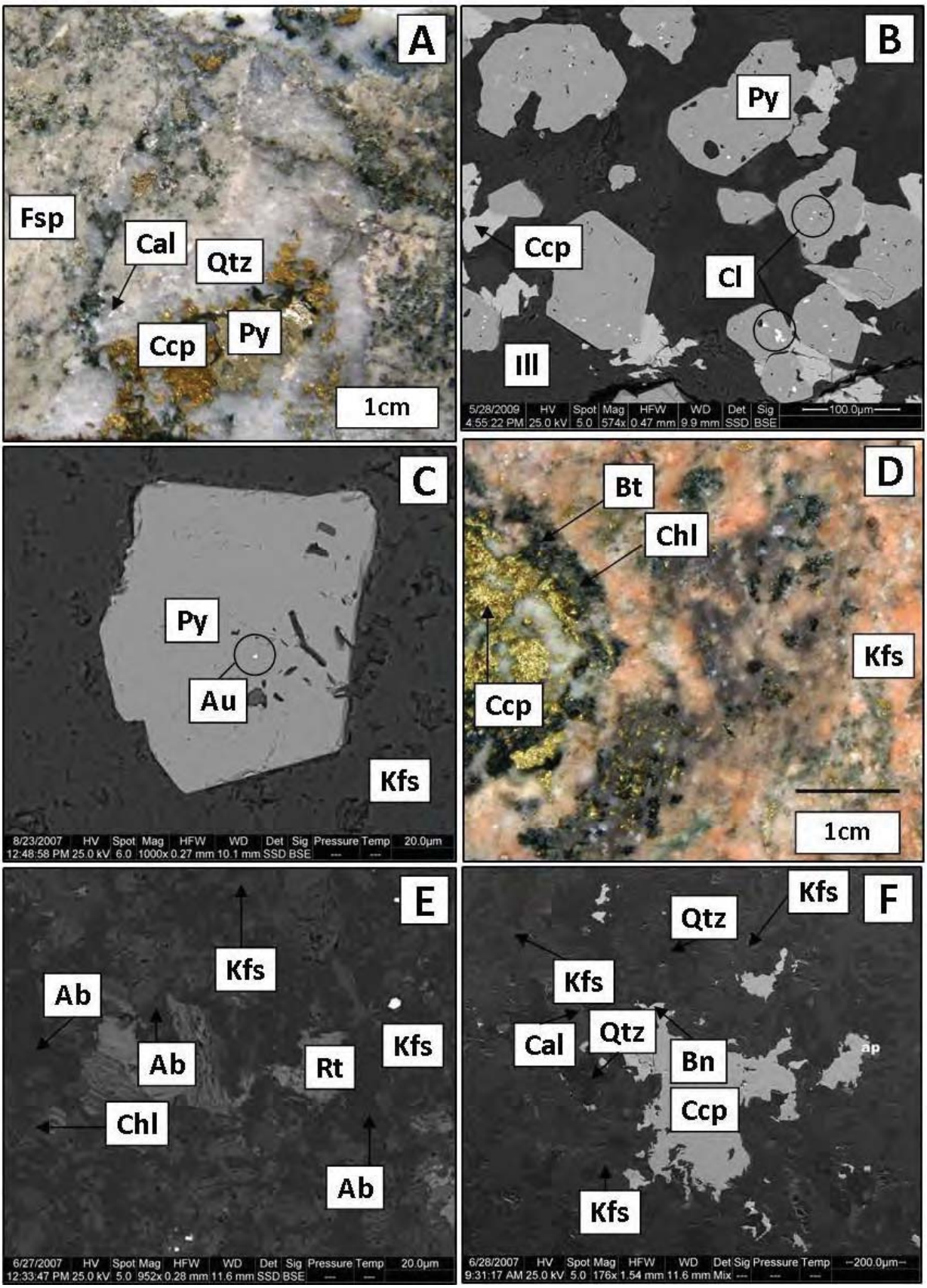

Figure 5.16A. CE110 186m. Coarse pyrite in Type B vein with Ccp, Qtz and Cal **B.** CE109 337m. Inclusions of Cl (PbSe) in Py **C.** CE109 206.50m. Inclusion of Au in pyrite **D.** CE110 Photograph of K-feldspar alteration **E.** CE143 1408.5m. Kfs and Ab occurring together with irregular grain boundaries **F.** CE143 1335m. K-feldspar and quartz occurring together with irregular boundaries. *For mineral abbreviations see Appendix 1.1.*

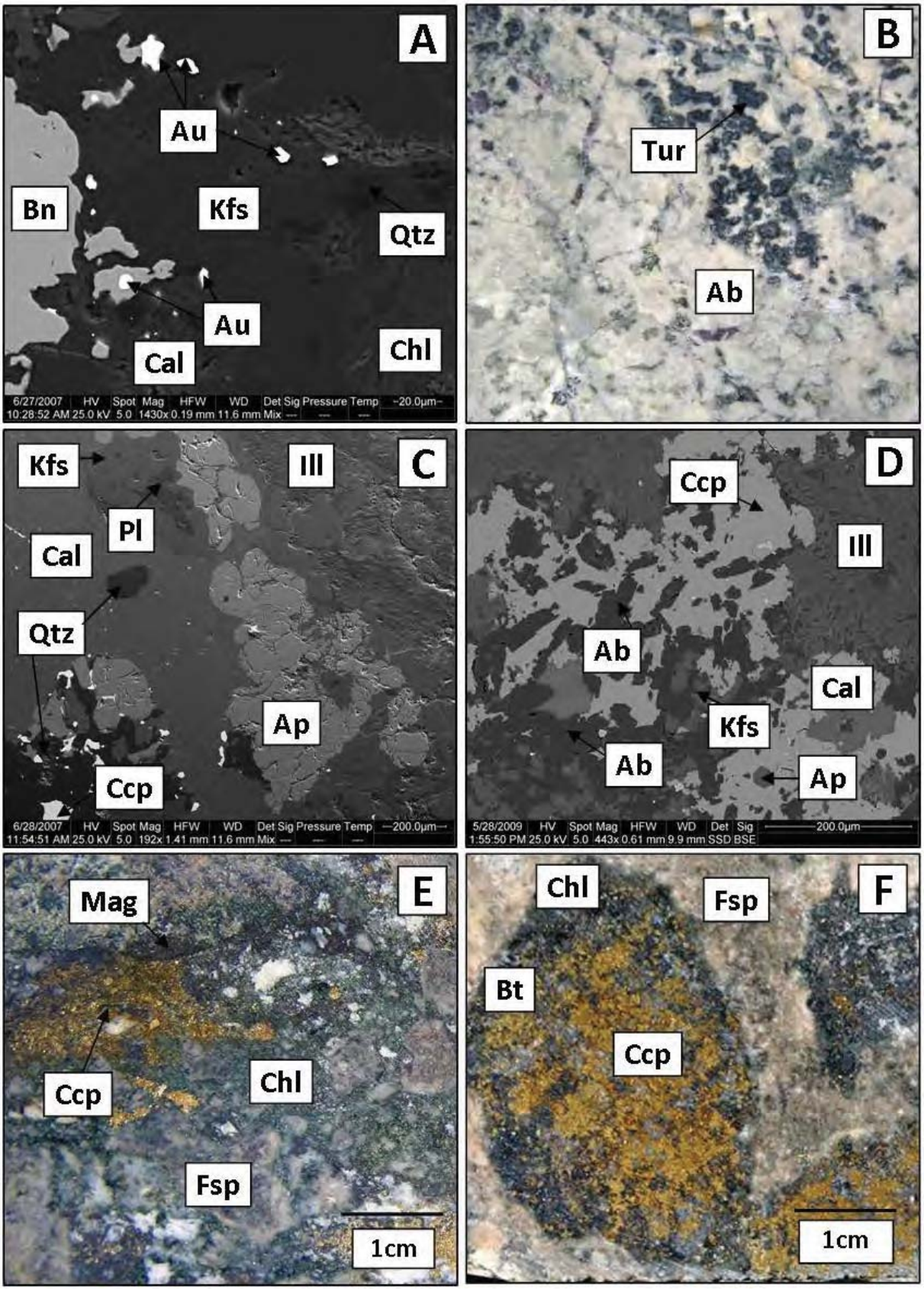

Figure 5.17A. CE143 1408m. Kfs in vein selvage with inclusions of Au **B.** CE110 173.65m. Photograph showing Ab in drill core (image width 5.5cm) **C.** CE143 1335m Kfs with remnant cores of Pl **D.** Remnant phenocrysts of Pl that have now been pseudomorphed by Al **E.** fine-grained Chl in rounded clots with Bt and Ccp with a matrix altered by Kfs. **F.** Volcaniclastic breccia with Chl and Ccp infill. *For mineral abbreviations see Appendix 1.1.*

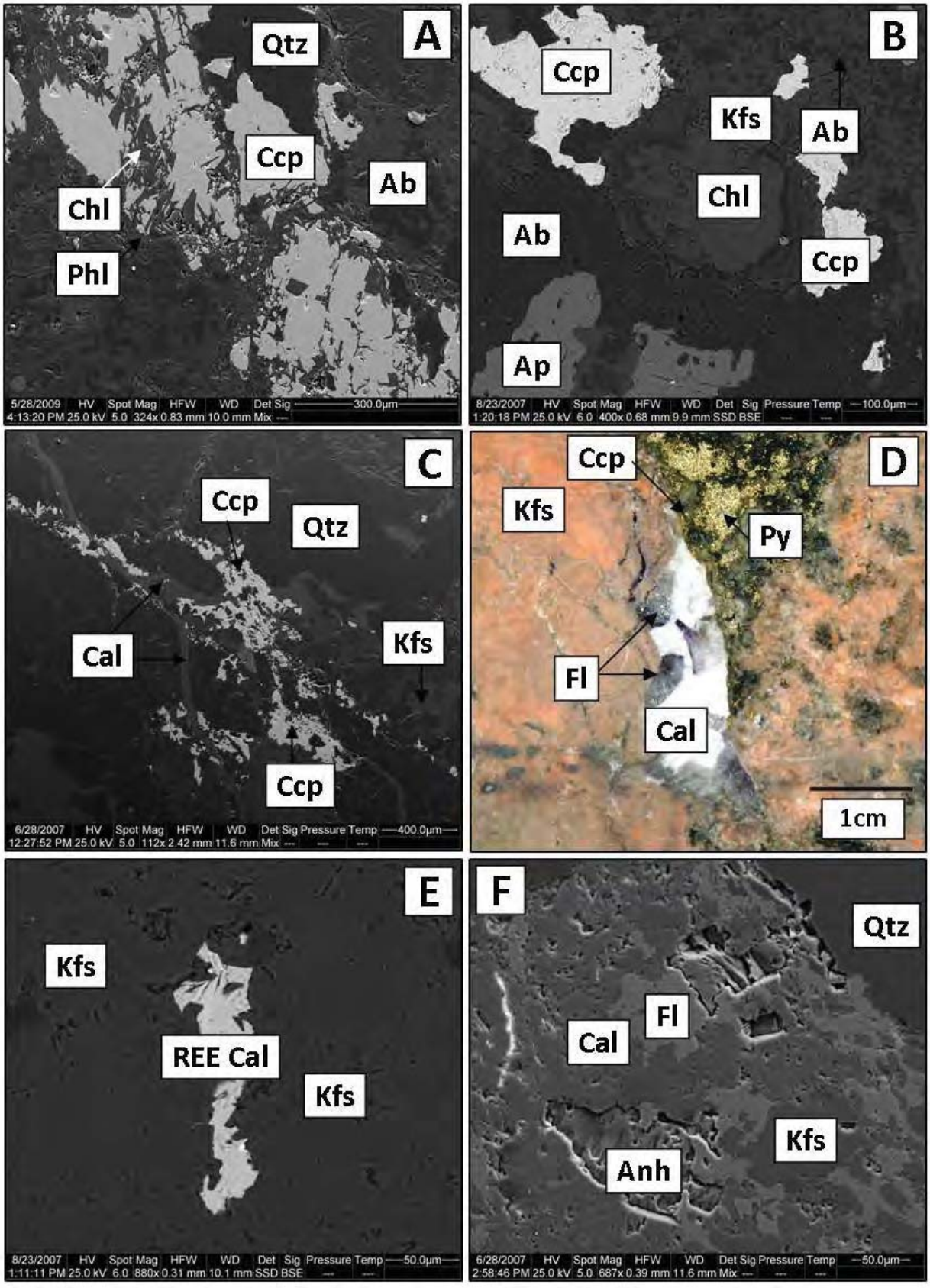

Figure 5.18A. CE143 1339.50m. BSE image illustrating Chl in fault gauge material with pseudo-clasts of Ccp-Qtz and Kfs-Ab **B.** CE109_207.50m. BSE image illustrating Chl alteration **C.** CE143 1381.50m. BSE image illustrating Type C Cal veinlet cross cutting all pre-existing minerals and textures **D.** Late stage Fl-Cal clot cross-cutting ksp altered rock **E.** CE109 206.50. BSE image of REE bearing Cal in Kfs **F.** CE143 1393.50m. BSE image of Anh-Cal-Fl-Kfs in Type B vein. *For mineral abbreviations see Appendix 1.1.*

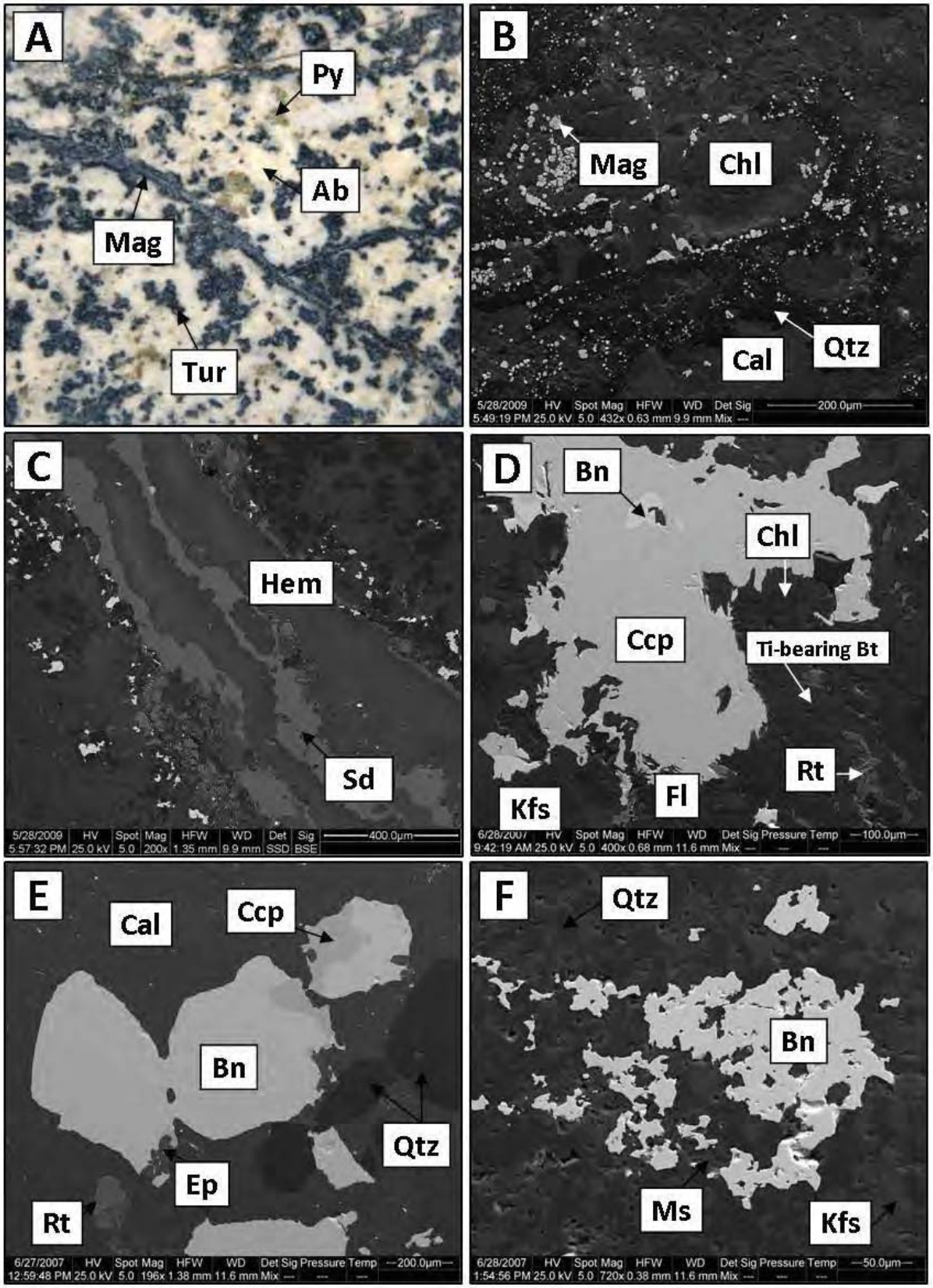

Figure 5.19A. CE110 199.00m Al-Tur alteration cross-cut by Mag Type A veinlet (image width is 5.5cm) **B.** CE098 386.50m. BSE image illustrating euhedral Mag with Chl, Qtz and Cal **C.** CE082 284.50m BSE image illustrating late stage Hem veinlets with Fe-Cal **D.** CE143 1335.00m. BSE image illustrating Rt occurring proximal to Ti-bearing Bt **E.** CE143 1408. BSE image illustrating euhedral Qtz crystals in Type B veins with Bn-Ccp-Ep-Cal-Rt **F.** CE143 1381.50m. BSE image illustrating Qtz-Kfs surrounding around disseminated Bn. *For mineral abbreviations see Appendix 1.1.*

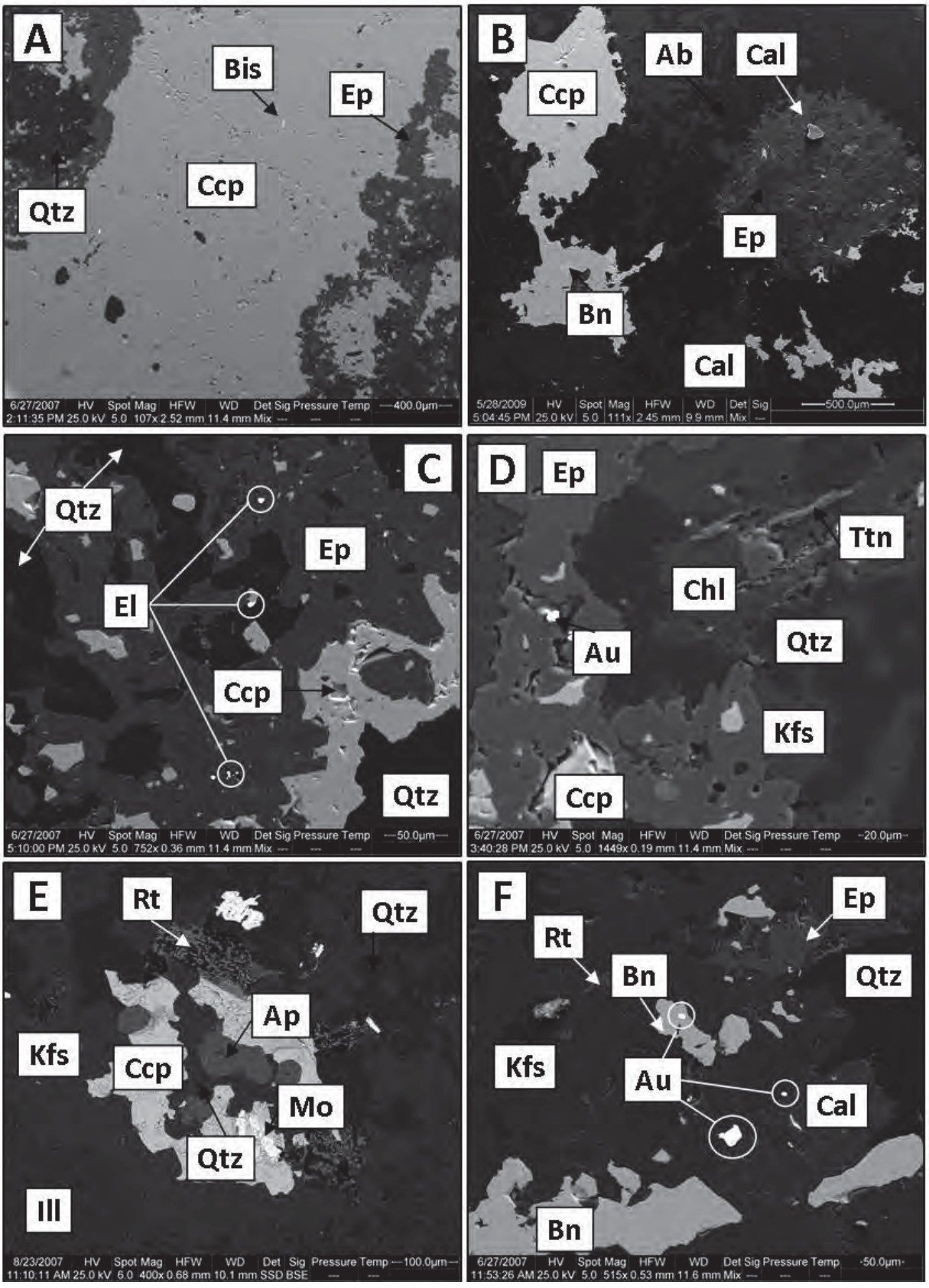

Figure 5.20A. CE143 1430.00m. BSE image illustrating a Type B vein with prismatic Ep and Qtz infilled with Ccp-bismithinide **B.** CE143 1420.00m BSE image illustrating clots of Ep-Cal **C.** CE143 1430.00m. BSE image illustrating El inclusions in Ep **D.** CE143 1430.00m BSE image illustrating Ttn along planar cleavage in Chl **E.** CE109 206.50m. BSE image illustrating a clot of Ccp-Ap-Qtz-Mo-Rt. **F.** CE143 1408m. BSE image illustrating au inclusions in Bn, Cal and Kfs. *For mineral abbreviations see Appendix 1.1.*

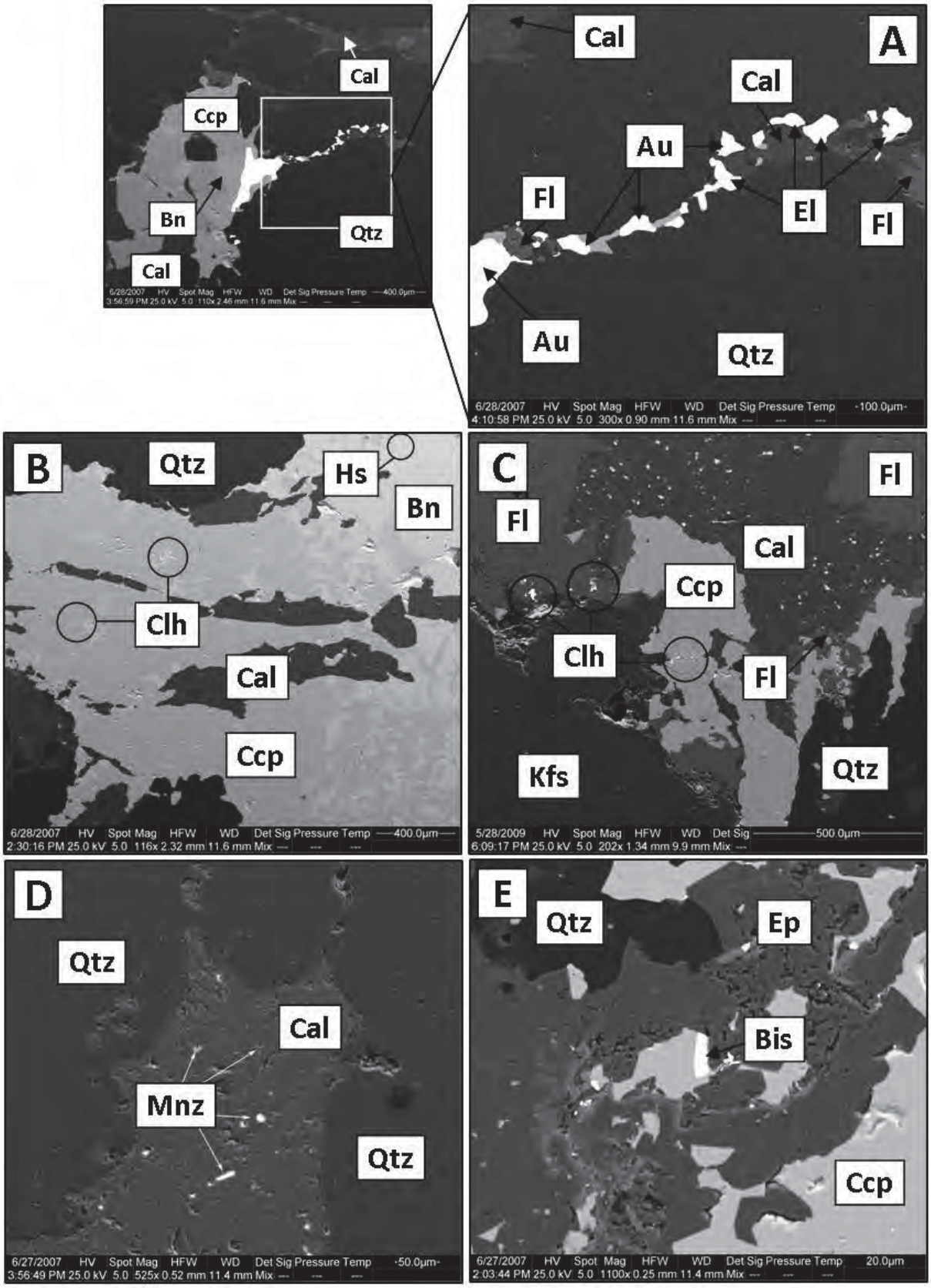

Figure 5.21A. CE143 1335m. Au and El in Type B vein, bordering Bn, Cal, Qtz and Fl **B.** CE143 1381.50m. Cl (PbSe) and Hs (AgTe) inclusions in Ccp and Bn **C.** CE110 205.50m. Cl inclusions in Ccp and Fl **D.** CE143 1430m. Mnz inclusions in Cal-Qtz Type B vein assemblage **E.** CE143 1430m. Bis (BiTe) inclusion in Ccp in Type B vein assemblage. *For mineral abbreviations see Appendix 1.1.*

5.3.2 Mineral spectra library: Cadia East

The creation of a representative mineral spectra library is an extremely important step in any MLA analysis. The mineral spectra library for Cadia East has been created using the method described in Chapter 3, section 3.5.2 in order to ensure that the most representative spectra for each mineral have been selected. The minerals at Cadia East have been grouped together to ease the process of data manipulation and interpretation of results (Table 5.10). These mineral groupings will be used for the XMOD and SPL-lite results in this chapter.

Table 5.10. Minerals grouped together for the analysis of MLA data from Cadia East.

Mineral	Mineral Group	Mineral	Mineral Group	Mineral	Mineral Group
Fe chlorite	Chlorite	Bornite	Bornite	Titanite	Titanite
Mg chlorite	Chlorite	Albite	Albite	Epidote	Epidote
Ti chlorite	Chlorite	Fe biotite	Biotite	Fluorite	Fluorite
Pb selenide	Pb selenide	Mg biotite	Biotite	Hessite	Hessite
REE calcite	Calcite	Ti biotite	Biotite	Illite	Illite/Muscovite
Calcite	Calcite	Chalcopyrite	Chalcopyrite	Muscovite	Illite/Muscovite
Sr calcite	Calcite	Digenite	Digenite	Magnetite	Magnetite
Apatite	Apatite	Electrum	Gold minerals	Pyrite	Pyrite
Molybdenite	Molybdenite	Gold	Gold minerals	Rutile	Rutile
K-Feldspar	K-Feldspar	Plagioclase	Plagioclase	Monazite	Monazite
Quartz	Quartz	Tennanite	Tennanite	Tourmaline	Tourmaline
Barite	Barite	Bismuthinite	Bismuthinite		

5.3.3 Modal mineralogy: XMOD analysis

The MLA XMOD analysis is an automated point counting system designed to provide a fast and accurate representation of the modal mineralogy of a sample. The results from these analyses can be used to create a mineralogical signature of each sample. At Cadia East 130 (3 x 3cm) tiles have undergone an XMOD analysis where 20 000 x-ray points per tile (one point every 47 pixels) have been measured using the method outlined in Chapter 3, section 3.5.3 (Appendix 5.3). The grid approach adopted by XMOD is designed to provide an unbiased mineralogical analysis of a sample.

The mineralogical abundances obtained from the XMOD analyses have been used to quantify the mineralogical signatures that are typical of various rock and/or alteration types. For example, Figure 5.22 shows XMOD analysis of two drill-core tiles from Cadia East. The tiles consist of a Type B vein (see Chapter 1, Figure 1.3) and biotite/chlorite alteration and are shown to have significantly different mineral abundances for quartz, chlorite/biotite, albite and illite/muscovite. Presented as pie charts, the mineralogical abundances for the selected Cadia east examples (see Table 5.8) are presented in Figure 5.23. From this figure the most commonly occurring minerals are K-feldspar, albite, illite/muscovite, quartz, biotite and chlorite.

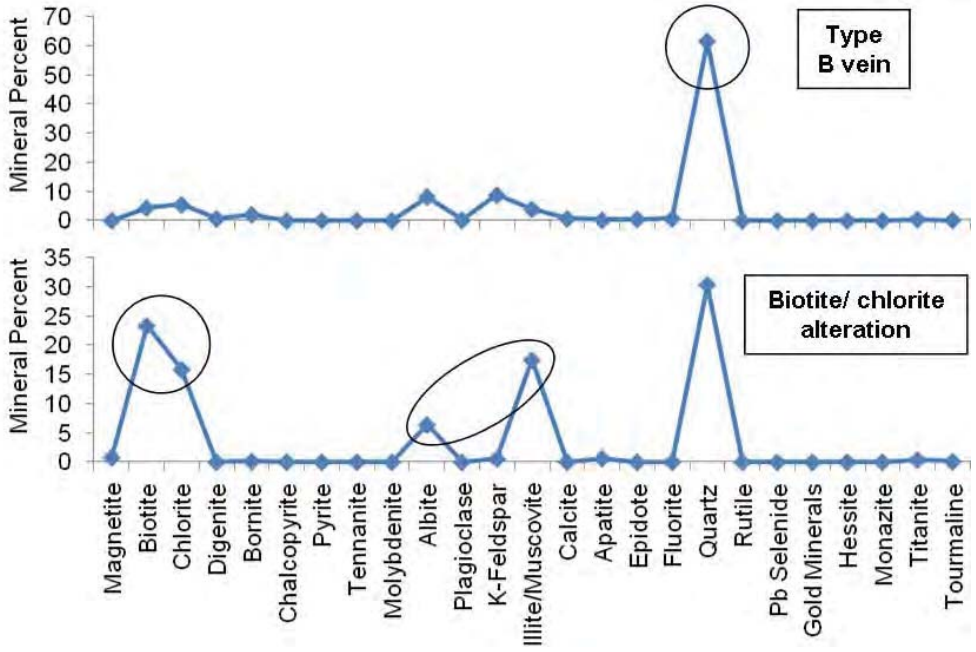

Figure 5.22. Mineralogical signatures created using XMOD analysis of drill-core tiles. Type B vein example (CE143 1293) shows an abundance of quartz. Example with dominant biotite/chlorite alteration (CE082 307) shows strong peaks for these minerals as well as albite, illite/muscovite and quartz.

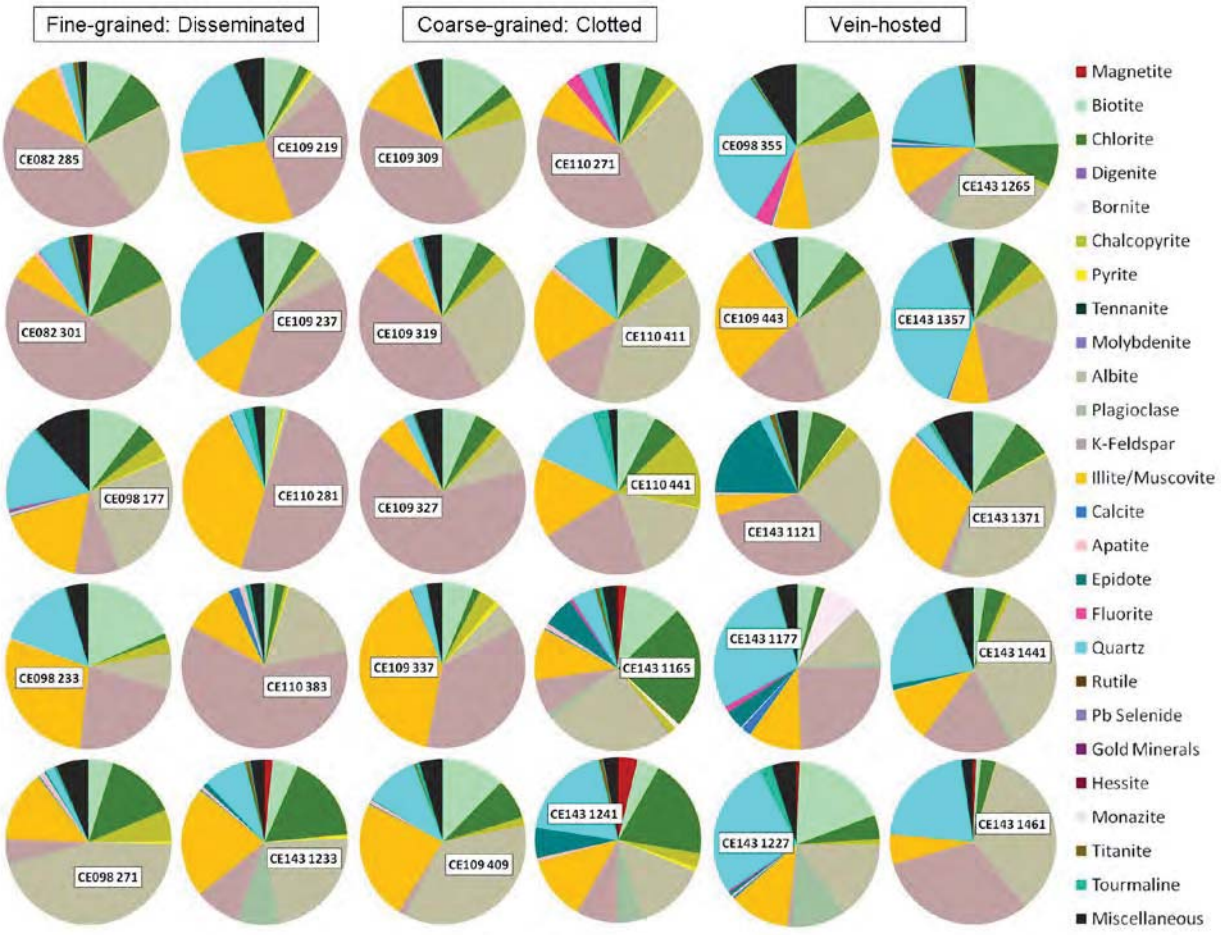

Figure 5.23. Pie charts illustrating the results of XMOD analyses undertaken on 30 examples from Cadia East (Table 5.8). Mineral groups are defined in Table 5.10. The most dominant minerals are K-feldspar, albite, illite/muscovite, quartz, biotite and chlorite.

5.3.4 Size analysis of Cu-sulphide minerals

The size analysis in this section is presented here as area, length and width, Phase Specific Surface Area (PSSA) and the smallest enclosing circle. The results for the size analysis of bornite are only presented where a sufficient number of PhRegs is available in the sample. This information was considered important to collect because the analysis of mineral size is considered to directly impact the ease at which those minerals can be released from a rock (Jones, 1987; Petruk, 2005).

Area

The area of each chalcopyrite PhReg has been converted to an Equivalent Circle Diameter (ECD) and divided into size fractions that follow a $\sqrt{2}$ distribution of sizes (see chapter 2, section 2.6.1). The size trends for each example are plotted as size distribution curves as well as cumulative size distribution curves. The curves are coloured based on their meso-scale class (see Table 5.11; *fine-grained disseminations- blue: coarse-grained clots- red: vein-hosted- green).*

The distribution of ECD size fractions presented in Figure 5.24 for chalcopyrite indicates that there are three dominant trends in chalcopyrite size (1, 3 and 4), but also show the presence of multimodal populations (2, 5 and 6) which can be masked when only cumulative plots are used (Figure 5.25). These six distribution curves are described in Table 5.12. For bornite only eight examples contained sufficient bornite to display ECD distribution curves (Figures 5.26 and 5.27). From these, three trends were previously observed in chalcopyrite (1, 2 and 4) and one was not (7).

Table 5.11. The results of area, length and width for the chalcopyrite and bornite PhRegs from each drill-core tile example from Cadia East (see Table 5.8). Size fractions have been measured as Equivalent Circle Diameter. Width refers to the corresponding chalcopyrite or bornite PhReg which has the maximum length in that drill-core tile.

Sample		Chalcopyrite									Bornite						
		(n)	<75 µm	75-150 µm	150-300 µm	300-600 µm	600-1200 µm	>1200 µm	Max length	Width	(n)	<75 µm	75-150 µm	150-300 µm	300-600 µm	600-1200 µm	>1200 µm
Fine-grained	CE082 285	2151	92.09	7.91	0.00	0.00	0.00	0.00	43.00	38.00	nil	0.00	0.00	0.00	0.00	0.00	0.00
	CE082 301	2024	36.85	35.09	19.93	8.13	0.00	0.00	162.35	109.69	28	100	0.00	0.00	0.00	0.00	0.00
	CE098 177	6244	16.91	16.31	21.40	34.38	11.01	0.00	397.38	326.23	nil	0.00	0.00	0.00	0.00	0.00	0.00
	CE098 233	4737	11.84	15.82	24.01	22.54	6.12	19.67	811.00	745.00	nil	0.00	0.00	0.00	0.00	0.00	0.00
	CE098 271	15249	17.03	12.82	19.04	31.40	19.72	0.00	702.00	201.00	nil	0.00	0.00	0.00	0.00	0.00	0.00
	CE109 219	1742	21.01	27.07	34.73	17.18	0.00	0.00	195.00	151.95	2	100	0.00	0.00	0.00	0.00	0.00
	CE109 237	1122	20.67	26.88	27.52	24.93	0.00	0.00	180.86	100.54	nil	0.00	0.00	0.00	0.00	0.00	0.00
	CE110 281	2184	41.93	15.68	10.29	21.06	11.04	0.00	309.68	202.62	1	100	0.00	0.00	0.00	0.00	0.00
	CE110 383	762	11.03	19.72	34.06	26.04	9.15	0.00	430.12	187.93	nil	0.00	0.00	0.00	0.00	0.00	0.00
	CE143 1233	2330	36.21	16.35	19.62	27.82	0.00	0.00	148.00	111.00	nil	0.00	0.00	0.00	0.00	0.00	0.00
Coarse-grained	CE109 309	8144	13.12	12.71	19.08	21.96	19.28	13.85	715.00	454.00	nil	0.00	0.00	0.00	0.00	0.00	0.00
	CE109 319	3393	6.50	10.85	27.59	27.00	22.08	5.97	855.84	106.17	3	100	0.00	0.00	0.00	0.00	0.00
	CE109 327	1891	8.73	15.14	24.78	37.13	14.22	0.00	595.26	247.71	2	100	0.00	0.00	0.00	0.00	0.00
	CE109 337	6683	12.01	11.85	22.44	22.16	11.85	19.69	994.35	598.56	1	100	0.00	0.00	0.00	0.00	0.00
	CE109 485	1019	5.01	2.39	2.44	0.00	12.48	77.67	960.00	400.00	94	100	0.00	0.00	0.00	0.00	0.00
	CE110 271	1801	4.79	5.22	9.28	13.15	7.00	60.56	759.00	626.00	1	100	0.00	0.00	0.00	0.00	0.00
	CE110 411	7770	13.01	15.19	26.65	28.99	12.24	3.93	649.42	462.49	nil	0.00	0.00	0.00	0.00	0.00	0.00
	CE110 441	24523	9.60	10.36	18.31	17.68	12.82	31.23	2182.55	1212.84	3	100	0.00	0.00	0.00	0.00	0.00
	CE143 1165	2400	9.86	8.76	21.30	11.13	32.81	16.14	689.35	419.91	19373	72.80	13.72	8.70	4.78	0.00	0.00
	CE143 1241	19571	39.07	15.72	17.41	10.85	3.58	13.38	629.59	284.78	29	0.00	0.00	0.00	0.00	0.00	0.00
Vein-hosted	CE098 355	1202	1.40	1.93	2.10	4.80	5.62	84.16	3002.59	620.41	59	38.43	61.57	0.00	0.00	0.00	0.00
	CE109 443	2951	27.19	13.86	16.51	22.26	20.17	0.00	322.00	264.00	nil	0.00	0.00	0.00	0.00	0.00	0.00
	CE143 1121	3411	6.72	4.38	3.84	7.51	3.70	73.85	1326.78	281.56	4355	69.52	19.75	10.73	0.00	0.00	0.00
	CE143 1177	125	23.35	10.30	18.57	47.78	0.00	0.00	147.00	75.00	5609	5.76	4.77	6.34	6.03	31.31	45.79
	CE143 1227	4626	20.75	11.26	13.51	11.35	0.00	43.13	832.65	405.42	nil	0.00	0.00	0.00	0.00	0.00	0.00
	CE143 1265	3390	20.46	13.49	20.47	12.49	33.09	0.00	862.54	171.74	nil	0.00	0.00	0.00	0.00	0.00	0.00
	CE143 1357	2284	3.49	2.71	4.19	8.02	16.76	64.82	1599.00	1076.00	553	80.75	19.25	0.00	0.00	0.00	0.00
	CE143 1371	1296	46.69	19.40	12.96	20.95	0.00	0.00	146.36	130.57	nil	0.00	0.00	0.00	0.00	0.00	0.00
	CE143 1441	2620	15.91	6.69	13.90	13.25	50.26	0.00	418.87	207.20	46	15.91	6.69	13.90	13.25	50.26	0.00
	CE143 1465	3900	43.58	13.95	7.96	9.20	25.32	0.00	383.06	237.10	nil	0.00	0.00	0.00	0.00	0.00	0.00

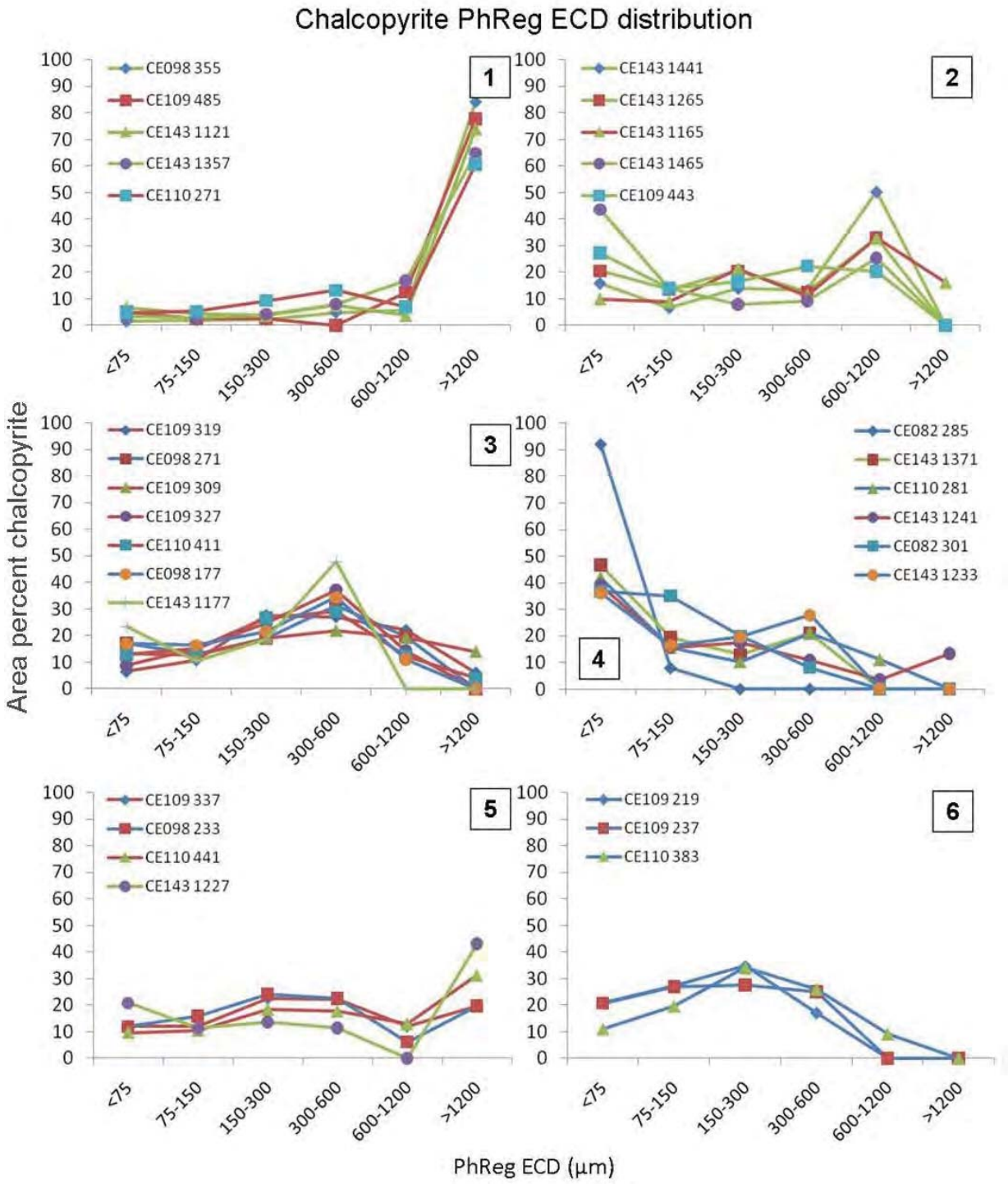

Figure 5.24. Distribution of chalcopyrite PhReg sizes for the selected Cadia East examples (Table 5.8). PhReg sizes have been determined from MLA SPL-lite images and converted to an Equivalent Circle Diameter (ECD). The results have been presented based on examples that exhibit similar trends. All samples have been area weighted to reduce bias towards smaller PhRegs. *Blue:* fine-grained *disseminated, red:* coarse-grained aggregates, *green:* vein-hosted.

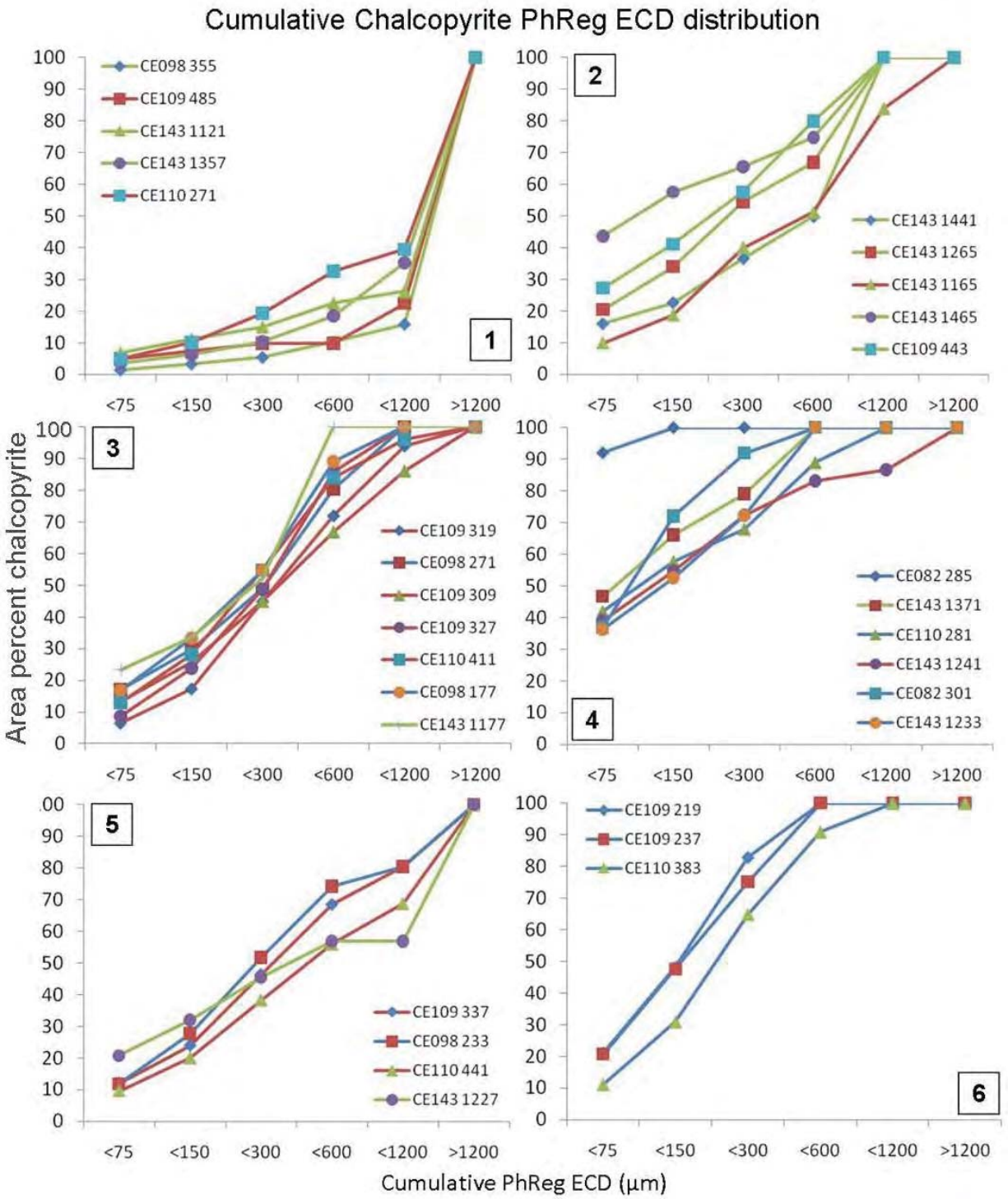

Figure 5.25. Cumulative distribution of chalcopyrite PhReg sizes for the selected Cadia East examples (Table 5.8). PhReg sizes have been determined from MLA SPL-lite images and converted to an Equivalent Circle Diameter (ECD). The results have been presented based on examples that exhibit similar trends. *blue: fine-grained disseminations, red: coarse-grained clots, green: vein-hosted*

Table 5.12. The characteristics of size distribution trends for chalcopyrite and bornite from Cadia East.

Trend	Minerals that exhibit this trend	Bimodal	Description
1	Chalcopyrite and bornite	No	> 80% of sample exceeds an ECD of 1200 µm.
2	Chalcopyrite and bornite	Yes	20-50% of sample has an ECD between 600 and 1200 µm. 10-50% of sample has an ECD <75 µm. < 20% of sample exceeds an ECD of 1200 µm.
3	Chalcopyrite	Yes	20-50% of sample has an ECD between 300 and 600 µm. <20% of sample exceeds an ECD of 1200 µm. 5-25% of sample has an ECD <75 µm.
4	Chalcopyrite and bornite	Yes	>35% of sample has an ECD <75 µm. 0-30% of sample has an ECD between 300 and 600 µm.
5	Chalcopyrite	Yes	20-40% of sample has an ECD between 150 and 600 µm. 20-40% of sample exceeds and ECD of 1200 µm. 10-20% of sample has an ECD of <75 µm.
6	Chalcopyrite	No	0% of sample exceeds an ECD of 1200 µm. 65-60% of sample has an ECD between 75 and 1200µm.
7	Bornite	No	100% of sample has an ECD <150 µm.

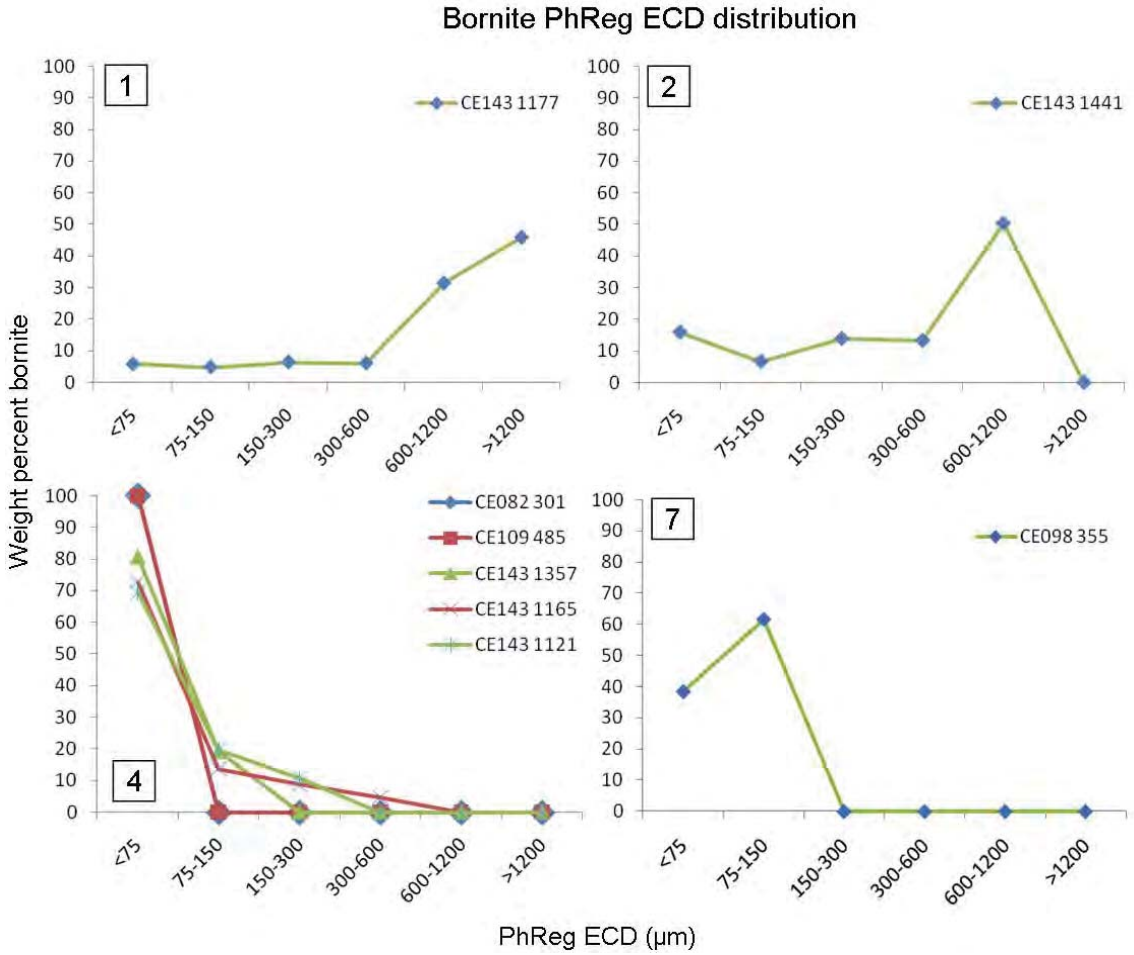

Figure 5.26. Distribution of bornite PhReg sizes for the selected Cadia East examples (Table 5.8). PhReg sizes have been determined from MLA SPL-lite images and converted to an Equivalent Circle Diameter (ECD). The results have been presented based on examples that exhibit similar trends. *blue: fine-grained disseminations, red: coarse-grained clots, green: vein-hosted*

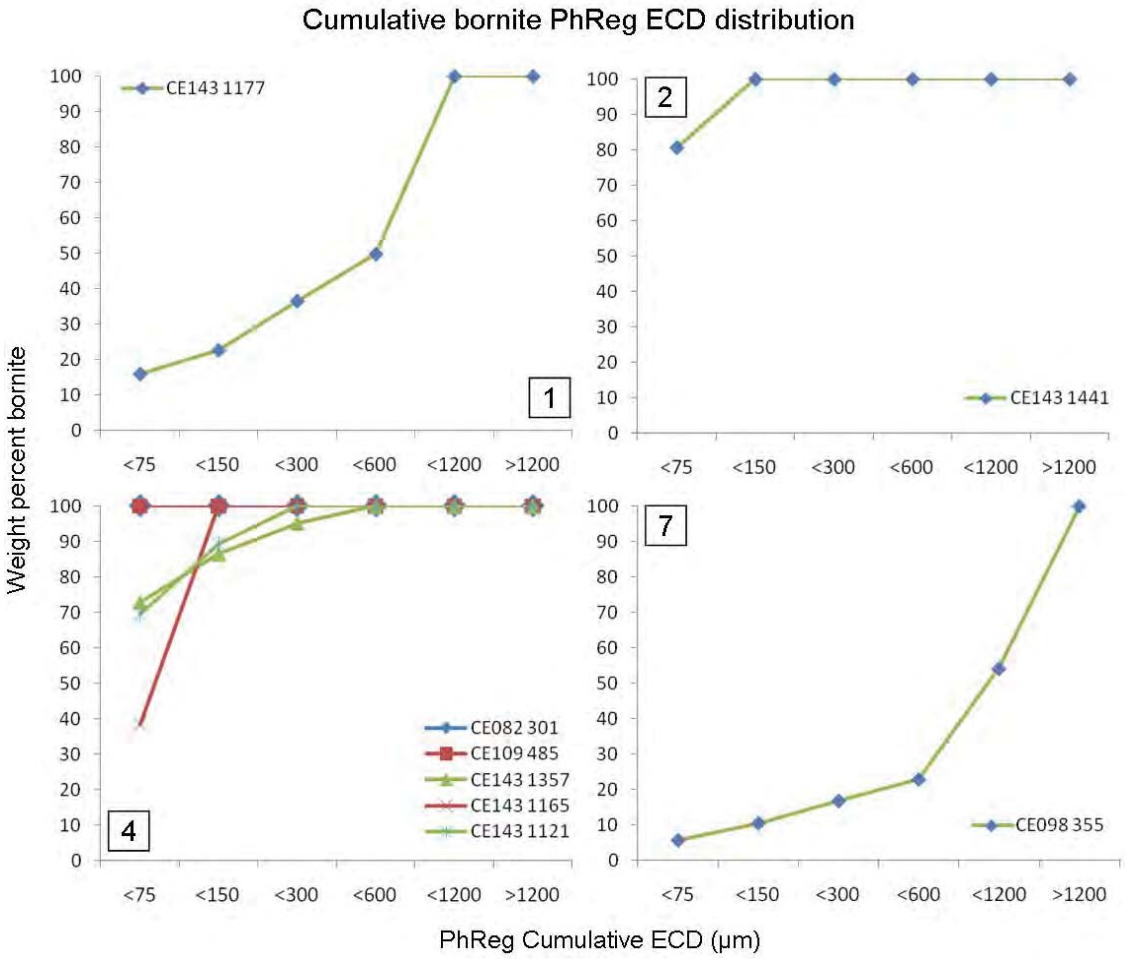

Figure 5.27. Cumulative distribution of bornite PhReg sizes for the selected Cadia East examples (Table 5.8). PhReg sizes have been determined from MLA SPL-lite images and converted to an Equivalent Circle Diameter (ECD). The results have been presented based on examples that exhibit similar trends. *blue: fine-grained disseminations, red: coarse-grained clots, green: vein-hosted*

Length and Width

At the micro-scale the shape boundaries of mineral PhRegs are better defined than when observed at the meso-scale. The high resolution of the images produced from the MLA means that the length and width measurements are more informative at this scale. At this scale it is expected that elongate mineral shapes and features such as those produced from veins or veinlets can be distinguished using the length and width data. Figure 5.28 shows the length and width of the chalcopyrite PhRegs from CE109 319, an example that is predominantly made up of coarse-grained chalcopyrite in veinlets (see Figure 5.13). The chalcopyrite PhRegs that correspond to veinlets in this example plot along the 4:1 length: width ratio boundary.

The length and width of all of the chalcopyrite PhRegs for the 30 selected drill-core tiles (Table 5.8) have been plotted in Figure 5.29. In this figure it is clear that the chalcopyrite from the fine-grained examples predominantly clusters between 1 and 400 pixels (844 µm) and rarely exceeds a length to width ration of 2:1. The chalcopyrite from the coarse-grained examples shows a spread of data which is predominantly < 1000 pixels (2110 µm) length and with a length to width ration < 3:1. The chalcopyrite that is vein-hosted exhibits a cluster of smaller PhRegs (<600 pixels; 1266 µm) with a number of larger more elongate Phregs with a length to width ratio up to 6:1.

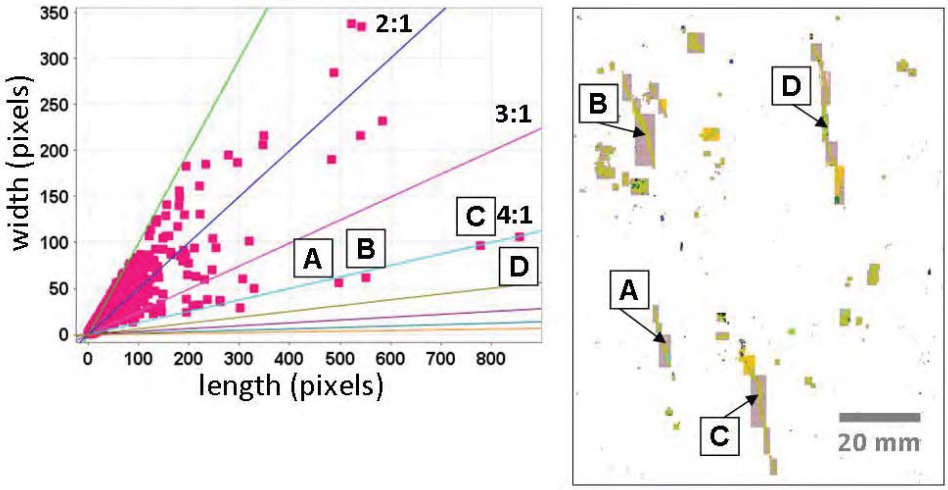

Figure 5.28. The length and width data of CE109 319 (left). Four points **A**, **B**, **C** and **D** represent chalcopyrite objects produced from veinlets. The classified SPL-lite image of the corresponding chalcopyrite objects **A-D** can be seen in the image on the right. The pixel length is 4.02 µm.

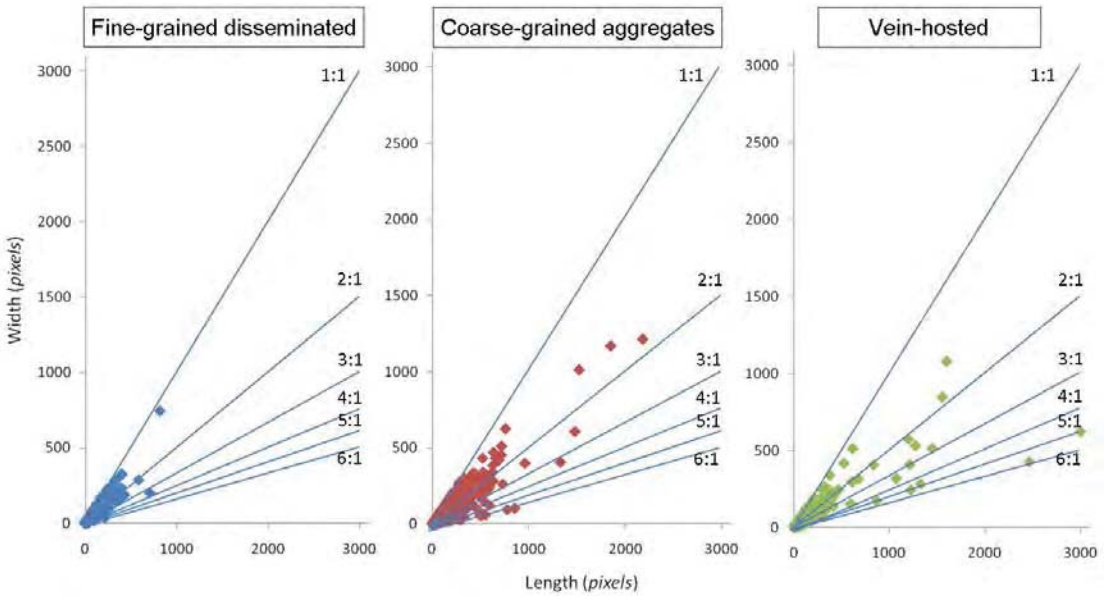

Figure 5.29. Length and width of all chalcopyrite PhRegs in each of the fine-grained disseminated, coarse-grained aggregates and vein-hosted Cadia East examples.

Phase Specific Surface Area

The PSSA values for each of the Cadia East drill-core tiles are presented in Figure 5.30 as box plots for fine-grained disseminations, coarse-grained clots and vein-hosted chalcopyrite. The box plots present PSSA values for every chalcopyrite PhReg in each drill-core tile. This allows the entire chalcopyrite population of each tile to be observed. A low PSSA value implies a simple PhReg boundary or a large PhReg size and a high PSSA value implies a complex PhReg boundary or a small PhReg size. Figure 5.30 shows that overall the examples of tiles classified as fine-grained disseminated have a lower average PSSA (except CE143 1233) than the coarse-grained aggregates and vein-hosted chalcopyrite. The examples with the lowest median PSSA are CE109 327, CE110 383 and CE109 237. The examples with the highest median PSSA are CE143 1233, CE143 1227 and CE143 1241.

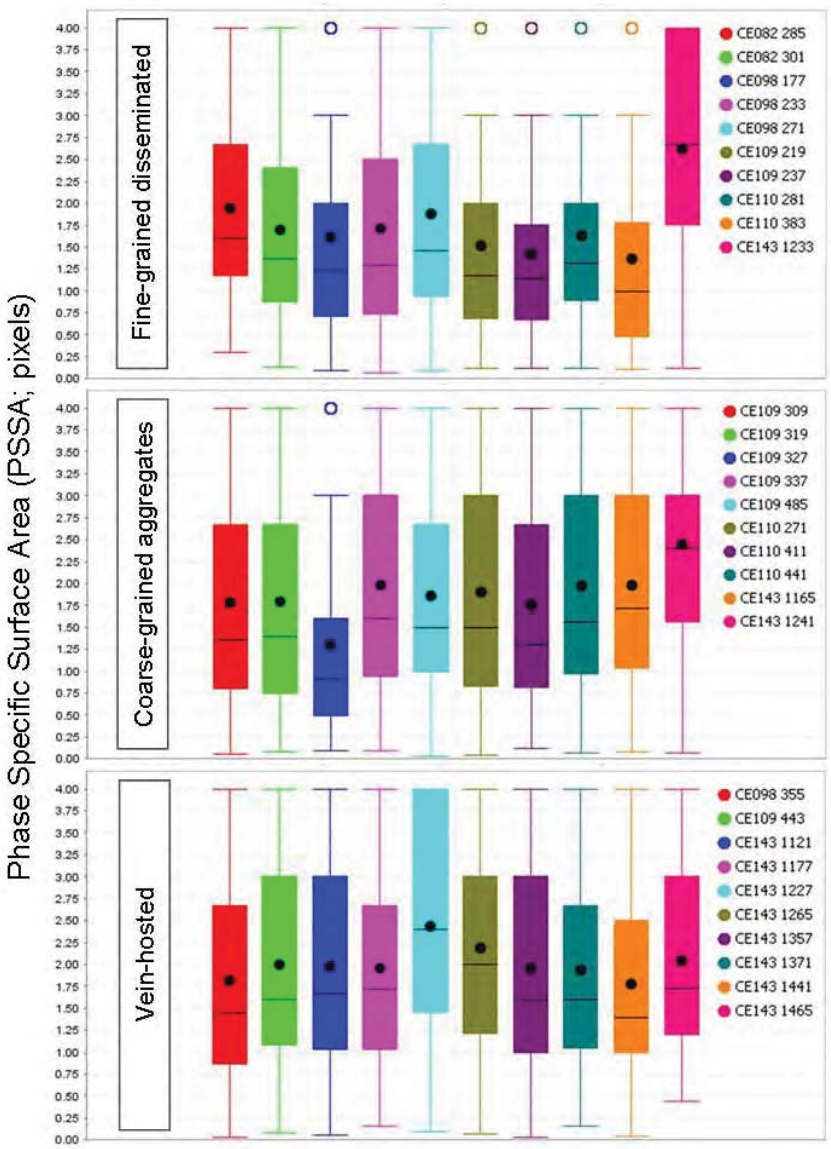

Figure 5.30 (*left*). Box plots illustrating the PSSA of the fine-grained disseminated, coarse-grained aggregates and vein-hosted chalcopyrite populations (see Table 5.8). Median is shown by the *black circles*, mean is shown by the *black lines*.

Smallest enclosing ellipse

The smallest enclosing ellipse has been calculated for each chalcopyrite PhReg. The value for this perimeter is produced by calculating the diameter of the equivalent ellipse and then growing that ellipse until the object is fully encompassed. The ratio of the diameter of the enclosing ellipse to the equivalent ellipse is the value that is returned (see Definiens user manual, page 122). A value of one indicates that the enclosing ellipse perfectly surrounds the equivalent ellipse. The higher the value the larger the enclosing ellipse and the more complex the object boundary is. This varies from the traditional method of calculating this parameter and is essentially a measure of border complexity rather than size.

The results of the smallest enclosing ellipse for the Cadia East examples have been plotted as box plots in Figure 5.31. Interestingly, the lowest overall median values occurred in the vein-hosted chalcopyrite. The highest smallest enclosed ellipse values were observed in the fine-grained disseminated chalcopyrite, however only slightly above the coarse-grained aggregates of chalcopyrite. This indicates that the fine-grained disseminated and coarse-grained aggregates of chalcopyrite have more complex PhReg boundaries than those that are vein-hosted when measured by this method.

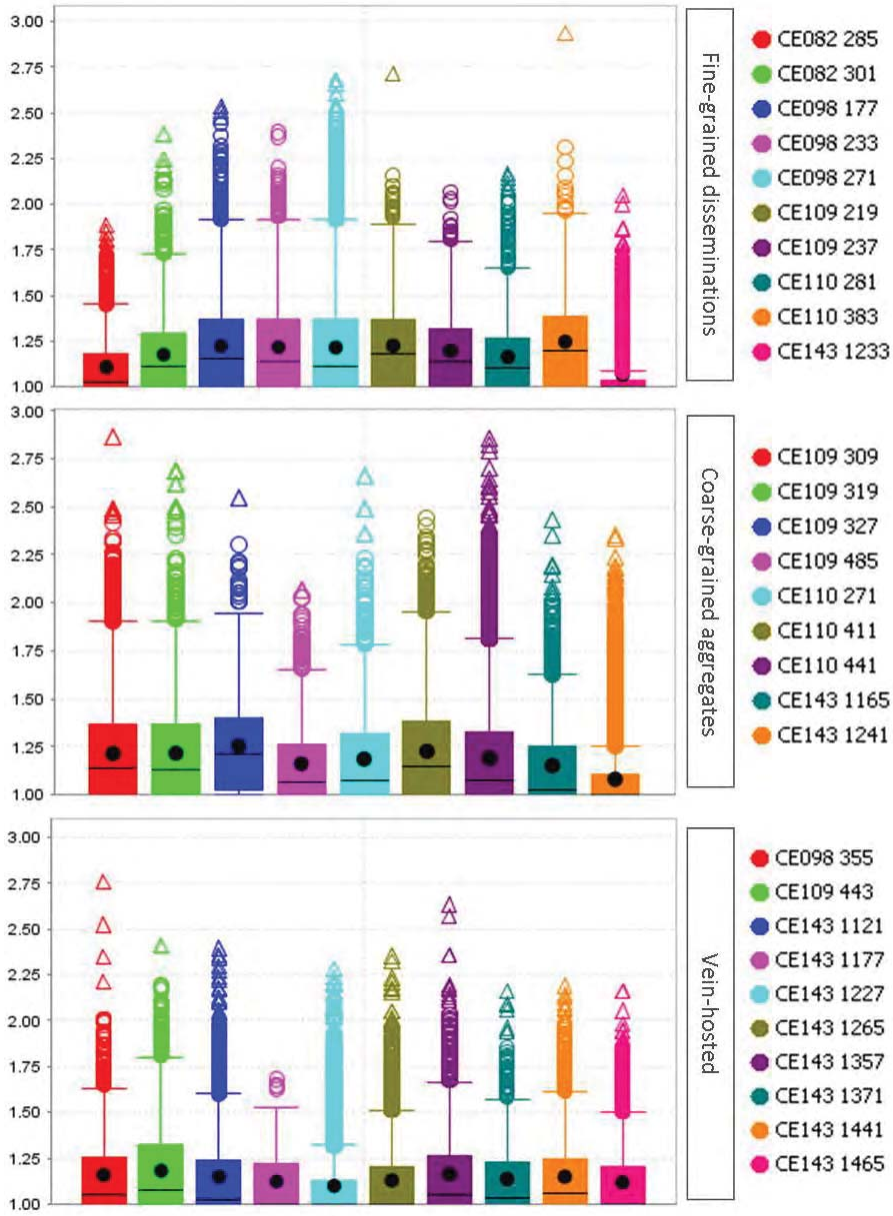

Figure 5.31 (*left*). Box plots illustrating the smallest enclosing ellipse of the fine-grained disseminated, coarse-grained aggregates and vein-hosted chalcopyrite populations (see Table 5.8). Median is shown by the *black circles*, mean is shown by the *black lines*.

5.3.5 Gangue minerals associated with Cu-sulphide minerals and molybdenite

The gangue minerals that are associated with the chalcopyrite, bornite and molybdenite minerals can have a direct effect on the ease with which these minerals can be liberated and recovered (e.g. Jones, 1987). In this section these mineral associations have been quantified using mineral maps of intact minerals and textures produced by the MLA. It was recognised early in this research that even for small samples, such as the 3 x 3 cm drill-core tiles used here, there are variable proportions of different minerals associated with Cu-sulphide minerals even within the same sample. In order to recognise the dominant mineralogical signatures a more sophisticated statistical approach was required than a simple correlation matrix.

The mineral associations for Cadia East have been determined by calculating the proportions of minerals within a one pixel rim of the mineral PhReg of interest. Using this data, a Principal Components Analysis (PCA) has been applied to all of the chalcopyrite PhRegs extracted from SPL-lite analyses at Cadia East (~250,000 chalcopyrite PhRegs). This allows the most commonly

occurring mineralogical signatures (combinations of minerals that occur with copper sulphide minerals) to be determined. Examples presented here in this section illustrate the mineralogical associations that can be calculated for an individual sample or a large quantity of samples within a group.

The PCA was undertaken using DataDesk data analysis software. The analysis indicated that the minerals associated with chalcopyrite at Cadia East were not as complex as initially thought, considering the degree of overlapping alteration events that are present (Wilson, 2003; Kitto, 2005). Figure 5.32 illustrates a snapshot of a 3 dimensional rotating plot of the PCA results. It shows that the dominant minerals associated with chalcopyrite are albite; biotite-chlorite; illite-muscovite; K-feldspar. Based on these findings, the dominant minerals that occur with chalcopyrite have been plotted in Figure 5.33 for each of the Cadia East examples (see Table 5.8).

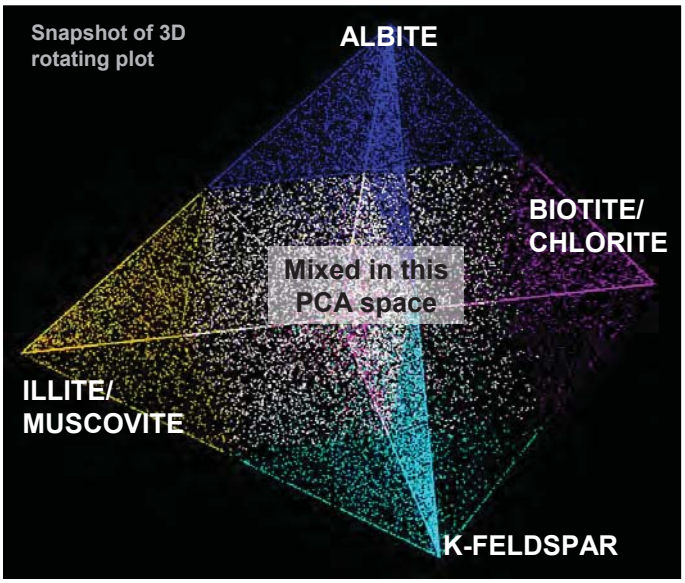

Figure 5.32. Screen shot taken from DataDesk which shows the distribution of minerals associated with chalcopyrite in 3 dimensions (PC1 – PC3). From this plot it can be seen that the dominant minerals associated with chalcopyrite are albite, illite-muscovite, biotite-chlorite and K-feldspar.

The approach for analyzing the minerals that are associated with bornite differs to that used for chalcopyrite. For chalcopyrite there were significantly more individual PhRegs to successfully perform a PCA, however considering that the results for chalcopyrite indicated predominantly binary and ternary associations, the data for bornite can easily be manipulated to establish if the bornite minerals at Cadia East also follow this trend. A total of 65,168 bornite PhRegs have been extracted from drill-core tile data from Cadia East. The most common minerals associated with bornite are epidote, albite, illite-muscovite, chlorite-biotite, K-feldspar, quartz and chalcopyrite respectively. Other less common associated minerals include carbonate, fluorite and magnetite. Any given sample can have examples of a number of different bornite associations. Figure 5.34 shows the weighted proportions of minerals associated with bornite for CE098 227. The mineral associations for the Cadia East examples (Table 5.8) are shown in Figure 5.35. In this figure, peaks are observed with the vein assemblage minerals carbonate, epidote, quartz and chalcopyrite as well as albite, illite-muscovite and fluorite.

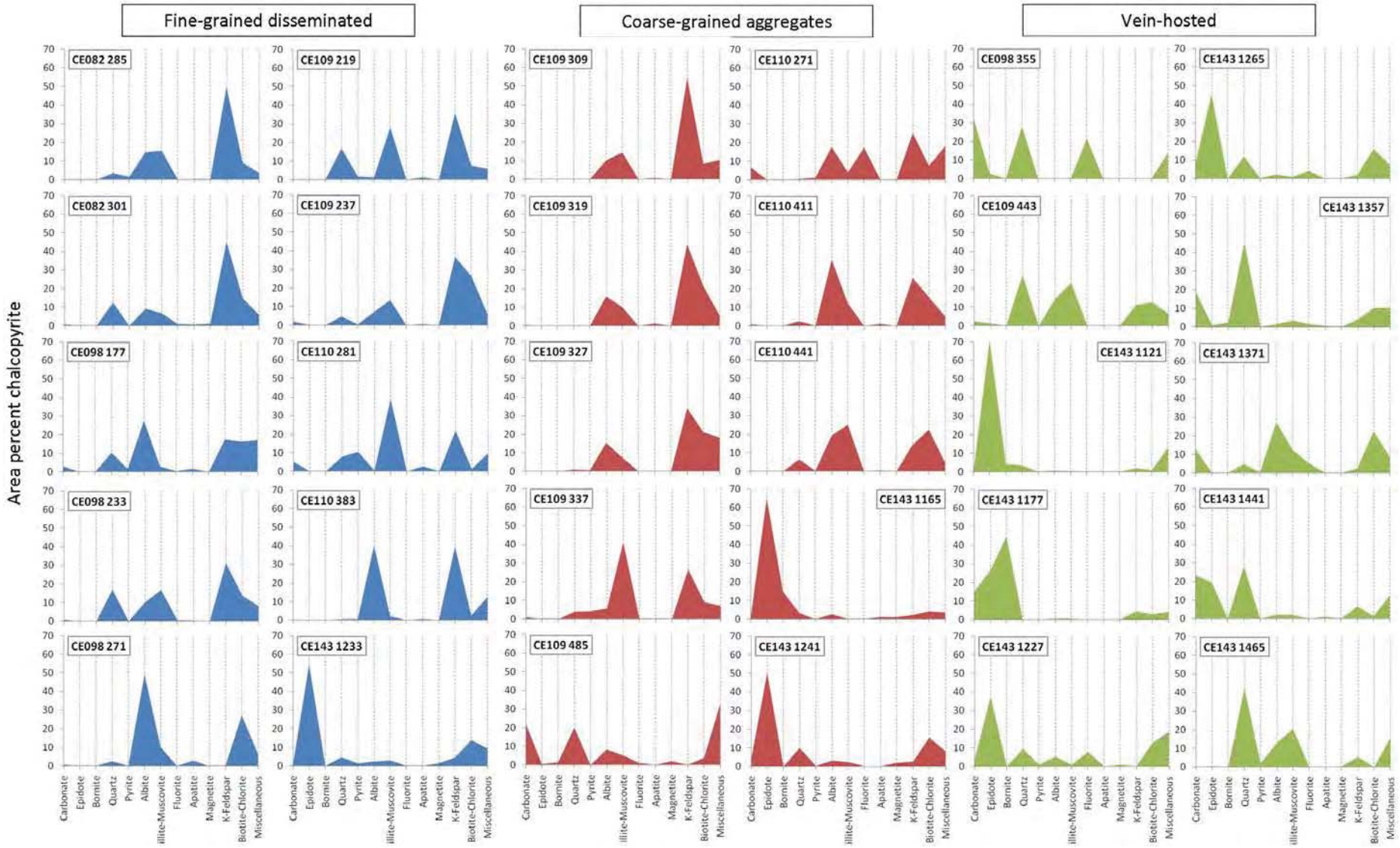

Figure 5.33. Area percent of minerals associated with chalcopyrite for Cadia East examples (see Table 5.8). Only the most commonly occurring mineral associated have been plotted as determined through the PCA.

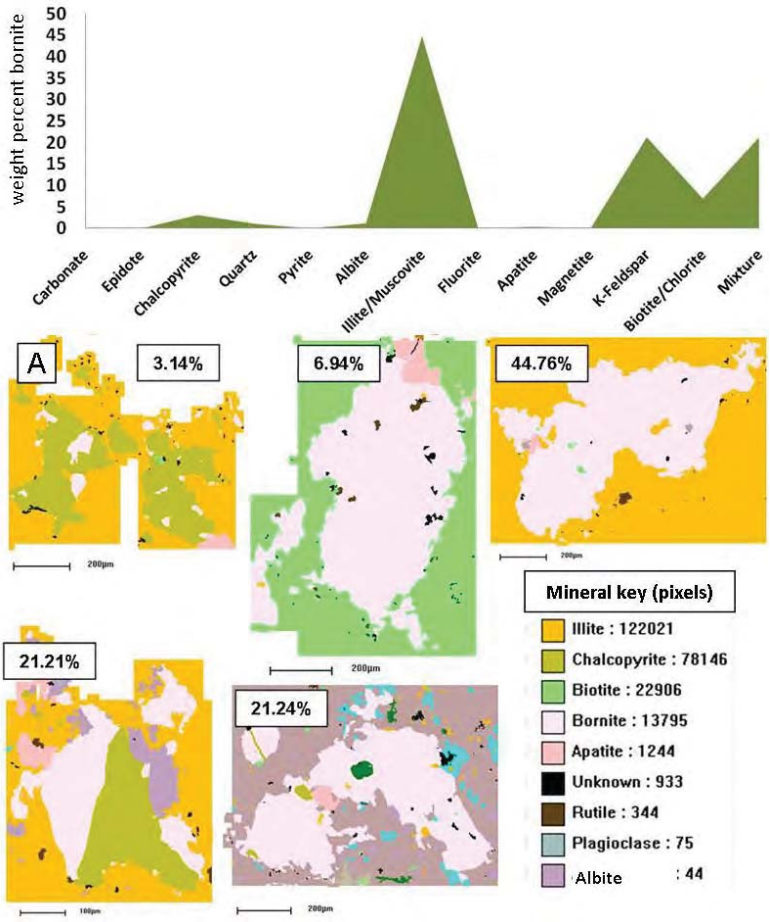

Figure 5.34. The minerals associated with bornite PhRegs for the example CE098 227. Mineral associations have been defined based on SPL-lite analysis. SPL-lite images below the graph illustrate the types of mineral associations that are present and the abundance. For example A shows bornite is associated with 3.14% (mineral).

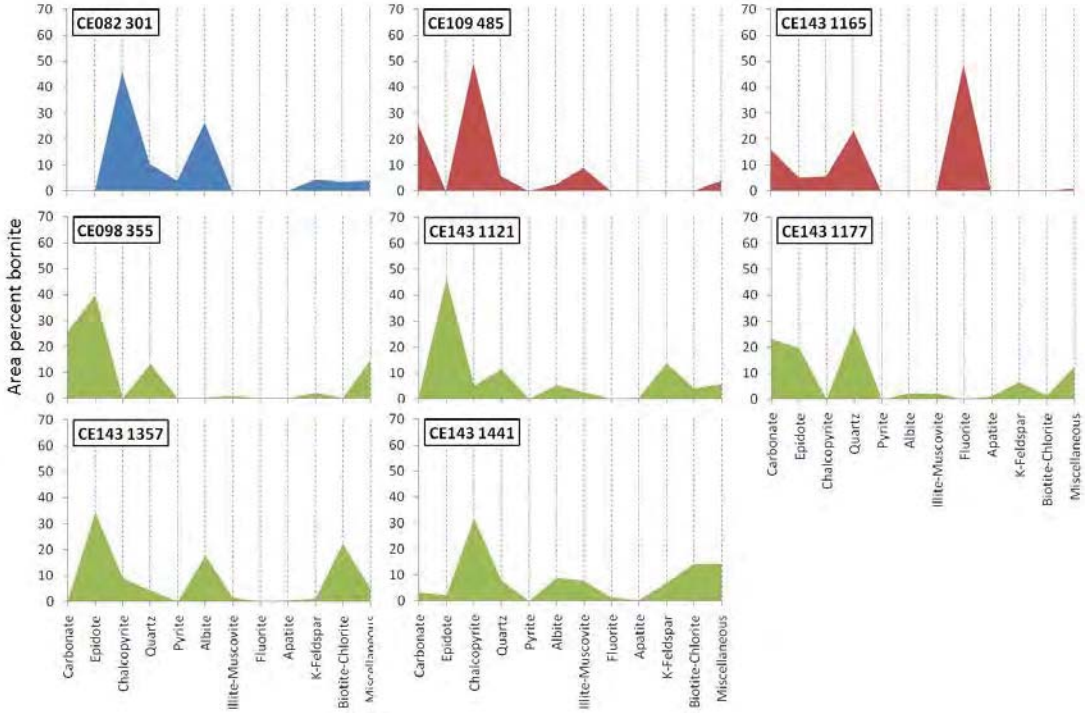

Figure 5.35. Area percent of minerals associated with bornite for Cadia East examples (see Table 5.8). Graphs are coloured based on their meso-scale texture class (*fine-grained disseminations – blue; coarse-grained clots – red; vein-hosted – green*).

Based on the bornite PhRegs that have been extracted using the SPL-lite method, the dominant minerals associated with bornite have been determined. For 65,168 bornite PhRegs (*all exceeding a classified size of 4 pixels, where one pixel equals a diameter of 4.22 μm*), the dominant mineral associations are:

Mineral	Percent of total sample
Epidote	18.52
Quartz	18.34
Carbonate	13.61
K-feldspar	8.13
Illite-muscovite	7.44
Chalcopyrite	5.90
Chlorite-biotite	5.36
Albite	5.52
Digenite	3.80
Fluorite	0.47
Electrum and gold	0.03
Miscellaneous and other minerals	12.88

Molybdenite

In recent years, the metal price for molybdenum has risen substantially making it a valuable commodity within many copper and gold deposits. Many companies have opted to install molybdenum processing plants to maximise profits within their operations (e.g. Bingham Canyon). At Cadia East, the molybdenum grade is relatively low in most areas of the deposit (for example the five drill-holes used in this study the average molybdenum grade is 66.71 ppm), however if it is easily extracted it may prove to be a valuable asset over the life of the mine.

Based on the molybdenite PhRegs that have been extracted using the SPL-lite method, the dominant minerals associated with molybdenite have been determined. For 3600 molybdenite PhRegs (*all exceeding a classified size of 4 pixels, where one pixel equals a diameter of 4.22 μm*), the dominant mineral associations are:

Mineral	Percent of total sample
K-feldspar	16.42
Chlorite-biotite	13.22
Illite-muscovite	9.62
Albite	8.75
Quartz	4.52
Carbonate	4.19
Chalcopyrite	3.44
Bornite	3.00
Miscellaneous and other minerals	36.84

5.3.6 Shape analysis

The descriptive analysis of mineral shapes has been widely used in various fields of geology for many years (sedimentary geology, igneous petrology). The various shape classification systems and nomenclature typically used in geology have been outlined in Chapter 2. The recent advances in digital imaging systems combined with increased computing power and software capabilities have lead to many mineralogical and textural attributes being quantified. However this has not been extended into the area of shape analysis where very little work is routinely undertaken. This is

namely due to it being a difficult attribute to quantify and whilst most shapes are assigned a numerical value the relevance of these values is not clear (such as length or area). A full shape analysis of all of the intact chalcopyrite phases at Cadia East is not within the scope of this research. However, a selection of intact mineral PhRegs have been analysed to assess which measures of shape are more useful and relevant for further work in this area in the future.

Thirty intact chalcopyrite PhRegs have been selected from SPL-lite images from Cadia East (Figure 5.36). These examples represent a range of shapes and sizes observed in intact textures. The shape attributes that have been analysed correspond to those that can be extracted using the Definiens developer software and fall into the following broad shape categories:

- Perimeter characteristics
- Length and Width
- Objects related to simple shapes
- Shape Index
- Shape attributes extracted using polygon analysis
- Shape attributes extracted using skeleton analysis

An evaluation of each shape parameter as a tool for quantifying rock and mineral properties has been summarized in Table 5.13. A more detailed description of each attribute and the corresponding results are detailed in Appendix 5.9.

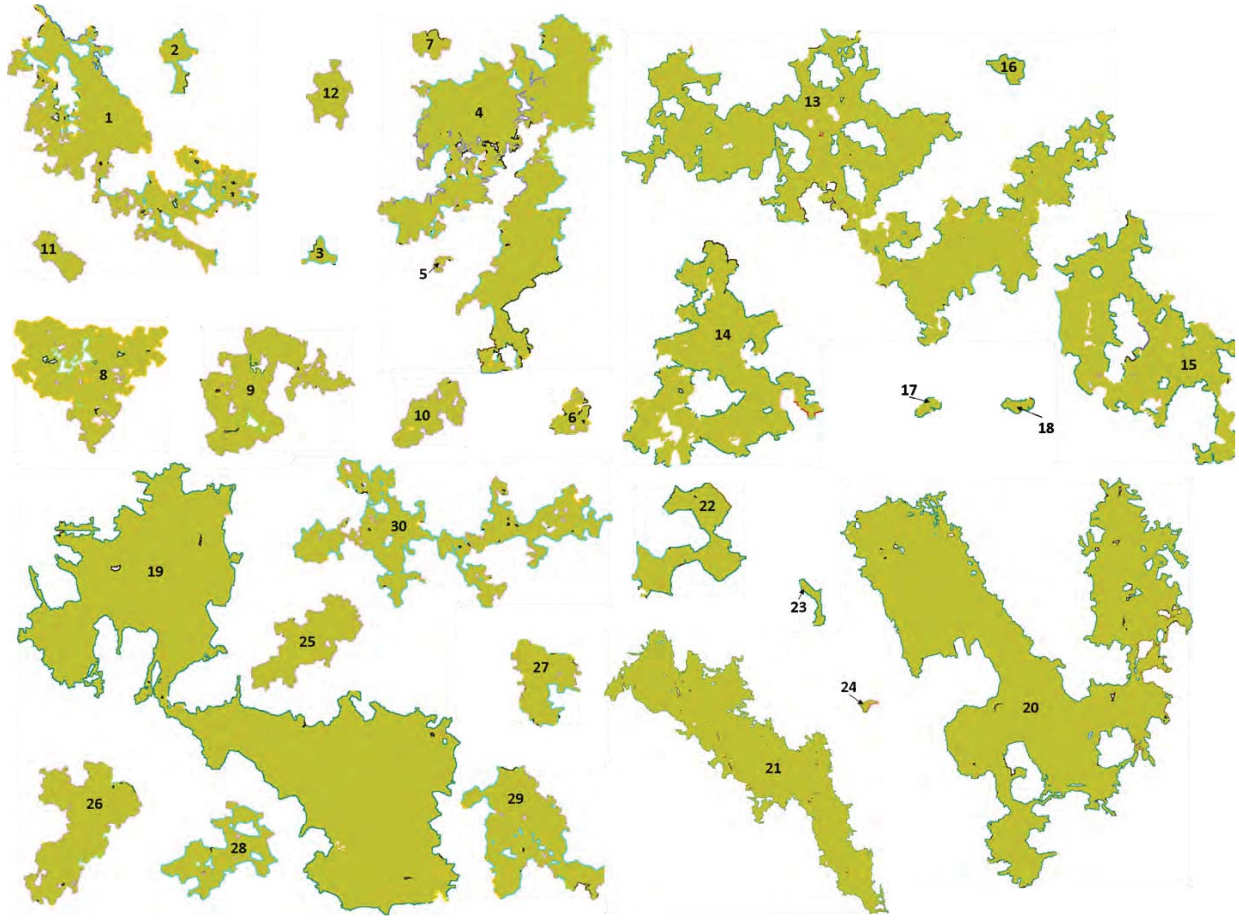

Figure 5.36. Examples of chalcopyrite that have undergone shape analysis using Definiens software. Each phase was produced using the MLA SPL-lite technique. The results of the shape analyses are presented in Appendix 5.8.

Table 5.13. Evaluation of shape attributes appropriate for the analysis of intact mineral and rock features.

Shape Attribute	Actual attribute being measured	Attributes for comparison	Graphical presentation	Comments (this study)
Border Length	Perimeter	Area	Scatter plot against area	Perimeter/ Area = PSSA (see Chapter 2, Section 2.61).
Border Index	Perimeter complexity	Area, number of inner objects	Scatter plot, probability plot	Good measure of perimeter complexity
Asymmetry	Elongateness	Length and Width	Scatter plot of Length/Width	Good measure of object elongateness. Measures of asymmetry correspond to various length/width ratios
Length	Length of the equivalent ellipse	Width, Asymmetry	Scatter plot	Good measure for recognising elongate object features such as veins, veinlets and laminations
Width	Width of the equivalent ellipse	Length, Asymmetry	Scatter plot	Good measure for recognising elongate object features such as veins, veinlets and laminations
Main direction	The main direction of the object measured as an angle		Stereonet and rose diagram	Good measure of the objects main direction and has potential for recognising vein orientations, laminations, dimensional preferred orientation of minerals and other mineralogical features where the objects have retained their original orientation.
Elliptical Fit	Compactness and similarity to the elliptical form	Rectangular fit	Probability plot	
Largest enclosed circle	The ratio of the radius of the largest enclosing ellipse to radius of the elliptical area equivalent		Probability plot	The value is calculated in a way that makes it difficult to compare to other values and use for the shape analysis of minerals. Strongly affected by mineral inclusions.
Smallest enclosing circle	The ratio of the radius of the smallest enclosing ellipse to the elliptical area equivalent		Probability plot	See above
Rectangular Fit	Compactness and similarity to the rectangular form	Elliptical fit	Probability plot	Could be potentially useful for the recognition of euhedral blocky minerals such as magnetite and pyrite as well as feldspar phenocrysts.
Roundness	Shape complexity and measure of circular or elliptical form		Probability plot	The ratio between the smallest enclosing and largest enclosed ellipse radius a good measurement for analysing the shapes of object populations
Compactness	Compactness and rectangularity	Elliptical fit	Probability plot	Similar results to rectangular fit
Density	Compactness and similarity to square form	Elliptical fit	Probability plot	May be useful for the recognition of cubic minerals such as magnetite and pyrite, however for the shape analysis of object populations is not very useful.
Shape Index	Shape complexity		Probability plot	Difficult to analyse for object populations
Inner polygon Analysis	Number of inner polygons, total area of inner polygons and average area of inner polygons	Asymmetry, length and width	Distribution curve of the area of inner objects divided by the area of the object	Very good indicator of inclusions and vein style mineralisation.
Polygon edge analysis	Number of edges, average length of edges, longest edge length	Asymmetry, length and width, area	Probability plot of longest edge, longest edge plotted against ECD	The longest edge is a good indicator for liberation potential and the perimeter complexity as it can represent particles with a large exposed surface relative to the length of the particle perimeter.
Polygon compactness	Compactness of polygon object	Rectangularity	Probability plot	Good correlation with compactness of original object shape
Skeleton-main line	The length of the main line of the object including and excluding inner objects. Measure of size and how fractal an object is	Area and length	Scatter plot	The main line (including cycles) is a good measure of the shape complexity and how fractal an object is.
Skeleton-branching	Degree of skeleton branching and perimeter complexity	Weighted area	Scatter plot	A good measure of object perimeter complexity
Skeleton-segments	Average segment size	ECD, area	Probability plot and scatter plot	A good measure of the average size of areas that only consist of the object e.g. areas that are only clean chalcopyrite with no inclusions
Skeleton-curvature	The length of the main line	Length of main line		Only objects with the same main line length can be compared for curvature values

The analysis of shape presented in this section has shown a wide range of measures that can be useful given the right mineral textures and type of information that is being sought. Like many of the quantified textural parameters, one attribute does not typically tell the whole story and needs to be used in conjunction with other parameters such as size and mineral association. The ability for the results to be plotted so that the results can be readily interpreted is also important for many of these attributes, especially those that are reported as a ratio or ranked against a known shape (e.g. elliptical fit and largest enclosed circle). For the purpose of this research and future studies it is important that shape attributes are able to be observed as populations.

The analysis of a rock sample will without doubt contain a number of different minerals, grains and populations. This has been shown already with the analysis of size and mineral associations in previous sections; this is also true for mineral shapes. The analysis of quantified mineral shapes as a tool for predicting potential variability in mineral processing behaviours will only be useful if the data can be evaluated and presented for entire mineral populations. Based on the results of the shape analysis presented earlier in this section an example will be shown for 3393 chalcopyrite PhRegs from one SPL-lite analysis at Cadia East (CE109 319; Figure 5.37).

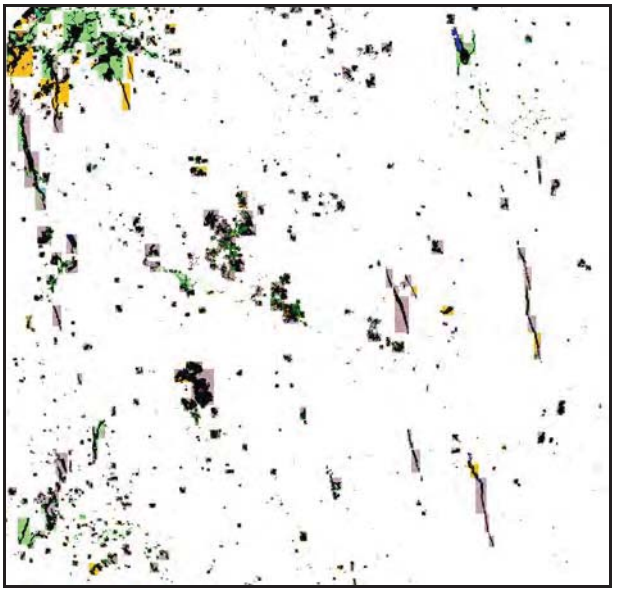

Figure 5.37. Classified mineral map obtained from MLA analysis using the SPL-lite method. The chalcopyrite PhRegs that have been used as an example of a shape analysis of an entire population are shown in *black*. The size of the drill-core tile analysed is 3×3 cm.

The shape attributes that have been measured are asymmetry, length, width, main direction, rectangular fit, elliptical fit, border index, inner polygon analysis, polygon edge analysis and the area skeleton segment analysis. The results of these analyses are plotted in Figure 5.39 (A-F) and the following conclusions can be made:

- There are several large chalcopyrite objects that have a polygon edge that exceeds 150 µm (Figure 5.38A).
- There are three size populations in this example that can be observed in the length versus width plot (Figure 5.38B); fine-grained, coarse-grained and coarse-grained veins or veinlets.
- A majority of the chalcopyrite objects are elongate. This is shown in the rectangular fit versus elliptical fit, where most of the data shown by the contoured graph have a rectangular fit > 0.7 and an elliptical fit > 0.4 (Figure 5.38C and D).
- There are three populations of objects with variable inclusion characteristics; one population with many small inner objects (< 50 pixels), one population with few large inner objects (> 50 pixels) and large population with few inner objects (see Figure 5.38E).

There are two populations with different perimeter complexities: one population has a simple perimeter and plots away from the population with complex perimeter in Figure 5.38F.

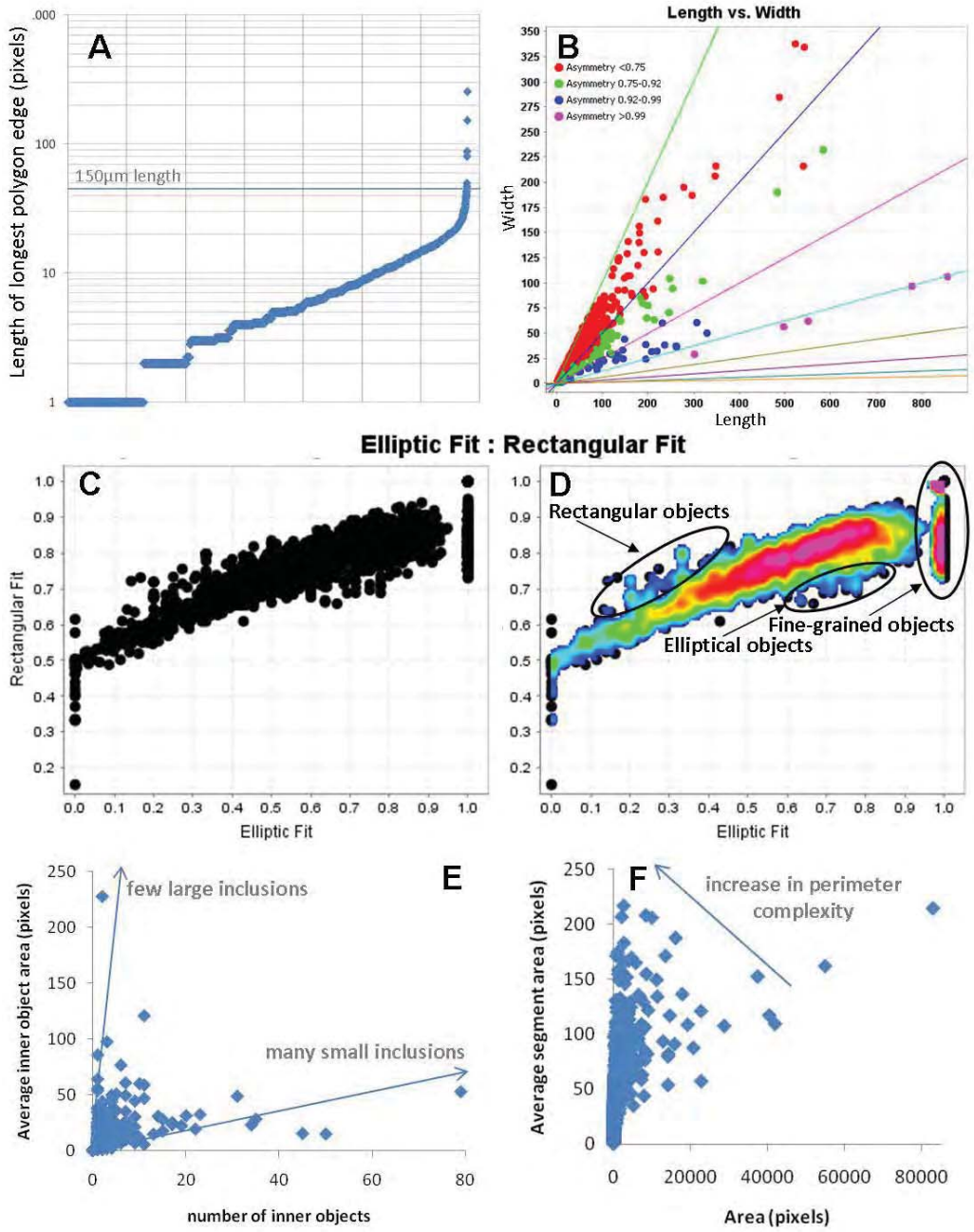

Figure 5.38. Graphs plotting data for chalcopyrite in example CE109 319 from Cadia East. **A.** Length of the longest polygon edge from shortest to longest **B.** Length versus width, colours represent various values of asymmetry **C. E**lliptical fit versus rectangular fit **D.** Contoured data for elliptical fit versus rectangular fit **E.** Number of inner polygon objects versus the average area of the inner polygon objects **F.** Area of the chalcopyrite object versus the average skeleton segment area. Pixel width is 4.22 µm.

In this section it has been shown that a quantified shape analysis can be undertaken on individual chalcopyrite PhRegs as well as populations. In this area of textural analysis study, there is still much further work to be undertaken towards linking these shape parameters to actual physical properties and producing a comprehensive study on a much larger scale. The data for this type of study has been produced within this research; however detailed analysis is not within the scope of this research.

5.3.7 Analysis of gold and silver bearing minerals

The detection of gold and silver minerals using MLA techniques requires special operating conditions, as discussed by many authors (e.g. Goodall and Scales, 2007; Lastra, 2007). These include a reduced beam size to detect smaller grains, a longer count time to collect a clean spectrum, high image resolution to clearly detect boundaries between different mineral phases. The analyses undertaken in this project did not use such settings. This would require extremely long machine operating times and cost, especially considering the main focus was towards the characterisation of the copper sulphide mineralogy. However, the conditions that were used for the MLA analyses in this project have proved to be sufficient to identify and classify 85 gold and electrum phases as well as 24 hessite phases. The data relating to the minerals associated with the gold, electrum and hessite provide an unbiased evaluation of the gold deportment and size as well as an insight into the minerals and textures that typically host these minerals.

Of 17 PhRegs of gold and 68 PhRegs of electrum that were analysed, 45 were completely encapsulated by another mineral (Figure 5.39) and 40 were located on the boundary between two minerals (e.g. Figure 5.40). The gold and electrum PhRegs located along the grain boundaries have a larger area than those encapsulated by a single mineral and possibly exhibit two populations, shown by the kink at 0.5 (N score) in Figure 5.41. The minerals that most commonly completely encapsulate gold and electrum are quartz (51.94 wt. %, 13 grains), chalcopyrite (18.11 wt. %, 14 grains), albite (8.54 wt. %, 5 grains) and illite (7.35 wt. %, 2 grains).

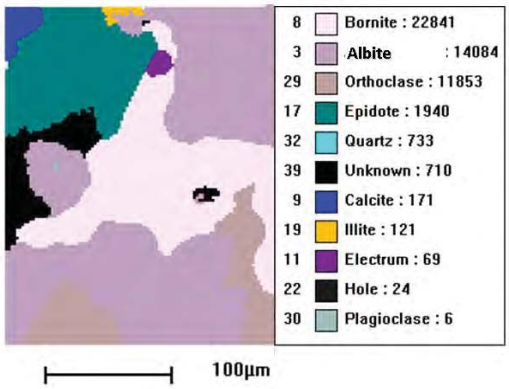

Figure 5.39. Example of a SPL-lite image showing electrum located on the grain boundary of epidote and bornite.

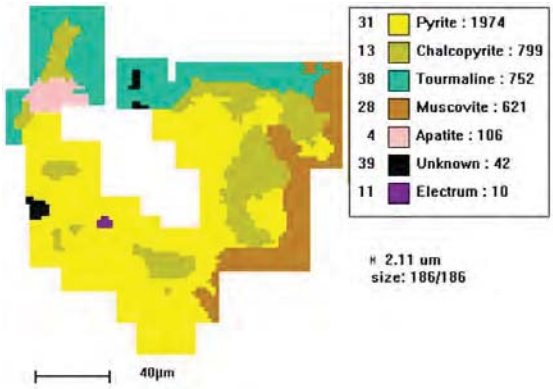

Figure 5.40. Example of a SPL-lite image showing electrum encapsulated within pyrite.

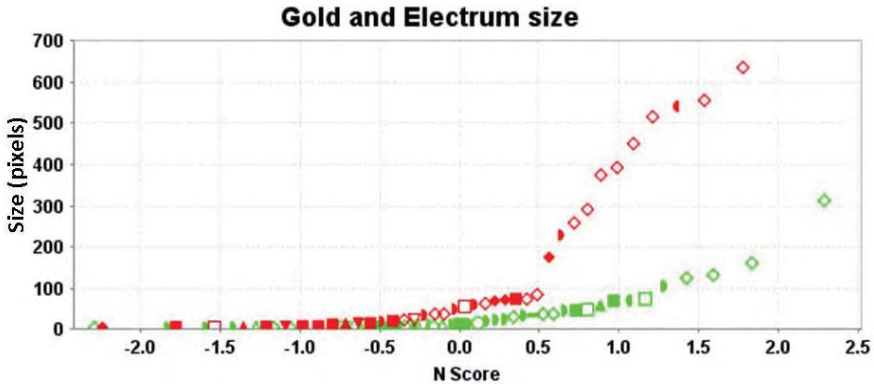

Figure 5.41. Area of the gold and electrum PhReg minerals classified with the MLA SPL-lite technique. The *red* points indicate gold and electrum that are located along mineral boundaries. The *green* points are gold and electrum that are completely encapsulated by other minerals. The N score is calculated by ranking each point from smallest to largest, zero is the median point. Pixel size is 4.22 µm in length.

The analysis of the mineral hessite using SPL-lite analysis found that it most commonly occurs as small inclusions in chalcopyrite and bornite (see section 5.3.1). Hessite PhRegs identified during SPL-lite anlysis typically do not exceed 20 μm in diameter, similar to the sizes observed in gold and electrum minerals. Of the drill-core tiles analysed from Cadia East only 24 hessite PhRegs have been observed, 70.30 wt. % of these are completely enclosed by other minerals. 29.70 wt. % are situated on the boundary between two minerals. 62.91 wt. % of the hessite PhRegs are associated with either bornite or chalcopyrite. These results imply that only the larger PhRegs of hessite are being identified by the SPL-lite method.

5.3.8 Summary

130 drill-core tiles have undergone MLA XMOD and SPL-lite analysis using the measurement protocol used for the tile measurements (see chapter 3, section 3.5) for the drill-holes CE082, CE098, CE109, CE110 and CE143 from Cadia East. From these analyses 35 minerals were identified. From the mineral maps produced using the SPL-lite analysis, quantified mineralogical and textural information has been extracted for chalcopyrite, bornite, molybdenite, gold and electrum (using the Definiens Developer software). The mineralogical and textural information extracted were modal mineralogy (XMOD), area, length, width, PSSA, smallest enclosing ellipse and the minerals associated with chalcopyrite, bornite and molybdenite. Thirty examples were selected based on the meso-scale visual texture classification presented in the previous chapter (fine-grained disseminations; coarse-grained clots; vein-hosted). A summary of the micro-scale results for Cadia East are presented later in this Chapter in section 5.6.

5.4 Results of MLA analysis: Ernest Henry

Based on the method described in Chapter 3, section 3.5, quantified mineralogical and textural attributes considered to potentially influence mineral processing behaviours have been measured from mineral maps created using the MLA. In total, 311 3 × 3 cm drill-core tiles have undergone MLA analysis from drill-holes EH432, EH446, EH556, EH574, EH633 and EH635. As with Cadia East, thirty examples have been selected for XMOD, gangue mineral association and size analysis (Table 5.14; Figure 5.42). The thirty Ernest Henry examples have been selected based on the outcomes of the meso-scale texture analysis (see Chapter 4, section 4.6) and are the same as the examples used previously in section 5.2 for the analysis using optical microscopy.

The Ernest Henry mineralogy has been determined using the MLA in the automated SEM mode and has been documented as a library of mineral spectra (Appendix 5.9). The spectra library has been compiled according to the methods and procedures outlined in Chapter 3, section 3.5.2. As with Cadia East, the objective of the library is to present all of the minerals and their variations that are present in the selected samples and to provide an understanding of the mineralogical and textural relationships that are present in the Ernest Henry ore body. As discussed in section 3.5.1, a thorough understanding of the mineralogy and textures present allows the appropriate analytical technique to be selected for MLA analysis (e.g. XMOD and SPL-lite, see Chapter 3, section 3.5).

Table 5.14. Examples used for MLA analysis at Ernest Henry. The texture class refers to the meso-scale visual classification. The number of chalcopyrite (ccp) PhRegs refers to the number of PhRegs that are present in that example.

Mottled (Fine-grained)			Mottled (Coarse-grained)			Massive		
Example	Texture	N (ccp)	Example	Texture	N (ccp)	Example	Texture	N (ccp)
EH432 253.15	F3	8134	EH432 376.10	F1	4557	EH432 213.07	MaM	3652
EH446 353.00	F3	10525	EH432 377.00	F1	2559	EH446 398.35	MaF	1457
EH556 592.00	F3	11031	EH446 386.10	F3	3311	EH574 765.00	MaM	14218
EH556 706.05	F3	1312	EH446 399.00	F1	3913	EH574 783.00	MaF	455
EH574 578.90	F2	567	EH446 471.50	F3	4720	EH574 798.00	MaF	118
EH574 586.00	F2	4817	EH574 596.00	F1	1331	EH574 800.00	MaF	343
EH574 594.00	F2	4567	EH633 999.00	F3	5675	EH633 887.00	MaM	12511
EH633 879.00	MF4	4060	EH635 923.00	F3	1914	EH633 915.00	MaM	6140
EH635 919.00	MF4	3761	EH635 945.00	F3	3923	EH633 1159.00	MaF	281
EH635 921.00	F2	7303	EH635 985.00	F3	1778	EH635 933.00	MaM	4161

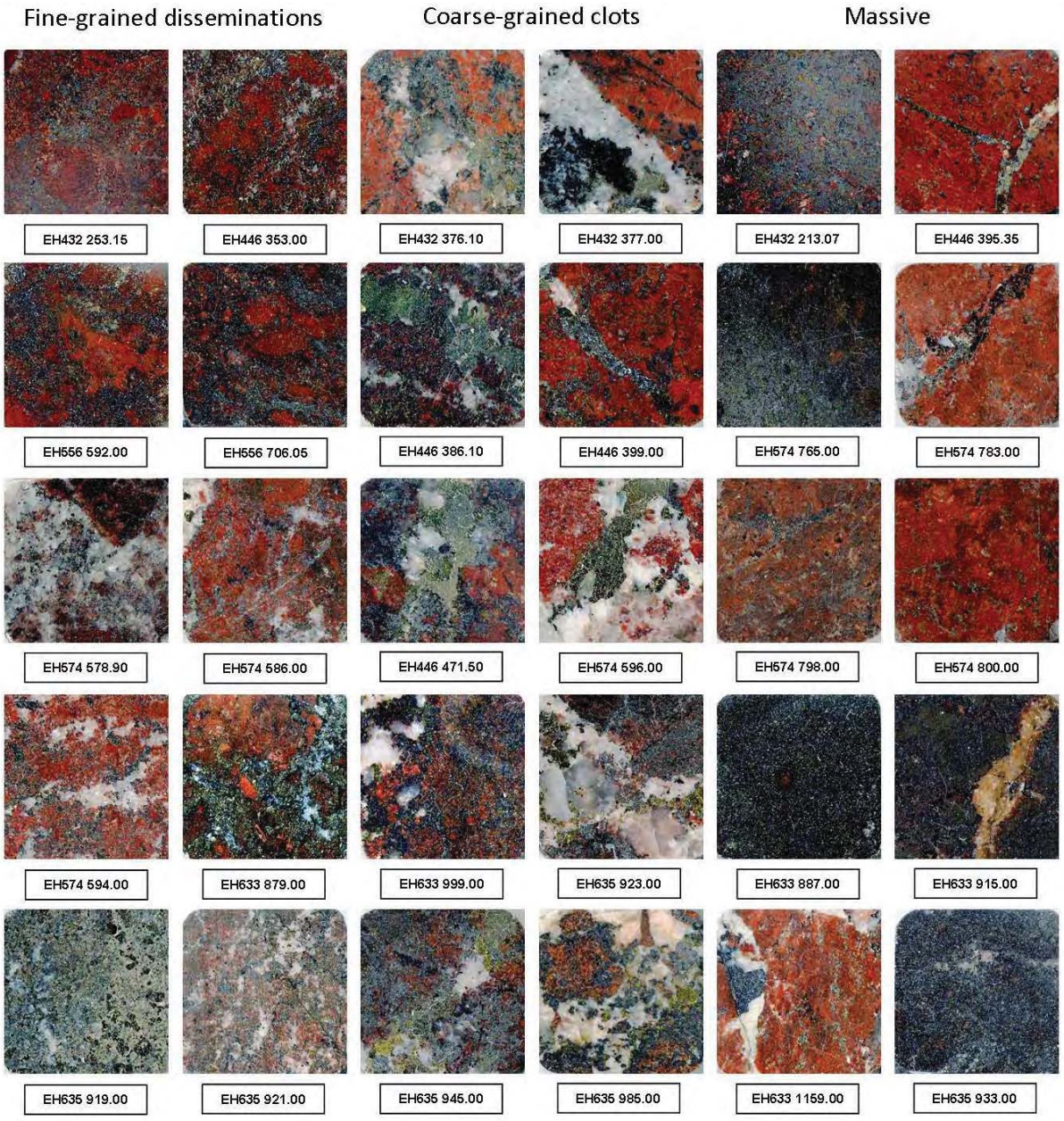

Figure 5.42. Scanned photographs of the 30 drill-core tiles selected for detailed analysis from Ernest Henry. Each tile is 3 × 3 cm.

The results of MLA analyses undertaken on samples from Ernest Henry are presented in this section as follows:

5.4.3 Modal mineralogy: XMOD analysis

5.4.4 Size analysis of chalcopyrite: measured as Equivalent Circle Diameter (ECD), length and width

5.4.5 Gangue minerals associated with chalcopyrite

5.4.6 Analysis of gold and silver bearing minerals

Additional information is in appendices:

5.10 Modal mineralogy calculated from XMOD analysis of drill-core tiles: Ernest Henry

5.11 Mineralogical and textural attributes of chalcopyrite calculated from SPL-lite analysis of drill-core tiles: Ernest Henry

5.12 Gold and Electrum analysis from SPL-lite analysis: Ernest Henry

5.4.1 Ernest Henry mineralogy

Previous studies undertaken at Ernest Henry by Mark et al. (2006) defined the mineralogy in the upper sections of the ore body. Since then new holes into the deeper portions of the ore body have been drilled and provide additional information regarding the mineralogy at Ernest Henry (drill-holes EH633 and EH635).

The mineralogy that has been defined for Ernest Henry as part of this research is presented as sulphide minerals, oxide minerals, silicates, mica minerals, feldspar minerals, carbonate minerals and rare minerals as summarized in Table 5.15.

Table 5.15. Ernest Henry mineralogy determined using the MLA in SEM mode.

Mineral		Meso-scale	Micro-scale
Sulphide minerals	Chalcopyrite	Chalcopyrite occurs as coarse-grains (<5cm) in mineralised clots with pyrite, calcite, quartz and magnetite (Figure 5.43A). It also occurs as sparse fine-grained disseminations (<2mm) with quartz and calcite in the matrix of fragmental units (Figure 5.43A) and as finer disseminations (<1mm) within reddened feldspar clasts of fragmental units (Figure 5.43B).	At higher magnifications, the chalcopyrite within mineralised clots is observed as irregular grains between more euhedral crystals of quartz, magnetite and pyrite (Figure 5.43C). The fine-grained disseminations occur as irregular sub-rounded to sub-angular grains within feldspathic clasts in fragmental units (Figure 5.43D); within massive feldspar or magnetite units (Figure 5.43E and 5.43F) and with calcite and quartz in the matrix of the fragmental units (Figure 5.43G).
	Arsenopyrite	Only observed at the micro-scale.	Occurs as small inclusions with chalcopyrite, pyrite and magnetite.
	Pyrite	Pyrite occurs as coarse euhedral grains (<3 cms) in mineralised clots with chalcopyrite, calcite, quartz and magnetite (Figure 5.43A). It also occurs as sparse fine-grained disseminations (<2mm) with quartz and calcite in the matrix of fragmental units (Figure 5.43A) and as finer disseminations (<1mm) within reddened feldspar clasts of fragmental units (Figure 5.43B).	At higher magnifications pyrite within mineralised clots occurs as coarse euhedral grains with crystals of quartz, magnetite, calcite and chalcopyrite (Figure 5.43G). The fine-grained disseminations occur as irregular sub-rounded grains within feldspathic clasts of fragmental units; within massive feldspar or magnetite units (Figure 5.43E and 5.43F) and with calcite and quartz in the matrix of the fragmental units (Figure 5.43G).
	Molybdenite	Only observed at the micro-scale.	Occurs as very small inclusions within chalcopyrite and K-feldspar (Figure 5.43H).
	Bornite	Only observed at the micro-scale.	Occurs as very small inclusions (<10 μm) within chalcopyrite.
	Galena	Only observed at the micro-scale.	Occurs as very small euhedral grains (<20 μm)

Mineral		Meso-scale	Micro-scale
			typically with chalcopyrite (Figure 5.43I).
	Sphalerite	Only observed at the micro-scale.	Occurs as rare fine grained inclusions (10's μm) typically with albite and K-feldspar.
Oxide minerals	Magnetite	Magnetite occurs as euhedral crystals (<5mm) in mineralised clots with chalcopyrite, pyrite, quartz and calcite (Figure 5.43A) as well as massive units 10's of metres thick (Figure 5.43J).	At higher magnifications magnetite is observed as euhedral crystals within mineralised clots (Figure 5.43H) and as coarse grains with chlorite (Figure 5.43E).
	Hematite	Hematite is observed where it has oxidized from magnetite (Figure 5.43K) and as well as finely disseminated with feldspar minerals (Figure 5.43K).	Cannot be distinguished from magnetite using the MLA.
	Rutile	Only observed at the micro-scale.	Occurs as small grains (<50 μm) typically with titanite and chlorite (Figure 5.43H)
Silicate minerals	Quartz	Quartz occurs as prismatic inward terminating crystals in mineralised clots with magnetite, pyrite, calcite and chalcopyrite as well as with calcite ± magnetite in the matrix of the fragmental units (Figure 5.43A).	At higher magnifications quartz is observed as euhedral crystals with calcite, magnetite, magnetite, chalcopyrite and pyrite (Figure 5.43C) as well as irregularly shaped grains with K-feldspar (Figure 5.43D).
	Tourmaline	Only observed at the micro-scale	Tourmaline occurs as small euhedral crystals (50-400 μm) and is commonly associated with carbonate minerals (Figure 5.44B).
	Titanite	Only observed at the micro-scale.	(Figure 5.43H)
	Garnet	Garnet typically occurs as coarse grained aggregates with skarn minerals (magnetite and actinolite; Figure 5.44C).	At higher magnifications garnet is observed as sub rounded grains surrounded by magnetite, biotite and quartz crystals (Figure 5.44 H).
	Actinolite	Actinolite occurs as small emerald green fibrous crystals in the matrix of fragmental units. It typically occurs with calcite and quartz (Figure 5.44C and 5.44D).	At higher magnifications actinolite is observed as layers of fine-grained fibrous crystals (Figure 5.45A)
Mica minerals	Biotite	Biotite occurs as fine-grained black crystals with magnetite (Figure 5.44D).	At higher magnification biotite is observed as individual euhedral grains (Figure 5.43G) as well as with chlorite and typically occurs on the grain boundaries of magnetite and less commonly chalcopyrite (Figure 5.44E).
	Chlorite	Chlorite occurs as fine-grained drak green – black crystals in the matrix of fragmented units (Figure 5.44F).	At higher magnification chlorite typically is observed on the grain boundaries of magnetite (Figure 5.44G) and occurs with biotite (Figure 5.44E).
Carbonate minerals	Calcite	Calcite occurs as coarse euhedral crystals in mineralised clots with chalcopyrite, pyrite, magnetite and quartz (Figure 5.44A) as well as in the matrix of fragmental units with quartz (Figure 5.44D).	A higher magnifications calcite is observed as coarse crystals with quartz in the matrix of fragmental units (Figure 5.45B) as well as with quartz, magnetite, pyrite, and chalcopyrite in mineralized clots (Figure 5.43G).
	Ankerite	Only observed at the micro-scale.	Ankerite typically occurs in mineralized clots with chalcopyrite, magnetite, quartz and calcite (Figure 5.44B).
	Dolomite	Only observed at the micro-scale.	Dolomite typically occurs in mineralized clots with chalcopyrite, magnetite, quartz and calcite (Figure 5.44B).
	Siderite	Siderite occurs as coarse grains (10's of cms) in vein assemblages and in the matrix of fragmental units.	At higher magnifications siderite is observed as anhedral grains in mineralised clots with chalcopyrite, pyrite, magnetite, quartz and calcite (Figure 5.44B).
	REE bearing carbonate	Only observed at the micro-scale.	Occurs as fibrous aggregates with rutile, uranium minerals and titanite (Figure 5.45C).
	Scheelite	Only observed at the micro-scale.	Scheelite occurs as sub-rounded grains within mineralized clots typically within chalcopyrite (Figure 5.45B).
Others	Fluorite	Only observed at the micro-scale.	Fluorite occurs as euhedral crystals < 500 μm diameter

Mineral		Meso-scale	Micro-scale
			with chalcopyrite or magnetite (Figure 5.45D).
	Barite	Barite typically occurs in thick veins (cms; Figure 5.43B) and as minor occurrences in mineralised clots with chalcopyrite, pyrite, calcite, magnetite and quartz.	At higher magnifications barite is observed with chalcopyrite (Figure 5.43I) and as late stage veins cross-cutting chalcopyrite.
Feldspar minerals	K-Feldspar	K-feldspar occurs as reddened clasts in the fragmental units (Figure 5.44D). The clasts vary from well-defined to mottled boundaries. It also occurs as massive units 10's of metres thick (Figure 5.45E).	At higher magnifications K-feldspar is observed as coarse crystals replacing pre-existing textures (Figure 5.45E) as well as very fine-grained phenocrysts that comprise the clasts of the fragmental units (Figure 5.45F).
	Albite	Albitic feldspar is observed as clasts within the fragmental units, however is difficult to be distinguished from K-feldspar in hand specimen without sodium cobaltinitrite staining (Hayes and Clugman, 1959).	At higher magnifications albite is observed as coarse phenocrysts within the K-feldspar altered clasts of the fragmental units (Figure 5.45F).
	Hyalophane	Hyalophane occurs as clasts within the fragmental units, however is difficult to be distinguished from K-feldspar or albite in hand specimen.	Hyalophane typically occurs with K-feldspar (Figure 5.45B).
Rare minerals	Electrum	Only observed at the micro-scale.	Electrum occurs as small rounded grains encapsulated within chalcopyrite, magnetite, quartz, calcite, K-feldspar and pyrite (Figure 5.46A) It also occurs along the grain boundaries of these minerals (Figure 5.46B).
	Gold	Only observed at the micro-scale.	Gold occurs as small rounded grains encapsulated within chalcopyrite, magnetite, calcite, K-feldspar, quartz and pyrite (Figure 5.46C). It also occurs along the grain boundaries of these minerals.
	Monazite	Only observed at the micro-scale.	Monazite occurs as fine-grained sub-angular crystals typically encapsulated within K-feldspar or albite (Figure 5.46D).
	U-bearing minerals	Only observed at the micro-scale.	Occur as small inclusions in rutile (Figure 5.45C)
	Sulpharsenite	Only observed at the micro-scale.	Occur as small inclusions in magnetite and chalcopyrite (Figure 5.46E).
	Fe-rich cobaltite	Only observed at the micro-scale.	Occurs as small inclusions within mineralised clots, in between grains of pyrite, chalcopyrite, magnetite, quartz and calcite.

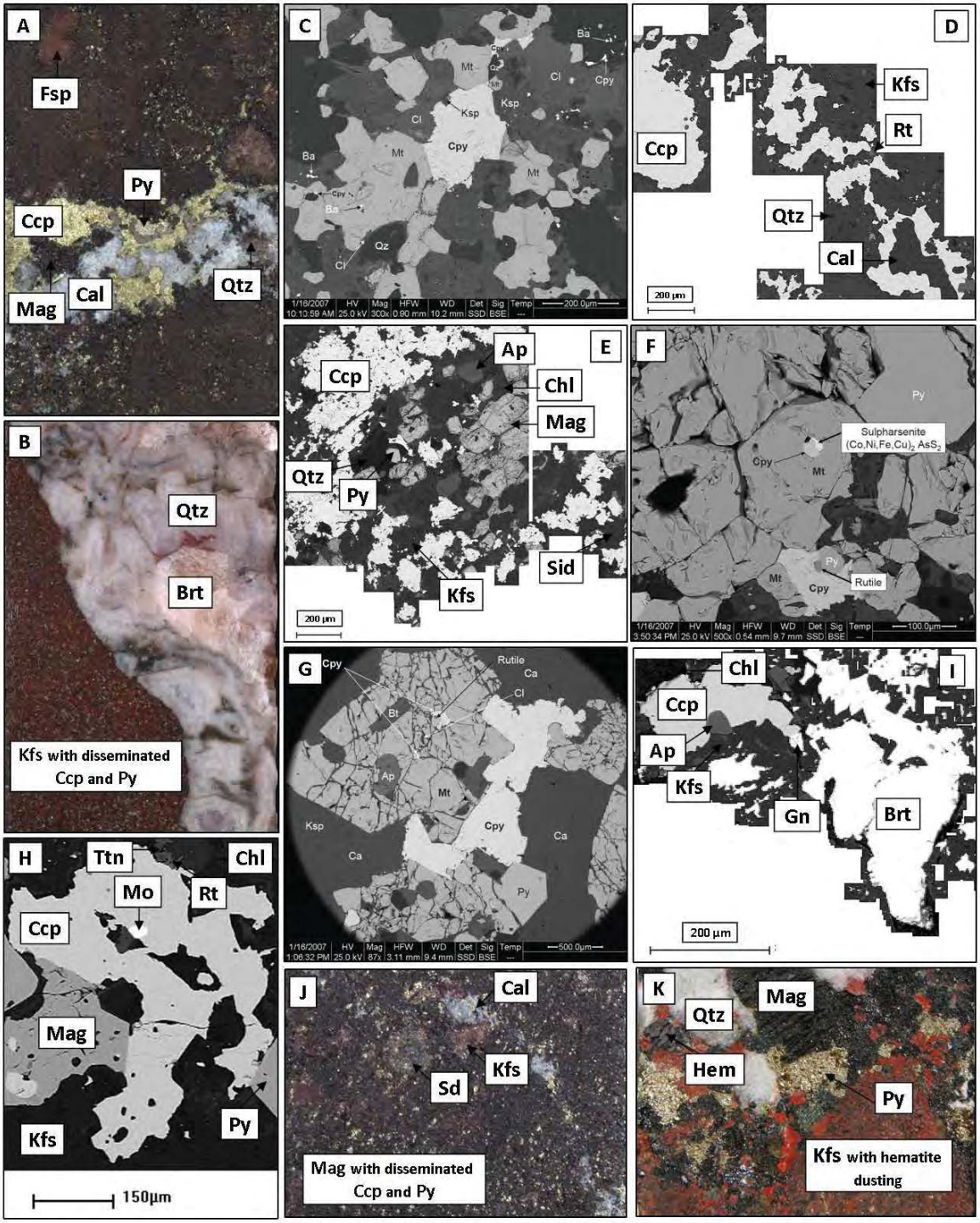

Figure 5.43. Photographs and BSE images of minerals and textures from Ernest Henry. Figures C, F and G courtesy of Dr.Julie Hunt, mineral abbreviations are Ba - Barite; Cl - Chlorite; Cpy - Chalcopyrite; Ksp – K-feldspar; Mt - Magnetite; Py – Pyrite; Qz – Quartz. All other abbreviations are listed in Appendix 1.1 **A.** Mineralised clot consisting of chalcopyrite, pyrite, magnetite, quartz and calcite, hosted by feldspar altered fragmental unit with fine-grained disseminated chalcopyrite and pyrite. *Image width is 5.5cm* **B.** Thick quartz and barite vein cross cutting massive K-feldspar altered rock with fine-grained disseminations of chalcopyrite and pyrite. *Image width is 5.5cm* **C.** BSE image showing a mineralised clot consisting of chalcopyrite, quartz and magnetite **D.** Disseminated Ccp within a Kfs altered clast within a fragmental rock unit **E.** Ccp within Mag-Chl altered host rock **F.** Ccp with Mag and Py in mineralized clot as well as encapsulated with sulpharsonite in magnetite **G.** Magnetite, chalcopyrite and calcite in the matrix of the fragmental units **H.** Fine-grained molybdenite inclusion in chalcopyrite with magnetite **I.** Fine-grained Gn with Ccp and Brt **J.** Fine-grained Mag with Kfs and Fsp in a massive magnetite altered rock **K.** Mineralised clot consisting of Mag-Qtz-Py.

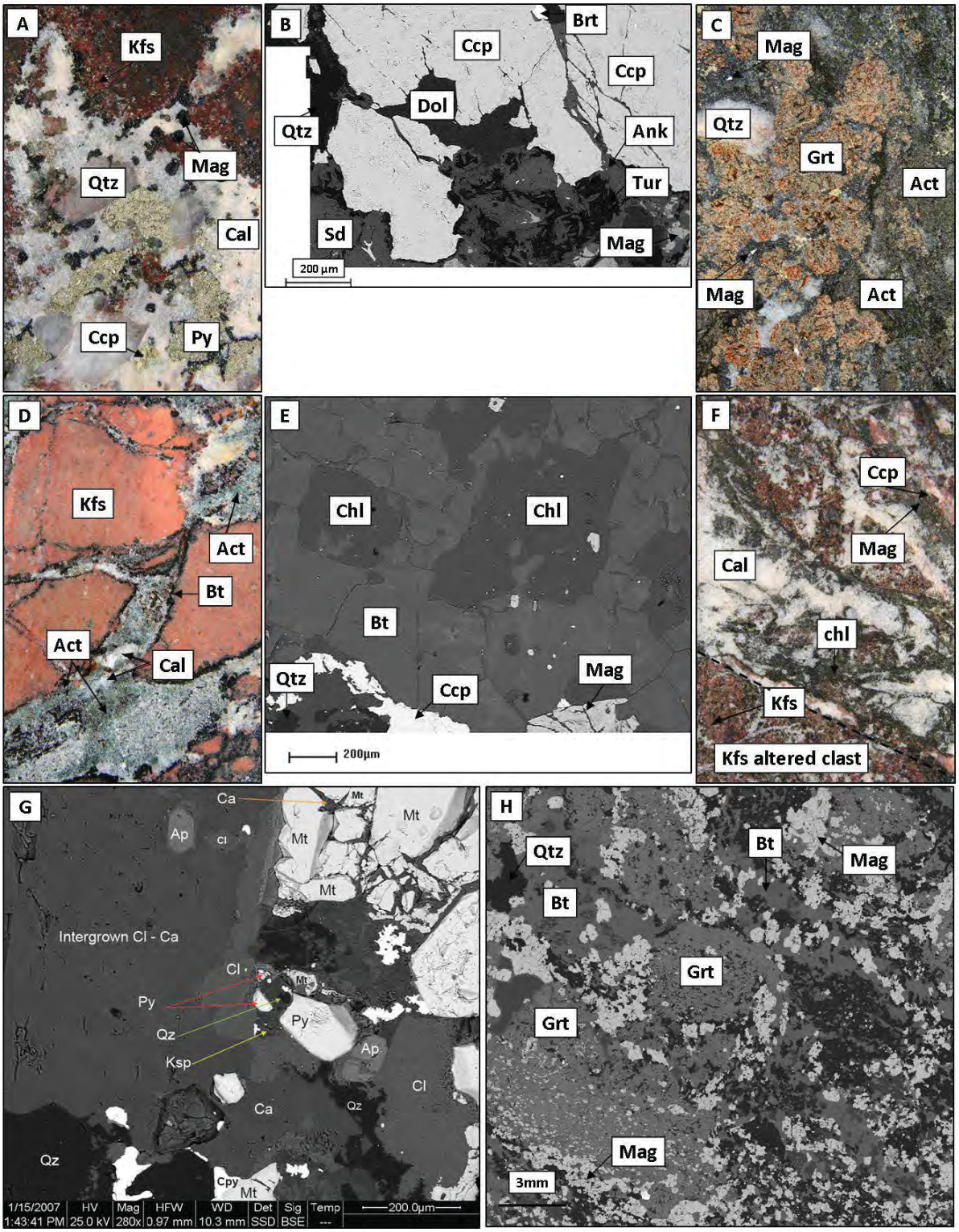

Figure 5.44. Photographs and BSE images of minerals and textures from Ernest Henry. Figure G is courtesy of Dr.Julie Hunt, mineral abbreviations are Ap – Apatite; Ca – Calcite; Cl - Chlorite; Cpy - Chalcopyrite; Ksp – K-feldspar; Mt - Magnetite; Py – Pyrite; Qz – Quartz. All other abbreviations are listed in Appendix 1.1. *The widths of figures A, C, D and F are 5.5 cm.* **A.** Mineralised clot with euhedral crystals of quartz and magneite, calcite, pyrite and chalcopyrite **B.** BSE image showing toumaline, ankerite and dolomite cross-cutting chalcopyrite **C.** Garnet and actinolite mineralisation **D.** K-feldspar altered clasts rimmed by biotite with actinolite and calcite comprising the matrix minerals **E.** BSE image illustrating chlorite and biotite mineral textures **F.** Fragmental unit with K-feldspar altered clasts with diffuse boundaries and a matrix consisting of calcite, chlorite and magnetite **G.** BSE image showing chlorite alteration penetrating a mineralized clot consisting of pyrite, magnetite, quartz and chalcopyrite **H.** BSE image showing porphyroblastic garnets with biotite, quartz and magnetite.

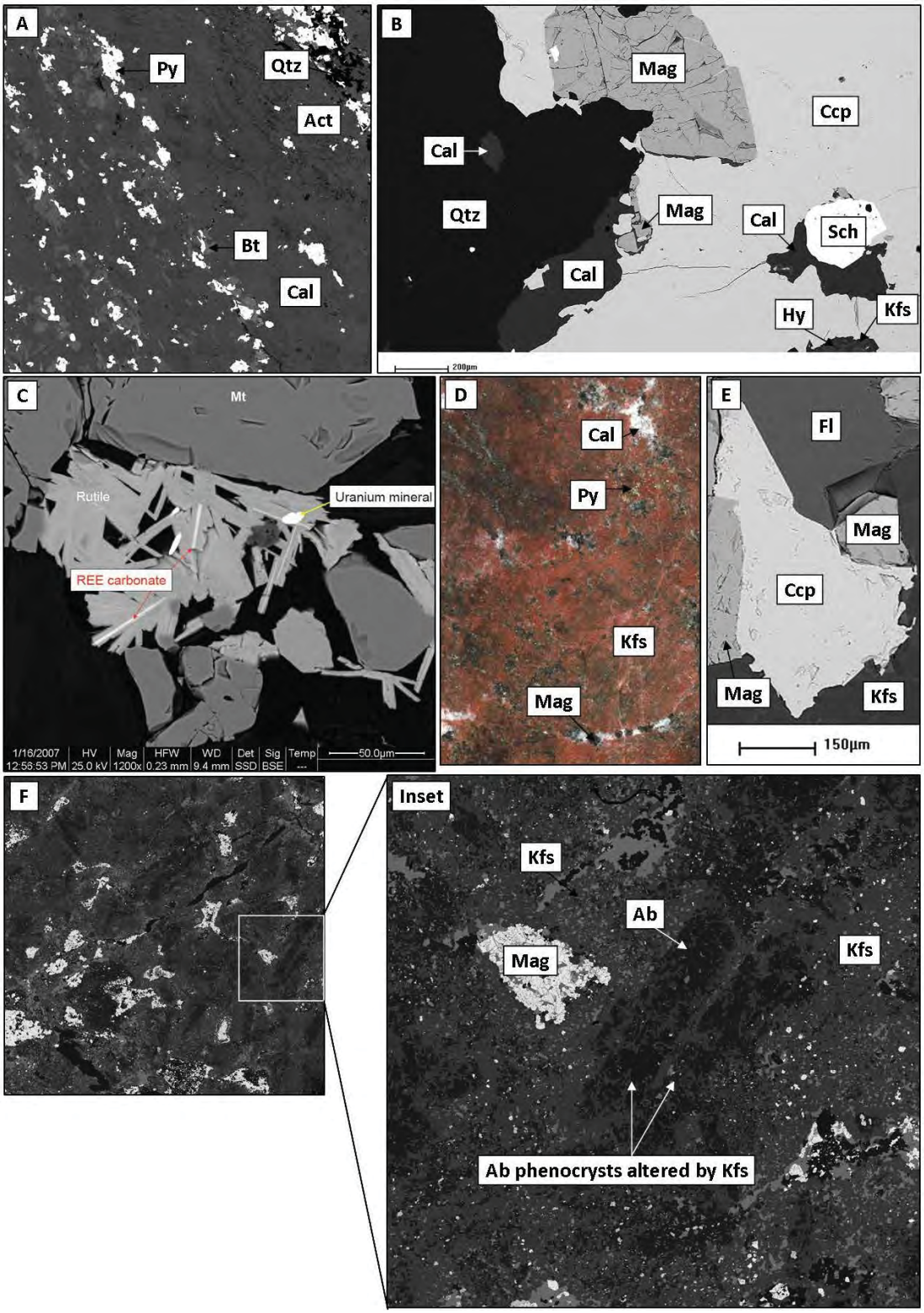

Figure 5.45. Photographs and BSE images of minerals and textures from Ernest Henry. Figures C is courtesy of Dr.Julie Hunt (Mt – Magnetite). *Other mineral abbreviations are listed in Appendix 1.1.* **A.** BSE image showing laminations of actinolite, quartz, pyrite, biotite and calcite. *Image width is 3cm* **B.** BSE image showing a scheelite-calcite inclusion in chalcopyrite as well as hyalophane and K-feldspar occurring together **C.** BSE image showing euhedral crystals of rutile with inclusions of uranium bearing minerals and REE bearing carbonate **D.** Example showing massive K-feldspar red rock alteration with small veinlets of magnetite and calcite as well as fine-grained disseminations of pyrite. *Image width is 5.5 cm* **E.** BSE image showing coarse grained euhedral fluorite with magnetite, chalcopyrite and K-feldspar **F.** BSE image, inset shows two phenocrysts of albite with the mineral edges being replaced with K-feldspar. The K-feldspar occurs as fine-grained euhedral crystals.

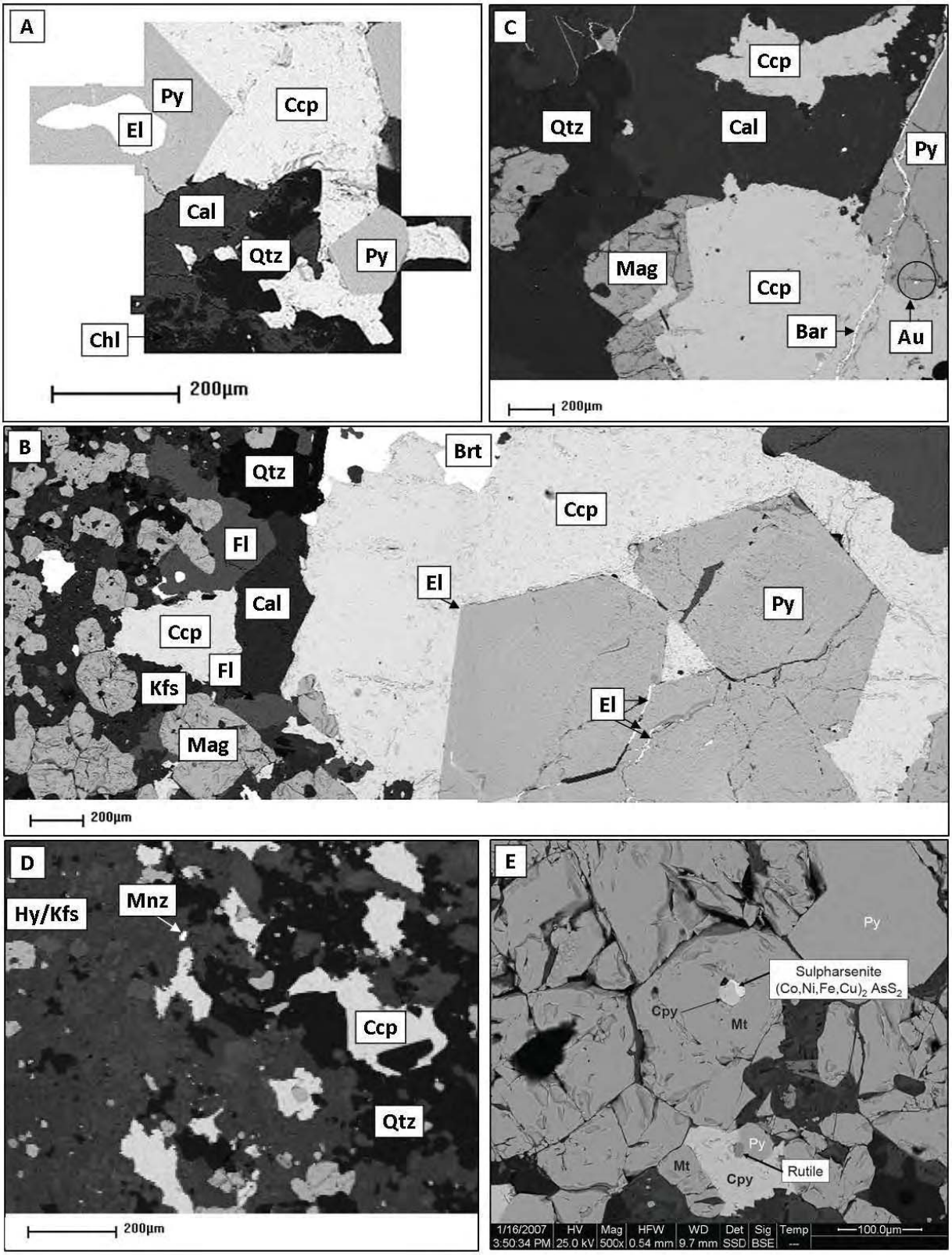

Figure 5.46. Photographs and BSE images of minerals and textures from Ernest Henry. Figures E is courtesy of Dr.Julie Hunt (Cpy – chalcopyrite; Mt – Magnetite; Py - pyrite). *Mineral abbreviations are listed in Appendix 1.1* **A.** BSE image illustrating electrum within pyrite **B.** BSE image illustrating micro-veinlets of electrum between two crystals of pyrite as well as a small inclusion on the boundary between chalcopyrite and pyrite **C.** BSE image showing a small gold inclusion within pyrite (*black circle*) **D.** BSE image showing monazite within K-feldspar and hyalophane alteration **E.** BSE image showing an inclusion of sulpharsenite and chalcopyrite within magnetite.

5.4.2 Mineral spectra library: Ernest Henry

The creation of a representative mineral spectra library is an extremely important step in any MLA analysis. The mineral spectra library for Ernest Henry has been created using the method described in Chapter 3, section 3.5.2 in order to ensure that the most representative spectra for each mineral have been selected. The minerals at Ernest Henry have been grouped together to simplify the process of data manipulation and interpretation of results (Table 5.16). These mineral groupings will be used in discussions relating to XMOD and SPL-lite results in this chapter.

Table 5.16. Mineral groups that have been created for the analysis of MLA data from Ernest Henry.

Mineral	Mineral Group	Frequency	Mineral	Mineral Group	Frequency
Actinolite	Actinolite	Rare	Gold	Gold	Rare
Albite	Feldspar	Common	Hyalophane	Feldspar	Common
Anhydrite	Anhydrite	Rare	K-Feldspar	K-Feldspar	Common
Ankerite	Carbonate	Rare	Magnetite	Magnetite	Common
Apatite	Apatite	Common	Siderite	Siderite	Common
Arsenopyrite	Arsenopyrite	Rare	Monazite	Monazite	Rare
Barite	Barite	Common	Molybdenite	Molybdenite	Rare
Biotite	Biotite	Common	Pyrite	Pyrite	Common
Bornite	Bornite	Rare	Quartz	Quartz	Common
Calcite	Carbonate	Common	REE carbonate	Carbonate	Rare
Chalcopyrite	Chalcopyrite	Common	Rutile	Rutile	Rare
Chlorite-Mg	Chlorite	Common	Scheelite	Scheelite	Rare
Chlorite-Fe	Chlorite	Common	Spessartine	Garnet	Rare
Clay	Clay	Common	Sphalerite	Sphalerite	Rare
Dolomite	Carbonate	Rare	Sulpharsenite	Sulpharsenite	Rare
Electrum	Electrum	Rare	Titanite	Titanite	Rare
Fe-Cobaltite	Fe-Cobaltite	Rare	Tourmaline	Tourmaline	Rare
Fluorite	Fluorite	Rare	U-minerals	U- minerals	Rare
Galena	Galena	Rare	Zircon	Zircon	Rare

5.4.3 Modal mineralogy: XMOD analysis

As described previously in Chapter 3, the XMOD is an automated point counting system designed to provide a fast and accurate representation of the modal mineralogy of a sample. The results from these analyses can be used to create a mineralogical signature of each sample. At Ernest Henry, 311 tiles have undergone XMOD analysis where 20,000 x-ray points per tile (one every 47 pixels) have been measured using the method outlined in Chapter 3, section 3.5.3 (Appendix 5.10). The grid approach adopted by XMOD provides an unbiased mineralogical analysis of a sample.

The mineralogical abundances obtained from the XMOD analyses have been used to quantify the mineralogical signatures that are typical of various rock and/or alteration types. For example, Figure 5.47 shows three XMOD analyses of drill-core tiles from Ernest Henry. The tiles consist of a magnetite rich, feldspar rich and pyrite rich sample. Presented as pie charts, the mineralogical abundances for the selected Ernest Henry examples (see Table 5.19) are presented in Figure 5.48. In this figure the most abundant minerals are K-feldspar, carbonate, quartz, pyrite, magnetite and hyalophane.

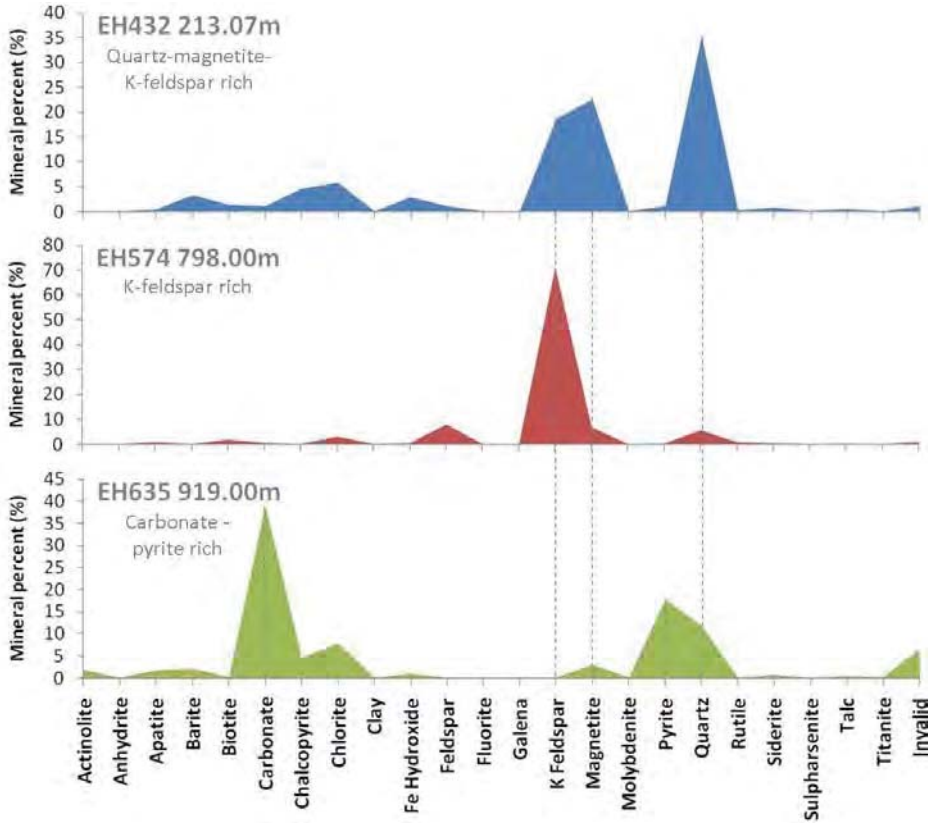

Figure 5.47. Graphs illustrating the mineralogical signatures for three drill-core tiles at Ernest Henry. The modal mineralogy has been determined using XMOD analysis.

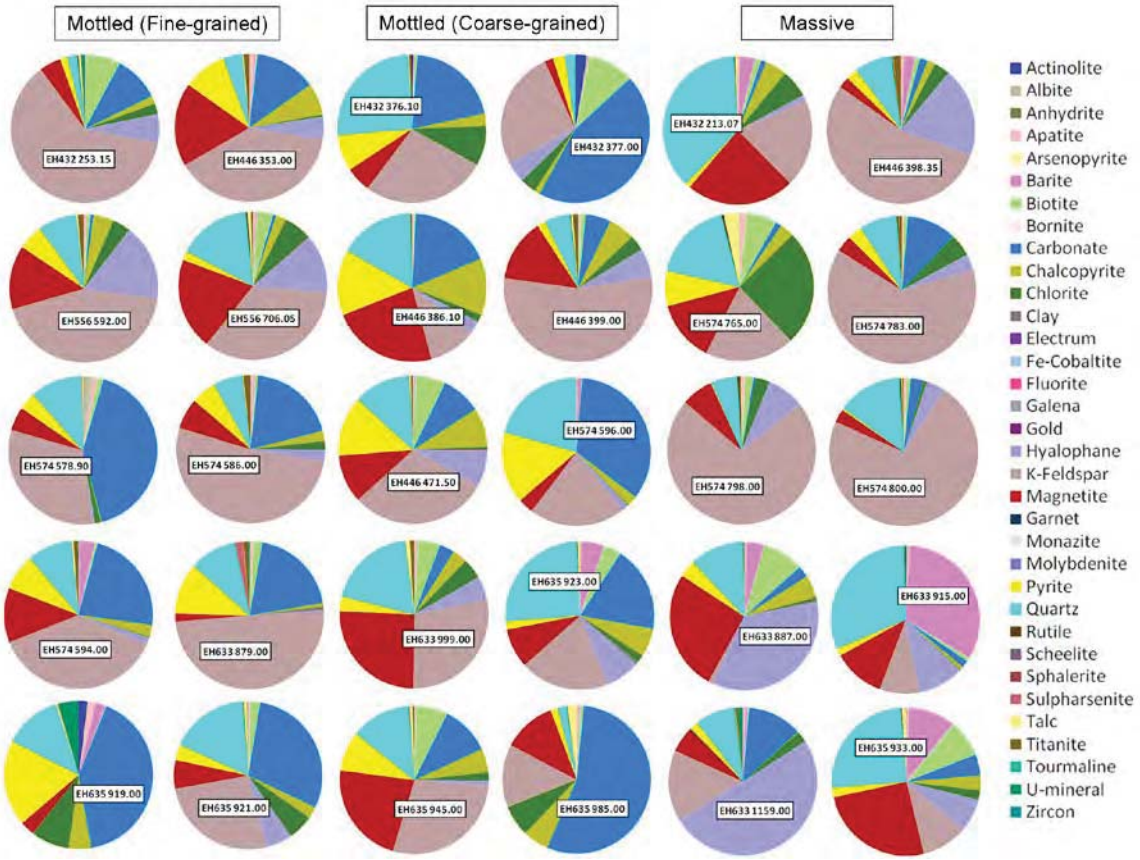

Figure 5.48. Pie charts illustrating the results of XMOD analyses undertaken on 30 examples from Ernest Henry (Table 5.22). Mineral groups are defined in Table 5.24. The dominant minerals are K-feldspar, carbonate, quartz, pyrite, magnetite and hyalophane.

5.4.4 Size analysis of chalcopyrite

The size of each chalcopyrite PhReg has been measured from the mineral maps produced from SPL-lite images of 311 drill-core tiles from Ernest Henry. The attributes were extracted using Definiens Developer software and follow the methods outlined in Chapter 3, section 3.5. Presented here in this section are the results for area, length and width of 30 selected examples outlined in Table 5.22. The data presented in this section are presented in the same format as the results of size analyses obtained from optical microscopy images (see section 5.2.3).

Area

The area of each chalcopyrite PhReg has been converted from a pixel to an Equivalent Circle Diameter (ECD; µm). The ECD size distributions are presented as size distribution curves (Figure 5.49 – *left*) as well as cumulative size distribution curves (Figure 5.49 – *right*) for examples of fine-grained mottled texture classes, coarse-grained mottled texture classes and the massive texture classes (see Table 5.19). Each size distribution has been coloured based on the meso-texture class assigned in the previous chapter (F1 – Orange; F2 – Green; F3 – Blue; MF4 – Red; MaM – Purple; MaF – Olive).

Based on the PhReg size distribution curves in Figure 5.49, the examples selected from the mottled fine-grained texture class show broadly similar trends with most examples exhibiting no chalcopyrite PhReg >1200 µm ECD and 50-80% of chalcopyrite with a PhReg ECD between 150 – 600 µms. The coarse-grained mottled examples show one trend with significant coarse-grained chalcopyrite (48-70% >1200 µms) and others that exhibit bimodal chalcopyrite populations i.e. coarse-grained chalcopyrite as well as a fine-grained population with a local maximum between 300-600 µms. In terms of how chalcopyrite size could potential mineral processing behaviours, the chalcopyrite PhRegs have been measured as the abundance of chalcopyrite larger than the predicted grind size for Ernest Henry(>150 µm). It is predicted that chalcopyrite with an ECD larger than 150 µm would expose sufficient surface area on a particle to float and be recovered. Chalcopyrite with an ECD <150 µm would require >25% chalcopyrite exposed on a particle surface to float and be recovered (Bradshaw, D.; pers. comm). For the meso-scale texture classes, the abundance of chalcopyrite with an ECD >150 µm are: F1 - 80.68% (4 samples); F2 - 64.76% (5 samples); F3 - 79.17% (9 samples); MaF - 47.39% (5 samples); MaM - 47.98% (5 samples); MF4 - 65.42% (2 samples).

The size distribution curves (Figure 5.49 – left) show that a number of the examples contain both fine- and coarse-grained chalcopyrite (e.g. EH432 377.00; EH633 1159.00; EH633 999.00). To better observe the size distribution trends, the drill-core tiles have been grouped based on similar PhReg size distribution trends. Figure 5.50 and Figure 5.51 show the distributions plotted as size distribution curves and as cumulative size distribution curves respectively. There are seven trends that have been characterised based on the proportions of different size fractions (Table 5.17). These results are discussed later in section 5.5.2.

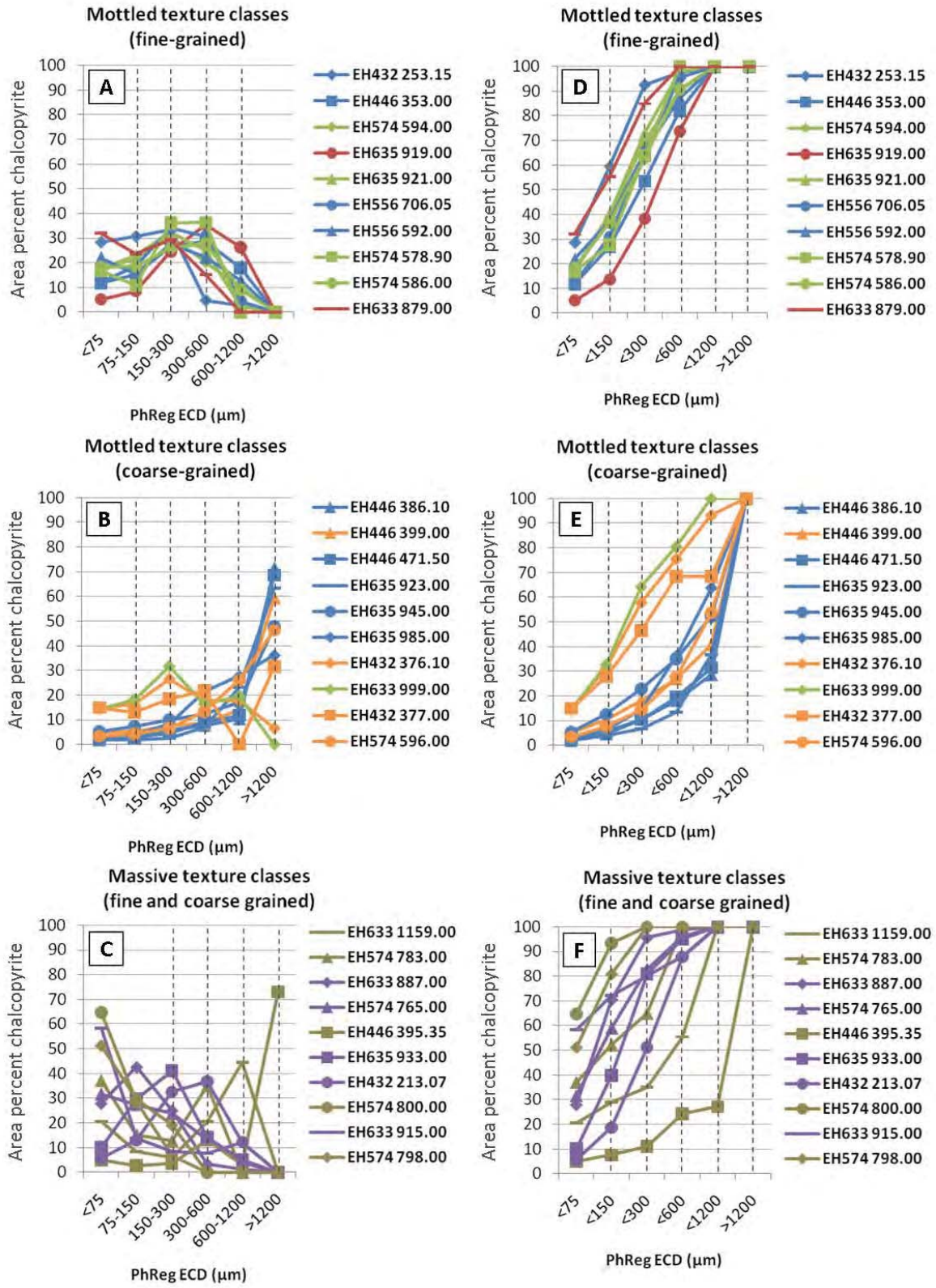

Figure 5.49. PhReg size distribution curves measured from SPL-lite MLA mineral maps and converted to an ECD. Each example has been coloured based on the corresponding meso-scale texture class assigned to the sampled interval in the previous chapter (F1 – Orange; F2 – Green; F3 – Blue; MF4 – Red; MaM – Purple; MaF – Olive).

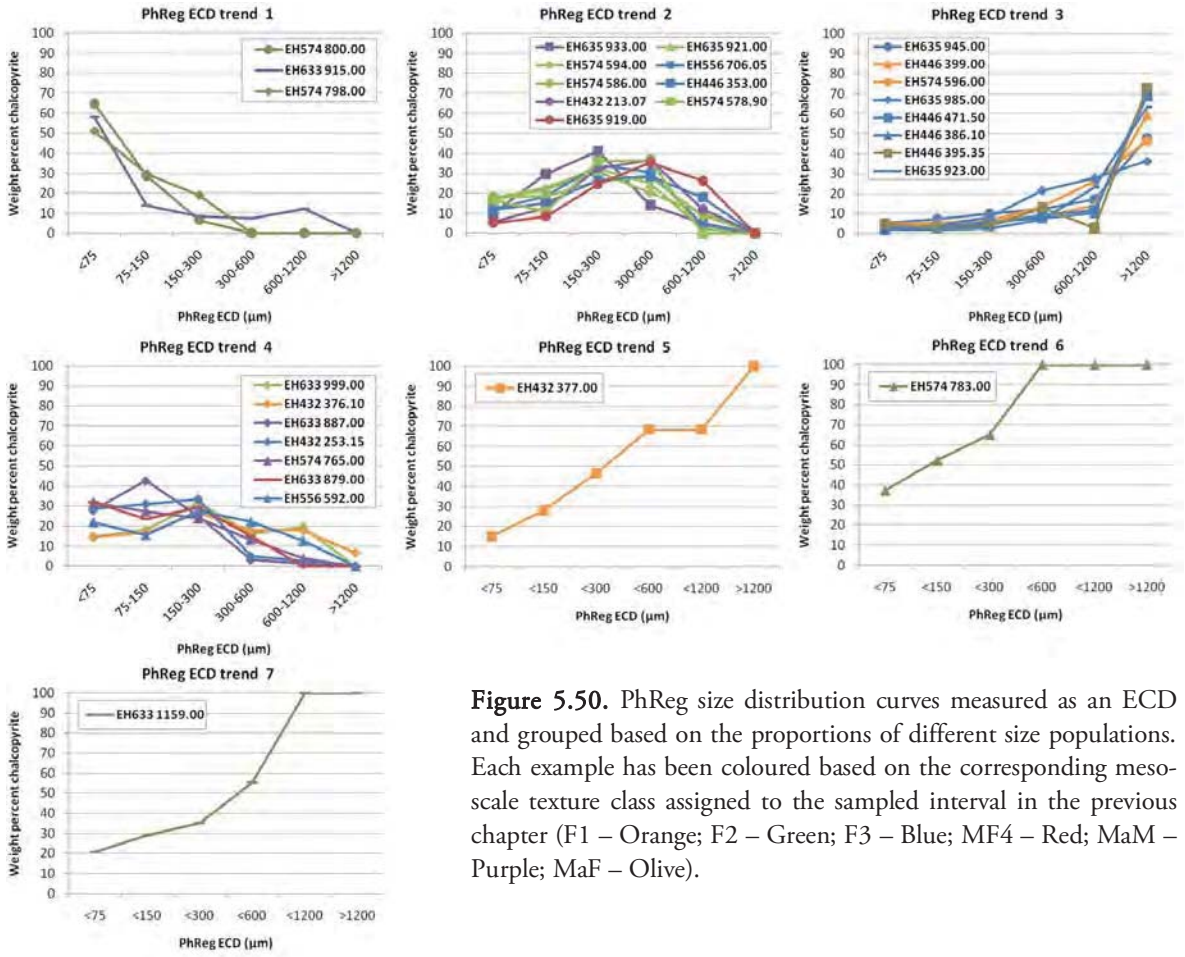

Figure 5.50. PhReg size distribution curves measured as an ECD and grouped based on the proportions of different size populations. Each example has been coloured based on the corresponding meso-scale texture class assigned to the sampled interval in the previous chapter (F1 – Orange; F2 – Green; F3 – Blue; MF4 – Red; MaM – Purple; MaF – Olive).

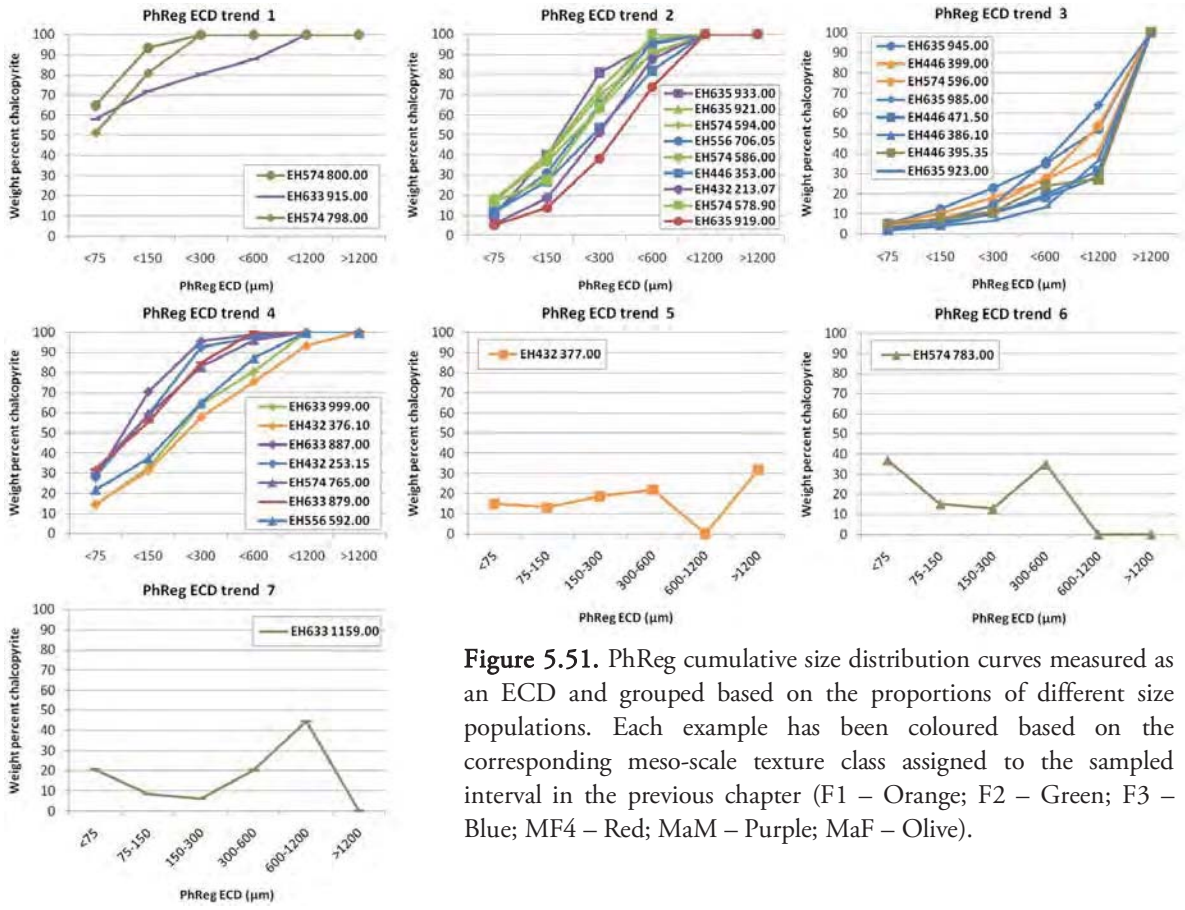

Figure 5.51. PhReg cumulative size distribution curves measured as an ECD and grouped based on the proportions of different size populations. Each example has been coloured based on the corresponding meso-scale texture class assigned to the sampled interval in the previous chapter (F1 – Orange; F2 – Green; F3 – Blue; MF4 – Red; MaM – Purple; MaF – Olive).

Table 5.17. Characteristics of chalcopyrite PhReg size trends obtained from MLA analysis.

ECD Trend	Characteristics
1	Fine-grained. Chalcopyrite ECD <1200 μm. 50-70% of chalcopyrite has an ECD <75 μm.
2	Fine-medium grained. 50-90% of chalcopyrite has an ECD of 75-600 μm.
3	Coarse-grained. 35-75% chalcopyrite has an ECD >1200 μm.
4	Bimodal distribution. 30-70% of chalcopyrite has an ECD of <150 μm with no chalcopyrite exceeding an ECD of 1200 μm (except for EH432 376.10).
5	Bimodal distribution. 68% chalcopyrite with ECD <600 μm and 32% >1200 μm.
6	Bimodal distribution. 40% chalcopyrite with ECD <150 μm and 46% between 150-600 μm.
7	Bimodal distribution. 30% chalcopyrite with ECD <150 μm and 65% between 300-1200 μm.

Length and Width

During the meso-scale textural analysis, the maximum length and corresponding width was used to determine whether a sample was fine- or coarse-grained. Here the maximum length and width has been calculated from each of the SPL-lite minerals maps outlined in Table 5.19 and presented in Figure 5.53. This figure shows that for both the fine- and coarse-grained mottled textures the chalcopyrite PhRegs with the longest length have length to width ratios between 1:1 and 3:1. For the massive examples, several examples exhibit length to width ratios > 3:1.

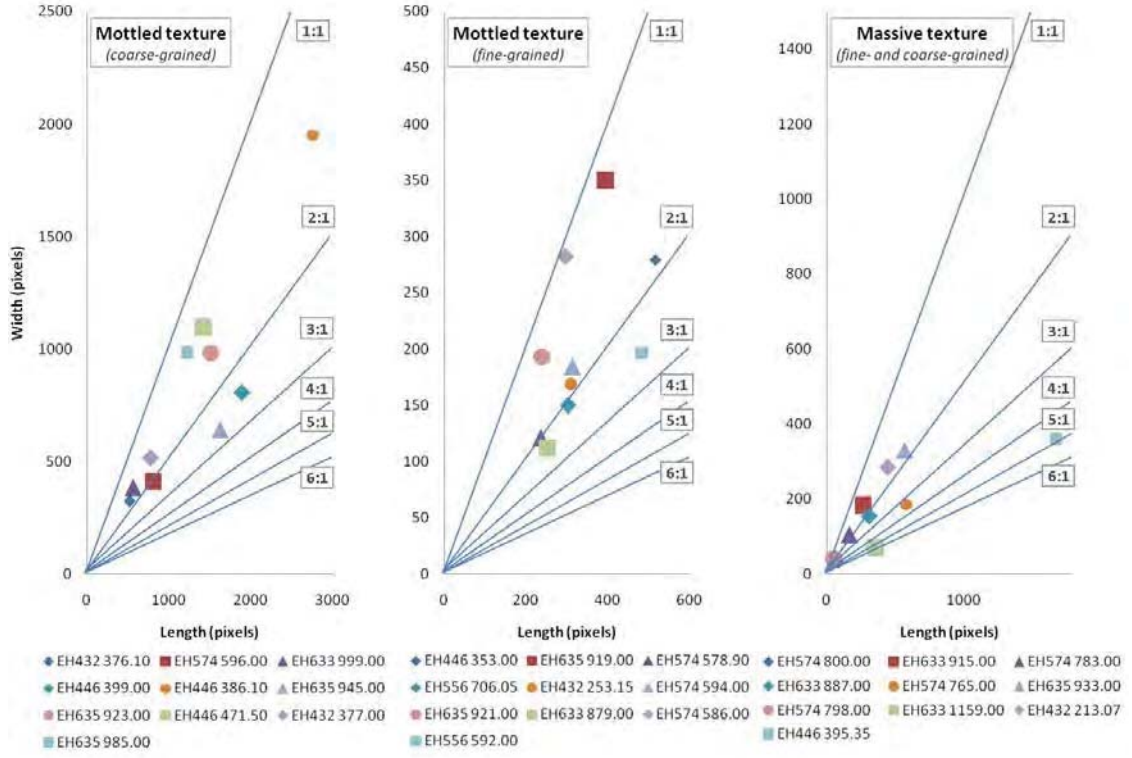

Figure 5.52. Maximum chalcopyrite PhReg length and corresponding widths for the Ernest Henry drill-core examples presented in Table 5.17.

5.4.5 Gangue minerals associated with chalcopyrite

The gangue minerals associated with chalcopyrite at Ernest Henry have been determined using the MLA in SPL-lite mode (see section 5.2.4). The abundance of a mineral associated with chalcopyrite is measured from the one pixel rim (4.22 μm) surrounding the chalcopyrite PhReg. Each mineral is weighted against the size of the chalcopyrite compared to the total chalcopyrite of that sample. To be consistent with the methods used in the optical microscopy analysis at Ernest Henry a PCA was

undertaken on all of the chalcopyrite PhRegs for EH635 (n = 298 443) in order to establish what the most common minerals to occur with chalcopyrite are.

The principal components analysis undertaken on MLA results for EH635 shows that 94% of the variation in minerals associated with chalcopyrite is accounted for in the first four Principal Components. The minerals that make up these principal components are shown in Table 5.23. The first two principal components have been plotted as a density plot in Figure 5.53. This figure consists of ~200,000 individual chalcopyrite PhRegs (PhRegs < 5 pixels have been removed for more efficient processing and to reduce the sampling bias to small PhRegs). The distance between areas of high density in Figure 5.53 indicates the strength of the relationship between different minerals. Ideally, principal components one and two would account for more of the sample variability, however this was the best result that could be obtained and the degree to which mineral contributes to the overall variability in the minerals typically associated with chalcopyrite is indicated as the '% population variability' in Table 5.18.

Table 5.18. The minerals present in the first four principal components calculated for Ernest Henry. This analysis has established that the dominant minerals associated with chalcopyrite are magnetite, quartz, pyrite, carbonate and K-feldspar.

Mineral	PC 1	PC 2	PC 3	PC 4
Magnetite	0.577	-0.601	0.104	0.017
Quartz	0.015	0.430	0.649	0.539
Pyrite	0.161	0.340	-0.750	0.427
Carbonate	0.246	0.546	0.052	-0.716
K-feldspar	-0.762	-0.200	-0.050	-0.118
% population variability	28.50	23.50	21.60	20.40

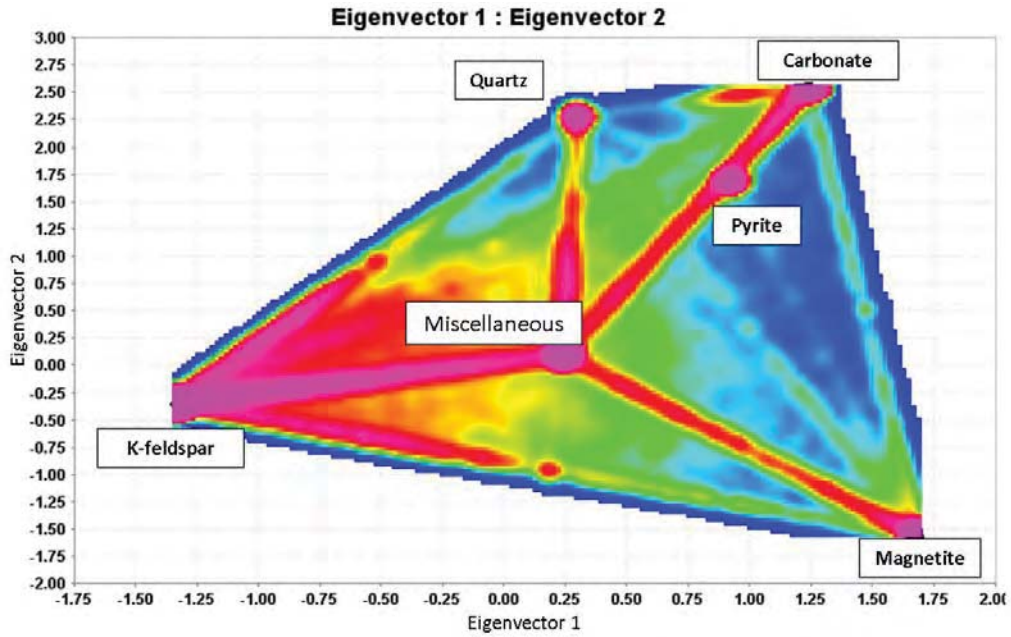

Figure 5.53. Density plot illustrating the minerals associated with chalcopyrite for eigenvectors 1 and 2. The chalcopyrite data used to perform the PCA were extracted from SPL-lite images of EH635.

The additional advantages of principal components plots are that individual samples or groups of samples can be plotted in order to establish their dominant mineral relationships with chalcopyrite. This is shown in Figure 5.54 where principal components one and two have been

plotted for the chalcopyrite PhRegs for one example of each the meso-scale texture classes that were defined in the previous chapter (see Table 5.19).

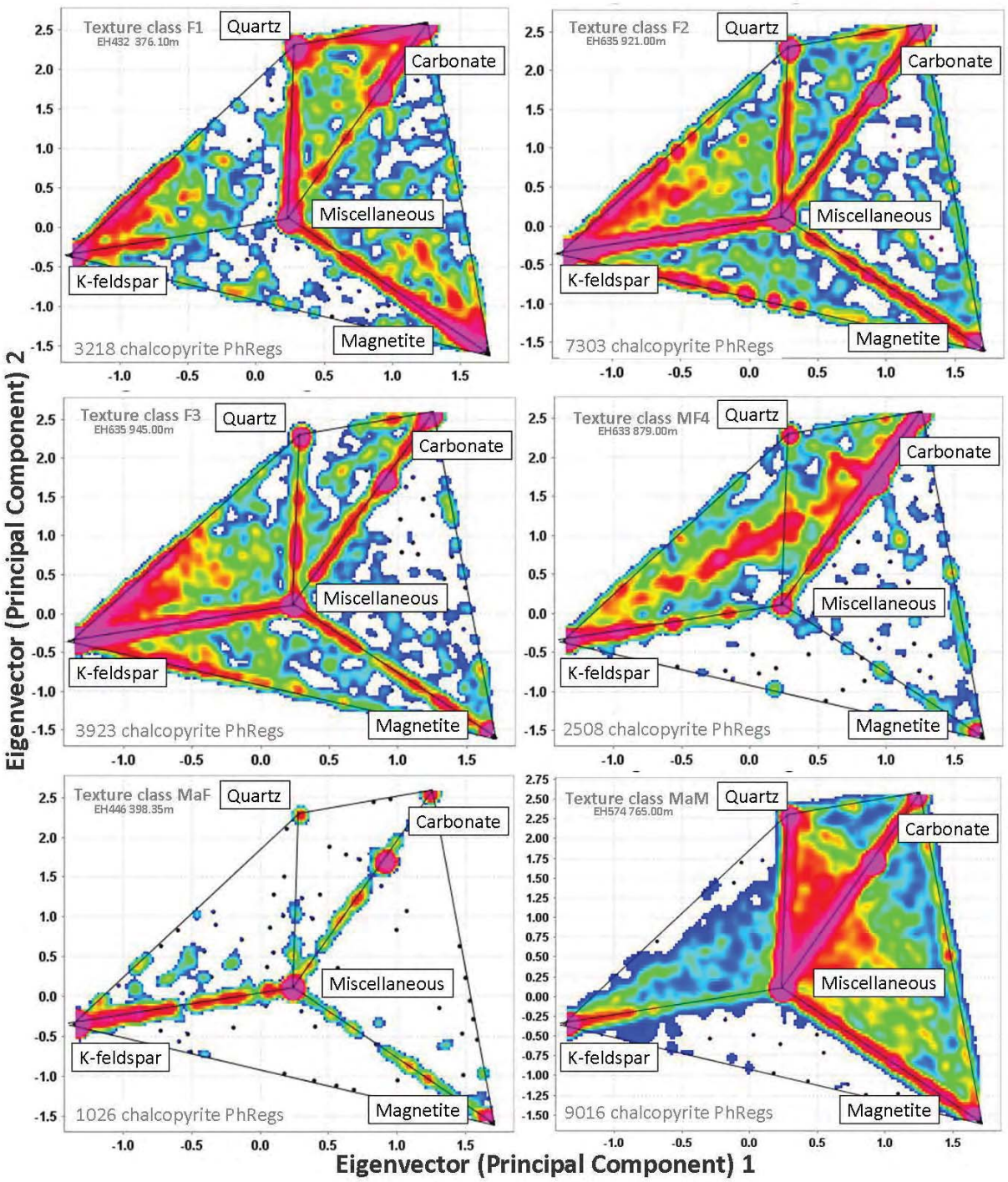

Figure 5.54. Density plots of Principal Component 1 and Principal Component 2 showing the minerals associated with chalcopyrite for the meso-scale texture classes at Ernest Henry.

Table 5.19. Descriptions of results for the Principal Component density plots shown in Figure 5.67 for each meso-scale texture class for Ernest Henry.

Texture	Example	Texture Characteristics	PCA characteristics
F1	EH432 376.10m	> 90% feldspar in modal mineralogy	Chalcopyrite strongly associated with magnetite-carbonate minerals-quartz-pyrite
F2	EH635 921.00m	> 80% magnetite in modal mineralogy	Chalcopyrite strongly associated with K-feldspar-carbonate minerals
F3	EH635 945.00m	60-90% feldspar in modal mineralogy	Chalcopyrite strongly associated with K-feldspar
MF4	EH633 879.00m	0-60% feldspar with carbonate/quartz % > magnetite or pyrite % in modal mineralogy	Chalcopyrite strongly associated with pyrite
MaF	EH446 398.35m	0-60% feldspar with magnetite % > carbonate/quartz or pyrite % in modal mineralogy	Chalcopyrite strongly associated with K-feldspar
MaM	EH574 765.00m	0-60 % feldspar with pyrite % > carbonate/quartz or magnetite % in modal mineralogy	Chalcopyrite strongly associated with magnetite-carbonate-quartz-pyrite-mixtures

Changes in mineral association with grain size

The analysis of chalcopyrite size presented in the previous section (Section 5.4.4) showed that there were multiple size fractions of chalcopyrite present, some of which occur within the same sample. In order to establish whether different sizes of chalcopyrite exhibit unique mineralogical signatures, density plots of the first two principal components have been created for the size fractions determined during the size analysis in section 5.4.4 (Figure 5.55). The size fractions are: fine-grained: ECD <150 µm; medium-grained: ECD between 150-600 µm; coarse-grained ECD >600 µm.

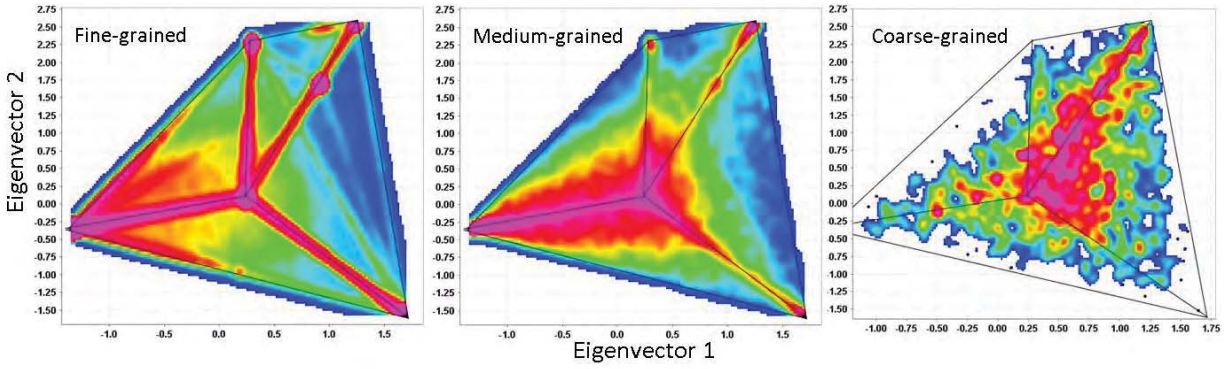

Figure 5.55. Density plots of Eigenvector 1 and 2 illustrating the dominant minerals associated with chalcopyrite at different sizes for all sampled drill-holes. The fine-grained chalcopyrite is <150 µm ECD (n = 742234 PhRegs), medium-grained is 150-600 µm ECD (n = 45693 PhRegs) and coarse-grained is >600 µm ECD (n = 1935 PhRegs). The areas of high density (*pink*) correspond to different minerals (see Figure 5.54).

Figure 5.55 shows that for the fine-grained chalcopyrite, K-feldspar is the dominant associated mineral. Areas of high density around the magnetite, quartz, carbonate and pyrite regions indicate that these minerals are also strongly associated with chalcopyrite of this size fraction. The dominant minerals associated with the medium-grained chalcopyrite are K-feldspar and miscellaneous (of the most dominant minerals) that trend towards magnetite, quartz and carbonate. The coarse-grained population has a strong carbonate-pyrite association which trends towards the quartz and magnetite end members. These minerals are consistent with the coarse-grained clots that have been described in the meso-scale analysis for Ernest Henry (Chapter 4). As the size of chalcopyrite increases, the association with carbonate-pyrite-magnetite-quartz becomes more pronounced.

The disadvantage of displaying the mineral association data as a density plot is that it is not weighted by the size of each chalcopyrite PhReg, and therefore is dominated by small grains that will not be recovered in flotation. Figure 5.56 shows the proportions of minerals that are associated with chalcopyrite in each of the size fractions. In this figure, it can be seen that magnetite and K-feldspar are the dominant minerals associated with chalcopyrite in the fine-grained populations. This dominance decreases as the chalcopyrite PhReg size increases. The minerals associated with the coarse-grained chalcopyrite that in abundance are carbonate and magnetite.

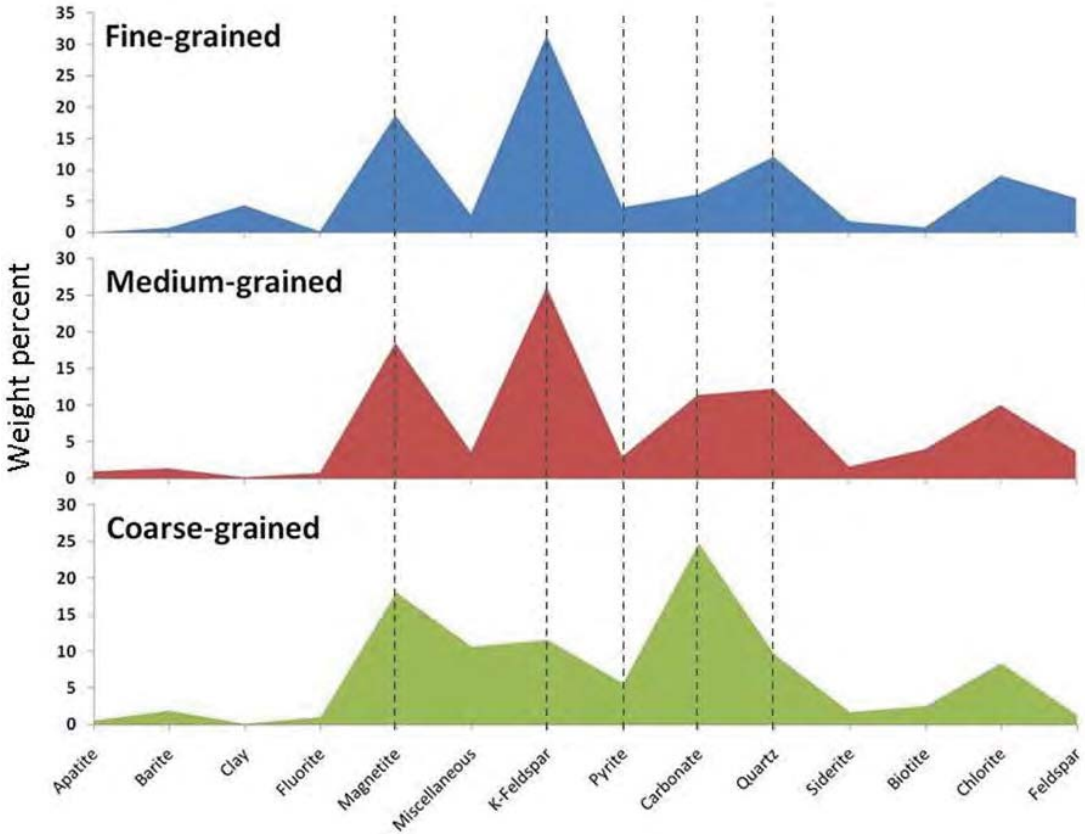

Figure 5.56. Abundances of gangue minerals associated with different sizes of chalcopyrite. Chalcopyrite PhReg data was extracted from SPL-lite analysis at Ernest Henry. The fine-grained chalcopyrite is <150 μm ECD (n = 742234 phases), medium-grained is 150-600 μm ECD (n = 45693 phases) and coarse-grained is >600 μm ECD (n = 1935 phases).

5.4.6 Analysis of gold and silver bearing minerals

The gold and silver bearing minerals that occur at Ernest Henry are gold and electrum. Using the SPL-lite method of the MLA and the procedures outlined in Chapter 3, section 3.5. 311 drill-core tiles were analysed for the presence of gold and electrum. From these tiles, 389 grains of electrum and 126 grains of gold were identified from 176 different tiles. The minerals that host the gold and electrum have been identified and are summarised in Table 5.20. The average size and the number of occurrences (n) have also been summarised. Where only one mineral is present, the gold or electrum grain is completely encapsulated. Multiple minerals indicate that the grain is on the boundary between these minerals. The overall average ECD of electrum is 8.20 μm and of gold is 13.47 μm. The most common minerals for electrum to be hosted in are pyrite, chalcopyrite-pyrite, chalcopyrite, magnetite, chalcopyrite-magnetite, K-feldspar, quartz and calcite. The most common minerals for gold to be hosted by are magnetite, K-feldspar, calcite, pyrite, hyalophane, quartz and chalcopyrite.

Table 5.20. Minerals associated with electrum and gold at Ernest Henry and their average size measured as an ECD. Where there is only one occurrence of an association a standard deviation cannot be measured and is noted as N/A.

Mineral Associations	Electrum			Gold		
	Average Size (ECD)	Standard deviation	N	Average Size (ECD)	Standard deviation	N
Biotite	8.85	2.47	3			
Calcite	56.45	8.50	11	109.33	7.56	9
Calcite - Fluorite	28.00	N/A	1			
Chalcopyrite	14.94	2.76	50	52.75	6.69	4
Chalcopyrite - Biotite	23.50	0.00	2			
Chalcopyrite - Calcite	42.00	3.11	2	20.00	N/A	1
Chalcopyrite - Chlorite	10.50	6.35	2	25.00	N/A	1
Chalcopyrite - Clay	30.00	N/A	1			
Chalcopyrite - Dolomite	23.00	N/A	1			
Chalcopyrite - Fe Cobaltite	6.00	N/A	1	22.00	N/A	1
Chalcopyrite - Fluorite	8.00	N/A	1			
Chalcopyrite - Hyalophane	4.00	N/A	1	23.00	N/A	1
Chalcopyrite - K Feldspar	13.40	2.66	5	12.00	8.49	2
Chalcopyrite – K Feldspar – Apatite	5.00	N/A	1			
Chalcopyrite – Magnetite	24.60	3.45	18	155.00	0.64	2
Chalcopyrite – Magnetite – Calcite	12.00	N/A	1			
Chalcopyrite – Magnetite – Chlorite	6.00	N/A	1			
Chalcopyrite – Magnetite – K Feldspar	12.00	N/A	1			
Chalcopyrite – Pyrite	20.50	2.58	74	28.50	11.09	2
Chalcopyrite – Pyrite – Arsenopyrite	161.00	N/A	1			
Chalcopyrite – Pyrite - Calcite				30.00	N/A	1
Chalcopyrite - Pyrite - Clay	62.00	N/A	1			
Chalcopyrite - Pyrite - Magnetite	112.00	N/A	1			
Chalcopyrite - Pyrite - Quartz	31.50	5.51	2			
Chalcopyrite - Quartz	14.30	2.19	4	37.50	0.89	2
Chalcopyrite - Quartz - Rutile	21.00	N/A	1			
Chalcopyrite - Unknown	15.70	2.37	3			
Chlorite	18.00	3.05	4	88.00	11.09	3
Chlorite - Quartz	4.00	N/A	1			
Chlorite - Sulfarsenite	11.00	N/A	1			
Clay				48.00	N/A	1
Dolomite				59.00	N/A	1
Electrum						
Gold - Unknown	361.00	N/A	1	350.00	N/A	1
Hyalophane				99.20	12.21	5
K Feldspar	36.40	7.71	15	80.60	0.44	15
K-Feldspar – Apatite – Titanite				53.00	N/A	1
K-Feldspar – Biotite				86.00	N/A	1
K-Feldspar - Chlorite				70.00	N/A	1
K Feldspar - Hyalophane	12.00	N/A	1			
K-Feldspar – Hyalophane - Calcite				38.00	N/A	1
K Feldspar - Quartz	7.00	N/A	1	21.74	4.25	2
Magnetite	41.70	6.73	28	12.19	13.40	18
Magnetite - Calcite	114.50	11.66	2	29.92	10.44	2
Magnetite - Chlorite	26.00	3.48	2	22.94	1.11	2
Magnetite – Fluorite				12.70	N/A	1
Magnetite - Hyalophane				16.63	N/A	1
Magnetite - K-Feldspar	55.50	6.47	4	14.40	2.87	3
Magnetite - K-Feldspar - Hyalophane - Biotite				10.75	N/A	1
Magnetite - K-Feldspar - Hyalophane - Quartz				61.21	N/A	1
Magnetite - Quartz	135.70	8.35	3	8.36	N/A	1
Magnetite - Siderite				32.16	N/A	1
Pyrite	54.10	9.03	85	12.78	8.83	8
Pyrite - Biotite	7.00	N/A	1	13.01	N/A	1
Pyrite - Calcite	37.30	1.15	3			
Pyrite - Dolomite	24.00	3.12	2			
Pyrite - Dolomite - Ankerite	33.00	N/A	1			
Pyrite - Fluorite - Calcite				8.98	N/A	1
Pyrite - K Feldspar - Quartz				5.18	N/A	1

Mineral Associations	Electrum			Gold		
	Average Size (ECD)	Standard deviation	N	Average Size (ECD)	Standard deviation	N
Pyrite - Hyalophane	38.00	N/A	1			
Pyrite - Magnetite	46.00	N/A	1	11.82	N/A	1
Pyrite - Quartz	70.00	N/A	1			
Pyrite - Siderite - Dolomite	236.00	N/A	1			
Pyrite - Sulfarsenite	11.00	N/A	1			
Pyrite - Unknown	6.00	N/A	1	10.87	N/A	1
Quartz	39.10	5.46	12	11.10	2.28	5
Quartz - Calcite	87.00	N/A	1	6.75	4.36	2
Quartz - Chalcopyrite	144.00	N/A	1			
Quartz - Chlorite				12.29	3.48	2
Quartz - Chlorite - Gold	15.00	N/A	1			
Quartz - Titanite	5.00	1.90	2			
Rutile	9.00	N/A	1			
Rutile - Biotite	16.00	0.86	2			
Rutile - Pyrite	12.00	N/A	1			
Siderite				10.37	N/A	1
Tourmaline	37.00	N/A	1			
Tourmaline - Unknown	159.00	N/A	1			
Unknown	187.70	10.02	11	12.89	10.69	12

5.5 Summary of micro-scale mineralogy and texture: Ernest Henry

The aim of the micro-scale analysis undertaken at Ernest Henry was to establish if the mineralogical and textural attributes that were observed at the meso-scale from both visual and machine based methods (Chapter 4) could also be observed at the micro-scale. Two different technologies were used; the higher cost and higher resolution Mineral Liberation Analyser (MLA) and the Leica DM6000 optical microscope which is lower resolution, but a much cheaper and faster system to run as a routine application. In total, optical microscopy and MLA analyses were undertaken on 311 drill-core tiles that represented a range of mineralogical and textural styles observed at Ernest Henry. The images produced from optical microscopy analyses allowed 10 minerals or mineral groups to be classified into mineral maps (Table 5.3). These mineral maps were then able to be analysed using Definiens Developer to produce quantified information regarding modal mineralogy, chalcopyrite size, and chalcopyrite mineral associations. The results of these analyses were presented in section 5.2 and are summarized here in Table 5.21.

The use of the MLA in SEM mode means that a library of mineral spectra was able to be created. This procedure allowed 38 minerals to be identified (Table 5.16) and provided detailed information regarding the minerals and textures present at Ernest Henry (see section 5.4.1). Information regarding the modal mineralogy, size of chalcopyrite and the gangue minerals associations were quantified using the MLA in SPL-lite and XMOD mode (see Chapter 3, section 3.5.1). The results of these analyses were presented in section 5.4 and are summarized here in Table 5.22.

Based on the outcomes of the micro-scale analyses using both the optical microscope and the MLA, the advantages and disadvantages of each measurement platform are apparent. The MLA allows the quantified identification of minerals which can be used as a tool for validating a rule set for optical microscopy classification. Alternatively, it can also be used to determine the limitations of the PhReg size that can be classified from optical microscopy images. While the optical microscope does have its limitations it does provide a more cost effective option for the fast routine analysis of mineralogical and textural attributes. As discussed in Chapter 3 (section 3.3.1) it is important not to

over interpret results for minerals that cannot be easily distinguished. In this study, mineral groups have been created based on the minerals that may be included in the classification. The most accurate classifications for optical microscopy mineral maps are those that can be identified clearly using reflected light microscopy. For Ernest Henry these are chalcopyrite, pyrite, magnetite and hematite.

Table 5.21. Summary of micro-scale optical microscopy mineralogical and textural analyses for Ernest Henry.

Mineralogical or Textural attribute	Measure	Results	Comments
Size	Area	Three trends identified as well as two bimodal distributions (Figure 5.7). Consistent with the three trends that were identified in the meso-scale visual core logging (Chapter 4, section 4.3). Examples shown in Figure 5.57.	Results were converted to an Equivalent Circle Diameter and presented as a size distribution curve and cumulative distribution curve.
	Length and Width	Two length and width trends identified. The coarser of the two trends can be used to distinguish coarse-grained mineralised clots from samples at Ernest Henry.	Measured as the maximum length and corresponding width of chalcopyrite in each sample. This measure is particularly useful for determining vein hosted and coarse-grained mineralisation.
Modal Mineralogy		The most dominant mineralogical signatures are Red feldspar; quartz; barite and carbonate minerals; magnetite, hematite and mafic minerals; chalcopyrite, pyrite, magnetite and hematite; pyrite and chalcopyrite; barite and hematite.	Mineralogical signatures were determined visually and using a PCA of 311 drill-core tiles.
Gangue mineral associations	Chalcopyrite	The most dominant minerals associated with chalcopyrite are magnetite and mafic minerals; quartz, pyrite and carbonate minerals; red feldspar; quartz.	Calculated using a PCA of ~326 000 chalcopyrite PhRegs. The mineral associations are consistent with the minerals associated with chalcopyrite minerals identified in the meso-scale visual logging i.e. mineralised clots; massive red feldspar; massive magnetite and minerals from mottled textures (carbonate minerals and quartz).
Changes in mineral associations with size	Chalcopyrite	The abundance of the minerals pyrite and red feldspar associated with chalcopyrite increases as the size decreases. The abundance of the minerals carbonates, quartz and magnetite associated with chalcopyrite increases with size.	Four examples were selected based on mineralogical differences observed in Figure 5.11.

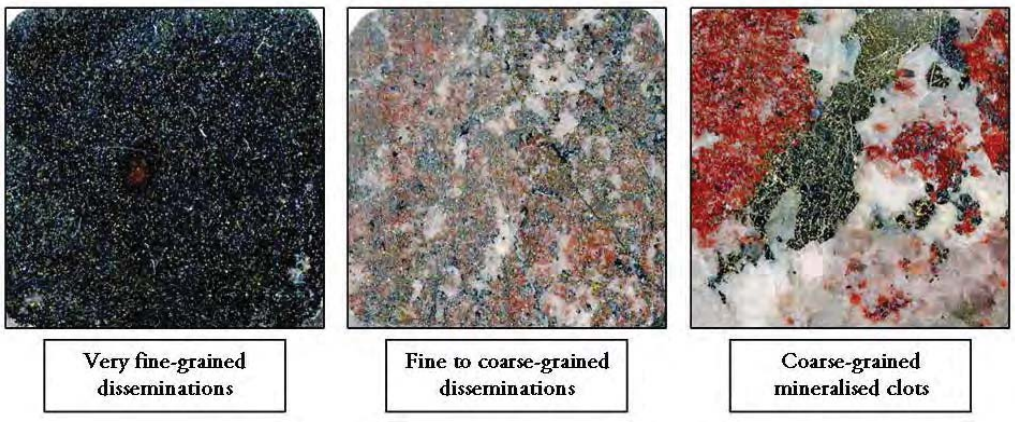

Figure 5.57. Examples of drill-core tiles showing very fine-grained, fine-coarse grained and coarse-grained mineralised clots that represent the chalcopyrite PhReg ECD trends 1, 2 and 3 respectively. All drill-core tiles have a width of 3cm.

Table 5.22. Summary of micro-scale MLA mineralogical and textural analyses for Ernest Henry.

Mineralogical or Textural attribute	Measure	Results	Comments
Size	Area	Three trends identified as well as four bimodal distributions (Figure 5.50). Consistent with the three trends that were identified in the meso-scale visual core logging (Chapter 4, section 4.3). Examples shown in Figure 5.57.	Results were converted to an Equivalent Circle Diameter and presented as a size distribution curve and cumulative distribution curve.
	Length and Width	Two length and width trends identified. The coarser of the two trends can be used to distinguish coarse-grained mineralised clots from samples at Ernest Henry.	Measured as the maximum length and corresponding width of each sample. This measure is particularly useful for determining vein hosted and coarse-grained mineralisation.
Modal Mineralogy	XMOD	The dominant mineralogical signatures are K-feldspar, carbonate, quartz, pyrite, magnetite and hyalophane.	MLA in SEM mode identified 38 minerals. Modal mineralogy has been calculated for 311 drill-core tiles (see Appendix 5.10).
Gangue mineral associations	Chalcopyrite	The dominant mineralogical signatures are magnetite; quartz; carbonate minerals; K-feldspar. These associations were plotted for each of the meso-scale texture classes (Figure 5.54).	Calculated using a PCA on ~298 000 PhRegs from EH635. The mineral associations are consistent with the minerals associated with chalcopyrite minerals identified in the meso-scale visual logging and optical microscopy .
Changes in mineral associations with size	Chalcopyrite	The fine-grained chalcopyrite maintains binary associations with all minerals shown in Figure 5.53. The medium-grained chalcopyrite is associated with K-feldspar, quartz, carbonate minerals and magnetite. For the coarse-grained chalcopyrite only the carbonate minerals and mixed mineral signatures are present (see Figure 5.55).	The changes in mineral associations with size for chalcopyrite were plotted for all of the chalcopyrite PhRegs from all drill-holes.
Rare minerals	Gold and electrum	Average ECD of electrum and gold was 8.20 μm and 13.47 μm respectively. The most common minerals associated with electrum are pyrite, chalcopyrite-pyrite, chalcopyrite, magnetite, chalcopyrite-magnetite, K-feldspar, quartz and calcite respectively. The most common minerals associated with gold are magnetite, K-feldspar, calcite, pyrite, hyalophane, quartz and chalcopyrite respectively.	389 grains of electrum and 126 grains of gold were identified using SPL-lite analysis. The distinction between gold and electrum has direct implications for the recovery of these minerals. Electrum will float more efficiently than gold (Allan and Woodcock, 2001).

5.6 Summary of micro-scale mineralogy and texture: Cadia East

The aim of the micro-scale analysis undertaken at Cadia East was to establish if the mineralogical and textural attributes that were observed at the meso-scale (Chapter 4) could also be observed at the micro-scale using the MLA. In order to determine this, MLA analyses were undertaken on 130 drill-core tiles that represented a range of mineralogical and textural styles observed at Cadia East. Using the MLA in SEM mode a library of mineral spectra was created. This procedure allowed 35 minerals to be identified (Table 5.10) and provided detailed information regarding the minerals and textures present at Cadia East (see section 5.3.1). Information regarding the modal mineralogy, size of Cu - sulphide mineral and their gangue minerals associations as well as shape were quantified using the MLA in SPL-lite and XMOD mode (see Chapter 3, section 3.5.1). The results of these analyses were presented in section 5.3 and are summarized here in Table 5.23.

Table 5.23. Summary of micro-scale mineralogical and textural analyses for Cadia East.

Mineralogical or Textural attribute	Measure	Results	Comments
Size	Area	Three trends identified as well as three bimodal distributions (Figure 5.24). Consistent with the three trends that were identified in the meso-scale visual core logging (Chapter 4, section 4.2).	Results were converted to an Equivalent Circle Diameter and presented as a size distribution curve and cumulative distribution curve.
	Length and Width	Fine-grained examples had the smallest maximum lengths, coarse-grained had the largest widths and the vein-hosted had the largest maximum lengths.	Measured as the maximum length and corresponding width of each sample. This measure is particularly useful for determining vein hosted and coarse-grained mineralisation.
	PSSA	PSSA shows minor variation between the median of individual samples.	PSSA as a measure is not appropriate for intact minerals or as a tool for distinguishing between samples with different grain boundary complexities.
	Smallest Enclosing Ellipse	Fine and coarse-grained disseminated chalcopyrite have more complex boundaries than the vein-hosted chalcopyrite.	As tool for distinguishing between mineral textures this measure is not suitable.
Gangue mineral associations	Chalcopyrite	The most dominant minerals associated with chalcopyrite are albite, chlorite/biotite, illite/ muscovite and K-feldspar with lesser epidote, quartz, pyrite, magnetite and calcite/fluorite.	Calculated using a PCA of ~250 000 chalcopyrite PhRegs. The mineral associations were predominantly associated with one mineral or mineral group. The mineral associations are consistent with the most dominant alteration assemblages and the minerals associated with Cu-sulphide minerals identified in the meso-scale visual logging.
	Bornite	The most dominant minerals associated with bornite are epidote, albite, illite/muscovite, chlorite/biotite, K-feldspar, quartz and chalcopyrite respectively.	Given the binary nature of the mineral associations at Cadia East, the most dominant mineral associations were calculated simply by manipulating the data set.
	Molybdenite	The most dominant minerals associated with molybdenite are K-feldspar, chlorite/biotite, illite/ muscovite, albite, quartz, carbonate, chalcopyrite and bornite respectively.	The minerals associated with molybdenite were calculated as a weight percent of the total molybdenite using 3600 molybdenite PhRegs.
Shape Attributes	Evaluation of shape attributes	Length of the longest polygon Length versus width Asymmetry Elliptical fit Rectangular fit Number of inner polygons Average area of inner polygons Average skeleton segment area	Shape analyses were performed on 30 examples of intact mineral PhRegs from Cadia East that represent variable sizes and shapes. The detailed results are found in Appendix 5.8 and a worked example using one drill-core tile is shown in Figure 5.38.
Rare Minerals	Gold and Electrum	17 grains of Au and 68 grains of electrum were identified. Of these grains 45 were completely encapsulated by one mineral and 40 occurred on the grain boundary between multiple minerals.	The gold and electrum minerals were identified using the MLA in SPL-lite mode. Gold and electrum were identified in upper and deeper sections of Cadia East. In the upper section, they typically occur in the pyrite and less chalcopyrite. In the deeper sections the gold minerals occur in both vein hosted minerals as well as within and proximal to disseminated chalcopyrite and bornite. Where gold and electrum were shown to occur along grain boundaries, two size fractions were identified: fine-grained (area <463.7µm ECD *or 100 pixels*) and coarse-grained (area >463.7µm ECD). The latter is vein-hosted.

Based on the results obtained from the SPL-lite analysis of chalcopyrite and bornite several mineralogical and textural attributes were consistent with those initially observed in the visual logging of drill-core. The dominant gangue minerals associated with chalcopyrite and bornite are consistent with the four major texture classes that were created:

1. Mafic-hosted: chlorite/biotite, magnetite and epidote
2. Felsic-hosted: albite, illite/muscovite, K-feldspar and quartz
3. Vein-hosted: quartz, calcite, fluorite and epidote
4. Fault-hosted: chlorite/biotite (but also dependent on primary rock type)

The three size distribution trends were identified from the analysis of chalcopyrite PhRegs, based on the chalcopyrite association data it can be concluded that the fine and medium grained trends were classified as the 'fine-grained disseminations' in the meso-scale logging. The coarse-grained distribution trend is concluded to be associated with the 'coarse-grained aggregates' and the 'vein-hosted' chalcopyrite in the meso-scale logging.

5.7 Summary

In Chapter 4, mineralogical and textural characteristics were identified and measured at the meso-scale in drill-core. In this chapter, the aim was to identify the same mineralogical and textural attributes i.e. modal mineralogy, size and mineral associations, however at the micro-scale. The micro-scale analysis was undertaken on both Cadia East and Ernest Henry, however only Ernest Henry had both optical microscopy and MLA analyses performed. The results for Ernest Henry were presented in section 5.2 (optical microscopy) and 5.4 (MLA) and a summary of the outcomes in section 5.5. The results for Cadia East were presented in section 5.3 (MLA only) and a summary of the outcomes in section 5.6. In the next chapter, particulate samples from the Cadia East deposit will be analysed using the optical microscopy method (see Chapter 3, section 3.4). This will determine whether the intact mineralogical and textural signatures observed at the meso-scale and here at the micro-scale are still preserved after the breakage process.

Chapter Six

Mineralogy and texture of particulate rocks: Micro-scale

6.1 Introduction

A 'particulate sample' is the result of crushing/ grinding a mass of rock to many discrete rock fragments (Jones, 1987). A particulate rock sample is considered to provide a more representative analysis than a 'chunk' of the bulk rock that it has been derived from. In metallurgical practice, particulate samples are taken from large composites of drill-core (up to 100 metres) to allow physical tests to be performed. The bulk nature of these samples however means that the natural mineralogical and textural variability within the rock can be disguised by the blending process. To overcome this (within the AMIRA P843 project), particulate samples have been selected at a smaller scale to coincide with the existing assay intervals (2 metres). By choosing to perform many small-scale analyses as opposed to fewer large scale bulk-rock tests, a block model can potentially be populated with a larger number of results that are less likely to disguise the inherent mineralogical and textural variability of the rock.

Within this project, three size fractions have been selected for mineralogical and textural analysis using optical microscopy and image analysis. These size fractions are shown in Table 6.1 and a comparison of the optical and MLA techniques are presented in the next section (6.2). Three finer size fractions have also been sampled for MLA analyses which have been performed Cathy Evans within the AMIRA P843 project for the purpose of predicting flotation behaviours (Evans, 2010). These size fractions are not discussed here.

Table 6.1. Size fractions of particulate samples selected for optical microscopy and MLA analysis within the AMIRA P843 project.

	Optical Microscopy (this research)			MLA (Evans, 2010)		
Size Fraction	-3.36 +2.36 mm	-1.18 +0.85 mm	-0.43 +0.30 mm	-150 +75µm	-75 +38µm	<38µm

This chapter discusses mineral maps of particulate samples that have been produced from optical microscopy images in order to extract quantified mineralogical and textural information about each sample. This information allows the mineralogy and texture of each sample to be compared with other attributes of the same sampled area (2 metres) such as assays, on-site geological logging, meso-scale mineralogy and texture (Chapter 4). While particulate samples are considered to be more representative than an intact rock sample of the same size (i.e. a drill-core tile or thin section), statistical analyses based on the number of particles per sample indicate that multiple samples of some size fractions are required to be representative. In the sampling theory defined by Pierre Gy particulate samples are further subdivided into lots, particles, increments, samples and subsamples (Pitard, 1993). For the purpose of this research the author acknowledges the work of Gy however particulate samples in this chapter refer to the size fractions outlined in Table 6.1. This is discussed further in section 6.3.

For the purpose of this research, quantified mineralogical and textural attributes have been extracted from images of one thin section of each size fraction (38 samples). Multiple thin sections of each sample are not within the scope of this project. However, it is considered an important next step for the development of automated optical microscopy as a tool for the routine extraction of mineralogical and textural data that could potentially be used to populate block models with more accurate mineralogical and textural information. The results of the particulate rock analyses are presented in this chapter as follows:

- 6.2 Optical microscopy and MLA comparison for particulate rock samples
- 6.3 Sampling statistics
- 6.4 Optical microscopy analysis of particulate rock samples: Cadia East

Microsoft Excel spreadsheets containing all of the data used in this chapter are presented in Appendix 6.1.

6.2 Optical microscopy and MLA comparison for particulate rock samples

The micro-scale mineralogical and textural analysis of particulate samples can be optimised by using the optical microscope and the MLA for the sample types that they are most suited to. The MLA is considered to be more accurate in terms of mineral identification and resolution than the optical microscope and is therefore more suited to finer-grained particulate samples that are below the resolution limitations of the optical microscope (Table 6.1). The automated optical microscope however is faster and cheaper to operate than the MLA and is more suited to coarse-particulate samples with simple mineralogy (i.e. binary, ternary or quaternary composition).

A comparison of the run times and the classification times for each instrument are shown in Table 6.2, the image resolution of the optical microscope is half that of the MLA, however the analysis and classification times are at least 10 times faster. Where the routine analysis of particulate samples using the MLA has been costly and time consuming, the optical microscopy system offers a cost and time effective solution. This is however not without its limitations and a compromise between analysis time, cost and instrument resolution is required and will vary between different ore types and deposit styles.

Table 6.2. Comparison of run times and classification times of the MLA in XBSE mode and the automated optical microscopy system (Berry, 2008).

	Analysis by MLA-XBSE			Optical Microscopy Analysis		
Size Fraction	3.36-2.36mm	1.18-0.85 mm	0.43-0.30 mm	3.36-2.36 mm (R)	1.18-0.85 mm (S)	0.43-0.30 mm (T)
Run time	5 hours 82 frames	8 hours 132 frames	4 hours 108 frames	25 minutes 110 frames	25 minutes 110 frames	25 minutes 110 frames
Classification time	1.5 hours	1.5 hours	1.5 hours	15 minute	30 minutes	60 minutes
Resolution	1 pixel = 2μm for this comparison			1 pixel = 3.94 μm		

In order to show the limitations of each system a sample has been analysed using both the optical microscope and the MLA on three size fractions. From these three size fractions the modal mineralogy results calculated from each mineral map are shown in Table 6.3. The results show that for this sample, quartz/feldspar is underestimated by the optical system and chlorite/biotite is overestimated. The minerals maps of the smaller size fractions overestimate the chalcopyrite and pyrite abundances compared to the MLA. These discrepancies can be attributed to several factors:

- The optical microscope has a lower resolution than the MLA. Figure 6.1 shows the same chalcopyrite PhReg extracted from mineral maps produced from the MLA (left) and the optical microscope (right). The difference in resolution between the instruments is shown by the MLA PhReg exhibiting a more complex boundary.
- Mineral edge effects (described in Chapter 3, section 3.4.2) produced by the optical microscope create mineral edges with optical properties different to those of the mineral itself. This can result in wrongly classified minerals as well as under or overrepresented minerals in a sample.
- Mineral intergrowths (such as chlorite/biotite) especially where the grain size is smaller than the MLA beam size, can lead to the mixed spectra being produced and an increase in invalid or unidentifiable spectra.

The MLA is a quantified analysis and does not solely rely on the mineral identification skills of a geologist. This can be utilized during the initial stages of creating an optical microscopy classification. For example, where an optical classification is not representative of a particular mineral, an analysis of the same sample using the MLA will result in large discrepancies in the mineral abundances between the two analyses. If this occurs, the optical classification can be amended until the error between the two results is reduced.

Table 6.3. Comparison of results determined using the MLA in XBSE mode and the optical microscopy system. The results were obtained using the same three size fractions for CE107 128-130m (Image comparison courtesy of Ron Berry).

	MLA (XBSE)			Optical Microscope		
	-3.36+2.36mm (%)	-1.18+0.85mm (%)	-0.43+.30mm (%)	-3.36+2.36mm (%)	-1.18+0.85mm (%)	-0.43+0.30mm (%)
Chalcopyrite	1.80	1.60	1.90	1.50	1.90	2.20
Pyrite	0.00	0.10	0.10	0.00	0.20	0.10
Quartz/Feldspar	84.70	71.00	63.20	81.10	67.40	61.00
Muscovite	0.70	2.60	2.40	3.10	2.30	3.80
Chlorite/Biotite	10.50	19.10	27.80	12.20	26.10	31.90
Carbonate	0.10	0.40	1.20	1.90	1.60	0.70

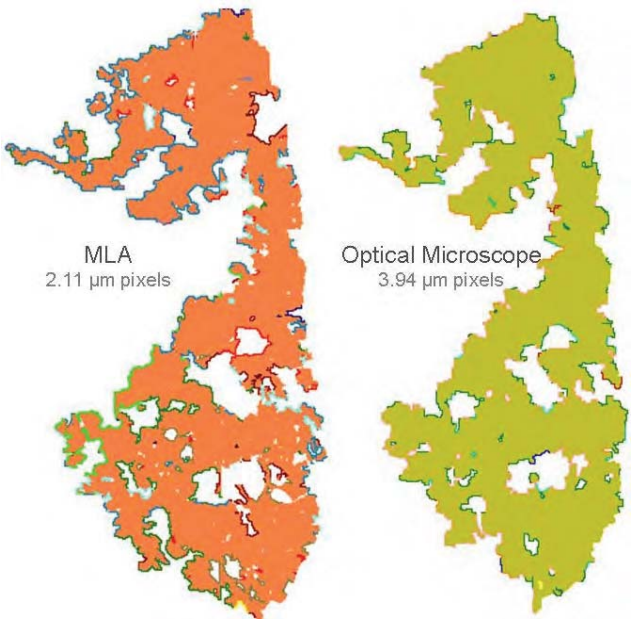

Figure 6.1. Chalcopyrite PhReg extracted from classified mineral maps produced by the MLA (*left*) and the optical microscope (after image analysis; *right*).

There are a number of factors need to be taken into consideration when deciding on which system is most suitable for the routine analysis of particulate samples. These include the cost of the analysis, the time taken to produce and run a sample and the quality of the data that is produced. The only difference in sample preparation is the time taken to carbon coat the sample (approximately 20 minutes). The cost of an MLA system is more expensive than the optical microscope and the maintenance and materials required are much higher in cost. However, the quality of the data is much higher when the correct image resolution and analysis time are allowed. In order to make the MLA more cost effective in terms of fast routine analyses, the image resolution could be reduced and sample run time reduced. This means that less time is taken to collect each mineral spectrum and clean spectra are not produced for comparison to the mineral spectra library. This may result in the misclassification of minerals (mainly minerals with variable compositions such as the micas and silicates). An example of a particulate sample analysed using the XBSE method and a fast run time is shown in Figure 6.2. The areas where the frames join can clearly be seen due to one or both of the minerals on each side of the frame being misclassified. If the minerals were of similar composition e.g. two feldspars, this may not be of such a concern, however in this case the minerals are anorthoclase and illite which have considerably different physical properties. Anorthoclase is a hard mineral with a Moh's hardness of 6 and specific gravity = 2.59 gm/cc, illite is a soft mineral with a Moh's hardness of 1-2 and a specific gravity of 2.75 gm/cc. Considering this it is assumed that these minerals will have very different implications for crushing, liberation and flotation.

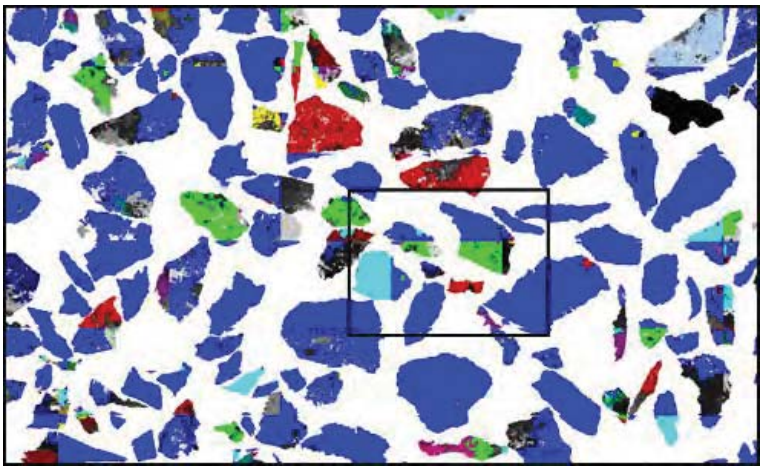

Figure 6.2. Example of a classified image from the MLA using a fast run time. This has resulted in insufficient time to measure a clean spectrum and as a result the minerals have been misclassified on either side of the frame join. Anorthoclase - *dark blue*, illite - *light blue*.

6.3 Sampling statistics

Sampling is the single most important factor in any analytical procedure (Jones, 1987). There are two formulae that can be used prior to sampling in order to reduce error. The first is Gy's sampling theory which is used to calculate the mass of a specimen needed to provide a required degree of accuracy (Pitard, 1993). The second formula is used to calculate the relative error itself, however this formula can be reverse engineered to calculate the number of particles that need to be analysed to be within the acceptable limits of error (e.g. within the 95% confidence interval) for a given mineral of interest. This formula is:

$$N = \frac{4q}{pE^2}$$

Where:
N = number of particle (or point) counts
p = proportion of the selected mineral
q =1-p
E = relative error = e/p
e = 2σ

This formula is only relevant to the proportion of a mineral in a given particle and appropriate where the particles follow a binomial distribution and each particle is independent i.e. p equals the likelihood of an event occurring or not occurring. For the analysis of particulate samples in this chapter, p will be the proportion of particles that contain chalcopyrite (or bornite; calculated independently). When the proportion of particles containing a given mineral is known, the number of particles required to achieve a given relative error can be calculated. The Relative Error (E) is shown in Table 6.4 for various abundances of mineral x (for this research x would be chalcopyrite or bornite). The margins of error at 2 and 3 standard deviations are shown and highlighted grey. The relative errors have been calculated for each size fraction of the 41 samples used in this chapter. The

average relative errors (E%) for chalcopyrite for the size fractions R (-3.36 + 2.36mm), S (-1.18 + 0.85mm) and T (-0.43 + 0.30mm) are 30.97, 18.74 and 13.95 respectively (For detailed results see Appendix 6.2).

There are a number of ways that the error can be improved including reducing the particle size or taking more samples. Within this project, the number of particles can be increased by combining the R, S and T size fractions and hence reducing the error.The error (with respect to mineral proportion) can also be reduced by making p the proportion of particles that contain chalcopyrite or bornite. Based on the average proportions of chalcopyrite, the approximate number of particles that would be required for each size fraction and the number of thin sections that would be needed for the data from the classified images to be representative are shown in Table 6.5. With respect to measuring primary grain size and the shape of minerals within a particle, the particle size must be at least 5 times greater than the expected PhReg size. For example, the S size fraction can only report accurate primary size information for mineral PhRegs <170µm (Table 5.6). Another consideration is that the size fractions that have been used in this research are coarser than the sizes typically used during a detailed mineralogical analysis (MLA). If these coarse particles were to be reduced in size by 50% then the number of particles would increase by a factor of 8. This would result in the T size fraction and a majority of the S size fraction having a relative error of < 5%. This can be achieved quite easily using digital images by using a masking technique. Within the AMIRA P843 project, this technique has been used on XBSE images of particulate samples (Evans, 2011).

The results presented in this chapter are considered to be proof of concept. It is important to recognise that if this new application of optical microscopy is to be implemented as a cheap, routine style of analysis on site, then a larger scale study will be required in the future and a number of considerations taken into account. All textural studies require compromise. For an accurate measure of mineral abundance, a fine grain size gives greater precision without much data loss. However for textural measurements the primary texture must be preserved. For the two mines studied here, the final grind size is ~ 150 µm. In describing texture relevant to this final grind size it is considered essential to have a particle size > 5 × 150 µm. This leads to the compromise of using samples that have small numbers of particles and large sampling errors. The decision here was that a large number of imprecise measurements were preferable to a single high precision number. Gy's formula is relevant to modal abundance. The extension of this formula to other textural parameters such as PhReg size, shape and association is not simple. The best way to estimate such errors is to subsample the measured population and use this to estimate the variance.

Table 6.4. The number of particles (N) required for various proportions of particles that contain mineral x (P) and the relative errors (E). Particle numbers are rounded to the nearest whole number.

Proportion of particles containing mineral x (p)	Number of particles required for Relative Error (E):																
	50%	40%	30%	20%	10%	9%	8%	7%	6%	5% 2σ	4%	3%	2% 3σ	1%	0.75%	0.50%	0.25%
0.005	3184	4975	8844	19900	79600	98272	124375	162449	221111	318400	497500	884444	1990000	7960000	14151111	31840000	127360000
0.01	1584	2475	4400	9900	39600	48889	61875	80816	110000	158400	247500	440000	990000	3960000	7040000	15840000	63360000
0.015	1051	1642	2919	6567	26267	32428	41042	53605	72963	105067	164167	291852	656667	2626667	4669630	10506667	42026667
0.02	784	1225	2178	4900	19600	24198	30625	40000	54444	78400	122500	217778	490000	1960000	3484444	7840000	31360000
0.03	517	808	1437	3233	12933	15967	20208	26395	35926	51733	80833	143704	323333	1293333	2299259	5173333	20693333
0.04	384	600	1067	2400	9600	11852	15000	19592	26667	38400	60000	106667	240000	960000	1706667	3840000	15360000
0.05	304	475	844	1900	7600	9383	11875	15510	21111	30400	47500	84444	190000	760000	1351111	3040000	12160000
0.06	251	392	696	1567	6267	7737	9792	12789	17407	25067	39167	69630	156667	626667	1114074	2506667	10026667
0.07	213	332	590	1329	5314	6561	8304	10845	14762	21257	33214	59048	132857	531429	944762	2125714	8502857
0.08	184	288	511	1150	4600	5679	7188	9388	12778	18400	28750	51111	115000	460000	817778	1840000	7360000
0.09	162	253	449	1011	4044	4993	6319	8254	11235	16178	25278	44938	101111	404444	719012	1617778	6471111
0.1	144	225	400	900	3600	4444	5625	7347	10000	14400	22500	40000	90000	360000	640000	1440000	5760000
0.15	91	142	252	567	2267	2798	3542	4626	6296	9067	14167	25185	56667	226667	402963	906667	3626667
0.2	64	100	178	400	1600	1975	2500	3265	4444	6400	10000	17778	40000	160000	284444	640000	2560000
0.25	48	75	133	300	1200	1481	1875	2449	3333	4800	7500	13333	30000	120000	213333	480000	1920000
0.3	37	58	104	233	933	1152	1458	1905	2593	3733	5833	10370	23333	93333	165926	373333	1493333
0.35	30	46	83	186	743	917	1161	1516	2063	2971	4643	8254	18571	74286	132063	297143	1188571
0.4	24	38	67	150	600	741	938	1224	1667	2400	3750	6667	15000	60000	106667	240000	960000
0.45	20	31	54	122	489	604	764	998	1358	1956	3056	5432	12222	48889	86914	195556	782222
0.5	16	25	44	100	400	494	625	816	1111	1600	2500	4444	10000	40000	71111	160000	640000
0.6	11	17	30	67	267	329	417	544	741	1067	1667	2963	6667	26667	47407	106667	426667
0.7	7	11	19	43	171	212	268	350	476	686	1071	1905	4286	17143	30476	68571	274286
0.8	4	6	11	25	100	123	156	204	278	400	625	1111	2500	10000	17778	40000	160000
0.9	2	3	5	11	44	55	69	91	123	178	278	494	1111	4444	7901	17778	71111

Table 6.5. The numbers of particles and thin sections that are required for a relative error of < 5%. Abbreviations: ccp – chalcopyrite, E – error. Size fractions: R (-3.36+2.36mm), S (-1.18+0.85mm), T (-0.43+0.30mm).

Size Fraction	Average percent of particles with ccp	Average # of particles in a thin section	# of particles required for E <10%	# of thin sections needed to be analysed	Particle size / 5
R	32.07	135	847	6	500 µm
S	18.16	725	1802	3	170 µm
T	7.63	3033	5314		60 µm

6.4 Optical microscopy analysis of particulate rock samples: Cadia East

The rule set for the classification of particulate samples analysed using the optical microscopy system at Cadia East includes 13 minerals or mineral groups (Figure 6.3) as well as potential image artefacts (opaque objects, transparent areas, edge effects, pits) and glue products. The 38 samples that are discussed in this chapter have been taken from same drill-holes that were used for the meso- and micro-scale (intact rocks) analyses at Cadia East (CE082, CE098, CE109, CE110 and CE143). These samples are listed in Table 6.6 with their corresponding Cu, CuCN and Au grades, mineral grades, lithology (as logged by site geologists) and meso-scale textural class (Chapter 4, section 4.5).

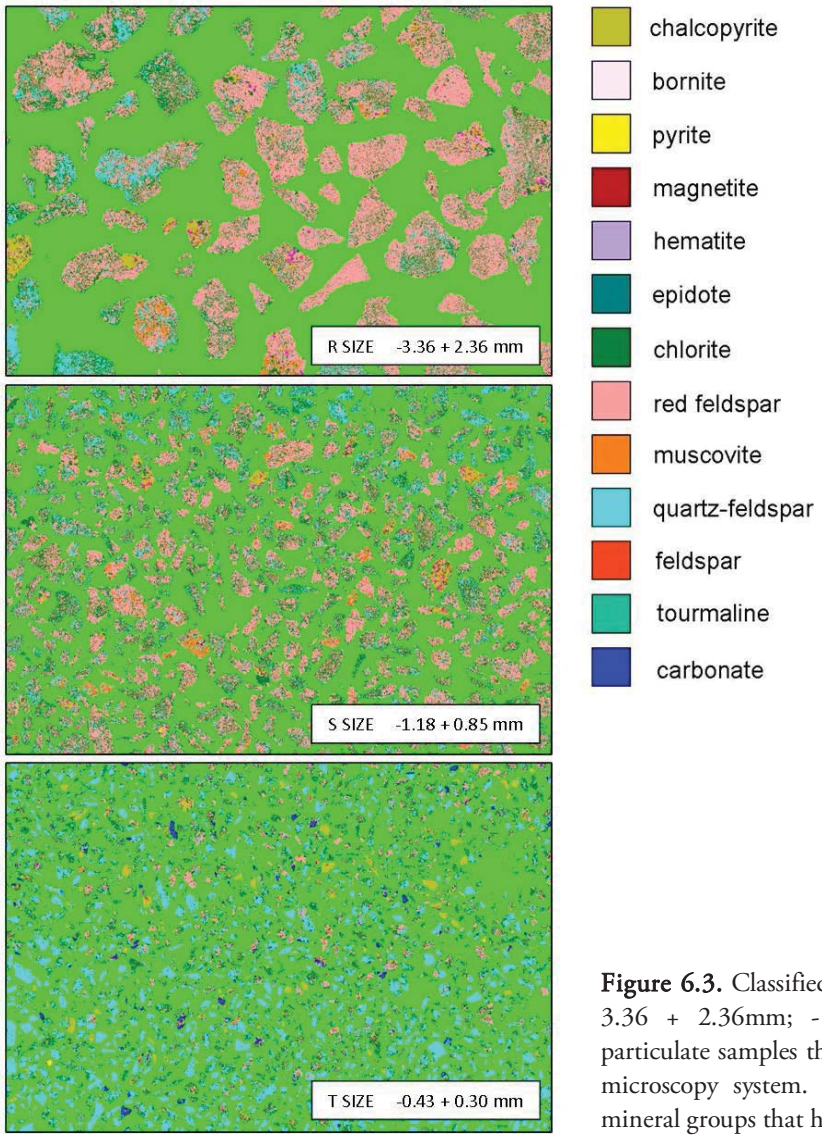

Figure 6.3. Classified mineral maps of the 3 size fractions (-3.36 + 2.36mm; -1.18 +0.85mm; -0.43 +0.30mm) of particulate samples that have been analysed using the optical microscopy system. Also shown are the 13 minerals and mineral groups that have been used in the classification.

Table 6.6. Particulate samples from Cadia East that have been used in this chapter with their associated elemental and mineral grades, lithologies (logged by site geologists) and meso-scale texture class.

Sample	Grade (ppm)			Mineral Grade				Lithology	Meso-scale Texture class
	Au	Cu	Cu CN	Ccp	Bn	Mo	Py		
CE082 190-192m	0.16	5770	316	1.58	0.05	0.01	1.25	Volcanicalstics - conglomerate	M2M
CE082 220-222m	0.16	3910	245	1.06	0.04	0.01	1.23	Volcanicalstics - conglomerate	M2M
CE082 284-286m	0.08	4530	413	1.19	0.07	0.02	0.40	Volcanicalstics - conglomerate	M2M
CE082 300-302m	0.07	3310	488	0.82	0.08	0.01	0.02	Volcanicalstics - conglomerate	V1
CE098 202-204m	0.21	15900	463	4.46	0.07	0.04	0.84	Altered/ Not identifiable	M3C
CE098 218-220m	0.23	10600	795	2.83	0.13	0.00	2.83	Volcanicalstics - conglomerate	M2M
CE098 226-228m	0.85	14400	7027	2.13	1.11	0.03	0.00	Volcanicalstics - conglomerate	M2C
CE098 328-330m	2.89	6990	617	1.84	0.1	0.03	0.10	Volcaniclastics - Bedded	V1
CE098 334-336m	0.42	4090	215	1.12	0.03	0.02	0.15	Feldspar Porphyry	V2
CE109 206-208m	0.87	8310	577	2.23	0.09	0.02	0.80	Feldspar Porphyry / Volcaniclastics - Bedded	M5
CE109 212-214m	0.94	10500	341	2.93	0.05	0.03	0.32	Volcanicalstics - conglomerate	FM1
CE109 218-220m	0.87	12600	331	3.54	0.05	0.05	0.94	Volcanicalstics - conglomerate	FM1
CE109 236-238m	0.45	6430	460	1.72	0.07	0.02	0.94	Volcanicalstics - conglomerate	FM1
CE109 244-246m	0.55	4580	121	1.29	0.02	0.01	1.77	Volcanicalstics - conglomerate	FM1
CE109 254-256m	1.39	13200	401	3.70	0.06	0.03	0.98	Volcanicalstics - conglomerate	FM1
CE109 292-294m	0.9	13700	1275	3.59	0.20	0.05	0.42	Volcanicalstics - conglomerate	MIXED
CE109 302-304m	0.38	8190	295	2.28	0.05	0.03	0.25	Pyroxene – Feldspar Porphyry	FM1
CE109 308-318m	0.92	16000	705	4.42	0.11	0.08	0.76	Pyroxene – Feldspar Porphyry	FM1
CE109 318-320m	0.26	17800	457	5.01	0.07	0.05	0.4	Volcanicalstics - conglomerate	FM1
CE109 358-360m	0.07	24900	1088	6.88	0.17	0.07	1.79	Volcaniclastic	FM1
CE109 366-368m	0.63	22500	559	6.34	0.09	0.01	1.34	Volcanicalstics - conglomerate	MIXED
CE109 388-390m	0.18	3480	410	0.89	0.06	0.00	1.61	Volcanicalstics - conglomerate	MIXED
CE109 434-436m	0.52	4110	213	1.13	0.03	0.01	0.80	Feldspar Porphyry	V1
CE109 442-444 m	0.48	5380	284	1.47	0.04	0.12	0.54	Feldspar Porphyry	V1
CE110 180-182m	0.19	4630	790	1.11	0.12	0.01	0.50	Volcaniclastics - Bedded	MIXED
CE110 230-232m	0.03	1485	199	0.37	0.03	0	3.74	Volcaniclastics - Bedded	M5
CE110 270-272m	0.26	8520	253	2.39	0.04	0.01	2.57	Volcanicalstics - conglomerate	FM1
CE110 350-352m	0.7	15600	404	4.39	0.06	0.01	2.59	Volcaniclastic	FM1
CE143 1138-1140m	0.45	4480	1151	0.96	0.18	0.01	0.00	Feldspar Porphyry	FZ2
CE143 1212-1214m	0.01	2120	213	0.55	0.03	0	0.03	Feldspar Porphyry	V1
CE143 1240-1242m	0.94	8090	631	2.15	0.1	0.03	1.80	Volcanicalstics - conglomerate	M3C
CE143 1282-1284m	0.92	4990	3140	0.53	0.50	0.00	0.05	Volcanics - Massive	M2M
CE143 1316-1318m	1.54	3150	1793	0.39	0.28	0.00	1.55	Volcaniclastic	MIXED
CE143 1338-1340m	3.06	8600	408	2.37	0.06	0.00	3.20	Volcaniclastic	MIXED
CE143 1380-1382m	5.25	5210	662	1.31	0.1	0.00	0.00	Volcaniclastics - Bedded	V2
CE143 1400-1402m	6.39	9000	5183	1.1	0.82	0.01	0.00	Volcaniclastic	V1
CE143 1420-1422m	4.19	6220	1693	1.31	0.27	0.00	0.14	Monzonite	V3
CE143 1448-1450m	0.83	1040	474	0.16	0.07	0.00	0.00	Monzonite	V3

The mineralogical and textural attributes that have been extracted and calculated in the analysis of particulate samples differ from those previously used for the analysis of intact rocks (drill-core tiles and half drill-core; see Chapters 4 and 5). In addition to the attributes measured for the valuable minerals (chalcopyrite and bornite), data regarding the particle shape, size, composition and the degree to which a mineral has been liberated (i.e. how much of the valuable mineral is exposed on the surface) can now be measured. This allows a comparison between the minerals and textures observed in the intact rocks to those that are present in the equivalent particulate samples. The attributes that have been measured for the particulate samples at Cadia East are described in Table 6.7.

Table 6.7. Mineralogical and textural attributes that have been measured for the particulate samples that are presented in this chapter. Each attribute has been calculated for each size fraction (R, S and T).

PARTICLE	Mineralogical and textural characteristic	Measures	Section
	Composition	Percent chalcopyrite and bornite in particle	6.4.1
		Mineralogical composition of particle	
	Size	Area	6.4.2
		Phase Specific Surface Area (PSSA)	
CHALCOPYRITE & BORNITE	Size	Area	6.4.3
	Liberation potential	Percent chalcopyrite and bornite exposed on particle surface	6.4.4

6.4.1 Particle composition

The particle composition is a measure of the mineral components of which each particle consists of. The composition of a sample provides valuable information regarding the potential breakage characteristics the rock in which it came from (Jones, 1987). Different minerals will preferentially break into different size fractions, depending on their hardness, form and cleavage properties. It is predicted that different abundances of minerals and their interactions with each other control the ease with which a rock can be crushed and milled, from which a valuable mineral can be liberated.

In this section the mineralogical composition of particles has been calculated from the classified mineral maps for the R, S and T size fractions of 38 samples (Table 6.6). In order to determine the most commonly occurring particles compositions a PCA was undertaken using all of the particles from the samples (152 353 particles in total). The PCA accounts for 82.10% of the variability in particle composition within the first four principal components (see Appendix 6.2). Figure 6.4 illustrates principal component 1 versus principal component 2 as well as principal component 3 versus principal component 4 for all particles. Areas within each graph have been labeled according to where a particle of a given mineral composition will plot. This figure illustrates that chlorite and red feldspar are the most commonly occurring particle compositions followed by quartz/feldspar, chalcopyrite, bornite and pyrite. Additionally, these plots can be used to illustrate individual samples as well as samples of specific size fractions. Figure 6.5 (*top left*) illustrates the first four principal components plotted for each of the R, S and T size fractions. The changes in particle composition reflect the preferential breakage characteristics of samples from Cadia East during the initial crushing process (King, 2001). In particular, Figure 6.5 shows that for the coarser particles (R size) the particle compositions predominantly consist of red feldspar trending towards particles consisting of several minerals. As the particles become finer (T size), the particles predominately consist of red feldspar, chlorite or a mixture of these two minerals, this is illustrated by the tie line between these two minerals.

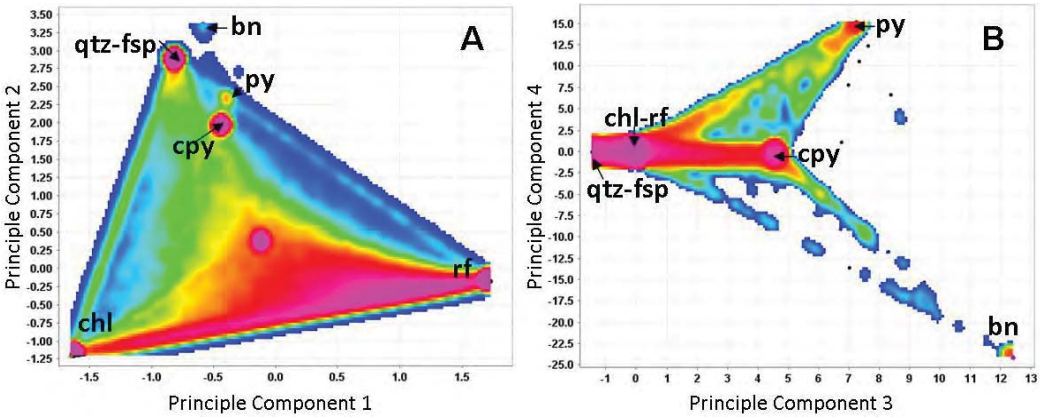

Figure 6.4 PC analysis of particle composition. **A.** Principal component 1 versus principal component 2 **B.** Principal component 3 versus principal component 4. n=152 353 particles. Mineral abbreviations: bn-bornite; chl-chlorite; cpy-chalcopyrite; fsp-feldspar; py-pyrite; qtz-quartz.

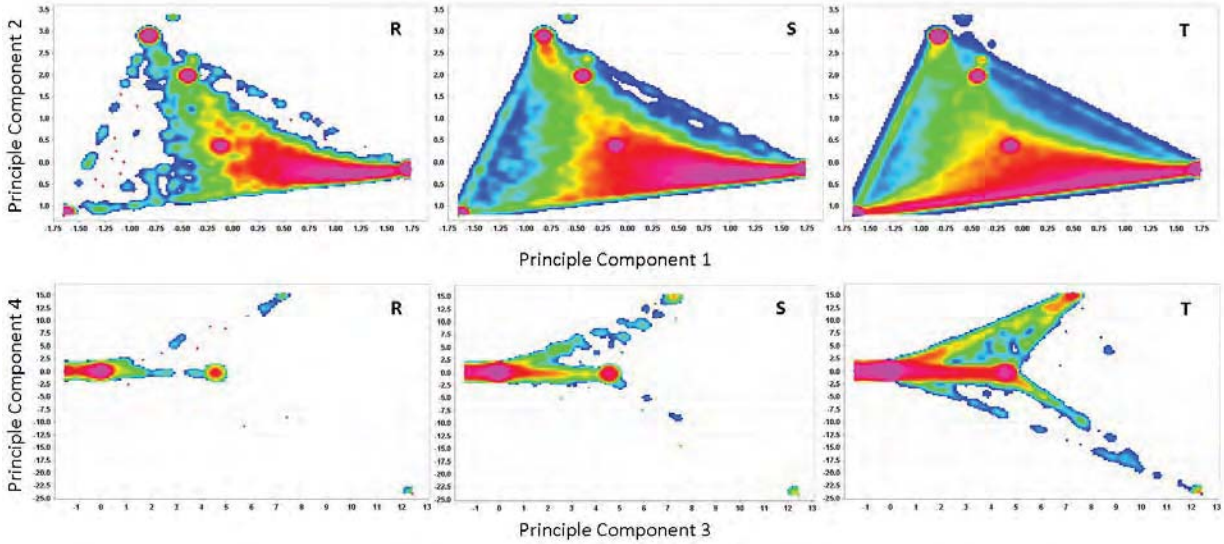

Figure 6.5. The mineralogical variability for the particles sizes R, S and T as determined using a PCA. For mineral positions refer to Figure 6.4.

Based on the particle compositions determined from Figures 6.4 and 6.5 each particle has been assigned a name based on their mono- or multi- mineralogical composition. Each particle has been assigned a mineral composition where it contains ≥ 90% of the mineral or mineral components. The area percent of each particle composition in a sample has been calculated (Appendix 6.3); the most abundant particle compositions are red feldspar-chlorite (36.67%), red feldspar-quartz/feldspar-chlorite (32.99%), chlorite-muscovite-red feldspar (7.03), red feldspar (3.23%), red feldspar-chlorite-chalcopyrite (2.26%) and chlorite-quartz/feldspar (1.46%). All other particle compositions consist of <1.00% of the total particle population. While these are the most common particle compositions it is expected that each sample will contain varying proportions of these particle types (especially where multiple textures are present within the one sample).

Previously in Chapter 4, 13 different meso-scale textures were identified. Of the 38 particulate samples that were analysed using optical microscopy, nine of the meso- texture classes were present (the textures not present are M1, M3M, M4 and FZ1). For each of these textures the average area percent of the most common particle composition types were calculated; these results are shown in Table 6.8 and illustrated in Figure 6.6. Considering that the coarse particulate size, the

mineral compositions of these particles are considered to represent the stronger mineral components of the rock and are predicted to be the minerals that will need to be reground and hence require more energy to process.

Table 6.8. The average abundance of particle compositions for each of the meso-scale texture classes recognised in the particulate samples (see Chapter 4).

Meso-scale texture class	SIZE	M2M	M2C	M3C	M5	FM1	V1	V2	V3	FZ2
Number of samples		5	1	2	2	11	6	2	2	1
Red feldspar- chlorite	R	55.18	9.32	34.66	59.46	26.44	27.53	36.96	0.97	25.77
	S	52.66	4.74	40.61	49.51	24.76	45.37	54.74	48.94	73.73
	T	68.43	6.51	43.61	53.91	29.24	47.91	32.71	43.21	77.74
Red feldspar- quartz/feldspar- chlorite	R	15.53	48.93	51.72	11.45	44.40	41.96	22.28	47.95	63.33
	S	19.75	46.85	27.87	27.45	38.02	24.44	24.95	38.83	3.60
	T	10.14	54.18	35.36	16.36	30.94	19.95	51.21	32.76	0.38
Chlorite- muscovite- red feldspar	R	12.00	22.68	4.26	14.79	4.79	6.13	0.12	4.42	0.00
	S	6.14	15.46	9.40	8.41	5.82	8.75	4.36	1.91	6.17
	T	6.83	8.42	2.21	13.79	9.08	9.36	5.37	2.96	11.22
Red feldspar	R	7.94	0.00	2.24	6.83	0.88	3.95	19.98	0.01	0.00
	S	8.58	0.03	0.79	4.12	0.51	9.64	5.37	2.39	12.41
	T	3.63	0.45	1.60	4.76	1.05	5.40	2.64	5.37	2.34
Red feldspar- chlorite- chalcopyrite	R	0.91	4.19	0.14	0.70	4.74	1.04	0.00	0.00	5.86
	S	1.37	0.77	4.59	3.14	3.39	0.81	0.46	0.36	0.55
	T	2.29	0.97	3.71	1.13	3.41	1.70	0.56	0.51	0.93
Chlorite- quartz/feldspar	R	0.00	1.31	1.91	0.00	0.94	0.48	0.43	0.00	0.06
	S	0.03	0.42	0.18	0.49	4.87	0.15	0.09	0.18	0.00
	T	0.06	0.22	0.25	0.01	4.63	0.30	1.51	1.80	0.00
Chalcopyrite- chlorite- muscovite- red feldspar	R	0.00	4.46	0.56	2.08	2.16	1.22	0.00	4.09	0.00
	S	1.50	0.54	0.41	0.75	0.99	0.32	0.28	0.00	0.56
	T	0.41	0.81	0.50	0.98	0.92	0.32	0.04	0.00	0.59
Red feldspar- quartz/feldspar- muscovite	R	0.12	0.00	0.00	0.00	0.00	0.44	0.00	5.65	0.00
	S	0.22	4.04	1.38	0.00	5.82	0.31	0.63	0.11	0.00
	T	0.08	4.42	0.20	0.17	9.08	0.51	0.48	0.23	0.00
Quartz/feldspar	R	0.00	0.00	0.01	0.00	0.45	0.24	0.00	0.72	0.03
	S	0.00	0.01	0.62	0.00	2.70	0.09	0.12	0.59	0.00
	T	0.04	0.28	0.63	0.05	1.41	0.22	0.11	1.67	0.00
Red feldspar- muscovite	R	0.22	0.50	0.00	0.00	0.06	0.02	0.00	1.41	0.00
	S	1.30	1.63	0.00	0.15	0.14	1.54	0.33	0.18	0.15
	T	1.57	1.34	0.28	1.86	0.64	1.12	0.71	0.30	1.34
Red feldspar- quartz/feldspar	R	0.00	0.00	0.00	0.00	0.00	0.00	0.01	2.64	0.02
	S	0.18	0.09	0.37	0.00	0.53	0.78	0.17	0.54	0.01
	T	0.24	1.00	0.25	0.13	0.61	0.88	1.66	1.67	0.00
Chlorite	R	0.01	0.00	0.00	0.01	0.00	0.00	0.00	0.00	0.01
	S	0.25	0.01	0.05	0.02	0.06	0.03	0.01	0.03	0.02
	T	1.28	0.04	0.35	0.32	1.27	1.58	0.11	0.14	0.41
Chalcopyrite	R	0.00	0.00	0.00	0.00	0.11	0.00	0.00	0.00	0.00
	S	0.02	0.00	0.12	0.00	0.08	0.09	0.00	0.00	0.00
	T	0.06	0.00	0.29	0.02	0.49	0.42	0.02	0.13	0.25
SUM	R	91.91	91.39	95.50	95.32	84.97	83.10	79.78	67.86	95.08
	S	92.00	74.59	86.39	94.04	87.69	92.29	91.51	94.06	97.20
	T	95.06	89.24	89.24	93.49	92.77	89.67	97.13	90.75	95.20

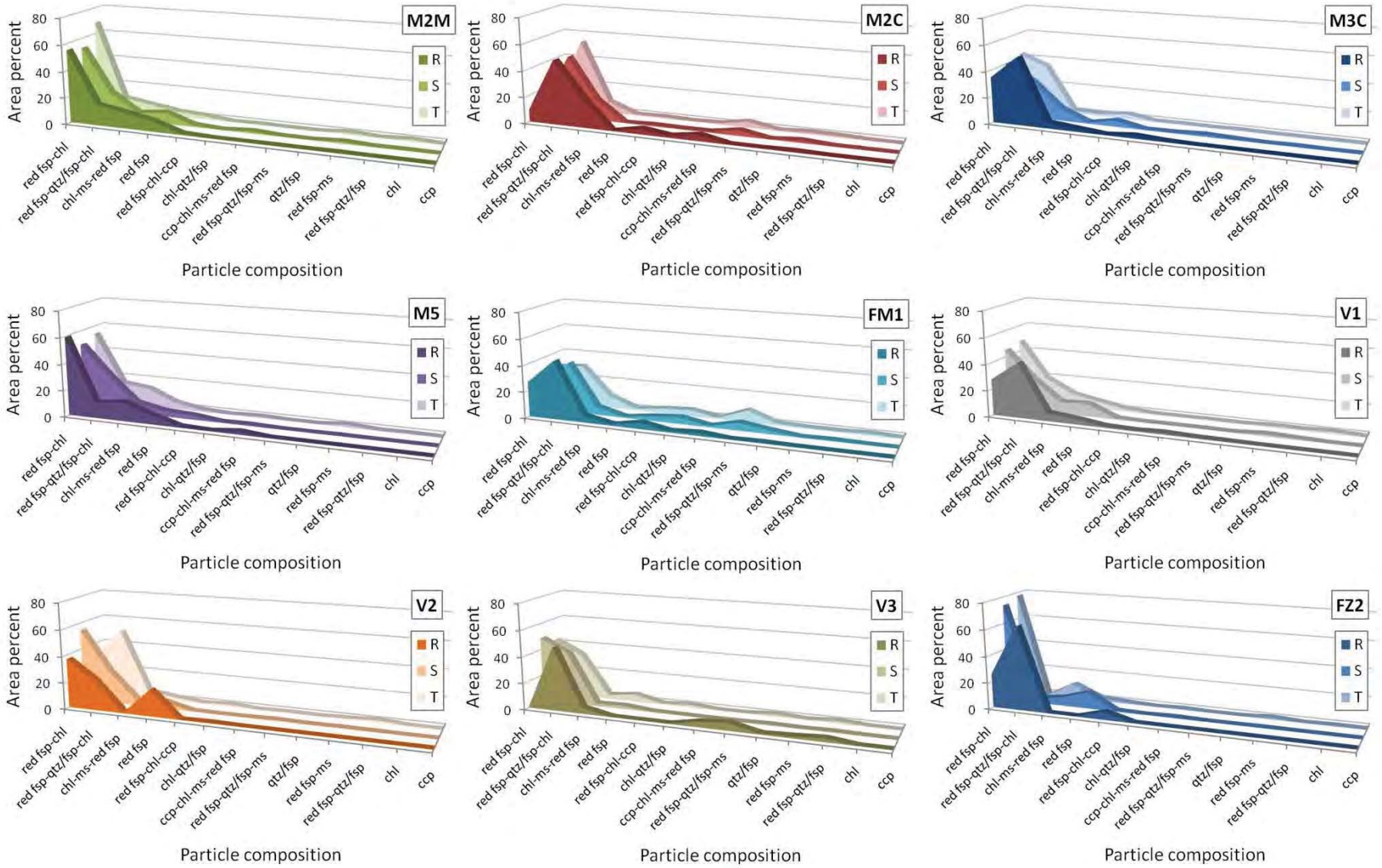

Figure 6.6. Area percent of particle compositions for each of the meso-scale texture classes (see Table 6.9). For mineral abbreviations refer to Appendix 1.1.

6.4.2 Particle size

The size of particles and their distributions are commonly used in the calculation of rock strength parameters used in the routine physical tests undertaken by mining companies (Wills and Napier-Munn, 2006). In this research, the size of each of the particles for each size fraction and sample have been measured as the particle area (converted to an ECD) as well as the Phase Specific Surface Area (PSSA; see chapter 2, section 2.6.1). However, given that only three size fractions have been analysed using the optical microscope there is insufficient data to observe any significant changes in distribution of particle size. If these data were to be used for this purpose in the future it would either need to be integrated with the results of particle size from the MLA or require the measurement of additional coarse size fractions that can also be measured using the optical microscope (i.e. > 0.3mm). In addition to this the use of sieved samples means that any variations in PSSA are likely to only be a measure of how much a given particle shape deviates from a sphere. It is for this reason that the results regarding particle size have been omitted from this chapter.

6.4.3 Size of chalcopyrite and bornite

The size of the target (valuable) minerals (chalcopyrite and bornite) has a strong impact on the degree of liberation that will be achieved when an ore is ground into different size fractions (e.g. Schaik et al., 2004). For example, if the size of the intact chalcopyrite is fine, then the exposure of chalcopyrite on a particle surface will increase as the particle size is reduced. Therefore, it is expected that the coarse-grained generations of chalcopyrite or bornite such as those identified in drill-core as coarse-grained clots and vein-hosted will exhibit a higher degree of liberation than the fine-grained disseminated chalcopyrite (see Chapter 4, section 4.2.1). In this section, the size of chalcopyrite and bornite have been measured as area (pixels) and then converted to an ECD (see Chapter 2, Figure 2.5). It is expected that a reduction in particle size will also result in the reduction of chalcopyrite size given that the area of the chalcopyrite (or bornite) cannot exceed the area of the host particle. Figure 6.7 shows the size distribution trends of chalcopyrite and bornite for the R, S and T size fractions (from all 38 samples). For the 75-150 µm size fraction it is predicted that at a grind size of 150 µm (as at Cadia East) a PhReg of chalcopyrite or bornite with a size of 75 µm will be exposed on the surface in most cases. In Figure 6.7 it is shown that:

- 79.08% of the chalcopyrite within the T-sized particles have an ECD > 75µm
- 81.30% of the chalcopyrite within the S-sized particles have an ECD > 75µm
- 82.81% of the chalcopyrite within the R-sized particles have an ECD > 75µm
- 40.14% of the bornite within the T-sized particles have an ECD > 75µm
- 11.01% of the bornite within the S-sized particles have an ECD > 75µm
- 36.74% of the bornite within the R-sized particles have an ECD > 75µm

A second influencing factor is whether the copper sulphide minerals are clustered or isolated. It is predicted that these effects will vary between different texture classes.

It is expected that the size of chalcopyrite and bornite will reduce with a reduction in particle size. However the degree that the chalcopyrite size will reduce and how amenable to liberation and flotation that it is, is considered to be a function of the particle texture and its mineral components. Figure 6.8 and 6.9 shows the changes in the size of chalcopyrite and bornite minerals respectively for

each of the R, S and T size fractions. For chalcopyrite, the texture classes M2M, M5, V1 and V2 showed the most reduction in PhReg size with particle size with texture classes FM1, M2C and V3 exhibiting similar size distribution trends across the R, S and T size fractions. For bornite, Figure 6.9 shows that texture class V1 is the only class to contain coarse-grained bornite, with all other classes, particularly FM1, M3C and M5 containing very fine-grained bornite. This has direct implications for bornite liberation potential. Where the bornite is very fine-grained, unless it is clustered together with other Cu-sulphide minerals, it is unlikely to be exposing enough of the particle surface to be picked up during flotation process.

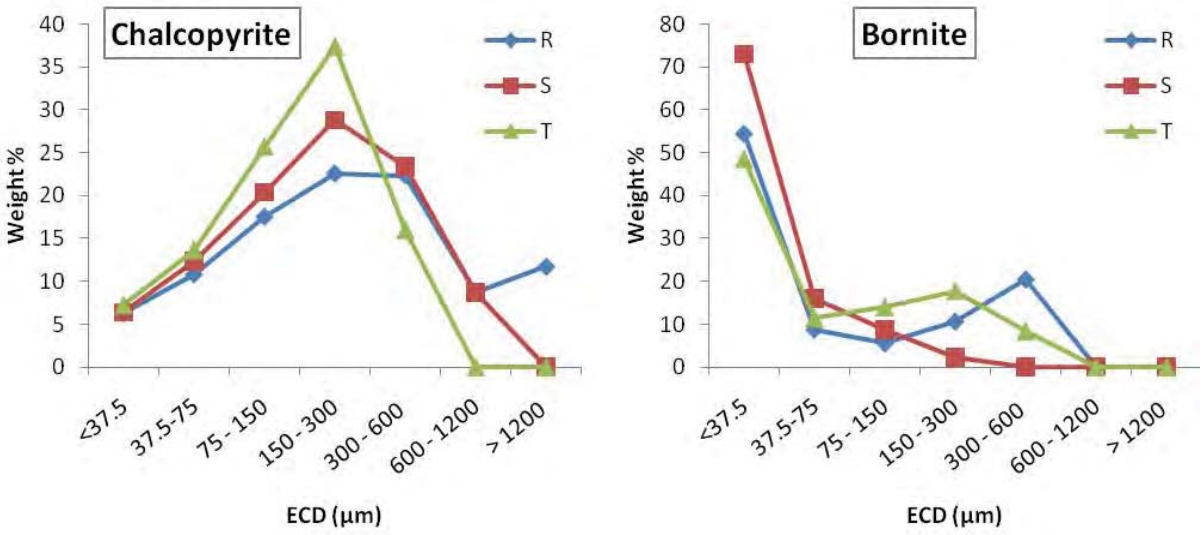

Figure 6.7. Size distribution trends for chalcopyrite and bornite for size fractions R, S and T. The size has been measured as an ECD and each PhReg has been weighted as a proportion of the total size fraction sample. N = 17884 (chalcopyrite R size), 16751 (chalcopyrite S size), 19374 (chalcopyrite T size), 6373 (bornite R size), 4885 (bornite S size), 4776 (bornite T size).

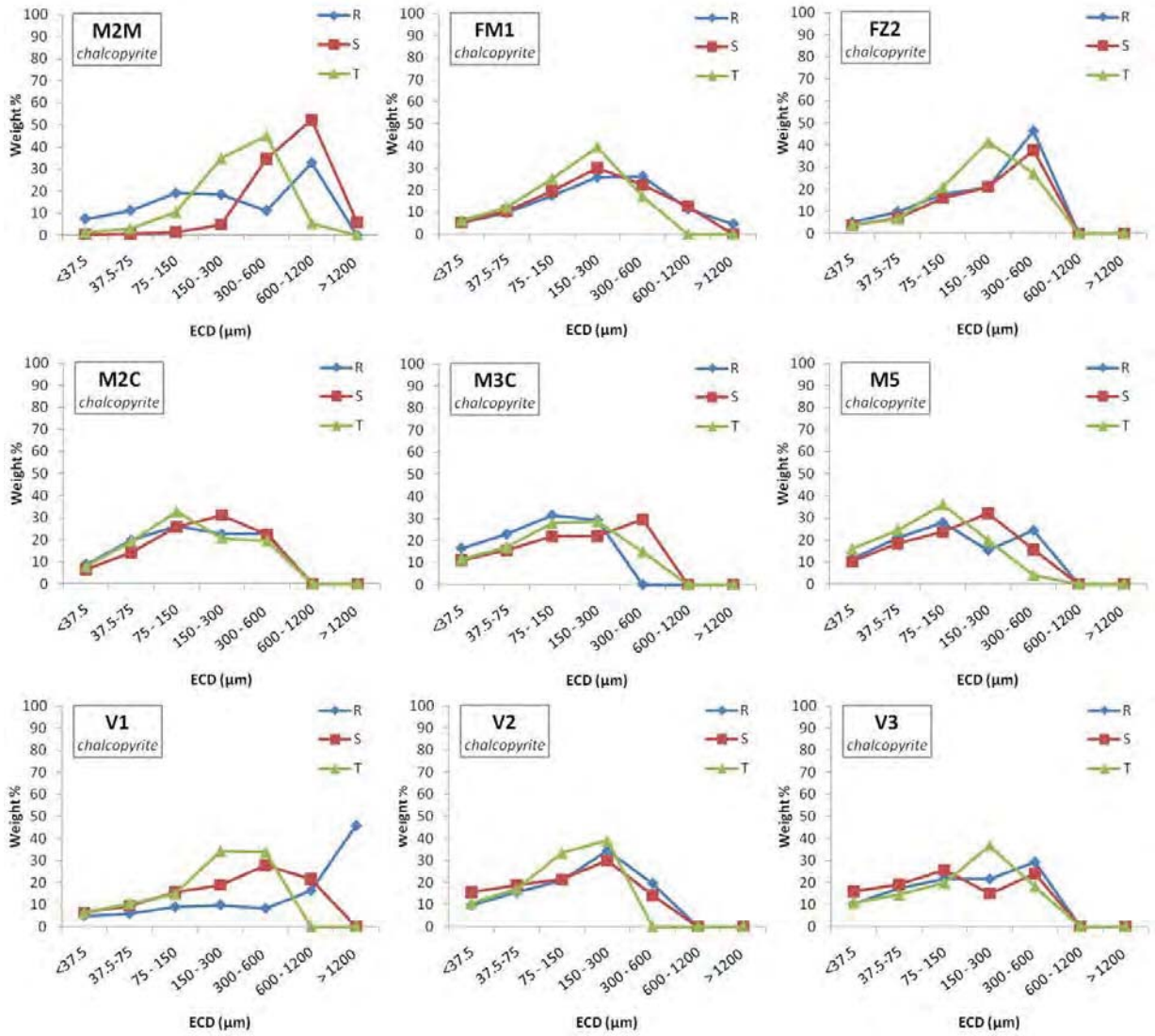

Figure 6.8. The size distribution trends of chalcopyrite for the R, S and T size fractions of each of the nine texture classes represented in the particulate samples (see Table 6.7).

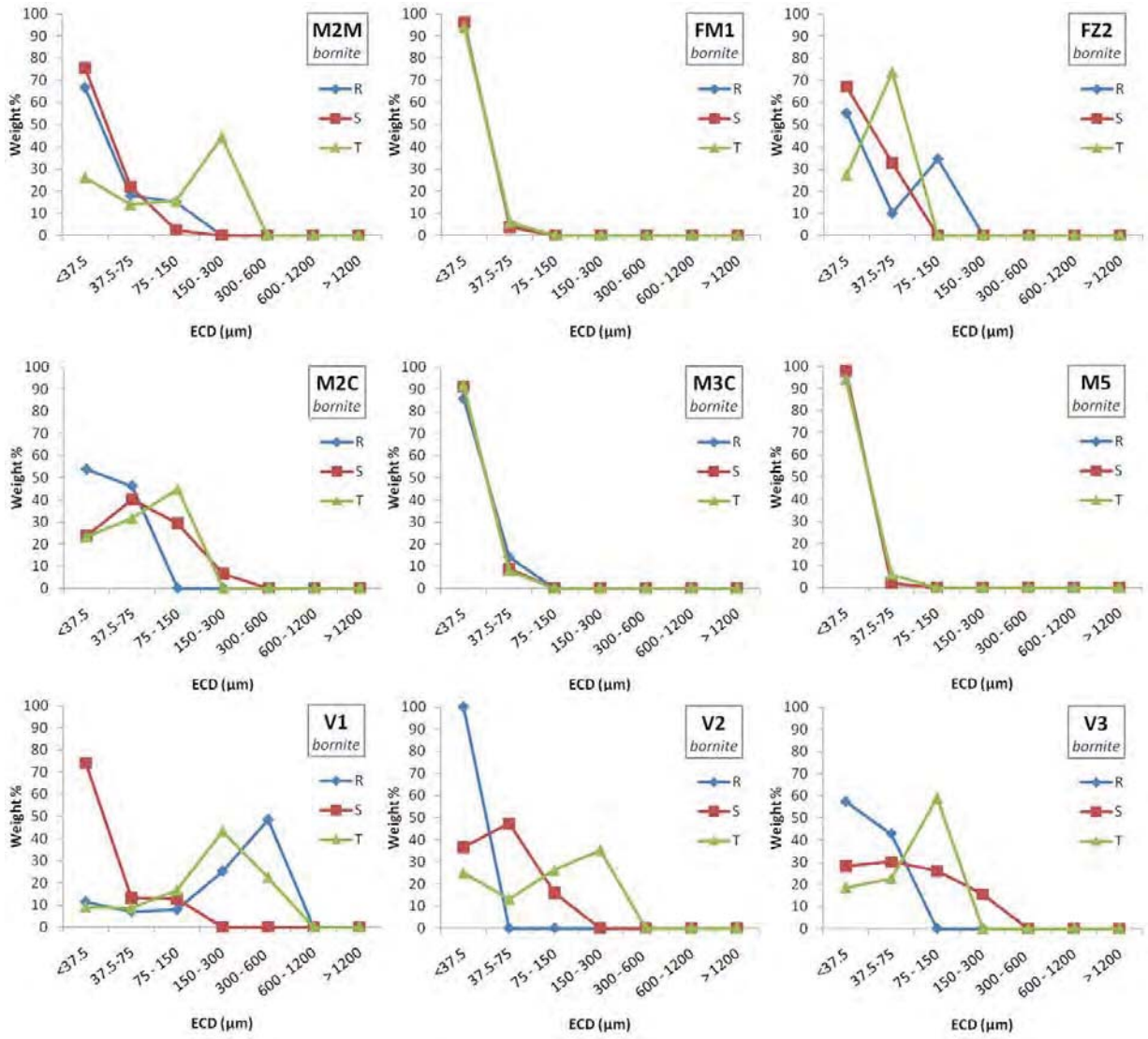

Figure 6.9. The size distribution trends of bornite for the R, S and T size fractions of each of the nine texture classes represented in the particulate samples (see Table 6.7).

6.4.4 Particle surface exposure of liberated chalcopyrite and bornite

The exposed surface of a mineral that is required for successful flotation and recovery is dependent on the mineral type. For chalcopyrite, which is considered to be 'free floating', the percent of chalcopyrite that is required to be exposed on the particle surface is 25% (Professor Dee Bradshaw, pers. comm.). Other factors that may influence the liberation potential of a particle are the distribution of the copper sulphide minerals within that particle. For example, are there multiple fine-grained copper-sulphide minerals exposed on the particle surface or one coarse grain? Are the copper-sulphide minerals completely encapsulated within the particle? The measures of liberation that have been used for the Cadia East particulate samples are described in Table 6.9. These results have been compiled based on their meso-scale texture class in order to assess whether some textures exhibit a greater liberation potential than others (Table 6.10). The surface exposed has been calculated as a combined total of bornite and chalcopyrite. The weight percent of particles with >25% of the surface area liberated, <25% of the surface area liberated and the particles where the copper sulphide minerals are completely locked for chalcopyrite and bornite respectively.

Table 6.9. Descriptions of measures of liberation potential and their implications for mineral processing behaviours.

Measurements of liberation potential	Implications
Particle perimeter consists of > 25% chalcopyrite and bornite	Likely to float and be recovered
Average number of chalcopyrite and bornite objects within a particle	Provides an indication of the chalcopyrite and bornite distribution within the particles
Particle perimeter consists of < 25% chalcopyrite and bornite	Unlikely to float and be recovered. May require grinding to a smaller particle size
Percentage of locked chalcopyrite and bornite	Will not float. Will require grinding to a smaller particle size to be recovered

Table 6.10. Results of the analyses of chalcopyrite and bornite exposed on the particle surfaces of the R, S and T size fractions for each of the meso-scale texture classes (see Table 6.6). Mineral abbreviations: ccp – chalcopyrite; bn – bornite.

TEXTURE CLASS	Particle Size	N (PhRegs)		Average number PhRegs per particle		Median number PhRegs per particle		Percent of sample with ccp +bn exposed on particle surface >25%		Percent of sample with ccp + bn exposed on particle surface <25%		Percent of sample with ccp + bn locked within the particle	
		ccp	bn	ccp	bn	ccp	bn	ccp	bn	ccp	bn	ccp	bn
M2M	R	1119	454	6.87	6.78	2	3	26.22	21.31	69.16	55.98	4.63	22.71
	S	1970	655	3.62	3.20	2	2	49.88	33.87	46.54	57.56	3.58	8.57
	T	2079	175	2.20	1.67	1	1	55.28	15.95	42.05	81.60	2.67	2.45
M2C	R	458	130	8.33	5.20	4	3	0.04	0.00	90.25	59.30	9.71	40.70
	S	436	252	2.58	2.96	2	2	9.87	3.85	80.75	75.89	9.38	20.26
	T	557	245	1.98	2.29	1	1	29.75	19.71	57.46	61.31	12.79	18.98
M3C	R	878	248	13.72	8.86	2	7	0.25	0.00	90.57	77.67	9.19	22.33
	S	2144	283	4.47	2.48	2	1	48.53	42.72	47.64	51.65	3.83	5.63
	T	2562	448	2.39	2.24	1	1	50.21	54.00	46.90	43.80	2.89	2.20
M5	R	879	227	7.51	4.20	3	2	0.18	0.15	92.01	93.38	7.80	6.47
	S	1019	214	2.35	3.71	2	1	17.20	10.38	72.43	68.03	10.38	21.59
	T	1075	135	1.99	1.38	1	1	44.60	30.02	48.63	59.74	6.77	10.24
FM1	R	7038	3330	11.21	11.85	1	1	24.11	23.36	73.46	73.90	2.43	2.74
	S	6377	2021	3.59	3.39	2	2	55.72	51.44	41.46	44.18	2.82	4.38
	T	9240	2816	1.89	2.10	3	4	73.53	71.69	24.93	25.53	1.54	2.77
FZ2	R	215	87	13.44	12.43	3	6	0.00	0.00	78.55	79.47	21.45	21.43
	S	107	52	3.24	3.47	2	2	69.95	43.65	27.69	41.07	2.36	15.28
	T	146	4	20.9	1.00	1	1	85.62	23.08	13.17	76.92	1.21	0.00
V1	R	1735	608	8.90	6.68	3	2	61.60	3.64	35.18	84.86	3.23	11.50
	S	1239	244	3.28	2.52	2	1	60.75	39.41	36.13	47.20	3.13	13.39
	T	1890	341	1.76	1.79	1	1	76.53	85.54	21.34	14.07	2.13	0.39
V2	R	237	33	8.46	3.00	3	1	0.04	0.00	80.21	83.13	19.75	16.87
	S	365	40	3.15	2.86	2	1	32.73	83.50	61.15	16.50	6.13	0.00
	T	331	50	2.03	1.79	1	1	44.64	8.16	49.52	90.41	5.85	1.43
V3	R	718	110	17.10	7.33	3	2	0.10	0.00	95.21	95.45	4.69	4.55
	S	235	110	2.53	1.96	1	1	30.49	33.04	60.28	52.89	9.23	14.07
	T	311	66	1.92	2.07	1	2	72.48	55.73	23.37	39.90	4.14	4.37

In terms of liberation and recovery potential, the ideal situation for an ore type would be 100% of the chalcopyrite and bornite exposed on >25% of the particle surfaces and no Cu-sulphide minerals completely locked within particles. For chalcopyrite, the meso-scale texture classes with the most favorable liberation potential are V1, FM1, M2M, FZ2, M3C, V3 and V2 respectively. For bornite, the meso-scale texture classes with the most favorable liberation potential are FM1, V1, M3C, V3 and M2M respectively.

6.5 Summary

The analysis of particulate rock samples has allowed mineralogical and textural information to be extracted from samples that are considered to be more representative than non-particulate samples. In this chapter, particulate samples were analysed using optical microscopy images. The optical microscope provides a faster and cheaper alternative to the MLA, making it more amenable to becoming a cost-effective platform for the routine analysis of particulate samples on site. As discussed in section 6.2, the optical microscopy method still requires a skilled operator and needs to be cross validated with more accurate methods such as the MLA in BSE mode. In this section three size fractions were analysed for a total of 38 samples (Table 6.7) from Cadia East. Of these samples nine of the meso-scale texture classes outlined in Chapter 4 (section 4.5) were present. Using the image analysis software Definiens Developer, quantified information regarding the particle composition, particle size, chalcopyrite and bornite size as well the degree of liberation were extracted.

In order to establish the most commonly occurring particle composition types for Cadia East, a PCA was performed on a total of ~152 000 particles. This determined that the most dominant particle composition types were red feldspar-chlorite, red feldspar-quartz/feldspar-chlorite, chlorite-muscovite-red feldspar, red feldspar and red feldspar-chlorite-chalcopyrite respectively. The distribution of these particle compositions was shown to vary between meso-scale texture types (Table 6.8) and between particle size fractions. For particle size, the PSSA was also measured for each sample as well as being compiled for each meso-scale texture class. This analysis showed that texture classes M2C and M5 had the lowest overall PSSA, indicating the lowest exposed surface area compared to particle area of all of the textures and hence the lowest liberation potential.

In order to measure the liberation potential of the particulate samples, the size of the chalcopyrite and bornite within the particles was analysed as well as the percentage of chalcopyrite and bornite exposed on the particle surface. This found that for all textures, the percent of Cu-sulphide minerals exposed on the particle surface increased with decreasing particle size. This also confirmed that texture does have an influence on liberation potential with the meso-scale texture classes V1, FM1, M2M and M3C exhibiting greater liberation potential.

Chapter Seven

Discussion and Conclusions

7.1 Introduction

The analysis of ore types using image classification and analysis has a significant advantage in the production of quantified mineralogical and textural information suitable for predicting variability in mineral processing behaviours. Combining image analysis software with automated microscopy platforms and the GEOTEK MSCL, has proved to be a powerful means for the routine collection of mineralogical and textural information relevant to the mining environment. The challenges that arise from the integration of multiple measurements platforms and the data obtained at different scales and sample sizes are discussed in this chapter (section 7.2). The conclusions that have been drawn from this research are summarised in section 7.3. Finally, recommendations for further work regarding mineralogy and texture in the field of geometallurgy are in section 7.4.

7.2 Integration of meso- and micro- scale information

The aim of this research was to establish whether quantified mineralogical and textural information can be used to predict changes in the mineral processing behaviours of Cu-Au style deposits. Several methods were tested across meso- and micro-scales (GEOTEK MSCL, optical microscopy and Mineral Liberation Analyser). The technologies were selected based on their potential to produce high resolution classified digital images. Semi-quantitative and quantitative mineralogical and textural information was extracted. The integration of these technologies and their data is fundamental if the routine analysis of mineralogy and texture are to be implemented in the mining industry. There are a number of challenges in comparing and using the data from the multiple sources tested in this research. These include:

- sample type: intact rock samples versus particulate rock samples
- scale: meso-scale versus micro-scale
- instrument resolution and accuracy, and

- the selection of a method that is suitable to a specific ore type

Sample selection type

Sample selection is the one of the most important decisions regarding any type of analytical procedure. With respect to extracting quantified mineralogical and textural data, there are several key factors that will influence the type of sample that will be selected for imaging. These are:

- What is the purpose of the data that will be collected? For example, if the data is being collected to populate a block model with mineralogical and textural parameters then representative samples need to be collected routinely, therefore particulate samples should be used.
- What data resolution is required? For example, if the data being collected is to determine the mineralogical associations of chalcopyrite with a diameter of <50 μm, then classified SEM images would be recommended and not high resolution meso-scale images.
- How many samples will need to be collected for the data to be statistically valid? This is particularly important where data is being integrated into a working block model and the data needs to be valid and JORC (Joint Ore Reserves Committee) compliant. This decision could have financial implications if the number of samples required becomes too expensive to maintain on a routine basis.
- What mineralogical and textural information is to be measured? For example, if data is required about the grain size prior to breakage then a large particle size is required to avoid modifying the measured parameter during sample preparation.

Meso-scale versus micro-scale

The scale of the geological features that is measured is not only important with respect to knowing the size limitations of the sample preparation, but also in determining how the data extracted can be used. The factors that need to be considered here are:

- What other types of mineralogical data can meso- or micro-scale data be compared to? This is an important factor to consider with respect to the validation of mineralogical and textural results. For example, assay data can be used to validate the precision of meso-scale classification rule set. Alternatively, the MLA can be used to validate an optical microscopy image analysis method. Other data available for comparison include geochemical analyses, qXRD data, and electron microprobe and laser ablation analyses.
- Can the results from two different sample types be compared to each other? This is particularly important considering that the interval each sample is taken from may be significantly different. For example, the results obtained from a classified mineral map measuring one meter could not be directly compared to the results of an SPL-lite image of a 3 x 3cm drill-core tile. The main issue is the representivity of a 3 x 3 cm image.

Instrument resolution and accuracy

The resolution and accuracy of an instrument is extremely important in determining the limitations of the results that an instrument will produce. For example, a classified image with a 50 μm pixel

width will not provide data for any minerals with grain size <50 μm. Key consideration regarding instrument resolution and accuracy include:

- Knowing the instrument precision and accuracy of the measurement platform
- Knowing the resolution of the classified mineral map that will be produced
- Selecting the measurement platform suitable for the level of mineralogical and textural information required.

Selecting a method suitable to an ore type

A significant part of successfully analysing rocks for their mineralogical and textural attributes is the selection of the analytical techniques suited to the mineralisation style and data required. In addition to this, familiarity with the limitations of the techniques and instruments that are being used is extremely important. For Cadia East and Ernest Henry, analytical techniques were selected based on the styles of mineralisation determined through the visual logging of drill-core as well as the sample types that were available. These are outlined in Table 7.1.

Table 7.1. Summary of the techniques used for the analysis of minerals and their textures.

Textural scale	Analytical technique	Cadia East	Comments	Ernest Henry	Comments
Meso-	Visual logging of drill-core	Yes	NA	Yes	NA
	Machine-based logging, GEOTEK MSCL	No	Cadia East was the first site to undergo this method. As a result the outcomes were considered to be not fit for purpose and significant changes to the camera, lighting and image processing were made.	Yes	The image classification process worked particularly well at Ernest Henry due to the contrast in mineral colours within the rocks making it easier to distinguish between minerals
	Chemical assay	Yes	Routine analysis by Newcrest	Yes	Routine analysis by Xstrata
Micro-	Optical microscopy (intact rocks)	No	The alteration mineralogy and grain size was too fine in the rocks from Cadia East in their intact form. As a result this method was considered not amenable for this deposit.	Yes	The euhedral nature of the pyrite and magnetite crystals at Ernest Henry made the sulphide and oxide minerals at Ernest Henry particularly amenable to this technique.
	MLA (intact rocks)	Yes	NA	Yes	NA
	Optical microscopy (particulate rocks)	Yes	NA	No	Not within the scope of this project.
	MLA (particulate rocks)	No	The analysis of particulate samples ranging between 150 μm and <38 μm has been undertaken by Cathy Evans (Evans, 2010) as another part of AMIRA P843 project linking textural attributes to flotation behaviours.	No	The analysis of particulate samples using the MLA was not within the scope of this project.

7.3 Conclusions

The aim of this research was to develop a method for the quantified measurement and characterisation of mineralogical and textural attributes that can be used to predict variability in the mineral processing behaviours of copper-gold deposits. In order to achieve this outcome several new and emerging technologies were utilised including automated SEM-MLA and optical microscopy platforms as well as high resolution digital images combined with object-oriented image analysis software. Within this research classified mineral maps were produced at the meso- and micro- scales from these platforms and analysed to produce a large volume of quantified mineralogical and textural information. Presented in this section are the main outcomes from this research and the independent outcomes for Cadia East and Ernest Henry.

The main outcomes from this research are:

- The development of a method for the logging of mineralogical and textural attributes in drill-core relevant to mineral processing behaviours. Through the careful consideration of mineralogical and textural features observed at the meso-scale in drill-core, semi-quantified estimates of parameters were measured and integrated over assay intervals. Textural parameters were compared to chemical assays and other geological parameters such as alteration, lithology and structure. Several textural classes were established that correlate with liberation behaviour.
- The development of a method that utilises classified mineral maps from different measurement platforms across the meso- and micro scales. Within this research mineral maps were created using high resolution digital images from the GEOTEK MSCL (continuous core images with data integrated over assay intervals), multiple digital images from the automated Leica DM6000 automated optical microscope and the SEM-MLA in SPL-lite mode. This step was extremely important in the success of this research and allowed quantified information about both intact and particulate samples to be generated.
- A total of 1774 metres of drill-core was classified and quantified mineralogical and textural information extracted. To this authors knowledge there are no existing studies that have been undertaken on this scale.
- The use of classified mineral maps created from optical microscopy images. A total of 406 mineral maps of drill-core tiles were created and quantified mineralogy and texture extracted.
- The development of a method for creating a representative mineral spectra library for MLA analyses.
- The development of a method for calculating mineral abundances from elemental assay data.

Outcomes from Cadia East

The outcomes presented in this section are based on the mineralogical and textural analyses undertaken in this research which utilised; meso-scale visual logging of drill-core, micro-scale MLA analysis of drill-core tiles and optical microscopy analysis of particulate samples. The key results are:

- Meso-scale logging identified four major classes (and thirteen sub-classes) that are predicted to have unique mineral processing behaviours. These are Cu-sulphide minerals hosted by (1) quartz-calcite sheeted veins (2) mafic minerals (chlorite, biotite, magnetite, epidote or tourmaline) (3) felsic minerals (albite, K-feldspar, quartz, illite or muscovite) and (4) fault zones (chlorite or laumontite). The subclasses are typically variations in the textures and distribution of the gangue minerals. Three unique grain size populations were identified for chalcopyrite and bornite (1) fine-grained disseminations (2) coarse-grained aggregates and (3) vein-hosted.
- XMOD analysis of 130 drill-core tiles showed that the most commonly occurring minerals are K-feldspar, illite/muscovite, quartz, biotite and chlorite which is consistent with the four major groups established in the meso-scale texture analysis.
- The analysis of 130 SPL-lite images identified the presence of three size distribution trends (as well as three bimodal distribution trends) consistent with meso-scale grain size populations. The dominant gangue mineral associations with chalcopyrite and bornite, identified using a Principal Components Analysis (PCA), were composed of one or two minerals. These are albite, chlorite/biotite, illite/muscovite and K-feldspar for chalcopyrite and epidote, albite, illite/muscovite, chlorite/biotite, K-feldspar, quartz and chalcopyrite for bornite.
- SPL-lite analysis identified the presence of gold and electrum. In the upper portion of Cadia East gold is typically encapsulated by pyrite and chalcopyrite. For Cadia East Deeps, the gold and electrum is typically vein hosted with Cu-sulphide minerals or within the vein selvage hosted by K-feldspar or quartz.
- The analysis of optical microscopy images of 38 particulate samples determined that the most common particle compositions were red feldspar-chlorite, red feldspar-quartz/feldspar-chlorite, chlorite-muscovite-red feldspar, red feldspar and red feldspar-chlorite-chalcopyrite respectively.

Outcomes from Ernest Henry

The outcomes presented in this section are based on the mineralogical and textural analyses undertaken in this research which utilised; meso-scale visual logging of drill-core, machine-based logging of drill-core, micro-scale MLA analysis and optical microscopy analysis of drill-core tiles. The key results are:

- Meso-scale visual logging identified nine textural classes that are predicted to have unique mineral processing behaviours. These were determined based on the gangue mineral textures (massive or fragmental), the dominant gangue minerals (feldspar, calcite, quartz, magnetite, pyrite) and the size of the chalcopyrite (fine-grained disseminated or coarse-grained clotted).
- 1454 classified mineral maps of drill-core were analysed for modal mineralogy, chalcopyrite area, chalcopyrite length and mineral associated with chalcopyrite. From these quantified measurements, three of the visual texture classes were able to be distinguished (MaF, MaM and MF4 and the remaining six grouped into three classes (F1 [MF1 and BF1], F2 [MF2 and BF2] and F3 [MF3 and BF3]).

- PCA of the results from 398 optical microscopy mineral maps identified that the most common mineralogical signatures to be red feldspar, quartz, barite-carbonate minerals, magnetite-hematite-mafic minerals, chalcopyrite-pyrite-magnetite-hematite and pyrite-chalcopyrite. Size distribution curves of chalcopyrite grains identified three distinct trends (and two bimodal distribution trends). PCA of ~326 000 chalcopyrite PhRegs determined that the most common minerals to be associated with chalcopyrite are magnetite-mafic minerals, quartz, pyrite-carbonate minerals, red feldspar and quartz.
- The most common minerals are K-feldspar, carbonate, quartz, pyrite, magnetite and hyalophane based on 311 XMOD analyses of drill-core tiles.
- The analysis of 311 SPL-lite images identified the presence of three size distribution trends (as well as four bimodal trends) consistent with meso-scale grain size populations. The dominant gangue mineral associations with chalcopyrite were identified using a PCA as magnetite, quartz, carbonate minerals and K-feldspar.
- SPL-lite analysis identified the presence of gold (126 grains) and electrum (389 grains). The average ECD for gold and electrum was 8.20 μm and 13.47 μm respectively. The most common minerals associated with electrum are pyrite, chalcopyrite-pyrite, magnetite, chalcopyrite-magnetite, K-feldspar, quartz and calcite. The most common minerals associated with gold are magnetite, K-feldspar, calcite, pyrite, hyalophane, quartz and chalcopyrite.

7.4 Recommendations for further work

Recommendations for further work based on the research presented in this thesis are:

1. A much larger database of measured liberation and recovery behaviour is required to fully calibrate and test predictions based the database developed in this project.
2. The methods and technologies presented in this thesis should be tested on other deposit styles.
3. A deposit scale mineralogical and textural study. This will allow mineralogical and textural data (including texture classes) to be integrated into a block model and their 3-dimensional distributions to be observed on a deposit scale.

References

Allan, G.C. and Woodcock, J.T., 2001. *A review of the flotation of native gold and electrum*. Minerals Engineering, **14**(9): 931-692.

Allen, J. R. L., 1971. *Transverse erosional marks of mud and rock: their physical basis and geological significance*. Sedimentary Geology, **5**(3-4): 167-385.

Arif, J. and Baker, T., 2004. *Gold paragenesis and chemistry at Batu Hijau, Indonesia: implications for gold-rich porphyry copper deposits*. Mineralium Deposita, **39**: 523-535.

Barton, P. B. Jr., 1991. *Ore textures: Problems and opportunities*. Mineralogical Magazine, **55**: 303-315.

Becker, M., Brough, C., Smith, D., Bradshaw, D., 2008. *Geometallurgical characteristaion of the Merensky Reef and Northam platinum mine; comparison of normal, pothole and transitional reef types*. International Congress for Automated Mineralogy, Brisbane, Queensland, Conference Proceedings. 391-399.

Berkman, D.A. (Ed), 2001, *Field geologist's manual,* Australian Institute of Mining and Metallurgy, Melbourne, 4th Edition, pp395.

Berry, R., 2008. *Mesoscale core imagery*. In: AMIRA P843 – Geometallurgical Mapping and Mine Modelling: Technical Report 2. 8.1- 8.8.

Berry, R., Walters, S.G. and McMahon, C., 2008. *Automated Mineral Identification by optical microscopy*. Ninth International Congress for Automated Mineralogy, Conference Proceedings. 91-94.

Blair, T. C. and McPherson, J. G., 1999. *Grain-size and textural classification of coarse sedimentary particles*. Journal of Sedimentary Research, **69**(1): 6-19.

Bojcevski, D., Vink, L., Johnson, N. W., Landmark, V., Johnston, M., Mackenzie J., Young, M.F., 1998. *Metallurgical characterisation of George Fisher ore textures and implications for mineral processing*. Mine to Mill, Brisbane, Conference Proceedings. 29-41.

Bojcevski, D., 2004. *Metallurgical characterisation of George Fisher meso-textures and micro-textures*. Masters Thesis, School of Engineering, The University of Queensland. 376pp.

Bonnici N., Hunt, J.A., Walters, S.G., Berry, R., and Collett, D., 2008. *Relating textural attributes to mineral processing – Developing a more effective approach for the Cadia East Cu-Au porphyry deposit*. Ninth International Congress for Automated Mineralogy, Conference Proceedings. 415-418.

Bonnici, N., Hunt, J., Walters, S., Berry, R., Kamenetsky, M., McMahon, C., Nguyen, K., 2009. *Integrating meso- and micro- textural information into mineral processing: An example from the Ernest Henry Iron-Oxide Copper-Gold deposit, Queensland, Australia*. 41st Annual Meeting of the Canadian Mineral Processors, Ottawa, Ontario, Conference Proceedings. 259-278.

Broch, E. and Franklin, J.A., 1972, *The point-load strength test*. International Journal of Rock Mechanics and Mining Sciences & Geomechanics Abstracts, **9(6):** 669 - 676

Bryant, E., 1982. *Behavior of grain size characteristics on reflective and dissipative foreshores, Broken Bay, Australia*. Journal of Sedimentary Research. **52**: 431-450.

Bucher, K., and Frey, M., 1994. *Petrogenesis of metamorphic rocks*. 6th edition © Springer-Verlag, Berlin, Heidelburg. 315pp.

Cashman, K.V. and Ferry, J.M., 1988. *Crystal size distribution (CSD) in rocks and the kinetics and dynamics of crystallization III. Metamorphic crystallization*. Contributions to Mineral Petrology. **99**: 401-415.

Cashman, K.V., and Marsh, B.D.,1988. *Crystal size distribution (CSD) in rocks and the kinetics and dynamics of crystallization II. Makaopuhi lava lake*. Contributions to Mineralogy and Petrology, **99**: 292-305.

Castroviejo, R., Brea, C., Pérez-Barnuevo, L., Catalina, J.C., Segundo, F., Bernhardt, H.J., Pirard, E., 2009. *Using computer vision for microscopic identification of ores with reflected light*. Society for Geology Applied to Mineral Deposits, Townsville, Australia, Conference Proceedings.

Chayes, F., 1956. Petrographic Modal Analysis. John Wiley and Sons, Inc, New York. 113p.

Cheetham, M.D., Keene, A.F., Bush, R.T., Sullivan, L.A., Erskine, W.D., 2008. *A comparison of grain-size analysis methods for sand-dominated fluvial sediments*. Sedimentology. **55**(6): 1905-1913.

Copeland, L.E. and Bragg, R.H., 1958. *Quantitative X-ray diffraction analysis*. Analytical Chemistry. **7**: 519-525.

Cottrell, A., 1975. *An introduction to metallurgy*, 2nd Edition, Edward Arnold, London, 548pp.

Craig, J.R. and Vaughan, D.J., 1981. *Ore microscopy and Ore Petrography*. John Wiley & Sons, NY. 406pp.

Dai, Z., Bos, J.A., Lee, A., Wells, P., 2008. *Mass balance and mineralogical analysis of flotation plant survey samples to improve plant metallurgy*. Minerals Engineering. **21**(12-14): 826-831.

Definiens Developer 7 Reference Book, © 2007 Definiens. All Rights reserved. 195pp.

Donskoi, E., Suthers, S.P., Fradd, S.B., Young, J.M., Campbell, J.J., Raynlyn, T.D., Clout, R.M.F., 2007. *Utilization of optical image analysis and automatic texture classification for iron ore particle analysis*. Minerals Engineering. **20**: 461-471.

Dou, M., 2002. *Automatic Mineral Identification using BSE and EDS signals from an SEM*. PhD Thesis, Julius Kruttschnitt Mineral Resource Centre, University of Queensland, Australia

Dowling, J.J., 1977. *A grain size spectra map*. Journal of Sedimentary Research. **47**(1): 281-284.

Dyer, K.R., 1970. *Grain size parameters for sandy-gravels*. Journal of Sedimentary Petrology. **40**: 616-620.

Erlich, R., and Weinberg, B., 1970. *An exact method for the characterization of grain shape*. Journal of Sedimentary Petrology. **40**: 205-212.

Evans, C., 2010. *Development of a methodology to estimate flotation seperability from ore microtexture,* PhD thesis, Sustainable Minerals Institute, University of Queensland.

Fandrich, R., Gu, Y., Burrows, D., Moeller, K., 2007. *Modern SEM-based mineral liberation analysis*. International Journal of Mineral Processing. **84**: 310-320.

Ferrara, G., Preti, U., Meloy, T.P., 1989. *Inclusion shape, mineral texture and liberation*. International Journal of Mineral Processing. **27**(3-4): 295-308.

Folk, R.L., 1951. Stages *of textural maturity in sedimentary rocks*. Journal of Sedminetary Research. **21**(3):127-130.

Gaspar, O. and Pinto, A., 1991. *The ore textures of the Neves-Corvo volcanogenic massive sulphides and their implications for ore beneficiation*. Mineralogical Magazine. **55**: 417-422.

Gay, S.L. and Latti, A.D., 2006. *Representation of particle multimineral distributions*. 23rd International Mineral Processors Conference, Instanbul, Turkey, Conference Proceedings. 237-241.

Gaudin, A.M., 1957. *Flotation 2nd Ed.* McGraw-Hill, New York. p262.

Gifkins, C.C., Herrmann, W., Large, R.R., 2005. *Altered Volcanic Textures: A guide to description and interpretation*. CODES Special Publication, University of Tasmania.

Gladstone C., and Sparks, R. S. J., 2002. *The significance of grain-size breaks in turbidites and pyroclastic density current deposits*. Journal of Sedimentary Research. **72**(1): 182-191.

Goldstein, G.I., Newbury, D.E., Echlin,P., Joy, D.C., Fiori, C., Lifshin, E. (1981). *Scanning electron microscopy and x-ray microanalysis*. New York: Plenum Press.

Goodall, W.R. and Scales, P.J., 2007. *An overview of the advantages and disadvantages of the determinations of gold mineralogy by automated mineralogy*. Minerals Engineering, **20**(5): 506-517.

Gottlieb, P., Wilkie, G., Sutherland, D., Ho-Tun, E., Suthers, S., Perera, K., Jenkins, B., Spencer, S., Butcher, A. and Rayner, J., 2000. *Using quantitative electron microscopy for process mineralogy applications*. Journal of Minerals, Metals and Materials Society. **52**(4): 24-25.

Grupta, A. and Yan, B.V., 2006. *Mineral processing design and operations: An introduction*. © Elsevier B.V. 719pp

Gu, Y., 2003. *Automated Scanning Electron Microscope Based Mineral Liberation Analysis*. Journal of Minerals & Materials Characterization & Engineering. **2**(1): 33-41.

Hasofer, A.M.,1963. *On the Reliability of Point-counter Method in Petrography*. Australian Journal of applied Science, **14**: 168-179.

Hayes, J.R. and Klugman, M.A., 1959. *Feldspar staining methods*, Journal of Sedimentary Research. **29**(2): 227-232.

Higgins, M.D., 1994. *Numerical modeling of crystal shapes in thin sections: Estimation of crystal habit and true size*. American Mineralogist. **79**:113-119.

Higgins, M.D., 2000. *Measurement of Crystal Size Distributions*. American Mineralogist. **85**: 1105-1116.

Higgins, M.D., 2002. *Closure in Crystal Size Distributions (CSD), verification of CSD calculations and the significance of CSD fans*. American Mineralogist. **87**: 171-175.

Higgins, M.D., 2006. *Use of appropriate diagrams to determine if crystal size distributions (CSD) are dominantly semi-logarithmic, logarithmic or fractal (scale invariant)*. Journal of Volcanology and Geothermal Research. 154: 8-16.

Higgins, M.D., 2006a. *Quantitative textural measurements in igneous and metamorphic petrology*. © Cambridge University Press. 270pp.

Higgins, M.D., and Chandrasekharam, D., 2007. *Nature of sub-volcanic magma chambers, Deccan province, India: Evidence from quantitative textural analysis of plagioclase megacrysts in the Giant plagioclase basalts*. Journal of Petrology. **48**:885-900.

Higgins, M.D. and Roberge, J., 2003. *Crystal Size Distribution (CSD) of plagioclase and amphibole from Soufriere Hills volcano, Montserrat: Evidence for dynamic crystallization/ textural coarsening cycles*. Journal of Petrology. **44**:1401-1411.

Howarth and Rowlands, 1987. *Quantitative assessment of Rock texture and correlation with drillability and strength properties*. Rock Mechanics and Rock Engineering. **20**:57-85.

Hudleston, P.J., 1973. *Fold morphology and some geometrical implications of theories of fold development.* Tectonophysics. **16**: 1-46.

Hunt, J.A., Berry, R., Walters, S., Bonnici, N., Kamenetsky, M., Nguyen, K. and Evans, C.L., 2008. *A new look at mineral maps and the potential relationships of extracted data to mineral processing behaviours*. 9th International Congress for Applied Mineralogy (ICAM), Brisbane, QLD. 429-432.

Hunt, J., Berry, R., Bonnici, N., Walters, S., Kamenetsky, M. and McMahon, C., 2009. *From drill core to processing – A geometallurgical approach to mineralogy and texture from meso- to micro- scale*. The proceeding of the 10th Biennial Meeting of the SGA, Townsville, 2009. 685-687.

Johnson, D.B., and Hallberg, K.B., 2005. *Acid mine drainage remediation options: A review*. Science of the total environment. 388 (1-2): 3-14.

Jolliffe, I.T., 2002. *Principle component analysis*. Springer-Verlag New York, Inc. 491pp.

Jones, M.P., 1987. *Applied mineralogy: A quantitative approach*. London; Norwell, MA., Graham and Trotman, 261pp

Jyothi, B.N., Babu, G.R., Krishna, I.V., 2008. *Object Oriented and Multi-Scale image analysis: Strengths, Weaknesses, Opportunities and Threats – A review*. Journal of Computer Science, **4**(9): 706-712.

Keary, P., 2001, Dictionary of Geology (2nd Edition), 2001, Penguin UK.

King, P., 2001. *Modeling and Simulation of mineral processing systems*. Elsevier, 402p.

Kitto, J C, 2005. *Lithostratigraphy, alteration and mineralisation of the Cadia East porphyry Au-Cu deposit, NSW*. Honours thesis, University of Tasmania, p136

Klein, C; Hurlbut, C.S Jr, 1977. *Manual of Mineralogy*, 20th edition. ©1977 (John Wiley & Sons).

Kleinhans, M.G., 2005. *Autogenic cyclicty of foreset sorting in experimental Gilbert-type deltas*. Sedimentary Geology, **181**(3-4): 215-224.

Klug, H.P. and Alexander, L.E., 1954. X-ray Diffraction Procedures for Polycrystalline and Amorphous Materials. John Willey and Sons, New York. 622pp.

Kodama, Y., 1994. *Downstream changes in the Lithology and Grain Size of Fluvial Gravels, the Watarase River, Japan: Evidence of the role of abrasion in Downstream Fining*. Journal of Sedimentary Research. **64A**: 68-75.

Komar, P.D., 1977. *Selective longshore transport rates of different grain-size fractions within a beach*. Journal of Sedimentary Petrology. **47**(4): 1444-1453.

Krumbein, W.C., 1934. *Size frequency distribution of sediments*. Journal of Sedimentary Petrology. **4**: 65-77.

Lancaster, N., 1986. *Grain-size characteristics of linear dunes in the southwestern Kalahari*. Journal of Sedimentary Petrology. **56**(3): 395-400.

Lane, G.R., Martin, C. And Pirard, E., 2008. *Techniques and applications for predictive metallurgy and ore characterization using optical image analysis*. Minerals Engineering. **21**(7): 568-577.

Lastra, R., 2002. *A comparison of liberation determinations by particle area percentage and exposed particle perimeter percentage in a flotation concentrator*. Journal of Minerals & Materials Characterization & Engineering. **1**(1): 31-37.

Lastra, R., 2007. Seven *practical cases of liberation analysis*. International Journal of Mineral Processing, **84**(1-4): 337-347.

Latti, D., Adair, B.J.I., 2001. *An assessment of stereological correction procedures*. Minerals Engineering, **14**(12): 1579-1587.

Launeau, P. and Cruden, A.R., 1998. *Magmatic fabric acquisition mechanisms in a syenite; results of a combined anisotropy of magnetic susceptibility and image analysis study*. Journal of Geophysical Research. **103**(B3): 5067-5089.

Lastra, R., Petruk, W., Wilson, J., 1998. *Image Analysis techniques and applications to mineral processing*. In: Modern Approaches to Ore and Environmental Mineralogy, Eds: Cabri and Vaughan © Mineralogical Association of Canada. 327-366.

Leigh, G.M., 1993. *The reconstruction method of Barbery; estimating particle shape and mineral texture from cross-sectional and line-scan data*. 3rd International Congress on Applied Mineralogy, Fremantle, Western Australia. Conference Proceedings. 50-53.

Leigh, G.M., 2008. *Automatic Ore Texture Analysis for Process Mineralogy*. Ninth International Congress for Automated Mineralogy, Conference Proceedings. 433-436.

Le Maitre, R.W., 2002. *Igneous Rocks: A classification and glossary of terms: Recommendations of International Union of Geological Sciences Subcommision on the systematics of Igenous rocks*. Cambridge university Press, 236pp.

Livingstone I., Bullard, J.E., Wiggs, G.F.S., Thomas, D.S.T., 1999. *Grain-size variation on dunes in the southwest Kalahari, Southern Africa*. Journal of Sedimentary Research. **69**(3): 546-552.

Mark, G, Oliver, H S, Williams, P J, 2006. Mineralogical and chemical evolution of the Ernest Henry Fe oxide-Cu-Au ore system, Cloncurry district, northwest Queensland, Australia, *Mineralium Deposita*, **40**: 769-801

McArthur, G.J., 1996. *Textural evolution of the Hellyer massive sulfide deposit*. Unpublished PhD thesis, University of Tasmania, Hobart, Australia. 272pp.

McBirney, A. R., 2007. *Igneous Petrology*. Boston: Jones and Bartlett publishers. 550pp.

McClaren, P. and Bowles, D., 1985. *The effects of sediment transport on grain-size distributions*. Journal of Sedimentary Research. **55**(4): 457-470.

MacKenzie, W.S. and Adams, A.E., 1994. *A colour atlas of rocks and minerals in thin section*. © Manson Publishing Ltd 1994. 192pp.

Macquarie Dictionary (5th edition), 2009, Macquarie Dictionary Publishers Pty Ltd.

Mock, A. and Jerram, D. A., 2005. *Crystal Size Distributions (CSD) in Three Dimensions: Insights from the 3D Reconstruction of a Highly Porphyritic Rhyolite*. Journal of Petrology. **46**(8): 1525-1541.

Moen, K., 2006. Quantitative measurements of mineral microstructures. Development, implementation and use of methods in applied mineralogy. PhD thesis, Norwegian University of Science and Technology, Faculty of Engineering Science and Technology.

MLA System User Operating Manual Module 3, 2005. Version 2.1a © Julius Kruttschnitt Minerals Resource Centre. 55pp.

Napier-Munn, T. J., S. Morrell, Morrison, R., Kojovic, T., 1996. *Mineral comminution circuits: Their operation and optimization.* Brisbane Australia, JKMRC University of Queensland, JKMRC Monograph Series in Mining and Mineral Processing 2, 413 p.

Napier-Munn, T.J. and Wills, B.A., 2005, Wills – Mineral Processing Technology, 7th Edition, JKMRC University of Queensland, 456pp,

Newcrest Mining staff, 1998. Cadia gold-copper deposits: geological update. Geological Society of Australia Abstracts No 49, p334.

Nickling, W.G., 1983. *Grain-size characteristics of sediment transported during dust storms*. Sedimentary Petrology. **53**: 1011-1024.

Oakey, R.J., Green, M., Carling, P.A., Lee, M.W.E., Sear, D.A., Warburton, J., 2005. Grain-shape analysis; a new method for determining representative particle shapes for populations of natural grains. Journal of Sedimentary Research. 75(6): 1065-1073.

Nichols, G., 2009. *Sedimentology and stratigraphy*. 2nd edition. © 2009 John Wiley and Sons. 419pp.

Pan, Y. and Higgins M.D., 2002. *Closure in crystal size distributions (CSD), verification of CSD calculations, and the significance of CSD fans*. American Mineralogist. **87**(8-9): 1242-1244.
Pawloski, G.A., 1985. *Quantitative determination of mineral content of geological samples by X-ray diffraction.* American Mineralogist. **70**: 663-667.

Petruk, W., 2005. *Applied mineralogy in the Mining Industry*. Elsevier Science BV, Amsterdam. 268pp.

Pettijohn, F.J., Potter, P.E. and Siever, R., 1972. *Sand and sandstone*. Springer-Verlag, Berlin, 618pp.

Pirard, E., 2004. *Microspectral imaging of ore minerals in optical microscopy*. Mineralogical Magazine. **68**(2):323-333.

Pirard, E., 2005. Image Anlaysis. In: Developments in Paleoenvirnmental Research. 7(1):59-86.

Pirard, E., Bernhardt, H.J., Catalina, J.C., Segundo, F., Castroviejo, R., 2008. *From spectrophotometry to multispectral imaging or ore minerals in visible and near infrared (VNIR) microscopy*. International Congress for Automated Mineralogy, Brisbane, Queensland, Conference Proceedings. 57-62.

Pirard, E., Vergara, N. and Chapeau, V., 2004. *Direct estimation of sieve size distributions from 2-D image analysis of sand particles*. Conference Proceedings, PARTEC 2004.

Pirard, E. and Dislaire, G., 2005. Robustness of Planar Shape Descriptors of Particles, 10th Annual Conferenence for the International, Conference Proceedings, PARTEC 2007.

Pirard, E., Leibichot, S and Krier, W., 2007. *Particle texture analysis using polarized light imaging and grey level intercepts*. International Journal of Mineral Processing. **84**: 299-309.

Pitard, F.F., 1993. Pierre Gy's Sampling Theory and Sampling Practice. Heterogeneity, Sampling Correctness, and Statistical Process Control © CRC Press. 488p

Pourhahramani, P., Forssberg, E., 2005. *Review of applied particle shape descriptors and produced particle shapes in grinding environments. Part II: The influence of comminution on the shape particle*. Mineral Processing and Extractive Metallurgy Review. **26**(2): 167-186.

Ramadorai, G., Hausen, D.M., Bucknam, C.H., 1991. *Metallurgical, analytical and mineralogical features of Carlin refractory ores*. Ore Geology Reviews. **6**(2-3): 119-132.

Ramdhor, P., 1980. *The ore minerals and their intergrowths 2nd Ed*. © Pergamon Press, 1980, Oxford; New York. 1269pp

Rosin, P.L., 1999. *Further Five-Point Fit Ellipse Fitting*. Graphical Models and Image Processing. **61**(5):245-259.

Rosin, P.L., 2003. *Measuring shape: ellipticity, rectangularity, and triangularity*. Machine Vision and Applications. **14**(3): 172-184

Rosin, P. and Rammler, B., (1933). *The laws governing the fineness of powdered coal*. Journal of the Institute of Fuels. 7: 29-36.

Russ, John, C. and Russ, J. Christian., 2007. *Introduction to image processing and analysis*. © Taylor & Francis Group, LLC, 821pp.

Ryan, A J, 1998. Ernest Henry copper-gold deposit, in *Geology of Australian and Papua New Guinea Mineral Deposits* (Eds: D A Berkmand and D H Mackenzie), pp 759-768 © The Australian Institute of Mining and Metallurgy, Melbourne.

Schaik, A. van, Reuter, M.A., Heiskanen, K., 2004. The influence of particle size reduction and liberation on the recycling rate of end-of-life vehicles, Minerals Engineering, 17: 331-347.

Schumann, R., 1940. *Principles of comminution. 1. Size distribution and surface calculations*. American Institute of Mining and Metallurgical Engineers. No.1187.

Serra, J., 1982. *Image analysis and mathematical morphology*. New York, Academic Press.

Solomon, M., 1963. *Counting and Sampling Errors in Modal Analysis by Point-counter*. Journal of Petrology, **4**: 367-382.

Streckeisen, A.L.,1974. *Classification and Nomenclature of Plutonic rocks. Recommendations of the IUGS Subcommision on the Systematics of Igneous Rocks*. Geologische Rundschau. Internationale Zeitschrift für Geologie. STittgart. **63**: 773-785.

Strohmayr, S J, Barns, K E, Brindley, S K, Munro, P D, 1998. Mineralogy Controlling Metallurgy at Ernest Henry Mining, in *Mine to Mill* conference proceedings, pp 13-17 © The Australian Institute of Mining and Metallurgy, Melbourne

Sutherland, D., 2007. *Estimation of mineral grain size using automated mineralogy*. Minerals Engineering, **20**: 452-460.

Tamura, T., 2004. *Preservation and grain-size trends of Holocene wave-dominated facies successions in eastern Japan: implications for high-resolution sequence stratigraphic analysis*. Journal of Sedimentary Research. **74**(5): 718-729.

Triebold, S., Kronz, A., Woerner, G., 2006. *Anorthite-calibrated backscattered electron profiles, trace elements, and growth textures in feldspars from the Teide-Pico Viejo volcanic complex (Tenerife)*. Journal of Volcanology and Geothermal Research. **154**(1-2): 117-130.

Triffett, B. and Bradshaw, D., 2008. *The role of morphology and host rock lithology on the flotation behaviour of molybdenite at Kennecott Utah Copper*. International Congress for Automated Mineralogy, Brisbane, Queensland, Conference Proceedings. 465-473.

Turner, F.J. and Verhoogen, J., 1960. *Igneous and metamorphic geology*, 2nd Edition, © McGraw-Hill Book Company Inc. 1960, New York, Toronto, London.

Van Alpin, C., 2007. *Automated mineralogical analysis of coal and ash products – Challenges and requirements*. Minerals Engineering, **20**(5): 496-505.

Vatandoost, A, Fullagar, P, Roach, M, 2008. *Automated multi-sensor petrophysical core logging*. Exploration Geophysics, **39**(3):181-188.

Vaughan, J.P. and Kyin, A., 2004. *Refractory gold ores in Archaean greenstones, Western Australia; mineralogy, gold paragenesis, metallurgical characterization and classification*. Mineralogical Magazine. 68(2): 255-277.

Veasey, T.J., Penhallow, A.L. and Elliott, A.J., 1989. *Mineralogy and mill performance optimization – a case study of south crofty tin mine*. Minerals Engineering. **2**(4): 471-480.

Verwaal, W. and Mulder, A., 1993, Estimating rock strength with the EQUOtip hardness tester: International Journal of Rock Mechanics and Mining Sciences & Geomechanics Abstracts, v. 30, p. 659-662.

Vink, L.,1997. *Textures of the Hilton North deposit, Queensland, Australia, and their relationship to liberation.* PhD Thesis, University of Queensland

Walters, S. and Kojovic, T., 2006. *Geometallurgical Mapping and Mine Modelling (GeM'") – the way of the future*. International Autogenous and Semi-Sutogenous Grinding Technology 2006, Vancouver Canada, 2006, Conference Proceedings. 411-425.

Walters, S., 2008. *An overview of new integrated geometallurgical research. Ninth International Congress for Applied Mineralogy*. ICAM Australia 2008, Brisbane, QLD 8-10 September. Conference Proceedings. 79-82.

Weibel, E.R.,1980. *Stereological Methods, Vol.2: Theoretical Foundations*. Academic Press. London. 340pp.

Wentworth, C.K., 1922. *A scale of grade and class terms for classic sediments*. Journal of Geology. **30**(5):377-392.

Wills, B.A. and Napier-Munn T., 2006. *Wills' Mineral Processing Technology. An introduction to the practical aspects of ore treatment and mineral recovery*, 7th edition. Elsevier Publishers. 456pp.

Wilson, A, 2003. The genesis and exploration context of porphyry Cu-Au deposits in the Cadia district, NSW. PhD thesis, CODES, University of Tasmania, p316

Wright, V.P., 1992. *A revised classification of limestones. Sedimentary Geology*. **76** (3-4): 177-185.

Xiao, Z. and Laplante, A.R., 2004. *Characterizing and recovering platinum group minerals – a review*. Minerals Engineering. **17**: 961-979.

Internet References

Australian Government AusAID, 2010. *AusGuide – A Guide to Program Management*. Retrieved from: http://www.ausaid.gov.au/ausguide/

British Geological Survey, 1999. *BGS Rock Classification Scheme: Metamorphic rocks*. Retrieved from: http://www.bgs.ac.uk/bgsrcs/home.html

British Geological Survey, 1999. *BGS Rock Classification Scheme: Igneous rocks*. Retrieved from: http://www.bgs.ac.uk/bgsrcs/home.html

Definiens, 2010. Understanding Images http://www.definiens.com/

EDAX home page, 2008. retrieved from: http://www.edax.com

Geoscience Australia, 2009. *Copper fact sheet*. Retrieved from: http://www.australianminesatlas.gov.au/

GEOTEK, 2000. Documentation for GEOTEK logger, www.GEOTEK.co.uk

JKTeck, 2010. *Mineral Liberation Copper Ores*. Retrieved from: http://www.jktech.com.au/Products_Services/Brochure_Files/MLA_CopperOres_006_EMAIL.pdf

MinAssist, 2006. *QEMSCAN*. Retrieved from: http://www.minassist.com.au/services/qemscan.html
SGS Group website, 2010. *Metallurgical Services*. Retrieved from: http://www.met.sgs.com/metallurgy_home_v2/services/met_mineralogical_services/explomin.htm

Newcrest Mining Ltd., 2010. *Mineral resources and reserves, 2009*. Retrieved from http://www.newcrest.com.au//pdf/FINAL%202009%20Resource%20and%20Reserve%20Statement.pdf

Syndicated Metals, 2010. *Projects: Mount Isa region*. Retrieved from: www.syndicatedmetals.com.au/projects-mtisa.php

Xstrata Copper, 2009. *News press release: Xstrata approved development of Ernest Henry underground mine and magnetite processing operation*. Retrieved from: http://www.xstrata.com/media/news/2009/12/03/08700CET/

Appendix 1.1

Mineral Abbreviations

The mineral abbreviations used in this thesis follow the recommendations by the IUGS Subcommision on the Systematics of Metamorphic Rocks: Web version 01.02.07 (Chace, 1956; Kretz, 1983). Minerals in italics are not listed in the IUGS Subcommision on the Systematics of Metamorphic Rocks.

Ab	Albite
Act	Actinolite
Afs	Alkali feldspar
Anh	Anhydrite
Ank	Ankerite
Ap	Apatite
Apy	Arsenopyrite
Au	Gold
Bis	Bismuthinite
Bn	Bornite
Brt	Barite
Bt	Biotite
Cal	Calcite
Cb	Carbonate mineral
Ccp	Chalcopyrite
Chl	Chlorite
Clh	Clausthalite
Cls	Celestite
Dg	Digenite
Di	Diopside
Dol	Dolomoite
El	Electrum
Enr	Enargite
Ep	Epidote
Fl	Fluorite
Fsp	Feldspar
Gn	Galena
Grt	Garnet
Hbl	Hornblende
Hem	Haemetite
Hs	*Hessite*
Hy	*Hyalophane*
Ill	Illite
Kfs	K-feldspar
Lmt	Laumontite
Mag	Magnetite
Mnz	Monazite
Mo	Molybdenite
Ms	Muscovite
Op	Opaque mineral
Or	Orthoclase
Phl	Phlogopite
Pl	Plagioclase
Px	Pyroxene
Py	Pyrite
Qtz	Quartz
REE	Rare Earth Elements
Rt	Rutile
Sch	Scheelite
Sd	Siderite
Ser	Sericite
Sp	Sphalerite
Tlc	Talc
Tt	Tetrahedrite
Ten	*Tennanite*
Ttn	Titanite
Tur	Tourmaline

Appendix 6
Texture Viewer (version 1)

K. Nguyen
JK Mineral Research Centre, University of Queensland
Email: k.nguyen@mailbox.uq.edu.au

Executive summary

Texture Viewer is a software program that allows researchers to analyse textures observed in classified images. The first version of Texture Viewer was officially released in August 2007 to GeM^{III} researchers. Following is an up-to-date summary and the application user manual.

Main features of the software

1. Texture Viewer uses standard MS-Windows image file formats such as: *.dib, *.bmp, *.tif, *.tga, *.gif, *.pcx, *.jpg, and *.png. as picture input. Texture Viewer re-writes the files as 24-bit colour depth images.
2. Texture Viewer can be used to analyse images of particles (such as MLA images) and images of intact rock (e.g. tiles).
3. Texture Viewer can be used to extract, group and analyse minerals of interest in a highly visual user environment. Minerals can be examined based on two main categories: (1) whole minerals or particles, and (2) surface perimeter. In each category, the size, distribution and phase association for the minerals of interest can be retrieved through a sorting tree.
4. Texture Viewer can be used to examine the shapes of minerals and particles. The following common particle shape descriptors have been built-in: phase specific surface area (PSSA), Equivalent Area Circle and Surface Dispersions. Other popular shape descriptors such as: major and minor axis will be included in the next version.
5. User-defined parameters (e.g. density, hardness, Young's modulus) can be input into Texture Viewer as mineral properties and used during analysis and sorting.
6. Texture Viewer allows users to place a selected mask over an image and view the results. There are two types of masks which can be applied to the image: (1) user-selected mask, e.g. geometric mask or random particle shapes and (2) square grid (digital sieve).
7. Results from Texture Viewer analyses are displayed and reported in MS-Excel file format.

Limitations of the software

The followings are limitations of the current version of Texture Viewer:

- maximum particles in an image: 40,000
- maximum image resolution: 7000 pixels (W) x 7000 pixels (H)
- maximum sorting levels: 20
- maximum number of mineral properties (e.g. density, hardness) that can be input: 15.

These articles have been removed for copyright or proprietary reasons.

GeMIII (Amira P843) Technical Report 1 – February, 2008 (Texture viewer user manual) copyright Julius Kruttschnitt Mineral Research Centre 2007,
and,
GeMIII (Amira P843) Technical Report 2 – November, 2008 (Texture viewer user manual) copyright Julius Kruttschnitt Mineral Research Centre 2007

Texture Viewer User Manual

Version 1.0

16th August 2007

Contents

Contact: Khoi Nguyen, Julius Kruttschnitt Mineral Research Centre - The University of Queensland - Australia

Phone: 61 7 3365 5849
Fax: 61 7 3365 5999
Email Address: jkmrc@uq.edu.au
Web Site: http://www.jkmrc.uq.edu.au/